RICE UNIVERSITY

Design, Synthesis, and Monitoring of Light-Activated Motorized Nanomachines

by

Pinn-Tsong Chiang

A THESIS SUBMITTED
IN PARTIAL FULFILLMENT OF THE
REQUIREMENTS FOR THE DEGREE

Doctor of Philosophy

APPROVED, THESIS COMMITTEE

James M. Tour, Chair
T.T. and W.F. Chao Professor of
Chemistry, Professor of Computer
Science, and Professor of Mechanical
Engineering and Materials Science

Angel A. Martí
Assistant Professor of
Chemistry and Bioengineering

Rafael Verduzco
Assistant Professor of Chemical and
Biomolecular Engineering

HOUSTON, TEXAS
February 2013

Abstract

Design, Synthesis, and Monitoring of Light-Activated Motorized Nanomachines

by

Pinn-Tsong Chiang

Our group has developed a family of single molecules termed nanocars, which are aimed at performing controllable motion on surfaces. In this work, a series of light-activated motorized nanomachines incorporated with a MHz frequency light-activated unidirectional rotary motor were designed and synthesized. We hope the light-activated motor can serve as the powering unit for the nanomachines, and perform controllable translational motion on surfaces or in solution.

A series of motorized nanovehicles intended for scanning tunneling microscopy (STM) imaging were designed and synthesized. A *p*-carborane-wheeled motorized nanocar was synthesized and monitored by STM. Single-molecule imaging was accomplished on a Cu(111) surface. However, further manipulations did lead to motor induced lateral motion. We attributed this result to the strong molecule-surface interactions between the *p*-carborane-wheeled nanocar and the Cu(111) surface and possible energy transfer between the rotary motor and the Cu(111) surface. To fine-tune the molecule-surface interactions, an adamantane-wheeled motorized nanocar and a three-wheel nanoroadster were designed and synthesized. In addition, the STM substrates will be varied and different combinations of molecule-surface interactions will be studied.

As a complimentary imaging method to STM, single-molecule fluorescence microscopy (SMFM) also provides single-molecule level resolution. Unlike STM experiment requires ultra-high vacuum and conductive substrate, SMFM experiment is conducted at ambient conditions and uses non-conductive substrate. This imaging method allows us to study another category of molecule-surface interactions. We plan to design a fluorescent motorized nanocar that is suitable for SMFM studies. However, both the motor and fluorophore are photochemically active molecules. In proximity, some undesired energy transfer or interference could occur. A cyanine 5- (cy5-) tagged motorized nanocar incorporated with the MHz motor was designed and synthesized in order to minimize the potential energy transfer or interference between the motor and the fluorophore. The SMFM study of this cy5-tagged motorized nanocar is currently undergoing.

The design of light-activated motorized nanocar inspired the design of nanosubmarines. We used fluorescence quenching and fluorescence correlation spectroscopy (FCS) to study the diffusion of single molecules. The fluorescence quenching experiments of $Ru(bpy)_3^{+2}$ by a quenching nanosubmarine was conducted, but no motor induced acceleration of the molecule were observed. Another fluorescent nanosubmarine was monitored by FCS, and no increase of diffusion coefficient was found. Finally, a 1-D channel approach was adopted for decreasing the effects of Brownian motion, and acceleration of nanosubmarine was observed.

Acknowledgments

If I choose one word that best describes my Ph.D. studies, it is “odessey”. Obtaining a doctoral degree was not only working hard, composing a thesis, and getting a diploma. It is more like a trailblazer exploring new territories—always expecting something unexpected to happen. Looking back to the past few years at Rice, I am truly thankful for God’s grace and guidance, all my mentors, coleagues, friends and family who participated in this journey.

Thank you to Dr. Tour for your training, patience, and love (in disguise). I dedicate Hebrew 12:6 to you. It says “*My son, do not make light of the Lord’s discipline, and do not lose heart when he rebukes you, because the Lord disciplines the one he loves, and he chastens everyone he accepts as his son.*”

Thank you to Dr. Martí for your research collaborations, service in my committee, and many great advises not limit to academic. You are like my big brother who I can share with and look up to.

Thank you to Dr. Verduzco, Dr. Engel, and Dr. Billups for your service in my Ph.D. thesis defense and qualifying exam committee. Special thanks to your critical suggestions and evaluations of my work.

Thank you to Dr. Leohnard, Dr. Link, Dr. Kolomiesky, and Dr. Pasquali for the collaborations and discussions.

Thank you to Dr. James for correcting my writings and solving my requests in the group. You are the lubricant to keep the group operates smoothly.

Thank you to Dr. Alemany for not just teaching me NMR. You showed me the meaning of carefulness and critical thinking.

Thank you to all Tour Group members I worked with. In particular, the nanocar subgroup members, Guillaume, Jason, Jazmin, Edmund, and Victor, I will cherish the time we worked together.

Thank you to my parants and parants in law. Thank you for your unreserved supports to me and Yi-Yu. As our first born is on his way, we will appreciate you more and more.

Thank you to my wife, Yi-Yu, for marrying me and taking a life-long adventure with me. Thank you for sharing every moment with me. You and the unborn son are the ultimate reason that motivates me. I love you.

Thank you to my Lord and Savior Jesus Christ, for His unconditional love and unfathomable wisdom. Although life is full of unexpectedness, I am sure you will lead my way forever.

"*Things which eye has not seen and ear has not heard,*

and which have not entered the heart of man,

all that God has prepared for those who love him."

— 1 Corinthians 2:9

Table of Contents

List of Symbols and Abbreviations

Ac	Acetyl
AFM	atomic force microscopy
ATP	adenosine triphosphate
ATR	attenuated total reflectance
Boc	*tert*-butoxycarbonyl
BODIPY	4,4-difluoro-4-bora-3a,4a-diaza-*s*-indacene
bp	boiling point
br	broad (spectral)
Bu	butyl
calcd	calculated
℃	degree Celsius
cm	centimeter(s)
cm^{-1}	wavenumbers
cod	*cis,cis*-1,5-cyclooctadiene
d	doublet
D	diffusion constant
δ	chemical shift in parts per million
DCC	*N,N'*-dicyclohexylcarbodiimide
dd	doublet of doublet
DMAP	4-(dimethylamino)pyridine
DMF	dimethylformamide

ε	extinction coefficient
eq	equation
equiv	equivalence
Et	ethyl
FCS	fluorescence correlation spectroscopy
FRET	fluorescence resonance energy transfer
FTIR	Fourier transform infrared
g	gram(s)
h	hour(s)
HOMO	highest occupied molecular orbital
HRMS	high-resolution mass spectroscopy
Hz	hertz
IPA	isopropyl alcohol
J	coupling constant (in NMR spectroscopy)
KHMDS	potassium bis(trimethylsilyl)amide
L	liter(s)
λ_{abs}	maximum absorption wavelength
λ_{em}	maximum absorption wavelength
lit.	literature value
LUMO	lowest occupied molecular orbital
M	molar or moles per liter; mega
m	meter(s); mili; multiplet
MALDI	matrix-assisted desorption ionization

μ	micro
Me	methyl
Mes	2,4,6-trimethylphenyl (mesityl)
mg	milligram(s)
min	minute(s)
mol	mole(s)
mp	melting point
m/z	mass-to-charge ratio
NBS	*N*-bromosuccinimide
NHC	*N*-heterocyclic carbene
NIS	*N*-iodosuccinimide
nm	nanometer(s)
NMR	nuclear magnetic resonance
OPE	oligo(phenylene ethynylene)
p	pentet
Ph	phenyl
ppm	parts per million
%	percent
q	quartet (spectral)
ROMP	ring-opening metathesis polymerization
Φ_F	quantum yield of fluorescence
RIE	reactive ion etching
rt	room temperature

s	second(s); singlet (spectral)
SMFM	single-molecule fluorescence microscopy
STM	scanning tunneling microscopy
t	triplet (spectral)
TBAF	tetrabutylammonium fluoride
TEA	triethylamine
tert	tertiary
THF	tetrahydrofuran
TIPSA	triisopropylsilyl acetylene
TMS	trimethylsilyl
TMSA	trimethylsilyl acetylene
TOF	time-of-flight
TRITC	tetramethylrhodamine isothiocyanate
UV	ultraviolet
vis	visible

CHAPTER 1

Toward a Light-Driven Motorized Nanocar:

Synthesis and Initial Imaging of Single Molecules

Note: This chapter was copied and modified in whole with permission from a paper that I co-authored.[1]

1.1. Introduction

Organic synthesis has recently been applied to the construction of single-molecule machines. These nanomachines include, for example, switches,[2] shuttles,[3] and muscles[4] that were designed to perform their namesake functions at the molecular level when proper external stimuli are applied. We recently developed a family of nanovehicles termed nanocars[5,6] that were designed to operate on surfaces and to be studied at the single-molecule level. They were imaged by scanning tunneling microscopy (STM) on metallic surfaces[7] and non-conducting glass surfaces using single-molecule fluorescence microscopy (SMFM).[8,9] The ultimate purpose of our research has been to synthesize nanomachines that can transport nanocargo (materials or information) from one place to another on a surface. The first nanocar, which comprised a chassis and two axles mounted with four C_{60} wheels, exemplified structurally controlled directional movement on a surface due to rolling of the wheels.[10,11] The motion could be thermally (heated substrate surface) or electrically (STM-tip field) induced, thus opening the way to molecular-structure-defined motion at the nanoscale. Our next goal was to synthesize a nanomachine that can convert energy input (light or chemically powered)[12] into controlled motion on a surface. Hence, we prepared the first generation motorized nanocar (**1**),[13] intended to harvest light as fuel (Figure 1). In designing nanocar **1** we replaced the oligo(phenylene ethynylene) (OPE) chassis of the first C_{60}-wheeled nanocar with a light-driven unidirectional molecular motor. Also, we opted for *p*-carborane wheels because C_{60} quenched the photoisomerization process of the molecular motor.[13-15] We intended for the paddle-like rotor to interact with the surface and thereby generate force to propel the nanocar upon irradiation.

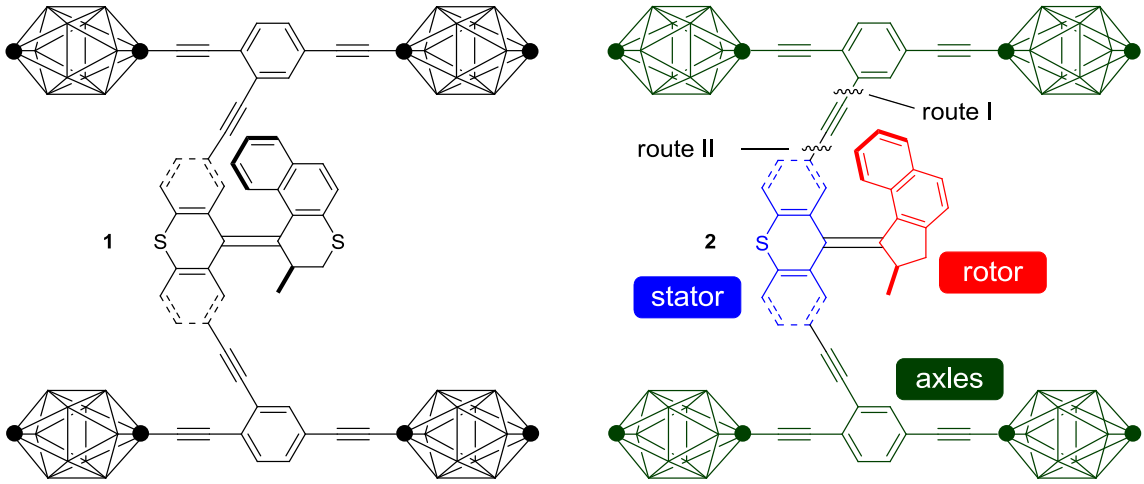

Figure 1.1. Structure of motorized nanocars. **Figure 1.1.** (Left) Structure of first generation motorized nanocar **1**. The *p*-carborane wheels have BH at every intersection except the black pointed vertices, which represent C and CH positions, *ipso* and *para*, respectively, relative to the alkyne. (Right) Structure of the second generation motorized nanocar **2**. Synthesis of **2** involved assembling the rotor (red), the stator (blue), and the axles (green) that bear carborane wheels.

1.2. Design of the Second Generation Motorized Nanocar

The kinetic parameters of the helical inversion process of nanocar **1** in solution, the rate determining step of the motor rotation, were obtained by proton NMR. The result was similar to the data obtained by Feringa and co-workers for the motor bearing two methoxy groups at the 2- and 7-positions on the thioxanthene stator.[16] These results were encouraging since the relatively bulky *p*-carborane-containing axles did not alter the rotation of the motor. However, the slow rotation of the motor, 202 h for a complete rotation at ambient temperature (1.8 rotations/h at 65 °C),[13] was a problem for surface

studies.

Hence, a molecular motor with a lower energy barrier to rotation process was needed. Feringa and co-workers determined that fine-tuning of the original motor of the first generation nanocar greatly enhanced the rotation rate by replacing the thiopyran rotor with a cyclopentanylidene rotor.[17,18] This increased the rotation rate by 10^{12}, producing a MHz unidirectional molecular motor. Accordingly, we designed the second generation motorized nanocar **2** (Figure 1). Here, we report the synthesis of **2** and its imaging by STM at low temperatures. This is a powerful method for the investigation of single nano-machines on a surface,[19] because thermal motion is suppressed. Moreover, it permits manipulation of single functional molecules by inducing internal changes,[20] lateral motion on a surface[21] or chemical modifications.[22] Furthermore, the changes within one and the same molecule upon light illumination from outside the ultrahigh vacuum chamber can be studied.[23] The molecular functions can thus be probed at the single molecular level with the complete information of the atomic-scale environment of each individual molecule.

1.3. Syntheis of the Core Molecular Motor

Scheme 1.1. Synthesis of molecular motor **9**.

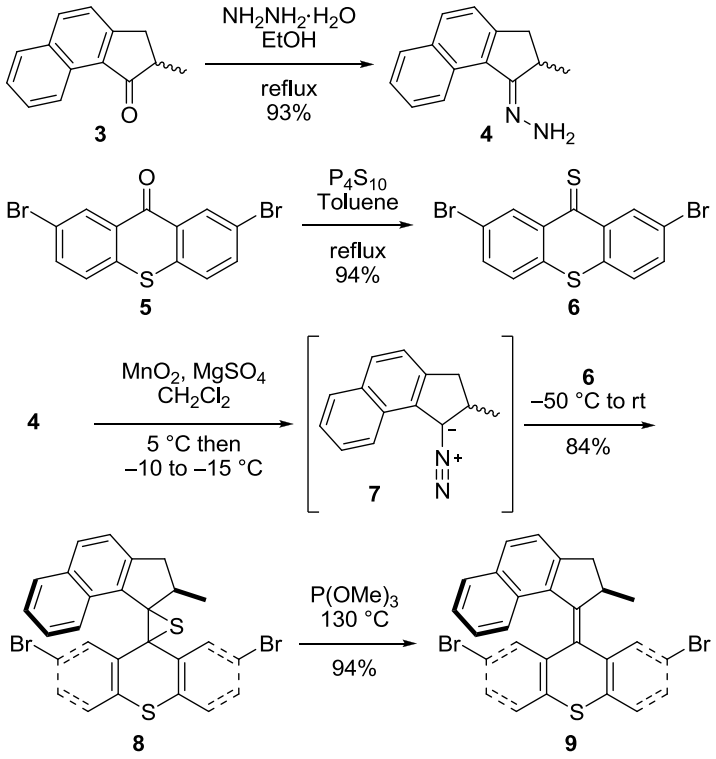

Our plan to synthesize nanocar **2** involved a modular approach in which the coupling of the axles and the stator represent the last step. According to Scheme 1.1., heating ketone **3** to reflux in an ethanol and hydrazine solution produced the rotor, hydrazone **4**.[24] The conversion of ketone **5** into thione **6** was improved by decreasing both the concentration and the reaction time from that in the published procedure.[13] The key step, generation of the sterically hindered double bond between the rotor and the stator, utilized the Barton-Kellogg coupling. Hydrazone **4** was oxidized to the unstable diazo intermediate **7** using manganese dioxide with careful temperature control. The inorganic residue was removed by filtration in a Schlenk-type set-up. Thione **6** was added

portionwise to the deep-purple filtrate. A [2+3] cycloaddition occurred and evolution of nitrogen gas indicated the formation of episulfide **8**. The white solid episulfide **8** was then treated with trimethyl phosphite in a screw-capped tube at 130 ℃ to afford molecular motor **9** in both chiral forms. As we plan to investigate individual molecules on surfaces, it was unnecessary to resolve the enantiomers.

1.4. NMR Characterization of Molecular Motor

We confirmed the structural integrity of key intermediate motor **9** using NMR techniques. All of the protons of motor **9** were unambiguously assigned with the assistance of correlation spectroscopy (COSY), nuclear Overhauser enhancement spectroscopy (NOESY), distortionless enhancement by polarization transfer spectroscopy (DEPT), heteronuclear single-quantum correlation spectroscopy (HSQC) and heteronuclear multiple-bond correlation spectroscopy (HMBC) experiments as detailed by the nuclear Overhauser enhancement (NOE) correlation arrows in Figure 2a and the accompanying spectrum.

The chemical shift difference steadily decreases between corresponding protons on the two benzene rings on the thioxanthenene stator: $\Delta\delta$ (H_a, $H_{a'}$) = 1.10 ppm, $\Delta\delta$ (H_b, $H_{b'}$) = 0.23 ppm and $\Delta\delta$ (H_c, $H_{c'}$) = 0.04 ppm, consistent with the steadily increasing distance of these pairs from the rotor. The chemical shifts of protons H_h, H_i and H_a reflect the shielding effect caused by the presence of an aromatic ring directly above H_a or directly below H_h and H_i. Compared to H_h and H_i, the most shielded aromatic protons in precursors **3** and **4** are at δ7.49-7.52[25] and δ7.32-7.38,[24] respectively; compared to H_a, the most shielded aromatic protons in precursors **5** and **6** are at δ7.43[26] and δ7.46,[13]

respectively. Interestingly, no NOE signals were found between H_a, H_i and H_a, H_h; this can be rationalized by the helical structure of the rotor as seen in Figure 2b. Proton H_i exhibits the most complex lineshape among the aromatic protons (more clearly shown in the Supporting information); not only does H_i couple to H_f, H_g, and H_h, but the COSY experiment also reveals coupling between H_i and each of the CH_2 protons.

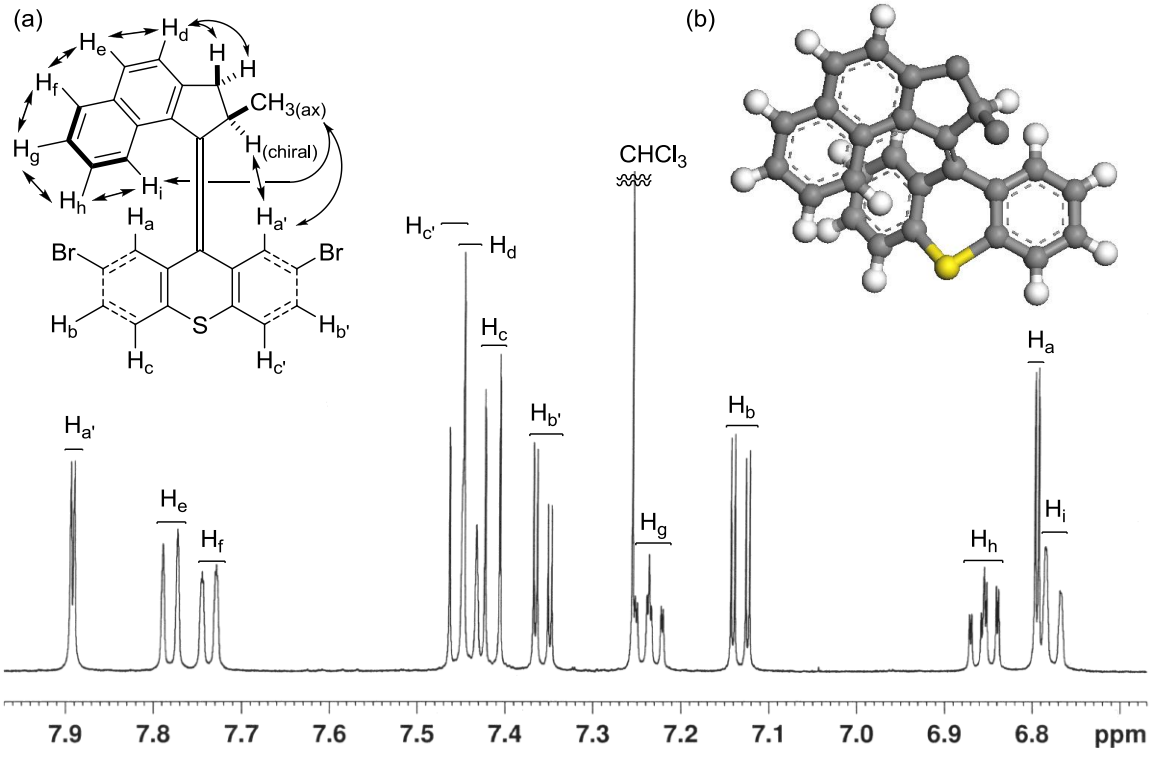

Figure 1.2. (a) Partial ^{1}H NMR (500 MHz, $CDCl_3$) at 295 K of molecular motor **9**. Selected NOE signals (double-headed arrows) were used to assign individual proton signals in the aromatic region as indicated in the top left structure. (b) Ball-and-stick model of the energy-minimized (*R*)-isomer of motor **9** (Materials Studio with forcite force field).

1.5. Assembly Line of the Second Generation Motorized Nanocar

We attempted the final assembly (Scheme 1.2., route I) of nanocar **2** using a method similar to our synthesis of nanocar **1**.[13] However, the subtle structural differences between the motors produced a remarkable difference in reactivities. Sonogashira coupling between trimethylsilylacetylene (TMSA) and **9** using conventional $Pd(PPh_3)_2Cl_2$ and CuI conditions did not afford the desired bis-coupled product, probably due to steric hindrance between the bromine atoms and the naphthalene rotor unit. Thus, a more reactive catalyst developed by Fu and co-workers[27] was used, but the result was disappointing because of a high degree of decomposition. Therefore, the more stable alkyne source, triisopropylsilylacetylene (TIPSA) was reacted with dibromide **9**. In a mixture of 6:1 NEt_3/THF as base and solvent, the Sonogashira coupling smoothly gave TIPS-protected bis-acetylene motor **10** in excellent yield. Compound **10** was deprotected using TBAF, producing dialkyne **11** in quantitative yield. Sonogashira coupling was used between dialkyne **11** and previously reported axle **12**[13] using $Pd(PPh_3)_4$ and CuI as catalysts to produced nanocar **2** in moderate yield. Therefore, we tried a more convergent synthetic pathway (Scheme 2, route II) by utilizing Sonogashira coupling between motor **9** and alkynylated axle **13**[7] by applying conditions analogous to those for the synthesis of **10**. Motorized nanocar **2** was thus obtained but in lower overall yield than that obtained from route I.

Scheme 1.2. Synthesis of the second generation motorized nanocar **2** through two different approaches

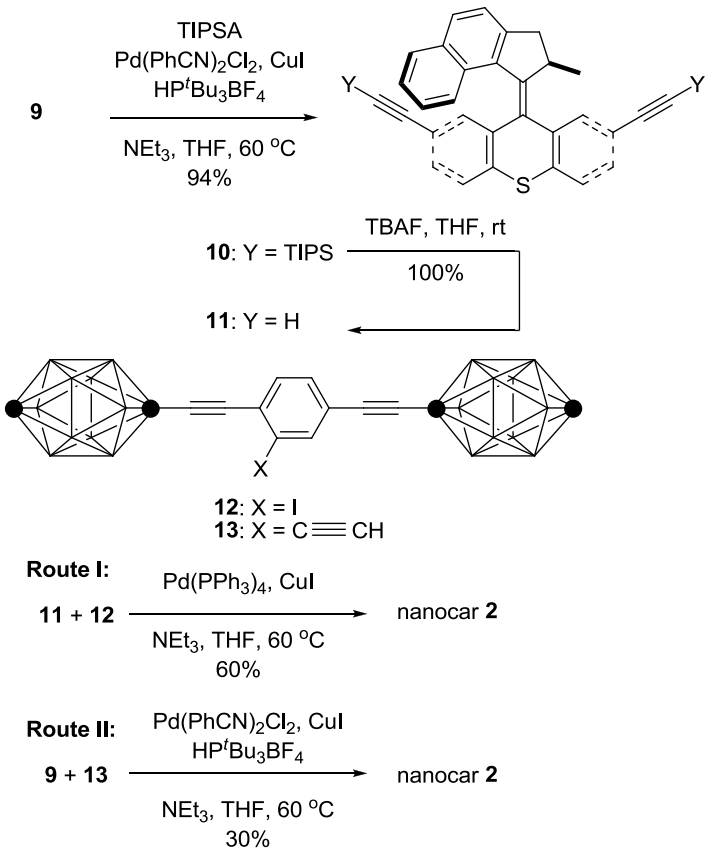

1.6. STM Imaging of the Motorized Nanocar 2

We evaporated nanocar **2** thermally under ultrahigh vacuum conditions onto a clean Cu(111) surface with large, flat terraces and imaged the surface by low temperature STM. If very low coverages are chosen, we find clean terraces and all molecules adsorbed at the step edges. This shows that the molecules, although being rather large and thus exhibiting significant interaction with the metal surface, are mobile at room temperature and diffuse to the step edges where they are bound more strongly than on a terrace. However, for a clear insight into molecular motion upon external stimuli, as STM

manipulation or light illumination, adsorption of the molecules on a flat terrace is preferred, because the environment is equal for all molecules and the diffusion barrier is lower. Hence, we have deposited larger coverages of molecules onto the surface to saturate the step edges and force the molecules to adsorb on the terraces. On the resulting surface (Figure 3a) single molecules are indeed found (as marked by circles). In addition to them, we also observe a significant number of small protrusions that might represent single carborane groups, which are either present in small amounts in the molecular substance, but due to their small weight appear in large numbers on the surface,[28] or result from molecular fragmentation during deposition. Furthermore, islands are present on the terraces, which contain nanocar **2** molecules and unidentified small species in a disordered fashion.

When studying in detail the single molecules on a clean terrace (Figure 1.3.b and d), we find characteristic appearances that consist of five lobes, four from the wheels and one from the motor. As some of the bonds in the chassis of the nanocar are rotatable, the two axles of the molecule can be either crossed (Figure 3b-c) or parallel (Figure 3d-e). When comparing the measured dimensions with those from gas phase simulations, there is a particularly good agreement for the lengths of the axles (d_1 and d_3), whereas the distances between opposite carborane wheels (d_2 and d_4) are slightly off. We assign this effect to the intramolecular flexibility of the central motor. Hence, the molecular appearance in STM images and the measured dimensions reveal that intact nanocar **2** molecules are present on the surface. The first illumination experiments were done at a wavelength of 248 nm and exposure times of up to 45 min at a pulse rate of 10 Hz (incidence angle of about 70° from the surface normal). However, no lateral motion of

the molecules could be induced, monitoring the exactly same surface area that was imaged before the light exposure.

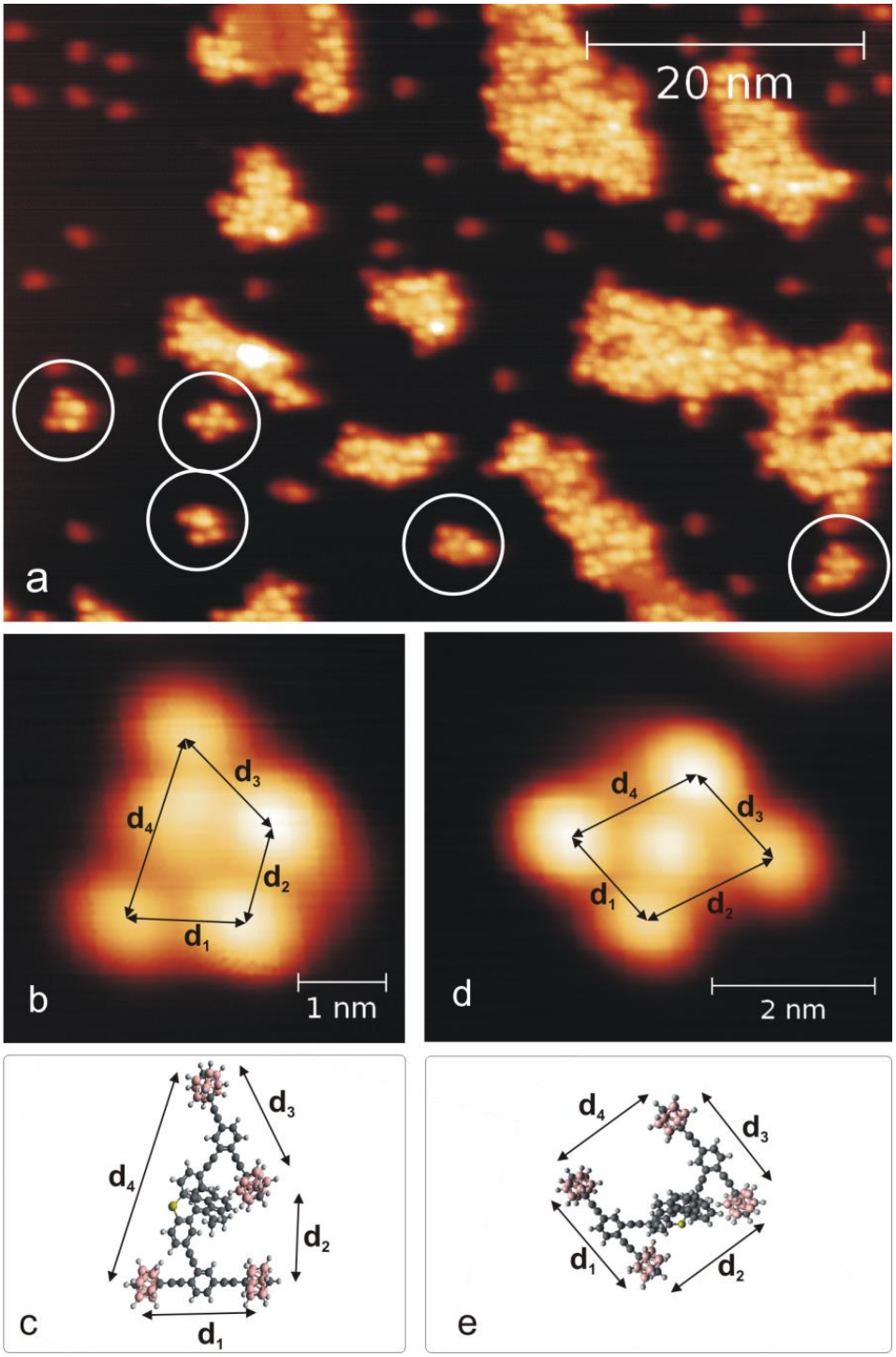

Figure 1.3. STM images of nanocar **2** on Cu(111) and calculated gas phase structures (HyperChem 7 software). (a) Overview image of the surface (white circles indicate wheels and motors of single molecules, partially adsorbed at defects). Intramolecular dimensions, determined from STM images, are compared with the calculated gas phase structure. Crossed axes: d_1 = 1.33 nm in the STM image (b) (and 1.38 nm in the calculation (c)), d_2 = 1.10 nm (1.07 nm), d_3 = 1.39 nm (1.38 nm), d_4 = 2.15 nm (2.29 nm). Parallel axles (d and e): d_1 = 1.38 nm in the STM image (d) (and 1.38 nm in the calculation (e)), d_2 = 1.65 nm (1.42 nm), d_3 = 1.37 nm (1.38 nm), d_4 = 1.70 nm (1.51 nm).

1.7. Conclusion

In this work, we successfully synthesized and did preliminary STM imaging of second generation motorized nanocar **2**. We imaged single molecules after deposition onto Cu(111), revealing that – despite their size and complexity – it is possible to transfer them intact onto a surface under ultrahigh vacuum conditions. Their appearance in the STM images is in good agreement with the molecular dimensions in the gas phase and, according to their chemical structure, two typical conformations are identified. However, lateral motion on the surface, in particular by activating the molecular motor, could not be achieved in our initial experiments. This was probably due to the strong coupling interaction between the nanocar **2** and the Cu(111) surface. Future experiments will also focus on using different metallic and non-metallic surfaces to modify the molecule-surface coupling in a controlled way. As a complementary imaging method, SMFM has been used to monitor rolling motion of many fluorescent nanocars synthesized in our

group.[8,9] We are investigating possibility of making the fluorescent motorized nanocars that have excitations and emission at a usable region.

1.8. Contributions

I finished and optimized all the synthetic tasks based on the previous work of Jason M. Guerrero. Jazmin Godoy helped on synthesizing nanocar **2** with route II. Johannes Mielke, Dr. Carlos J. Villagómez, and Dr. Alex Saywell did the STM imaging in the laboratory of Leonhard Grill at Fritz-Haber-Institute, Berlin. Dr. Lawrence B. Alemany analyzed the structure of **9** by NMR.

1.9. Experimental Section

1.9.1. The Motorized Nanocar 2 STM Imaging Procedure

The scanning tunnelling microscopy (STM) experiments have been performed in an ultra-high vacuum (UHV) chamber with a base pressure of 10^{-10} mbar. The Cu(111) surface has been cleaned through repeated cycles of Ar^+ sputtering and annealing at 400 °C. The molecules were thermally evaporated from a Knudsen cell, held at about 300 °C onto the Cu(111) surface (at 50 °C). The STM images were taken in an Omicron low temperature (LT) STM working at 5.7 K using a tungsten tip. All images have been taken using a tip bias of –1 V and a tunnelling current of 1 pA. Gas phase calculations have been performed using the HyperChem 7 software.

1.9.2 Experimental data for compounds 2, 4, 6, 8, 9, 10, 11, 15, 18, and 19.

General Methods. ^{1}H NMR and ^{13}C NMR spectra were recorded at 400 or 500 and 100 or 125 MHz, respectively. Chemical shifts (δ) are reported in ppm from tetramethylsilane (TMS). FTIR spectra were recorded using a Nicolet FTIR Infrared Microscope with ATR objective with 2 cm^{-1} resolution. All glassware was oven-dried overnight prior to use. Reagent grade tetrahydrofuran (THF) and ether (Et_2O) was distilled from sodium benzophenoneketyl under N_2 atmosphere. Triethylamine (NEt_3), dichloromethane (CH_2Cl_2) and 1,2-dichloroethane were distilled from calcium hydride (CaH_2) under N_2 atmosphere. THF and NEt_3 were degassed with a stream of argon for 15 min before being used in the Sonogashira coupling reactions. All palladium-catalyzed reactions were carried out under argon atmosphere, while other reactions were performed under N_2 unless otherwise noted. Trimethylsilylacetylene (TMSA) was donated by FAR Research Inc. or Petra Research. All other chemicals were purchased from commercial suppliers and used without further purification. Flash column chromatography was performed using 230-400 mesh silica gel from EM Science. Thin layer chromatography (TLC) was performed using glass plates pre-coated with silica gel 40 F_{254} 0.25 mm layer thickness purchased from EM Science.

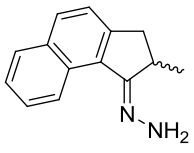

Hydrazone 4.[23] To an oven dried round-bottom flask charged with ketone **3**[23] (1.96 g, 10 mmol) was added EtOH (20 mL) and hydrazine monohydrate (10 mL) through a condenser. The mixture was heated at reflux for 3 d. The cooled reaction mixture was extracted with Et_2O (100 mL) and water (100 mL × 3). The organic layer was dried over

$MgSO_4$ and concentrated under vacuum to afford hydrazone **4** as yellow solid (1.95 g, 93%). Spectroscopic data were identical to those in the literature. *Caution:* since hydrazone **4** is reactive toward acetone, all containers used should be completely acetone-free.

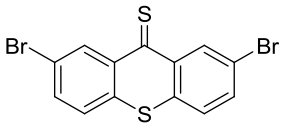

2,7-Dibromo-thioxanthene-9-thione (6).[12] To an oven dried two-neck round-bottom flask charged with thioxanthenone **5**[12] (3.25 g, 8.78 mmol) and P_4S_{10} (10 g, 22.5 mmol) was added toluene (250 mL) and the mixture was heated at reflux for 2 d. The mixture was filtered while hot, and the filtrate was collected. The brownish solid that formed upon cooling was filtered, and solid was collected and dried under vacuum (3.2 g, 94 %). Spectroscopic data were identical to those reported in the literature.

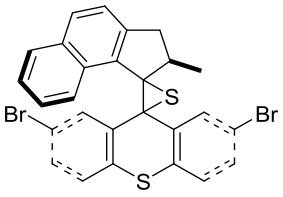

Episulfide 8. To an oven dried three-neck round-bottom flask charged with hydrazone **4** (0.99 g, 4.7 mmol) and $MgSO_{4(s)}$ (0.49 g, 4.1 mmol) was added CH_2Cl_2 (25 mL). To this suspension was added quickly MnO_2 (1.62 g, 18.8 mmol, Sigma-Aldrich > 90%) at *ca*. 5 ℃. The reaction flask was immediately immersed and stirred in a cold bath ranging from −15 ℃ to −10 ℃ for 1.5 h. After this period, the reaction mixture was cooled to −50 ℃ and then transferred to a Schlenk filtration tube connected to an oven dried three-

neck round-bottom flask. The deep-purple filtrate that contained intermediate **7** was collected, and the Schlenk tube was rinsed with pre-cooled CH_2Cl_2 (20 mL, −50 ℃). To the flask containing the combined filtrate, thione **6** (0.97 g, 2.5 mmol) was added portionwise until no more N_2 evolved. The mixture was stirred for an additional 0.5 h at ambient temperature. The mixture was poured into MeOH (80 mL) with vigorous stirring and a white precipitate formed. The solid was filtered, and the filter cake was washed with MeOH (30 mL) and dried under vacuum to afford the desired compound **8** (1.19 g, 84%): m.p. 204 ℃ (decomp); FTIR (neat) 3078, 3070, 3050, 2974, 2954, 2934, 2898, 2866, 2840, 1616, 1580, 1568, 1556, 1514, 1456, 1436, 1382, 1372, 1252, 1212, 1160, 1132, 1112, 1080, 1052, 1024 cm^{-1}; ^1H NMR (400 MHz, $CDCl_3$) δ 8.89 (d, *J* = 8.8 Hz, 1H), 8.00 (d, *J* = 2.0 Hz, 1H), 7.83 (d, *J* = 2.0 Hz, 1H), 7.56 (d, *J* = 8.2 Hz, 1H), 7.54 (d, *J* = 7.8 Hz, 1H), 7.40–7.34 (m, 2H), 7.29 (d, *J* = 8.2 Hz, 1H), 7.26–7.20 (m, 1H), 7.18 (d, *J* = 8.2 Hz, 1H), 6.84 (dd, J_1 = 8.2 Hz, J_2 = 2.0 Hz, 1H), 6.77 (d, *J* = 8.2 Hz, 1H), 3.43 (dd, J_1 = 6.6 Hz, J_2 = 15.4 Hz, 1H), 2.44 (d, *J* = 15.6 Hz, 1H), 1.57 (qd, J_1 = 6.9 Hz, J_2 = 6.6 Hz), 1.12 (d, *J* = 6.9 Hz, 3H); ^{13}C NMR (100 MHz, $CDCl_3$) δ 142.5, 140.9, 136.2, 135.3, 134.4, 134.1, 132.6, 131.8, 130.81, 130.76, 130.1, 129.7, 129.4, 128.2, 127.8, 127.6, 124.5, 124.4, 124.0, 123.4, 120.9, 120.0, 72.2, 60.8, 40.5, 38.1, 21.8; HRMS (APCI) *m*/*z* calcd for $[M+H]^+$ $C_{27}H_{19}Br_2S_2$ 564.9295, found 564.9275.

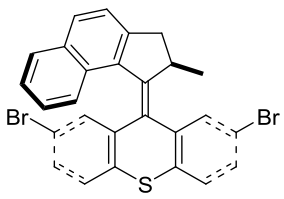

2,7-Dibromo-9-(2-methyl-2,3-dihydro-1H-cyclopenta[a]naphthalen-1-ylidene)-9H-thioxanthene (molecular motor 9). To a 200 mL screw-capped tube charged with episulfide **8** (524 mg, 0.960 mmol) was added trimethyl phosphite (9.6 mL), and the mixture was stirred at 130 °C for 14 h. After the reaction mixture was cooled to room temperature, MeOH (30 mL) was added. The precipitate was filtered and washed with MeOH (20 mL). The solid was purified by column chromatography (silica gel, 10% CH_2Cl_2 in hexanes) to afford compound **9** as a pale yellow solid (485 mg, 94%): m.p. 245–246 °C; FTIR (neat) 3072, 3046, 3032, 3008, 2952, 2920, 2859, 2848, 1616, 1612, 1576, 1568, 1558, 1548, 1540, 1512, 1452, 1440, 1394, 1380, 1362, 1346, 1284, 1256, 1204, 1196, 1180, 1152, 1140, 1128, 1084, 1074, 1052 cm^{-1}; HRMS (APCI) *m*/*z* calcd for $[M+H]^+$ $C_{27}H_{19}Br_2S$ 532.9574, found 532.9550. For NMR spectroscopic data, see analyses in section **1.9.3.**

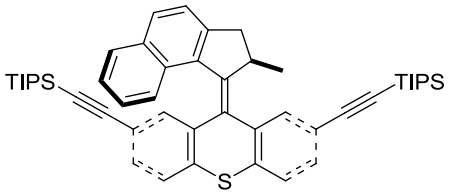

(9-(2-Methyl-2,3-dihydro-1H-cyclopenta[a]naphthalen-1-ylidene)-9H-thioxanthene-2,7-diyl)bis(ethyne-2,1-diyl)bis(triisopropylsilane) (molecular motor 10). To a 20 mL screw-capped tube charged with molecular motor **9** (190 mg, 0.356 mmol), $Pd(PhCN)_2Cl_2$ (20.8 mg, 0.054 mmol), $HP^tBu_3BF_4$ (31.1 mg, 0.107 mmol) and CuI (20.4 mg, 0.107 mmol) were added NEt_3 (3 mL), THF (0.5 mL) and TIPSA (0.61 mL, 2.75 mmol). The reaction was stirred at 60 °C for 12 h and then cooled to room temperature. The mixture was quenched with saturated ammonium chloride aqueous solution

($NH_4Cl_{(aq)}$; 20 mL) and extracted with Et_2O (30 mL). The organic phase was washed with water (30 mL), dried over $MgSO_4$, and filtered, and the filtrate was concentrated under vacuum. The crude product was purified by column chromatography (silica gel, 10% CH_2Cl_2 in hexanes) to afford the desired product **10** as a pale yellow solid (245 mg, 94%): m.p. 154–156 °C; FTIR (neat) 2942, 2920, 2888, 2860, 2148, 1620, 1588, 1548, 1512, 1454, 1386, 1366, 1212, 1164, 1136, 1076, 1052, 1012 cm^{-1}; ^1H NMR (500 MHz, $CDCl_3$) δ 7.83 (d, J = 1.7 Hz, 1H), 7.71 (d, J = 8.2 Hz, 1H), 7.65 (br d, J = 8.2 Hz, 1H), 7.52 (dd, J_1 = 8.0 Hz, J_1 = 0.3 Hz, 1H), 7.46 (dd, J_1 = 8.0 Hz, J_2 = 0.5 Hz, 1H), 7.41 (d, J = 8.2 Hz, 1H), 7.34 (dd, J_1 = 8.2 Hz, J_2 = 1.7 Hz, 1H), 7.16 (ddd, J_1 = 7.4 Hz, J_2 = 7.4 Hz, J_3 = 1.3 Hz, 1H), 7.07 (dd, J_1 = 8.0 Hz, J_2 = 1.7 Hz, 1H), 6.84–6.79 (m, 1H), 6.77 (dd, J_1 = 8.0 Hz, J_2 = 0.6 Hz, 1H), 6.72 (dd, J_1 = 1.8 Hz, J_2 = 0.5 Hz, 1H), 4.22 (qd, J_1 = 6.8 Hz, J_2 = 6.0 Hz,1H), 3.68 (dd, J_1 = 15.6 Hz, J_2 = 6.0 Hz, 1H), 2.65 (d, J = 15.6 Hz, 1H), 1.15 (br s, 21H), 0.91 (br s, 21H), 0.84 (d, J = 6.8 Hz, 3H); ^{13}C NMR (125 MHz, $CDCl_3$) δ 147.4, 145.7, 139.4, 137.5, 136.2, 135.4, 134.6, 133.0, 132.5, 131.2, 130.4, 129.7, 129.2, 128.6, 128.0, 127.7, 127.1, 126.4, 125.8, 124.8, 124.3, 123.5, 121.9, 121.6, 106.9, 106.3, 91.4, 90.3, 39.7, 37.5, 19.8, 18.7, 18.5, 11.3, 11.1; HRMS (APCI) m/z calcd for $[M+H]^+$ $C_{49}H_{61}SSi_2$ 737.4033, found 737.4003.

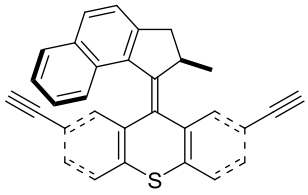

2,7-Diethynyl-9-(2-methyl-2,3-dihydro-1H-cyclopenta[a]naphthalen-1-ylidene)-9H-thioxanthene (molecular motor 11). To an oven-dried three-neck round-bottom flask

charged with molecular motor **10** (120 mg, 0.163 mmol) was added TBAF (1.2 mL, 1 M solution in THF) and THF (2.4 mL). The reaction was stirred for 1.5 h at room temperature. The mixture was extracted with CH_2Cl_2 (25 mL) and water (30 mL). The organic layer was dried over $MgSO_4$, concentrated, and purified by column chromatography (silica gel, 25% CH_2Cl_2 in hexanes) to afford desired compound **11** as a pale yellow solid (69 mg, 100%): m.p. 230 °C (decomp); FTIR (neat) 3286, 3072, 3046, 3032, 3008, 2956, 2952, 2918, 2898, 2860, 2846, 2106, 1616, 1586, 1548, 1512, 1448, 1386, 1312, 1264, 1204, 1162, 1140, 1132, 1062, 1052, 1028 cm^{-1}; ^1H NMR (400 MHz, $CDCl_3$) δ 7.90 (d, J = 1.6 Hz, 1H), 7.76 (d, J = 8.4 Hz, 1H), 7.72 (d, J = 8.0 Hz, 1H), 7.55 (d, J = 8.0 Hz, 1H), 7.51 (d, J = 7.6 Hz, 1H), 7.44 (d, J = 8.0 Hz, 1H), 7.36 (dd, J_1 = 8.0 Hz, J_2 = 0.8 Hz, 1H), 7.21 (ddd, J_1 = 8.0 Hz, J_2 = 8.0 Hz, J_3 = 1.6 Hz, 1H), 7.13 (dd, J_1 = 8.0 Hz, J_2 = 2.0 Hz, 1H), 6.86–6.76 (m, 3H), 4.23 (qd, J_1 = 7.2 Hz, J_2 = 6.4 Hz, 1H), 3.65 (dd, J_1 = 15.6 Hz, J_2 = 6.4 Hz, 1H), 3.16 (s, 1H), 2.69 (s, 1H), 2.65 (d, J = 15.6 Hz, 1H), 0.80 (d, J = 7.2 Hz, 3H); ^{13}C NMR (100 MHz, $CDCl_3$) δ 147.6, 146.2, 139.8, 137.6, 136.7, 136.1, 134.4, 133.1, 132.1, 131.3, 130.6, 129.9, 129.7, 128.6, 128.0, 127.8, 127.4, 126.4, 125.7, 124.9, 124.4, 123.7, 120.4, 120.3, 83.4, 82.7, 77.9, 77.0, 39.7, 37.9, 19.5; HRMS (APCI) m/z calcd for $[M+H]^+$ $C_{31}H_{21}S$ 425.1364, found 425.1359.

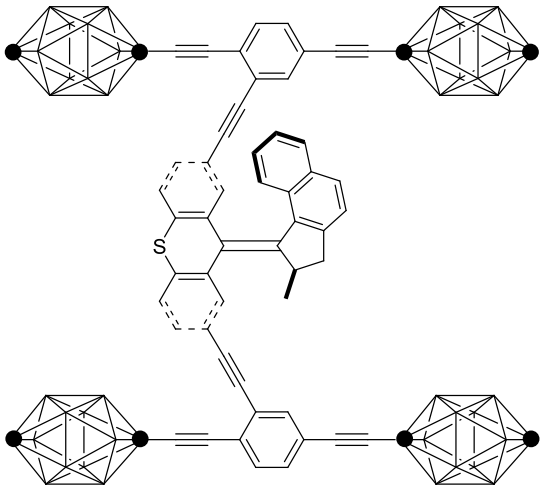

***p*-Carborane-wheeled motorized nanocar 2.** Route I: An oven dried 10 mL Schlenk-tube equipped with a stir bar was charged with molecular motor **11** (45 mg, 0.106 mmol)**,** axle **12** (128 mg, 0.238 mmol), $Pd(PPh_3)_4$ (9.8 mg, 8.5 μmol), and CuI (3.3 mg, 17 μmol) to which were added NEt_3 (0.15 mL) and THF (1 mL). The reaction mixture was stirred at 60 ℃ for 16 h, and then it was cooled to room temperature. The mixture was quenched with saturated $NH_4Cl_{(aq)}$ (20 mL) and extracted with CH_2Cl_2 (30 mL). The organic phase was washed with water (30 mL), dried over anhydrous $MgSO_4$, filtered, and the filtrate was concentrated under vacuum. The crude product was purified by column chromatography (silica gel, 8% CH_2Cl_2 in hexanes) to yield **2** as a pale yellow solid (78 mg, 60%). Route II: Inside a glovebox, a 20 mL screw-capped tube equipped with a stir bar was charged with molecular motor **9** (26 mg, 49 μmol), axle **13** (63 mg, 0.146 mmol), $Pd(PhCN)_2Cl_2$ (4 mg, 10 μmol), $HP^tBu_3BF_4$ (5.7 mg, 20 μmol), CuI (4 mg, 20 μmol), NEt_3 (3 mL), and THF (1 mL). The reaction mixture was stirred at 60 ℃ for 16 h, and then it was cooled to room temperature. The mixture was quenched with saturated $NH_4Cl_{(aq)}$ (20 mL) and extracted with CH_2Cl_2 (30 mL). The organic phase was washed with water (30 mL), dried over anhydrous $MgSO_4$, filtered, and the filtrate was

concentrated under vacuum. The crude product was purified by column chromatography (silica gel, 5% CH_2Cl_2 in hexanes) to yield **2** as a pale yellow solid (18 mg, 30%): m.p. 200 °C (decomp); FTIR (neat) 3060, 2956, 2924, 2866, 2846, 2610, 2208, 1594, 1488, 1454, 1140, 1062 cm^{-1}; ^1H NMR (500 MHz, CD_2Cl_2) δ 8.03 (d, J = 1.7 Hz, 1H), 7.81 (d, J = 8.2 Hz, 1H), 7.73 (d, J = 8.2 Hz, 1H), 7.70–7.65 (m, 2H), 7.53 (d, J = 8.2 Hz, 1H), 7.48–7.45 (m, 2H), 7.28–7.25 (m, 2H), 7.23 (ddd, J_1 = 7.4 Hz, J_2 = 7.2 Hz, J_3 = 1.5 Hz, 1H), 7.18 (dd, J_1 = 8.1 Hz, J_2 = 1.7 Hz, 1H), 7.14–7.10 (m, 2H), 7.06 (dd, J_1 = 8.0 Hz, J_2 = 1.8 Hz, 1H), 6.94 (dd, J_1 = 2.0 Hz, J_1 = 0.4 Hz, 1H), 6.93–6.87 (m, 2H), 4.34 (qd, J_1 = 6.8 Hz, J_2 = 6.3 Hz, 1H), 3.84 (dd, J_1 = 15.6 Hz, J_2 = 6.3 Hz, 1H), 3.20–1.60 (br m, 45H), 0.86 (d, J = 6.8 Hz, 3H); ^{13}C NMR (125 MHz, CD_2Cl_2) δ 148.3, 147.4, 140.9, 138.5, 137.5, 137.2, 135.6, 135.4, 134.8, 133.7, 132.8, 132.5, 132.1, 131.52, 131.50, 131.22, 131.19, 130.3, 129.9, 129.3, 128.6, 128.5, 128.3, 127.2, 126.9, 126.8, 126.3, 125.6, 124.9, 124.5, 124.4, 124.1, 122.6, 122.3, 121.5, 121.3, 94.7, 94.3, 91.7, 91.5, 88.4, 88.2, 87.5, 86.8, 78.4, 78.3, 78.2, 78.0, 69.7 (br), 69.6 (br), 61.2 (br), 40.4, 38.6, 19.9; HRMS (APCI) m/z calcd for $[M+H]^+$ $C_{59}H_{69}{}^{10}B_7{}^{11}B_{33}S$ 1242.9096, found 1242.9124.

1.9.3. NMR analyses of molecular motor 9.

A combination of standard 1D ^1H, ^{13}C, and DEPT-135 ^{13}C experiments and standard 2D ^1H-^1H COSY, ^1H-^1H NOE, ^1H-^{13}C HSQC, and ^1H-^{13}C HMBC experiments obtained on a 500 MHz spectrometer yielded the assignments for **9** discussed below and illustrated in Figure 2 of the main text.

The ^1H spectrum immediately differentiated the two CH_2 protons from the aliphatic CH proton by the distinctive large geminal coupling constant (15.6 Hz)

exhibited by the CH_2 protons at δ3.652 and δ2.664. Only the downfield CH_2 proton exhibited a detectable *J* coupling (6.2 Hz) to the methine proton (δ4.186), which, exhibited a five-line pattern because of additional *J* coupling (6.9 Hz) to the methyl protons (δ0.832).

The ^1H and COSY experiments revealed two groups of signals that each contained three coupled aromatic protons (H_a, H_b, H_c and $H_{a'}$, $H_{b'}$, $H_{c'}$), two coupled protons (H_d and H_e), and four coupled protons (H_f, H_g, H_h, H_i) two of which (δ7.737 and δ6.776) were also coupled to a proton (δ7.781) in the adjacent H_d-H_e ring.

H_a-H_b-H_c ring protons or $H_{a'}$-$H_{b'}$-$H_{c'}$ ring protons: δ6.794, d (*J* = 2.10 Hz) of d (*J* = 0.35 Hz); δ7.132, d (*J* = 8.30 Hz) of d (*J* = 2.10 Hz); δ7.414, d (*J* = 8.30 Hz) of d (*J* = 0.35 Hz).

$H_{a'}$-$H_{b'}$-$H_{c'}$ ring protons or H_a-H_b-H_c ring protons: δ7.357, d (*J* = 8.25 Hz) of d (*J* = 2.10 Hz); δ7.455, d (*J* ≈ 8.3 Hz) of d (*J* ≈ 0.2 Hz); δ7.892, d (*J* = 2.05 Hz) plus unresolved fine structure.

H_d-H_e ring protons: δ7.440, d (*J* ≈ 8.2 Hz, broad signals); δ7.781, d (*J* = 8.15 Hz, broad signals).

H_f-H_g-H_h-H_i ring protons: δ6.776, d (*J* = 8.55 Hz, broad complex signals); δ6.855, d (*J* = 8.55 Hz) of d (*J* = 6.70 Hz) of d (*J* = 1.25 Hz); δ7.236, d (*J* = 8.15 Hz) of d (*J* = 6.70 Hz) of d (*J* = 1.15 Hz); δ7.737, d (*J* = 8.15 Hz) of d (*J* = 1.25 Hz) of d (*J* ≈ 0.6 Hz) plus unresolved fine structure.

In the H_a-H_b-H_c and $H_{a'}$-$H_{b'}$-$H_{c'}$ spin systems, the protons exhibiting only small *J* values (≤ 2.1 Hz) were attributed to H_a and $H_{a'}$ because the couplings were over at least

four bonds. H_b ($H_{b'}$) was tentatively differentiated from H_c ($H_{c'}$) on the assumption that $^4J_{HH}$ to H_a ($H_{a'}$) would be larger than $^5J_{HH}$ to H_a ($H_{a'}$).

The upfield CH_2 proton exhibited correlations to H_d and H_e, while the downfield CH_2 proton also exhibited correlations to two of the four protons (δ7.236 and δ6.776) in the H_f-H_g-H_h-H_i ring. The long-range couplings to both of the methylene protons presumably account for the breadth of the H_d and H_e signals. The complexity of the δ7.737 and δ6.776 signals (more than just a d of d of d from couplings within the H_f-H_g-H_h-H_i ring) arises from the long-range coupling of the δ7.737 and δ6.776 protons to the δ7.781 proton in the H_d-H_e ring and the long-range coupling of the δ6.776 proton with both of the methylene protons.

The aliphatic methine proton (δ4.186) exhibited a correlation to the aromatic signal at δ7.892 but not to the signal at δ6.794.

The NOE experiment revealed critical information on the spatial proximity of various protons. In particular:

- The presence of an NOE between the proton at δ7.892 and various aliphatic protons and the absence of an NOE between the proton at δ6.794 and various aliphatic protons enabled secure assignments for $H_{a'}$ (δ7.892) and H_a (δ6.794) to be made. NOEs were observed between $H_{a'}$ and the aliphatic methine proton (δ4.186), between $H_{a'}$ and the methyl protons (δ0.832), and between $H_{a'}$ and the methylene proton at δ2.664.
- The presence of an NOE between the aromatic proton at δ7.440 and each of the methylene protons and the absence of an NOE between the aromatic proton at

δ7.781 and each of the methylene protons enabled secure assignments for H_d (δ7.440) and H_e (δ7.781) to be made.

- The presence of an NOE between the aromatic protons at δ7.781 and δ7.737 enabled the latter signal to be assigned to H_f, which provided a secure starting point for sequentially assigning the signals of the H_g (δ7.236), H_h (δ6.855), and H_i (δ6.776) protons through NOE. H_i also exhibited an NOE to the methyl protons.
- The presence of an NOE between δ6.794 and δ7.132 and between δ7.132 and δ7.414 confirmed the H_a (δ6.794), H_b (δ7.132), and H_c (δ7.414) assignments. Similarly, the presence of an NOE between δ7.892 and δ7.357 and between δ7.357 and δ7.455 confirmed the $H_{a'}$ (δ7.892), $H_{b'}$ (δ7.357), and $H_{c'}$ (δ7.455) assignments.
- Among the aliphatic protons, the methyl protons exhibited an NOE to the methine proton and to each of the methylene protons; the methylene protons exhibited an NOE between themselves; but only one methylene proton (3.652) exhibited an NOE to the methine proton. This established their cis orientation and the cis orientation of the methylene proton at δ2.664 and the methyl group.

The DEPT-135 ^{13}C experiment immediately differentiated the CH and CH_2 carbons and differentiated the aromatic CH carbons from the fully substituted aromatic and alkene carbons. The two closest aromatic CH signals differed by only 0.034 ppm.

The ^{1}H-^{13}C HSQC experiment then gave specific, pairwise $^{1}H/^{13}C$ assignments for the 12 aromatic CH, aliphatic CH, CH_2, and CH_3 groups (H_a δ6.794 / C_a δ131.542, H_b δ7.132 / C_b δ129.190, H_c δ7.414 / C_c δ128.664, $H_{a'}$ δ7.892 / $C_{a'}$ δ130.654, $H_{b'}$ δ7.357 / $C_{b'}$ δ129.109, $H_{c'}$ δ7.455 / $C_{c'}$ δ129.143, H_d δ7.440 / C_d δ123.738, H_e δ7.781 / C_e δ130.895,

H_f δ7.737 / C_f δ128.062, H_g δ7.236 / C_g δ124.510, H_h δ6.855 / C_h δ125.003, H_i δ6.776 / C_i δ125.709, methine H δ4.186 / C δ37.763, methylene H δ3.652 and δ2.664 / C δ39.678, and methyl H δ0.832 / C δ19.642).

The ^{1}H-^{13}C HMBC experiment provided at least partial assignments for the ten fully substituted aromatic carbons and the two fully substituted alkene carbons.

The quaternary ^{13}C signal at δ125.818 exhibited a distinctive set of correlations to H_a, $H_{a'}$, H_c, $H_{c'}$ that enabled it to be assigned to the alkene carbon in the sulfur-containing ring.

Each of the three quaternary aromatic carbons in the H_a-H_b-H_c ring exhibited at least one correlation to H_a, H_b, or H_c (δ141.564 with H_c at δ7.414, δ134.322 with H_b at δ7.132 and with H_a at δ6.794, and δ120.611 with all three of these protons) and exhibited no other long-range correlations. Each of the three quaternary aromatic carbons in the $H_{a'}$-$H_{b'}$-$H_{c'}$ ring exhibited the corresponding correlations to $H_{a'}$, $H_{b'}$, or $H_{c'}$ (δ139.425 with $H_{c'}$ at δ7.455, δ134.785 with $H_{b'}$ at δ7.357 and with $H_{a'}$ at δ7.892, and δ120.354 with all three of these protons) and exhibited no other long-range correlations. The aliphatic methine carbon exhibited a correlation to $H_{a'}$ at δ7.892 but not to H_a at δ6.794 (just as the aliphatic methine proton exhibited a correlation in the COSY experiment to $H_{a'}$ but not to H_a).

Only the signal at δ148.160 exhibited a long-range correlation to the methyl protons, which was the basis for assigning this signal to the alkene carbon in the five-membered ring. This carbon also exhibited correlations to the aliphatic methine proton and both methylene protons. Each of the quaternary carbon signals at δ134.084 and δ146.309 exhibited correlations to the aliphatic methine proton, both methylene protons,

H_d, and H_e; these carbon signals are assigned to the two quaternary aromatic carbons in the five-membered ring. The signal at δ134.084 was tentatively assigned to the carbon next to the alkene because it, unlike the signal at δ146.309, exhibited long-range correlations to the H_f-H_g-H_h-H_i ring ($^4J_{CH}$ to H_f at δ7.737 and $^3J_{CH}$ to H_i at δ6.776).

Each of the aromatic CH signals at δ123.738 and δ130.895 exhibited long-range correlations to each of the methylene protons, consistent with their assignments above.

The two remaining quaternary signals at δ128.597 and δ133.121 were assigned to the ring junction carbons in the naphthalene moiety. Each exhibited long range correlations to each of the six protons in the naphthalene moiety. The signal at δ128.597 was tentatively assigned to the ring junction nearest the five-membered ring because this carbon exhibited correlations to both methylene protons and a weak correlation to the aliphatic methine proton, while the signal at δ133.121 exhibited only a weak correlation to one of the methylene protons.

Experimental Details of NMR Analyses. A Bruker Avance-500 spectrometer using a broadband observe probe with a z-axis gradient coil and the standard Bruker pulse programs indicated was used for these analyses. ^{1}H (zg30): 30° pulse, 13.11-s FID, 5-s relaxation delay, 16 scans, no line broadening. COSY (cosygpqf): 2048 increments for an F_1 digital resolution = 0.0049 ppm, 12 scans/increment, FID acquisition time = 0.41 s for an F_2 digital resolution = 0.0024 ppm, relaxation delay = 1.5 s. NOE (noesygpph), mixing time = 1 s, 2048 increments for an F_1 digital resolution = 0.0049 ppm, 4 scans/increment, FID acquisition time = 0.41 s for an F_2 digital resolution = 0.0024 ppm, relaxation delay = 1 s. A second NOE experiment with a mixing time of 1.75 s and 8

scans/increment did not yield any additional information. ^{13}C (zgpg): 90° pulse, 6.60-s FID, 5-s relaxation delay, 664 scans, 0.10-Hz line broadening. DEPT-135 ^{13}C (dept135): optimized for $^{1}J_{CH}$ = 145 Hz, 6.60-s FID, 5-s relaxation delay, 128 scans, 0.10-Hz line broadening. ^{1}H-^{13}C HSQC (hsqcetgp): optimized for $^{1}J_{CH}$ = 145 Hz, 2048 increments for ^{13}C digital resolution = 0.069 ppm (zero-filled once), 16 scans/increment. The ^{13}C digital resolution was just enough to enable pairwise ^{1}H/^{13}C assignments for the ^{13}C signals at δ129.109, δ129.143, and δ129.190. ^{1}H-^{13}C HMBC (hmbcgplpndqf): optimized for $^{1}J_{CH}$ = 145 Hz, optimized for long-range J_{CH} = 6.25 Hz, 2048 increments for ^{13}C digital resolution = 0.077 ppm (zero-filled once), 48 scans/increment.

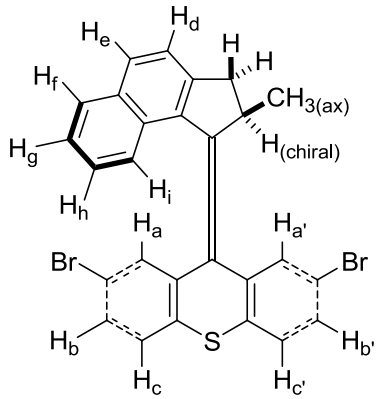

9

1.10. References

1. Chiang, P.-T.; Mielke, J.; Godoy, J.; Guerrero, J. M.; Alemany, L. B.; Villagómez, C. J.; Saywell, A.; Grill, L.; Tour, J. M. Toward a Light-Driven Motorized Nanocar: Synthesis and Initial Imaging of Single Molecules. *ACS Nano* **2012**, *6*, 592-597.

2. Chiang, P.-T.; Cheng, P.-N.; Lin, C.-F.; Liu, Y.-H.; Lai, C.-C.; Peng, S.-M.; Chiu, S.-H. A Macrocycle/Molecular-Clip Complex That Functions as a Quadruply Controllable Molecular Switch. *Chem.−Eur. J.* **2006**, *12*, 865-876.

3. Badjić, J. D.; Balzani, V.; Credi, A.; Silvi, S.; Stoddart, J. F. A Molecular Elevator. *Science* **2004**, *303*, 1845-1849.

4. Chuang, C.-J.; Li, W.-S.; Lai, C.-C.; Liu, Y.-H.; Peng, S.-M.; Chao, I.; Chiu, S.-H. A Molecular Cage-Based [2]Rotaxane That Behaves as a Molecular Muscle. *Org. Lett.* **2008**, *11*, 385-388.

5. Shirai, Y.; Morin, J.-F.; Sasaki, T.; Guerrero, J. M.; Tour, J. M. Recent Progress on Nanovehicles. *Chem. Soc. Rev.* **2006**, *35*, 1043-1055.

6. Vives, G.; Tour, J. M. Synthesis of Single-Molecule Nanocars. *Acc. Chem. Res.* **2009**, *42*, 473-487.

7. Villagómez, C. J.; Sasaki, T.; Tour, J. M.; Grill, L. Bottom-up Assembly of Molecular Wagons on a Surface. *J. Am. Chem. Soc.* **2010**, *132*, 16848-16854.

8. Khatua, S.; Guerrero, J. M.; Claytor, K.; Vives, G.; Kolomeisky, A. B.; Tour, J. M.; Link, S. Micrometer-Scale Translation and Monitoring of Individual Nanocars on Glass. *ACS Nano* **2009**, *3*, 351-356.

9. Khatua, S.; Godoy, J.; Tour, J. M.; Link, S. Influence of the Substrate on the Mobility of Individual Nanocars. *J. Phys. Chem. Lett.* **2010**, *1*, 3288-3291.

10. Shirai, Y.; Osgood, A. J.; Zhao, Y.; Kelly, K. F.; Tour, J. M. Directional Control in Thermally Driven Single-Molecule Nanocars. *Nano Lett.* **2005**, *5*, 2330-2334.

11. Shirai, Y.; Osgood, A. J.; Zhao, Y.; Yao, Y.; Saudan, L.; Yang, H.; Yu-Hung, C.; Alemany, L. B.; Sasaki, T.; Morin, J.-F.; Guerrero, J. M.; Kelly, K. F.; Tour, J. M. Surface-Rolling Molecules. *J. Am. Chem. Soc.* **2006**, *128*, 4854-4864.

12. Godoy, J.; Vives, G.; Tour, J. M. Toward Chemical Propulsion: Synthesis of Romp-Propelled Nanocars. *ACS Nano* **2010**, *5*, 85-90.

13. Morin, J.-F.; Shirai, Y.; Tour, J. M. En Route to a Motorized Nanocar. *Org. Lett.* **2006**, *8*, 1713-1716.

14. Sasaki, T.; Tour, J. M. Synthesis of a New Photoactive Nanovehicle: A Nanoworm. *Org. Lett.* **2008**, *10*, 897-900.

15. Shirai, Y.; Sasaki, T.; Guerrero, J. M.; Yu, B.-C.; Hodge, P.; Tour, J. M. Synthesis and Photoisomerization of Fullerene− and Oligo(Phenylene Ethynylene)−Azobenzene Derivatives. *ACS Nano* **2007**, *2*, 97-106.

16. Koumura, N.; Geertsema, E. M.; van Gelder, M. B.; Meetsma, A.; Feringa, B. L. Second Generation Light-Driven Molecular Motors. Unidirectional Rotation Controlled by a Single Stereogenic Center with near-Perfect Photoequilibria and Acceleration of the Speed of Rotation by Structural Modification. *J. Am. Chem. Soc.* **2002**, *124*, 5037-5051.

17. Klok, M.; Boyle, N.; Pryce, M. T.; Meetsma, A.; Browne, W. R.; Feringa, B. L. Mhz Unidirectional Rotation of Molecular Rotary Motors. *J. Am. Chem. Soc.* **2008**, *130*, 10484-10485.

18. Kulago, A. A.; Mes, E. M.; Klok, M.; Meetsma, A.; Brouwer, A. M.; Feringa, B. L. Ultrafast Light-Driven Nanomotors Based on an Acridane Stator. *J. Org. Chem.* **2009**, *75*, 666-679.

19. Grill, L.; Rieder, K.-H.; Moresco, F.; Jimenez-Bueno, G.; Wang, C.; Rapenne, G.; Joachim, C. Imaging of a Molecular Wheelbarrow by Scanning Tunneling Microscopy. *Surf. Sci.* **2005**, *584*, L153-L158.

20. Grill, L.; Rieder, K.-H.; Moresco, F.; Stojkovic, S.; Gourdon, A.; Joachim, C. Exploring the Interatomic Forces between Tip and Single Molecules During Stm Manipulation. *Nano Lett.* **2006**, *6*, 2685-2689.

21. Grill, L.; Rieder, K. H.; Moresco, F.; Rapenne, G.; Stojkovic, S.; Bouju, X.; Joachim, C. Rolling a Single Molecular Wheel at the Atomic Scale. *Nat. Nanotech.* **2007**, *2*, 95-98.

22. Hla, S.-W.; Bartels, L.; Meyer, G.; Rieder, K.-H. Inducing All Steps of a Chemical Reaction with the Scanning Tunneling Microscope Tip: Towards Single Molecule Engineering. *Phys. Rev. Lett.* **2000**, *85*, 2777-2780.

23. Comstock, M. J.; Levy, N.; Kirakosian, A.; Cho, J.; Lauterwasser, F.; Harvey, J. H.; Strubbe, D. A.; Fréchet, J. M. J.; Trauner, D.; Louie, S. G.; Crommie, M. F. Reversible Photomechanical Switching of Individual Engineered Molecules at a Metallic Surface. *Phys. Rev. Lett.* **2007**, *99*, 038301.

24. ter Wiel, M. K. J.; Vicario, J.; Davey, S. G.; Meetsma, A.; Feringa, B. L. New Procedure for the Preparation of Highly Sterically Hindered Alkenes Using a Hypervalent Iodine Reagent. *Org. Biomol. Chem.* **2005**, *3*, 28-30.

25. ter Wiel, M. K. J.; van Delden, R. A.; Meetsma, A.; Feringa, B. L. Increased Speed of Rotation for the Smallest Light-Driven Molecular Motor. *J. Am. Chem. Soc.* **2003**, *125*, 15076-15086.

26. Coleman, M. P.; Boyd, M. K. S-Pixyl Analogues as Photocleavable Protecting Groups for Nucleosides. *J. Org. Chem.* **2002**, *67*, 7641-7648.

27. Hundertmark, T.; Littke, A. F.; Buchwald, S. L.; Fu, G. C. $Pd(PhCN)_2Cl_2/P(t\text{-}Bu)_3$: A Versatile Catalyst for Sonogashira Reactions of Aryl Bromides at Room Temperature. *Org. Lett.* **2000**, *2*, 1729-1731.

28. Rapenne, G.; Grill, L.; Zambelli, T.; Stojkovic, S. M.; Ample, F.; Moresco, F.; Joachim, C. Launching and Landing Single Molecular Wheelbarrows on a Cu(100) Surface. *Chem. Phys. Lett.* **2006**, *431*, 219-222.

Dibromo molecular motor. In CDCl3 with 0.05% TMS.

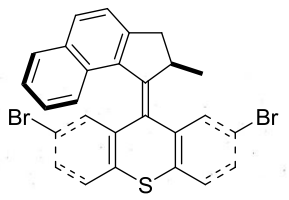

9


```
Current Data Parameters
NAME      DibromoMotor_H
EXPNO                  1
PROCNO                 1

F2 - Acquisition Parameters
Date_           20100726
Time               16.45
INSTRUM            spect
PROBHD   5 mm PABBO BB-
PULPROG             zg30
TD                131072
SOLVENT             CDCl3
NS                     16
DS                      0
SWH              5000.000 Hz
FIDRES           0.038147 Hz
AQ              13.1073503 sec
RG                  287.4
DW                100.000 use
DE                  6.00 use
TE                295.2 K
D1             5.00000000 sec
TD0                    1

======== CHANNEL f1 ========
NUC1                   1H
P1                  8.60 use
PL1                -3.00 dB
SFO1         500.1320000 MHz

F2 - Processing parameters
SI                262144
SF           500.1300155 MHz
WDW                   no
SSB                    0
LB                  0.00 Hz
GB                     0
PC                  1.00
```

Dibromo molecular motor. In CDCl3 with 0.05% TMS.

3436.54
3435.24
3429.79
3428.14
3426.69
3421.24
3419.99
3399.33
3398.98
3397.18
3396.88
3393.03
3384.48

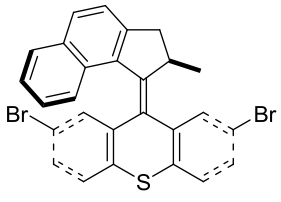

9

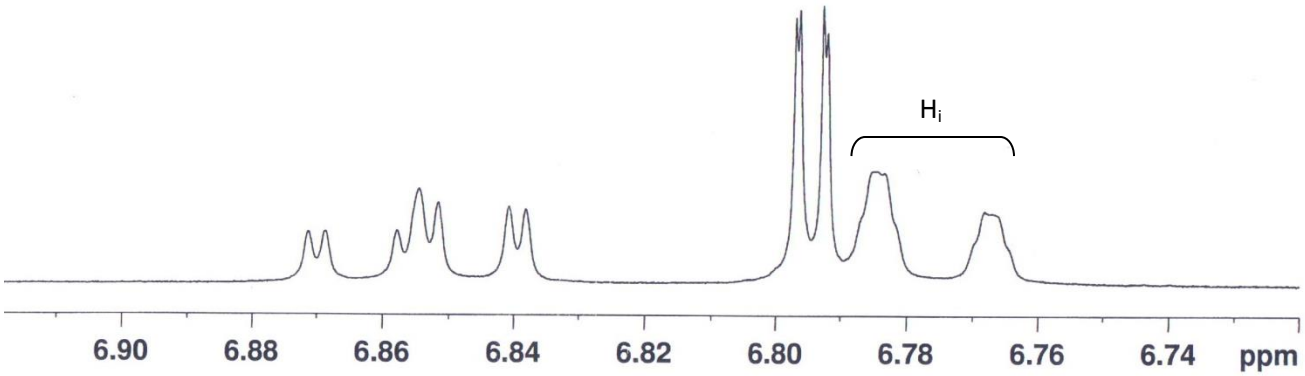

BRUKER

```
Current Data Parameters
NAME      DibromoMotor_H
EXPNO                 1
PROCNO                1

F2 - Acquisition Parameters
Date_          20100726
Time              16.45
INSTRUM           spect
PROBHD   5 mm PABBO BB-
PULPROG            zg30
TD               131072
SOLVENT            CDCl3
NS                    16
DS                     0
SWH            5000.000 Hz
FIDRES            0.038147 Hz
AQ            13.1073503 sec
RG                287.4
DW               100.000 usec
DE                 6.00 usec
TE                295.2 K
D1            5.00000000 sec
TD0                    1

======== CHANNEL f1 ========
NUC1                  1H
P1                 8.60 usec
PL1               -3.00 dB
SFO1         500.1320000 MHz

F2 - Processing parameters
SI                262144
SF         500.1300155 MHz
WDW                   no
SSB                    0
LB                0.00 Hz
GB                     0
PC                1.00
```

Dibromo molecular motor. In CDCl3 with 0.05% TMS.

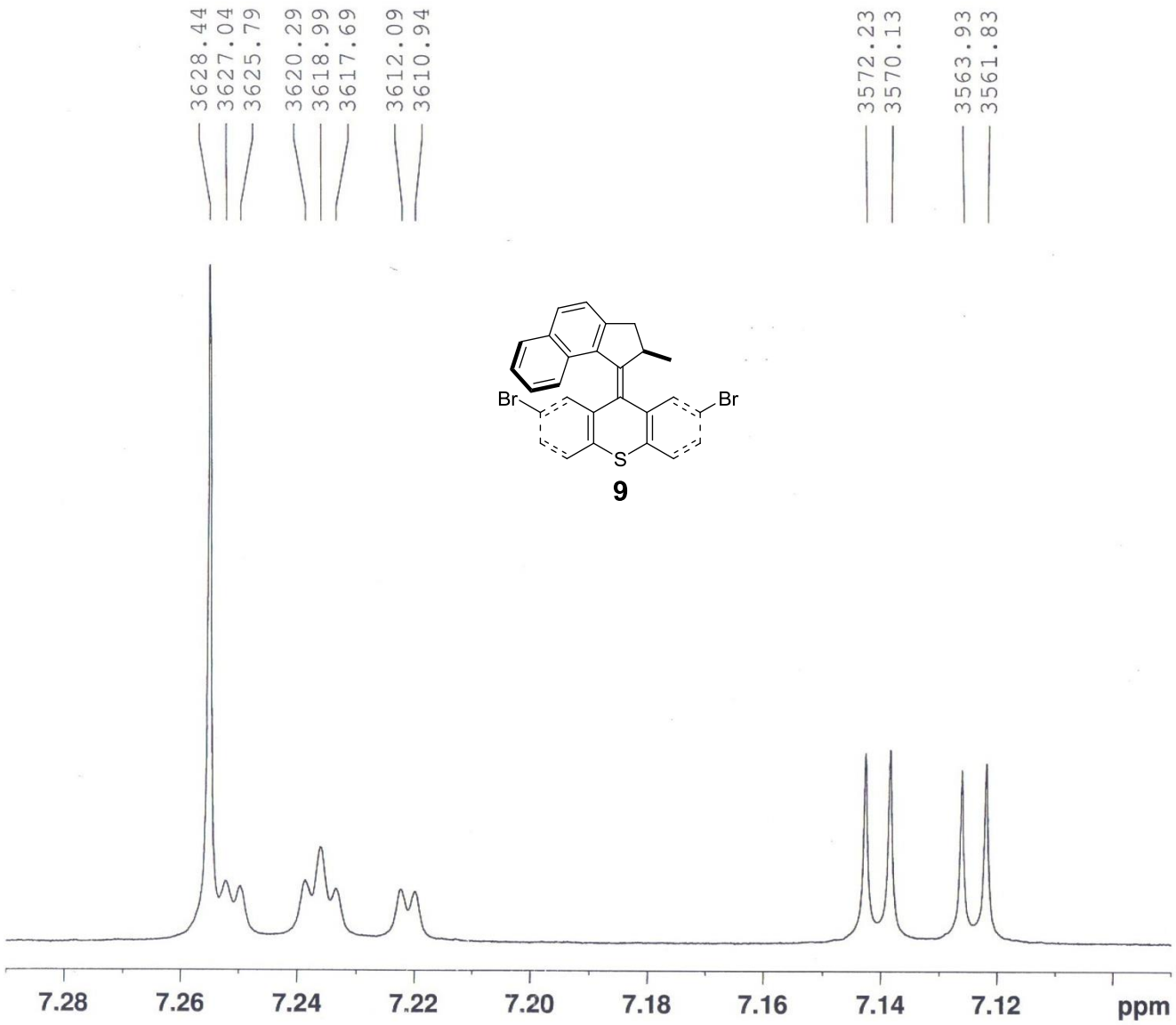

Current Data Parameters
NAME DibromoMotor_H
EXPNO 1
PROCNO 1

F2 - Acquisition Parameters
Date_ 20100726
Time 16.45
INSTRUM spect
PROBHD 5 mm PABBO BB-
PULPROG zg30
TD 131072
SOLVENT CDCl3
NS 16
DS 0
SWH 5000.000 Hz
FIDRES 0.038147 Hz
AQ 13.1073503 sec
RG 287.4
DW 100.000 usec
DE 6.00 usec
TE 295.2 K
D1 5.00000000 sec
TD0 1

======== CHANNEL f1 ========
NUC1 1H
P1 8.60 usec
PL1 -3.00 dB
SFO1 500.1320000 MHz

F2 - Processing parameters
SI 262144
SF 500.1300155 MHz
WDW no
SSB 0
LB 0.00 Hz
GB 0
PC 1.00

Dibromo molecular motor. In CDCl3 with 0.05% TMS.

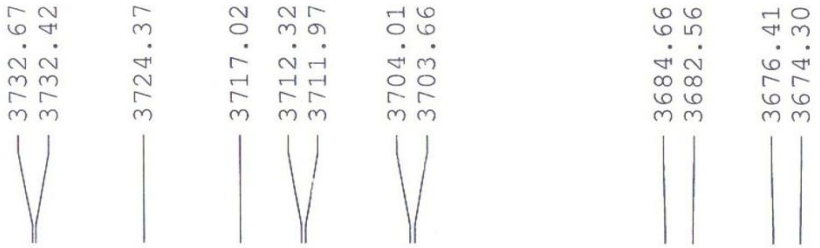

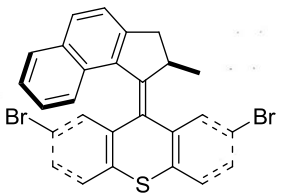

9

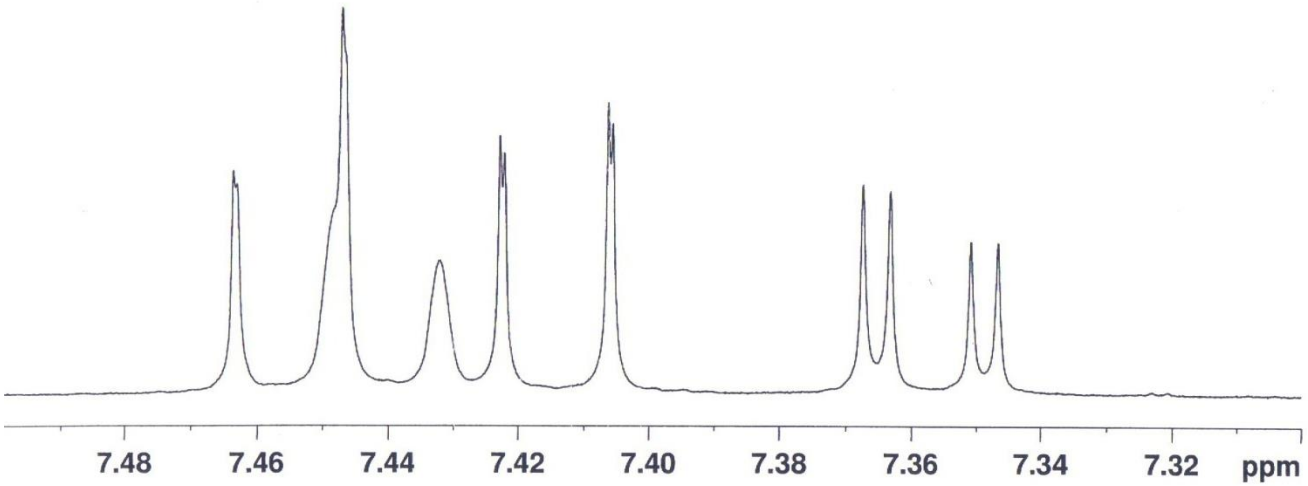

BRUKER

```
Current Data Parameters
NAME      DibromoMotor_H
EXPNO                  1
PROCNO                 1

F2 - Acquisition Parameters
Date_           20100726
Time               16.45
INSTRUM            spect
PROBHD   5 mm PABBO BB-
PULPROG             zg30
TD                131072
SOLVENT             CDCl3
NS                     16
DS                      0
SWH           5000.000 Hz
FIDRES           0.038147 Hz
AQ            13.1073503 sec
RG                 287.4
DW              100.000 usec
DE                6.00 usec
TE                295.2 K
D1            5.00000000 sec
TD0                    1

======== CHANNEL f1 ========
NUC1                   1H
P1                  8.60 usec
PL1                -3.00 dB
SFO1        500.1320000 MHz

F2 - Processing parameters
SI                262144
SF          500.1300155 MHz
WDW                   no
SSB                    0
LB                0.00 Hz
GB                     0
PC                  1.00
```

Dibromo molecular motor. In CDCl3 with 0.05% TMS.

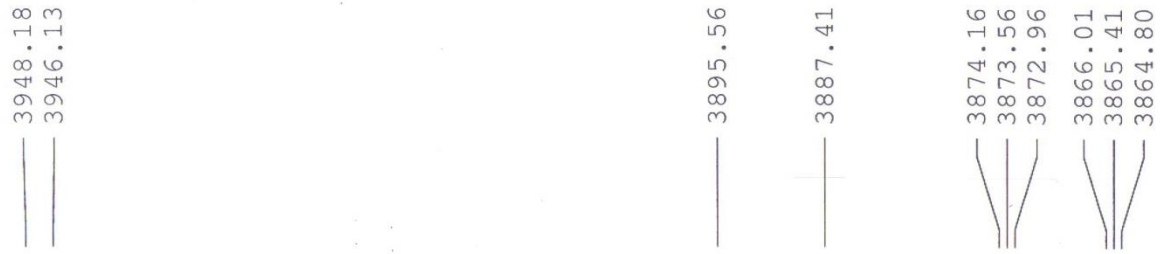

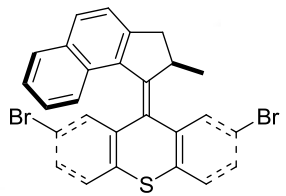

9

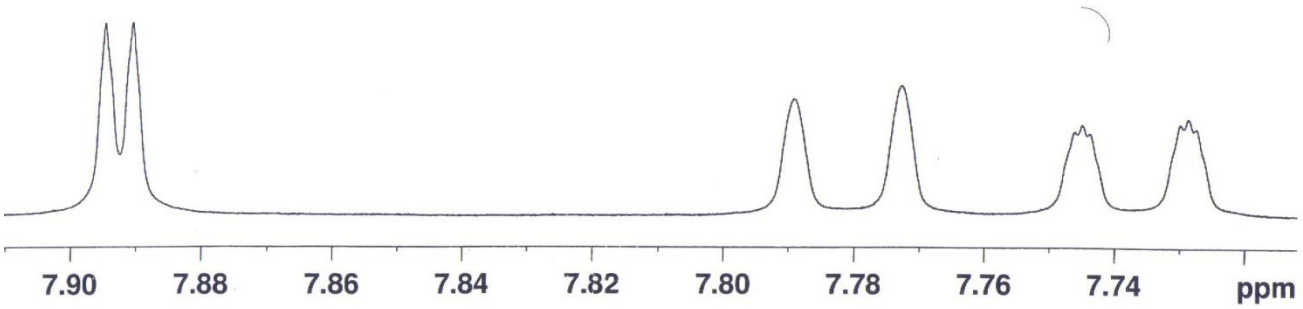


```
Current Data Parameters
NAME      DibromoMotor_H
EXPNO                  1
PROCNO                 1

F2 - Acquisition Parameters
Date_           20100726
Time               16.45
INSTRUM            spect
PROBHD   5 mm PABBO BB-
PULPROG             zg30
TD                131072
SOLVENT             CDCl3
NS                    16
DS                     0
SWH             5000.000 Hz
FIDRES             0.038147 Hz
AQ             13.1073503 sec
RG                 287.4
DW               100.000 usec
DE                 6.00 usec
TE                295.2 K
D1             5.00000000 sec
TD0                    1

======== CHANNEL f1 ========
NUC1                  1H
P1                 8.60 usec
PL1               -3.00 dB
SFO1        500.1320000 MHz

F2 - Processing parameters
SI                262144
SF          500.1300155 MHz
WDW                   no
SSB                    0
LB                 0.00 Hz
GB                     0
PC                 1.00
```

Dibromo molecular motor. In CDCl3 with 0.05% TMS.
90degree pulse, 6.60-s FID, 5-s relaxation delay. 664 scans. lb = 0.1 Hz.
All 24 aromatic and alkene signals are resolved.

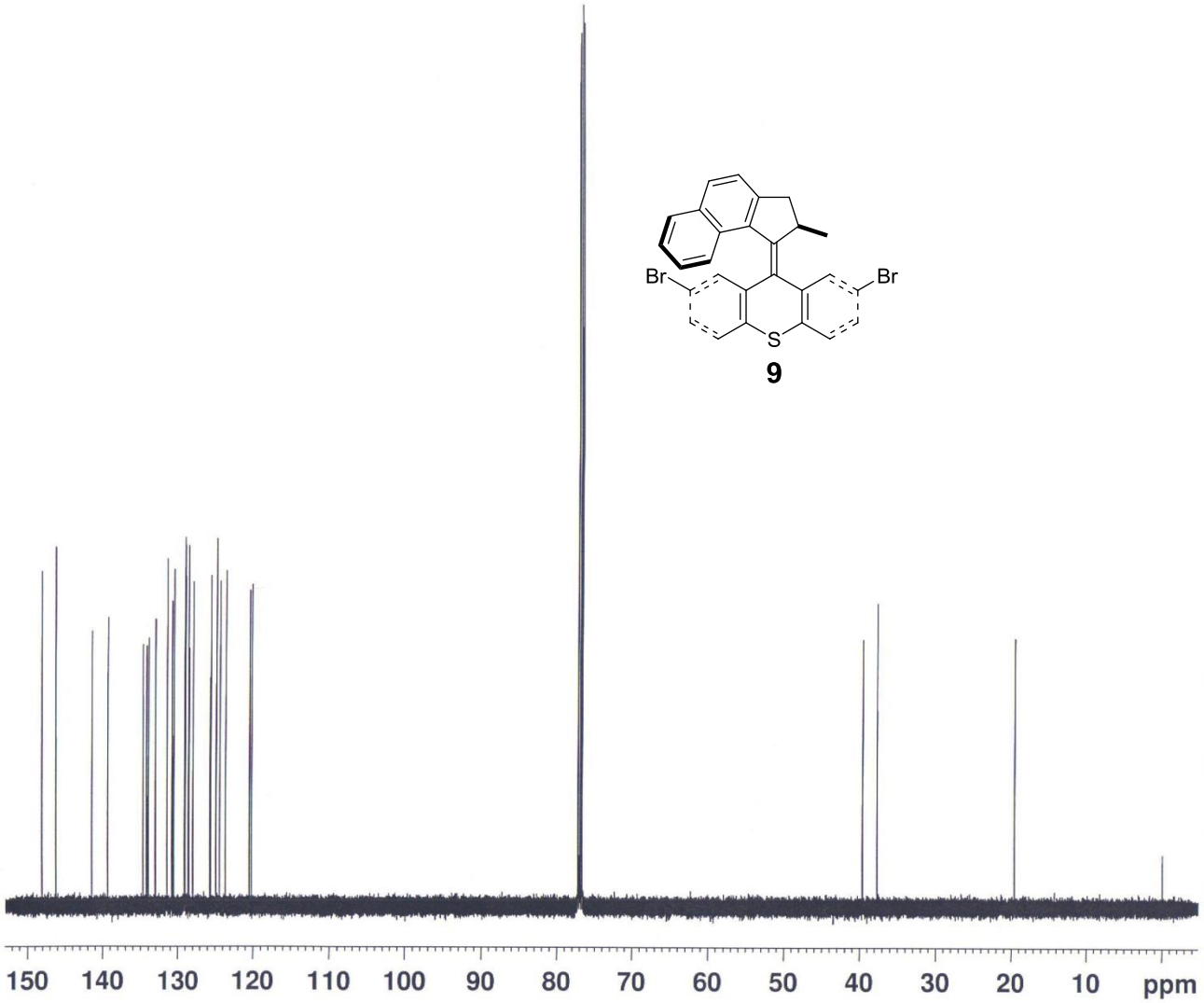

9

```
Current Data Parameters
NAME      DibromoMotor_C
EXPNO                  1
PROCNO                 1

F2 - Acquisition Parameters
Date_           20100727
Time                8.14
INSTRUM            spect
PROBHD   5 mm PABBO BB-
PULPROG             zgpg
TD                262144
SOLVENT            CDCl3
NS                   664
DS                     0
SWH            19841.270 Hz
FIDRES          0.075688 Hz
AQ             6.6061039 sec
RG                9195.2
DW                25.200 usec
DE                 6.00 usec
TE                296.2 K
D1             5.00000000 sec
d11            0.03000000 sec
DELTA          4.90000010 sec
TD0                    1

======== CHANNEL f1 ========
NUC1                  13C
P1                   9.50 usec
PL1                  4.00 dB
SFO1         125.7671100 MHz

======== CHANNEL f2 ========
CPDPRG2           waltz16
NUC2                  1H
PCPD2              80.00 usec
PL2                -3.00 dB
PL12               19.50 dB
PL13               19.50 dB
SFO2         500.1320000 MHz

F2 - Processing parameters
SI                262144
SF         125.7577914 MHz
WDW                   EM
SSB                    0
LB                  0.10 Hz
GB                     0
PC                  1.40
```

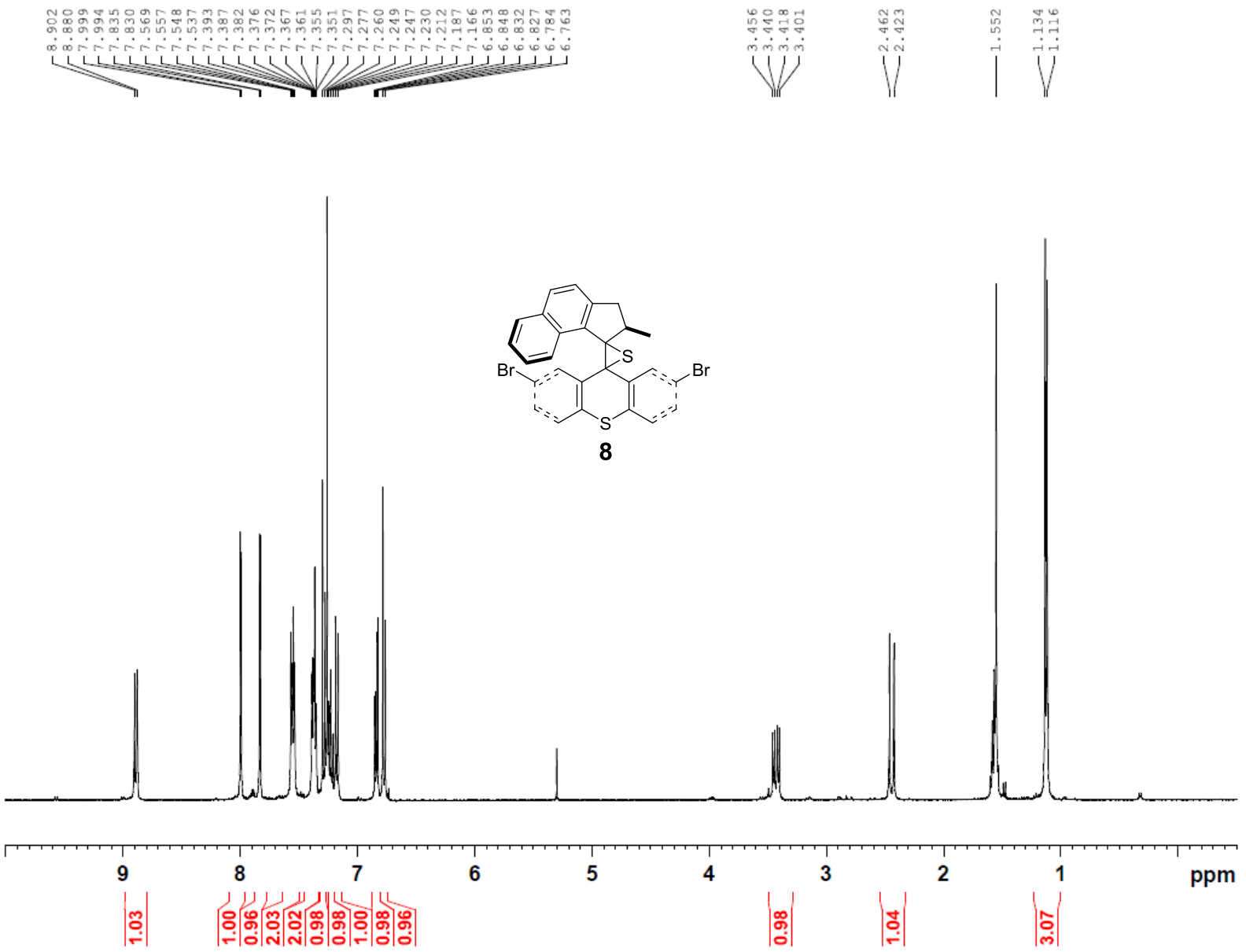
8.902
8.880
7.999
7.994
7.835
7.830
7.569
7.557
7.548
7.537
7.393
7.387
7.382
7.376
7.372
7.367
7.361
7.355
7.351
7.297
7.277
7.260
7.249
7.247
7.230
7.212
7.187
7.166
6.853
6.848
6.832
6.827
6.784
6.763
3.456
3.440
3.418
3.401
2.462
2.423
1.552
1.134
1.116
Br
S
S
Br
8
9
8
7
6
5
4
3
2
1
ppm
1.03
1.00
0.96
2.03
2.02
0.98
0.98
1.00
0.98
0.96
0.98
1.04
3.07

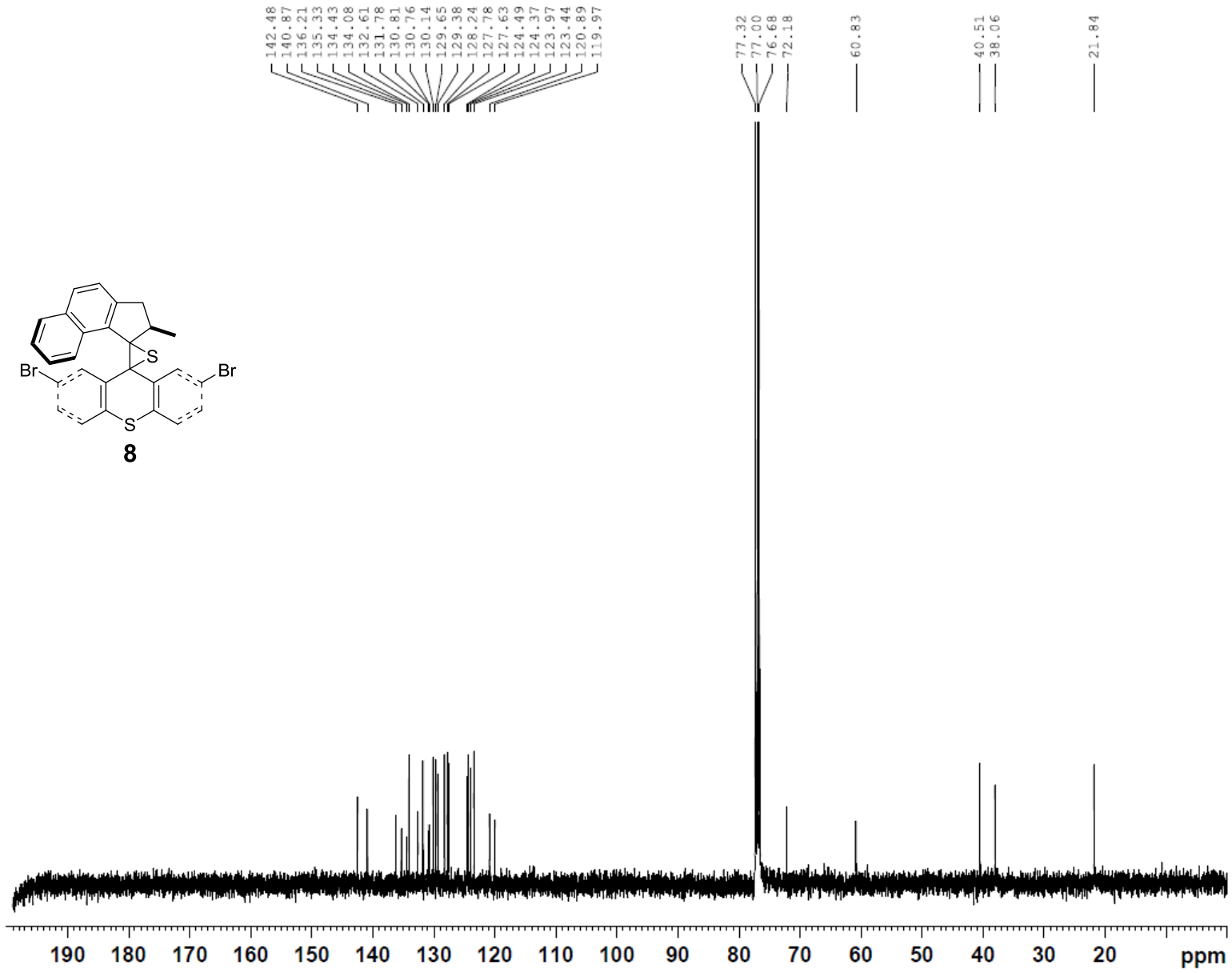
142.48
140.87
136.21
135.33
134.43
134.08
132.61
131.78
130.81
130.76
130.14
129.65
129.38
128.24
127.78
127.63
124.49
124.37
123.97
123.44
120.89
119.97
77.32
77.00
76.68
72.18
60.83
40.51
38.06
21.84
Br
Br
S
S
8
190
180
170
160
150
140
130
120
110
100
90
80
70
60
50
40
30
20
ppm

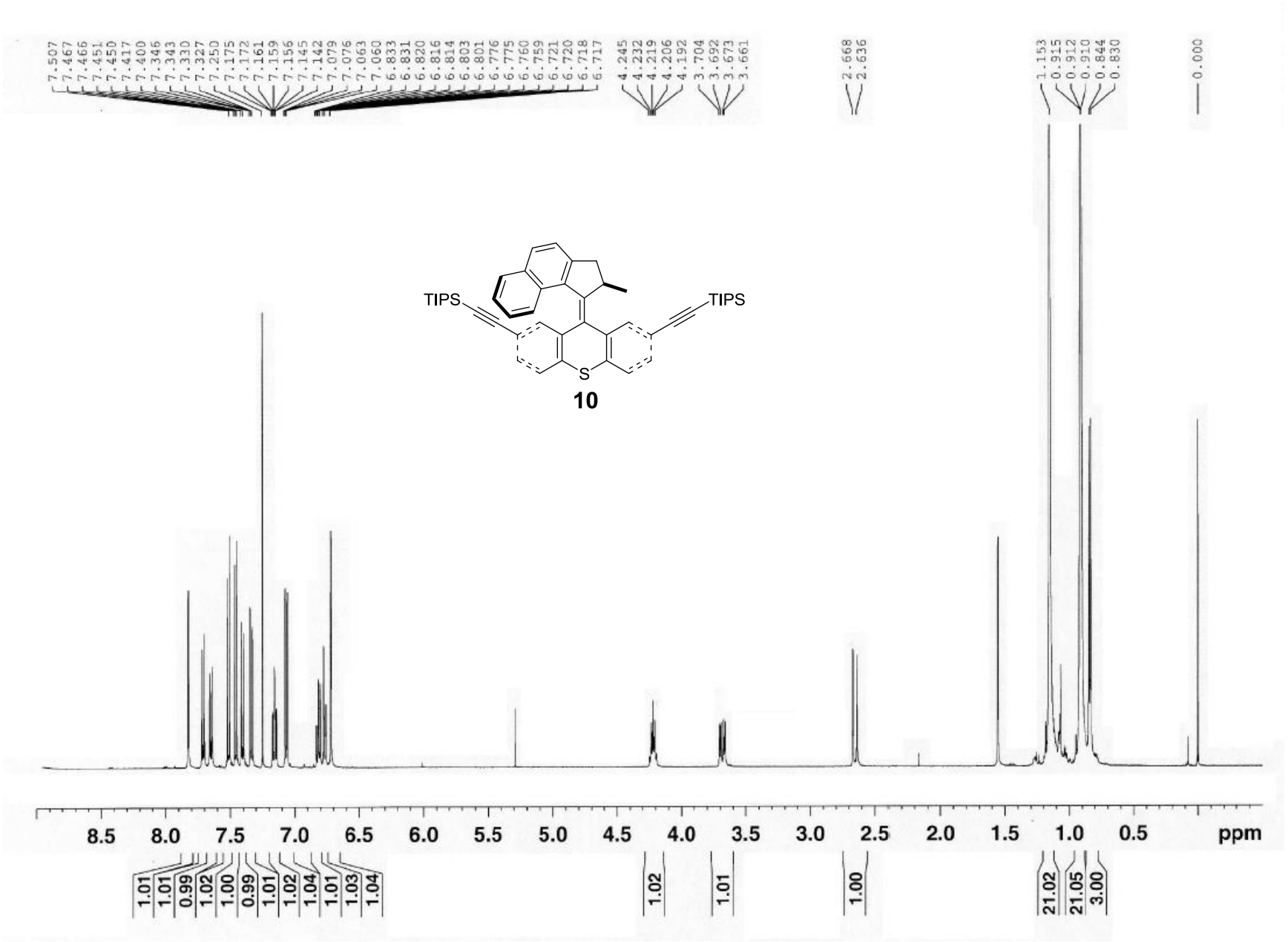
7.507
7.467
7.466
7.451
7.450
7.417
7.400
7.346
7.343
7.330
7.327
7.250
7.175
7.172
7.161
7.159
7.156
7.145
7.142
7.079
7.076
7.063
7.060
6.833
6.831
6.820
6.816
6.814
6.803
6.801
6.776
6.775
6.760
6.759
6.721
6.720
6.718
6.717
4.245
4.232
4.219
4.206
4.192
3.704
3.692
3.673
3.661
2.668
2.636
1.153
0.915
0.912
0.910
0.844
0.830
0.000
TIPS
TIPS
S
10
8.5
8.0
7.5
7.0
6.5
6.0
5.5
5.0
4.5
4.0
3.5
3.0
2.5
2.0
1.5
1.0
0.5
ppm
1.01
1.01
0.99
1.02
1.00
0.99
1.01
1.02
1.04
1.01
1.03
1.04
1.02
1.01
1.00
21.02
21.05
3.00

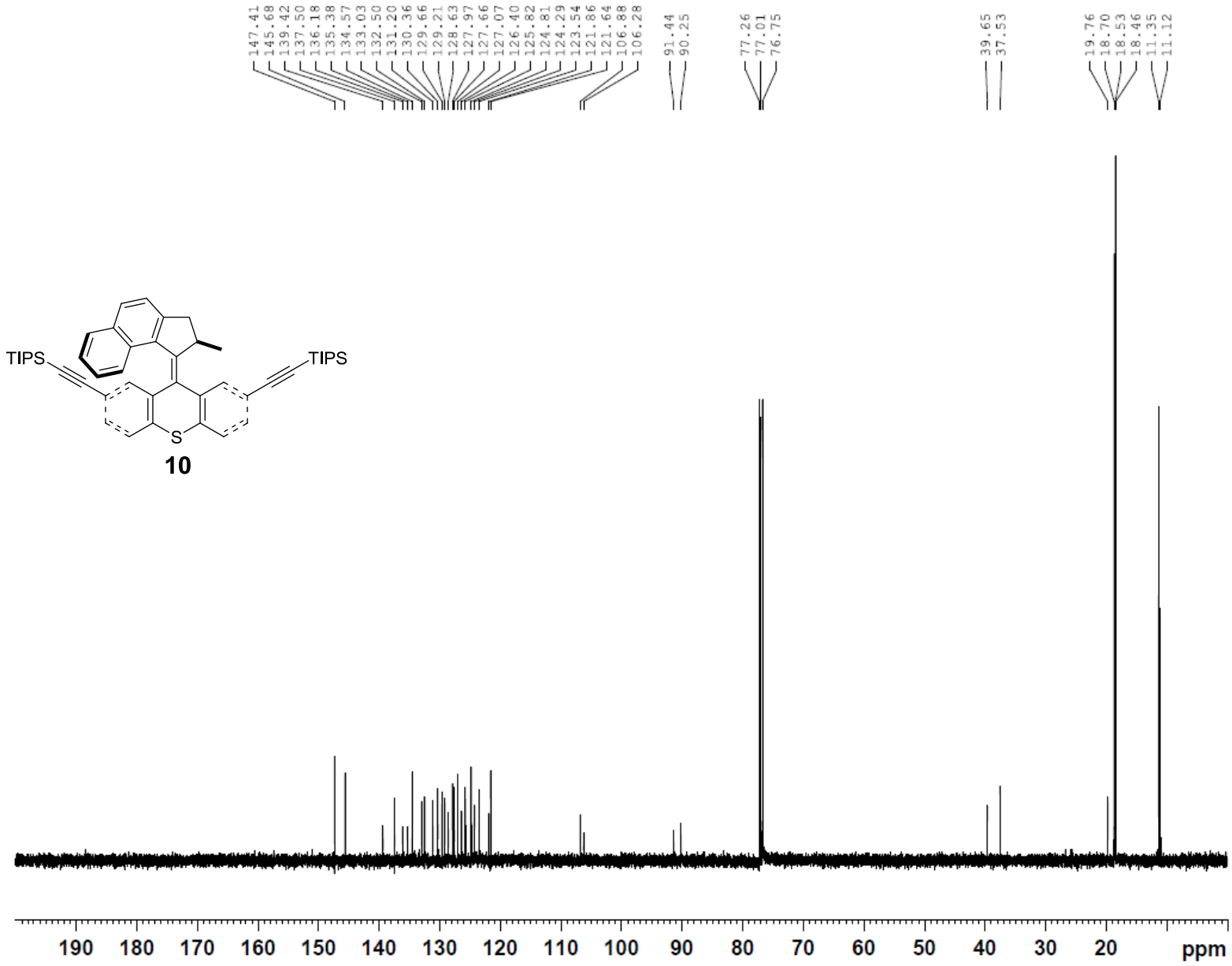
147.41
145.68
139.42
137.50
136.18
135.38
134.57
133.03
132.50
131.20
130.36
129.66
129.21
128.63
127.97
127.66
127.07
126.40
125.82
124.81
124.29
123.54
121.86
121.64
106.88
106.28
91.44
90.25
77.26
77.01
76.75
39.65
37.53
19.76
18.70
18.53
18.46
11.35
11.12
TIPS
TIPS
S
10
190
180
170
160
150
140
130
120
110
100
90
80
70
60
50
40
30
20
ppm

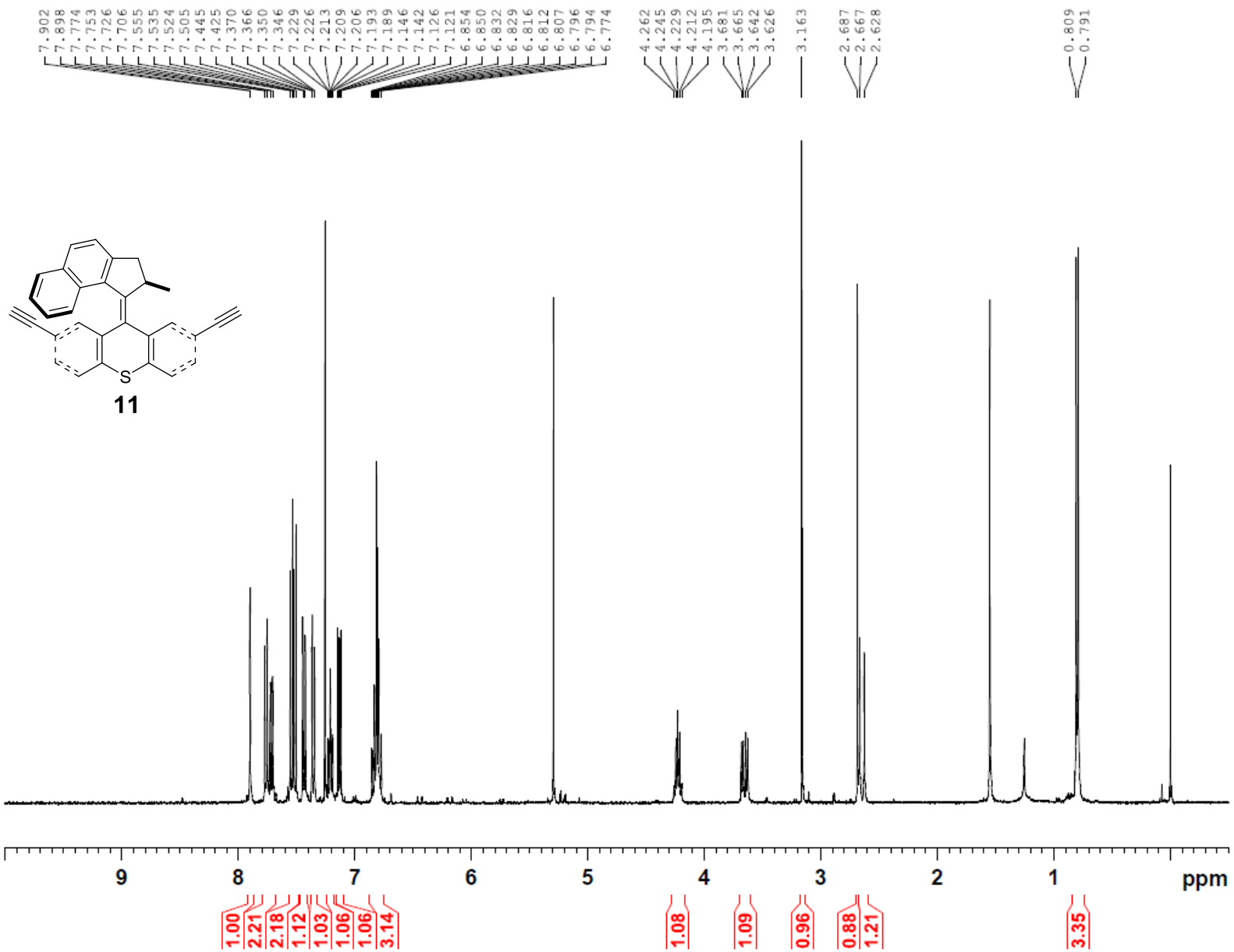
7.902
7.898
7.774
7.753
7.726
7.706
7.555
7.535
7.524
7.505
7.445
7.425
7.370
7.366
7.350
7.346
7.229
7.226
7.213
7.209
7.206
7.193
7.189
7.146
7.142
7.126
7.121
6.854
6.850
6.832
6.829
6.816
6.812
6.807
6.796
6.794
6.774
4.262
4.245
4.229
4.212
4.195
3.681
3.665
3.642
3.626
3.163
2.687
2.667
2.628
0.809
0.791
S
11
9
8
7
6
5
4
3
2
1
ppm
1.00
2.21
2.18
1.12
1.03
1.06
1.06
3.14
1.08
1.09
0.96
0.88
1.21
3.35

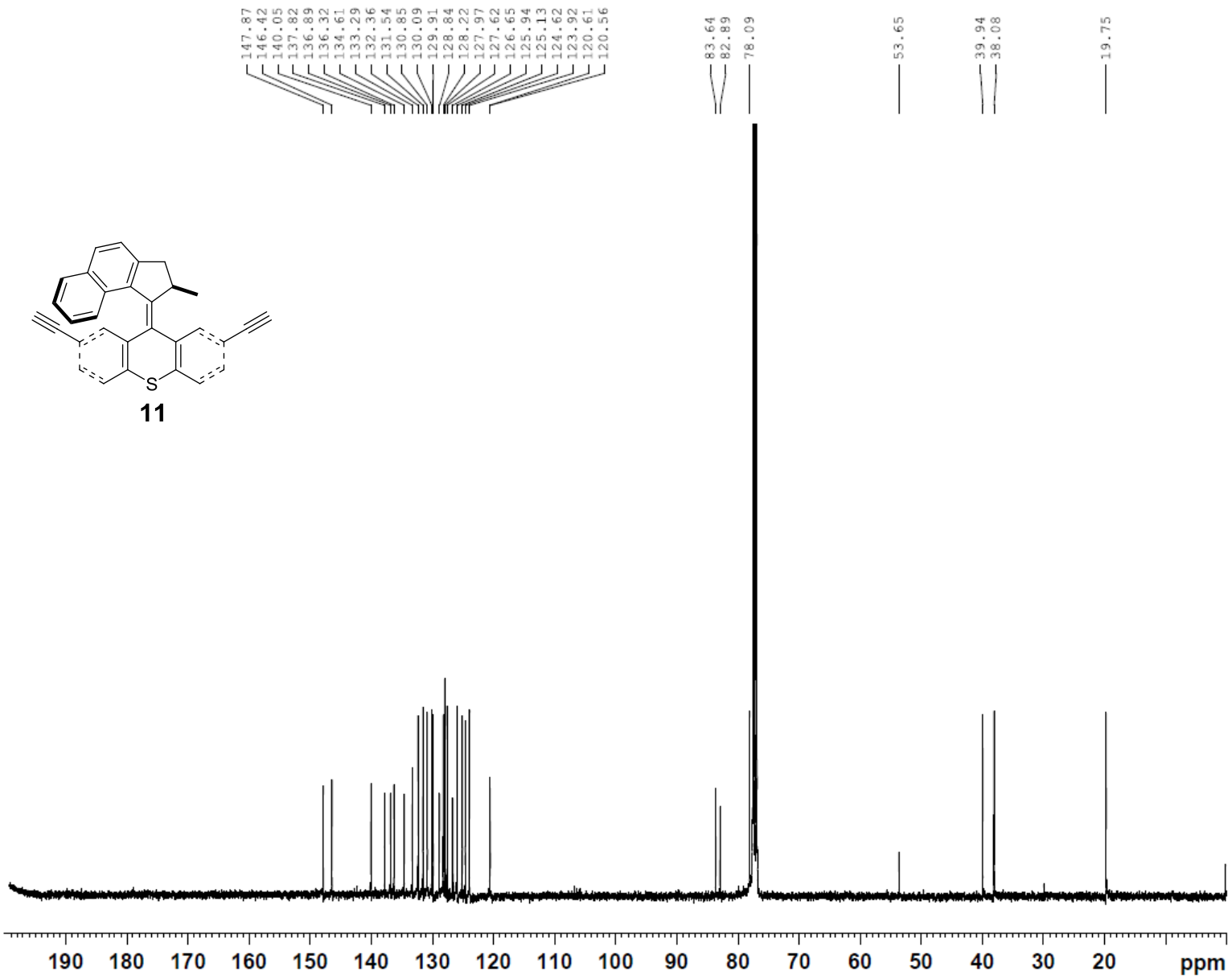
147.87
146.42
140.05
137.82
136.89
136.32
134.61
133.29
132.36
131.54
130.85
130.09
129.91
128.84
128.22
127.97
127.62
126.65
125.94
125.13
124.62
123.92
120.61
120.56
83.64
82.89
78.09
53.65
39.94
38.08
19.75
S
11
190
180
170
160
150
140
130
120
110
100
90
80
70
60
50
40
30
20
ppm

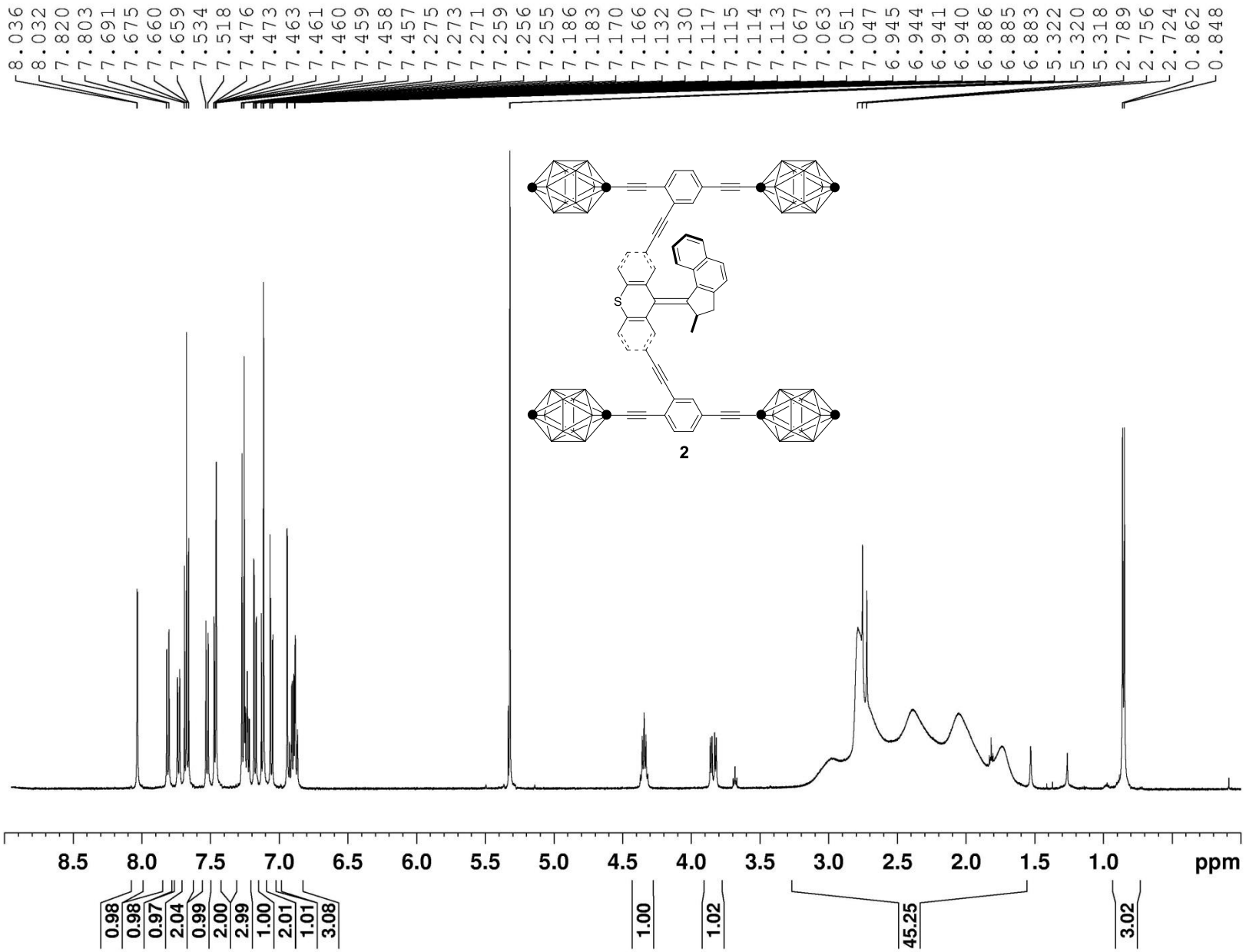
8.036
8.032
7.820
7.803
7.691
7.675
7.660
7.659
7.534
7.518
7.476
7.473
7.463
7.461
7.460
7.459
7.458
7.457
7.275
7.273
7.271
7.259
7.256
7.255
7.186
7.183
7.170
7.166
7.132
7.130
7.117
7.115
7.114
7.113
7.067
7.063
7.051
7.047
6.945
6.944
6.941
6.940
6.886
6.885
6.883
5.322
5.320
5.318
2.789
2.756
2.724
0.862
0.848
S
2
8.5
8.0
7.5
7.0
6.5
6.0
5.5
5.0
4.5
4.0
3.5
3.0
2.5
2.0
1.5
1.0
ppm
0.98
0.98
0.97
2.04
0.99
2.00
2.99
1.00
2.01
1.01
3.08
1.00
1.02
45.25
3.02

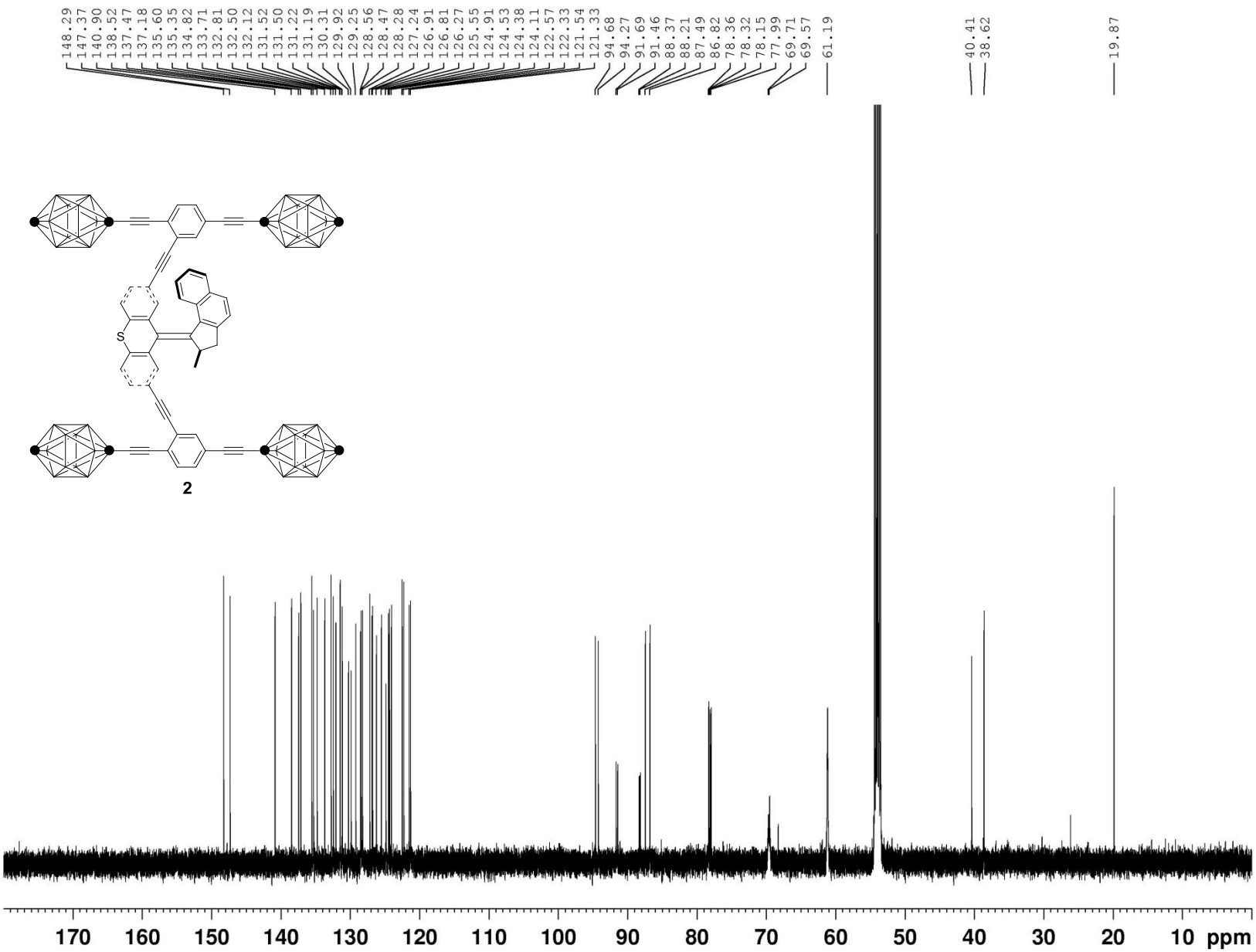
148.29
147.37
140.90
138.52
137.47
137.18
135.60
135.35
134.82
133.71
132.81
132.50
132.12
131.52
131.50
131.22
131.19
130.31
129.92
129.25
128.56
128.47
128.28
127.24
126.91
126.81
126.27
125.55
124.91
124.53
124.38
124.11
122.57
122.33
121.54
121.33
94.68
94.27
91.69
91.46
88.37
88.21
87.49
86.82
78.36
78.32
78.15
77.99
69.71
69.57
61.19
40.41
38.62
19.87
S
2
170
160
150
140
130
120
110
100
90
80
70
60
50
40
30
20
10
ppm

CHAPTER 2

Fine-Tuning the Molecule-Surface Interactions between Motorized Nanovehicles and Conductive Surfaces

2.1. Introduction

Developing synthetic molecular machines has become an extremely interesting and challenging task for chemists.[1,2] Recently, a family of single-molecule nanocars[3,4] was developed in our group, aiming to construct nanovehicles that ultimately can controllably carry nanocargos. One of our short term goals is to design and synthesize self-propelled nanovehicles that can convert external energy into mechanical force and further generate controllable translational motion on surfaces. To meet this goal, we designed and synthesized motorized nanocars incorporating unidirectional rotary motors that are intended to assimilate photonic or electric energy to propel themselves on surfaces.[5,6] The initial single-molecule imaging by STM techniques was accomplished. However, we are not yet able to manipulate on-surface translational motion by applying external energy.[5] In a STM experiment, not only the surface but also the STM tip exhibits short range interaction with the deposited molecule.[7] Thus, the combination of interactions between molecule, surface, light, electric field, and STM tip become very complicated.[7,8] As a result, finding the suitable experimental conditions is extremely challenging for the future design of self-propelled molecular machines.

Feringa and co-workers had successfully demonstrated a four-wheeled molecule (meso-(*R*,*S*-*R*,*S*)-**1**) that performs translational motion on a Cu(111) surface (Figure 1).[9] Molecule **1** consists of four unidirectional molecular rotary motor as wheels, and the rotation of the motorized wheels was induced by tunneling electrons from the STM tip. Sequential electronic and vibrational excitation produced continuous and defined conformational changes of the motor. Consequently, the motor rotation propelled the four-wheeled molecule with directional preference.

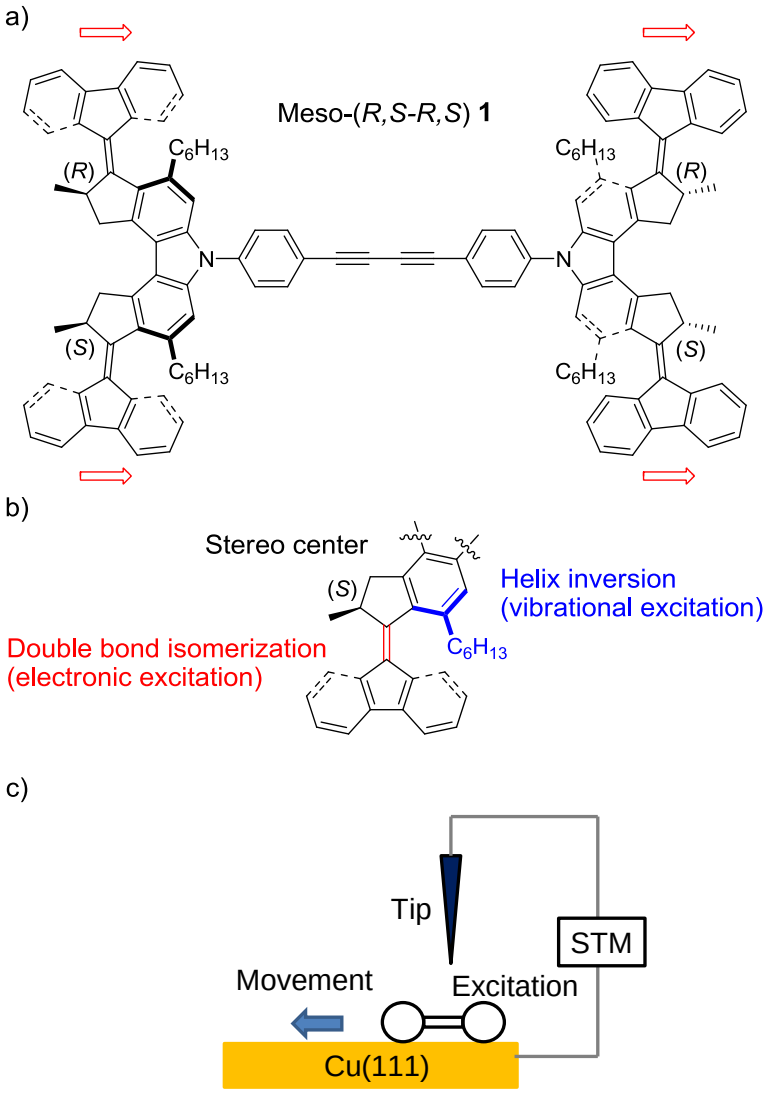

Figure 2.1. Structure of the four-wheeled molecule. (a) Structure of the meso-(*R*,*S*-*R*,*S*) isomer **1**. Red arrows indicate the direction in which the rotary action of the individual motor units propels the molecule. (*R*) and (*S*) indicate the absolute configurations at the stereogenic centers. The black solid and dashed wedges of the cartoon indicate the orientations of the methyl groups, respectively. (b) Structural details of the rotary motor unit. The double bond (red) functions as the axle in rotation and undergoes *trans*-to-*cis* isomerization when electronically excited. Interconversion between helical conformers, arising from steric overcrowding in the region highlighted in blue, is achieved by vibrational excitation. The

stereocenter in the cyclopentane ring determines the stability of each conformer and the direction of rotation of the motor. (c) Schematic representation of the experiment. The bias voltage U is applied to the sample. The electrons tunneling through the molecule excited the vibrational and electronic states and thus induce translational movement on the surface.

2.2. Fine-tuning the molecule-surface interactions

In contrast to the design of **1**, the nanocars have highly symmetrical molecules as wheels and rely on the rolling mechanism for translational motions.[10,11] Our initial experiments of inducing the motor rotation of the *p*-carborane-wheeled motorized nanocar **2** (Figure 2) deposited on Cu(111) did not yield translational motion. We attribute this result to the rather strong molecule-surface interactions, including the high diffusion barrier of *p*-carborane rolling motion on Cu(111),[5] and/or energy transfer from the excited motor to the metallic surface.

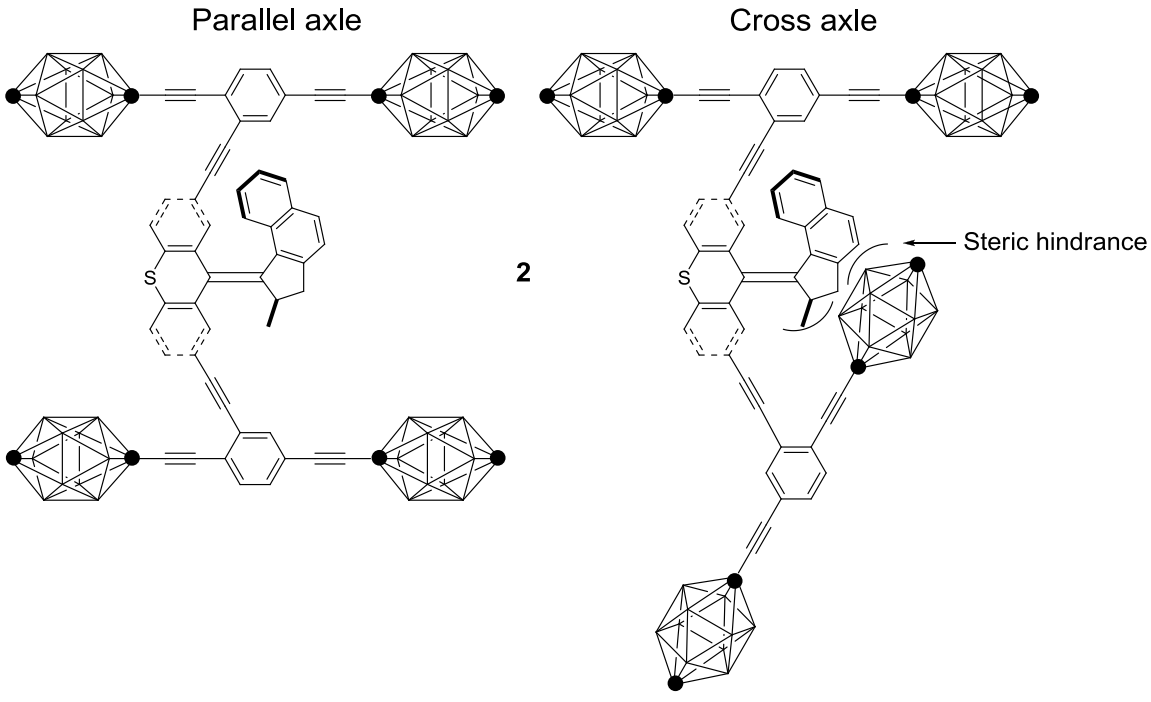

Figure 2.2. Structure of the *p*-carborane-wheeled motorized nanocar **2**. Nanocar **2** exhibited two possible landing conformations on a Cu(111) surface: parallel axle (left) and cross axle (right) conformers. Note that in the cross axle conformer, the rotor and the axle existed steric hindrance that might interfere with the motor rotation. Attempts to achieve motor-propelled motion of nanocar **2** were made by irradiating UV-lights and manipulating by STM tip. No lateral motion or switching between the two conformers was found.

The high diffusion barrier of *p*-caborane on a Cu(111) surface was also found in our previous studies of a *p*-carborane-wheeled nanocar **3** (Figure 3).[12] We had tried to use STM tip-generated electric field to push or drag the nanocar **3** and wished to study the rolling motion of nanocar **3**. However, no electric field induced rolling motion was achieved. Only conformational switching between the parallel axle and the cross axle conformers was found. Likewise, the parallel axle and cross axle conformers were also found in the STM imaging of nanocar **2**. In the cross axle conformer of nanocar **2**, steric hindrance exists between the axle and the rotor that interfere with the motor rotation. Unlike nanocar **3**, we did not accomplish switching between the two conformers of nanocar **2** by the STM tip.

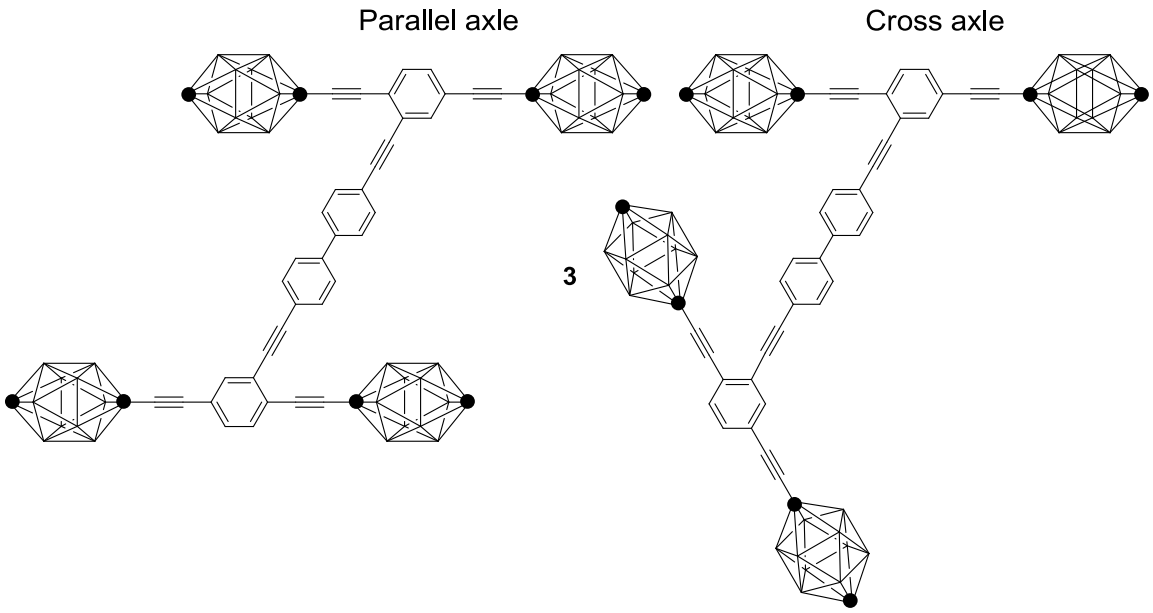

Figure 2.3. Structure of the STM assembled *p*-carborane-wheeled nanocar **3**. STM manipulations on a Cu(111) surface were done to study the rolling motion of nanocar **3** through electric field gradients induced by the tip. However, only switching between the parallel axle and cross axle conformers was achieved. Note that no rolling motion was induced, which indicated the *p*-carborane wheel molecules exhibit rather strong molecule-surface interactions on Cu(111).

The success of motion in **1** exemplified the possibility of generating motor-propelled translational motion. However, **1** has a different structural design when compared to nanocars, and the molecule-surface interactions are different. Finding the adequate molecule-surface interaction is important for nanocar because the translational motion relies on rolling to give directionality. If the molecule-surface interaction is too weak, then the nanocar will slide on a surface and the directionality will be lost. On the other hand, strong molecule-surface interaction will increase the energy barrier for rolling and might impact the rotation of motor.

The following parameters can be varied for fine-tuning the molecule-surface interaction:

1. The wheel type
2. The number of the wheels
3. The surface type.

Since the first C_{60}-bearing nanocar,[10,11] many endeavors were made to find molecules, such as *p*-carborane,[6] organometallic,[13] and adamantane,[14] that are suitable as wheels. By choosing different wheels, nanovehicles give different interactions to a surface. Another hybrid-wheel concept was developed in the design of nanodragster **4** (Figure 4).[15] It consists of a *p*-carborane-wheeled axle and a C_{60}-wheeled axle. Compared to the first C_{60}-wheeled nanocar, the molecule-surface interactions is expected to be weaker. In contrast to the C_{60} nanocar which required 470 K for the thermally activated translational motion on an Au(111) surface, the nanodragster only needed 350 K to start travelling across an Au(111) surface.

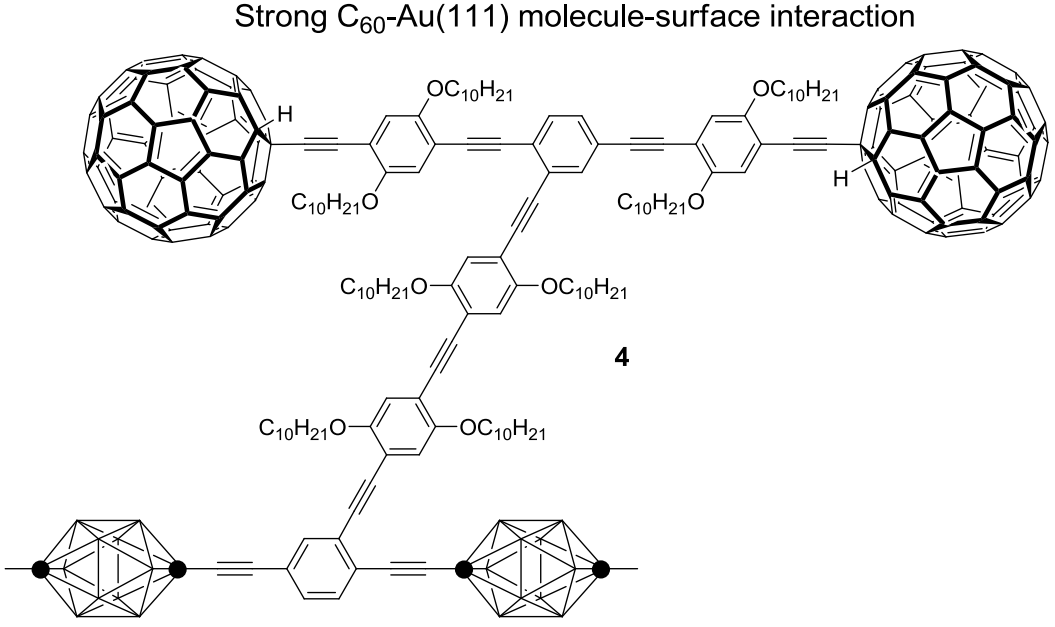

Figure 2.4. Structure and design of the nanodraster **4**. A hybrid-wheel concept was developed in the design of the nanodragster. The molecule included a C_{60}-axle and a *p*-carborane-axle. The C_{60} wheels give strong interaction with gold surface, and the *p*-carborane wheels help maintain the directionality of the nanovehicle. The nanodragster started to show thermally driven translational motion at 350 K.[16] By contrast, the four C_{60}-wheeled nanocar required 470 K for the thermally driven translational motion to be observed.

The number of the wheels can also impact the molecule-surface interactions. We can make adjustments to the design of nanovehicles.

Lastly, varying the surface type also impacts the molecule-surface interaction. In addition to switching between different metallic surfaces, depositing a thin film of NaCl on a metal surface is a method to modify the surface yet allows STM measurements to be done. The thin film decouples the molecule-metal surface electronic interactions, and the increased lifetime of tunneling electrons also increases the yield of STM tip manipulated reactions.[8,17]

2.3. Design of the adamantane-wheeled motorized nanocar and three-wheel nanoroadster

Recently, single-molecule fluorescence microscopic (SMFM) diffusion studies of the adamantane-wheeled boron-dipyrromethene- (BODIPY-) based nanocar **5** were carried out on a glass surface. The results showed 67 (±10)% of the nanocar **5** were mobile on a glass surface under ambient conditions. In the same environment, 54 (±7)% of the *p*-carborane-wheeled model **6** moved.[14] This increase of mobility reflected a decrease of the adamantane-

glass interaction compared to the *p*-carborane-glass interaction. Despite the decrease of molecule-surface interaction, the highly mobile nanocar **5** still retains the rolling mechanism.

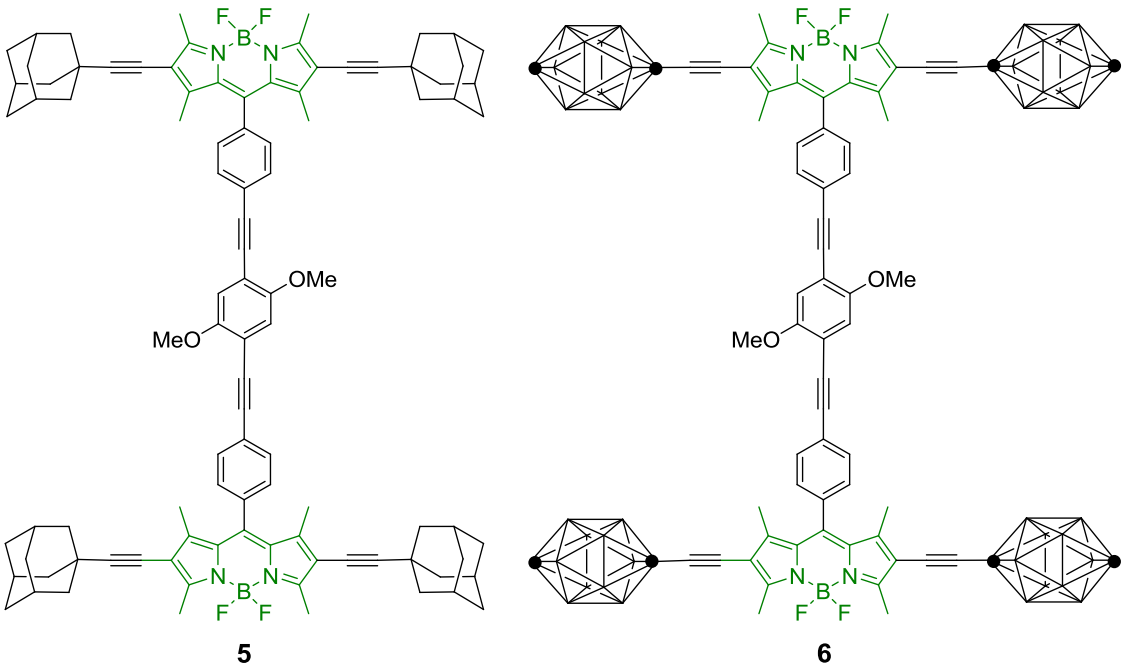

Figure 2.3. Structure of the BODIPY-based nanocars **5** and **6**. The SMFM studies indicated that both nanocars performed micrometer scale translational motion on a glass surface with the rolling mechanism. By switching from *p*-carborane to adamantane, the wheel-glass interaction is decreased. As expected, nanocar **5** showed higher mobility than nanocar **6**.

Nanocar **5** immediately stimulated the design of the adamantane-wheeled motorized nanocar **7** (Figure 4). By switching the wheels of motorized nanocar from *p*-carborane to adamantane, the surface-molecule interaction of **7** is anticipated to decrease compare to its parent nanocar **2**. Based on the STM imaging result of nanocar **2**, we expect two possible landing conformations, the parallel axle and the cross axle conformer, for nanocar **7**. In the cross axle conformer, steric hindrance between the axle and the rotor might inhibit the motor

rotation. Nevertheless, the adamantane-wheeled nanocar **7** with the correct landing conformation is possible in performing motor propelled translational motion.

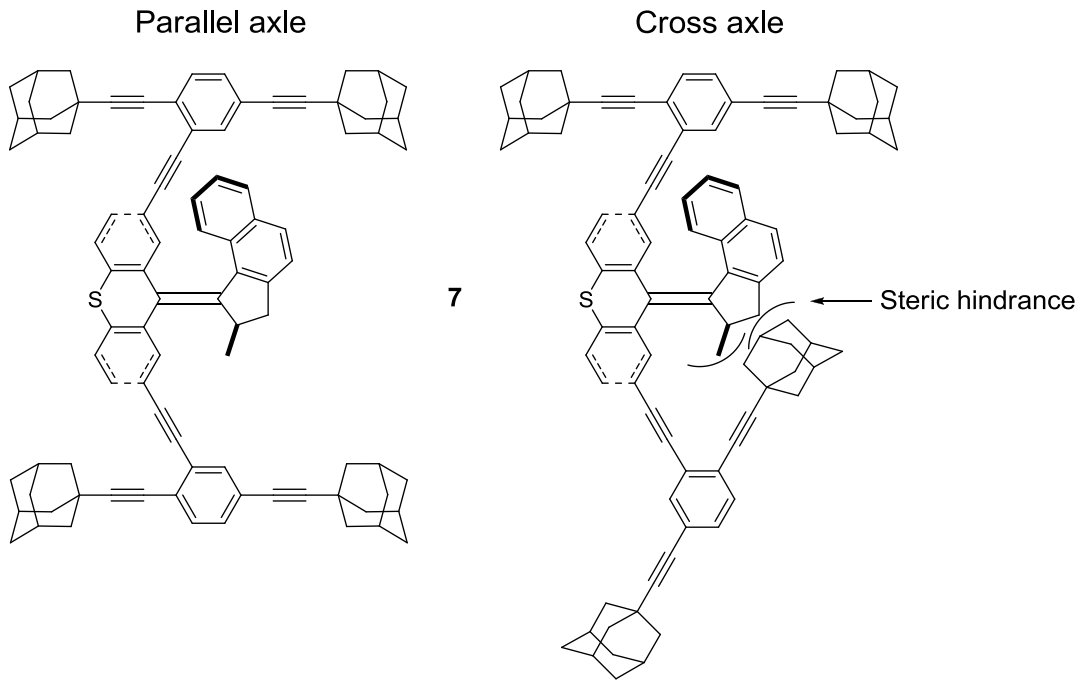

Figure 2.4. Structure and the two possible conformers of the adamantane-wheeled motorized nanocar **7**. The cross axle conformer showed possible steric hindrance that might inhibit the motor rotation.

In addition to switching from *p*-caborane to adamantane wheels, it was planned to reduce the number of wheels. Inspired by the hybrid-wheel approach of the nanodraster **4** and the motorized-wheel design found in **1**, a three-wheel nanoroadster **8** (Figure 5) was designed. The strategy was to put one adamantane-wheeled axle and one motor wheel. We expect the three-wheel design will still maintain the directionality preference as in previous nanocars. Also, the nanoroadster **8** was anticipated to have two landing conformers, the parallel wheel and the cross wheel conformations, on a surface. Note that the axle is attached at the 3-

position of the stator in the nanoroadster **8** rather than at the 2-position as in nanocar **7**. This design would avoid the possibility of steric hindrance between the axle and the motor that might interfere with the motor rotation.

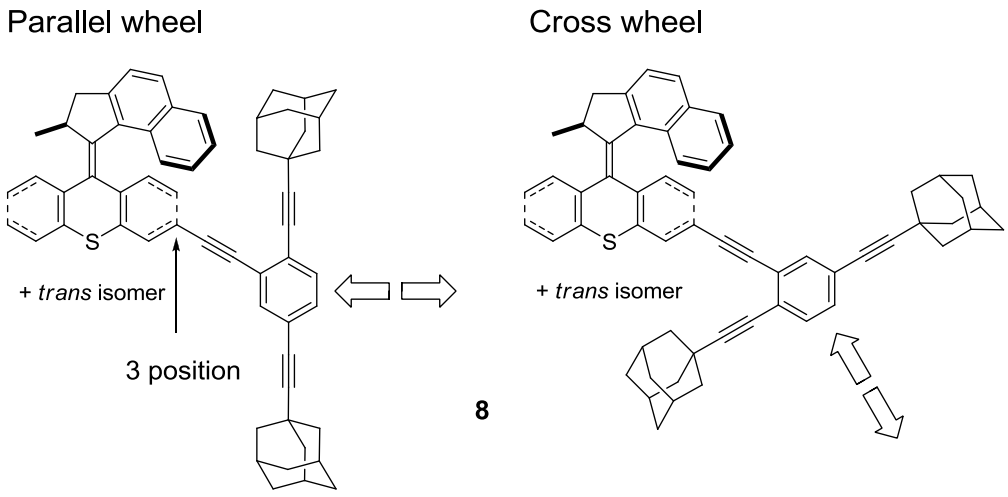

Figure 2.5. Structure of the three-wheel nanoroadster **8**. The nanoroadster was synthesized with one adamantane axle, and the motor served as another wheel. Similar to the motorized nanocars **2** and **7**, nanoroadster **8** has a parallel wheel conformer (left) and a cross axle conformer (right). Note that the axle is connected to the motor at the 3-position. Compared to nanocar **7**, there is less possibility of steric hindrance between the axle and the motor that would interfere with the motor rotation.

2.4. Synthesis of the adamantane-wheeled motorized nanocar

The preparation of nanocar **7** (Scheme 2.3.) involved a similar synthetic sequence for making the *p*-carborane-wheeled motorized nanocar **2**.[5] To synthesize the adamantane-wheeled axle **9**, a selective Sonogashira coupling on the iodine site of 2-bromo-1,4-diiobenzene **10**[6] between 1-ethylnyladamantane **11** was carried out. Subsequently, treating **9**

with *tert*-butyllithium followed by 1,2-diioethane afforded the iodo-axle **12**. Finally, a double Sonogashira coupling between **12** and motor **13** yielded adamantane-wheeled motorized nanocar **7**.

Scheme 2.3. Synthesis of the adamantane-wheeled motorized nanocar **7**.

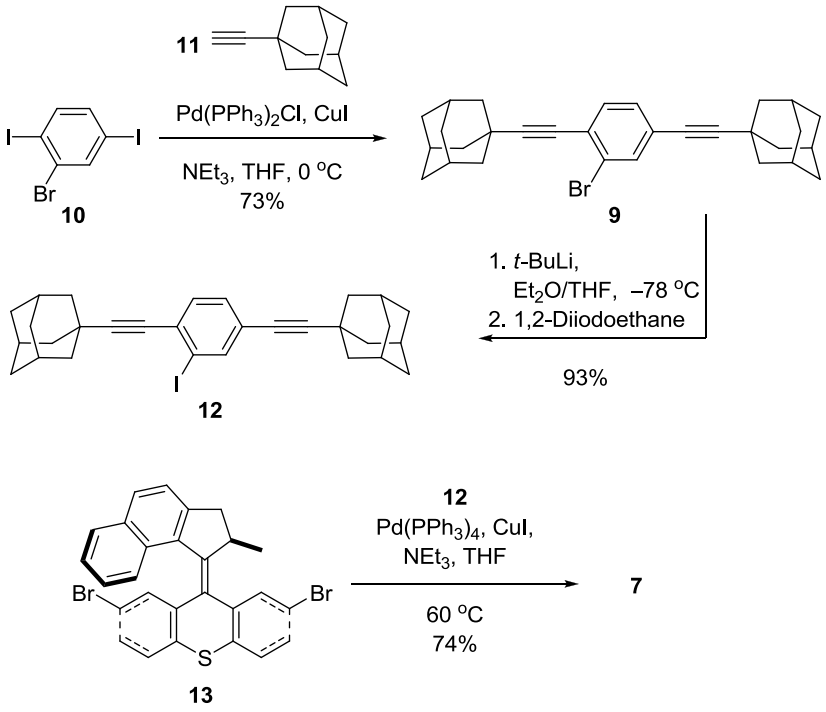

2.5. Synthesis of the Three-Wheel Nanoroadsters

The 3-bromothioxanthen-9-one **14** was prepared according to the literature procedure.[18] The ketone **14** was converted to thione **15** with the treatment of P_4S_{10} in toluene at reflux. Hydrazone **16**[5] was oxidized to the unstable diazo intermediate using manganese dioxide with careful temperature control. The inorganic residue was removed by filtration in a Schlenk-type set-up. Thione **15** was added portionwise to the deep-purple filtrate. A [2+3] cycloaddition occurred and evolution of nitrogen gas indicated the formation of episulfide **17**.

The episulfide **17** was obtained as a mixture of *trans*- and *cis*-isomers form because the stator **15** is dissymmetric. The molecular motor **18** was then made from desulfurization of **17** with trimethyl phosphite in a screw-capped tube at 130 ℃. Note that motor **18** was obtained as a mixture of *trans*- and *cis*-diastereomers and both diastereomers consist of two enantiomers. However, the diastereomers were not separated because the *trans*- and *cis*-forms of **18** can interconvert in the presence of light. The structural similarity of the *trans*- and *cis*-diasteromers also makes the separation very difficult. Because molecules were to be investigated individually on surfaces, it was unnecessary to resolve the enantiomers.

Scheme 2.4. Synthesis of the 3-bromomolecular motor **18**

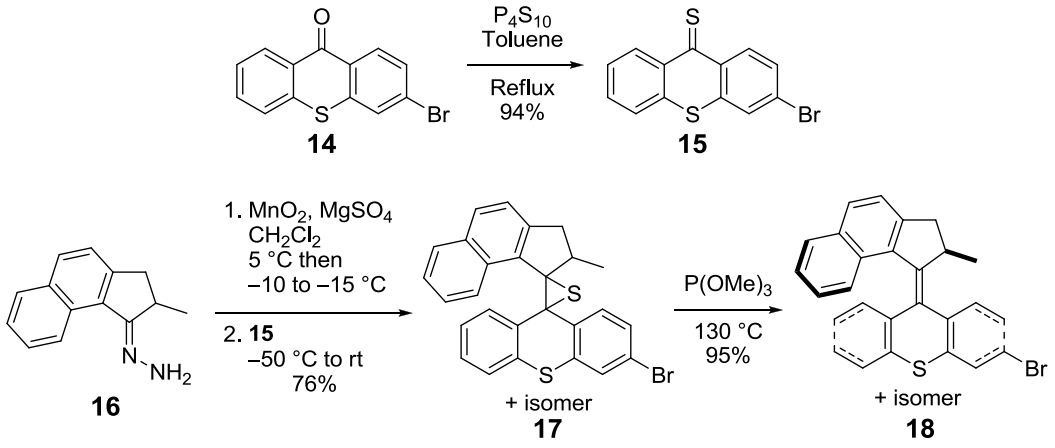

Further Sonogahira coupling between the motor **18** and the triisopropylsilyl- (TIPS-) acetylene gave a good yield of **19**. The TIPS protective group was removed by adding tetrabutylammonium fluoride (TBAF) to afford motor **20**. Finally, motor **20** was coupled with axle **12** and yielded the desired the nanoroadster **8**.

Scheme 2.5. Synthesis of the three-wheel nanoroadster **8**.

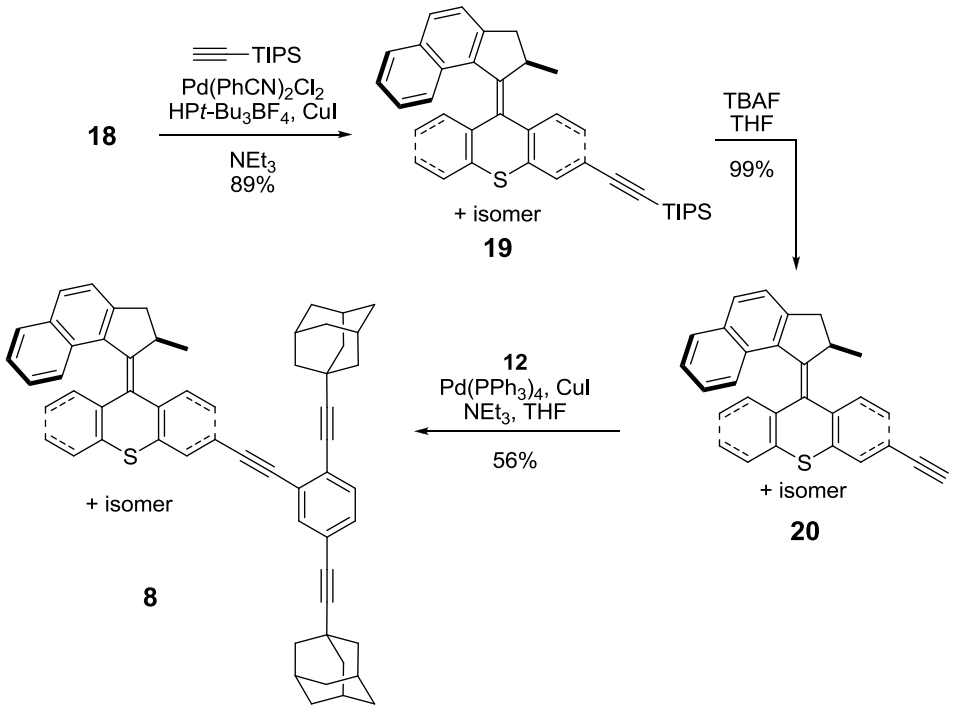

2.6. Imaging and Manipulations of the Adamantane-Wheeled Motorized Nanocar

The adamatane-wheeled motorized nanocar **7** was successfully imaged by STM on both Cu(111) (Figure 6) and Au(111) surfaces. Although evaporating single molecules onto metal surfaces is possible, the surface coverage of the nanocar **7** molecule was low. Compared to the *p*-carborane-wheeled nanocars **2**, more debris was found. This indicated that the adamantane-wheeled nanocar **7** was less stable than the *p*-carborane-wheeled nanocar **2** at the evaporation temperature, and that the deposition method used was inferior to the original dosing valve method.[10,11]

Note that no parallel axle nanocars **7** were found on surface terraces but only on the metal step edges. Although a single-molecule cross axle **7** was found on a terrace, it was an exception. During the evaporation process nanocar molecules were firstly randomly

deposited on a surface. Like nanocar **2**, the nanocars **7** are also mobile at room temperature. Hence, based on the evidence, all nanocars moved to the step edges, where the molecules bound more strongly than on terraces. Unlike nanocar **2**, it is difficult to evaporate enough nanocar **7** to saturate all the step edges. Consequently, it is difficult to find molecules that were adsorbed on a terrace, which is preferable for further manipulations.

Nevertheless, the nanocar **7** was illuminated at wavelengths of 266 nm and 355 nm, but no motion was observed on both surfaces. Voltage pulses were applied to the molecules with the tip of the STM up to ±4 V, at which the voltage dissociated the molecules, without inducing directed motion or reversible change in the motor of the nanocar **7**. Switching between parallel axle and cross axle conformations was not observed.

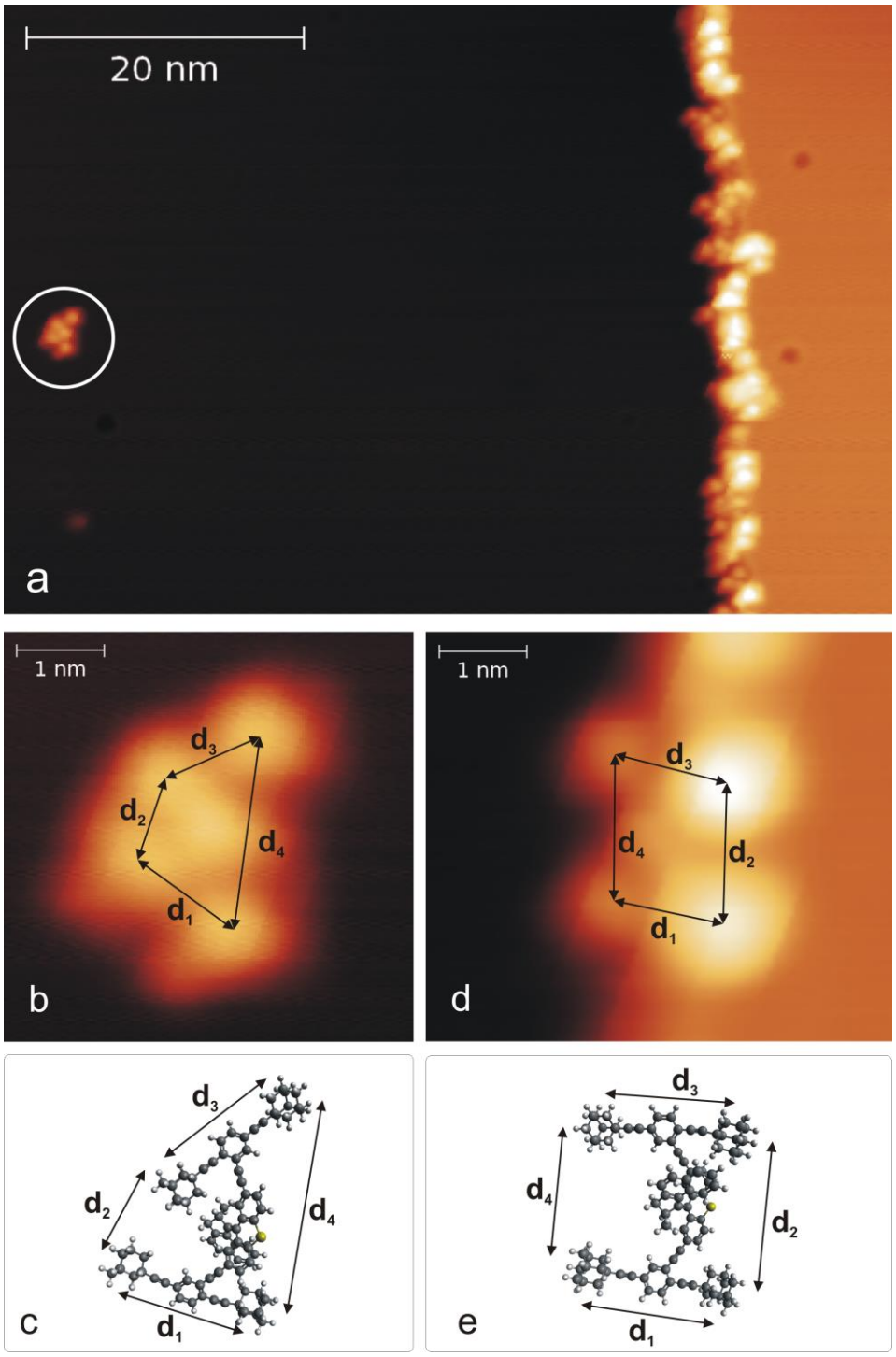

Figure 2.6. STM images of adamantane-wheeled nanocar **7** on Cu(111) and calculated gas phase structures (HyperChem 7 software). (a) Overview image of the surface (white circles indicate wheels and motors of single molecules, partially adsorbed at defects). Intramolecular

dimensions, determined from STM images, are compared with the calculated gas phase structure. Crossed axes: d_1 = 1.17 nm in the STM image (b) (and 1.33 nm in the calculation (c)), d_2 = 0.95 nm (0.95 nm), d_3 = 1.28 nm (1.34 nm), d_4 = 2.32 nm (2.13 nm). Parallel axles (d and e): d_1 = 1.32 nm in the STM image (d) (and 1.32 nm in the calculation (e)), d_2 = 1.64 nm (1.61 nm), d_3 = 1.30 nm (1.32 nm), d_4 = 1.70 nm (1.48 nm).

2.7. Attempts at Imaging the *p*-Carborane-Motorized Nanocar on a NaCl modified Cu(111) Surface

The STM imaging and manipulation results of *p*-carborane-wheeled motorized nanocar **2** and adamantane-wheeled motorized nanocar **7** showed no motor propelled motion on unmodified metal surfaces. Recently, growing a thin film of NaCl on metal surfaces has become a popular method for surface modifications. The presence of NaCl film decreases the molecule-substrate interaction, yet allows the tunneling current between the tip and the conducting surface to be measured.

For the two motorized nanocars **2** and **7**, cleaner sample preparation was achieved for the *p*-carborane-wheeled model **2**. Therefore, we tried depositing nanocar **2** on a NaCl modified surface. However, finding the optimal evaporation condition was very difficult. Even worse, the molecule-NaCl interactions were very weak. It was not possible to obtain a single STM image of the *p*-carborane-wheeled nanocar **2** on a NaCl modified surface because the tip dragged or pushed the deposited molecule/fragments in the scanning mode.

2.8. Conclusion and Future Work

In this work, we designed new nanovehicles for fine-tuning the molecule-surface interactions. An adamantane-wheeled motorized nanocar **7** was synthesized, and STM imaging and manipulations were done. Due to the difficulties of STM sample preparation, nanocar **7** was difficult to find on terraces. Using a NaCl-modified metal substrate, attempts at imaging *p*-carborane-wheeled motorized nanocar **2** were done. Yet the NaCl surface exhibits very weak molecule-surface interactions that inhibit the obtaining of an STM image. In future studies, we will image the three-wheel nanoroadster **8** on different surfaces. The smaller molecule weight of the nanoroadster could result in cleaner preparation of STM samples.

2.9. Contributions

I designed and synthesized the nanovehicles. Johannes Mielke in the laboratory of Leonhard Grill at Fritz-Haber-Institute, Berlin designed and performed all the STM experiments.

2.10. Experimental Section

2.10.1. The Nanocar 6 STM Imaging Procedure

The STM experiments have been performed in an ultra-high vacuum (UHV) chamber with a base pressure of 10^{-10} mbar. The Cu(111) surface has been cleaned through repeated cycles of Ar^+ sputtering and annealing at 400 °C. The molecules were thermally evaporated from a Knudsen cell, held at about 300 °C onto the Cu(111) surface (at 50 °C). The STM images were taken in an Omicron low temperature (LT) STM working at 5.7 K using a tungsten tip. All images were taken using a tip bias of –1 V and a tunnelling current of 1 pA. Gas phase calculations have been performed using the HyperChem 7 software.

2.10.2. The Nanocar 2 STM Imaging Procedure on a NaCl-Modified Surface

An Au(111) sample was cleaned by standard Ar^+ sputtering (as described above) and subsequent annealing at 400 ℃. NaCl was thermally evaporated from a quartz crucible (510 ℃) onto the clean Au(111) held at about room temperature. The coverage was chosen such that both NaCl double layer regions and gold regions could easily be found on the surface. The sample was transferred into the STM where it was cooled down to 5 K and the quality of the NaCl film could be checked. If everything was sufficiently clean, the *p*-carborane nanocars **2** were evaporated directly into the STM (sample at 5.5 K) from a tantalum crucible, held at temperatures between 260 ℃ and 300 ℃.

2.10.3. Experimental Data for Compounds 2, 7, 8, 9, 12, 15, 17, 18, 19, and 20.

General Methods. ^{1}H NMR and COSY were obtained at 500 MHz. ^{13}C, DEPT-90, and DEPT-135 spectra were recorded at and 125 MHz. Chemical shifts (δ) are reported in ppm from tetramethylsilane (TMS). FTIR spectra were recorded using a FTIR Infrared Microscope with ATR objective with 2 cm^{-1} resolution. All glassware was oven-dried overnight prior to use. Reagent grade tetrahydrofuran (THF) and ether (Et_2O) were distilled from sodium benzophenone ketyl under N_2 atmosphere. Triethylamine (NEt_3), and dichloromethane (CH_2Cl_2) were distilled from calcium hydride (CaH_2) under a N_2 atmosphere. Trimethyl phosphite was distilled over sodium metal and stored over molecular sieves 4Å . THF and NEt_3 were degassed with a stream of argon for 15 min before being used in the Sonogashira coupling reactions. All palladium-catalyzed reactions were carried out under argon atmosphere, while other reactions were performed under N_2 unless otherwise

noted. All chemicals were purchased from commercial suppliers and used without further purification. Flash column chromatography was performed using 230-400 mesh silica gel from EM Science. Thin layer chromatography (TLC) was performed using glass plates pre-coated with silica gel 40 F_{254} 0.25 mm layer thickness purchased from EM Science. Melting points of **15**, **17**, **18**, **19**, and **20** were not recorded because they exist as mixtures of two isomers.

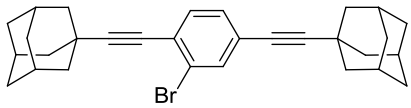

2-Bromo-1,4-bis(1-adamantylethynyl)benzene (9). A round-bottom flask was charged with 2-bromo-1,4-diiobenzene **10** (1.635 g, 4 mmol), 1-ethynyladamantane **11** (1.38 g, 8.60 mmol), $Pd(PPh_3)_2Cl_2$ (140 mg, 0.20 mmol), and CuI (76 mg, 0.40 mmol). THF (20 mL) was added and the mixture was cooled to 0 ℃. NEt_3 (5 mL) was added in one portion, and the reaction was allowed to stir at rt for 16 h. The mixture was quenched with saturated $NH_4Cl_{(aq)}$ (30 mL) and extracted with CH_2Cl_2 (50 mL). The organic phase was washed with water (30 mL), dried over anhydrous $MgSO_4$, filtered, and the filtrate was concentrated under vacuum. The crude product was purified by column chromatography (silica gel, hexanes) to yield **9** as a white solid (1.385 g, 73%): m.p. 216–218 ℃; FTIR (neat) 2900, 2848, 2660, 2224, 1588, 1524, 1484, 1468, 1448, 1340, 1316, 1100, 1040 cm^{-1}; ^1H NMR (500 MHz, $CDCl_3$) δ 7.58 (dd, J_1 = 1.6 Hz, J_2 = 0.4 Hz, 1H), 7.29 (dd, J_1 = 8.0 Hz, J_2 = 0.4 Hz, 1H), 7.21 (dd, J_1 = 8.0 Hz, J_2 = 1.6 Hz, 1H), 2.15–1.85 (m, 18H), 1.75–1.65 (m, 12H); ^{13}C NMR (125 MHz, $CDCl_3$) δ 135.00 (CH), 132.44 (CH), 129.97 (CH), 125.17, 124.96, 124.48, 104.54, 100.90, 78.27,

78.05, 42.66 (CH_2), 42.57 (CH_2), 36.35 (CH_2), 36.32 (CH_2), 30.47, 30.15, 27.94 (CH), 27.93 (CH); MS (MALDI) *m*/*z* calcd for $[M]^+$ $C_{30}H_{33}Br$ 472.2, found 472.5.

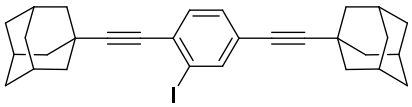

2-Iodo-1,4-bis(1-adamantylethynyl)benzene (12). An oven-dried three-necked round-bottom flask equipped with a stir bar charged with THF (20 mL) was cooled to −78 ℃, and to which a *tert*-butyllithium solution (1.7 M in pentane, 4.1 mL, 5.8 mmol) was added. A solution of **9** (1.18 g, 2.50 mmol) in THF (10 mL) was added dropwise, and the mixture was stirred at −78 ℃ for 1 h, and then 1,2-diiodoethane (1.51 g, 4.25 mmol) was added in one portion. The mixture was allowed to gradually warm to rt, and the mixture was stirred overnight. To the mixture was then added saturated sodium thiosulfate aqueous solution ($NaS_2O_{3(aq)}$, 30 mL), and the aqueous phase extracted with CH_2Cl_2 (50 mL). The organic phase was washed with water (50 mL) and dried over anhydrous $MgSO_4$, and concentrated under vacuum. The crude product was purified by column chromatography (silica gel; hexanes) to afford the desired product **12** as a white solid (1.21 g, 93%): m.p. 220–222 ℃; FTIR (neat) 2900, 2848, 2660, 2224, 1740, 1588, 1520, 1480, 1464, 1448, 1364, 1344, 1316, 1216, 1100, 1032 cm^{-1}; ^1H NMR (500 MHz, $CDCl_3$) δ 7.84 (dd, J_1 = 1.5 Hz, J_2 = 0.5 Hz, 1H), 7.27 (dd, J_1 = 8.0 Hz, J_2 = 0.5 Hz, 1H), 7.24 (dd, J_1 = 8.0 Hz, J_2 = 1.5 Hz, 1H), 2.05–1.90 (m, 18H), 1.75–1.65 (m, 12H) ; ^{13}C NMR (125 MHz, $CDCl_3$) δ 141.22 (CH), 131.34 (CH), 130.77 (CH), 129.28, 124.42, 103.65, 100.96, 100.91, 82.05, 77.80, 42.7 (CH_2), 42.67 (CH_2), 36.37 (CH_2), 36.33 (CH_2), 30.48, 30.16, 27.94 (CH), 27.93 (CH); MS (MALDI) *m*/*z* calcd for $C_{30}H_{33}I$ $[M]^+$ 520.2, found 520.1.

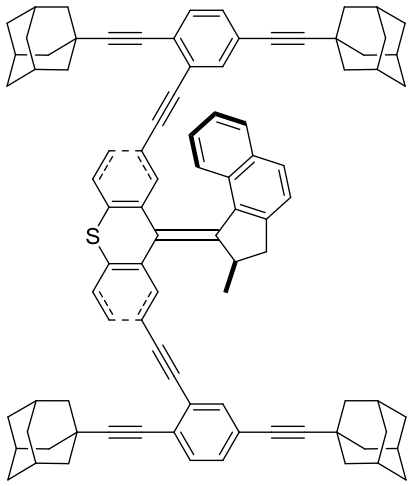

Adamantane-Wheeled Motorized Nanocar (7). An oven dried 10 mL Schlenk-tube equipped with a stir bar was charged with molecular motor **13** (45 mg, 0.106 mmol), axle **12** (208 mg, 0.400 mmol), $Pd(PPh_3)_4$ (9.8 mg, 8.5 μmol), and CuI (3.3 mg, 17 μmol) to which was added NEt_3 (148 μL) and THF (1 mL). The reaction mixture was stirred at 60 ℃ for 16 h, and then it was cooled to room temperature. The mixture was quenched with saturated $NH_4Cl_{(aq)}$ (20 mL) and extracted with CH_2Cl_2 (30 mL). The organic phase was washed with water (30 mL), dried over anhydrous $MgSO_4$, filtered, and the filtrate was concentrated under vacuum. The crude product was purified by column chromatography (silica gel, 10% CH_2Cl_2 in hexanes) to yield **7** as a yellow solid (95 mg, 74%): m.p. 245 ℃ (decomp); FTIR (neat) 3052, 2900, 2848, 2660, 2212, 1596, 1486, 1452, 1320, 1100, 1052 cm^{-1}; ^1H NMR (500 MHz, $CDCl_3$) δ 7.94 (d, J = 1.7 Hz, 1H), 7.77 (d, J = 8.2 Hz, 1H), 7.73–7.69 (m, 2H), 7.57 (dd, J_1 = 8.1 Hz, J_2 = 0.4 Hz, 1H), 7.45–7.40 (m, 2H), 7.34 (dd, J_1 = 8.1 Hz, J_2 = 0.5 Hz, 1H), 7.26 (dd, J_1 = 8.1 Hz, J_2 = 1.7 Hz, 1H), 7.23 (dd, J_1 = 1.6 Hz, J_2 = 0.6 Hz, 1H), 7.21 (dd, J_1 = 8.1 Hz, J_2 = 1.8 Hz, 1H), 7.21–7.17 (m, 2H), 7.16 (dd, J_1 = 8.1 Hz, J_2 = 1.7 Hz, 1H), 6.89-6.82 (m, 3H), 4.28 (qd, J_1 = 6.8 Hz, J_2 = 6.1 Hz, 1H), 3.64 (dd, J_1 = 15.5 Hz, J_2 = 6.1 Hz, 1H),

2.66 (d, J = 15.5 Hz, 1H), 2.04–1.93 (m, 24H), 1.93–1.89 (m, 6H), 1.87–1.83 (m, 6H), 1.77–1.65 (m, 24H), 0.82 (d, J = 6.8 Hz, 3H); ^{13}C NMR (125 MHz, $CDCl_3$) δ 147.30, 146.13, 140.12, 137.87, 136.18, 135.66, 134.79 (CH), 134.65 (CH), 134.35, 133.11, 131.75 (CH), 131.44 (CH), 131.34 (CH), 131.00 (CH), 130.87 (CH), 130.71 (CH), 130.60 (CH), 129.53 (CH), 129.16 (CH), 128.66, 128.13 (CH), 127.79 (CH), 127.46 (CH), 126.85, 125.80 (CH), 125.57, 125.42, 125.32, 125.01, 124.88 (CH), 124.42 (CH), 123.61 (CH), 123.16, 122.89, 121.81, 121.75, 104.08, 103.78, 100.26, 100.02, 92.68, 92.22, 88.80, 88.13, 78.61, 78.58, 78.23, 78.06, 42.91 (CH_2), 42.753 (CH_2), 42.745 (CH_2), 42.73 (CH_2), 39.70 (CH_2), 37.90 (CH), 36.39 (CH_2), 36.343 (CH_2), 36.336 (CH_2), 36.32 (CH_2), 27.98 (CH), 27.958 (CH), 27.955 (CH), 27.948 (CH), 19.58 (CH_3); MS (MALDI) m/z calcd for $[M]^+$ $C_{91}H_{84}S^+$ 1208.6, found 1208.7.

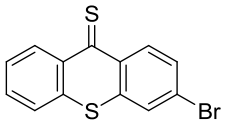

3-Bromo-thioxanthene-9-thione (15). To an oven dried three-neck round-bottom flask charged with ketone **14** (874 mg, 3.00 mmol) and P_4S_{10} (3.33 g, 7.50 mmol) was added toluene (40 mL) and the mixture was heated at reflux for 2 d. The mixture was filtered while hot, and the filtrate was collected. The solvent was removed under vacuum, and solid was collected as a brownish solid (865 mg, 94 %): m.p. 154–157 ℃; FTIR (neat) 3068, 3050, 2998 1574, 1554, 1522, 1446, 1426, 1370, 1282, 1256, 1192, 1156, 1120, 1098, 1082, 1006 cm^{-1}; ^{1}H NMR (500 MHz, $CDCl_3$) δ 8.96 (ddd, J_1 = 8.4 Hz, J_2 = 1.4 Hz, J_3 = 0.5 Hz, 1H), 8.83 (dd, J_1 = 9.0 Hz, J_2 = 0.4 Hz, 1H), 7.73 (dd, J_1 = 2.0 Hz, J_2 = 0.4 Hz, 1H), 7.62 (ddd, J_1 = 8.1 Hz, J_2 = 6.9 Hz, J_3 = 1.4 Hz, 1H), 7.55 (ddd, J_1 = 8.1 Hz, J_2 = 1.4 Hz, J_3 = 0.5 Hz, 1H),

7.51 (dd, J_1 = 9.0 Hz, J_2 = 2.0 Hz, 1H), 7.45 (ddd, J_1 = 8.4 Hz, J_2 = 6.9 Hz, J_3 = 1.4 Hz, 1H); ^{13}C NMR (125 MHz, $CDCl_3$) δ 210.17, 137.38, 136.26, 134.90 (CH), 133.34 (CH), 133.26, 131.94 (CH), 131.07, 130.43 (CH), 128.08 (CH), 127.62, 127.33 (CH), 125.95 (CH); HRMS (APCI) *m*/*z* calcd for $[M+H]^+$ $C_{13}H_7BrS^+$ 306.9245, found 306.9250. This thione was used without further purification.

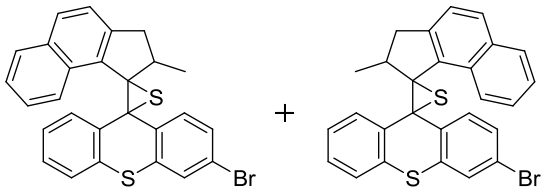

trans isomer *cis* isomer

Episulfide 17. To an oven dried three-neck round-bottom flask charged with hydrazone **16**[5] (946 mg, 4.5 mmol) and $MgSO_{4(s)}$ (473 mg, 3.92 mmol) was added CH_2Cl_2 (20 mL). To this suspension was added quickly MnO_2 (1.56 g, 18.0 mmol, Sigma-Aldrich > 90%) at *ca*. 5 ℃. The reaction flask was immediately immersed and stirred in a cold bath ranging from −15 ℃ to −10 ℃ for 1.5 h. After this period, the reaction mixture was cooled to −50 ℃ and then transferred to a Schlenk filtration tube connected to an oven dried three-neck round-bottom flask. The deep-purple filtrate that contained the intermediate was collected, and the Schlenk tube was rinsed with pre-cooled CH_2Cl_2 (10 mL, −50 ℃). To the flask containing the combined filtrate, thione **15** (400 mg, 1.30 mmol) was added portionwise until no more N_2 evolved. The mixture was stirred for an additional 0.5 h at ambient temperature. The organic phase was evaporated, and the residue was purified by column chromatography (silica gel, 10% CH_2Cl_2 in hexanes) to yield desired compound as a white solid (480 mg, 76%): FTIR (neat) 3054, 2964, 2924, 2864, 2842, 1572, 1450, 1436, 1372, 1080, 1032 cm^{-1}; ^{1}H NMR (500 MHz, $CDCl_3$) δ 8.97–8.91 (m, 1H), 7.89 (ddd, J_1 = 7.8 Hz, J_2 = 1.4 Hz, J_3 = 0.4 Hz,

0.5H), 7.76 (dd, J_1 = 8.3 Hz, J_2 = 0.3 Hz, 0.5H), 7.69 (ddd, J_1 = 7.7 Hz, J_2 = 1.5 Hz, J_3 = 0.4 Hz, 0.5H), 7.60–7.50 (m, 2H); 7.59 (dd, J_1 = 2.0 Hz, J_2 = 0.3 Hz, 0.5H), 7.56 (dd, J_1 = 8.3 Hz, J_2 = 0.3 Hz, 0.5H), 7.43 (ddd, J_1 = 7.6 Hz, J_2 = 1.3 Hz, J_3 = 0.5 Hz, 0.5H), 7.42 (dd, J_1 = 8.3 Hz, J_2 = 2.0 Hz, 0.5H), 7.32 (ddd, J_1 = 7.7 Hz, J_2 = 7.5 Hz, J_3 = 1.3 Hz, 0.5H), 7.25 (ddd, J_1 = 7.6 Hz, J_2 = 7.5, J_3 = 1.5 Hz, 0.5H), 7.24-7.15 (m, 3H), 7.11 (dd, J_1 = 2.0 Hz, J_2 = 0.3 Hz, 0.5H), 7.01 (dd, J_1 = 8.3 Hz, J_2 = 2.0 Hz, 0.5H), 6.96 (ddd, J_1 = 7.6 Hz, J_2 = 1.2 Hz, J_3 = 0.4 Hz, 0.5H), 6.92 (ddd, J_1 = 7.8 Hz, J_2 = 7.5 Hz, J_3 = 1.2 Hz, 0.5H), 6.76 (ddd, J_1 = 7.6 Hz, J_2 = 7.5 Hz, J_3 = 1.4 Hz, 0.5H), 3.47 (dd, J_1 = 15.4 Hz, J_2 = 6.4 Hz, 0.5H), 3.45 (dd, J_1 = 15.4 Hz, J_2 = 6.4 Hz, 0.5H), 2.42 (d, J = 15.4 Hz, 0.5H), 2.40 (d, J = 15.4 Hz, 0.5H), 1.58–1.49 (m, 1H), 1.08 (d, J = 6.4 Hz, 1.5H), 1.07 (d, J = 6.4 Hz, 1.5H); ^{13}C NMR (100 MHz, $CDCl_3$) δ 142.59, 142.52, 139.06, 138.72, 138.66, 137.78, 135.83, 134.89, 134.51, 134.27, 132.73, 132.67, 132.21 (CH), 131.27, 131.18, 131.05, 130.99, 130.86 (CH), 130.3 (CH), 129.54 (CH), 129.46 (CH), 129.43 (CH), 129.34 (CH), 129.15 (CH), 128.89 (CH), 128.75 (CH), 127.91 (CH), 127.67 (CH), 127.08 (CH), 126.92 (CH), 126.79 (CH), 126.71 (CH), 126.60 (CH), 126.09 (CH), 124.67 (CH), 124.43 (CH), 124.37 (CH), 124.35 (CH), 124.27 (CH), 124.2 (CH), 123.58 (CH), 123.56 (CH), 120.39, 119.93, 72.12, 72.05, 61.72, 61.67, 40.71 (CH), 40.67 (CH), 38.09 (CH_2), 38.01 (CH_2), 21.75 (CH_3), 21.67 (CH_3). HRMS (APCI) *m*/*z* calcd for $[M+H]^+$ $C_{27}H_{19}BrS_2^+$ 487.0184, found 487.0190.

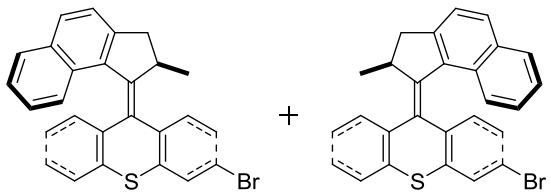

trans isomer *cis* isomer

3-Bromo-9-(2-methyl-2,3-dihydro-1*H*-cyclopenta[a]naphthalen-1-ylidene)-9*H*-thioxanthene (18). To a 200 mL screw-capped tube charged with episulfide **17** (390 mg, 0.80 mmol) was added trimethyl phosphite (8.0 mL, 68 mmol), and the mixture was stirred at 130 °C for 16 h. After the reaction mixture was cooled to room temperature, MeOH (30 mL) was added. The precipitate was filtered and washed with MeOH (20 mL). The solid was purified by column chromatography (silica gel, 10% CH_2Cl_2 in hexanes) to afford **18** as a pale yellow solid (344 mg, 95%): FTIR (neat) 3050, 2998, 2954, 2922, 2864, 2840, 1612, 1570, 1452, 1434, 1402, 1370, 1080 cm^{-1}; ^1H NMR (500 MHz, $CDCl_3$) δ 7.81–7.77 (m, 0.5H), 7.76 (dd, J_1 = 2.0 Hz, J_2 = 0.2 Hz, 0.5H), 7.74 (d, J = 8.3 Hz, 0.5H), 7.73 (d, J = 8.3 Hz, 0.5H), 7.30 (dd, J_1 = 2.0 Hz, J_2 = 0.3 Hz, 0.5H), 7.73-7.71 (m, 0.5H), 7.70-7.67 (m, 0.5H), 7.67-7.64 (br d, J = 8.3 Hz, 0.5H), 7.60 (ddd, J_1 = 7.8 Hz, J_2 = 1.3 Hz, J_3 = 0.4 Hz, 0.5H), 7.57 (ddd, J_1 = 7.8 Hz, J_2 = 1.2 Hz, J_3 = 0.5 Hz, 0.5H), 7.44 (dd, J_1 = 8.3 Hz, J_2 = 2.0 Hz, 0.5H), 7.43 (d, J = 2.0 Hz, 0.5H), 7.42 (d, J = 1.8 Hz, 0.5H), 7.35 (ddd, J_1 = 7.8 Hz, J_2 = 7.4 Hz, J_3 = 1.3 Hz, 0.5H), 7.23 (ddd, J_1 = 7.7 Hz, J_2 = 7.3 Hz, J_3 = 1.4 Hz, 0.5H), 7.22 (ddd, J_1 = 8.0 Hz, J_2 = 6.7 Hz, J_3 = 1.4 Hz, 0.5H), 7.16 (ddd, J_1 = 8.0 Hz, J_2 = 6.6 Hz, J_3 = 1.4 Hz, 0.5H), 7.02 (ddd, J_1 = 7.8 Hz, J_2 = 7.3 Hz, J_3 = 1.5 Hz, 0.5H), 6.90 (ddd, J_1 = 8.0 Hz, J_2 = 6.7 Hz, J_3 = 1.3 Hz, 0.5H), 6.87-6.81 (m, 1H), 6.78 (ddd, J_1 = 8.0 Hz, J_2 = 6.6 Hz, J_3 = 1.3 Hz, 0.5H), 6.73 (dd, J_1 = 8.2 Hz, J_2 = 2.0 Hz, 0.5H), 6.71 (ddd, J_1 = 8.2 Hz, J_2 = 7.7 Hz, J_3 = 0.5 Hz, 0.5H), 6.64 (ddd, J_1 = 7.7 Hz, J_2 = 7.3 Hz, J_3 = 1.2 Hz, 0.5H), 6.56 (dd, J_1 = 8.3 Hz, J_2 = Hz, 0.5H), 4.29 (qd, J_1 = 7.0 Hz, J_2 = 6.2 Hz, 0.5H), 4.21 (qd, J_1 = 7.0 Hz, J_2 = 6.2 Hz, 0.5H), 3.64 (dd, J_1 = 15.5 Hz, J_2 = 6.2 Hz, 1H, two sets of signals overlapping, the J values were measured as appeared), 2.63 (d, J = 15.5 Hz, 1H, two sets of signals overlapping, the J value was measured as appeared), 0.79 (d, J = 7.0 Hz, 1.5H), 0.78 (d, J = 7.0 Hz, 1.5H); ^{13}C NMR

(125 MHz, $CDCl_3$) δ 146.63, 146.58, 146.06, 146.01, 140.01, 139.30, 138.09, 137.75, 137.66, 136.99, 135.01, 134.88, 134.78, 134.77, 132.98, 132.94, 130.28 (CH), 130.24 (overlapping of two signals, both CH carbons), 129.95 (CH), 129.83 (CH), 129.40 (CH), 129.17 (CH), 128.94 (CH), 128.79, 128.70, 128.68 (CH), 127.86 (CH), 127.84 (CH), 127.79 (CH), 127.78 (CH), 127.57, 127.53 (CH), 127.48, 126.65 (CH), 126.50 (CH), 126.47 (CH), 126.19 (CH), 126.09 (CH), 126.08 (CH), 124.79 (CH), 124.78 (CH), 124.45 (CH), 124.20 (CH), 123.78 (CH), 123.75 (CH), 119.74, 119.33, 39.71 (CH_2), 39.70 (CH_2), 37.97 (CH), 37.85 (CH), 19.46 (CH_3), 19.41 (CH_3). HRMS (APCI) *m*/*z* calcd for $[M+H]^+$ $C_{27}H_{19}BrS^+$ 455.0464, found 455.0474.

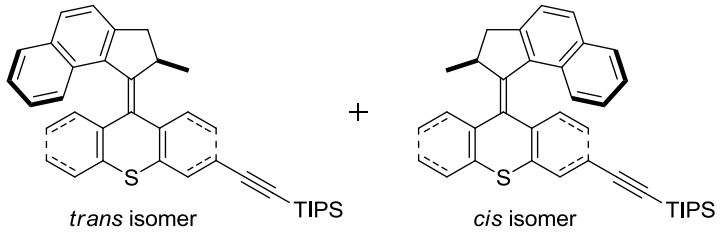

Triisopropyl((9-(2-methyl-2,3-dihydro-1*H*-cyclopenta[a]naphthalen-1-ylidene)-9*H*-thioxanthen-3-yl)ethynyl)silane (19). To a 20 mL screw-capped tube charged with molecular motor **18** (273 mg, 0.6 mmol), $Pd(PhCN)_2Cl_2$ (13.8 mg, 0.036 mmol), $HP^tBu_3BF_4$ (21.0 mg, 0.072 mmol) and CuI (13.7 mg, 0.072 mmol) were added NEt_3 (6 mL), and TIPSA (0.4 mL, 1.8 mmol). The reaction was stirred at 45 ℃ for 12 h and then cooled to room temperature. The mixture was quenched with saturated ammonium chloride aqueous solution ($NH_4Cl_{(aq)}$; 20 mL) and extracted with Et_2O (30 mL). The organic phase was washed with water (30 mL), dried over $MgSO_4$, and filtered, and the filtrate was concentrated under

vacuum. The crude product was purified by column chromatography (silica gel, 10% CH_2Cl_2 in hexanes) to afford the desired product **19** as a pale yellow solid (296 mg, 89%): FTIR (neat) 3054, 2942, 2890, 2864, 2162, 1612, 1456, 1436, 1382, 1266, 1236, 1068 cm^{-1}; ^1H NMR (500 MHz, $CDCl_3$) δ 7.80–7.77 (m, 0.43H), 7.74 (d, J = 8.0 Hz, 0.43H), 7.73–7.71 (m, 0.43H + 1.71H), 7.70 (dd, J_1 = 1.6 Hz, J_2 = 0.5 Hz, 0.43H), 7.70–7.67 (m, 0.57H), 7.59 (ddd, J_1 = 7.8 Hz, J_2 = 1.3 Hz, J_3 = 0.4 Hz, 0.43H), 7.56 (ddd, J_1 = 7.8 Hz, J_2 = 1.2 Hz, J_3 = 0.5 Hz, 0.57H), 7.44 (dd, J_1 = 8.0 Hz, J_2 = 1.6 Hz, 0.57H), 7.44–7.41 (m, 0.43H + 0.57H), 7.33 (ddd, J_1 = 7.8 Hz, J_2 = 7.4 Hz, J_3 = 1.3 Hz, 0.43H), 7.22 (ddd, J_1 = 7.7 Hz, J_2 = 7.3 Hz, J_3 = 1.4 Hz, 0.43H), 7.21 (ddd, J_1 = 8.0 Hz, J_2 = 6.2 Hz, J_3 = 1.9 Hz, 0.43H), 7.16 (ddd, J_1 = 8.1 Hz, J_2 = 6.7 Hz, J_3 = 1.3 Hz, 0.57H), 7.00 (ddd, J_1 = 7.8 Hz, J_2 = 7.3 Hz, J_3 = 1.5 Hz, 0.57H), 6.92–6.86 (m, 0.86H), 6.87–6.83 (m, 0.57H), 6.78 (ddd, J_1 = 8.1 Hz, J_2 = 6.7 Hz, J_3 = 1.3 Hz, 0.57H), 6.73 (dd, J_1 = 7.9 Hz, J_2 = 1.6 Hz, 0.43H), 6.71 (ddd, J_1 = 7.7 Hz, J_2 = 1.5 Hz, J_3 = 0.5 Hz, 0.57H), 6.68 (dd, J_1 = 7.9 Hz, J_2 = 0.5 Hz, 0.43H), 6.63 (ddd, J_1 = 7.7 Hz, J_2 = 7.3 Hz, J_3 = 1.2 Hz, 0.57H), 4.30 (dq, J_1 = 6.8 Hz, J_2 = 6.1 Hz, 0.43H), 4.24 (dq, J_1 = 6.8 Hz, J_2 = 6.1 Hz, 0.57H), 3.64 (dd, J_1 = 15.5 Hz, J_2 = 6.5 Hz, 1H, two sets of signals overlapping, the J values were measured as appeared), 2.62 (d, J = 15.5 Hz, 1H, two sets of signals overlapping, the J value was measured as appeared), 1.14 (br s, 11.97 H), 1.09 (br s, 9.03 H), 0.782 (d, J = 6.8 Hz, 1.71H), 0.777 (d, J = 6.8 Hz, 1.29 H); ^{13}C NMR (125 MHz, $CDCl_3$) δ 146.611, 146.605, 146.05, 146.00, 140.54, 140.05, 138.16, 137.74, 135.97, 135.62, 135.35, 135.04, 135.01, 134.93, 132.96, 132.95, 131.14 (CH), 130.87 (CH), 130.20 (CH), 130.19 (CH), 129.95 (CH), 129.78 (CH), 128.83, 128.82, 128.64 (CH), 128.27 (CH), 128.17, 128.16, 127.84 (CH), 127.79 (CH), 127.77 (CH), 127.75 (CH), 127.52 (CH), 127.46 (CH), 126.49 (CH), 126.39 (CH), 126.37 (CH), 126.23 (CH), 126.17 (CH), 126.09 (CH), 124.93 (CH),

124.77 (CH), 124.38 (CH), 124.18 (CH), 123.75 (CH), 123.74 (CH), 121.46, 121.19, 106.68, 106.43, 91.26, 91.07, 39.74, 39.73, 37.911 (CH), 37.906 (CH), 19.50, 19.46, 18.69 (CH_3), 18.643 (CH_3), 18.640 (CH_3), 11.32 (CH), 11.28 (CH). HRMS (APCI) *m*/*z* calcd for $[M+H]^+$ $C_{38}H_{40}SiS^+$ 557.2686, found 557.2682.

Note: 1. The original ^1H spectrum showed that one form of isomer is preferred over the other. The ratio of the two isomers was determined by the integration values of the singlets at 1.14 ppm and 1.09 ppm. The first ^1H, COSY, ^{13}C, and DEPT-135 spectra were obtained from a sample originally purified. 2. Because the two isomers can interconvert in presence of UV-light, the original NMR sample was irradiated with 365 nm UV-light (3 mW/cm^2) for 1 h. Additional ^1H and ^{13}C NMR spectra were obtained. Comparing the ^1H spectra before and after UV-light irradiation assisted the ^1H NMR assignments. 3. The ^{13}C NMR signal at δ 18.69 corresponds to the methyl groups of the triisopropylsilyl protecting group on *one* isomer. Peaks at δ 18.639, and 18.639 belong to the methyl groups on the triisopropylsilyl protecting group on *the other* isomer. The two more upfield signals were probably due to coupling to the stereogenic center. However, which specific isomer gives the splitted signals was not determined. 4. According to the assignments, the *trans*-isomer is the major before UV-light irradiation. Partial ^1H NMR assignments are summarized:

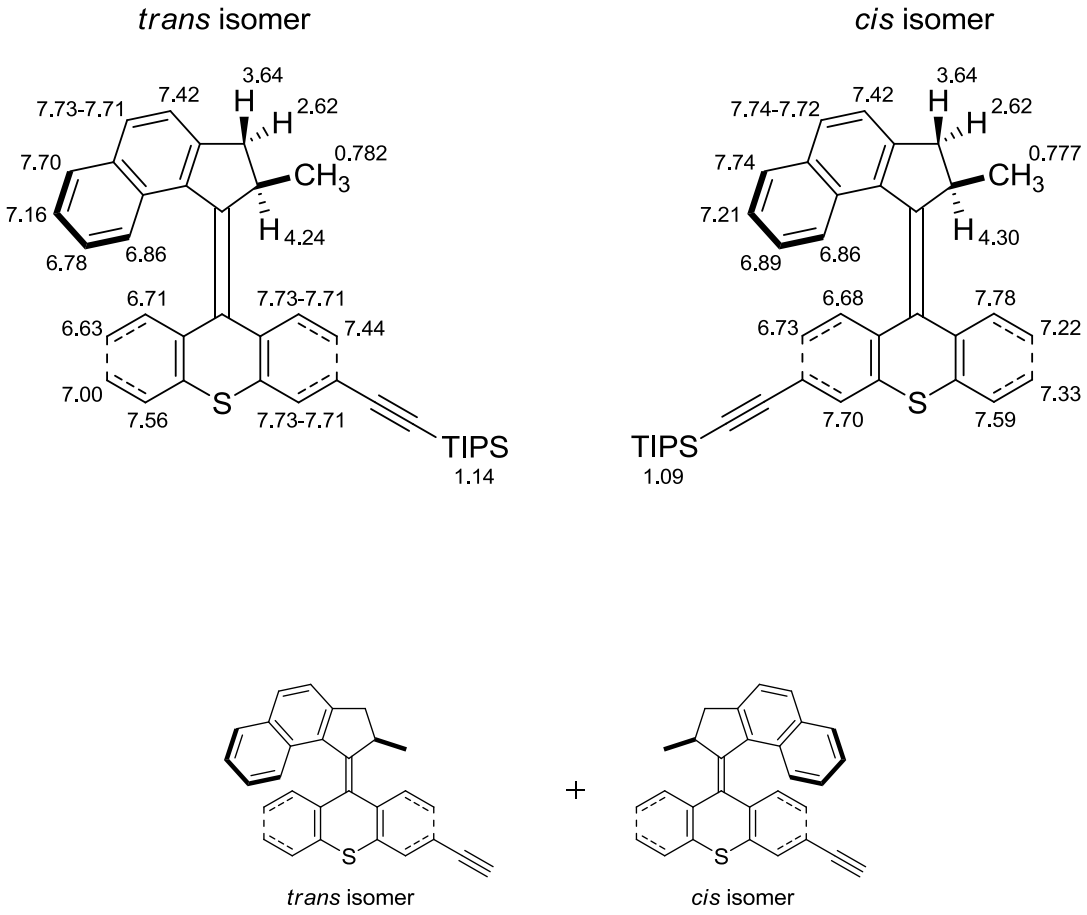

3-Ethynyl-9-(2-methyl-2,3-dihydro-1*H*-cyclopenta[a]naphthalen-1-ylidene)-9*H*-thioxanthene (20). To an oven-dried three-neck round-bottom flask charged with molecular motor **19** (223 mg, 0.4 mmol) was added THF (2.4 mL) and TBAF (0.6 mL, 1 M solution in THF). The reaction was stirred for 1.5 h at room temperature. The mixture was extracted with CH_2Cl_2 (25 mL) and water (30 mL). The organic layer was dried over $MgSO_4$, concentrated, and purified by column chromatography (silica gel, 25% CH_2Cl_2 in hexanes) to afford desired compound **20** as a pale yellow solid (158 mg, 99%): FTIR (neat) 3286, 3052, 3002, 2956, 2922, 2864, 2840, 2108, 1612, 1586, 1514, 1456, 1436, 1382, 1266, 1212, 1054, 1030 cm^{-1}; ^1H NMR (500 MHz, $CDCl_3$) δ 7.81–7.77 (m, 0.5H), 7.77–7.73 (m, 2H), 7.73–7.71 (m, 0.5H), 7.72–7.67 (m, 1H), 7.60 (ddd, J_1 = 7.8 Hz, J_2 = 1.3 Hz, J_3 = 0.4 Hz, 0.5H),

7.57 (ddd, J_1 = 7.8 Hz, J_2 = 1.2 Hz, J_3 = 0.5 Hz, 0.5H), 7.47-7.44 (m, 0.5H), 7.43 (d, J = 2.0 Hz, 0.5H), 7.42 (d, J = 2.1 Hz, 0.5H), 7.34 (ddd, J_1 = 7.8 Hz, J_2 = 7.4 Hz, J_3 = 1.3 Hz, 0.5H), 7.23 (ddd, J_1 = 7.7 Hz, J_2 = 7.4 Hz, J_3 = 1.4Hz, 0.5H), 7.20 (ddd, J_1 = 8.1 Hz, J_2 = 6.2 Hz, J_3 = 1.8 Hz, 0.5H), 7.16 (ddd, J_1 = 8.2 Hz, J_2 = 6.7 Hz, J_3 = 1.3 Hz, 0.5H), 7.01 (ddd, J_1 = 7.8 Hz, J_2 = 7.4 Hz, J_3 = 1.5 Hz, 0.5H), 6.88 (ddd, J_1 = 7.5 Hz, J_2 = 6.2 Hz, J_3 = 1.3 Hz, 0.5H), 6.87-6.83 (m, 1H), 6.79 (ddd, J_1 = 8.1 Hz, J_2 = 6.7 Hz, J_3 = 1.3 Hz, 0.5H), 6.74 (ddd, J_1 = 8.0 Hz, J_2 = 1.6 Hz, J_3 = 0.2 Hz, 0.5H), 6.72 (ddd, J_1 = 7.7 Hz, J_2 = 1.4 Hz, J_3 = 0.5 Hz, 0.5H), 6.66 (dd, J_1 = 8.0 Hz, J_2 = 0.5 Hz, 0.5H), 6.64 (ddd, J_1 = 7.7 Hz, J_2 = 7.4 Hz, J_3 = 1.2 Hz, 0.5H), 4.30 (dq, J_1 = 6.9 Hz, J_2 = 6.2 Hz, 0.5H), 4.23 (dq, J_1 = 6.9 Hz, J_2 = 6.2 Hz, 0.5H), 3.64 (dd, J_1 = 15.4 Hz, J_2 = 6.2 Hz, 1H, two sets of signals overlapping, the J values were measured as appeared), 2.62 (d, J = 15.5 Hz, 1H, two sets of signals overlapping, the J value was measured as appeared), 0.782 (d, J = 6.9 Hz, 1.5H), 0.777 (d, J = 6.9 Hz, 1.5 H) ; ^{13}C NMR (125 MHz, $CDCl_3$) δ 146.84, 146.79, 146.08, 146.05, 141.09, 139.95, 138.62, 137.58, 136.16, 135.84, 135.26, 134.96, 134.93, 134.84, 132.96, 132.95 (CH), 131.18, 130.93 (CH), 130.25 (overlapping of two signals, both CH carbons), 130.05 (CH), 129.91 (CH), 128.81, 128.76, 128.67 (CH), 128.43 (CH), 128.00, 127.96, 127.85 (CH), 127.81 (CH), 127.78 (CH), 127.77(CH), 127.57 (CH), 127.53 (CH), 126.56 (CH), 126.45 (CH), 126.43 (CH), 126.15 (CH), 126.122 (CH), 126.118 (CH), 124.84 (CH), 124.80 (CH), 124.44 (CH), 124.19 (CH), 123.74 (overlapping of two signals, both CH carbons), 119.90, 119.73, 83.20, 83.05, 77.65 (CH), 77.40 (CH), 39.73 (overlapping of two signals, both CH_2 carbons), 37.91 (CH), 37.90 (CH), 19.46 (CH_3), 19.43 (CH_3). HRMS (APCI) m/z calcd for $[M+H]^+$ $C_{29}H_{21}S$ 401.1358, found 401.1354.

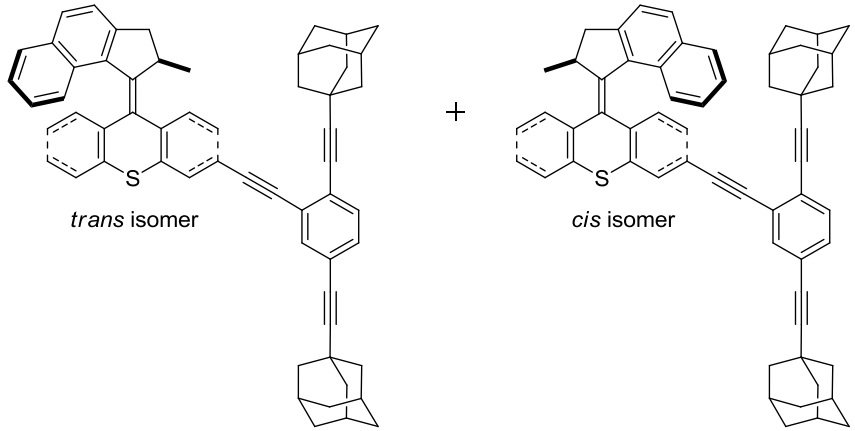

3-((2,5-Bis(1-adamantylethynyl)phenyl)ethynyl)-9-(2-methyl-2,3-dihydro-1*H*-cyclopenta[a]naphthalen-1-ylidene)-9*H*-thioxanthene (three-wheel nanoroadster 8). An oven dried 10 mL Schlenk-tube equipped with a stir bar was charged with molecular motor **20** (40 mg, 0.1 mmol)**,** axle **12** (78 mg, 0.4 mmol), $Pd(PPh_3)_4$ (4.6 mg, 4.0 μmol), and CuI (1.5 mg, 8.0 μmol) to which were added NEt_3 (0.25 mL) and THF (0.75 mL). The reaction mixture was stirred at 60 °C for 16 h, and then it was cooled to room temperature. The mixture was quenched with saturated $NH_4Cl_{(aq)}$ (10 mL) and extracted with CH_2Cl_2 (20 mL). The organic phase was washed with water (20 mL), dried over anhydrous $MgSO_4$, filtered, and the filtrate was concentrated under vacuum. The crude product was purified by column chromatography (silica gel, 20% CH_2Cl_2 in hexanes) to yield nanoroadster **8** as a yellow solid (44 mg, 56%): FTIR (neat) 2906, 2850, 2218, 1594, 1488, 1450, 1344, 1318, 1262, 1100 cm^{-1}; ^1H NMR (500 MHz, $CDCl_3$) δ 7.83 (dd, J_1 = 1.7 Hz, J_2 = 0.3 Hz, 0.5H), 7.82–7.77 (m, 1H), 7.80 (dd, J_1 = 1.6 Hz, J_2 = 0.5 Hz, 0.5H), 7.75 (d, J = 8.2, 0.5H), 7.74 (d, J = 8.2, 0.5H), 7.72–7.68 (m, 1H), 7.61 (ddd, J_1 = 7.8 Hz, J_2 = 1.3 Hz, J_3 = 0.4 Hz, 0.5H), 7.58 (ddd, J_1 = 7.8 Hz, J_2 = 1.2 Hz, J_3 = 0.5 Hz, 0.5H), 7.55 (dd, J_1 = 1.7 Hz, J_2 = 0.6 Hz, 0.5H), 7.35 (ddd, J_1 = 7.8 Hz, J_2 = 7.4 Hz, J_3 = 1.3 Hz, 0.5H), 7.33 (dd, J_1 = 8.1 Hz, J_2 = 0.6 Hz,

0.5H), 7.30 (dd, J_1 = 8.1 Hz, J_2 = 0.6 Hz, 0.5H), 7.26–7.18 (m, 2H), 7.17 (ddd, J_1 = 8.1 Hz, J_2 = 6.7 Hz, J_3 = 1.2 Hz, 0.5H), 7.02 (ddd, J_1 = 7.8 Hz, J_2 = 7.3 Hz, J_3 = 1.4 Hz, 0.5H), 6.92-6.85 (m, 1.5H), 6.79 (ddd, J_1 = 8.1 Hz, J_2 = 6.7 Hz, J_3 = 1.3 Hz, 0.5H), 6.79 (dd, J_1 = 8.0 Hz, J_2 = 1.6 Hz, 0.5H), 6.73 (ddd, J_1 = 7.7 Hz, J_2 = 1.4 Hz, J_3 = 0.5 Hz, 0.5H), 6.79 (dd, J_1 = 8.0 Hz, J_2 = 1.6 Hz, 0.5H), 6.69 (dd, J_1 = 8.0 Hz, J_2 = 0.5 Hz, 0.5H), 6.64 (ddd, J_1 = 7.7 Hz, J_2 = 7.3 Hz, J_3 = 1.2 Hz, 0.5H), 4.31 (qd, J_1 = 6.8 Hz, J_2 = 6.6 Hz, 0.5H), 4.28 (qd, J_1 = 6.8 6.6 Hz, J_2 = Hz, 0.5H), 3.66 (dd, J_1 = 15.5 Hz, J_2 = 6.6 Hz, 0.5H), 3.65 (dd, J_1 = 15.5 Hz, J_2 = 6.6 Hz, 0.5H), 2.64 (d, J = 15.5 Hz, 1H, two sets of signals overlapping, the J value was measured as appeared), 2.05–1.85 (m, 18H), 1.77–1.69 (m, 12H), 0.80 (d, J = 6.8 Hz, 1.5H), 0.79 (d, J = 6.8 Hz, 1.5H); ^{13}C NMR (125 MHz, $CDCl_3$) δ 146.72, 146.71, 146.06, 146.03, 140.52, 140.05, 138.04, 137.70, 136.07, 135.77, 135.37, 135.05, 135.03, 134.95, 134.74 (CH), 134.70 (CH), 132.96, 132.95, 131.63 (overlapping of two signals, both CH carbons), 131.00 (CH), 130.88 (overlapping of two signals, both CH carbons), 130.66 (CH), 130.21 (overlapping of two signals, both CH carbons), 129.45 (CH), 129.35 (CH), 128.84, 128.79, 128.69 (CH), 128.46 (CH), 128.16, 128.13, 127.87 (CH), 127.79 (CH), 127.77 (overlapping of two signals, both CH carbons), 127.55 (CH), 127.54 (CH), 126.5 (CH), 126.43 (CH), 126.39 (CH), 126.21 (CH), 126.14 (CH), 126.12 (CH), 125.52, 125.462, 125.459, 125.33, 124.91 (CH), 124.78 (CH), 124.49 (CH), 124.18 (CH), 123.76 (CH), 123.72 (CH), 123.15, 123.12, 121.27, 121.07, 104.14, 104.02, 100.23, 100.18, 92.62, 92.40, 88.74, 88.49, 78.62, 78.60, 78.24, 78.17, 42.94 (CH_2), 42.86 (CH_2), 42.74 (CH_2), 42.73 (CH_2), 39.79 (CH_2), 39.75 (CH_2), 37.94 (CH), 37.93 (CH), 36.41 (CH), 36.37 (CH), 36.36 (CH), 36.35 (CH), 30.50, 30.43, 30.15, 30.13, 28.02 (CH), 27.97 (CH), 27.96 (CH), 27.95 (CH), 19.464 (CH_3), 19.459 (CH_3); MS (MALDI) *m*/*z* calcd for $C_{59}H_{52}S$ $[M]^+$ 792.4, found 792.3.

2.11. References

1. Balzani, V.; Credi, A.; Raymo, F. M.; Stoddart, J. F. Artificial Molecular Machines. *Angew. Chem., Int. Ed.* **2000**, *39*, 3348–3391.

2. Kay, E. R.; Leigh, D. A.; Zerbetto, F. Synthetic Molecular Motors and Mechanical Machines. *Angew. Chem., Int. Ed.* **2007**, *46*, 72–191.

3. Shirai, Y.; Morin, J.-F.; Sasaki, T.; Guerrero, J. M.; Tour, J. M. Recent Progress on Nanovehicles. *Chem. Soc. Rev.* **2006**, *35*, 1043–1055.

4. Vives, G.; Tour, J. M. Synthesis of Single-Molecule Nanocars. *Acc. Chem. Res.* **2009**, *42*, 473–487.

5. Chiang, P.-T.; Mielke, J.; Godoy, J.; Guerrero, J. M.; Alemany, L. B.; Villagómez, C. J.; Saywell, A.; Grill, L.; Tour, J. M. Toward a Light-Driven Motorized Nanocar: Synthesis and Initial Imaging of Single Molecules. *ACS Nano* **2012**, *6*, 592–597.

6. Morin, J.-F.; Shirai, Y.; Tour, J. M. En Route to a Motorized Nanocar. *Org. Lett.* **2006**, *8*, 1713–1716.

7. Grill, L.; Rieder, K.-H.; Moresco, F.; Stojkovic, S.; Gourdon, A.; Joachim, C. Exploring the Interatomic Forces between Tip and Single Molecules During STM Manipulation. *Nano Lett.* **2006**, *6*, 2685–2689.

8. Liljeroth, P.; Swart, I.; Paavilainen, S.; Repp, J.; Meyer, G. Single-Molecule Synthesis and Characterization of Metal–Ligand Complexes by Low-Temperature STM. *Nano Lett.* **2010**, *10*, 2475–2479.

9. Kudernac, T.; Ruangsupapichat, N.; Parschau, M.; Macia, B.; Katsonis, N.; Harutyunyan, S. R.; Ernst, K.-H.; Feringa, B. L. Electrically Driven Directional Motion of a Four-Wheeled Molecule on a Metal Surface. *Nature* **2011**, *479*, 208–211.

10. Shirai, Y.; Osgood, A. J.; Zhao, Y.; Kelly, K. F.; Tour, J. M. Directional Control in Thermally Driven Single-Molecule Nanocars. *Nano Lett.* **2005**, *5*, 2330–2334.

11. Shirai, Y.; Osgood, A. J.; Zhao, Y.; Yao, Y.; Saudan, L.; Yang, H.; Yu-Hung, C.; Alemany, L. B.; Sasaki, T.; Morin, J.-F.; Guerrero, J. M.; Kelly, K. F.; Tour, J. M. Surface-Rolling Molecules. *J. Am. Chem. Soc.* **2006**, *128*, 4854–4864.

12. Villagómez, C. J.; Sasaki, T.; Tour, J. M.; Grill, L. Bottom-up Assembly of Molecular Wagons on a Surface. *J. Am. Chem. Soc.* **2010**, *132*, 16848–16854.

13. Vives, G.; Tour, J. M. Synthesis of a Nanocar with Organometallic Wheels. *Tetrahedron Lett.* **2009**, *50*, 1427–1430.

14. Chu, P.-L. E.; Wang, L.-Y.; Khatua, S.; Kolomeisky, A. B.; Link, S.; Tour, J. M. Synthesis and Single-Molecule Imaging of Highly Mobile Adamantane-Wheeled Nanocars. *ACS Nano* **2013**, *7*, 35–41.

15. Vives, G.; Kang, J.; Kelly, K. F.; Tour, J. M. Molecular Machinery: Synthesis of a "Nanodragster". *Org. Lett.* **2009**, *11*, 5602–5605.

16. Kang, J.; Vives, G.; Godoy, J.; Tour, J. M.; Kelly, K. F. Motions of Nanodragsters Manuscript in Preparation.

17. Swart, I.; Sonnleitner, T.; Niedenführ, J.; Repp, J. Controlled Lateral Manipulation of Molecules on Insulating Films by Stm. *Nano Lett.* **2012**, *12*, 1070–1074.

18. Coasts, S.; Dax, S. L.; DeCorte, B.; Liu, L.; McDonnell, M.; McNally, J. J., Tricyclic δ-Opioid Modulators. U.S. Patent 7,439,239, Oct. 21, 2008.

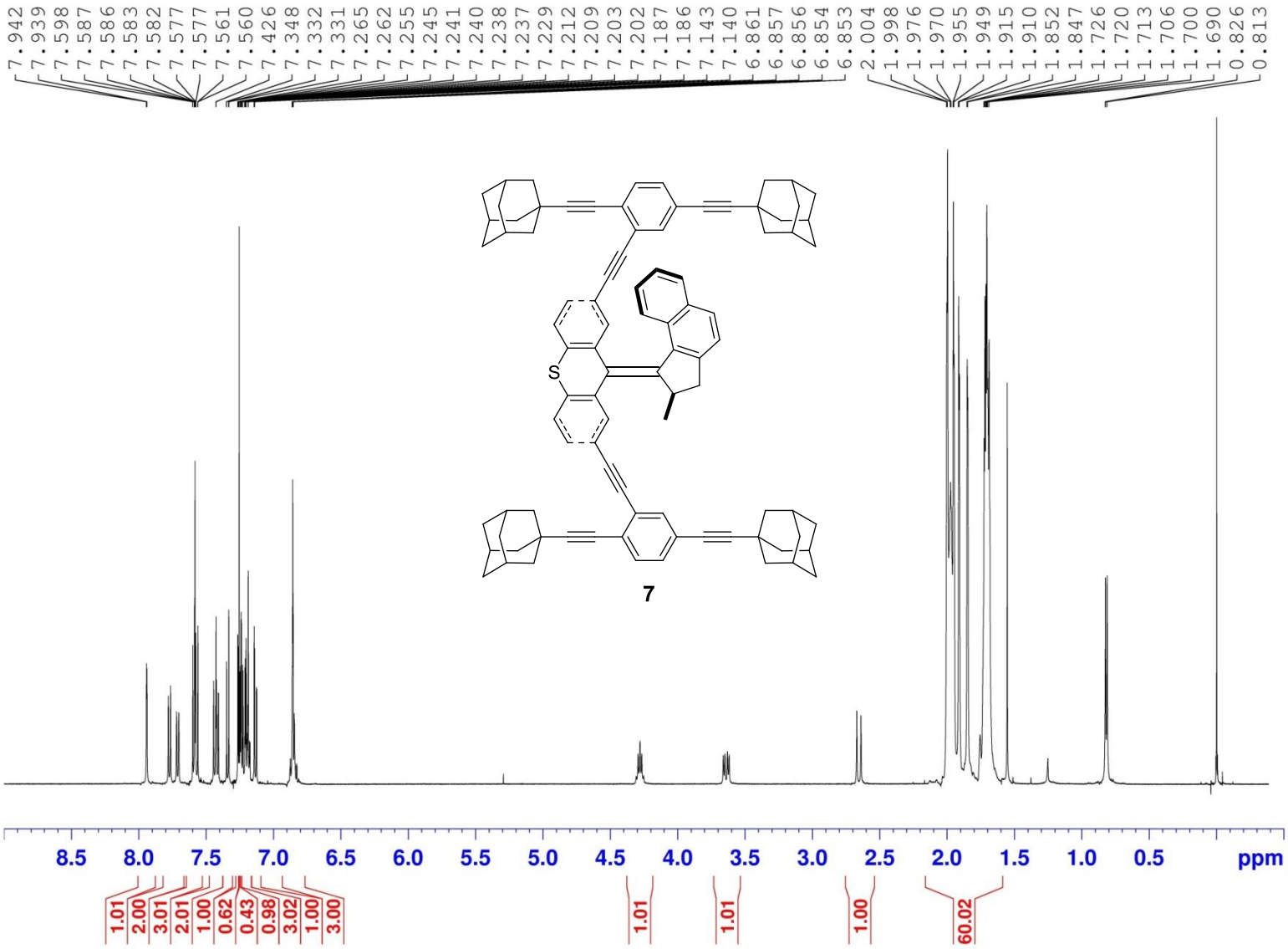
7.942
7.939
7.598
7.587
7.586
7.583
7.582
7.577
7.577
7.561
7.560
7.426
7.348
7.332
7.331
7.265
7.262
7.255
7.245
7.241
7.240
7.238
7.237
7.229
7.212
7.209
7.203
7.202
7.187
7.186
7.143
7.140
6.861
6.857
6.856
6.854
6.853
2.004
1.998
1.976
1.970
1.955
1.949
1.915
1.910
1.852
1.847
1.726
1.720
1.713
1.706
1.700
1.690
0.826
0.813
S
7
8.5
8.0
7.5
7.0
6.5
6.0
5.5
5.0
4.5
4.0
3.5
3.0
2.5
2.0
1.5
1.0
0.5
ppm
1.01
2.00
3.01
2.01
1.00
0.62
0.43
0.98
3.02
1.00
3.00
1.01
1.01
1.00
60.02

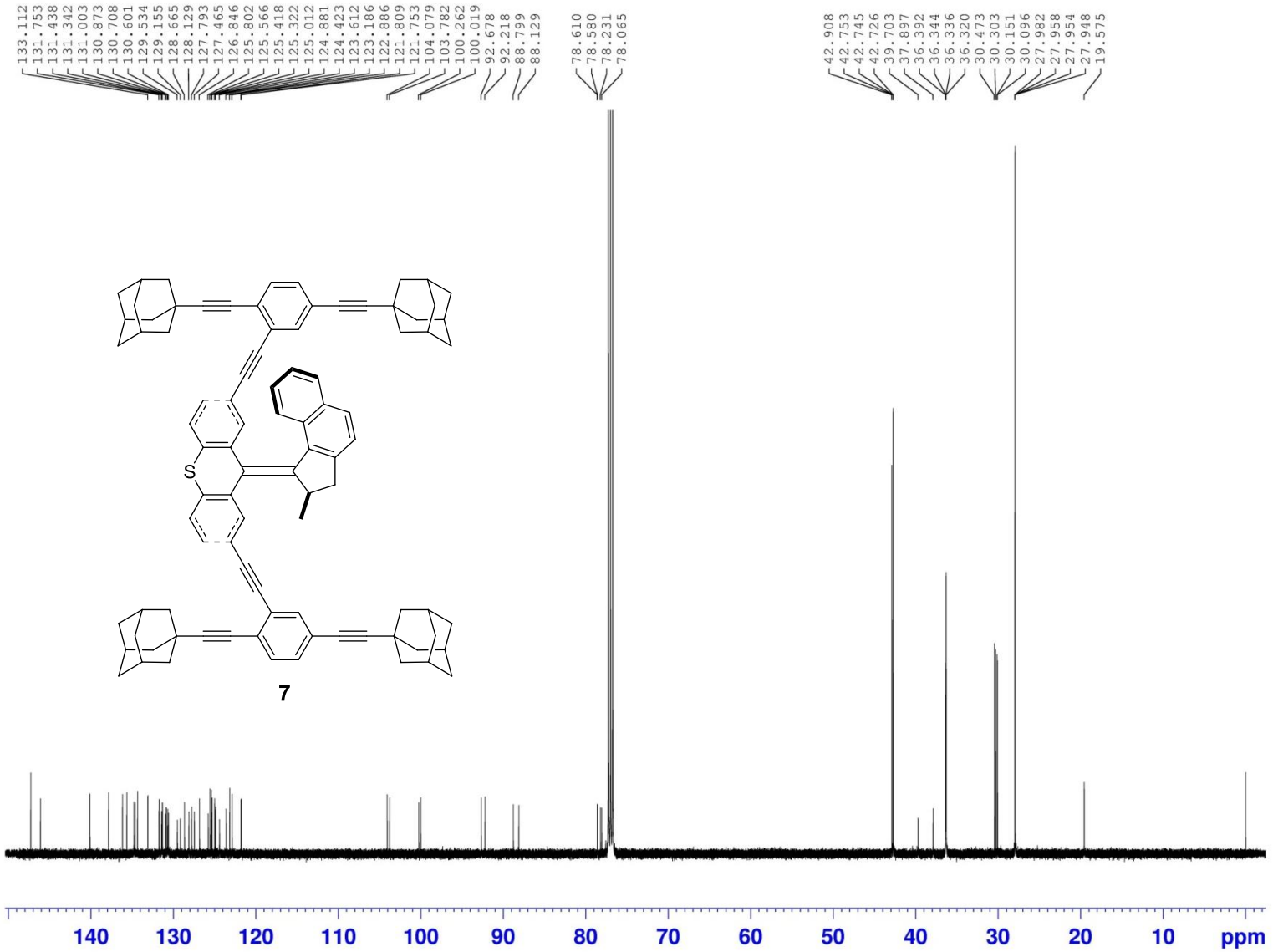
133.112
131.753
131.438
131.342
131.003
130.873
130.708
130.601
129.534
129.155
128.665
128.129
127.793
127.465
126.846
125.802
125.566
125.418
125.322
125.012
124.881
124.423
123.612
123.186
122.886
121.809
121.753
104.079
103.782
100.262
100.019
92.678
92.218
88.799
88.129
78.610
78.580
78.231
78.065
42.908
42.753
42.745
42.726
39.703
37.897
36.392
36.344
36.336
36.320
30.473
30.303
30.151
30.096
27.982
27.958
27.954
27.948
19.575
S
7
140
130
120
110
100
90
80
70
60
50
40
30
20
10
ppm

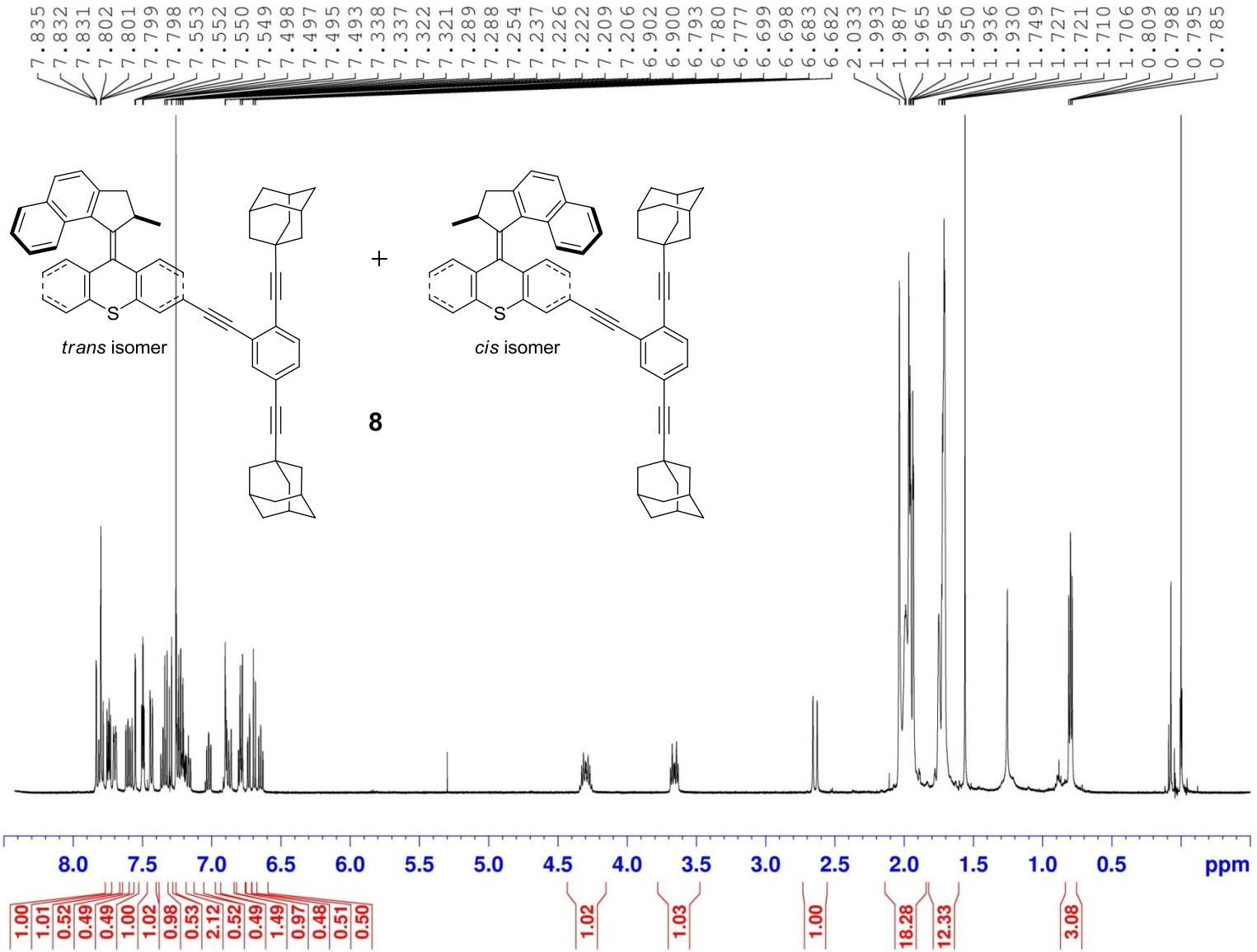
7.835
7.832
7.831
7.802
7.801
7.799
7.798
7.553
7.552
7.550
7.549
7.498
7.497
7.495
7.493
7.338
7.337
7.322
7.321
7.289
7.288
7.254
7.237
7.226
7.222
7.209
7.206
6.902
6.900
6.793
6.780
6.777
6.699
6.698
6.683
6.682
2.033
1.993
1.987
1.965
1.956
1.950
1.936
1.930
1.749
1.727
1.721
1.710
1.706
0.809
0.798
0.795
0.785
S
trans isomer
+
S
cis isomer
8
8.0
7.5
7.0
6.5
6.0
5.5
5.0
4.5
4.0
3.5
3.0
2.5
2.0
1.5
1.0
0.5
ppm
1.00
1.01
0.52
0.49
0.49
1.00
1.02
0.98
0.53
2.12
0.52
0.49
1.49
0.97
0.48
0.51
0.50
1.02
1.03
1.00
18.28
12.33
3.08

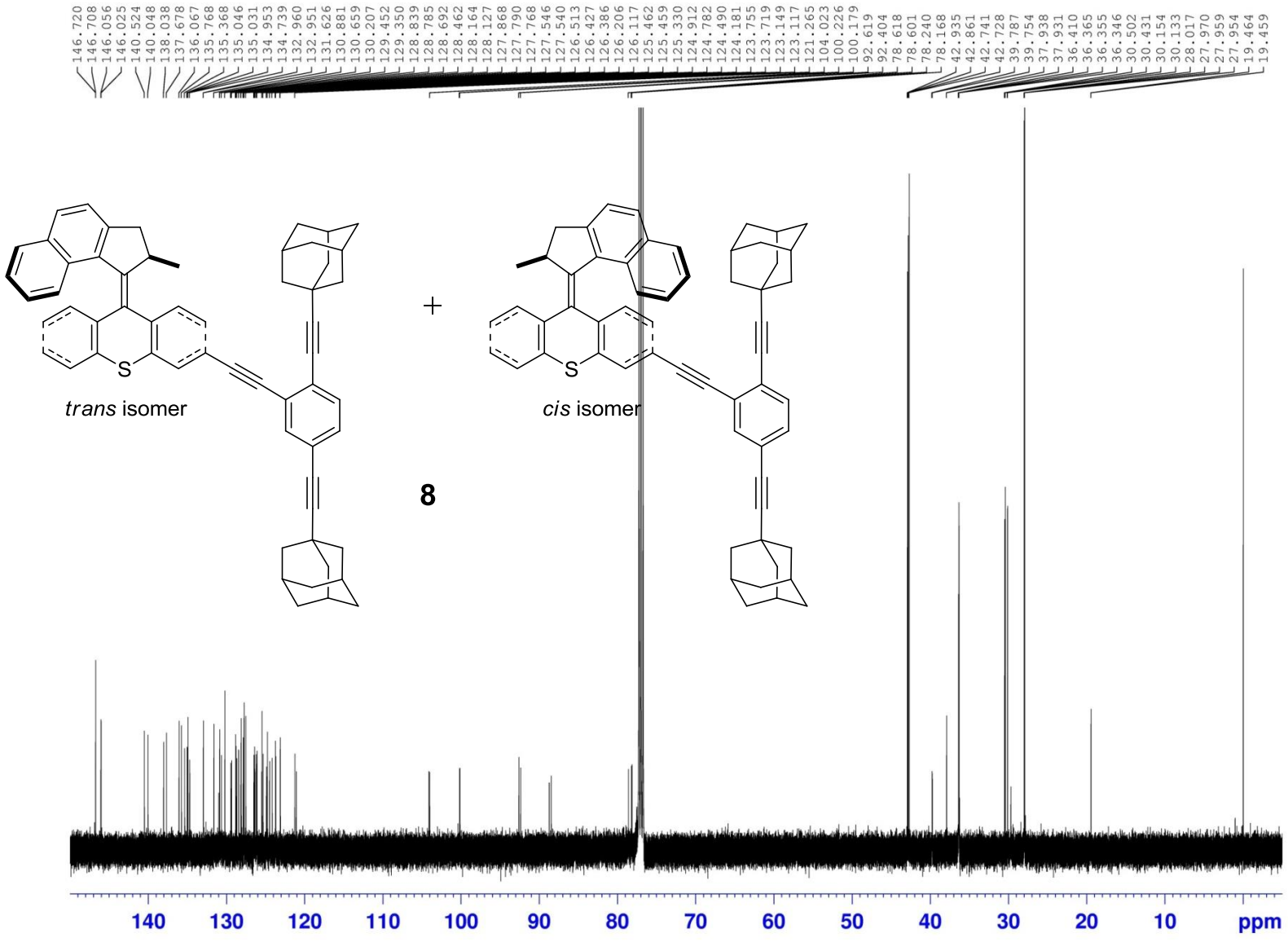
146.720
146.708
146.056
146.025
140.524
140.048
138.038
137.678
136.067
135.768
135.368
135.046
135.031
134.953
134.739
132.960
132.951
131.626
130.881
130.659
130.207
129.452
129.350
128.839
128.785
128.692
128.462
128.164
128.127
127.868
127.790
127.768
127.546
127.540
126.513
126.427
126.386
126.206
126.117
125.462
125.459
125.330
124.912
124.782
124.490
124.181
123.755
123.719
123.149
123.117
121.265
104.023
100.226
100.179
92.619
92.404
78.618
78.601
78.240
78.168
42.935
42.861
42.741
42.728
39.787
39.754
37.938
37.931
36.410
36.365
36.355
36.346
30.502
30.431
30.154
30.133
28.017
27.970
27.959
27.954
19.464
19.459
S
trans isomer
+
S
cis isomer
8
140
130
120
110
100
90
80
70
60
50
40
30
20
10
ppm

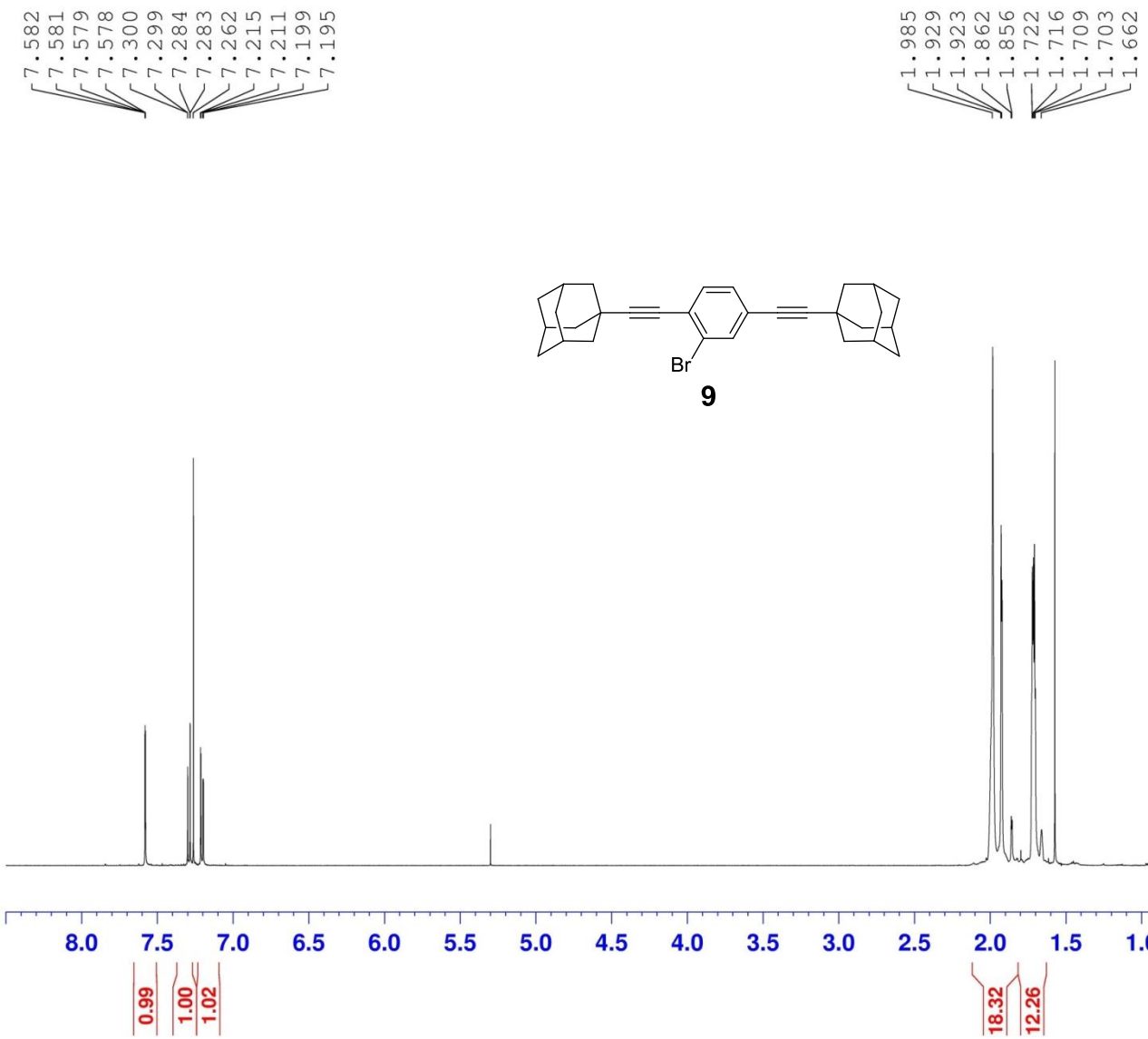
7.582
7.581
7.579
7.578
7.300
7.299
7.284
7.283
7.262
7.215
7.211
7.199
7.195
1.985
1.929
1.923
1.862
1.856
1.722
1.716
1.709
1.703
1.662
Br
9
8.0
7.5
7.0
6.5
6.0
5.5
5.0
4.5
4.0
3.5
3.0
2.5
2.0
1.5
1.0
0.5
ppm
0.99
1.00
1.02
18.32
12.26

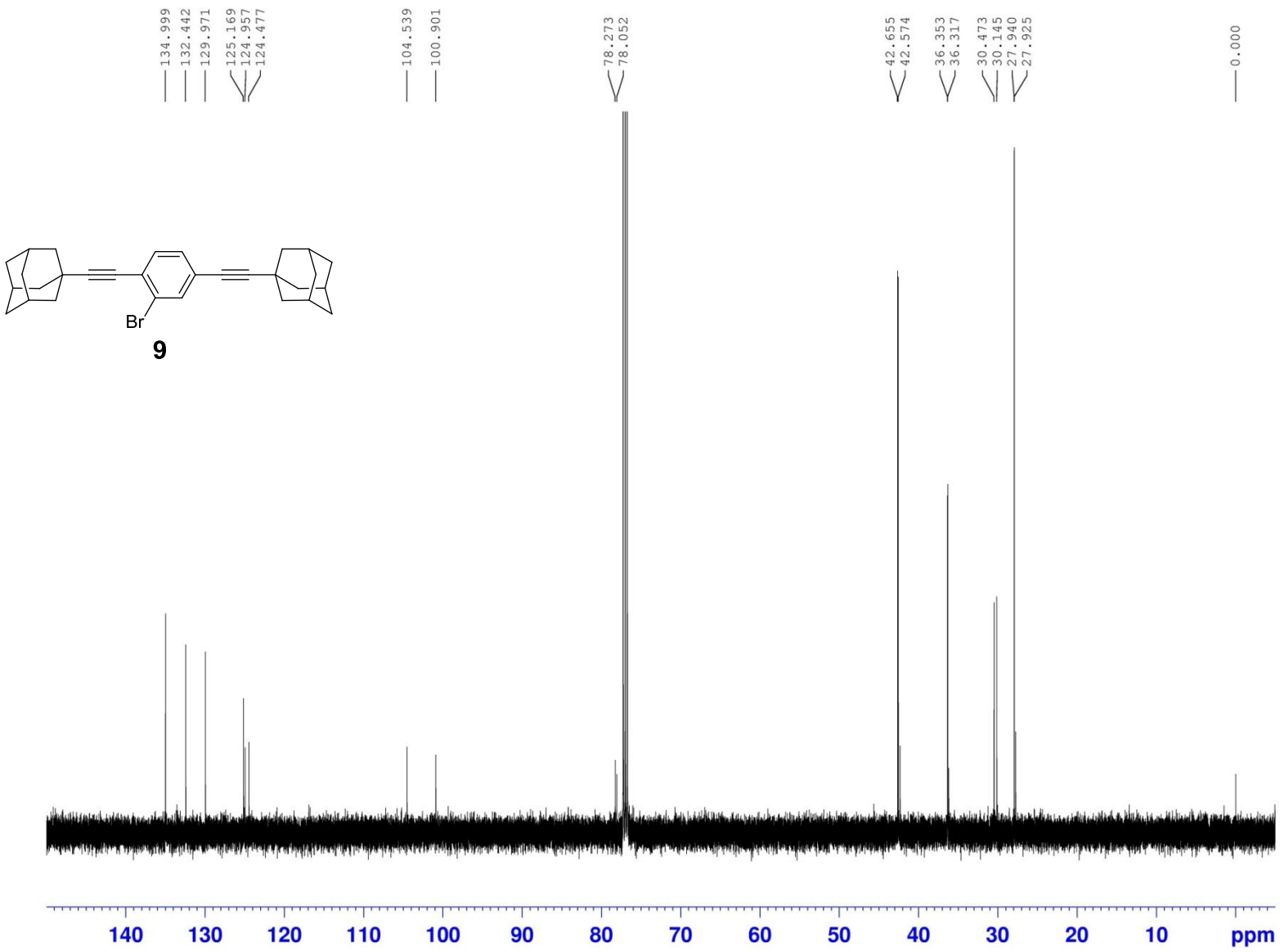
134.999
132.442
129.971
125.169
124.957
124.477
104.539
100.901
78.273
78.052
42.655
42.574
36.353
36.317
30.473
30.145
27.940
27.925
0.000
Br
9
140
130
120
110
100
90
80
70
60
50
40
30
20
10
ppm

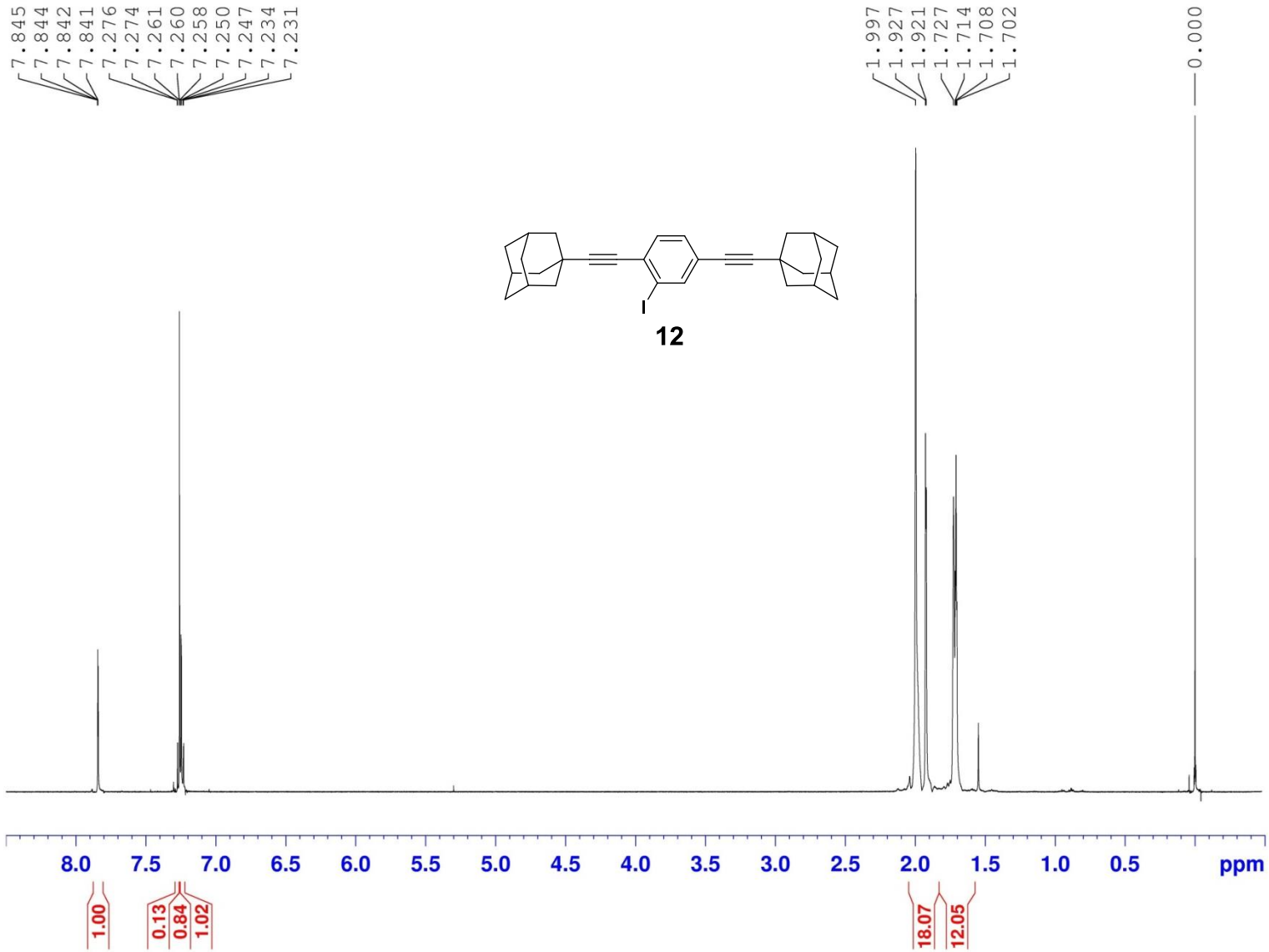
7.845
7.844
7.842
7.841
7.276
7.274
7.261
7.260
7.258
7.250
7.247
7.234
7.231
1.997
1.927
1.921
1.727
1.714
1.708
1.702
0.000
I
12
8.0
7.5
7.0
6.5
6.0
5.5
5.0
4.5
4.0
3.5
3.0
2.5
2.0
1.5
1.0
0.5
ppm
1.00
0.13
0.84
1.02
18.07
12.05

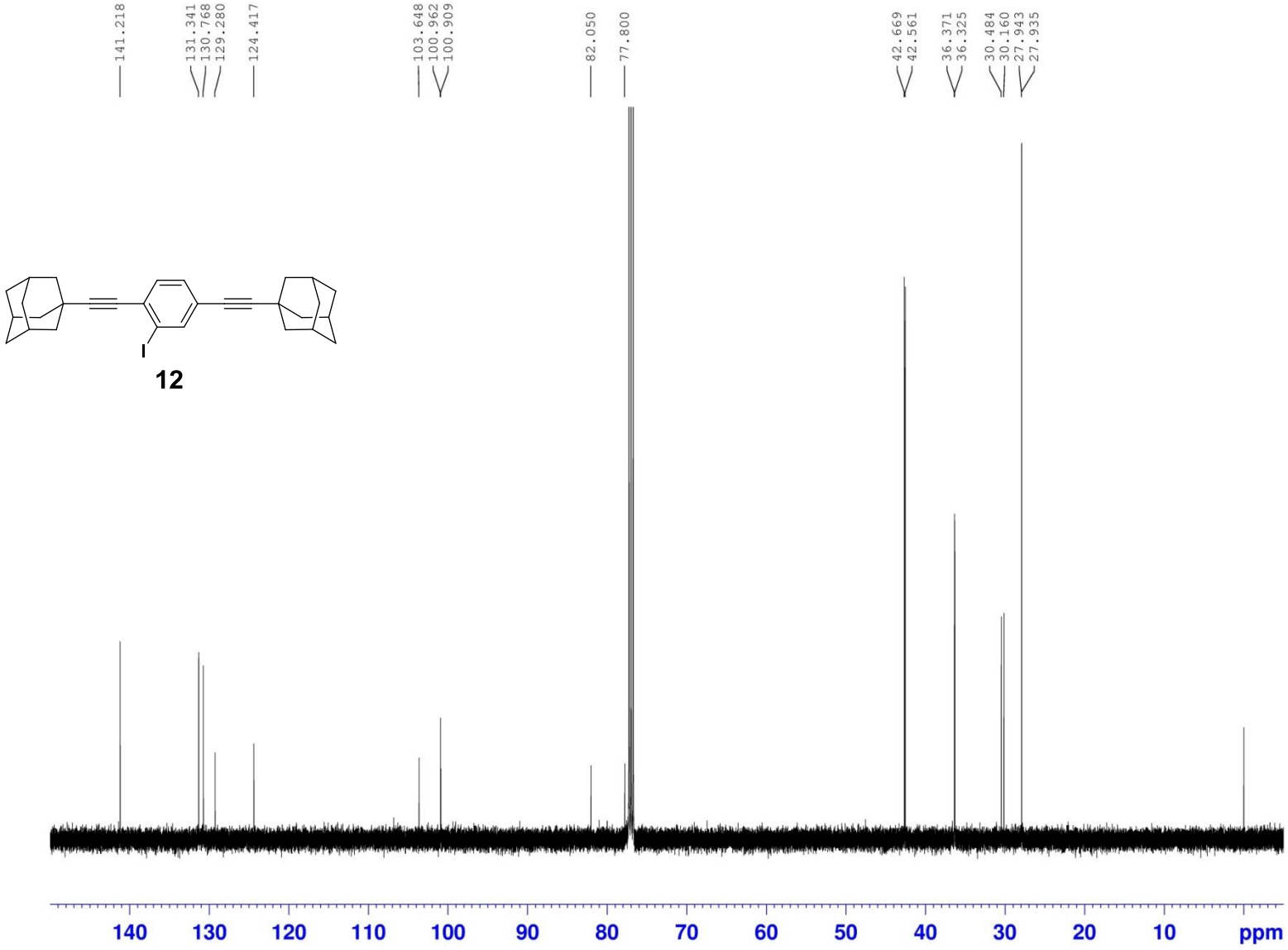
141.218
131.341
130.768
129.280
124.417
103.648
100.962
100.909
82.050
77.800
42.669
42.561
36.371
36.325
30.484
30.160
27.943
27.935
I
12
140
130
120
110
100
90
80
70
60
50
40
30
20
10
ppm

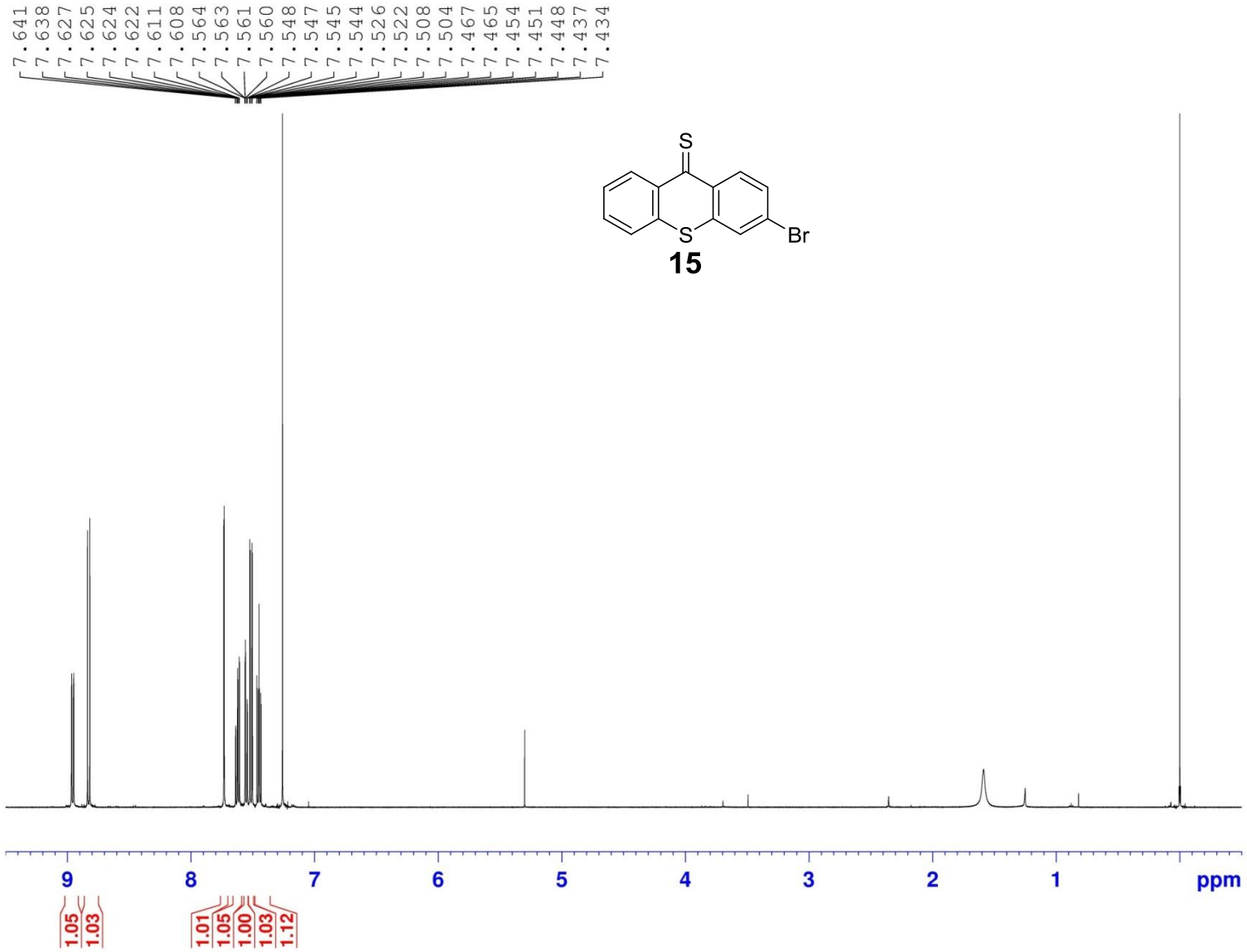
7.641
7.638
7.627
7.625
7.624
7.622
7.611
7.608
7.564
7.563
7.561
7.560
7.548
7.547
7.545
7.544
7.526
7.522
7.508
7.504
7.467
7.465
7.454
7.451
7.448
7.437
7.434
S
S
Br
15
9
8
7
6
5
4
3
2
1
ppm
1.05
1.03
1.01
1.05
1.00
1.03
1.12

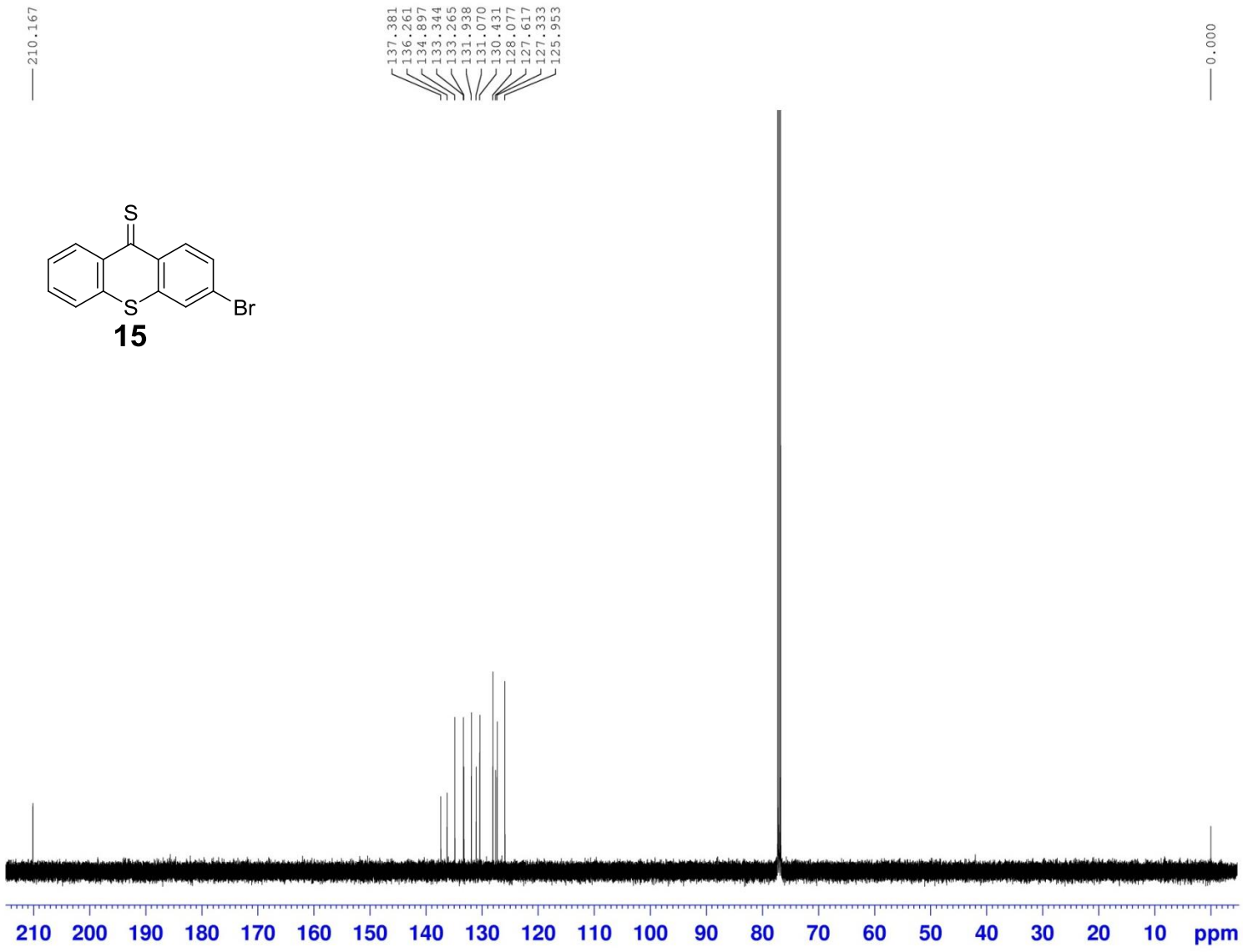
210.167
137.381
136.261
134.897
133.344
133.265
131.938
131.070
130.431
128.077
127.617
127.333
125.953
0.000
S
S
Br
15
210 200 190 180 170 160 150 140 130 120 110 100 90 80 70 60 50 40 30 20 10 ppm

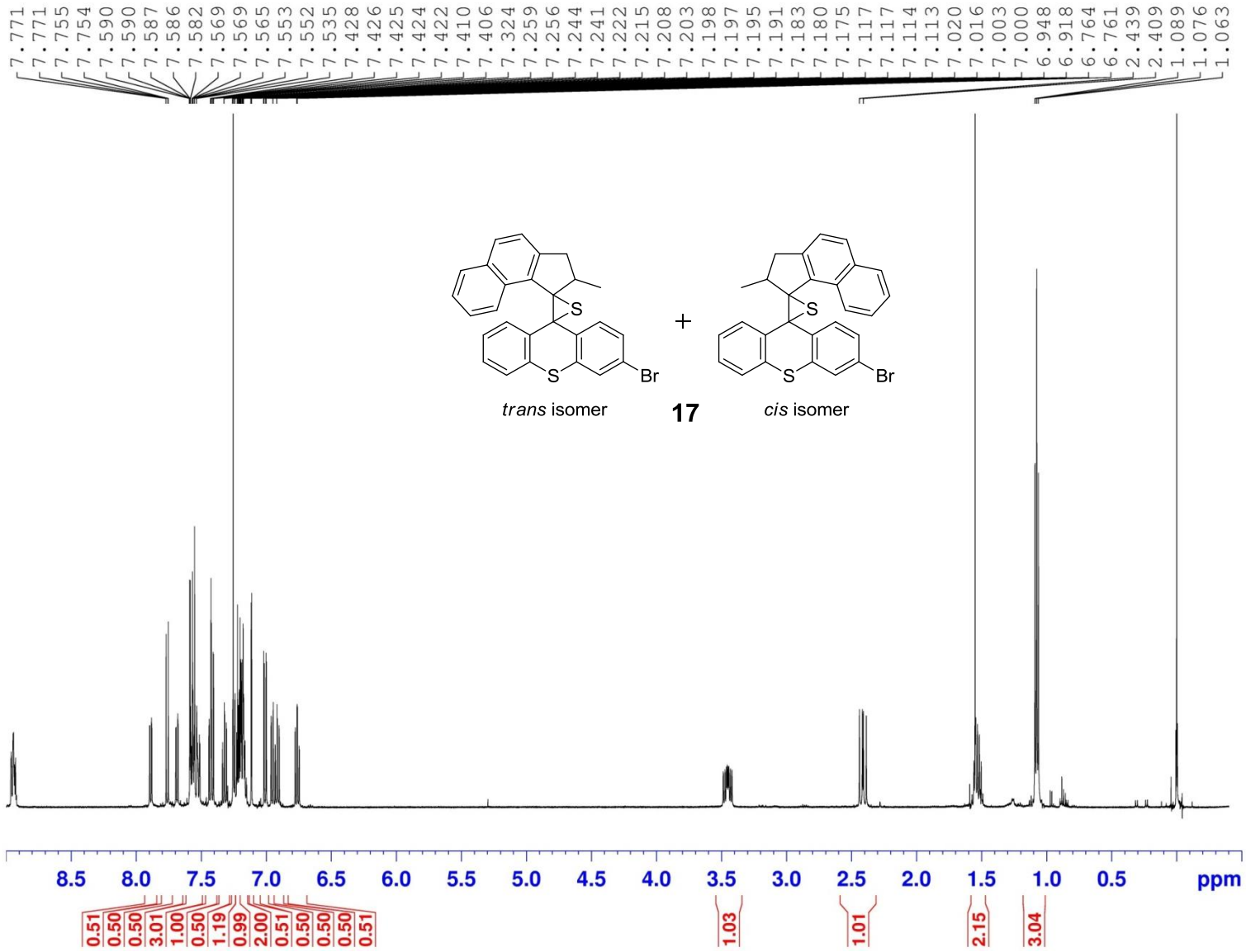
7.771
7.771
7.755
7.754
7.590
7.590
7.587
7.586
7.582
7.569
7.569
7.565
7.553
7.552
7.535
7.428
7.426
7.425
7.424
7.422
7.410
7.406
7.324
7.259
7.256
7.244
7.241
7.222
7.215
7.208
7.203
7.198
7.197
7.195
7.191
7.183
7.180
7.175
7.117
7.117
7.114
7.113
7.020
7.016
7.003
7.000
6.948
6.918
6.764
6.761
2.439
2.409
1.089
1.076
1.063
S
S
Br
trans isomer
17
+
S
S
Br
cis isomer
8.5
8.0
7.5
7.0
6.5
6.0
5.5
5.0
4.5
4.0
3.5
3.0
2.5
2.0
1.5
1.0
0.5
ppm
0.51
0.50
0.50
3.01
1.00
0.50
1.19
0.99
2.00
0.51
0.50
0.50
0.50
0.51
1.03
1.01
2.15
3.04

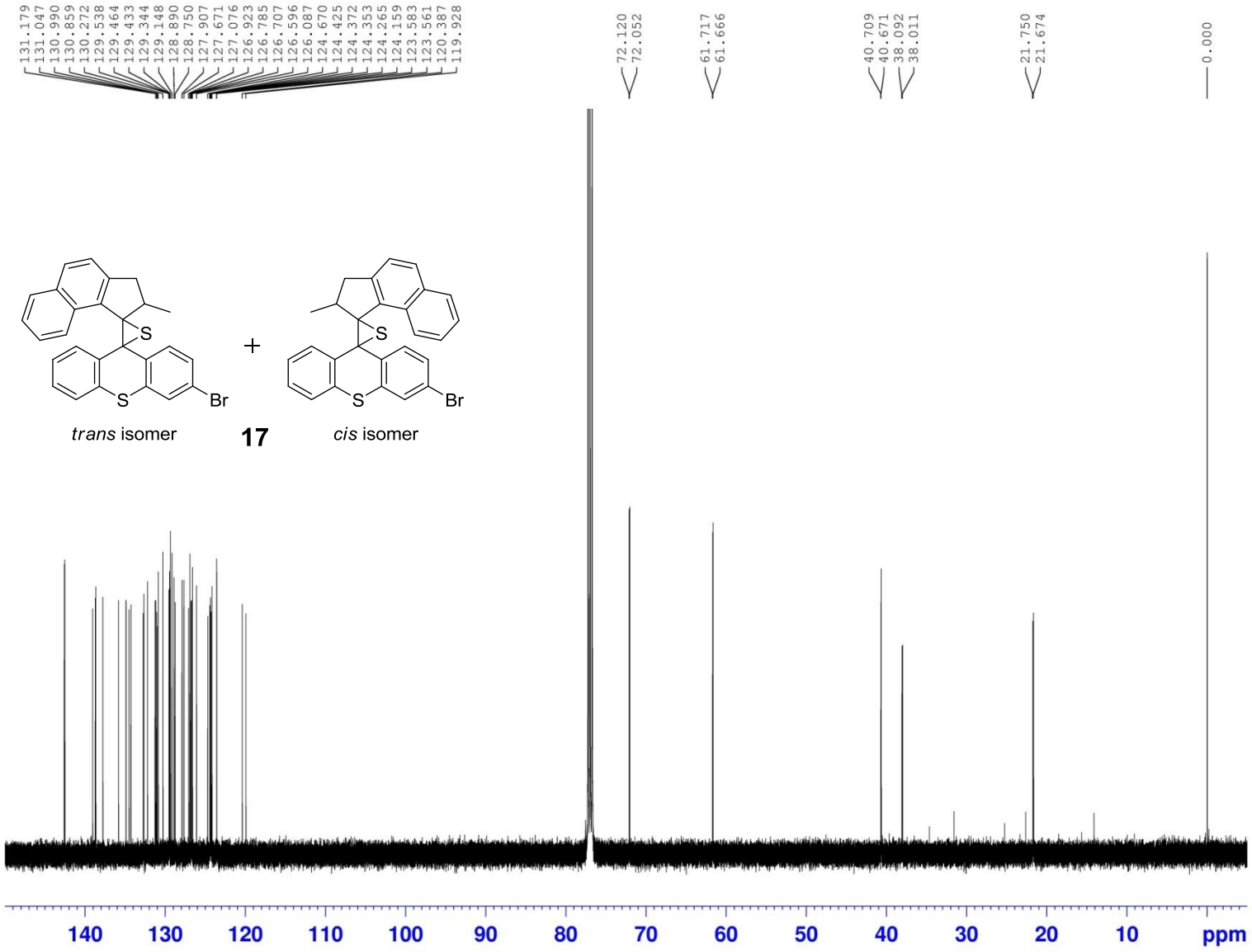
131.179
131.047
130.990
130.859
130.272
129.538
129.464
129.433
129.344
129.148
128.890
128.750
127.907
127.671
127.076
126.923
126.785
126.707
126.596
126.087
124.670
124.425
124.372
124.353
124.265
124.159
123.583
123.561
120.387
119.928
72.120
72.052
61.717
61.666
40.709
40.671
38.092
38.011
21.750
21.674
0.000
S
S
Br
+
S
S
Br
trans isomer
17
cis isomer
140
130
120
110
100
90
80
70
60
50
40
30
20
10
ppm

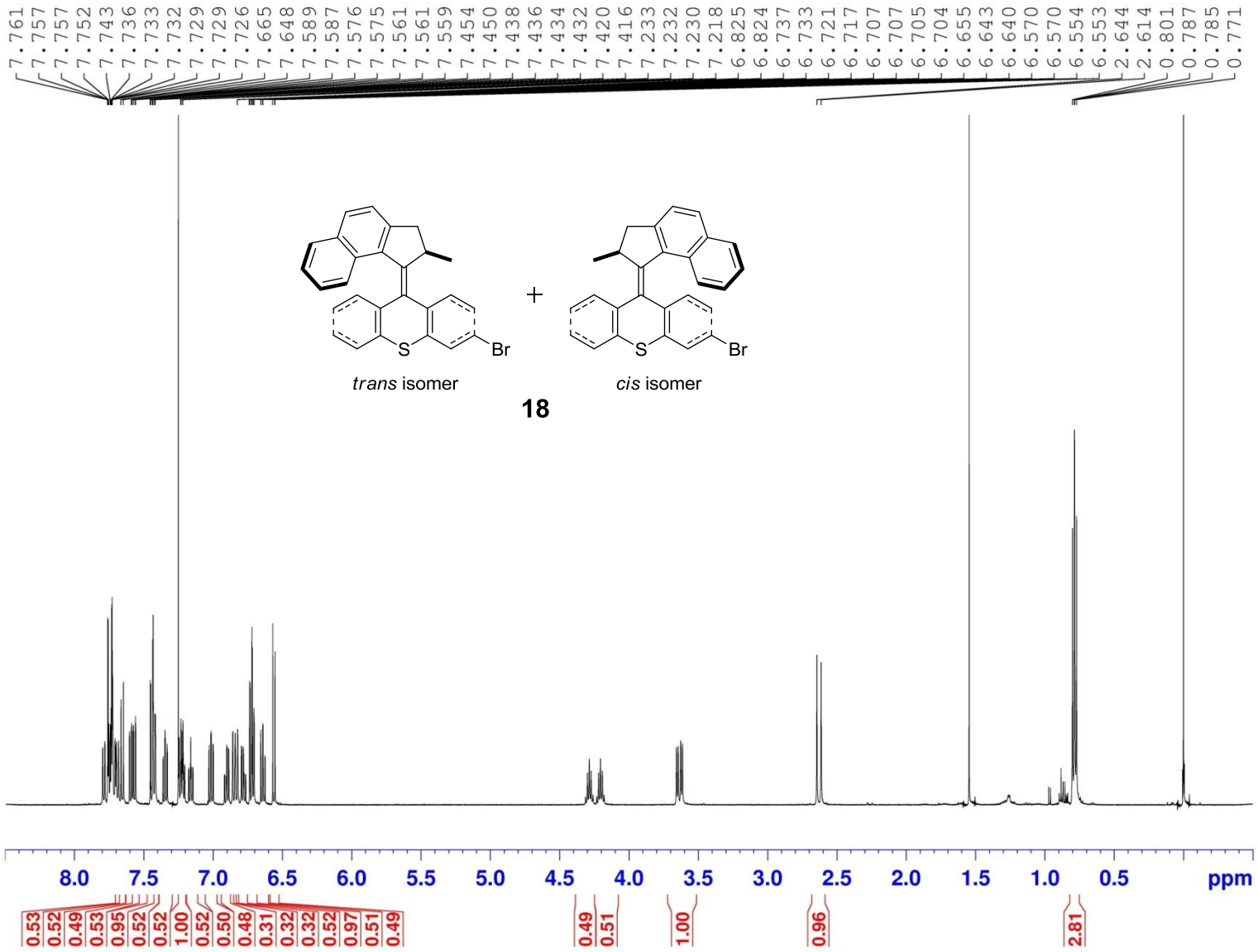

trans isomer + *cis* isomer

18

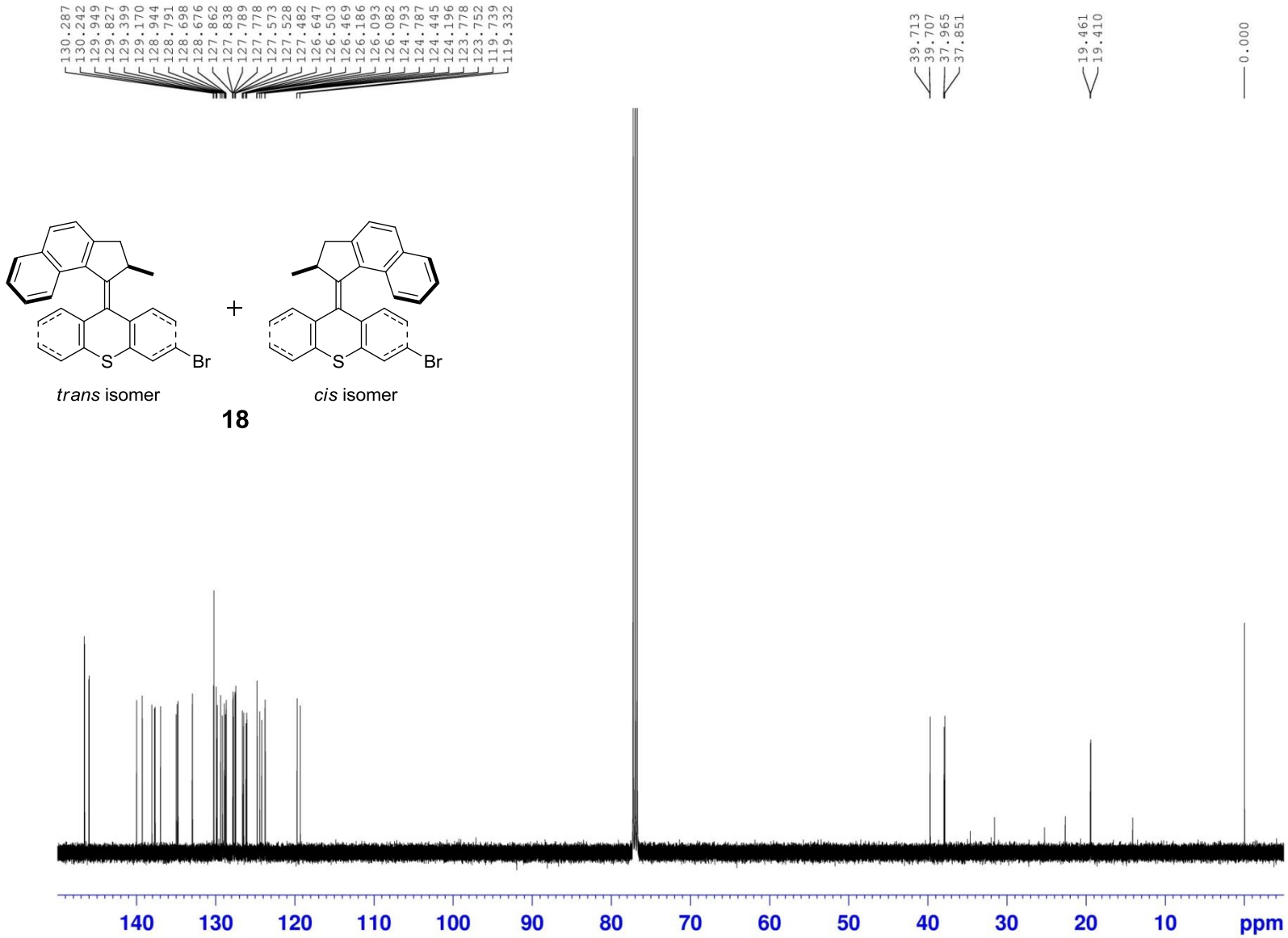

trans isomer + *cis* isomer

18

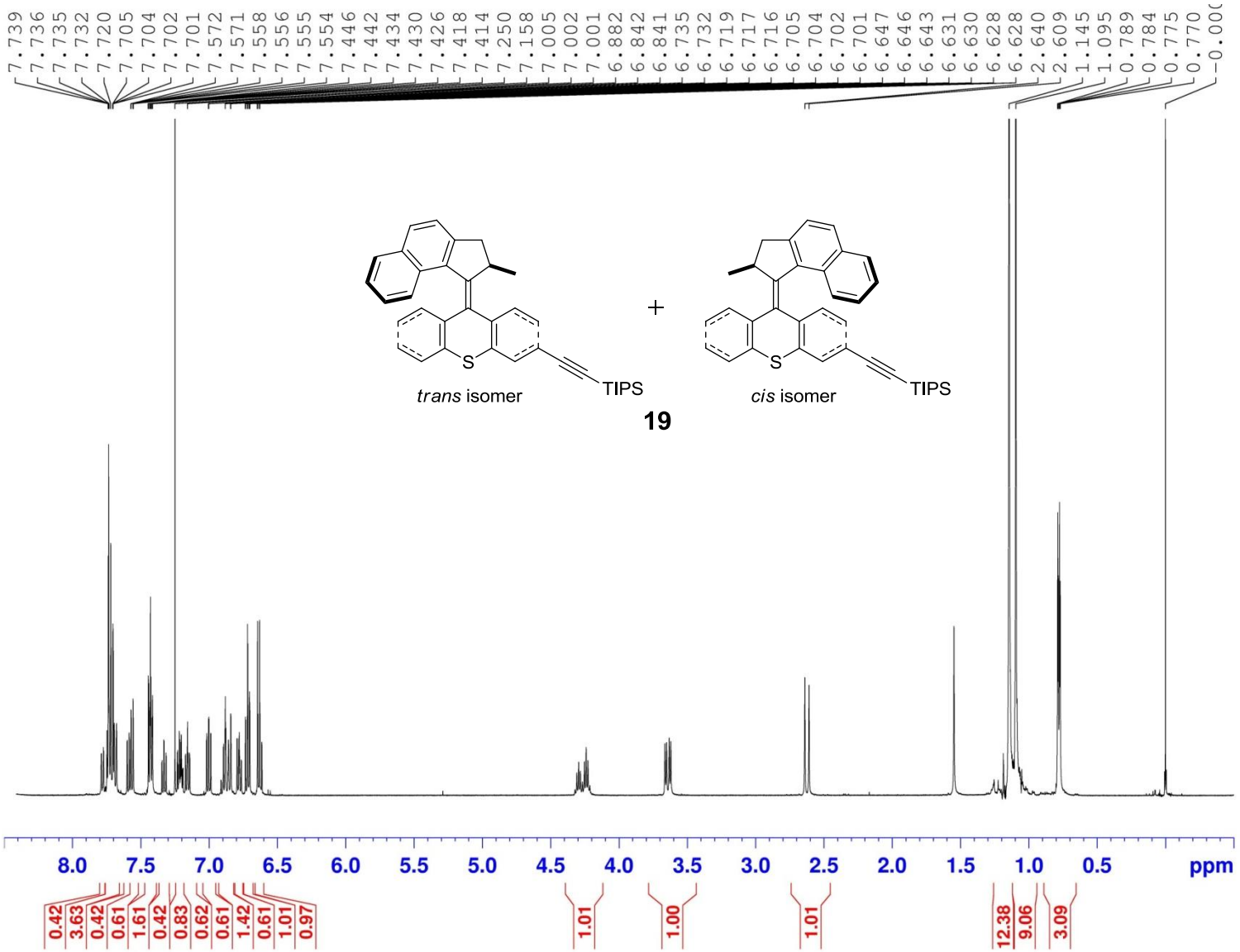
7.739
7.736
7.735
7.732
7.720
7.705
7.704
7.702
7.701
7.572
7.571
7.558
7.556
7.555
7.554
7.446
7.442
7.434
7.430
7.426
7.418
7.414
7.250
7.158
7.005
7.002
7.001
6.882
6.842
6.841
6.735
6.732
6.719
6.717
6.716
6.705
6.704
6.702
6.701
6.647
6.646
6.643
6.631
6.630
6.628
6.628
2.640
2.609
1.145
1.095
0.789
0.784
0.775
0.770
-0.000
S
TIPS
trans isomer
+
S
TIPS
cis isomer
19
8.0
7.5
7.0
6.5
6.0
5.5
5.0
4.5
4.0
3.5
3.0
2.5
2.0
1.5
1.0
0.5
ppm
0.42
3.63
0.42
0.61
1.61
0.42
0.83
0.62
0.61
1.42
0.61
1.01
0.97
1.01
1.00
1.01
12.38
9.06
3.09

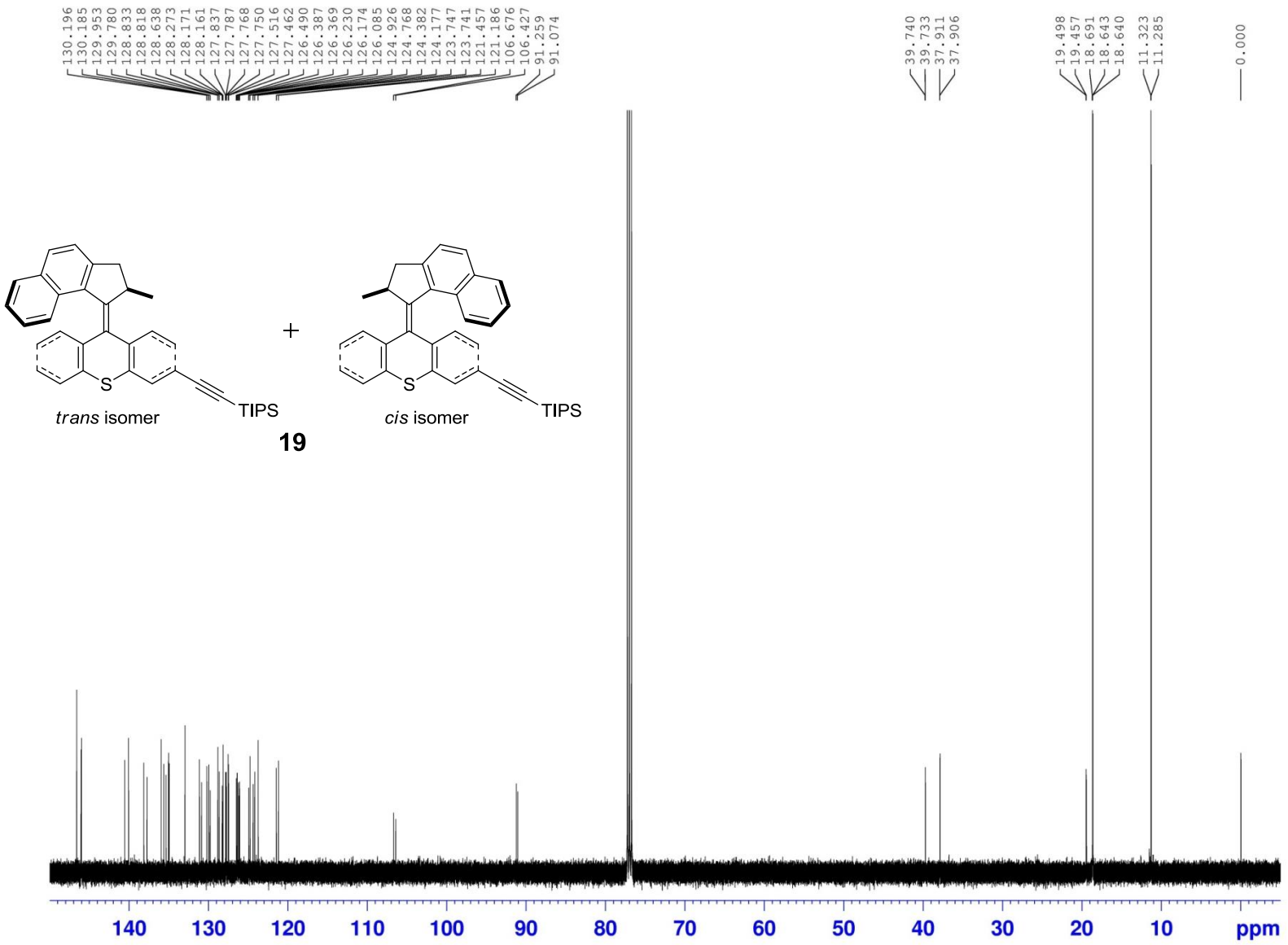
130.196
130.185
129.953
129.780
128.833
128.818
128.638
128.273
128.171
128.161
127.837
127.787
127.768
127.750
127.516
127.462
126.490
126.387
126.369
126.230
126.174
126.085
124.926
124.768
124.382
124.177
123.747
123.741
121.457
121.186
106.676
106.427
91.259
91.074
39.740
39.733
37.911
37.906
19.498
19.457
18.691
18.643
18.640
11.323
11.285
0.000
S
TIPS
trans isomer
+
S
TIPS
cis isomer
19
140
130
120
110
100
90
80
70
60
50
40
30
20
10
ppm

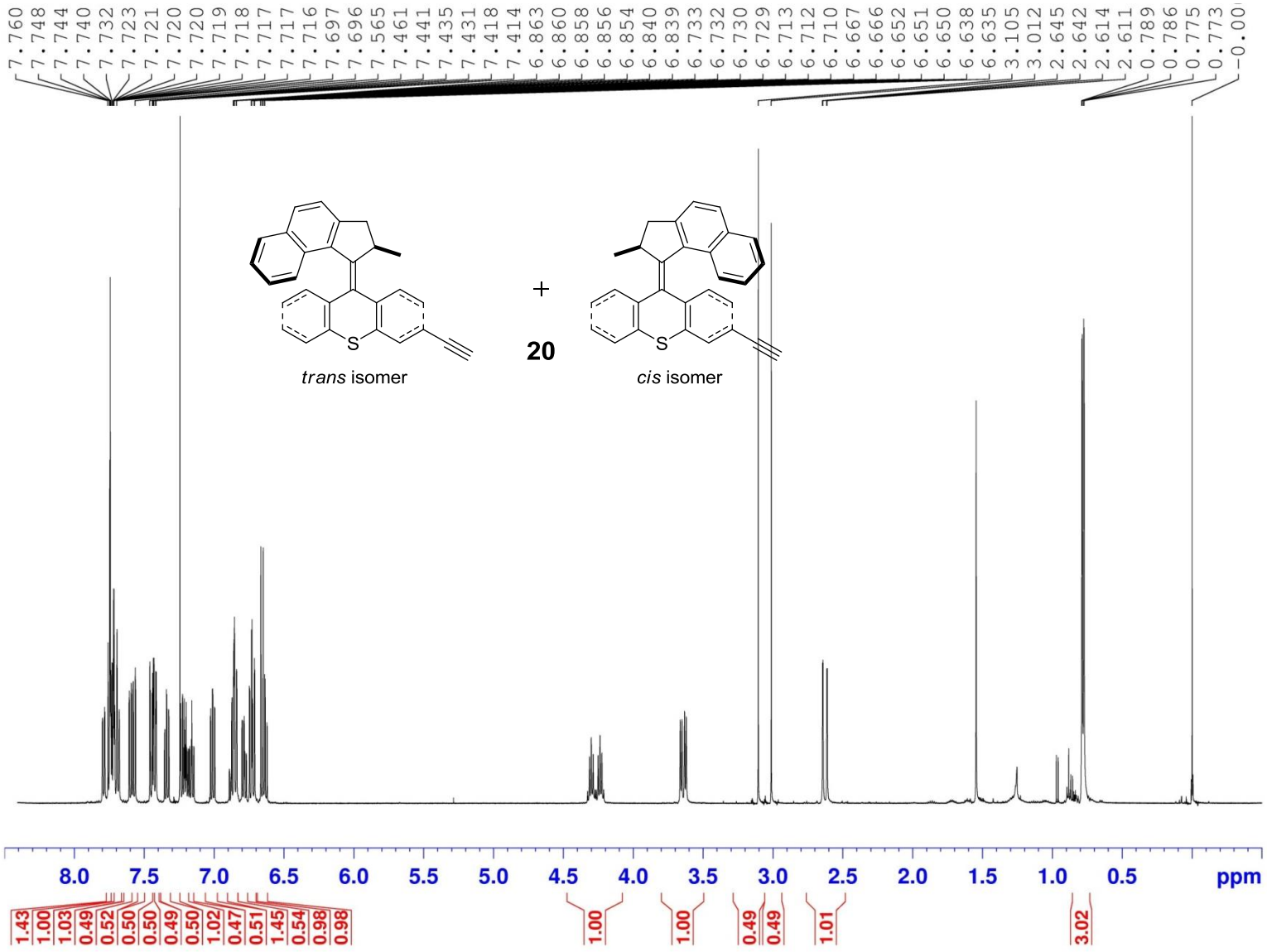
7.760
7.748
7.744
7.740
7.732
7.723
7.721
7.720
7.720
7.719
7.718
7.717
7.717
7.716
7.697
7.696
7.565
7.461
7.441
7.435
7.431
7.418
7.414
6.863
6.860
6.858
6.856
6.854
6.840
6.839
6.733
6.732
6.730
6.729
6.713
6.712
6.710
6.667
6.666
6.652
6.651
6.650
6.638
6.635
3.105
3.012
2.645
2.642
2.614
2.611
0.789
0.786
0.775
0.773
-0.00
S
trans isomer
+
20
S
cis isomer
8.0
7.5
7.0
6.5
6.0
5.5
5.0
4.5
4.0
3.5
3.0
2.5
2.0
1.5
1.0
0.5
ppm
1.43
1.00
1.03
0.49
0.52
0.50
0.50
0.49
0.50
1.02
0.47
0.51
1.45
0.54
0.98
0.98
1.00
1.00
0.49
0.49
1.01
3.02

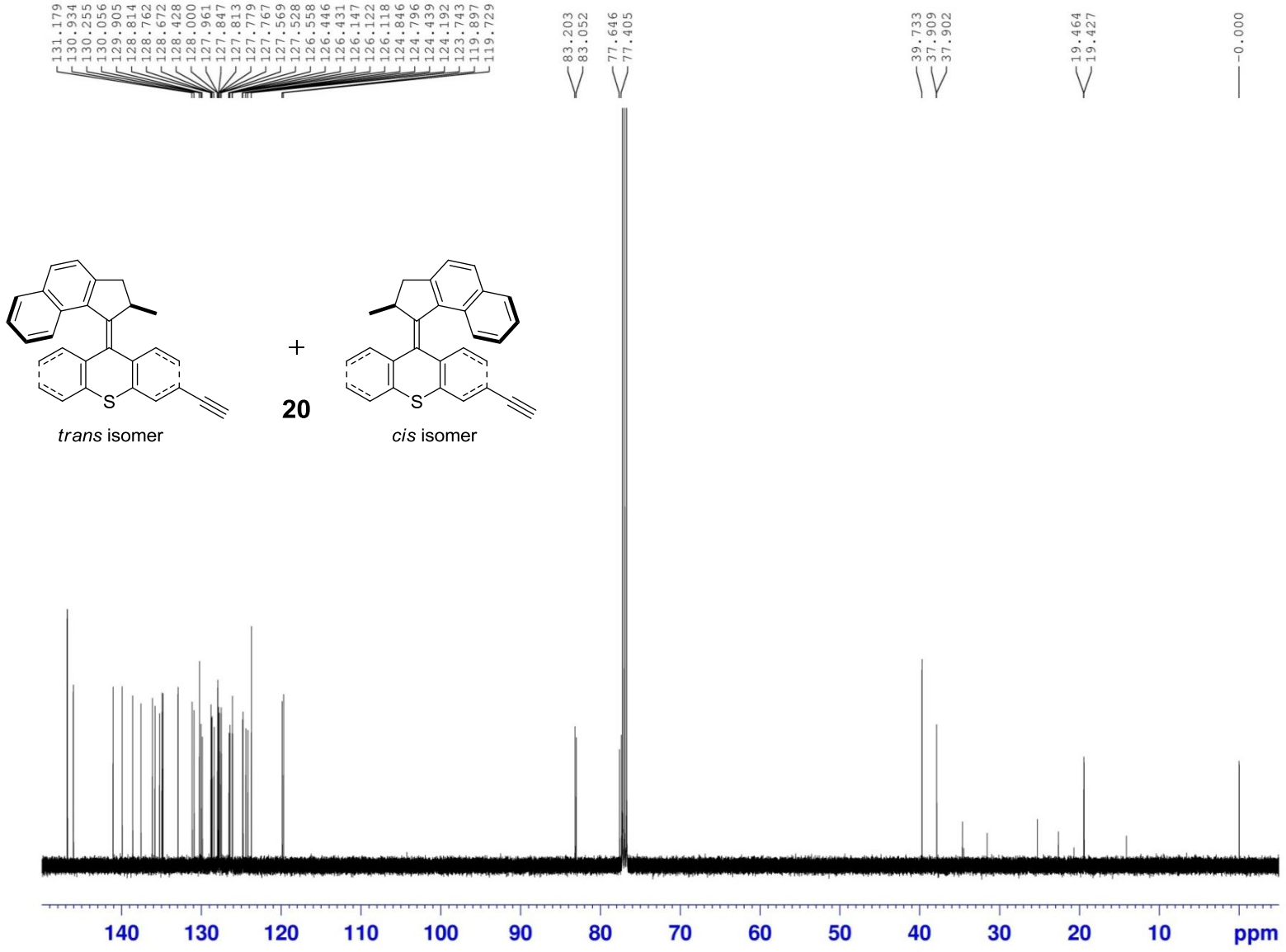
131.179
130.934
130.255
130.056
129.905
128.814
128.762
128.672
128.428
128.000
127.961
127.847
127.813
127.779
127.767
127.569
127.528
126.558
126.446
126.431
126.147
126.122
126.118
124.846
124.796
124.439
124.192
123.743
119.897
119.729
83.203
83.052
77.646
77.405
39.733
37.909
37.902
19.464
19.427
0.000
S
S
+
20
trans isomer
cis isomer
140
130
120
110
100
90
80
70
60
50
40
30
20
10
ppm

CHAPTER 3

Designs and Synthesis of a Cy5-Tagged Motorized Nanocar

3.1. Introduction

Thanks to advancements in microbiology, scientists gained tremendous understanding of many naturally occurring protein machines.[1] Mimicking nature, many sophisticated artificial molecular machines, such as, muscles[2-4] and an elevator,[5] were developed and performed work at the nanometer scale. These nanometer-sized machines respond to certain external stimuli, and perform programmed or directed functions. Our group has designed a family of nanovehicles named nanocars that are aimed to transport molecules on a surface.[6,7] Inspired by the rolling motion of C_{60},[8,9] the first nanocar was designed and successfully manipulated by scanning-tunneling microscopy (STM).[10] Complementary to STM, single-molecule fluorescent microscopy (SMFM) also provides single-molecule resolution.[11] Unlike STM, which requires conducting substrates and ultra-high vacuum, SMFM uses non-conducting substrates and ambient environments.[11] A family of fluorescent nanocars (Figure 1) were designed, synthesized and imaged.[11-13] These nanocars showed micrometer scale translational motion on glass surfaces, and the substrate-mobility relationships were also investigated.[12]

STM and SMFM imaging results indicated that our single-molecule nanocars rely on rolling mechanisms to achieve significantly higher mobility on surfaces. Despite the previous successes of nanocars, their motion was mostly driven by random thermal energy which produced 2-D thermally induced movements. In order to achieve controlled motion, a nanomachine that can convert an external energy input into a controllable movement is required. Although the use of an electric field to control the nanocar movement has been demonstrated,[10,14] the sizes of these nanomanipulators, for example, STM or atomic force microscopic (AFM) tips, are usually 8-9 orders of magnitude larger

than the individual nanoentities. Therefore, we sought here to study active transporters that have imbedded nanomotors that can be actuated by external energy.

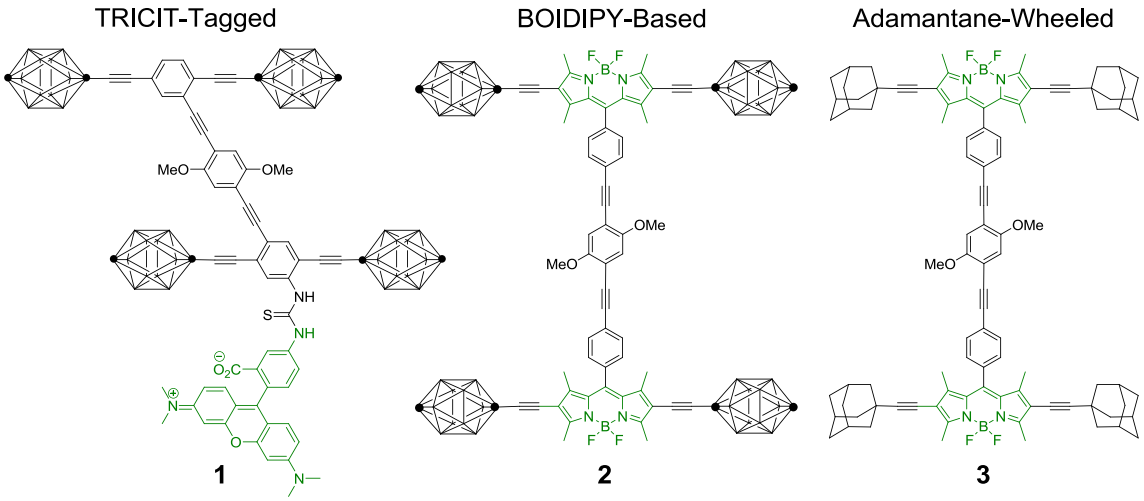

Figure 3.1. Structure of fluorescent nanocars. A tetramethylrhodamine isothiocyanate-(TRITC-) tagged fluorescent nanocar **1**, an intrinsically fluorescent boron-dipyrromethene (BODIPY-) based nanocar **2**, and an adamantane-wheeled BODIPY-nanocar **3** were designed, synthesized, and monitored. All fluorescent nanocars rely on rolling mechanism to achieve micrometer scale translational movement on glass surfaces. Among the three nanocars, nanocar **3** exhibits the highest mobility.

A few motorized nanovehicles[15,16] that are intended to assimilate light as the energy source, such as motorized nanocar **4**, were designed. This family of molecules included a light-driven molecular rotary motor affixed with chassis, axles, and wheels. Initial STM imaging experiments were done, however, no light- or electric field-induced lateral motion was observed.[16] This is probably due to the strong and complex interactions between the molecule, surface, light, electric field and STM tip.[17,18] As

discussed in chapter 2, a few modifications of the molecule design and the substrate were proposed in order to fine-tune the molecule-surface interactions for STM experiments. In addition to studying nanocars on conductive surfaces with STM, SMFM uses non-conductive substrates, which provides a different platform for studying molecule-surface interactions. We report here the design and synthesis of a fluorescent motorized nanocar intended for SMFM studies.

3.2. Design of the BODIPY-Based Motorized Nanocar

The first fluorescent motorized nanocar design was based on the structure of motorized nanocar **4**[16] and the BODIPY-based nanocar **3**.[13] Accordingly, a bent BODIPY-based motorized nanocar **5** was developed (Figure 3.2). The synthesis of nanocar **5** would be completed by coupling two adamantane-wheeled BODIPY-axles **6**[13] and the 2,7-dibromomolecular motor **7**. However, nanocar **5** was expected to demonstrate circling motion because the axles are not in a parallel configuration.[19]

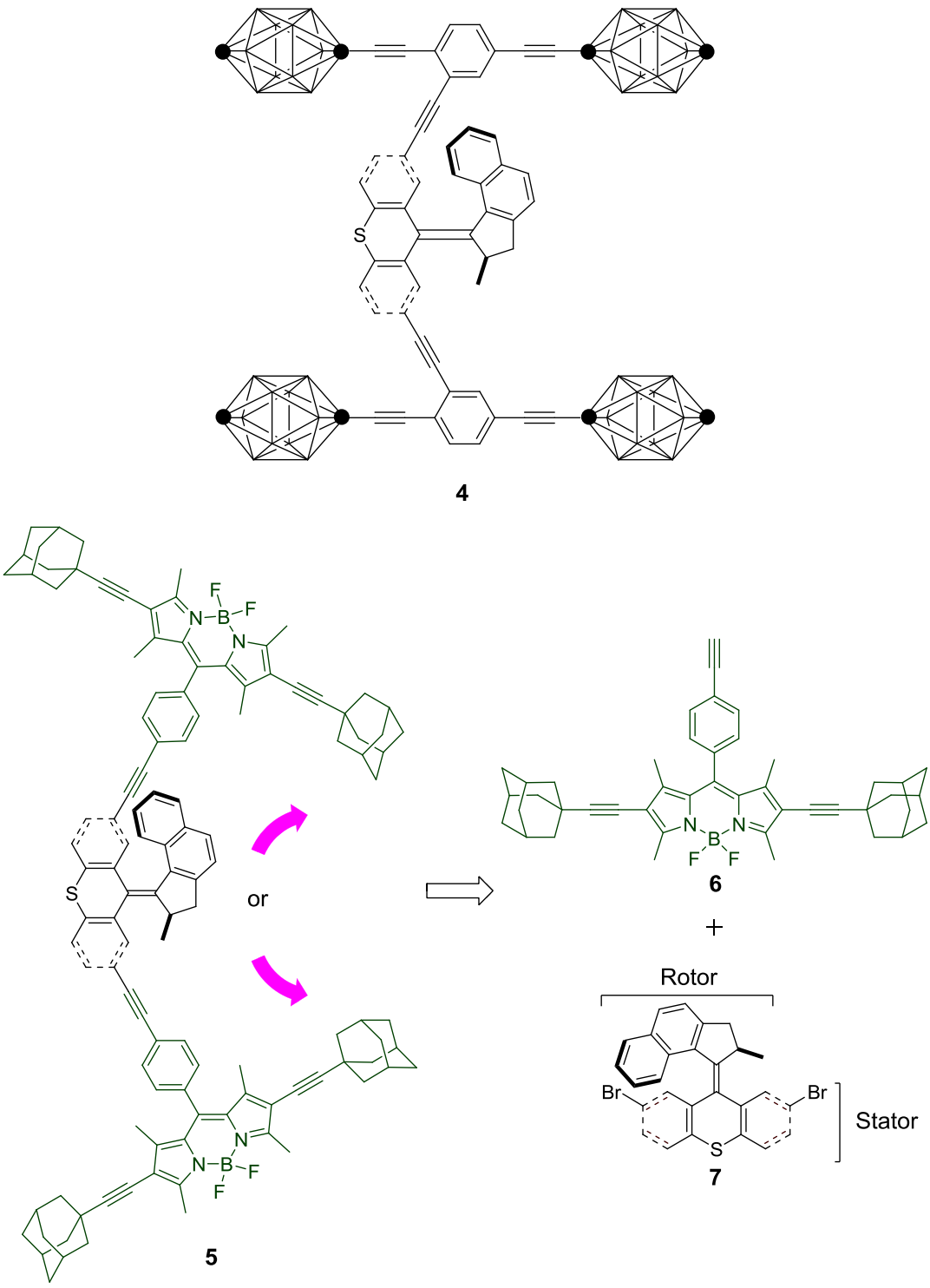

Figure 3.2. a) Structure of the *p*-carborane wheeled motorized nanocar **4**. b) Proposed structure and the synthetic plan of the bent BODIPY-based motorized nanocar **5**. Nanocar **5** can be assembled by coupling two adamantane-wheeled BODIPY axles **6** with the

light-driven unidirectional molecular motor **7** that bears two bromides at the 2,7-positions of the stator. Due to the non-parallel wheel orientation, the nanocar **5** is expected to move in circled motion (purple arrows; clockwise or counterclockwise directions, depending on the motor chirality and landing conformation).

An aligned configuration of the axles is required for linear translational motion. The structure of a linear BODIPY-based nanocar **8** was designed (Figure 3.3). The parallel axle configuration was expected to give linear translational motion on a surface. The synthetic challenge of this nanocar **8** is to construct a molecular motor **9** with two bromine atoms at the 2- and 6-positions. Note that motor **9** would be made as a mixture of *cis*- and *trans*-isomers because the Barton-Kellogg reaction used for forming the central double bond does not differentiate one diastereomer over the other. Additionally, both diastereomers consist of two enantiomers. The structural similarity makes the separation very difficult. However, since the molecules would be investigated individually on surfaces, it was unnecessary to resolve the diastereomers and enantiomers.

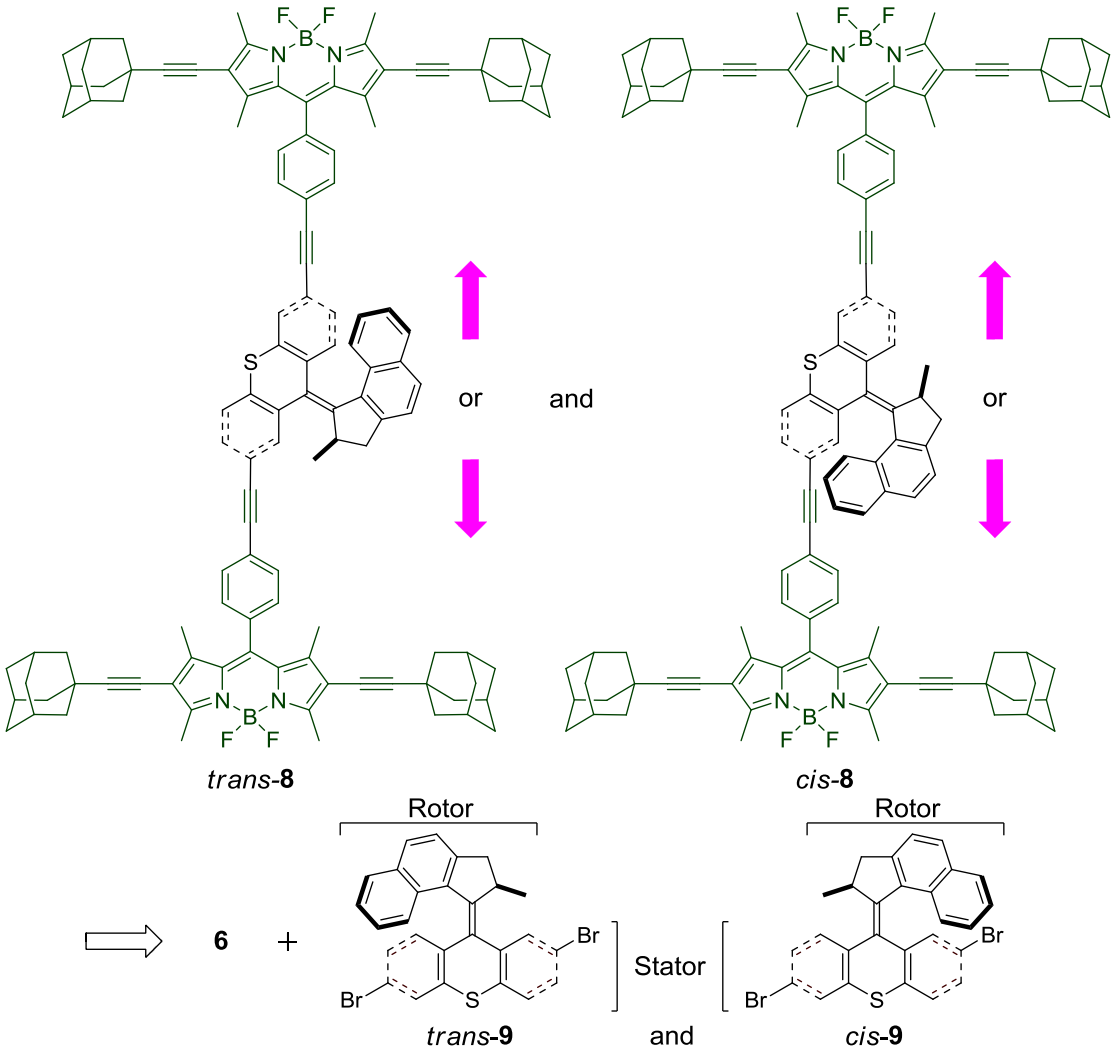

Figure 3.3. Proposed structure of the linear BODIPY-based motorized-nanocar **8**. To synthesize nanocar **8**, a light-driven molecular motor **9** with two bromides at the 2,6 positions of the stator was designed. Similar to nanocar **5**, nanocar **9** could be obtained by coupling axle **6** and motor **9**. Nanocar **8** would be prepared as a mixture of two geometrical isomers because *trans*-**9** and *cis*-**9** are synthesized in one pot, and the two forms are interconvertible in the presence of UV-light. Nanocar **8** was expected to move in either direction due to its parallel axle configuration.

3.3. Synthesis of the 2,6-Dibromomotor

Based on a literature approach (Scheme 3.1),[20] a nucleophilic aromatic substitution between thiol **10** and the benzonitrile **11** was used to form the skeleton **12** of the stator. Subsequent hydrolysis of the nitrile gave the carboxylic acid **13**. Friedel-Crafts cyclization yielded stator **14**, and the ketone was converted into thione **15** by P_4S_{10} in toluene at reflux. Formation of the motor involved oxidizing a hydrazone **16**[16,21] into the corresponding unstable diazo intermediate by manganese dioxide. The inorganic residue was removed by filtration in a Schlenk-type set-up. Thione **15** was added portionwise to the deep-purple filtrate. A [2+3] cycloaddition occurred and evolution of nitrogen gas indicated the formation of the 2,6-dibromoepisulfide **17**. Due to the dissymmetric bromide positions of stator, episulfide **17** was obtained in a mixture of two diastereomers. The *trans* and *cis* assignments were determined regarding the relative positions of the episulfide three-membered ring and the bromides. The molecular motor **9** was then made from desulfurization of **17** with trimethyl phosphite in a screw-capped tube at 130 ℃.

Scheme 3.1. Synthesis of the 2,6-dibromomotor **9**

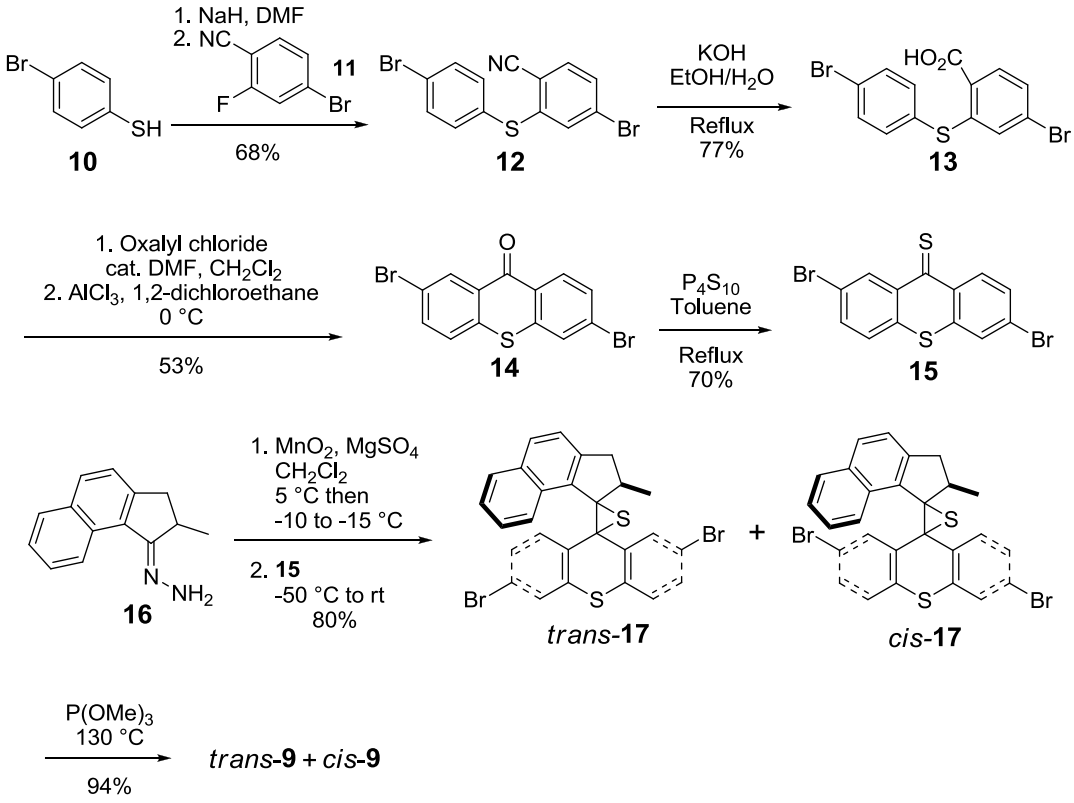

3.4. NMR Characterization of the 2,6-Dibromomotor 9

The ^{1}H NMR spectrum of a freshly prepared 2,6-dibromomotor **9** sample (Figure 3.4.) was compared to the previously synthesized and characterized motor **7**. While motor **7** had 12 proton signals in the aromatic region, 24 proton signals were found for motor **9**. The area of all proton signals in motor **9** were integrated, and two sets of 12 integrals with a ratio at 62:38 were obtained. This indicated that the motor **9** very likely exists as a mixture of *cis*- and *trans*-isomers with non-equal abundance. Another ^{1}H NMR spectrum of the 2,6-dibromotor was taken after one week. Interestingly, the ratio of the integrals changed to 50:50. The gradual change of the ratio may have been due to the presence of

UV-light in the ambient environment. The changes of signal intensities further confirmed the initial assignments of proton signals toward specific isomers.

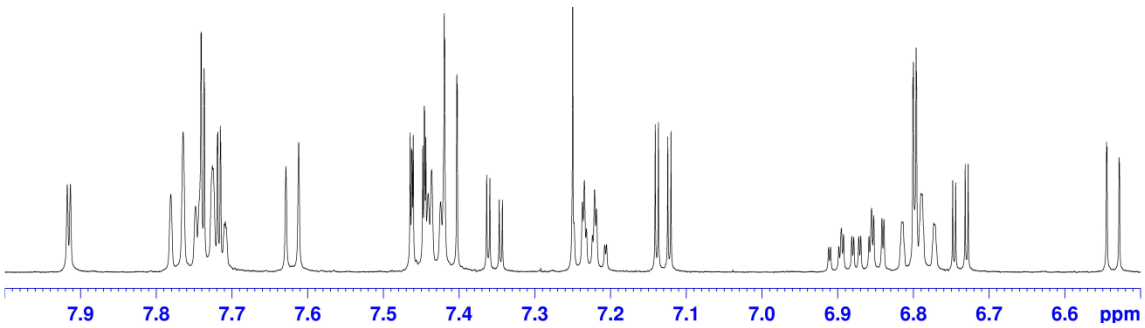

Figure 3.4. Partial ^{1}H NMR spectrum of the freshly prepared 2,6-dibromomotor **9**. Two sets of signals with integration ratio at 62:38, which correspond to *cis*- and *trans*-**9**, were observed.

Finally, all of the protons of the individual isomers of motor **9** were unambiguously assigned with the assistance of correlation spectroscopy (COSY), nuclear Overhauser enhancement spectroscopy (NOESY), distortionless enhancement by polarization transfer spectroscopy (DEPT), heteronuclear single-quantum correlation spectroscopy (HSQC) and heteronuclear multiple-bond correlation spectroscopy (HMBC) experiments. The assignments for both *cis*- and *trans*-**9** showed the characteristic patterns that reflect the motor helicity.[16] The initially more abundant isomer was determined to be *cis*-**9**.

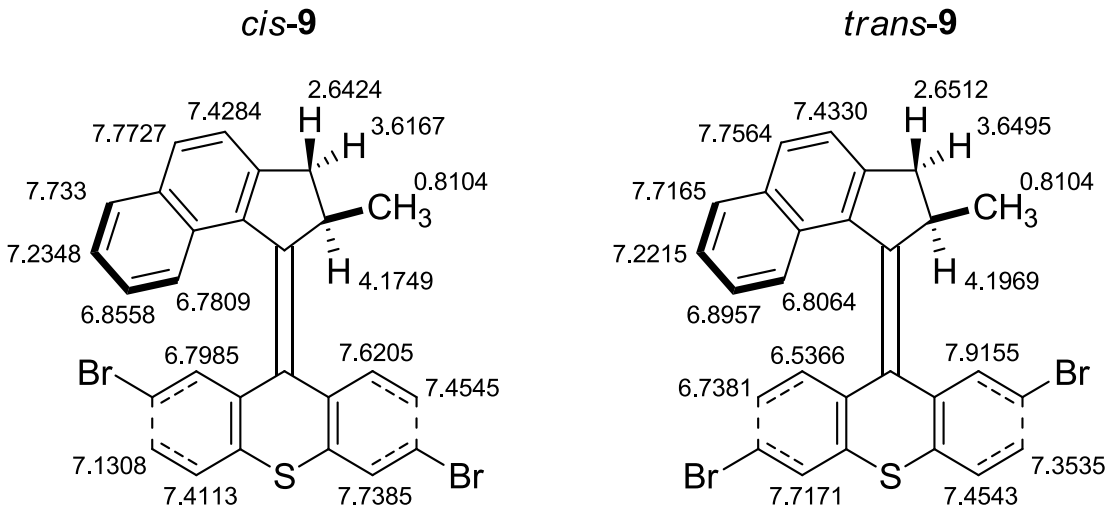

Figure 3.5. ^{1}H NMR (500 MHz, $CDCl_3$, 295K) assignments of *cis*-**9** and *trans*-**9**. The initially more abundant isomer was *cis*-**9**.

3.5. Photoisomerization Study of the BODIPY-Slow Motor Hybrid

Although motor **9** was successfully synthesized and characterized, the possible energy transfer between the motor and the BODIPY fluorophore needed to be evaluated before pursuing nanocar **8**. The UV-Vis absorption spectra of BODIPY-axle **6** showed noticeable absorption at the 365 nm area, which is required for motor rotation. The absorption overlap between the photochemically active motor and the BODIPY unit could decrease the quantum yield for motor photoisomerization. A stronger light source to accommodate the decrease in quantum yield might be useful, but the possibility of photobleaching would then be exacerbated.[22] In addition, the motor and the BODIPY-axles are nearby each other and connected via conjugated bonds.[23] Hence, the two photochemically active moieties could have through-bond or through-space energy transfer.

To further address this concern, a model compound **18** was designed (Scheme 3.2). Compared to the MHz frequency of rotation of motor **7** and **9**, the rotation rate of motor **19** was much slower because the energy barrier for the thermal helix inversion is much higher.[24] This enabled the study of its rotation by NMR spectroscopy.[15] Model **18** was synthesized by a Sonogashira coupling between a motor **19** and two BODIPY fluorophores, **20** in moderate yield.

Scheme 3.2. Synthesis of the BODIPY-slow motor hybrid **18**.

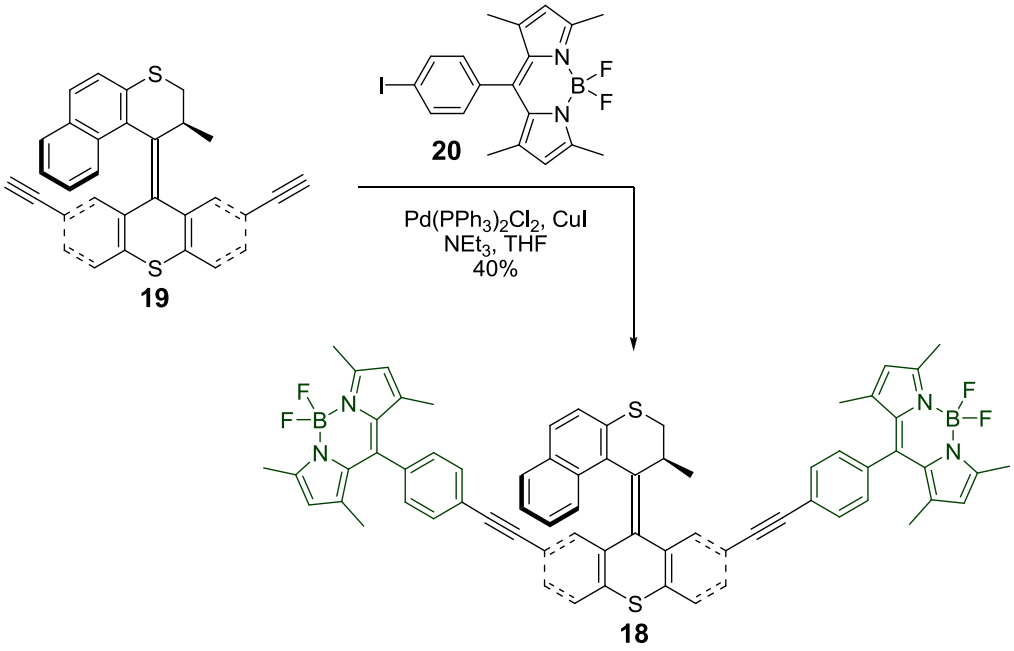

A rotation study of motor **19** was conducted as a reference experiment (Figure 3.6). A 1 mM sample of **19** was irradiated with 365 nm light (3 mW/cm^2) for 1 h. As shown by NMR analysis, 91% of motor **19** isomerized. A similar NMR photoisomerization experiment was done for model **18**. By comparison of the spectra before and after UV irradiation, 45% of the model **19** was found to be isomerized. This

indicated that the presence of BODIPY in **18** reduced the efficiency of photoisomerization.

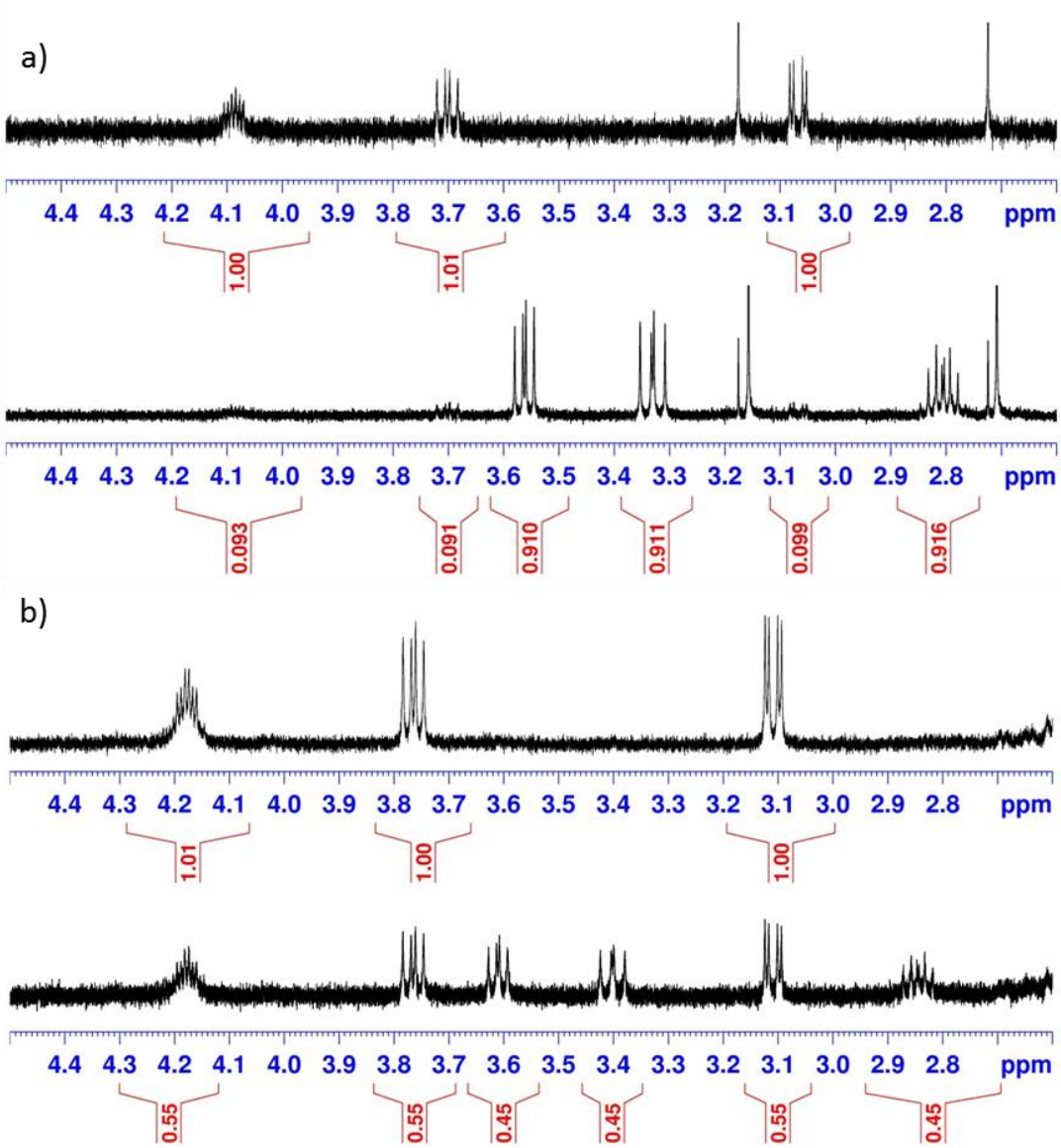

Figure 3.6. ^{1}H NMR photoisomerization study of a) the slow motor **19** and b) the BODIPY-motor hybrid **18** (500 MHz, $CDCl_3$, 295K, 1 mM). a) Top: **19** without irradiation of 365 nm light; bottom: **19** after 1 h irradiation of 365 nm light (3 mW/cm^2).

The integrations of the proton spectra showed 91% of motor **19** photoisomerized. b) Top: **18** without irradiation of 365 nm light; bottom: **18** after 1 h irradiation of 365 nm light. 45% of **18** isomerized after irradiation of 365 nm light (3 mW/cm^2). The presence of BODIPY fluorophore reduced the efficiency of photoisomerization.

3.6. Design of the Cy5-Tagged Motorized Nanocar

The rotation study of the BODIPY-slow motor hybrid **18** revealed that the presence of the conjugated bonded BODIPY fluorophores greatly reduced the motor photoisomerization efficiency. The absorption overlapping and the intramolecular energy transfer between the motor and the BODIPY fluorophores are likely to be the major causes. Thus, a fluorophore with minimum absorption at the 365 nm region, which is required the photoisomerization of the motor, is preferred. Inserting a spacer between the motor and the fluorophore might reduce the possibility of intramolecular energy transfer (either through-bond or through-space).[25]

To choose a potentially suitable fluorophore, a group of fluorophores organized by Lavis and Raines (Figure 3.7) was examined.[26] Since the laser sources available for the SMFM experiments are 514 nm, 532 nm and 638 nm, the UV-Vis absorption and fluorescent emission spectra of fluorophores in the above region were reviewed. The UV-Vis absorption spectrum of a cy5 dye[27,28] (Figure 3.8) showed that it has weak absorption at the 365 nm region, which is necessary for motor rotation. The maximum extinction coefficient (ε) of a cy5 dye is approximately at 640 nm, which is suitable for SMFM experiments. The fact that the motor absorbs weakly at the 365 nm region gives the motor the highest probability for harvesting photons. The strong absorptivity of the cy5 dye at

640 nm and the high quantum yield (Φ) make the dye bright (ε × Φ) and thus suitable for single-molecule fluorescent experiments.

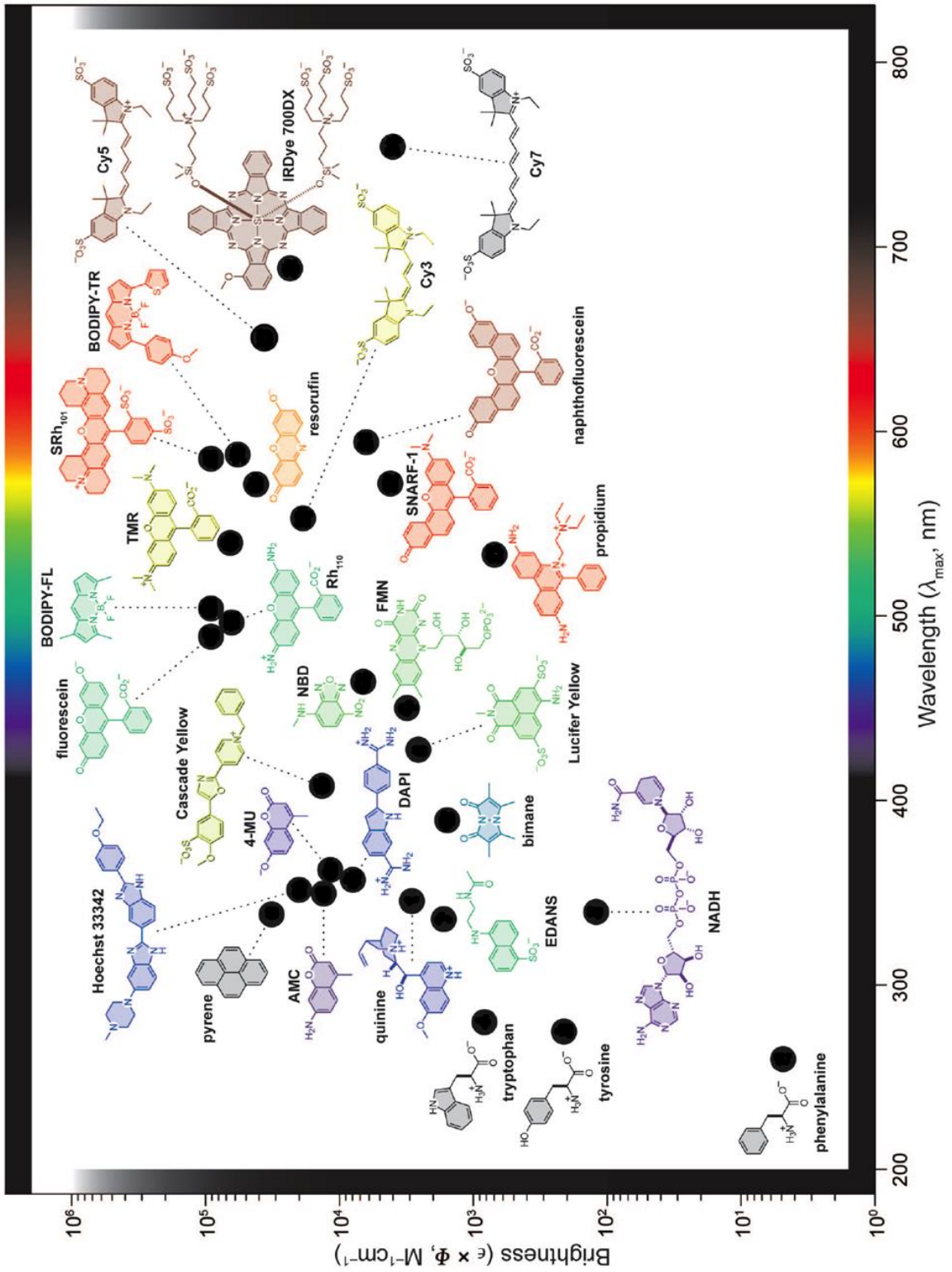

Figure 3.7. Plot of fluorophore brightness ($\varepsilon \times \Phi$) vs. the wavelength of maximum absorption (λ_{max}) for the major classes of fluorophores. The color of the structure indicates its wavelength of maximum emission (λ_{em}). Figure adapted with permission from reference 26. Copyright 2008 American Chemical Society.

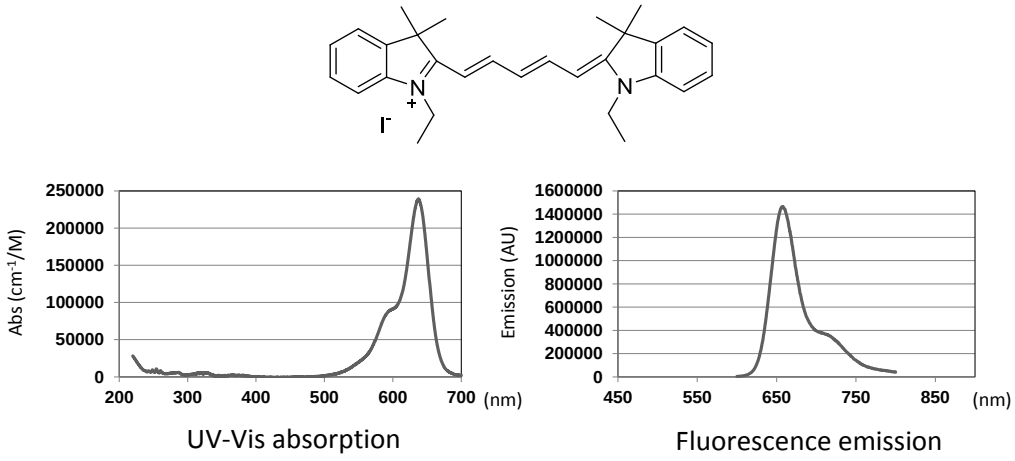

Figure 3.8. Structure, UV-vis absorption, and fluorescence spectra of a cy5 dye. The absorption spectrum indicated that cy5 absorption is weak in the 365 nm region, which is required for the motor photoisomerization. The maximum absorption of the cy5 dye is in the 640 nm region, which matches a laser source used in SMFM imaging.

A cy5-tagged motorized nanocar **20** was designed (Figure 3.9) resembling the design of the TRITC-tagged nanocar **1**. The chassis consists of a light-driven molecular motor, and a cy5 dye attached to the end of the structure via a non-conjugated spacer. The spacer is expected to provide a longer distance between the photochemically driven motor and the fluorescent dye, and consequently minimize undesired energy transfer.

Because the cy5 dye exhibits weak absorptivity in the 365 nm region, the efficiency of the motor photoisomerization of the nanocar **20** is expected to be highest.

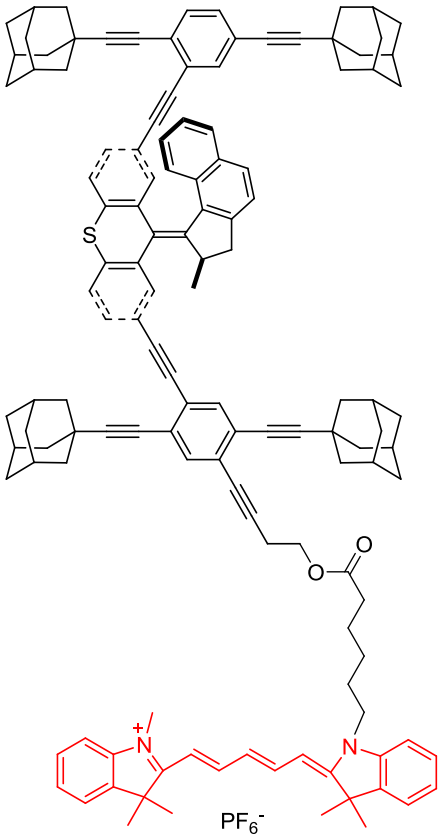

20

Figure 3.9. Design of a cy5-tagged motorized nanocar **20**. The nanocar **20** is based on the concept of TRITC-tagged nanocar **1** and the motorized nanocar **4**. The rotary motor relies on 365 nm light for the photoisomerization step. Therefore, we use a cy5 dye instead of a TRITC dye because a cy5 dye absorbs weakly in 365 nm region. Adding an aliphatic linker, which separates the photochemically active motor and the fluorescent dye, decreases the probability of through bond energy transfer.

The synthetic plan (Figure 3.10) for the nanocar **20** includes esterification of nanocar **21** with a hydroxyl group and cy5 dye **22** with its carboxylic acid. The chassis of nanocar **21** can be built by a statistical coupling between an iodo-axle **23**, motor **24** and a tetrasubstituted iodo-axle **25**. The challenges to this synthetic plan will be the preparation of the tetrasubstituted iodo-axle **25**, and the low yielding statistical coupling step for the formation of nanocar synthesis.

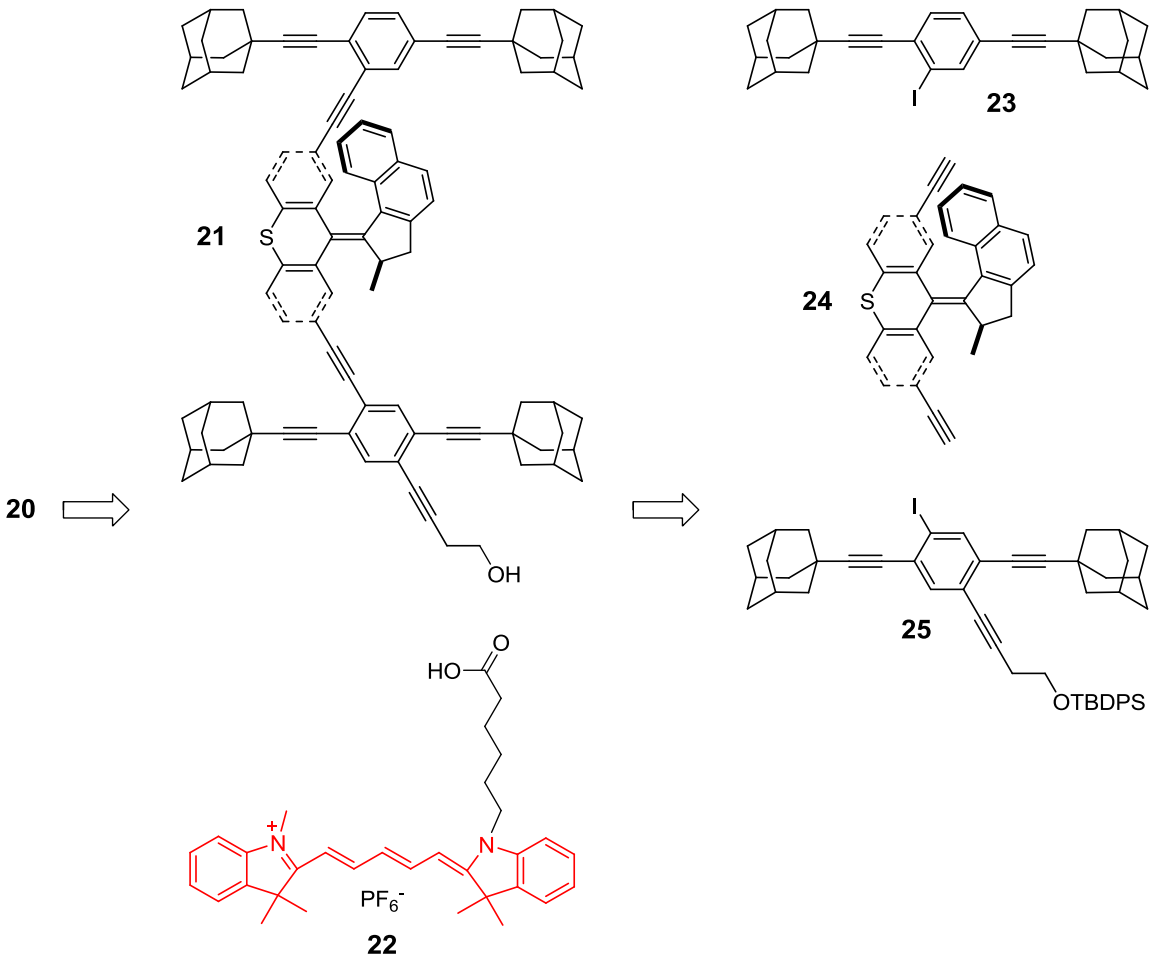

Figure 3.10. Retrosynthetic analysis of the cy5-tagged nanocar **20**. Nanocar **20** is planned to be assembled by an esterification reaction between a trailer nanocar **21** and a

cy5 dye **22**. A statistical coupling between a motor **24** and two different axles **23** and **25** will be used for the construction of nanocar **21**.

3.7. Synthesis of the Cy5-Tagged Motorized Nanocar 20

3.7.1. Toward the Tetrasubstituted Iodo-Axle 25

The first target for synthesis the cy5-tagged motorized nanocar **20** was the iodo-axle **25** (Scheme 3.3). A selective Sonogashira coupling of 1,4-diiodo-2,5-dibromobenzene **26** with 1-ethynyladamantane **27** was carried out. Subsequently, a halogen exchange of the resulting dibromoaxle **28** yielded the diiodoaxle **29** in excellent yield. Unfortunately, attempts at a selective mono-coupling reaction between the 4-(*t*-butyldimethylsilyloxy)-1-butyne **30** and the diiodoaxle **29** did not afford the desired product. This might be due to the poor solubility of diiodoaxle **29**. Hence, an alternative synthetic route was needed to obtain **25**.

Scheme 3.3. Toward the tetrasubstituted iodo-axle **25**

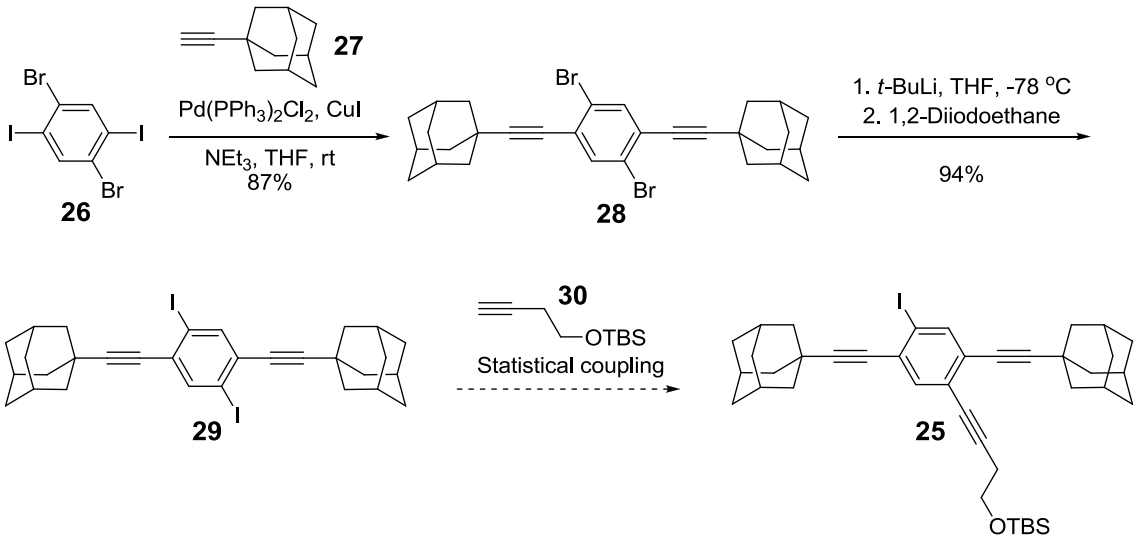

3.7.2. An Alternative Synthetic Route for the Iodo-Axle 25

Since axle **25** consists of an aryl iodide, it can be synthesized by a functional group interconversion from the corresponding aniline (Scheme 3.4). To make the aniline, 2,5-dibromo-4-nitroaniline **31** was prepared according to a five-step literature procedure.[29] A Sandmeyer reaction converted the aniline **31** into 2,5-dibromo-4-iodonitrobenzene **32** in good yield. A selective Sonogashira coupling reaction was carried out between the nitrobenzene **32** and 4-(*t*-butyldiphenylsilyloxy)-1-butyne. This reaction was optimized by using 1% palladium catalyst and 20% copper catalyst, yielding **33**. Interestingly, the major side product of this reaction was 2,5-dibromonitrobenzene, resulting from de-iodination of **32**. When a larger amount of palladium and a smaller amount of copper catalyst was used, the formation of 2,5-dibromonitrobenzene was favored.

Scheme 3.4. Synthesis of the iodo-axle **25**.

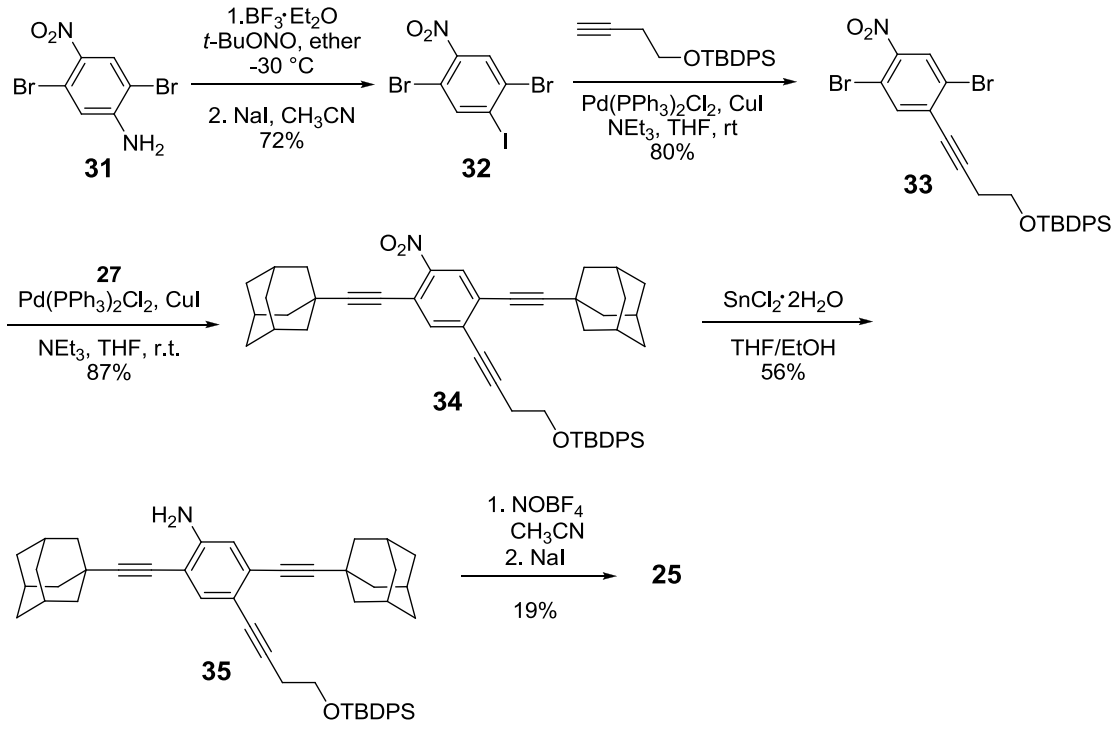

The axle precursor **33** was further coupled with 1-ethynyladamantane **27** to yield the nitrobenzene axle **34**. Aniline axle **35** was obtained by reducing **34** with tin(II) chloride dehydrate. Although a Sandmeyer reaction converting aniline **35** into iodo-axle **25** was used, the reaction was very low yielding (see note in experimental section). The overall yield to form axle **25** was only 5.3% from aniline **31**, which makes the synthetic route very inefficient.

3.7.3. The Wheel-Last Approach for Constructing the Nanocar Skeleton

In the previous synthetic route toward axle **25**, 1-ethynyladamantan **27** was introduced in the middle stage of the synthetic sequence. In contrast to this approach, another wheel-last strategy (Figure 3.11) was attempted. Instead of synthesizing the iodo-

axle **25**, another building block **36** was chosen. A Sonogashira coupling was planned to mix the axle **23** and the 2,5-dibromo-4-iodobenzene axle precursor **36** with the motor. It was expected that the Sonogashira couplings would only occur between the alkynes on motor **24** and the iodide sites on both **23** and **36**.

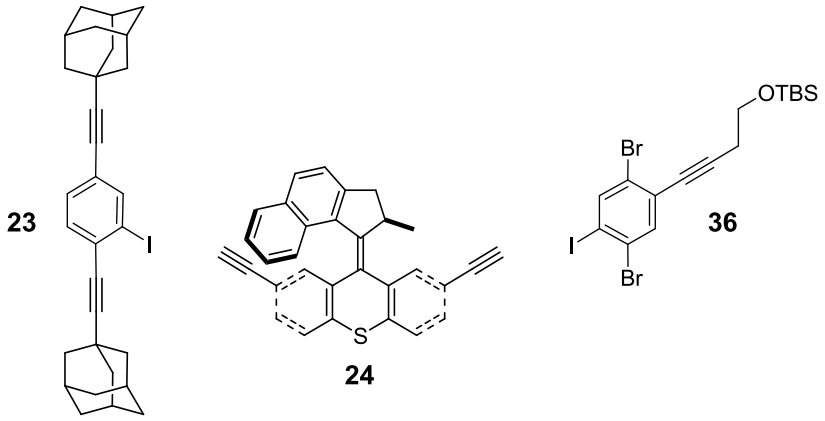

Figure 3.11. The wheel-last synthetic strategy for the formation of the nanocar skeleton. An axle precursor **36** was used instead of the iodo-axle **25**. The Sonogashira coupling reactions are expected to occur selectively on the iodide sites.

The axle precursor **36** was synthesized by a selective mono-coupling between 2,5-dibromo-1,4-diiodobenzene **26** and alkyne **30** in moderate yield (Scheme 3.5). Subsequently, a Sonogashira coupling between one equivalent of motor **24**, and two equivalents of both **23** and **36** was carried out attempting to synthesize the nanocar precursor **37**. Surprisingly, no desired compound **37** was obtained, and the only compound obtained was **38** with recovery of axle **23**. This indicated that the iodide site on **36** is more reactive than the iodide site on axle **23**. By adjusting the equivalence of **23** (2 equiv) and **26** (1 equiv), the nanocar precursor **37** was afforded in 39% yield.

Scheme 3.5. Synthesis of the nanocar skeleton

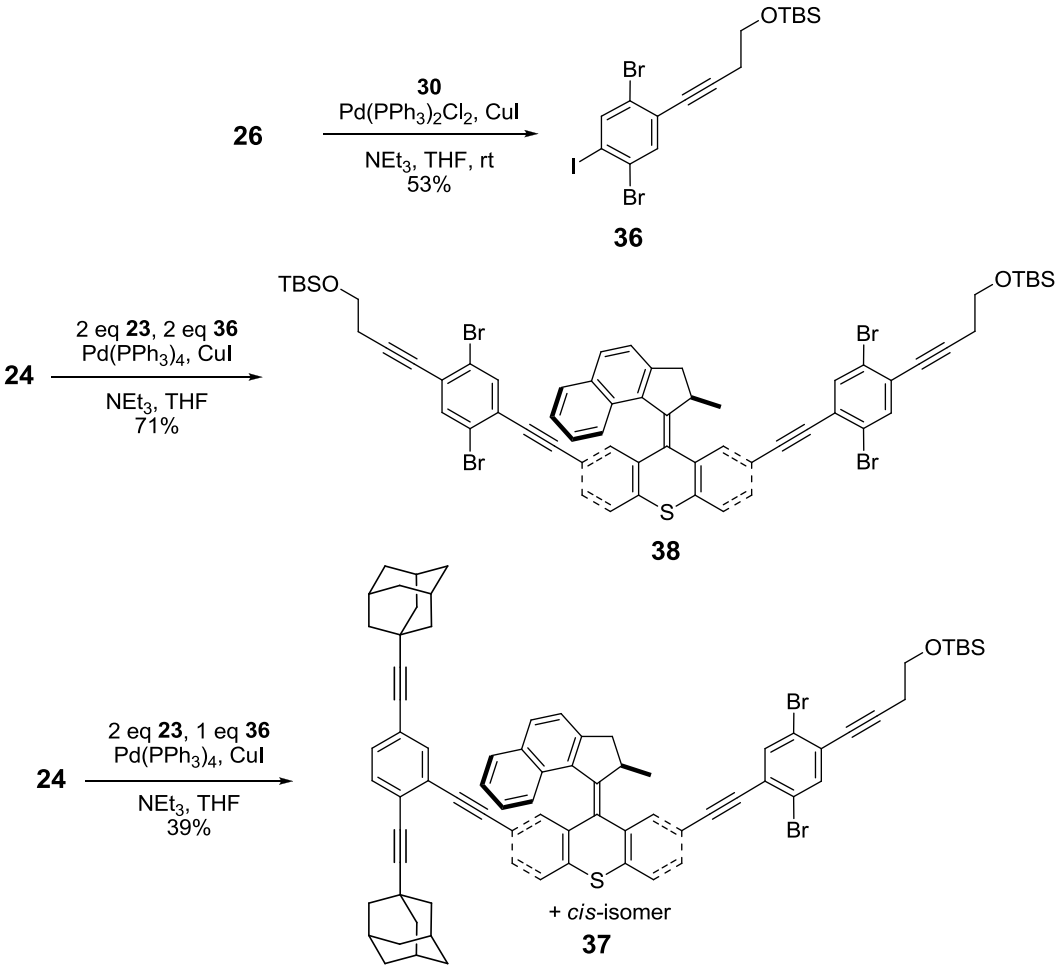

3.7.4. Synthesis and Rotation Study of the Cy5-Tagged Nanocar 20

The wheel-last synthetic approach of forming the nanocar skeleton successfully yielded the desired precursor **37**. The 1-ethylnyladamantane wheel **27** was mounted onto **37** by Sonogashira coupling using neat NEt_3 as solvent to give nanocar **39** in excellent yield. The hydroxyl protecting group of nanocar **39** was removed by a tetrabutylammonium fluoride (TABF) THF solution. A Steglich esterification of the resulting nanocar **21** was carried out with cy5 dye **22**,[30] and the cy5-tagged nanocar **20** was thus synthesized in excellent yield.

Scheme 3.6. Synthesis of the cy5-tagged nanocar **20**

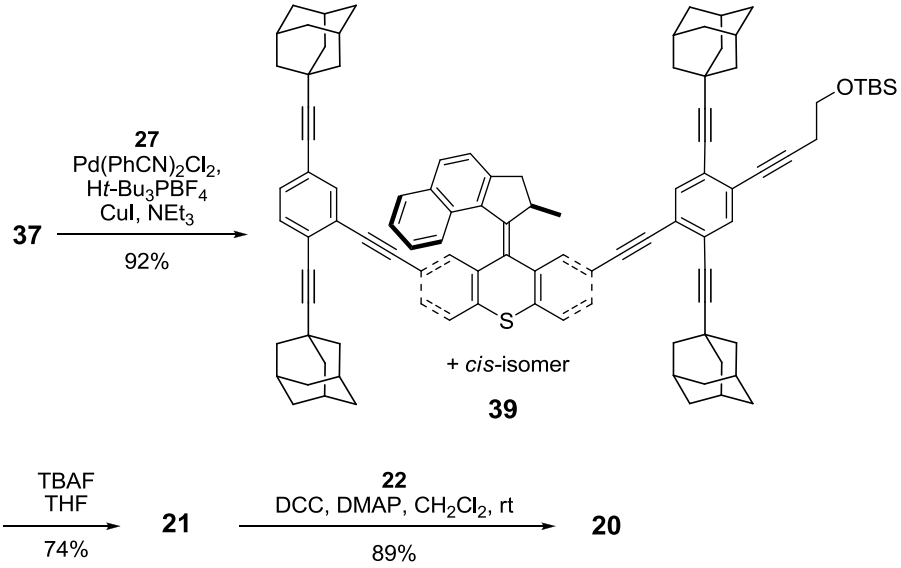

3.8. Synthesis of the Cy5-Tagged Motorized Nanocar with the Slow Motor

Similar to the synthetic protocol of nanocar **20**, a cy5-tagged motorized nanocar incorporating with a slow motor was synthesized (Scheme 3.7). The nanocar skeleton was constructed by a Sonogashira coupling between slow motor **19**, axle **23**, and axle precursor **36**. Nanocar precursor **40** was reacted with 1-ethynyladamantane **27** to form nanocar **41**. The TBS-protecting group was removed by TABF, resulting in nanocar **42**. Akin to forming cy5-tagged nanocar **20**, a Steglich esterification of the nanocar **42** was carried out with cy5 dye **22**. The cy5-tagged nanocar **43** would be used to test the photoisomerization efficiency.

Scheme 3.7. Synthesis of the cy5-tagged slow-motorized nanocar

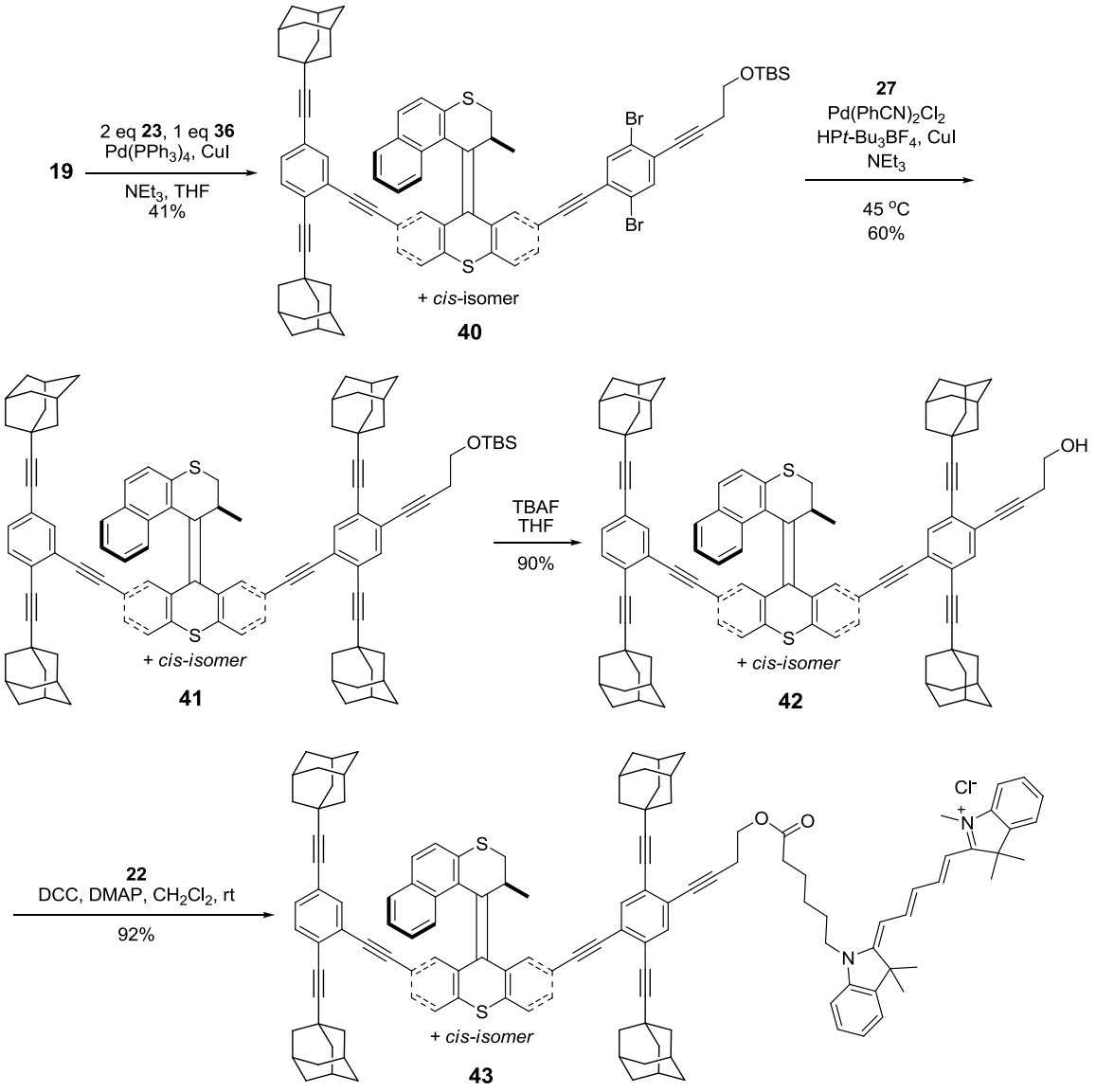

The photoisomerization step of the motor incorporated in the cy5-tagged motorized nanocar **43** was studied (Figure 3.12). After 1 h of irradiation with 365 nm light, the NMR spectrum showed 90% of the slow motor incorporated in **43** photoisomerized. Compared to the BODIPY-motor hybrid **18** photoisomerized, in which

45% of the slow motor photoisomerized, a significant increase percentage of motor photoisomerization was observed.

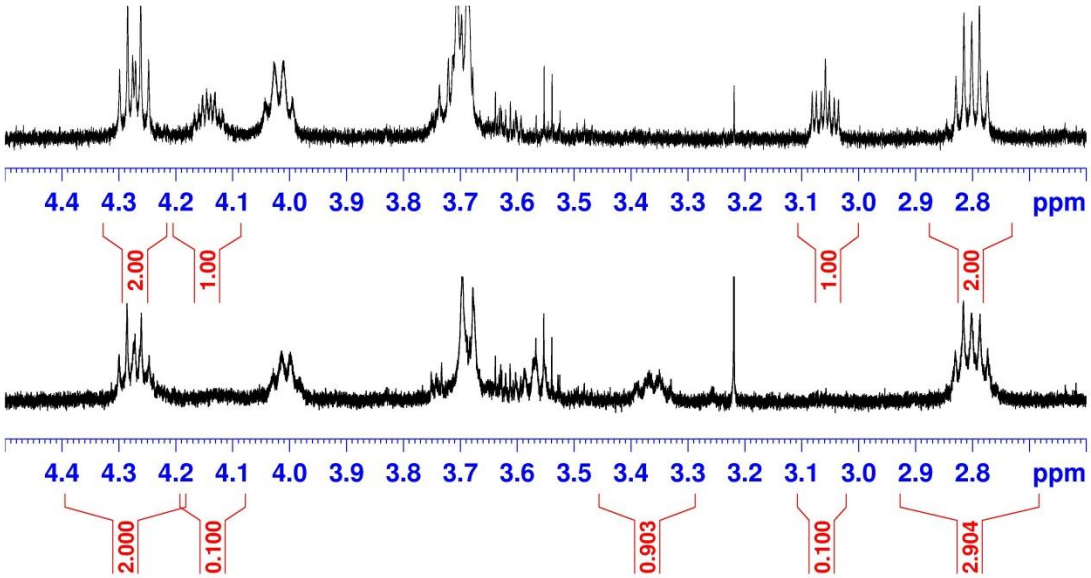

Figure 3.12. ^{1}H NMR rotation study of the cy5-tagged motorized nanocar **43** (partial NMR, CD_2Cl_2, 295K). Top: **43** without irradiation of 365 nm light; bottom: **43** after 1h irradiation of 365 nm light (3 mW/cm^2). The integrations showed that 90% of **43** underwent photoisomerization.

3.9. Conclusion

We have discussed the design and synthesis of fluorescent motorized nanocars that are suitable for SMFM studies. BODIPY-based motorized nanocars were designed. In order to investigate the photoisomerization efficiency, a slow motor-BODIPY hybrid **18** was synthesized. Our photoisomerization experiment showed that 45% of the model **18** photoisomerized. Compared to 91% of motor **19**, a decrease in photoisomerization

percentage is observed. The decrease of efficiency is due to the absorption overlap between the motor, the fluorophore and the connection by the conjugated network.

Secondly, a fluorescent-motorized nanocar **20**, designed to retain the motor photoisomerization efficiency in the presence of a fluorescent dye, was synthesized. We chose cy5 dye because it has minimum absorption in the 365 nm region, which is required for motor photoisomerization. Additionally, an aliphatic linker was also incorporated into the design of cy5-tagged nanocar **20**. A wheel-last synthetic strategy was used in the synthesis of the nanocar skeleton, and dissymmetric functionalization of the motor **24** was achieved. Based on the cy5-tagged motorized nanocar model **43**, 90% of the motor underwent photoisomerization, which indicated that the two photochemically active moieties can function with minimal overlapping light-based interactions.

3.10. Contribution

I designed all the BODIPY-based and the cy5-tagged nanocars. Jazmin Godoy synthesized the 2,6-dibromothioxane-9-one **14** and the BODIPY dyes **6** and **20**. Victor Garcia and Pin-Lei Edmund Chu participated in the preparation of fluorescent dyes **6** and 1-ethynyladamantane **27**. Dr. Lawrence Alemany did the NMR analysis for the 2,6-dibromomotor.

3.11. Experimental Section

3.11.1. General Procedure for Photoisomerization Study of 9, 18, and 43.

A 1 mM solution was prepared and its ^{1}H NMR spectrum was recorded at 500 MHz ($CDCl_3$ with 0.05% tetramethylsilane (TMS), 295 K, 128 scans, TMS half-height width <0.2 Hz). The NMR tube containing the solution was irradiated with 365 nm light for 1 h (3 mW/cm^2; Mineralight UVGL-25), and another ^{1}H NMR spectrum was recorded. The photoisomerization percentage was obtained by comparing integrals obtained from ^{1}H NMR spectra.

3.11.2. Experimental Data for Compounds 9, 12, 13, 14, 15, 17, 18, 20, 21, 25, 28, 29, 32, 33, 34, 35, 36, 37, 38, 39, 40, 41, 42, 43.

General Methods. ^{1}H NMR and ^{13}C NMR spectra were recorded at 400 or 500 and 100 or 125 MHz, respectively. Chemical shifts (δ) were reported in ppm from TMS. FTIR spectra were recorded using a FTIR Infrared Microscope with ATR objective with 2 cm^{-1} resolution. All glassware was oven-dried overnight prior to use. Reagent grade tetrahydrofuran (THF) and ether (Et_2O) were distilled from sodium benzophenoneketyl under N_2 atmosphere. Triethylamine (NEt_3), dichloromethane (CH_2Cl_2) and *N,N'*-dimethylforamide (DMF) were distilled from calcium hydride (CaH_2) under an N_2 atmosphere. THF and NEt_3 were degassed with a stream of argon for 15 min before being used in the Sonogashira coupling reactions. All palladium-catalyzed reactions were carried out under argon atmosphere, while other reactions were performed under N_2 unless otherwise noted. All chemicals were purchased from commercial suppliers and used without further purification. Flash column chromatography was performed using 230-400 mesh silica gel from EM Science. Thin layer chromatography (TLC) was performed using glass plates pre-coated with silica gel 40 F_{254} 0.25 mm layer thickness

purchased from EM Science. Note that melting points of **9**, **20**, **21**, **37**, **39**, **40**, **41**, **42**, **43** were not measured because they exist as a mixture of *cis* and *trans* isomers.

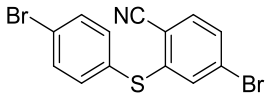

4-Bromo-2-(4-bromophenylthio)benzonitrile (12). A 250 mL round-bottom flask equipped with a stir bar was charged with NaH (360 mg, 60% NaH in mineral oil, 9.0 mmol). A solution of 4-bromothiophenol **10** (1.42 g, 7.50 mmol) in DMF (50 mL) was added, followed by addition of Zn dust (100 mg, 1.5 mmol). A light yellow solution was obtained. After stirring the mixture for 10 min at rt, 4-bromo-2-fluorobenzonitrile **11** (1.50 g, 7.50 mmol) was added as a solution in DMF (40 mL). After the mixture turned into a white suspension (~ 10 min), it was stirred overnight at rt. Water (100 mL) was added and the product was extracted with Et_2O (30 mL × 3). The combined organic phase was washed with water (50 mL × 5). After layer separation the organic fraction was dried over anhydrous $MgSO_4$ and the solvent was removed under vacuum. The crude product was purified using flash column chromatography (silica gel, 25% CH_2Cl_2 in hexanes) to give **12** as a white solid (1.88 g, 68%): m.p. 130–131 °C; FTIR (neat) 3062, 2934, 2850, 2218, 1738, 1716, 1572, 1540, 1454, 1376, 1086, 1066 cm^{-1}; ^1H NMR (400 MHz, $CDCl_3$) δ 7.59–7.55 (m, 2H), 7.49 (d, J = 8.3 Hz, 1H), 7.41 (dd, J_1 = 8.3 Hz, J_2 = 1.8 Hz, 1H), 7.39–7.34 (m, 2H), 7.21 (d, J = 1.8 Hz); ^{13}C NMR (100 MHz, $CDCl_3$) δ 143.83, 135.38, 134.59, 133.28, 132.17, 130.08, 129.74, 128.34, 124.19, 116.13, 111.34; HRMS (APCI) m/z calcd for $[M]^+$ $C_{13}H_7Br_2NS$ 366.8660, found 366.8669.

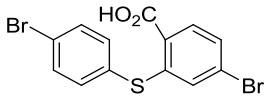

4-Bromo-2-(4-bromophenylthio)benzoic acid (13). A 250 mL round-bottom flask equipped with a stir bar and condenser was charged with **12** (1.80 g, 4.87 mmol). EtOH (72 mL) was added via syringe, followed by addition of 20% $NaOH_{(aq)}$ (90 mL). The mixture was stirred at reflux overnight, and the resulting yellow solution was cooled to rt. The mixture was acidified to pH ~3 using 4 M $HCl_{(aq)}$ and ether (150 mL) was added. The layers were separated, and the aqueous layer was extracted with ether (50 mL ×2). The combined organic phase was dried over $MgSO_4$ and the solvent was removed by rotary evaporation. Recrystallization of the crude product from boiling EtOH (20 mL) afforded **13** as a white solid (1.42 g, 77%): mp 209−211 °C; FTIR (neat) 3074, 2918, 2900–2500 (br), 1678, 1572, 1536, 1458, 1416, 1386, 1270, 1250, 1150, 1092, 1066, 1050, 1008 cm^{-1}; ^1H NMR (400 MHz, d_6-acetone) δ 7.97 (d, J = 8.3 Hz, 1H), 7.78–7.73 (m, 2H), 7.59–7.54 (m, 2H), 7.43 (dd, J_1 = 8.3 Hz, J_2 = 1.9 Hz, 1H), 6.90 (d, J = 1.9 Hz, 1H); ^{13}C NMR (100 MHz, d_6-acetone) δ 166.64, 145.76, 138.00, 133.93, 133.47, 131.98, 129.67, 128.31, 127.60, 126.58, 124.45; HRMS (ESI) *m*/*z* calcd for $[M-H]^-$ $C_{13}H_7Br_2O_2S$ 384.8545, found 384.8532.

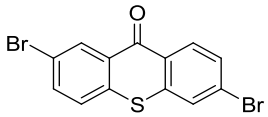

2,6-Dibromo-9*H*-thioxanthen-9-one (14). A 250 mL round-bottom flask equipped with a stir bar was charged with acid **13** (1.22 g, 3.14 mmol). Under a nitrogen atmosphere, hexanes (95 mL) were added, followed by oxalyl chloride (17.0 mL, 199 mmol) and

DMF (1 mL). The mixture was stirred at rt overnight. A clear solution and a white precipitate formed. The solution was decanted, and the solvent was removed by rotary evaporation. The acyl chloride intermediate was dissolved in 1,2-dichloroethane (150 mL). Under N_2, the resultant solution was cooled to 0 ℃. Aluminum chloride was added (788 mg, 5.92 mmol) to the reaction flask and the mixture was stirred at 0 ℃ for 1 h. The reaction was quenched with saturated $NH_4Cl_{(aq)}$ (20 mL) and the organic layer was collected and dried over $MgSO_{4(s)}$. The crude product was obtained by evaporating the organic layer. Recrystallization from boiling toluene (150 mL) afforded **14** as a pale yellow solid (583 mg, 53%): m.p. >250 ℃; FTIR (neat) 3016, 2970, 2904, 2850, 1788, 1626, 1576, 1452, 1366, 1228, 1216, 1092 cm^{-1}; ^1H NMR (500 MHz, $CDCl_3$) δ 8.73 (dd, J_1 = 2.3 Hz, J_2 = 0.4 Hz, 1H), 8.46 (dd, J_1 = 8.7 Hz, J_2 = 0.4 Hz, 1H), 7.76 (dd, J_1 = 1.9 Hz, J_2 = 0.4 Hz, 1H), 7.75 (dd, J_1 = 8.6 Hz, J_2 = 2.3 Hz, 1H), 7.61 (dd, J_1 = 8.7 Hz, J_2 = 1.9 Hz, 1H), 7.47 (dd, J_1 = 8.6 Hz, J_2 = 0.4 Hz, 1H); ^{13}C NMR (125 MHz, $CDCl_3$) δ 178.23, 138.45, 135.59, 135.35, 132.53, 131.57, 130.32, 130.18, 128.37, 128.07, 127.60, 127.59, 120.73; HRMS (ESI) *m*/*z* calcd for $[M+H]^+$ $C_{13}H_7Br_2OS$ 368.8584, found 368.8580.

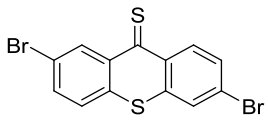

2,6-Dibromo-9*H*-thioxanthene-9-thione (15). An oven-dried round-bottom flask equipped with a reflux condenser was charged with **14** (370 mg, 1.0 mmol) and P_4S_{10} (1.33 g, 3.00 mmol). Toluene (30 mL) was added via syringe, and the suspension was heated to reflux overnight. The suspension was filtered while hot, and the filtrate was

collected. Upon cooling the desired compound precipitated as a brown solid (270 mg, 70%): m.p. 218–219 °C; FTIR (neat) 3070, 2994, 1634, 1582, 1572, 1544, 1518, 1444, 1376, 1304, 1256, 1176, 1156, 1134 1102, 1024 cm^{-1}; ^{1}H NMR (500 MHz, $CDCl_3$) δ 9.10 (dd, J_1 = 2.2 Hz, J_2 = 0.4 Hz, 1H), 8.80 (dd, J_1 = 9.0 Hz, J_2 = 0.4 Hz, 1H), 7.74 (dd, J_1 = 2.0 Hz, J_2 = 0.4 Hz, 1H), 7.72 (dd, J_1 = 8.5 Hz, J_2 = 2.2 Hz, 1H), 7.54 (dd, J_1 = 9.0 Hz, J_2 = 2.0 Hz, 1H), 7.45 (dd, J_1 = 8.5 Hz, J_2 = 0.4 Hz, 1H); ^{13}C NMR (125 MHz, $CDCl_3$) δ 208.37, 138.37, 136.08, 135.64, 135.00, 134.68, 132.81, 130.82, 129.80, 128.19, 128.00, 127.50, 121.65; HRMS (APCI) *m*/*z* calcd for $[M]^+$ $C_{13}H_7Br_2S_2$ 384.8350, found 384.8358.

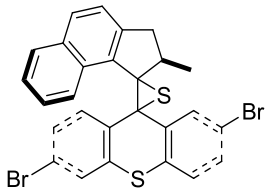

Episulfide 17. To an oven dried three-neck round-bottom flask charged with hydrozone **16**[21] (550 mg, 2.62 mmol) and $MgSO_{4(s)}$ (275 mg, 3.92 mmol) was added CH_2Cl_2 (20 mL). To this suspension was added quickly MnO_2 (1.56 g, 18.0 mmol) at *ca*. 5 °C. The reaction flask was immediately immersed and stirred in a cold bath ranging from −15 °C to −10 °C for 1.5 h. After this period, the reaction mixture was cooled to −50 °C and then transferred to a Schlenk filtration tube connected to an oven dried three-neck round-bottom flask. The deep-purple filtrate that contained the intermediate was collected, and the Schlenk tube was rinsed with pre-cooled CH_2Cl_2 (10 mL, −50 °C). To the flask containing the combined filtrate, thione **15** (320 mg, 0.83 mmol) was added portionwise until no more N_2 evolved. The mixture was stirred for an additional 0.5 h at ambient

temperature. The organic phase was evaporated and the residue was purified by column chromatography (silica gel, 10% CH_2Cl_2 in hexanes) to yield the desired compound as a white solid (375 mg, 80%). The pure *trans*-isomer could be isolated in small quantity by reprecipitation of the chromatographically purified product from CH_2Cl_2 and MeOH. The purified product was dissolved in a mixture of CH_2Cl_2 (5 mL) and MeOH (20 mL), and placed in a flask on a rotary evaporator. The CH_2Cl_2 was partially removed under vacuum without heating unitl a precipitate started to form. The solid was filtered, collected, and dried under vacuum and was identified as a pure *trans*-**17** by NMR. Characterization data for *trans*-**17**: m.p. 201–203 °C; FTIR (neat) 3076, 2966, 2932, 1578, 1516, 1452, 1430, 1384, 1370, 1082 cm^{-1}; ^1H NMR (500 MHz, $CDCl_3$) δ 8.92–8.88 (m, 1H), 8.00 (d, J = 2.1 Hz, 1H), 7.57 (d, J = 1.9 Hz, 1H), 7.57–7.53 (m, 2H), 7.54 (d, J = 8.2 Hz, 1H), 7.43 (dd, J_1 = 8.3 Hz, J_2 = 2.0 Hz, 1H), 7.37 (ddd, J_1 = 8.7 Hz, J_2 = 6.8 Hz, J_3 = 1.4 Hz, 1H), 7.23 (ddd, J_1 = 8.7 Hz, J_2 = 6.8 Hz, J_3 = 1.4 Hz, 1H), 7.18 (d, J = 8.2 Hz, 1H), 6.84 (dd, J_1 = 8.2 Hz, J_2 = 2.1 Hz, 1H), 6.77 (d, J = 8.2 Hz, 1H), 3.42 (dd, J_1 = 15.4 Hz, J_2 = 6.5 Hz, 1H), 2.43 (d, J = 15.4 Hz, 1H), 1.53 (qd, J_1 = 7.0 Hz, J_2 = 6.5 Hz, 1H), (d, J = 7.0 Hz, 3H); ^{13}C NMR (125 MHz, $CDCl_3$) δ 142.44, 138.17, 137.82, 136.43, 134.03 (CH), 134.01, 132.63, 130.83, 130.80, 130.43 (CH), 129.77 (CH), 129.63 (CH), 129.38 (CH), 129.35 (CH), 127.81 (CH), 127.67 (CH), 124.49 (CH), 124.35 (CH), 123.99 (CH), 123.47 (CH), 120.71, 120.03, 72.10, 60.92, 40.45 (CH), 38.06 (CH_2), 21.74 (CH_3); HRMS (APCI) m/z calcd for $[M+H]^+$ $C_{27}H_{18}S_2Br_2$ 564.9289, found 564.9296.

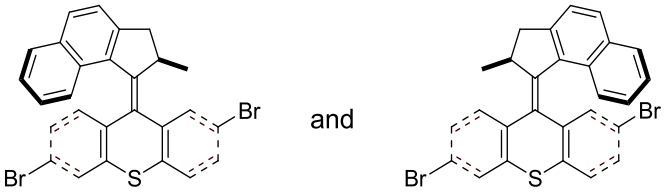

(2,6-Dibromo-9-(2-methyl-2,3-dihydro-1*H*-cyclopenta[a]naphthalen-1-ylidene)-2,3,4,5,6,7,8,9-octahydro-1*H*-thioxanthene (mixture of *cis*- and *trans*-motor 9). A 100 mL screw-capped tube equipped with a stir bar was charged with episulfide **17** (225 mg, 0.400 mmol). Trimethyl phosphite (4.0 mL, 34 mmol) was added and the screw-capped tube was assembled. The mixture was stirred at 130 ℃ for 16 h. After cooling to rt, MeOH (30 mL) was added with vigorous stirring for 5 min. The precipitate was filtered and washed with MeOH (20 mL). The solid was purified by column chromatography (silica gel, 10% CH_2Cl_2 in hexanes) to afford **9** as a light yellow solid (207 mg, 97%): FTIR (neat) 3048, 2922, 2662, 2840, 1605, 1576, 1538, 1448, 1374, 1176, 1154, 1082 cm^{-1}; HRMS (APCI) m/z calcd for $[M+H]^+$ $C_{27}H_{18}Br_2S$ 532.9569, found 532.9577. The ^1H NMR assignments are in Figure 3.5.

^{13}C assignments of 2,6-dibromomolecular motor **9**:

cis-**9**: Initially the major component

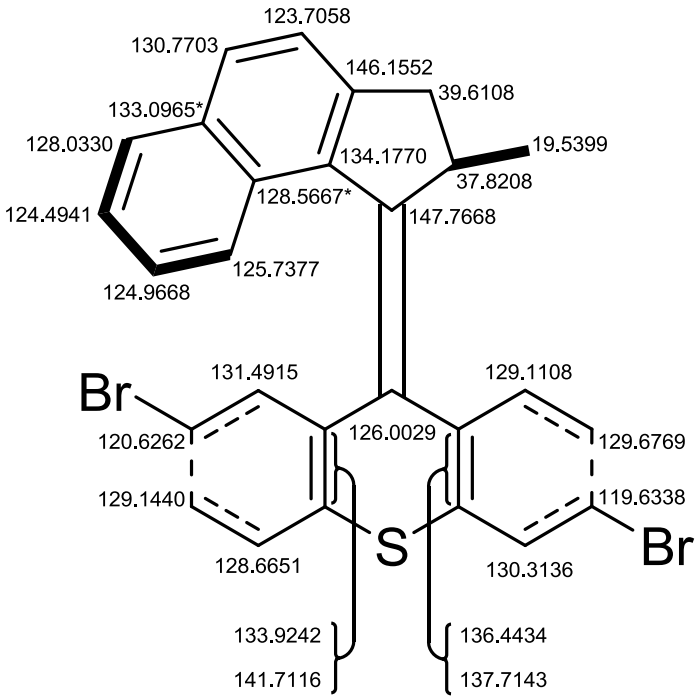

trans-**9**: Initially the minor component

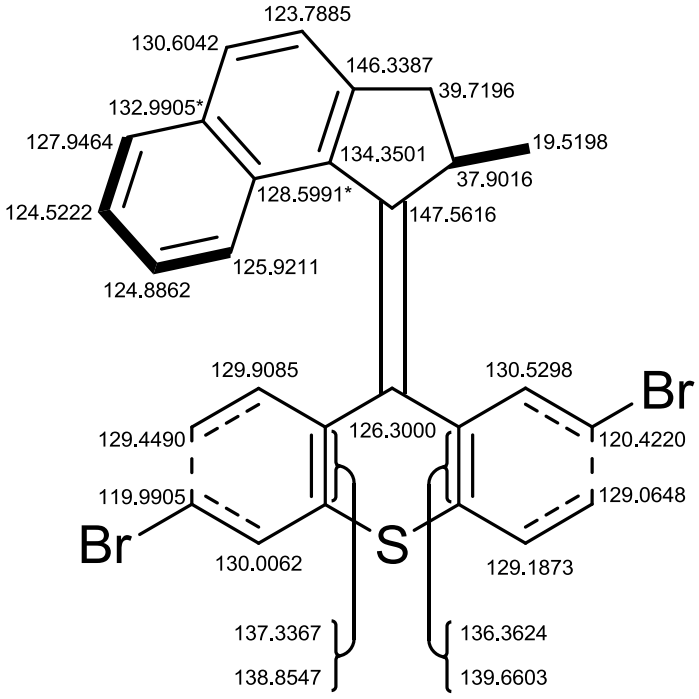

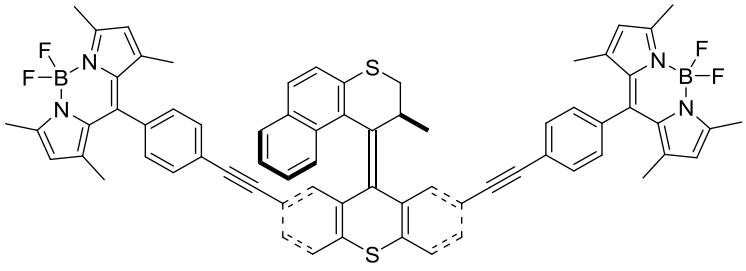

Slow-Motor BODIPY Hybrid 18. An oven dried 10 mL Schlenk-tube equipped with a stir bar was charged with motor **19** (31 mg, 0.70 mmol), BODIPY **20**[31] (124 mg, 0.280 mmol), $Pd(PPh_3)_4$ (8.0 mg, 0.0070 mmol), and CuI (2.6 mg, 0.014 mmol). THF (1.5 mL) and NEt_3 (0.50 mL) were added and the reaction mixture was stirred at 60 ℃ for 16 h. After cooling to rt, the reaction was quenched with saturated $NH_4Cl_{(aq)}$ (20 mL) and extracted with CH_2Cl_2 (30 mL). The organic phase was washed with water (30 mL), dried over anhydrous $MgSO_4$, filtered, and the filtrate was concentrated under vacuum. The crude product was purified by column chromatography (silica gel, 40% to 50% CH_2Cl_2 in hexanes) to yield **18** as an orange solid (30 mg, 40%): m.p. 175 ℃ (decomp.); FTIR (neat) 3052, 2922, 2852, 1542, 1510, 1468, 1410, 1370, 1306, 1260, 1210, 1154, 1120, 1082, 1052 cm^{-1}; ^1H NMR (500 MHz, $CDCl_3$) δ 7.79 (d, J = 1.7 Hz, 1H), 7.74–7.70 (m, 2H), 7.67 (br d, J = 8.7 Hz, 1H), 7.60 (d, J = 8.0 Hz, 1H), 7.62 (br d, J = 8.0 Hz, 1H), 7.54 (br d, J = 8.4 Hz, 1H), 7.50 (dd, J_1 = 8.0 Hz, J_2 = 1.7 Hz, 1H), 7.45 (J = 8.5 Hz, 1H), 7.46–7.43 (m, 2H), 7.35–7.31 (m, 2H), 7.27 (dd, J_1 = 8.0 Hz, J_2 = 0.4 Hz, 1H), 7.24–7.21 (m, 2H), 7.16 (ddd, J_1 = 8.0 Hz, J_2 = 6.9 Hz, J_3 = 1.1 Hz, 1H), 7.05 (ddd, J_1 = 8.3 Hz, J_2 = 7.0 Hz, J_3 = 1.3 Hz, 1H), 6.92 (dd, J_1 = 8.1 Hz, J_2 = 1.8 Hz, 1H), 6.52 (dd, J_1 = 1.8 Hz, J_2 = 0.4 Hz, 1H), 6.01 (s, 2H), 5.99 (s, 2H), 4.18 (dqd, J_1 = 7.5 Hz, J_2 = 6.9 Hz, J_3 = 3.5 Hz, 1H), 3.77 (dd, J_1 = 11.5 Hz, J_2 = 7.5 Hz, 1H), 3.11 (dd, J_1 = 11.5 Hz, J_2 = 3.5 Hz, 1H), 2.57 (s, 6H), 2.56 (s, 6H), 1.46 (s, 2H), 1.40 (s, 2H), 0.85 (d, J = 6.9 Hz, 3H); ^{13}C

NMR (125 MHz, $CDCl_3$) δ 155.85, 155.74, 142.98, 142.96, 140.83, 140.68, 138.38, 137.96, 136.71, 135.82, 135.57, 135.24, 134.77, 134.70, 132.38 (CH), 132.13 (CH), 132.11 (CH), 131.68, 131.19 (overlapping of two signals, both quaternary carbons), 130.93, 130.83, 130.62, 130.59 (CH), 130.09 (CH), 129.23 (CH), 128.34 (CH), 128.08 (CH), 127.87 (CH), 127.85 (CH), 127.83 (CH), 126.42 (CH), 126.06 (CH), 125.61 (CH), 124.57 (CH), 124.03, 123.93 (CH), 123.83, 121.40 (CH), 121.33 (CH), 121.07, 120.21, 90.28, 89.84, 89.70, 88.49, 37.22 (CH_2), 32.93 (CH), 19.33 (CH_3), 14.65 (CH_3), 14.63 (overlapping of two signals, both CH_3 carbons), 14.61 (CH_3). MS (MALDI) m/z calcd for $[M]^+$ $C_{69}H_{54}B_2F_4N_4S_2$ 1100.4, found 1100.3.

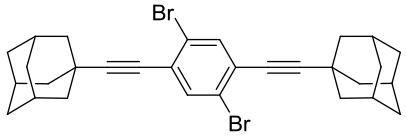

1,4-Bis(1-adamantylethynyl)-2,5-dibromodobenzene (28). A 50 mL round-bottom flask equipped with a stir bar was charged with 2,5-dibromo-1,4-diiobenzene (**26**) (980 mg, 2.0 mmol), 1-ethynyladamantane (**27**)[13] (670 mg, 4.2 mmol), $Pd(PPh_3)_2Cl_2$ (71 mg, 0.10 mmol), and CuI (38 mg, 0.20 mmol). THF (5.0 mL) was added and the mixture was cooled to 0 ℃. NEt_3 (2.0 mL) was added at 0 ℃, and the reaction was allowed to stir overnight while gradually warming to rt; solids formed upon stirring. The mixture was combined with saturated $NH_4Cl_{(aq)}$ (20 mL) and extracted with ether (50 mL). The remaining non-dissolved solids were collected by filtration and washed thoroughly with ether (50 mL). The solid was dried under vacuum and collected as the desired compound. The remaining organic phase was concentrated under vacuum then purified by column chromatography (silica gel; 4% CH_2Cl_2 in hexanes) to afford another fraction of pure

compound. The two fractions were combined as a white solid (958 mg, 87%): m.p. 240 °C (decomp); FTIR (neat) 2918, 2900, 2658, 2228, 1470, 1450, 1360, 1344, 1312, 1254, 1180, 1098, 1060 cm^{-1}; ^{1}H NMR (500 MHz, $CDCl_3$) δ 7.58 (s, 2H), 2.03–1.97 (m, 18H), 1.75–1.70 (m, 12H); ^{13}C NMR (125 MHz, $CDCl_3$) δ 135.75 (CH), 126.32, 123.71, 105.69, 77.34, 42.47 (CH_2), 36.32 (CH_2), 30.52, 27.90 (CH); MS (MALDI) *m*/*z* calcd for $C_{30}H_{32}Br_2$ $[M]^+$ 552.1, found 552.0.

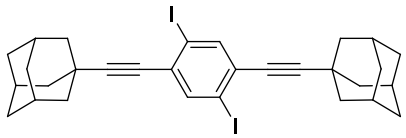

1,4-Bis(1-adamantylethynyl)-2,5-diiodobenzene (29). An oven-dried three-necked round-bottom flask equipped with a stir bar charged with the dibromoaxle **28** (720 mg, 1.3 mmol) and THF (12 mL) was cooled to −78 °C. To the flask was added dropwise a solution *tert*-butyllithium solution (1.7 M, 3.5 mL, 6.0 mmol) dropwise. The mixture was stirred at −78 °C for 1 h during which time the colorless suspension gradually became red. 1,2-diiodoethane (1.10 g, 3.90 mmol) was added in one portion, and the mixture was allowed to gradually warm and stir overnight. The non-dissolved solids were filtered, washed with ether (50 mL), collected, and dried under vacuum. The organic phase was washed with saturated $NaSO_{3(aq)}$ and evaporated under vacuum to yield a white solid. The two solids were combined and used without further purifications (790 mg, 94%): m.p. > 250 °C; FTIR (neat) 2900, 2846, 2224, 1460, 1450, 1340, 1312, 1254, 1180, 1098, 1046 cm^{-1}; ^{1}H NMR (500 MHz, $CDCl_3$) δ 7.79 (s, 2H), 2.02–1.96 (m, 18H), 1.74–1.70 (m, 12H); ^{13}C NMR (125 MHz, $CDCl_3$) δ 140.84 (CH), 130.68, 104.75, 100.17, 80.78, 42.44

(CH_2), 36.32 (CH_2), 30.51, 27.88 (CH); MS (MALDI) *m*/*z* calcd for $C_{30}H_{32}Br_2$ $[M]^+$ 552.1, found 552.0.

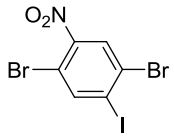

1,4-Dibromo-2-iodo-5-nitrobenzene (32). A 250 mL round-bottom flask equipped with a stir bar was charged with a solution of 2,5-dibromoaniline **31**[29] (10.4 g, 35.0 mmol) in ether (150 mL) and cooled to −30 °C. $BF_3{\cdot}OEt_2$ (17.6 mL, 140 mmol) was added and the mixture was stirred at −30 °C for 30 min. *tert*-Butylnitrite (16.8 mL, 122 mmol) was added and the reaction mixture was stirred for another 30 min at −30 °C. The diazonium salt that formed was filtered, washed with ether (50 mL) and quickly transferred to a 250 mL three-neck round-bottom flask. The diazonium salt was dissolved in CH_3CN (100 mL), and NaI (10.5 g, 70.0 mmol) was added to the solution in portions. The reaction was stirred for 1 h, and the organic solvent was removed under vacuum. The mixture was combined with ether (250 mL), and the organic phase washed with saturated $NaSO_{3(aq)}$ (50 mL) and water (150 mL). The organic phase was dried over anhydrous $MgSO_4$ and concentrated under vacuum. The crude compound was purified by column chromatography (silica gel; 2% to 3% CH_2Cl_2 in hexanes) to afford the desired compound as a white solid (10.4 g, 72%): m.p. 110–111 °C; FTIR (neat) 2846, 1564, 1540, 1510, 1460, 1430, 1338, 1310, 1262, 1136, 1106, 1042 cm^{-1}; ^1H NMR (500 MHz, $CDCl_3$) δ 8.26 (d; *J* = 0.2 Hz, 1H), 8.08 (d; *J* = 0.2 Hz, 1H); ^{13}C NMR (125 MHz, $CDCl_3$) δ 149.41 (significantly broader signal which corresponds to the carbon attached to the NO_2 group), 145.28 (CH), 129.57, 128.63 (CH), 113.44, 107.74; HRMS (APCI) *m*/*z*

calcd for $[M]^-$ $C_6H_2NO_2Br_2I$ 404.7502, found 404.7502. *Caution: The diazonium salt is potentially explosive. Handling behind a blast shield is recommended.*

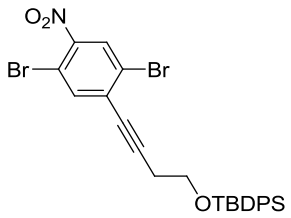

2,5-Dibromo-4-(4-(*tert*-butyldiphenylsilyloxy)but-1-ynyl)nitrobenzene (33). A 25 mL oven-dried round-bottom flask equipped with a stir bar was charged with the nitrobenzene **32** (2.03 g, 5.00 mmol), $Pd(PPh_3)_2Cl_2$ (33 mg, 0.050 mmol), and CuI (190 mg, 1.0 mmol). THF (15 mL), NEt_3 (5 mL) and 4-(*tert*-butyldiphenylsilyloxy)-1-butyne (1.56 mL, 5.00 mmol) was added. The reaction was stirred at rt overnight. The resulting mixture was partitioned between saturated $NH_4Cl_{(aq)}$ (50 mL) and CH_2Cl_2 (50 mL). The organic phase was washed with water (50 mL), brine (20 mL), dried over anhydrous $MgSO_4$, and concentrated under vacuum. The crude compound was purified by column chromatography (silica gel; 15% CH_2Cl_2 in hexanes) to afford the desired compound as a brown oil (2.35 g, 80%): FTIR (neat) 2956, 2932, 2856, 2232, 1556, 1520, 1472, 1460, 1428, 1384, 1336, 1270, 1106, 1070 cm^{-1}; ^1H NMR (500 MHz, $CDCl_3$) δ 8.08 (d, J = 0.3 Hz), 7.71 (d, J = 0.3 Hz, 1H), 7.70–7.65 (m, 4H), 7.46–7.35 (m, 6H), 3.90 (t, J = 6.6 Hz, 2H), 2.75 (t, J = 6.6 Hz, 2H), 1.07 (s, 9H); ^{13}C NMR (125 MHz, $CDCl_3$) δ 138.74 (CH), 135.57 (CH), 133.36 (overlapping of two signals, both CH carbons), 131.63, 129.80 (CH), 129.19 (CH), 127.75 (CH), 124.27, 112.96, 99.12, 78.21, 61.82 (CH_2), 26.78 (CH_3), 23.95 (CH_2), 19.24; HRMS (APCI) *m*/*z* calcd for $[M]^-$ $C_{26}H_{25}Br_2NO_3Si$ 584.9976, found 584.9982. The side product 2,5-dibromonitrobenzene was identified by GC/mass.

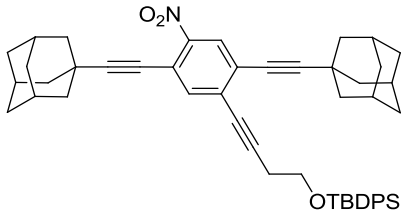

2,5-Bis(1-adamantylethynyl)-4-(4-(*tert*-butyldiphenylsilyloxy)but-1-ynyl)nitrobenzene (34). A 100 mL screw-capped tube was charged with **33** (2.35 g, 4.00 mmol), $Pd(PhCN)_2Cl_2$ (92 mg, 0.24 mmol), 1-ethylnyladamantane (1.92 g, 12.0 mmol), HP*t*-Bu_3BF_4 (139 mg, 0.480 mmol), CuI (91 mg, 0.48 mmol), THF (10 mL) and NEt_3 (10 mL). The reaction was stirred at 60 °C for 12 h and then cooled to rt. The mixture was combined with saturated $NH_4Cl_{(aq)}$ (30 mL) and partitioned between Et_2O (50 mL). The organic phase was washed with water (50 mL), brine (20 mL), dried over $MgSO_4$, and filtered, and the filtrate was concentrated under vacuum. The crude product was purified by column chromatography (silica gel, 20% CH_2Cl_2 in hexanes) to afford the desired product **34** as a slightly yellow solid (2.75 g, 92%): m.p. 88–91 °C; FTIR (neat) 2904, 2852, 2226, 1600, 1546, 1512, 1482, 1450, 1428, 1336, 1316, 1272, 1110 cm^{-1}; ^1H NMR (500 MHz, $CDCl_3$) δ 7.96 (d, *J* = 0.4 Hz), 7.70–7.65 (m, 4H), 7.49 (d, *J* = 0.4 Hz), 7.44–7.35 (m, 6H), 3.90 (t, *J* = 7.2 Hz), 2.75 (t, *J* = 7.2 Hz), 2.05–1.85 (m, 18H), 1.75–1.60 (m, 12H), 1.07 (s, 9H); ^{13}C NMR (125 MHz, $CDCl_3$) δ 147.96, 137.56 (CH), 135.51 (CH), 133.44 (two signals overlapping), 130.62, 129.76 (CH), 127.74 (CH), 127.49 (CH), 126.00, 117.83, 108.02, 105.70, 95.82, 78.99, 74.81, 62.30 (CH_2), 42.48 (CH_2), 42.19 (CH_2), 36.28 (CH_2), 36.24 (CH_2), 30.65, 30.38, 27.83 (CH_2), 27.81 (CH), 26.80 (CH), 23.85 (CH_2), 19.24; MS (MALDI) *m*/*z* calcd for $[M+H]^+$ $C_{50}H_{56}NO_3Si$ 746.4, found 746.3.

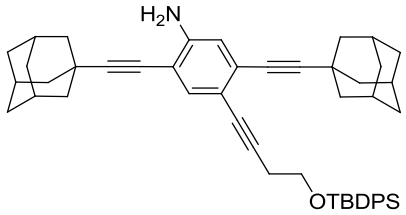

2,5-Bis(1-adamantylethynyl)-4-(4-(*tert*-butyldiphenylsilyloxy)but-1-ynyl)aniline (35). A 100 mL three-neck round-bottom flask equipped with a stir bar was charged with axle **34** (370 mg, 0.50 mmol), EtOH (5 mL), and THF (5 mL). $SnCl_2 \cdot H_2O$ (680 mg, 3.0 mmol) was added in portions, and the mixture was stirred overnight. The organic phase was removed under vacuum, and CH_2Cl_2 (50 mL) was added. The organic phase was passed through a celite plug. The reaction mixture was washed with CH_2Cl_2 (50 mL), and the organic phase was passed through the celite plug. The filtrate was collected, dried under vacuum, and purified by column chromatography (silica gel, 30% CH_2Cl_2 in hexanes) to afford the target compound as a white powder (200 mg, 56%): m.p. 92–94 °C; FTIR (neat) 3482, 3386, 2902, 2850, 2162, 1980, 1612, 1536, 1494, 1428, 1314, 1110 cm^{-1}; ^1H NMR (500 MHz, $CDCl_3$) δ 7.70–7.66 (m, 4H), 7.44–7.35 (m, 6H), 7.23 (d, *J* = 0.4 Hz), 6.66 (d, *J* = 0.4 Hz), 4.14 (br s, 2H), 3.88 (t, *J* = 7.6 Hz), 2.71 (t, *J* = 7.6 Hz), 2.05–1.85 (m, 18H), 1.75–1.60 (m, 12H); ^{13}C NMR (125 MHz, $CDCl_3$) δ 146.35, 135.52 (CH), 135.30 (CH), 133.67, 129.62 (CH), 127.67 (CH), 126.47, 116.57 (CH), 115.56, 108.35, 105.10, 102.46, 87.29, 80.26, 78.35, 74.90, 62.93 (CH_2), 42.99 (CH_2), 42.75 (CH_2), 36.34 (CH_2), 36.31 (CH_2), 30.43, 30.22, 27.96 (CH), 27.93 (CH), 26.82 (CH_3), 23.73 (CH_2), 19.22; MS (MALDI) *m*/*z* calcd for $[M+H]^+$ $C_{50}H_{58}NOSi$ 716.4, found 716.3.

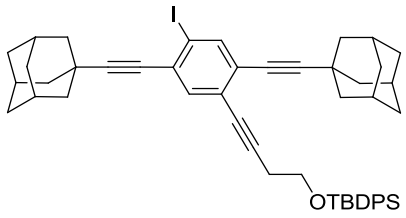

2,5-Bis(1-adamantylethynyl)-4-(4-(*tert*-butyldiphenylsilyloxy)but-1-ynyl)iodobenzene (25). To an oven-dried 50 mL three-neck round-bottom flask charged with **35** (360 mg, 0.50 mmol) in CH_3CN (2 mL) was added $NOBF_4$ at −30 °C. The mixture was allowed to stir for 30 min, and NaI (64 mg, 0.55 mmol) was added. The reaction mixture was warmed to rt, and the organic phase was removed under vacuum. The residue was combined H_2O (20 mL) and partitioned between CH_2Cl_2 (20 mL). The organic phase was washed with H_2O (30 mL), brine (10 mL), and dried under vacuum. The crude product was purified by column chromatography (silica gel, 5% to 10% CH_2Cl_2 in hexanes) to afford the desired product as a white solid (80 mg, 19%): m.p. 94–96 °C; FTIR (neat) 2900, 2850, 2226, 1982, 1614, 1490, 1450, 1428, 1374, 1316, 1190, 1110, 1030 cm^{-1}; ^1H NMR (500 MHz, $CDCl_3$) δ 7.79 (d, *J* = 0.4 Hz, 1H), 7.70–7.65 (m, 4H), 7.45-7.40 (m, 2H); 7.40–7.35 (m, 4H), 7.33 (d, *J* = 0.4 Hz, 1H), 3.88 (t, *J* = 7.4 Hz, 2H), 2.71 (t, *J* = 7.4 Hz, 2H), 2.05-1.80 (m, 18H), 1.75–1.60 (m, 12H), 1.06 (s, 9H); ^{13}C NMR (125 MHz, $CDCl_3$) δ 141.05 (CH), 135.52 (CH), 134.56 (CH), 133.55, 129.69 (CH), 129.17, 127.71 (CH), 126.37, 125.79, 104.41, 103.78, 99.63, 91.86, 81.49, 79.48, 76.94, 62.53 (CH_2), 42.62 (CH_2), 42.51 (CH_2), 36.35 (CH_2), 36.29 (CH_2), 30.46, 30.32, 27.91 (CH), 27.87 (CH), 26.81 (CH), 23.77 (CH_2), 19.23; MS (MALDI) *m*/*z* calcd for $[M+Na]^+$ $C_{50}H_{55}IOSiNa$ 716.4, found 716.3. Note: A protocol similar to synthesizing 2,5-dibromo-4-iodonitrobenzene **32** was tried. However, the diazonium salt intermediate was soluble in ether and thus no clean intermediate was obtained. This protocol only led to a

trace amount of **25**. It is known that $NOBF_4$ reacts with ethereal solvents, such as ether and THF.[32] Therefore, $NOBF_4$ might have reacted with the silyl-ether linkage and resulted in low yield of the product.

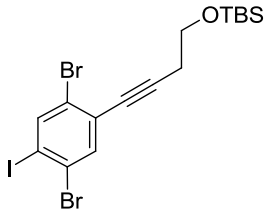

2,5-Dibromo-4-(4-(*tert*-butyldimethylsilyloxy)but-1-ynyl)iodobenzene (36). An oven-dried 25 mL round-bottom flask equipped with a stir bar was charged with 2,5-dibromo-1,4-diiobenzene (**26**) (1.25 g, 2.60 mmol), $Pd(PPh_3)_2Cl_2$ (42 mg, 0.06 mmol), and CuI (23 mg, 0.12 mmol). THF (4 mL) and NEt_3 (2 mL) were added, and the mixture was cooled to 0 ℃. 4-(*tert*-Butyldimethylsilyloxy)-but-1-yne (**30**) (0.41 mL, 2.0 mmol) was added at 0 °C. The reaction was stirred overnight while gradually warming up to rt. The resulting mixture was combined with saturated $NH_4Cl_{(aq)}$ (20 mL) and partitioned between CH_2Cl_2 (30 mL). The organic phase was dried over anhydrous $MgSO_4$ and concentrated under vacuum. The crude compound was purified by column chromatography (silica gel; 4% to 7% CH_2Cl_2 in hexanes) to afford the desired compound as a white solid (575 mg, 53%): m.p. 42–44 °C;FTIR 3080, 2950, 2928, 2882, 2856, 2236, 1470, 1444, 1424, 1384, 1326, 1252, 1216, 1100, 1056, 1004 cm^{-1} (neat); ^1H NMR (500 MHz, $CDCl_3$) δ 8.02 (d, *J* = 0.2 Hz, 1H), 7.64 (d, *J* = 0.2 Hz, 1H), 3.83 (t, *J* = 7.0 Hz, 1H), 2.66 (t, *J* = 7.0 Hz, 1H), 0.91 (s, 9H), 0.09 (s, 6H); ^{13}C NMR (125 MHz, $CDCl_3$) δ 142.43(CH), 136.00 (CH), 128.11, 127.30, 124.12, 100.54, 95.04, 78.61, 61.46

(CH_2), 25.87 (CH_3), 24.05 (CH_2), 18.32, −5.26 (CH_3); MS (MALDI) *m*/*z* calcd for $[M+Na]^+$ $C_{16}H_{21}Br_2IOSiNa$ 564.9, found 565.2.

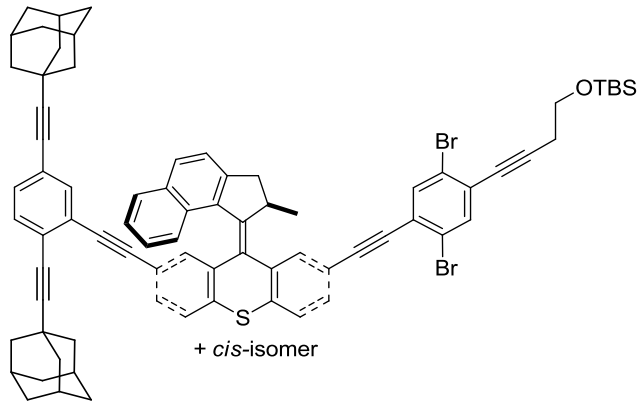

Nanocar precursor 37. An oven dried 10 mL Schlenk-tube equipped with a stir bar was charged with motor **24** (138 mg, 0.330 mmol)**,** iodoaxle **23** (338 mg, 0.650 mmol), the iodobenzene **36** (177 mg, 0.330 mmol), $Pd(PPh_3)_4$ (30 mg, 0.026 mmol), and CuI (10 mg, 0.052 mmol). NEt_3 (0.8 mL) and THF (2.5 mL) were added, and the mixture was stirred at 60 ℃ for 16 h. After cooling to rt, the mixture was partitioned between saturated $NH_4Cl_{(aq)}$ (20 mL) and CH_2Cl_2 (30 mL). The organic phase was washed with water (30 mL), dried over anhydrous $MgSO_4$, filtered, and the filtrate was concentrated under vacuum. The crude product was purified by column chromatography (silica gel, 20% to 30% CH_2Cl_2 in hexanes) to yield **37** as a yellow solid (155 mg, 39%): FTIR (neat) 2902, 2850, 2222, 1476, 1450, 1386, 1356, 1318, 1250, 1100, 1068 cm^{-1}; ^1H NMR (500 MHz, $CDCl_3$) δ 7.98 (d, *J* = 1.7 Hz, 0.5H), 7.92 (d, *J* = 1.6 Hz, 0.5H), 7.79–7.75 (m, 1.5H), 7.79–7.69 (m, 1H), 7.67 (br s, 0.5H), 7.61–7.57 (m, 1H), 7.59 (dd, J_1 = 1.7 Hz, J_2 = 0.5 Hz, 0.5 H), 7.57 (d, *J* = 0.3 Hz, 0.5H), 7.56 (d, *J* = 0.3 Hz, 0.5H), 7.53 (br s, 0.5H), 7.46–7.40 (m, 2.5H), 7.34 (dd, J_1 = 8.1 Hz, J_2 = 0.5 Hz, 0.5H), 7.27–7.24 (m, 1H), 7.22 (dd, J_1

= 8.1 Hz, J_2 = 1.8 Hz, 0.5H), 7.22–7.16 (m, 1H), 7.19 (dd, J_1 = 8.0 Hz, J_2 = 0.5 Hz, 0.5H), 7.18 (dd, J_1 = 8.0 Hz, J_2 = 1.8 Hz, 0.5H), 7.13 (dd, J_1 = 8.1 Hz, J_2 = 1.7 Hz, 0.5H), 6.88 (dd, J_1 = 1.8 Hz, J_2 = 0.4 Hz, 0.5H), 6.88–6.82 (m, 2.5H), 4.30 (qd, J_1 = Hz, J_2 = Hz, 0.5H), 4.24 (qd, J_1 = Hz, J_2 = Hz, 0.5H), 3.85 (t, J = 7.0 Hz, 1H), 3.82 (t, J = 7.1 Hz, 1H), 3.67 (dd, J_1 = 15.5 Hz, J_2 = 6.2 Hz, 0.5H), 3.65 (dd, J_1 = 15.6 Hz, J_2 = 6.2 Hz, 0.5H), 2.71 (t, J = 7.1 Hz, 1H), 2.67 (t, J = 7.0 Hz, 1H), 2.664 (d, J = 15.6 Hz, 0.5H), 2.657 (d, J = 15.5 Hz, 0.5H), 2.02–1.90 (m, 15H), 1.84–1.80 (m, 3H), 1.76–1.64 (m, 12H), 0.92 (s, 4.5H), 0.90 (s, 4.5H), 0.84 (d, J = 6.9 Hz, 1.5H), 0.82 (d, J = 6.9 Hz, 1.5H), 0.11 (s, 3H), 0.09 (s, 3H); ^{13}C NMR (125 MHz, $CDCl_3$) δ 147.64, 146,58, 146.17, 146.09, 139.98, 139.94, 137.96, 137.53, 137.28, 136.60, 136.37 (CH), 136.09 (CH), 135.96, 135.89 (CH), 135.49 (CH), 135.44, 134.72 (CH), 134.56 (CH), 134.47, 134.28, 133.16, 133.12, 131.88 (CH), 131.75 (CH), 131.53 (CH), 131.31 (CH), 131.04 (CH), 131.01 (CH), 130.84 (CH), 130.79 (CH), 130.64 (CH), 130.58 (CH), 129.60 (CH), 129.24 (CH), 129.23 (CH), 129.18 (CH), 128.65, 128.16 (CH), 128.09 (CH), 127.90 (CH), 127.81 (CH), 127.52 (CH), 127.46 (CH), 126.95, 126.58, 126.55, 126.46, 125.85, 125.82, 125.80 (CH), 125.78 (CH), 125.56, 125.39, 125.38, 125.08, 124.97 (CH), 124.96 (CH), 124.91 (CH), 124.47 (CH), 124.46 (CH), 123.78, 123.69 (CH), 123.65, 123.62 (CH), 123.58, 123.34, 123.21, 122.91, 121.89, 121.86, 120.61, 120.50, 104.06, 103.76, 100.28, 100.04, 96.12, 95.67, 95.64, 95.31, 92.65, 92.18, 88.91, 88.20, 87.49, 86.75, 79.17, 79.13, 78.61, 78.59, 78.27, 78.08; 61.55 (CH_2), 61.54 (CH_2), 42.94 (CH_2), 42.75 (CH_2), 42.74 (CH_2), 42.74 (CH_2), 39.72 (CH_2), 39.71 (CH_2), 37.88, 37.83, 36.41(CH_2), 36.350 (CH_2), 36.346 (CH_2), 36.30 (CH_2), 30.49, 30.29, 30.16, 30.11, 27.99 (CH), 27.97 (CH), 27.96 (CH), 27.95 (CH), 25.89 (CH), 25.88 (CH), 24.13 (CH_2), 24.08 (CH_2), 19.63 (CH_3), 19.59 (CH_3), 18.34,

18.32, –5.24 (CH_3), –5.26 (CH_3); MS (MALDI) *m/z* calcd for $[M+H]^+$ $C_{77}H_{73}Br_2OSSi$ 1231.4, found 1231.1.

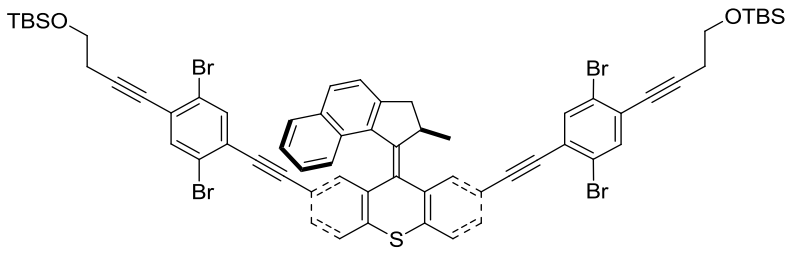

(4,4'-(4,4'-(9-(2-Methyl-2,3-dihydro-1H-cyclopenta[a]naphthalen-1-ylidene)-9H-thioxanthene-2,7-diyl)bis(ethyne-2,1-diyl)bis(2,5-dibromo-4,1-phenylene))bis(but-3-yne-4,1-diyl))bis(oxy)bis(*tert*-butyldimethylsilane) (38). The procedure is identical to that described for **37**. Motor **24** (42 mg, 0.10 mmol), iodoaxle **23** (104 mg, 0.200 mmol), the iodobenzene **36** (109 mg, 0.200 mmol), $Pd(PPh_3)_4$ (9.8 mg, 0.0080 mmol), and CuI (3.3 mg, 0.016 mmol), NEt_3 (0.3 mL) and THF (0.7 mL) were used. The product **38** was obtained as a yellow solid (89 mg, 71%): m.p. 194–196 °C; FTIR (neat) 2928, 2902, 2854, 2212, 1594, 1476, 1452, 1356, 1252, 1100, 1068, 1004 cm^{-1}; ^1H NMR (500 MHz, $CDCl_3$) δ 7.95 (d, J = 1.7 Hz, 1H), 7.79–7.75 (m, 2H), 7.71 (br d, J = 8.0 Hz, 1H), 7.67 (d, J = 0.2 Hz, 1H), 7.59 (d, J = 8.0 Hz, 1H), 7.56 (dd, J_1 = 8.1 Hz, J_2 = 0.4 Hz, 1H), 7.52 (d, J = 0.2 Hz, 1H), 7.44 (d, J = 8.2 Hz, 1H), 7.43 (dd, J_1 = 8.0 Hz, J_2 = 1.7 Hz, 1H), 7.43 (d, J = 0.2 Hz, 1H), 7.20 (ddd, J_1 = 8.1 Hz, J_2 = 6.4 Hz, J_3 = 1.6 Hz, 1H), 7.18 (dd, J_1 = 8.1 Hz, J_2 = 1.8 Hz, 1H), 6.87 (dd, J_1 = 1.8 Hz, J_2 = 0.5 Hz, 1H), 6.86 (ddd, J_1 = 8.5 Hz, J_2 = 6.4 Hz, J_3 = 1.2 Hz, 1H), 6.84–6.82 (m, 1H), 4.27 (td, J_1 = 6.9 Hz, J_2 = 6.2 Hz, 1H), 3.85 (t, J = 7.1 Hz, 2H), 3.82 (t, J = 7.0 Hz, 2H), 3.70 (dd, J_1 = 15.5 Hz, J_2 = 6.2 Hz, 1H), 2.71 (t, J = 7.0 Hz, 2H), 2.69–2.65 (m, 3H), 0.92 (s, 9H), 0.90 (s, 9H), 0.83 (d, J = 6.9 Hz, 3H), 0.11 (s, 6H), 0.09 (s, 6H); ^{13}C NMR (125 MHz, $CDCl_3$) δ 147.93, 146.19, 139.81,

137.59, 137.01, 136.37 (CH), 136.35, 136.08 (CH), 135.88 (CH), 135.48 (CH), 134.43, 133.15, 131.98 (CH), 130.90 (CH), 130.63 (CH), 129.37 (CH), 129.25 (CH), 128.63, 128.11 (CH), 127.89 (CH), 127.49 (CH), 126.97, 126.57, 126.22, 125.82, 125.78, 125.77 (CH), 124.99 (CH), 124.50 (CH), 123.81, 123.75 (CH), 123.65, 123.61, 123.34, 120.71, 120.57, 96.06, 95.64, 95.61, 95.32, 87.57, 86.82, 79.17, 79.13, 61.55 (CH_2), 61.53 (CH_2), 39.76 (CH_2), 37.85 (CH), 25.89 (CH), 25.88 (CH), 24.12 (CH_2), 24.08 (CH_2), 19.60 (CH), 18.34, 18.32, −5.24 (CH_3), −5.26 (CH_3); MS (MALDI) *m*/*z* calcd for $[M+H]^+$ $C_{63}H_{61}Br_4O_2SSi_2$ 1253.1, found 1253.0.

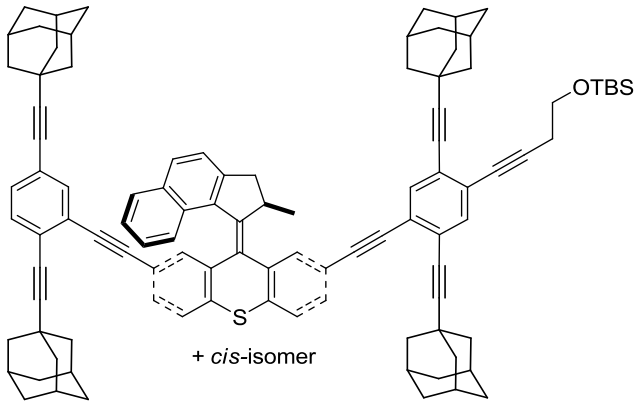

Nanocar 39. An oven dried 10 mL Schlenk-tube equipped with a stir bar was charged with nanocar precursor **37** (123 mg, 0.100 mmol)**,** 1-ethynyladamantane (**27**) (64 mg, 0.40 mmol), $Pd(PhCN)_2Cl_2$ (3.8 mg, 0.010 mmol), CuI (3.8 mg, 0.010 mmol), and HP*t*-Bu_3BF_4 (5.9 mg, 0.020 mmol). NEt_3 (1 mL) was added, and the mixture was stirred at 45 °C for 16 h. After cooling to rt, the mixture was partitioned between saturated $NH_4Cl_{(aq)}$ (20 mL) and CH_2Cl_2 (30 mL). The organic phase was washed with water (30 mL), dried over anhydrous $MgSO_4$, filtered, and the filtrate was concentrated under vacuum. The crude product was purified by column chromatography (silica gel, 20% to

30% CH_2Cl_2 in hexanes) to yield **39** as a yellow solid (128 mg, 92%): FTIR (neat) 2902, 2850, 2222, 1592, 1488, 1450, 1318, 1100 cm^{-1}; ^1H NMR (500 MHz, $CDCl_3$) δ 7.94 (d, *J* = 1.7 Hz, 0.5H), 7.92 (d, *J* = 1.6 Hz, 0.5H), 7.79–7.75 (d, *J* = 8.2 Hz, 1H, two sets of signals overlapping, the *J* value was measured as it appeared), 7.73–7.69 (d, *J* = 8.3 Hz, 1H, two sets of signals overlapping, the *J* value was measured as it appeared), 7.60–7.55 (m, 2H), 7.58 (dd, J_1 = 1.7 Hz, J_2 = 0.6 Hz, 0.5H), 7.56 (d, *J* = 0.5 Hz, 0.5H), 7.46 (d, *J* = 0.5 Hz, 0.5H), 7.44 (s, 0.5H), 7.43 (s, 0.5H), 7.42 (dd, J_1 = 7.9 Hz, J_2 = 1.8 Hz, 0.5H), 7.40 (dd, J_1 = 7.8 Hz, J_2 = 1.7 Hz, 0.5H), 7.34 (dd, J_1 = 8.1 Hz, J_2 = 0.6 Hz, 0.5H), 7.31 (d, *J* = 0.4 Hz, 0.5H), 7.25 (dd, J_1 = 8.1 Hz, J_2 = 1.7 Hz, 0.5H), 7.24 (dd, J_1 = 1.7 Hz, J_2 = 0.6 Hz, 0.5H), 7.217 (dd, J_1 = 7.9 Hz, J_2 = 1.7 Hz, 0.5H), 7.215 (d, *J* = 0.5 Hz, 0.5H), 7.21–7.16 (m, 1H), 7.20 (dd, J_1 = 7.9 Hz, J_2 = 1.8 Hz, 0.5H), 7.19 (dd, J_1 = 8.1 Hz, J_2 = 0.6 Hz, 0.5H), 7.13 (dd, J_1 = 8.0 Hz, J_2 = 1.7 Hz, 0.5H), 6.88-6.81 (m, 3H), 4.32-4.22 (m, 1H), 3.88–3.79 (m, 2H), 3.67–3.60 (dd, J_1 = 15.5 Hz, J_2 = 6.2 Hz, 1H, two sets of signals overlapping, the *J* value was measured as it appeared), 2.72–2.63 (m, 3H), 2.05–1.89 (m, 30H), 1.86–1.81 (m, 6H), 1.77–1.66 (m, 24H), 0.92 (s, 4.5H), 0.90 (s, 0.5H), 0.81 (d, *J* = 6.7 Hz, 3H, two sets of signals overlapping, the *J* value was measured as it appeared), 0.10 (s, 3H), 0.08 (s, 3H); ^{13}C NMR (125 MHz, $CDCl_3$) δ 147.33 (overlapping of two signals), 146.15, 146.13, 140.16, 140.11, 137.89, 137.85, 136.33, 136.15, 135.81, 135.63, 135.11 (CH), 134.79 (overlapping of two signals, both CH carbons), 134.72 (CH), 134.65 (CH), 134.64 (CH), 134.34, 134.34, 133.12 (overlapping of two signals, both quaternary carbons), 131.75 (CH), 131.45 (CH), 131.41 (CH), 131.34 (CH), 131.01 (CH), 130.87 (CH), 130.85 (CH), 130.72 (overlapping of two signals, both CH carbons), 130.61 (CH), 129.54 (CH), 129.52 (CH), 129.17 (CH), 129.13 (CH), 128.665, 128.660, 128.14 (CH),

128.13 (CH), 127.81 (CH), 127.79 (CH), 127.49 (CH), 127.47 (CH), 126.822, 126.817, 125.80 (CH), 125.78 (CH), 125.64, 125.56, 125.42, 125.36, 125.33, 125.23, 125.15, 125.08, 125.02, 124.89 (overlapping of two signals, both CH signals), 124.85, 124.54, 124.43 (overlapping of two signals, both CH carbons), 124.38, 123.62 (overlapping of two signals, both CH carbons), 123.19, 122.89, 121.83, 121.77, 121.69, 121.63, 104.16, 104.08, 103.86, 103.78, 103.75, 103.49, 100.26, 100.02, 93.82, 93.40, 92.67, 92.22, 92.21, 91.94, 88.82, 88.66, 88.15, 88.02, 80.00, 79.77, 78.61, 78.58, 78.24, 78.07, 77.67, 77.66, 77.62, 77.50, 62.08 (CH_2), 62.06 (CH_2), 42.91 (CH_2), 42.86 (CH_2), 42.80 (CH_2), 42.78 (CH_2), 42.76 (CH_2), 42.75 (CH_2), 42.73 (CH_2), 42.70 (CH_2), 39.71 (CH_2), 37.91 (CH), 36.39 (CH_2), 36.38 (CH_2), 36.35 (overlapping of four signals, all CH_2 carbons), 36.32 (CH_2), 36.31 (CH_2), 30.48, 30.46, 30.38, 30.32, 30.31, 30.29, 30.16, 30.10, 27.99 (CH), 27.96 (overlapping of three signals, all CH carbons), 27.96 (CH), 27.95 (overlapping of two signals, both CH carbons), 27.94 (CH), 25.91 (CH_3), 25.90 (CH_3), 24.06 (CH_2), 24.02 (CH_2), 19.56 (CH_3), 18.36, 18.34, −5.27 (CH_3), −5.29 (CH_3); MS (MALDI) *m*/*z* calcd for $[M]^+$ $C_{101}H_{102}OSSi$ 1390.7, found 1390.7.

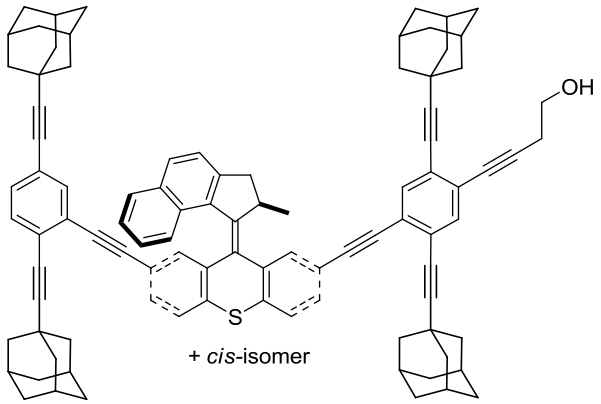

Nanocar 21. To an oven-dried 10 mL round-bottom flask charged with nanocar **39** (98 mg, 0.070 mmol) was added TBAF (0.08 mL, 1 M solution in THF) and THF (5 mL). The reaction was stirred for 1 h at room temperature. The mixture was partitioned between water (30 mL) and CH_2Cl_2 (25 mL). The organic layer was dried over $MgSO_4$, concentrated, and purified by column chromatography (silica gel, 50% CH_2Cl_2 in hexanes) to afford desired compound **21** as a pale yellow solid (67 mg, 74%): FTIR (neat) 3548, 2902, 2850, 2222, 1450, 1316, 1052 cm^{-1}; ^1H NMR (500 MHz, $CDCl_3$) δ 7.94 (d, *J* = 1.6 Hz, 0.5H), 7.93 (d, *J* = 1.7 Hz, 0.5H), 7.77 (d, *J* = 8.3 Hz, 1H, overlapping of two sets of signals, the *J* value was measured as it appeared), 7.71 (d, *J* = 8.2 Hz, 1H, overlapping of two sets of signals, the *J* value was measured as it appeared), 7.61–7.55 (m, 3H), 7.48 (br s, 0.5H), 7.45–7.42 (m, 1H), 7.42 (dd, J_1 = 8.1 Hz, J_2 = 1.7 Hz, 0.5H), 7.41 (dd, J_1 = 8.0 Hz, J_2 = 1.7 Hz, 0.5H), 7.36-7.32 (m, 1H), 7.26 (dd, J_1 = 8.0 Hz, J_2 = 1.7 Hz, 0.5H), 7.24–7.23 (m, 1H), 7.23–7.17 (m, 2.5H), 7.13 (dd, J_1 = 8.1 Hz, J_2 = 1.7 Hz, 0.5H), 6.88–6.82 (m, 3H), 4.32–4.24 (m, 1H), 3.88–3.76 (m, 2H), 3.64 (dd, J_1 = 15.5 Hz, J_2 = 6.1 Hz, 1H, overlapping of two sets of signals, the *J* value was measured as it appeared), 2.75 (t, *J* = 6.1 Hz, 1H), 2.67 (t, *J* = 6.1 Hz, 1H), 2.66 (d, *J* = 15.5 Hz, 1H, overlapping of two sets of signals, the *J* value was measured as it appeared), 2.05–1.80 (m, 36H), 1.77–1.65 (m, 24H), 0.82 (d, *J* = 6.8 Hz, 3H, overlapping of two sets of signals, the *J* value was measured as it appeared); ^{13}C NMR (125 MHz, $CDCl_3$) δ 147.35, 147.34, 146.17, 146.13, 140.17, 140.10, 137.90, 137.84, 136.41, 136.13, 135.90, 135.62, 135.12 (CH), 135.07 (CH), 134.93 (CH), 134.79 (CH), 134.71 (CH), 134.65 (CH), 134.330, 134.329, 133.12 (overlapping of two signals, both quaternary carbons), 131.76 (CH), 131.44 (CH), 131.42 (CH), 131.35 (CH), 131.02 (CH), 130.87 (CH), 130.86 (CH),

130.74 (CH), 130.72 (CH), 130.62 (CH), 129.55 (CH), 129.53 (CH), 129.18 (CH), 128.15 (CH), 128.66 (overlapping of two signals, both quaternary carbons), 128.13 (overlapping of two signals, both CH carbons), 127.83 (CH), 127.80 (CH), 127.51 (CH), 127.47 (CH), 126.82, 126.80, 125.79 (overlapping of two signals, both CH carbons), 125.55, 125.42, 125.41, 125.33, 125.26, 125.14, 125.02, 125.00, 124.96, 124.90 (overlapping of two signals, both CH carbons), 124.83, 124.67, 124.57, 124.44 (overlapping of two peaks, both CH carbons), 123.63 (CH), 123.61 (CH), 123.19, 122.90, 121.84, 121.78, 121.61, 121.56, 104.34, 104.08, 104.04, 104.01, 103.78, 103.75, 100.27, 100.03, 94.00, 93.58, 92.66, 92.20, 91.79, 91.50, 88.83, 88.56, 88.16, 87.93, 81.117, 81.111, 78.61, 78.58, 78.24, 78.07, 77.74, 77.70, 77.60, 77.42, 60.97 (CH_2), 60.94 (CH_2), 42.91 (CH_2), 42.85 (CH_2), 42.76 (CH_2), 42.75 (CH_2), 42.731 (CH_2), 42.725 (CH_2), 42.70 (CH_2), 42.69 (CH_2), 39.71 (CH_2), 37.92 (CH), 37.90 (CH), 36.40 (CH_2), 36.37 (CH_2), 36.35 (CH_2), 36.34 (CH_2), 36.32 (overlapping of two signals, both CH_2 carbons), 36.32 (CH_2), 36.30 (CH_2), 30.48, 30.47, 30.42, 30.36, 30.31, 30.30, 30.16, 30.10, 27.99 (CH), 27.962 (CH), 27.957 (CH), 27.955 (CH), 27.953 (CH), 27.946 (CH), 27.936 (CH), 27.93 (CH), 24.17 (CH_2), 24.14 (CH_2), 19.57 (overlapping of two signals, both CH_3 carbons); MS (MALDI) *m*/*z* calcd for $[M+Na]^+$ $C_{95}H_{88}OSNa$ 1299.7, found 1299.5.

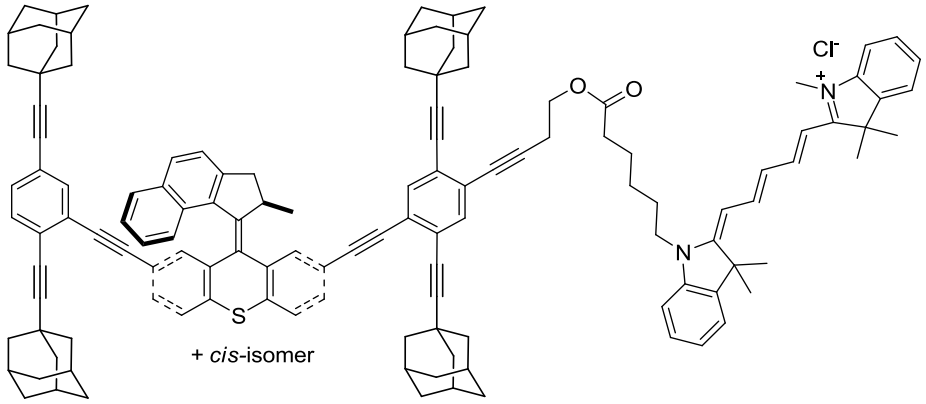

Cy5-tagged nanocar 20. An oven dried 10 mL Schlenk-tube equipped with a stir bar was charged with nanocar **21** (25.5 mg, 0.0200 mmol), cy5 dye **22** (12.5 mg, 0.0240 mmol), *N*,*N*′-dicyclohexylcarbodiimide (5.0 mg, 0.024 mmol) and 4-dimethylaminopyridine (2.6 mg, 0.024 mmol). CH_2Cl_2 (2 mL) was added, and the reaction was stirred at rt overnight in the absence of light. The mixture was purified by column chromatography (silica gel, 2% MeOH in CH_2Cl_2) to afford the cy5-tagged nanocar **20** as a blue solid (31.0 mg, 89%): FTIR (neat) 3404, 2902, 2850, 2220, 1732, 1480, 1450, 1370, 1334, 1216, 1144, 1090, 1040, 1016 cm^{-1}; ^1H NMR (500 MHz, $CDCl_3$) δ 8.09–8.01 (m, 2H), 8.00 (d, *J* = 1.7 Hz, 0.5H), 7.97 (d, *J* = 1.7 Hz, 0.5H), 7.813 (d, *J* = 8.2 Hz, 0.5H), 7.806 (d, *J* = 8.2 Hz, 0.5H), 7.78–7.73 (m, 1H), 7.66–7.60 (m, 2H), 7.57 (dd, J_1 = 1.7 Hz, J_2 = 0.6 Hz, 0.5H), 7.53 (d, *J* = 0.5 Hz, 0.5H), 7.50–7.47 (m, 1H), 7.46 (dd, J_1 = 8.0 Hz, J_2 = 1.7 Hz 0.5H), 7.44 (d, *J* = 0.5 Hz, 0.5H), 7.43–7.36 (m, 4.5H), 7.34 (d, *J* = 0.6 Hz, 0.5H), 7.29 (d, *J* = 0.5 Hz, 0.5H), 7.29–7.20 (m, 5H), 7.17 (d, *J* = 0.5 Hz, 0.5H), 7.15 (dd, J_1 = 8.1 Hz, J_2 = 1.7 Hz, 0.5H), 7.15–7.06 (m, 2.5H), 6.91–6.86 (m, 3H), 6.73–6.63 (m, 1H), 6.25–6.15 (m, 2H), 4.34–4.27 (m, 1H), 4.29 (t, *J* = 6.8 Hz, 1H), 4.25 (t, *J* = 6.8 Hz, 1H), 4.02–3.94 (m, 2H), 3.70–3.62 (m, 1H), 3.61 (s, 1.5H), 3.59 (s, 1.5H), 2.84 (t, *J* = 6.8 Hz, 1H), 2.79 (t, *J* = 6.8 Hz, 1H), 2.69 (d, *J* = 15.7 Hz, 0.5H), 2.68

(d, *J* = 15.7 Hz, 0.5H), 2.41 (t, *J* = 7.3 Hz, 1H), 2.38 (t, *J* = 7.3 Hz, 1H), 2.04–1.80 (m, 36H), 1.80–1.66 (m, 38H), 1.55–1.46 (m, 2H), 0.81 (d, *J* = 6.8 Hz, 3H); ^{13}C NMR (125 MHz, $CDCl_3$) δ 174.04, 174.00, 173.52 (overlapping of two signals, both quaternary carbons), 173.31, 173.28, 153.96 (overlapping of two signals, both CH carbons), 153.82 (CH), 153.79 (CH), 147.89, 147.88, 147.03, 146.93, 143.08, 143.06, 142.37, 142.31, 141.66, 141.62, 141.39, 141.37, 140.78, 140.69, 138.37, 138.30, 137.04, 136.76, 136.71, 136.41, 135.44 (CH), 135.15 (CH), 135.09 (CH), 135.05 (CH), 134.95 (CH), 134.86 (CH), 134.63, 134.60, 133.56, 133.55, 132.20 (CH), 131.89 (CH), 131.72 (CH), 131.68 (CH), 131.41 (CH), 131.28 (overlapping of two signals, both CH carbons), 131.11 (overlapping of two signals, both CH carbons), 131.05 (CH), 130.03 (CH), 129.99 (CH), 129.59 (CH), 129.53 (CH), 129.08, 129.07, 129.03 (CH), 129.00 (overlapping of three signals, all CH carbons), 128.47 (overlapping of two signals, both CH carbons), 128.31 (CH), 128.29 (CH), 128.17 (CH), 128.11 (CH), 127.22, 127.18, 126.15 (CH), 126.13 (CH), 125.87, 125.74, 125.71 (overlapping of two signals, both quaternary carbons), 125.67 (overlapping of four signals, all CH carbons), 125.63, 125.62, 125.60 (CH), 125.58, 125.57 (CH), 125.402, 125.398, 125.34 (CH), 125.32 (CH), 125.28, 125.00, 124.93, 124.74 (CH), 124.71 (CH), 124.26 (CH), 124.20 (CH), 123.75, 123.51, 122.72 (CH), 122.71 (CH), 122.60 (CH), 122.59 (CH), 122.09, 121.89, 121.82, 121.62, 111.02 (CH), 111.00 (CH), 110.91 (CH), 110.90 (CH), 105.01, 104.78, 104.74, 104.72, 104.57, 104.48, 103.81 (CH), 103.76 (CH), 103.68 (CH), 103.67 (CH), 100.95, 100.78, 94.44, 94.01, 93.03, 92.57, 92.03, 91.86, 89.06, 88.76, 88.38, 88.11, 82.27, 80.22, 78.74, 78.66, 78.45, 78.23, 77.82, 77.78, 77.69, 77.59, 62.60 (CH_2), 62.56 (CH_2), 49.864, 49.856, 49.75, 49.74, 44.62 (CH_2), 44.59 (CH_2), 43.31 (CH_2), 43.25 (CH_2), 43.18 (CH_2), 43.15

(CH_2), 43.14 (CH_2), 43.11 (CH_2), 43.08 (overlapping of two signals, both CH_2 carbons), 40.07 (CH_2), 40.06 (CH_2), 38.44 (CH_3), 38.40 (CH_3), 36.73 (CH_2), 36.68 (overlapping of two signals, both CH_2 signals), 36.67 (overlapping of three signals, all CH_2 signals), 36.66 (CH_2), 36.63 (CH_2), 34.20 (CH_2), 34.19 (CH_2), 30.911, 30.907, 30.83, 30.77, 30.75, 30.73, 30.59, 30.53, 28.52 (overlapping of two signals, both CH carbons), 28.51 (overlapping of two signals both CH carbons), 28.50 (CH), 28.48 (CH), 28.47 (CH), 28.46 (CH), 28.21 (overlapping of two signals, both CH_3 signals), 28.20 (CH_3), 28.18 (CH_3), 28.07 (overlapping of two signals, both CH_3 carbons), 27.47 (CH_2), 27.43 (CH_2), 26.77 (CH_2), 26.72 (CH_2), 24.95 (CH_2), 24.91 (CH_2), 20.56 (CH_2), 20.51 (CH_2), 19.64 (CH_3), 19.63 (CH_3); HRMS (ESI) *m*/*z* calcd for $[M–Cl]^+$ $C_{127}H_{125}O_2S$ 1741.9467, found 1741.9456.

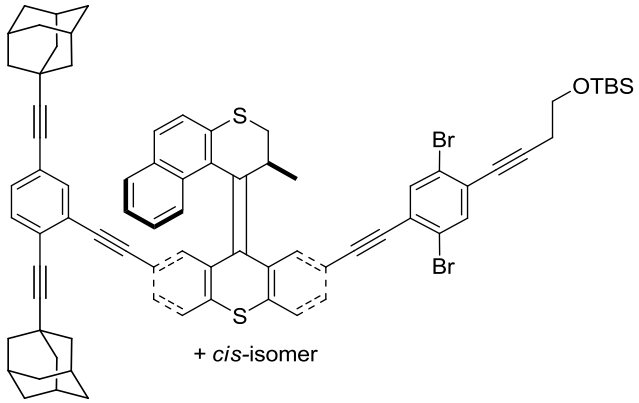

Nanocar precursor 40. The procedure is identical to that described for **36**. Motor **19** (170 mg, 0.370 mmol), the iodoaxle **23** (416 mg, 0.800 mmol), iodobenzene **36** (218 mg, 0.400 mmol), $Pd(PPh_3)_4$ (37 mg, 0.032 mmol), CuI (12 mg, 0.064 mmol), NEt_3 (1 mL) and THF (3 mL) were used. The product **40** was obtained as a yellow solid (208 mg, 41%): FTIR (neat) 2902, 2850, 2220, 1476, 1450, 1356, 1252, 1100, 1068 cm^{-1}; ^1H NMR

(500 MHz, $CDCl_3$) δ 7.78–7.76 (m, 1H), 7.77 (d, J = 0.2 Hz, 0.65H), 7.68 (d, J = 0.2H, 0.65H), 7.66–7.57 (m, 3.7H), 7.54–7.46 (m, 2.35H), 7.42 (d, J = 8.5 Hz, 0.65H), 7.41 (d, J = 8.5 Hz, 0.35H), 7.34 (dd, J_1 = 8.1 Hz, J_2 = 0.6 Hz, 0.35H), 7.31 (dd, J_1 = 1.7 Hz, J_2 = 0.6 Hz, 0.65H), 7.26 (dd, J_1 = 8.1 Hz, J_2 = 1.7 Hz, 0.35H), 7.25 (dd, J_1 = 8.1 Hz, J_2 = 0.5 Hz, 0.35H), 7.24 (dd, J_1 = 8.1 Hz, J_2 = 0.5 Hz, 0.65H), 7.23 (dd, J_1 = 8.1 Hz, J_2 = 0.6 Hz, 0.65H), 7.17 (dd, J_1 = 8.0 Hz, J_2 = 1.7 Hz, 0.65H), 7.13 (ddd, J_1 = 8.2 Hz, J_2 = 6.8 Hz, J_3 = 1.2 Hz, 0.35H), 7.12 (ddd, J_1 = 8.0 Hz, J_2 = 6.8 Hz, J_3 = 1.2 Hz, 0.65H), 7.02 (ddd, J_1 = 8.5 Hz, J_2 = 6.8 Hz, J_3 = 1.3 Hz, 1H, overlapping of two sets of signals, the J values were measured as it appeared), 6.92 (dd, J_1 = 8.1 Hz, J_2 = 1.8 Hz, 0.65H), 6.88 (dd, J_1 = 8.1 Hz, J_2 = 1.8 Hz, 0.35H), 6.53 (dd, J_1 = 1.8 Hz, J_2 = 0.5 Hz, 0.65H), 6.49 (dd, J_1 = 1.7 Hz, J_2 = 0.4 Hz, 0.35H), 4.16 (dqd, J_1 = 7.4 Hz, J_2 = 6.7 Hz, J_3 = 3.5 Hz, 0.35H), 4.12 (dqd, J_1 = 7.4 Hz, J_2 = 6.7 Hz, J_3 = 3.4 Hz, 0.65H), 3.86 (t, J = 7.0 Hz, 1.3H), 3.84 (t, J = 7.1 Hz, 0.7H), 3.74 (dd, J_1 = 11.5 Hz, J_2 = 7.4 Hz, 0.35H), 3.70 (dd, J_1 = 11.4 Hz, J_2 = 7.4 Hz, 0.65H), 3.09 (dd, J_1 = 11.5 Hz, J_2 = 3.5 Hz, 0.35H), 3.08 (dd, J_1 = 11.4 Hz, J_2 = 3.4 Hz, 0.7H), 2.71 (t, J = 7.0 Hz, 1.3H), 2.69 (t, J = 7.1 Hz, 0.7H), 2.04–1.82 (m, 18H), 1.75–1.64 (m, 12H), 0.925 (s, 5.85H), 0.916 (s, 3.15H), 0.83 (d, J = 6.7 Hz, 3H, overlapping of two sets of signals, the J value was measured as it appeared), 0.11 (s, 3.9H), 0.10 (2.1H); ^{13}C NMR (125 MHz, $CDCl_3$) δ 138.42, 138.31, 138.06, 137.82, 137.42, 136.39, 136.16, 136.15, 135.97, 135.83, 135.70, 135.64, 135.53, 135.47, 135.38, 134.80, 134.64 (overlapping of two signals), 134.16, 132.41, 131.99, 131.78, 131.60, 131.45, 131.16, 130.75, 130.74, 130.72, 130.70, 130.63, 130.56, 130.53, 130.51, 130.13, 129.87, 129.41, 128.92, 128.04, 128.02, 127.92, 127.88, 127.82, 127.74, 127.08, 126.59, 126.40, 126.39, 126.29, 125.97, 125.87 (overlapping of two signals), 125.67, 125.58, 125.56, 125.51,

125.39, 125.23, 125.11, 124.46, 124.37, 123.84 (overlapping of two signals), 123.79, 123.70, 123.67, 123.41, 123.22, 122.93, 121.76, 120.95, 120.48, 119.56, 104.21, 103.91, 100.33, 100.11, 95.82, 95.75, 95.57, 95.36, 92.31, 92.17, 89.25, 88.05, 87.84, 86.74, 79.16, 79.15, 78.63, 78.57, 78.20, 78.04, 61.55 (CH_2), 61.54 (CH_2), 42.76 (CH_2), 42.75 (overlapping of two signals, both CH_2 carbons), 42.74 (CH_2), 37.25 (CH_2), 37.08 (CH_2), 36.365 (CH_2), 36.355 (CH_2), 36.347 (CH_2), 36.33 (CH_2), 32.85 (CH), 32.81 (CH), 30.49, 30.33, 30.16, 30.15, 27.97 (overlapping of two signals), 27.96 (CH), 27.95 (CH), 25.890 (CH_3), 25.886 (CH_3), 24.13 (CH_2), 24.10 (CH_2), 19.27 (overlapping of two signals, both CH_3 carbons), 18.34, 18.33, −5.24 (CH_3), −5.25 (CH_3); MS (MALDI) *m*/*z* calcd for $[M+Na]^+$ $C_{77}H_{72}Br_2OS_2SiNa$ 1285.3, found 1285.0. Note: Nanocar precursor **40** existed as a mixture of two isomers, and the ratio was determined to be 65:35 by comparing the integrations of the *tert*-butyl groups and the silyl methyl groups in its ^1H NMR. ^{13}C and DEPT-135 NMR spectra of the first sample were recorded. After obtaining the spectra, the NMR sample was irradiated with 365 nm light for 16 h (3 mW/cm^2) and subsequently heated to 60 °C overnight in the absence of light. After this process, the ratio changed to 38:62. The ^1H, ^{13}C and DEPT-135 were recorded for the light irradiated sample. The assignments were made by comparing all the spectra. However, which isomer (*cis*- or *trans*-) was the initially major component was not determined.

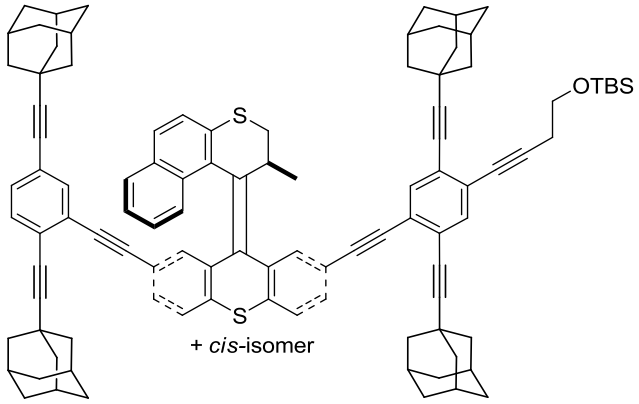

Nanocar 41. The procedure is identical to that described for **38**. Nanocar precursor **40** (127 mg, 0.100 mmol)**,** 1-ethynyladamantane (**27**) (64 mg, 0.40 mmol), $Pd(PPh_3)_4$ (3.8 mg, 0.010 mmol), CuI (3.8 mg, 0.010 mmol), HP*t*-Bu_3BF_4 (5.9 mg, 0.020 mmol) and NEt_3 (1 mL) were used. The product **41** was obtained as a yellow solid (85 mg, 60%): FTIR (neat) 2902, 2850, 2224, 1488, 1450, 1318, 1252, 1100 cm^{-1}; ^1H NMR (500 MHz, $CDCl_3$) δ 7.75 (d, J = 1.6 Hz, 0.38H), 7.74 (d, J = 1.6 Hz, 0.62H), 7.66–7.63 (m, 1H), 7.62–7.58 (m, 2.38H), 7.56 (d, J = 0.5 Hz, 0.62H), 7.53 (d, J = 8.4 Hz, 1H, overlapping of two sets of signals, the J value was measured as it appeared), 7.50–7.45 (m, 1H), 7.46 (d, J = 0.5 Hz, 0.62H), 7.429 (d, J = 8.5 Hz, 0.38H), 7.428 (d, J = 8.6 Hz, 0.62H), 7.345 (d, J = 0.5 Hz, 0.38H), 7.343 (dd, J_1 = 8.1 Hz, J_2 = 0.6 Hz, 0.38 H), 7.31 (dd, J_1 = 1.7 Hz, J_2 = 0.6 Hz, 0.62H), 7.29 (d, J = 0.5 Hz, 0.38H), 7.26 (dd, J_1 = 8.1 Hz, J_2 = 1.7 Hz, 0.38H), 7.24 (dd, J_1 = 8.1 Hz, J_2 = 0.4 Hz, 1H, overlapping of two sets of signals, the J values were measured as they appeared), 7.23 (dd, J_1 = 8.0 Hz, J_2 = 0.6 Hz, 0.62H), 7.17 (dd, J_1 = 8.0 Hz, J_2 = 1.7 Hz, 0.62H), 7.14–7.09 (m, 1H), 7.04–6.99 (m, 1H), 6.91 (dd, J_1 = 8.0 Hz, J_2 = 1.8 Hz, 0.62H), 6.90 (dd, J_1 = 8.1 Hz, J_2 = 1.8 Hz, 0.38H), 6.47 (dd, J_1 = 1.8 Hz, J_2 = 0.4 Hz, 0.62H), 6.46 (dd, J_1 = 1.7 Hz, J_2 = 0.4 Hz, 0.38H), 4.18–4.10 (m, 1H), 3.89–3.81 (m, 2H), 3.721 (dd, J_1 = 11.4 Hz, J_2 = 7.5 Hz, 0.38H), 3.716 (dd, J_1 = 11.5

Hz, J_2 = 7.5 Hz, 0.62H), 3.064 (dd, J_1 = 11.5 Hz, J_2 = 3.6 Hz, 0.38H), 3.061 (dd, J_1 = 11.5 Hz, J_2 = 3.7 Hz, 0.62H), 2.73–2.65 (m, 2H), 2.05–1.80 (m, 36H), 1.78–1.65 (m, 24H), 0.92 (s, 5.58H), 0.91 (s, 3.42H), 0.83 (d, J = 6.7 Hz, 3H), 0.10 (s, 3.72H), 0.09 (s, 2.28H); ^{13}C NMR (125 MHz, $CDCl_3$) δ 138.16, 138.15, 138.08, 138.02, 136.54, 136.37, 135.95, 135.92, 135.67, 135.65, 135.16 (CH), 134.89 (CH), 134.86 (CH), 134.71 (CH), 134.70 (CH), 134.56, 134.37, 132.75 (CH), 132.15 (CH), 131.89 (CH), 131.83 (CH), 131.80, 131.61, 131.59, 131.50 (CH), 131.12 (CH), 130.98, 130.97, 130.74, 130.71, 130.68 (CH), 130.67, 130.59, 130.58, 130.54 (CH), 130.50 (CH), 130.05 (CH), 130.04 (CH), 129.36 (CH), 129.10 (CH), 127.96 (CH), 127.95 (CH), 127.90 (CH), 127.89 (CH), 127.76, 127.74, 126.31 (CH), 126.28 (CH), 125.84 (CH), 125.77, 125.64 (CH), 125.63 (CH), 125.56 , 125.37, 125.32, 125.30, 125.26, 125.14, 125.11, 125.03, 124.86, 124.52, 124.35 (CH), 124.20, 123.91 (overlapping of two signals, both CH carbon), 123.22, 122.93, 121.68, 121.53, 120.88, 120.75, 104.25, 104.17, 103.94, 103.87, 103.81, 103.58, 100.33, 100.11, 94.48, 93.26, 92.34, 92.30, 92.06, 91.96, 89.17, 88.99, 87.99, 87.87, 80.00, 79.98, 78.63, 78.57, 78.19, 78.04, 77.66, 77.62, 77.47, 62.07 (overlapping of two signals, both CH_2 carbons), 42.94 (CH_2), 42.88 (CH_2), 42.80 (CH_2), 42.79 (CH_2), 42.75 (CH_2), 42.742 (CH_2), 42.739 (CH_2), 42.69 (CH_2), 37.25 (CH_2), 37.24 (CH_2), 36.35 (overlapping of eight signals, all CH_2 carbons), 32.96, 32.93, 30.48, 30.46, 30.39, 30.37, 30.32, 30.30, 30.16, 30.15, 27.97 (overlapping of two signals, both CH carbons), 27.96 (overlapping of two signals, both CH carbons), 27.95 (overlapping of two signals, both CH carbons), 27.93 (overlapping of two signals, both CH carbons), 25.913 (CH_3), 25.906 (CH_3), 24.06 (CH_2), 24.04 (CH_2), 19.29 (CH_3), 19.28 (CH_3), 18.36, 18.35, −5.27 (CH_3), −5.28 (CH_3); MS (MALDI) *m*/*z* calcd for $[M+Na]^+$ $C_{101}H_{102}OS_2SiNa$ 1445.7, found 1445.5. Note: The

starting material **40** used in this reaction existed as a mixture of two isomers with ratio to be 65:35. Nanocar **41** also existed as a mixture of two isomers, and the ratio was determined as 62:38 by comparing the integrations of the *tert*-butyl groups and the silyl methyl groups in its ^{1}H NMR. ^{13}C and DEPT-135 NMR spectra of the first sample were recorded. After obtaining the spectra, the NMR sample was irradiated with 365 nm light for 4 h (3 mW/cm^2) and subsequently heated to 60 °C overnight in the absence of light. After this process, the ratio changed to 50:50. The ^{1}H, ^{13}C and DEPT-135 were recorded for the light irradiated sample. The assignments were made by comparing all the spectra.

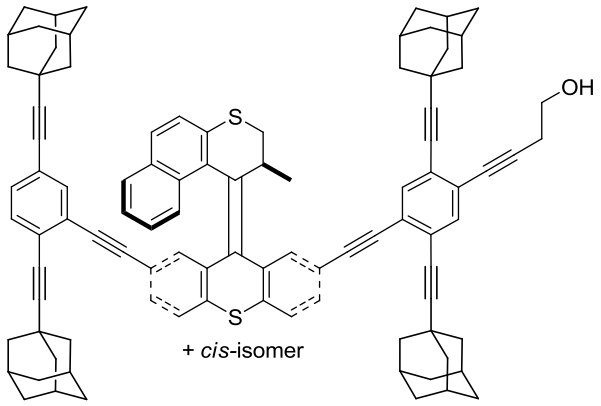

Nanocar 42. To an oven-dried three-neck round-bottom flask charged with nanocar **41** (55 mg, 0.038 mmol) was added a solution of TBAF (0.06 mL, 1.0 M in THF, 0.06 mmol) and THF (5 mL). The reaction was stirred for 1 h at room temperature. The mixture was poured into water (30 mL) and the precipitates were removed by filtration. The solids were washed thoroughly with water (30 mL), collected and dried under vacuum to afford the desired compound **42** as a pale yellow solid (46 mg, 90%): FTIR (neat) 3566, 2902, 2850, 2222, 1486, 1450, 1316, 1054 cm^{-1}; ^{1}H NMR (500 MHz, $CDCl_3$) δ 7.76 (d, *J* = 1.6 Hz, 0.4H), 7.48 (d, *J* = 1.6 Hz, 0.6 H), 7.65 (d, *J* = 8.6 Hz, 1H,

overlapping of two sets of signals, the *J* value was measured as it appeared), 7.62–7.58 (m, 3H), 7.53 (d, *J* = 8.5 Hz, 1H, overlapping of two sets of signals, the *J* value was measured as it appeared), 7.50–7.46 (m, 1.6H), 7.43 (d, *J* = 8.6 Hz, 1H, overlapping of two sets of signals, the *J* value was measured as it appeared), 7.37 (d, *J* = 0.4 Hz, 0.4H), 7.35 (dd, J_1 = 8.1 Hz, J_2 = 0.6 Hz, 0.4H), 7.32–7.30 (m, 1H), 7.27 (dd, J_1 = 8.1 Hz, J_2 = 1.7 Hz, 0.4H), 7.244 (dd, J_1 = 8.1 Hz, J_2 = 0.4 Hz, 0.4H), 7.241 (dd, J_1 = 8.1 Hz, J_2 = 0.4 Hz, 0.6H), 7.23 (dd, J_1 = 8.0 Hz, J_2 = 0.6 Hz, 0.6H), 7.18 (dd, J_1 = 8.1 Hz, J_2 = 1.7 Hz, 0.6H), 7.12 (ddd, J_1 = 8.1 Hz, J_2 = 6.9 Hz, J_3 = 1.1 Hz, 1H, overlapping of two sets of signals, the *J* values were measured as they appeared), 7.02 (ddd, J_1 = 8.5 Hz, J_2 = 6.8 Hz, J_3 = 1.2 Hz, 1H, overlapping of two sets of signals, the *J* values were measured as they appeared), 6.92 (dd, J_1 = 8.1 Hz, J_2 = 1.8 Hz, 0.6 H), 6.91 (dd, J_1 = 8.0 Hz, J_2 = 1.8 Hz, 0.4H), 6.49–6.46 (m, 1H), 4.19–4.11 (m, 1H), 3.87–3.78 (m, 2H), 3.726 (dd, J_1 = 11.4 Hz, J_2 = 7.4 Hz, 0.4H), 3.721 (dd, J_1 = 11.4 Hz, J_2 = 7.4 Hz, 0.6H), 3.071 (dd, J_1 = 11.4 Hz, J_2 = 3.5 Hz, 0.4H), 3.066 (dd, J_1 = 11.4 Hz, J_2 = 3.5 Hz, 0.6H), 2.76 (t, *J* = 6.1 Hz, 1.2H), 2.73 (t, *J* = 6.2 Hz, 0.8H), 2.05–1.85 (m, 36H), 1.76–1.67 (m, 24H), 0.83 (d, *J* = 6.8 Hz, 3H, overlapping of two signals, the *J* value was measured as it appeared); ^{13}C NMR (125 MHz, $CDCl_3$) δ 138.183, 138.179, 138.09, 138.02, 136.63, 136.36, 135.98, 135.91, 135.68, 135.67, 135.18 (CH), 135.15 (CH), 135.00 (CH), 134.89 (CH), 134.86 (CH), 134.72 (overlapping of two signals, both CH carbons), 134.65, 134.36, 131.88 (CH), 131.86 (CH), 131.81 (CH), 131.62, 131.60, 131.510 (CH), 131.507 (CH), 131.13 (CH), 130.98, 130.97, 130.76, 130.73, 130.693 (CH), 130.688 (CH), 130.599, 130.595, 130.54 (CH), 130.51 (CH), 130.07 (CH), 130.06 (CH), 129.37 (overlapping of two signals, both CH carbons), 127.96 (CH), 127.90 (CH), 127.78 (CH), 127.75 (CH), 126.33

(CH), 126.29 (CH), 125.86 (CH), 125.64 (overlapping of two signals, both CH carbons), 125.56, 125.45, 125.33, 125.25 (overlapping of two signals), 125.18, 125.13, 125.03, 124.97, 124.82, 124.64, 124.50, 124.37 (CH), 124.36 (CH), 123.92 (overlapping of two signals, both CH carbons), 123.23, 122.94, 121.70, 121.47, 120.90, 120.67, 104.44, 104.17, 104.13, 104.07, 103.87, 103.84, 100.34, 100.12, 93.66, 93.45, 92.34, 92.06, 91.87, 91.52, 89.18, 89.90, 88.01, 87.78, 81.15, 81.10, 78.64, 78.58, 78.20, 78.05, 77.75, 77.70, 77.56, 77.40, 60.98 (CH_2), 60.96 (CH_2), 42.94 (CH_2), 42.88 (CH_2), 42.76 (CH_2), 42.75 (CH_2), 42.744 (CH_2), 42.738 (CH_2), 42.73, 42.69 (CH_2), 37.26 (CH_2), 37.25 (CH_2), 36.37 (CH_2), 36.36 (overlapping of two signals, both CH_2 carbons), 36.350 (overlapping of two signals, both CH_2 carbons), 36.34 (overlapping of two signals, both CH_2 carbons), 36.328 (CH_2), 33.00 (CH), 33.95 (CH), 30.483, 30.48, 30.43, 30.42, 30.323, 30.319, 30.168, 30.155, 27.98 (CH), 27.96 (overlapping of four signals, all CH carbons), 27.95 (CH), 27.93 (overlapping of two signals, both CH carbons), 24.18 (CH_2), 24.16 (CH_2), 19.30 (CH_3), 19.28 (CH_3); MS (MALDI) *m*/*z* calcd for $[M+Na]^+$ $C_{95}H_{88}OS_2Na$ 1331.6, found 1331.5. Note: The starting material **41** used in this reaction existed as a mixture of two isomers with ratio to be 62:38. Nanocar **42** also existed as a mixture of two isomers, and the ratio was determined as 60:40 by comparing the integrations of the doublets at δ 7.76 and 7.74 and the doublets of doublets at δ 6.92 and 6.91 in its ^{1}H NMR. ^{13}C and DEPT-135 NMR spectra of the first sample were recorded. After obtaining the spectra, the NMR sample was irradiated with 365 nm light for 2 h (3 mW/cm^2) and subsequently heated to 60 °C overnight in the absence of light. After this process, the ratio changed to 50:50. The ^{1}H, ^{13}C and DEPT-135 were recorded for the light irradiated sample. The assignments were made by comparing all the spectra.

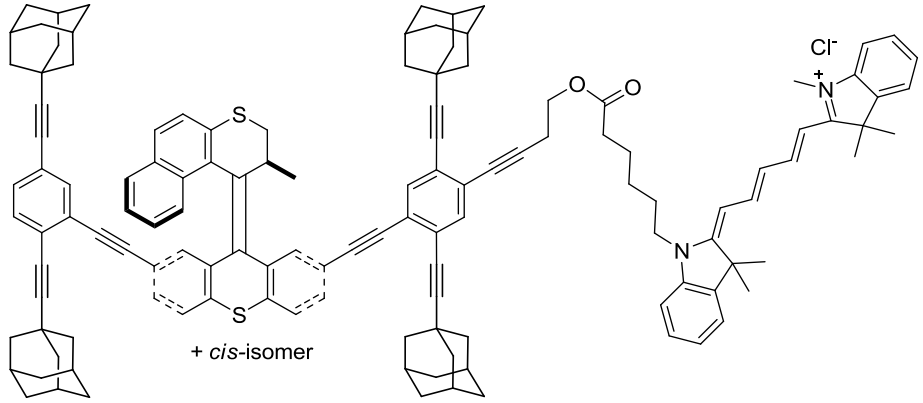

Cy5-tagged nanocar 43. The procedure is identical to that described for **20**. Nanocar **42** (20.0 mg, 0.0150 mmol)**,** cy5 dye **22** (9.3 mg, 0.018 mmol), *N*,*N*′-dicyclohexylcarbodiimide (3.7 mg, 0.018), 4-dimethylaminopyridine (2.2 mg, 0.018 mmol), and CH_2Cl_2 (1.8 mL) were used in the reaction. The cy5-tagged nanocar **43** was obtained as a blue solid (25.0 mg, 92%): FTIR (neat): 2902, 2850, 2220, 1734, 1482, 1450, 1370, 1334, 1218, 1144, 1092, 1040, 1016 cm^{-1}; ^1H NMR (500 MHz, $CDCl_3$) δ 8.09–8.00 (m, 2H), 7.79 (d, J = 1.6 Hz, 0.42H), 7.77 (d, J = 1.7 Hz, 0.58H), 7.71–7.61 (m, 2.58H), 7.59–7.54 (m, 2.16H), 7.54 (d, J = 0.5 Hz, 0.58H), 7.53 (dd, J_1 = 8.1 Hz, J_2 = 1.7 Hz, 0.42H), 7.49 (dd, J_1 = 8.1 Hz, J_2 = 1.7 Hz, 0.58H), 7.47–7.43 (m, 1.58H), 7.43–7.37 (m, 3.42H), 7.35 (dd, J_1 = 8.1 Hz, J_2 = 0.6 Hz, 0.42H), 7.33 (d, J = 0.5 Hz, 0.42H), 7.31 (d, J = 0.4 Hz, 0.58H), 7.30–7.23 (m, 4.42H), 7.19 (dd, J_1 = 8.0 Hz, J_2 = 1.7 Hz, 0.58H), 7.18–7.07 (m, 3.26H), 7.05 (ddd, J_1 = 8.5 Hz, J_2 = 6.8 Hz, J_3 = 1.3 Hz, 1H, overlapping of two sets of signals, the J values were measured as they appeared), 6.95 (dd, J_1 = 8.1 Hz, J_2 = 1.8 Hz, 0.58H), 6.91 (dd, J_1 = 8.1 Hz, J_2 = 1.8 Hz, 0.42H), 6.72–6.63 (m, 1H), 6.53–6.49 (m, 1H), 6.25–6.16 (m, 2H), 4.29 (t, J = 6.8 Hz, 1.16H), 4.26 (t,

J = 6.8 Hz, 0.84H), 4.20–4.13 (m, 1H), 4.03–3.95 (m, 2H), 3.76–3.70 (m, 1H), 3.62 (s, 1.74H), 3.50 (s, 1.26H), 3.09 (dd, J_1 = 11.5 Hz, J_2 = 3.6 Hz, 0.42H), 3.07 (dd, J_1 = 11.5 Hz, J_2 = 3.6 Hz, 0.58H), 2.84 (t, J = 6.8 Hz, 1.16H), 2.81 (t, J = 6.8 Hz, 0.84H), 2.41 (t, J = 7.3 Hz, 1.16H), 2.39 (t, J = 7.3 Hz, 0.84H), 2.05–1.80 (m, 36H), 1.80–1.66 (m, 38H), 1.56–1.48 (m, 2H), 0.811 (d, J = 6.8 Hz, 1.74H), 0.809 (d, J = 6.8 Hz, 1.26H); ^{13}C NMR (125 MHz, $CDCl_3$) δ 174.16, 174.13, 173.56, 173.54, 173.30, 173.28, 154.32, 154.30, 154.27, 154.22, 143.13, 143.12, 142.42, 142.37, 141.71, 141.68, 141.45, 141.43, 138.723, 138.716, 138.66, 137.30, 136.99, 136.43, 136.36 (overlapping of two signals), 135.64, 135.47, 135.29, 135.25, 135.24, 145.13, 135.04, 134.95, 132.23, 132.15, 132.14, 132.03, 132.00, 131.99, 131.51, 131.35, 131.33, 131.16, 131.12, 131.03, 130.98, 130.97, 130.48, 130.42, 129.69, 129.67, 128.975, 128.973, 128.970, 128.966, 128.26, 128.23, 128.21, 128.15, 128.12, 127.00, 126.95, 126.39, 126.38, 126.03 (overlapping of two signals), 125.87, 125.84, 125.75, 125.72, 125.67, 125.64, 125.62, 125.61, 125.60, 125.59, 125.58, 125.46, 125.42, 125.31, 124.95, 124.89, 124.834, 124.828, 124.37, 124.35, 123.76, 123.53, 122.72, 122.71, 122.585, 122.582, 121.99, 121.72, 120.96, 120.69, 110.94, 110.93, 110.89, 110.88, 105.10, 104.87, 104.81, 104.77, 104.62, 104.57, 103.88 (CH), 103.83 (CH), 103.65 (CH), 103.64 (CH), 100.98, 100.83, 94.15, 93.82, 92.77, 92.38, 92.07, 91.86, 89.36, 89.04, 88.29, 88.02, 82.27, 80.26, 78.72 (overlapping of two signals), 78.41, 78.22, 77.78, 77.77, 77.75, 77.59, 62.59 (CH_2), 49.84 (overlapping of two signals), 49.76, 49.75, 43.33 (CH_2), 43.28 (CH_2), 43.18 (overlapping of two signals, both CH_2 carbons), 43.14 (CH_2), 43.11 (overlapping of two signals, both CH_2 carbons), 43.09 (CH_2), 37.583 (CH_2), 37.575 (CH_2), 37.703 (overlapping of two signals, both CH2 carbons), 36.697 (CH_2), 36.69 (CH_2), 36.682 (overlapping of two signals, both CH_2

carbons), 36.675 (CH_2), 36.66 (CH_2), 34.194 (CH_2), 34.190 (CH_2), 33.42 (CH), 33.34 (CH), 30.92, 30.91, 30.84, 30.82, 30.764, 30.759, 30.60, 30.58, 28.53 (CH), 28.52 (CH), 28.511 (CH), 28.510 (CH), 28.50 (overlapping of two signals, both CH carbons), 28.47 (CH), 28.45 (CH), 28.163 (CH_3), 28.156 (CH_3), 28.02 (overlapping of two signals, both CH_3 carbons), 27.47 (CH_2), 27.45 (CH_2), 26.76 (CH_2), 26.73 (CH_2), 24.95 (CH_2), 24.93 (CH_2), 20.56 (CH_2), 20.53 (CH_2), 19.36 (CH_3), 19.32 (CH_3); HRMS (ESI) *m*/*z* calcd for $[M–Cl]^+$ $C_{127}H_{125}O_2S_2$ 1773.9177, found 1773.9197. Note: The starting material **42** used in this reaction existed as a mixture of two isomers with ratio to be 60:40. Cy5-tagged model nanocar **43** also existed as a mixture of two isomers, and the ratio was determined as 58:42 by comparing the integrations of the doublets at δ 7.79 and 7.77 and the doublets of doublets at δ 6.95 and 6.91 in its ^{1}H NMR. ^{13}C and DEPT-135 NMR spectra of the first sample were recorded. After obtaining the spectra, the NMR sample was irradiated with 365 nm light for 2 h (3 mW/cm^2) and subsequently heated to 60 °C overnight in the absence of light. After this process, the ratio changed to 50:50. The ^{1}H, ^{13}C and DEPT-135 were recorded for the light irradiated sample. The assignments were made by comparing all the spectra. However, 8 carbon signals in the aromatic region cannot be identified or assigned due to severely overlapping of signals.

3.12. References

1. Kinbara, K.; Aida, T. Toward Intelligent Molecular Machines: Directed Motions of Biological and Artificial Molecules and Assemblies. *Chem. Rev.* **2005**, *105*, 1377–1400.

2. Huang, T. J.; Brough, B.; Ho, C.-M.; Liu, Y.; Flood, A. H.; Bonvallet, P. A.; Tseng, H.-R.; Stoddart, J. F.; Baller, M.; Magonov, S. A Nanomechanical Device Based on Linear Molecular Motors. *Appl. Phys. Lett.* **2004**, *85*, 5391–5393.

3. Liu, Y.; Flood, A. H.; Bonvallet, P. A.; Vignon, S. A.; Northrop, B. H.; Tseng, H.-R.; Jeppesen, J. O.; Huang, T. J.; Brough, B.; Baller, M.; Magonov, S.; Solares, S. D.; Goddard, W. A.; Ho, C.-M.; Stoddart, J. F. Linear Artificial Molecular Muscles. *J. Am. Chem. Soc.* **2005**, *127*, 9745–9759.

4. Chuang, C.-J.; Li, W.-S.; Lai, C.-C.; Liu, Y.-H.; Peng, S.-M.; Chao, I.; Chiu, S.-H. A Molecular Cage-Based [2]Rotaxane That Behaves as a Molecular Muscle. *Org. Lett.* **2008**, *11*, 385–388.

5. Badjić, J. D.; Balzani, V.; Credi, A.; Silvi, S.; Stoddart, J. F. A Molecular Elevator. *Science* **2004**, *303*, 1845–1849.

6. Vives, G.; Tour, J. M. Synthesis of Single-Molecule Nanocars. *Acc. Chem. Res.* **2009**, *42*, 473–487.

7. Shirai, Y.; Morin, J.-F.; Sasaki, T.; Guerrero, J. M.; Tour, J. M. Recent Progress on Nanovehicles. *Chem. Soc. Rev.* **2006**, *35*, 1043–1055.

8. Beton, P. H.; Dunn, A. W.; Moriarty, P. Manipulation of C_{60} Molecules on a Si Surface. *Appl. Phys. Lett.* **1995**, *67*, 1075–1077.

9. Keeling, D. L.; Humphry, M. J.; Fawcett, R. H. J.; Beton, P. H.; Hobbs, C.; Kantorovich, L. Bond Breaking Coupled with Translation in Rolling of Covalently Bound Molecules. *Phys. Rev. Lett.* **2005**, *94*, 146104.

10. Shirai, Y.; Osgood, A. J.; Zhao, Y.; Kelly, K. F.; Tour, J. M. Directional Control in Thermally Driven Single-Molecule Nanocars. *Nano Lett.* **2005**, *5*, 2330–2334.

11. Khatua, S.; Guerrero, J. M.; Claytor, K.; Vives, G.; Kolomeisky, A. B.; Tour, J. M.; Link, S. Micrometer-Scale Translation and Monitoring of Individual Nanocars on Glass. *ACS Nano* **2009**, *3*, 351–356.

12. Khatua, S.; Godoy, J.; Tour, J. M.; Link, S. Influence of the Substrate on the Mobility of Individual Nanocars. *J. Phys. Chem. Lett.* **2010**, *1*, 3288–3291.

13. Chu, P.-L. E.; Wang, L.-Y.; Khatua, S.; Kolomeisky, A. B.; Link, S.; Tour, J. M. Synthesis and Single-Molecule Imaging of Highly Mobile Adamantane-Wheeled Nanocars. *ACS Nano* **2013**, *7*, 35–41.

14. Shirai, Y.; Osgood, A. J.; Zhao, Y.; Yao, Y.; Saudan, L.; Yang, H.; Yu-Hung, C.; Alemany, L. B.; Sasaki, T.; Morin, J.-F.; Guerrero, J. M.; Kelly, K. F.; Tour, J. M. Surface-Rolling Molecules. *J. Am. Chem. Soc.* **2006**, *128*, 4854–4864.

15. Morin, J.-F.; Shirai, Y.; Tour, J. M. En Route to a Motorized Nanocar. *Org. Lett.* **2006**, *8*, 1713–1716.

16. Chiang, P.-T.; Mielke, J.; Godoy, J.; Guerrero, J. M.; Alemany, L. B.; Villagómez, C. J.; Saywell, A.; Grill, L.; Tour, J. M. Toward a Light-Driven Motorized Nanocar: Synthesis and Initial Imaging of Single Molecules. *ACS Nano* **2012**, *6*, 592–597.

17. Grill, L.; Rieder, K.-H.; Moresco, F.; Stojkovic, S.; Gourdon, A.; Joachim, C. Exploring the Interatomic Forces between Tip and Single Molecules During STM Manipulation. *Nano Lett.* **2006**, *6*, 2685–2689.

18. Liljeroth, P.; Swart, I.; Paavilainen, S.; Repp, J.; Meyer, G. Single-Molecule Synthesis and Characterization of Metal−Ligand Complexes by Low-Temperature STM. *Nano Lett.* **2010**, *10*, 2475–2479.

19. Sasaki, T.; Osgood, A. J.; Alemany, L. B.; Kelly, K. F.; Tour, J. M. Synthesis of a Nanocar with an Angled Chassis. Toward Circling Movement. *Org. Lett.* **2007**, *10*, 229–232.

20. Coasts, S.; Dax, S. L.; DeCorte, B.; Liu, L.; McDonnell, M.; McNally, J. J., Tricyclic δ-Opioid Modulators. U.S. Patent 7,439,239, Oct. 21, 2008.

21. ter Wiel, M. K. J.; Vicario, J.; Davey, S. G.; Meetsma, A.; Feringa, B. L. New Procedure for the Preparation of Highly Sterically Hindered Alkenes Using a Hypervalent Iodine Reagent. *Org. Biomol. Chem.* **2005**, *3*, 28–30.

22. For an photobelching interactive tutorial, see:
http://micro.magnet.fsu.edu/primer/java/fluorescence/photobleaching/

23. Ueno, Y.; Jose, J.; Loudet, A.; Pérez-Bolívar, C.; Anzenbacher, P.; Burgess, K. Encapsulated Energy-Transfer Cassettes with Extremely Well Resolved Fluorescent Outputs. *J. Am. Chem. Soc.* **2010**, *133*, 51–55.

24. Klok, M.; Boyle, N.; Pryce, M. T.; Meetsma, A.; Browne, W. R.; Feringa, B. L. Mhz Unidirectional Rotation of Molecular Rotary Motors. *J. Am. Chem. Soc.* **2008**, *130*, 10484–10485.

25. Shirai, Y.; Sasaki, T.; Guerrero, J. M.; Yu, B.-C.; Hodge, P.; Tour, J. M. Synthesis and Photoisomerization of Fullerene− and Oligo(Phenylene Ethynylene)−Azobenzene Derivatives. *ACS Nano* **2007**, *2*, 97–106.

26. Lavis, L. D.; Raines, R. T. Bright Ideas for Chemical Biology. *ACS Chem. Biol.* **2008**, *3*, 142–155.

27. Dixon, J. M.; Taniguchi, M.; Lindsey, J. S. Photochemcad 2: A Refined Program with Accompanying Spectral Databases for Photochemical Calculations. *Photochem. Photobiol.* **2005**, *81*, 212–213.

28. The software was downloaded from http://www.photochemcad.com/.

29. DMF and 1,4-dioxane were heated up to 100 ℃ but most axle 29 did not dissolve. The very poor solubility is probably due to the highly symmetrical axle structure.

30. Kosynkin, D. V.; Tour, J. M. Phenylene Ethynylene Diazonium Salts as Potential Self-Assembling Molecular Devices. *Org. Lett.* **2001**, *3*, 993–995.

31. Kvach, M. V.; Ustinov, A. V.; Stepanova, I. A.; Malakhov, A. D.; Skorobogatyi, M. V.; Shmanai, V. V.; Korshun, V. A. A Convenient Synthesis of Cyanine Dyes: Reagents for the Labeling of Biomolecules. *Eur. J. Org. Chem.* **2008**, *2008*, 2107–2117.

32. Connelly, N. G.; Geiger, W. E. Chemical Redox Agents for Organometallic Chemistry. *Chem. Rev.* **1996**, *96*, 877–910.

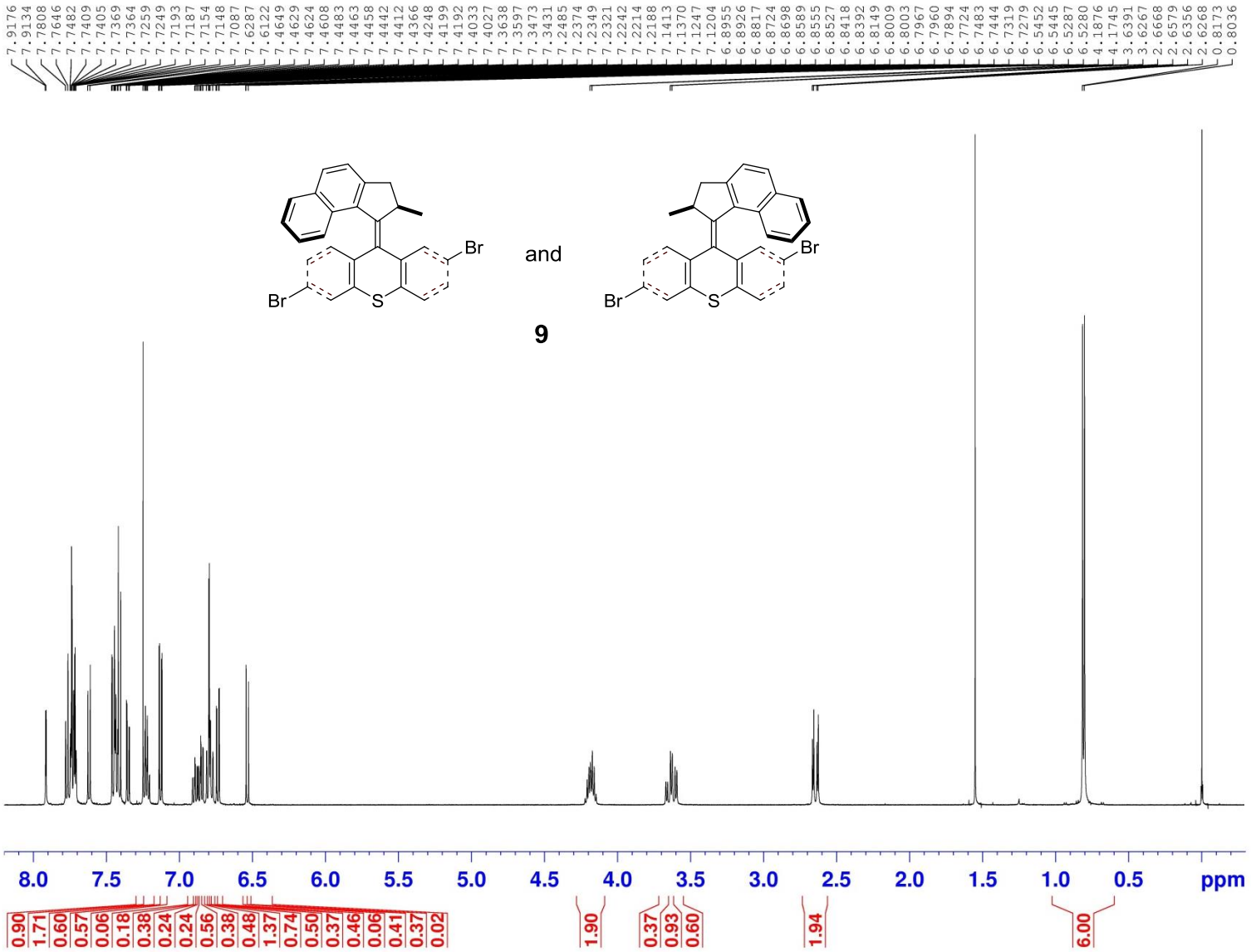
7.9176
7.9134
7.7808
7.7646
7.7482
7.7409
7.7405
7.7369
7.7364
7.7259
7.7249
7.7193
7.7187
7.7154
7.7148
7.7087
7.6287
7.6122
7.4649
7.4629
7.4624
7.4608
7.4483
7.4463
7.4458
7.4442
7.4412
7.4366
7.4248
7.4199
7.4192
7.4033
7.4027
7.3638
7.3597
7.3473
7.3431
7.2485
7.2374
7.2349
7.2321
7.2242
7.2214
7.2188
7.1413
7.1370
7.1247
7.1204
6.8955
6.8926
6.8817
6.8724
6.8698
6.8589
6.8555
6.8527
6.8418
6.8392
6.8149
6.8009
6.8003
6.7967
6.7960
6.7894
6.7724
6.7483
6.7444
6.7319
6.7279
6.5452
6.5445
6.5287
6.5280
4.1876
4.1745
3.6391
3.6267
2.6668
2.6579
2.6356
2.6268
0.8173
0.8036
Br
Br
S
and
Br
Br
S
9
8.0
7.5
7.0
6.5
6.0
5.5
5.0
4.5
4.0
3.5
3.0
2.5
2.0
1.5
1.0
0.5
ppm
0.90
1.71
0.60
0.57
0.06
0.18
0.38
0.24
0.24
0.56
0.38
0.48
1.37
0.74
0.50
0.37
0.46
0.06
0.41
0.37
0.02
1.90
0.37
0.93
0.60
1.94
6.00

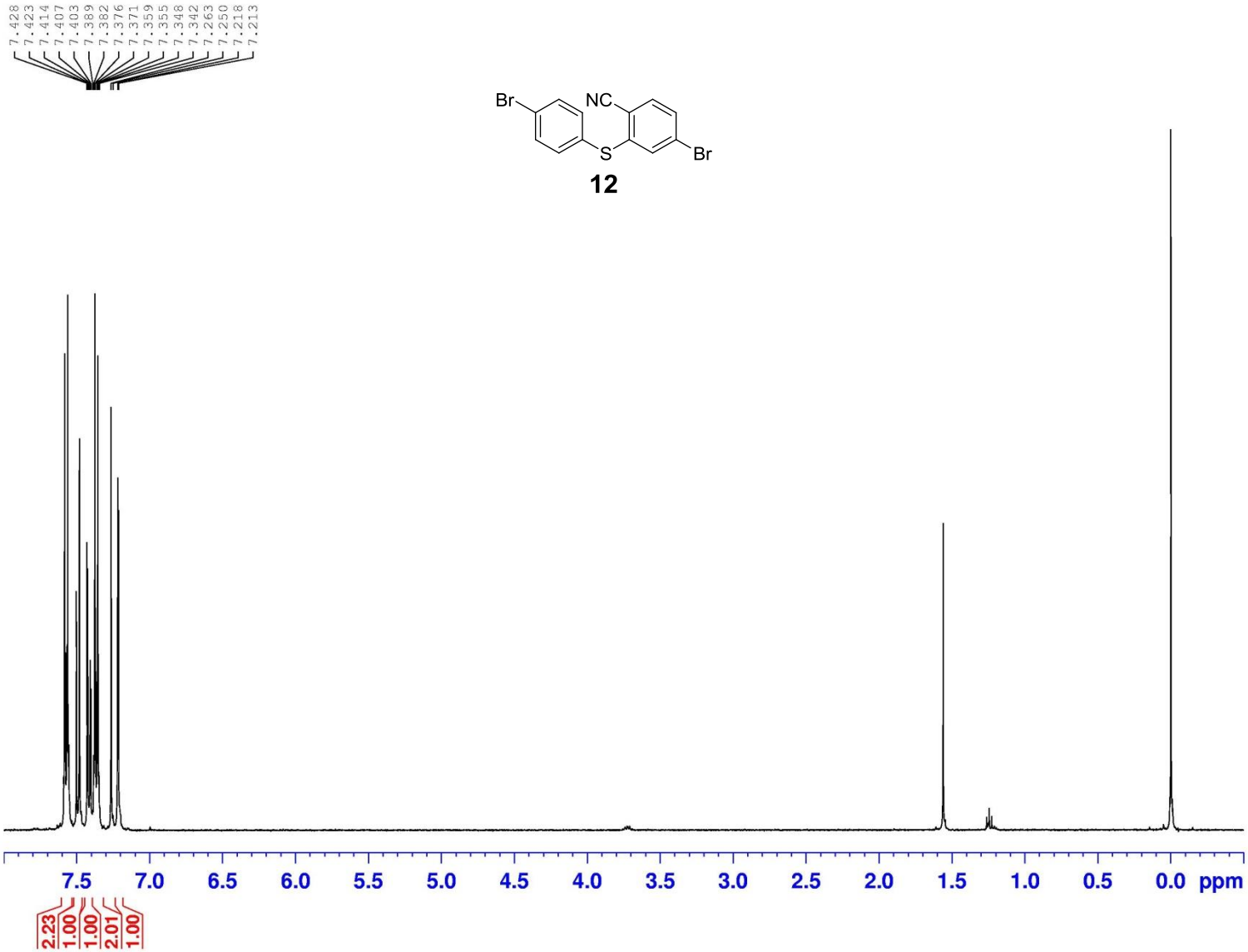
7.428
7.423
7.414
7.407
7.403
7.389
7.382
7.376
7.371
7.359
7.355
7.348
7.342
7.263
7.250
7.218
7.213
Br
NC
S
Br
12
7.5
7.0
6.5
6.0
5.5
5.0
4.5
4.0
3.5
3.0
2.5
2.0
1.5
1.0
0.5
0.0
ppm
2.23
1.00
1.00
2.01
1.00

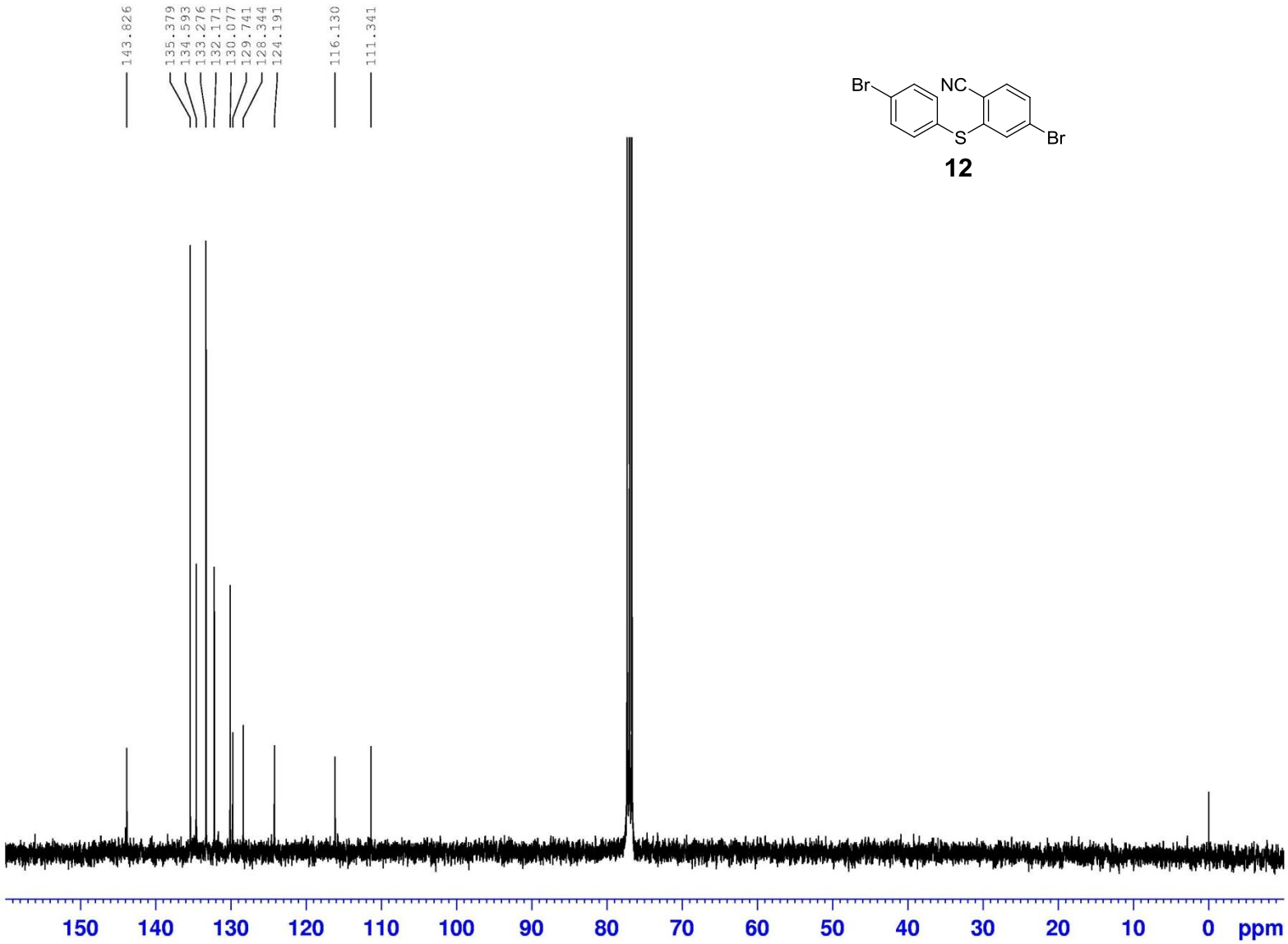
143.826
135.379
134.593
133.276
132.171
130.077
129.741
128.344
124.191
116.130
111.341
Br
NC
S
Br
12
150
140
130
120
110
100
90
80
70
60
50
40
30
20
10
0
ppm

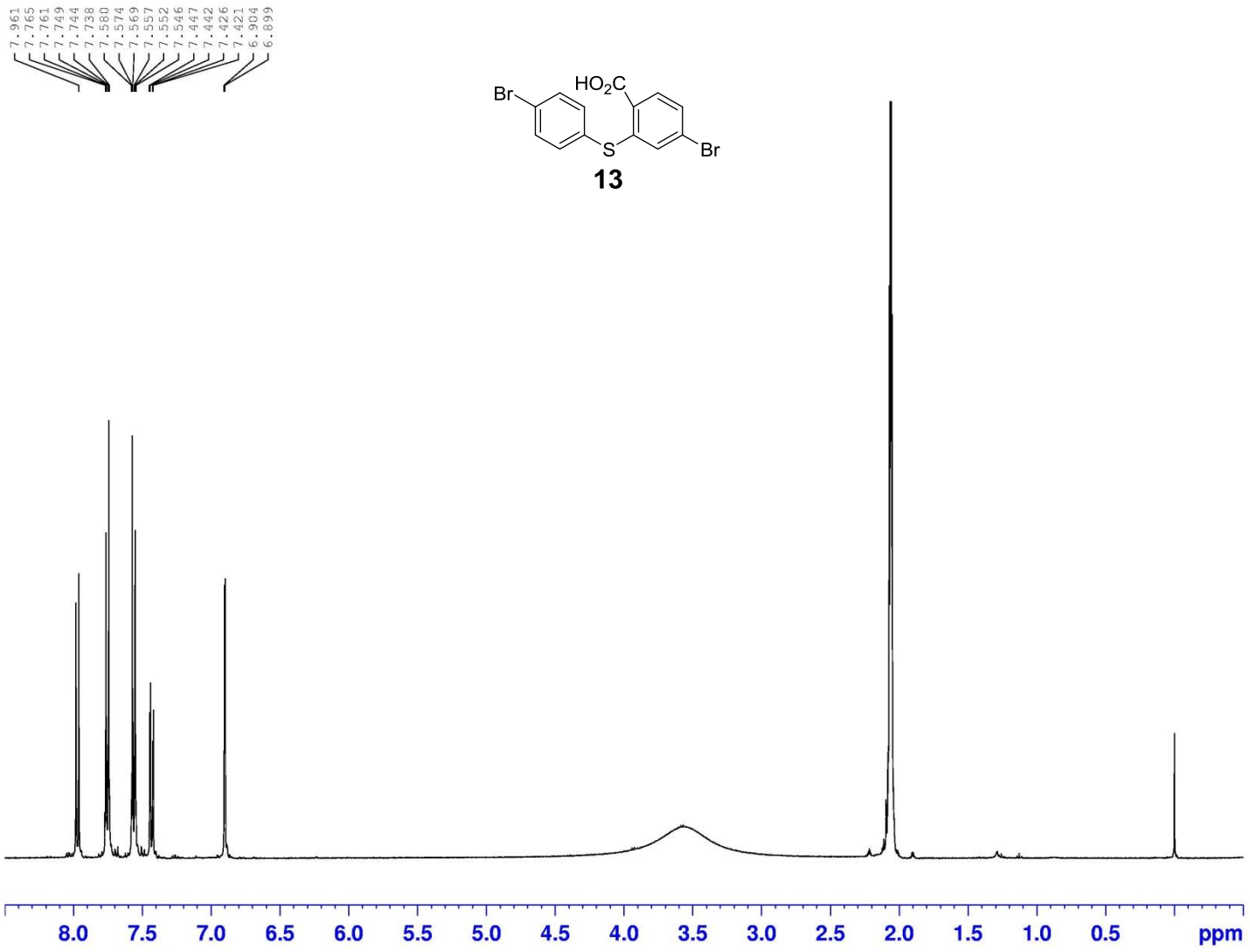
7.961
7.765
7.761
7.749
7.744
7.738
7.580
7.574
7.569
7.557
7.552
7.546
7.447
7.442
7.426
7.421
6.904
6.899
HO2C
Br
S
Br
13
8.0
7.5
7.0
6.5
6.0
5.5
5.0
4.5
4.0
3.5
3.0
2.5
2.0
1.5
1.0
0.5
ppm

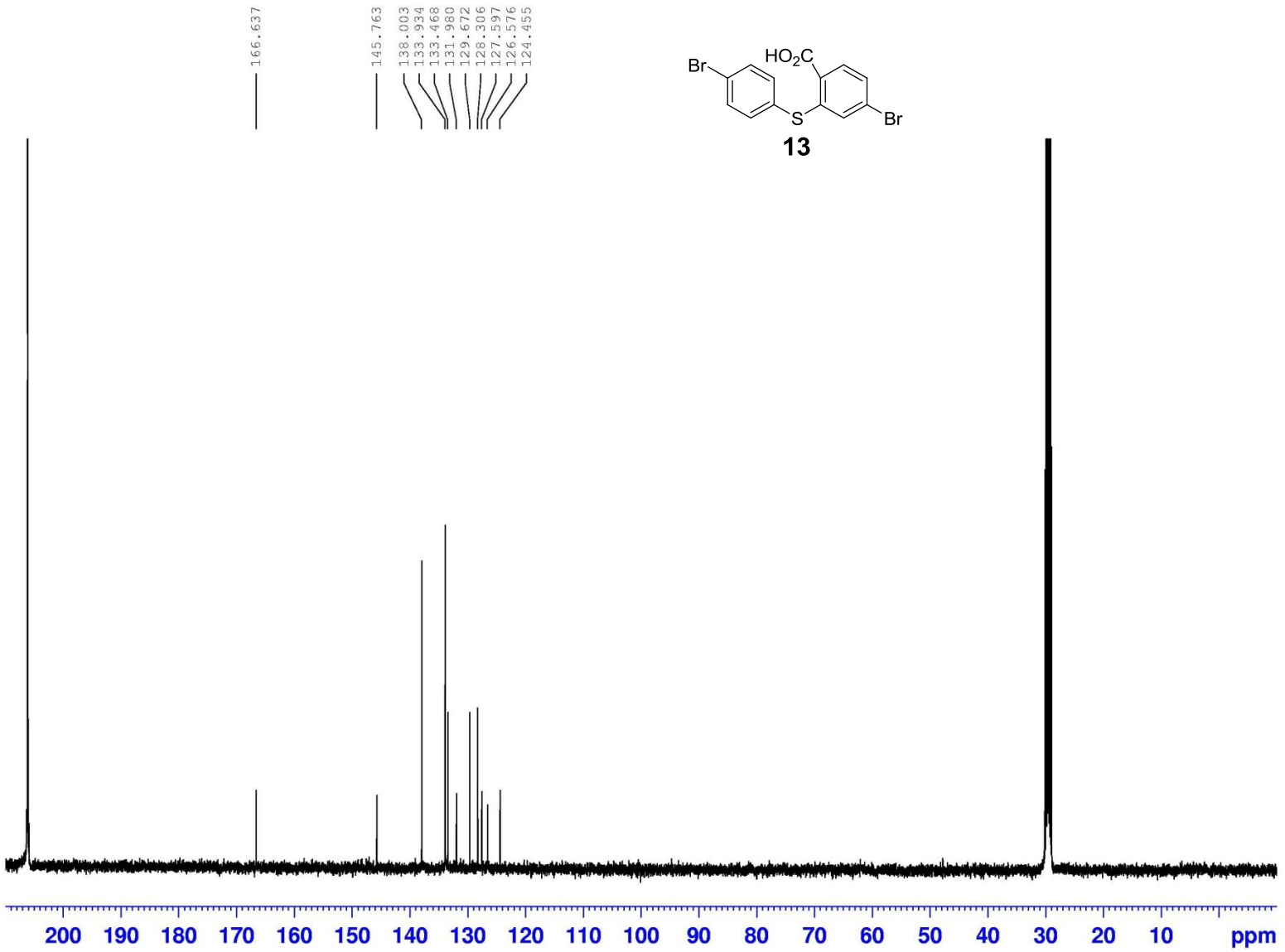
166.637
145.763
138.003
133.934
133.468
131.980
129.672
128.306
127.597
126.576
124.455
Br
HO2C
S
Br
13
200 190 180 170 160 150 140 130 120 110 100 90 80 70 60 50 40 30 20 10 ppm

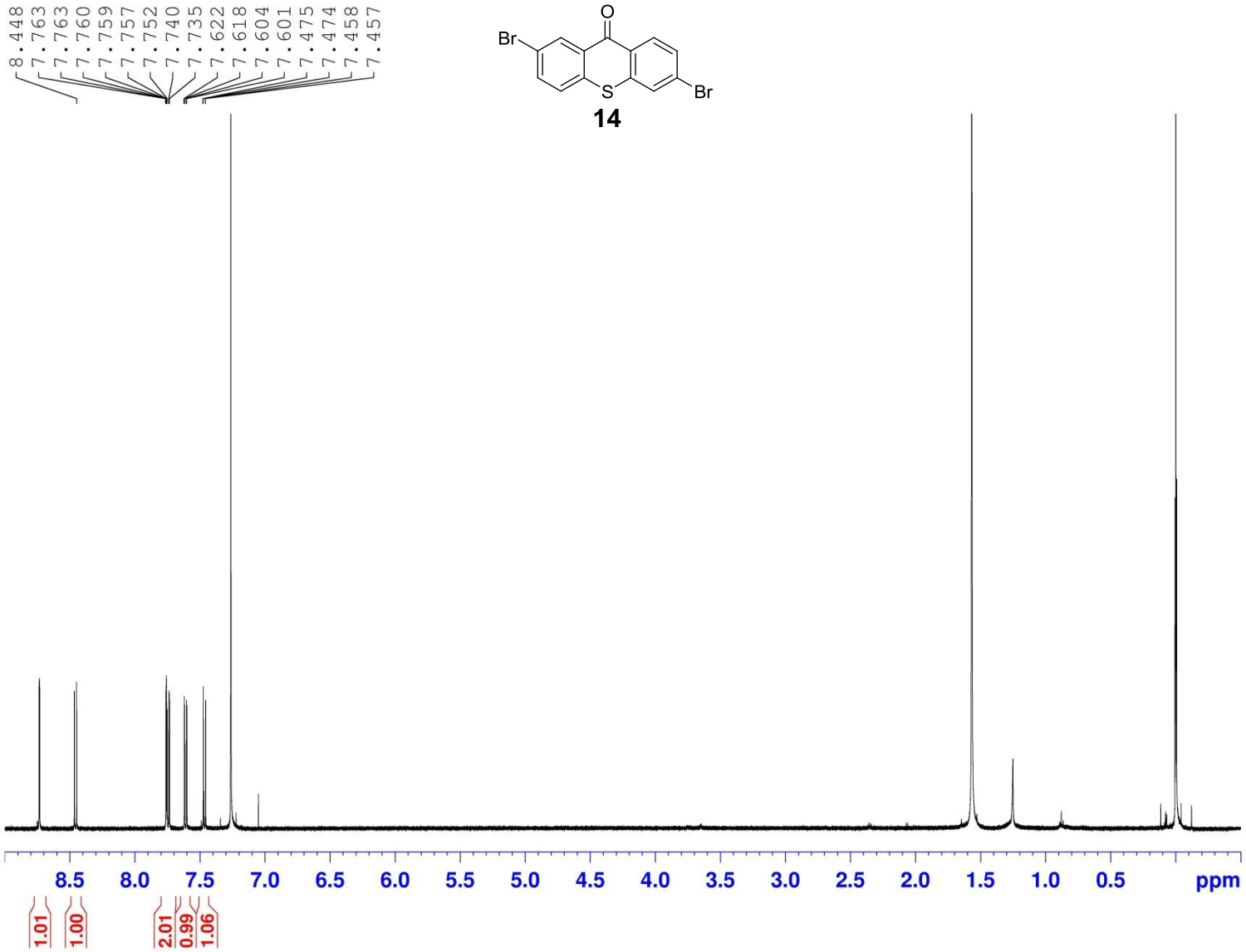
8.448
7.763
7.763
7.760
7.759
7.757
7.752
7.740
7.735
7.622
7.618
7.604
7.601
7.475
7.474
7.458
7.457
O
Br
S
Br
14
8.5
8.0
7.5
7.0
6.5
6.0
5.5
5.0
4.5
4.0
3.5
3.0
2.5
2.0
1.5
1.0
0.5
ppm
1.01
1.00
2.01
0.99
1.06

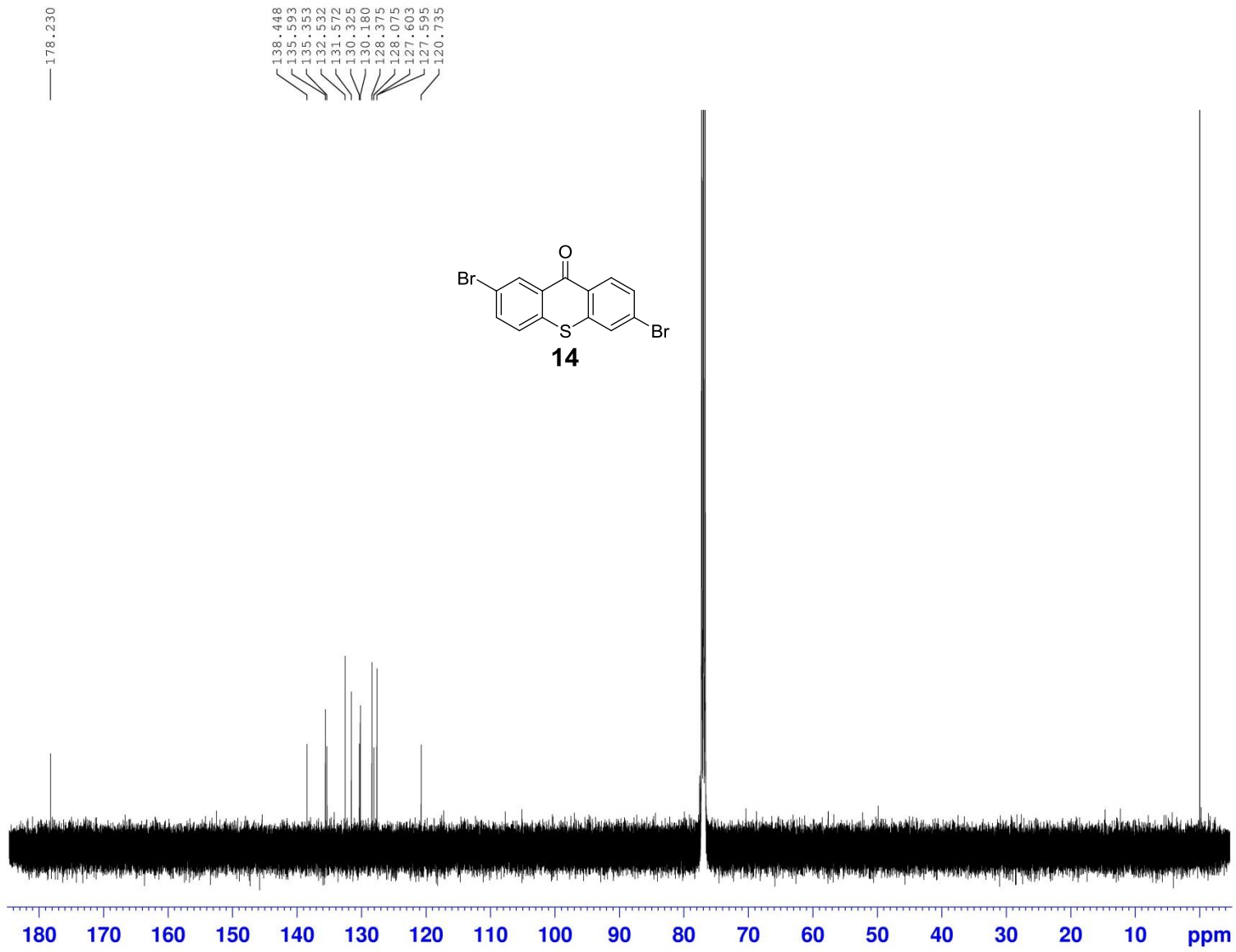
178.230
138.448
135.593
135.353
132.532
131.572
130.325
130.180
128.375
128.075
127.603
127.595
120.735
O
Br
S
Br
14
180
170
160
150
140
130
120
110
100
90
80
70
60
50
40
30
20
10
ppm

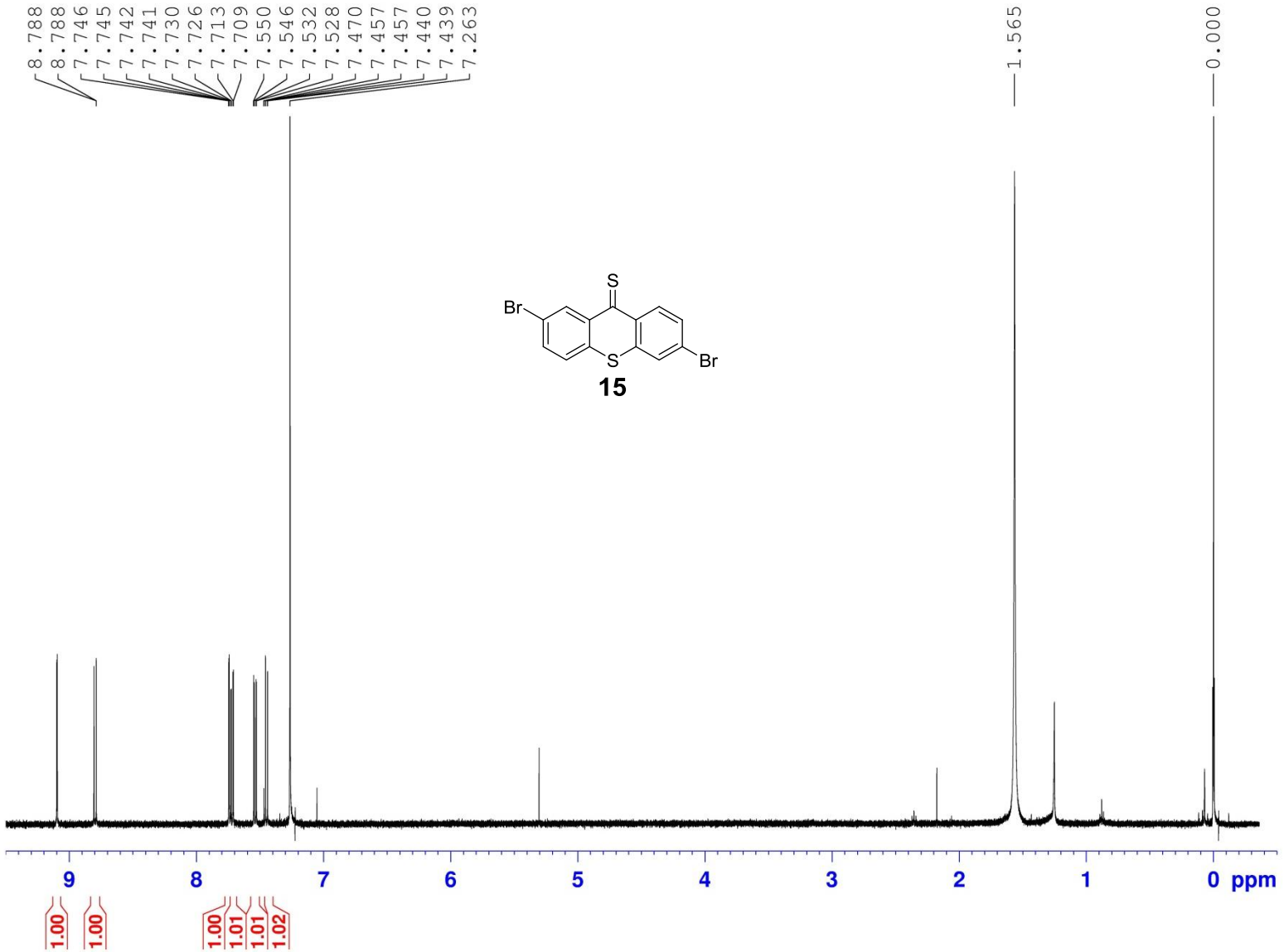
8.788
8.788
7.746
7.745
7.742
7.741
7.730
7.726
7.713
7.709
7.550
7.546
7.532
7.528
7.470
7.457
7.457
7.440
7.439
7.263
1.565
0.000
S
Br
S
Br
15
9
8
7
6
5
4
3
2
1
0 ppm
1.00
1.00
1.00
1.01
1.01
1.02

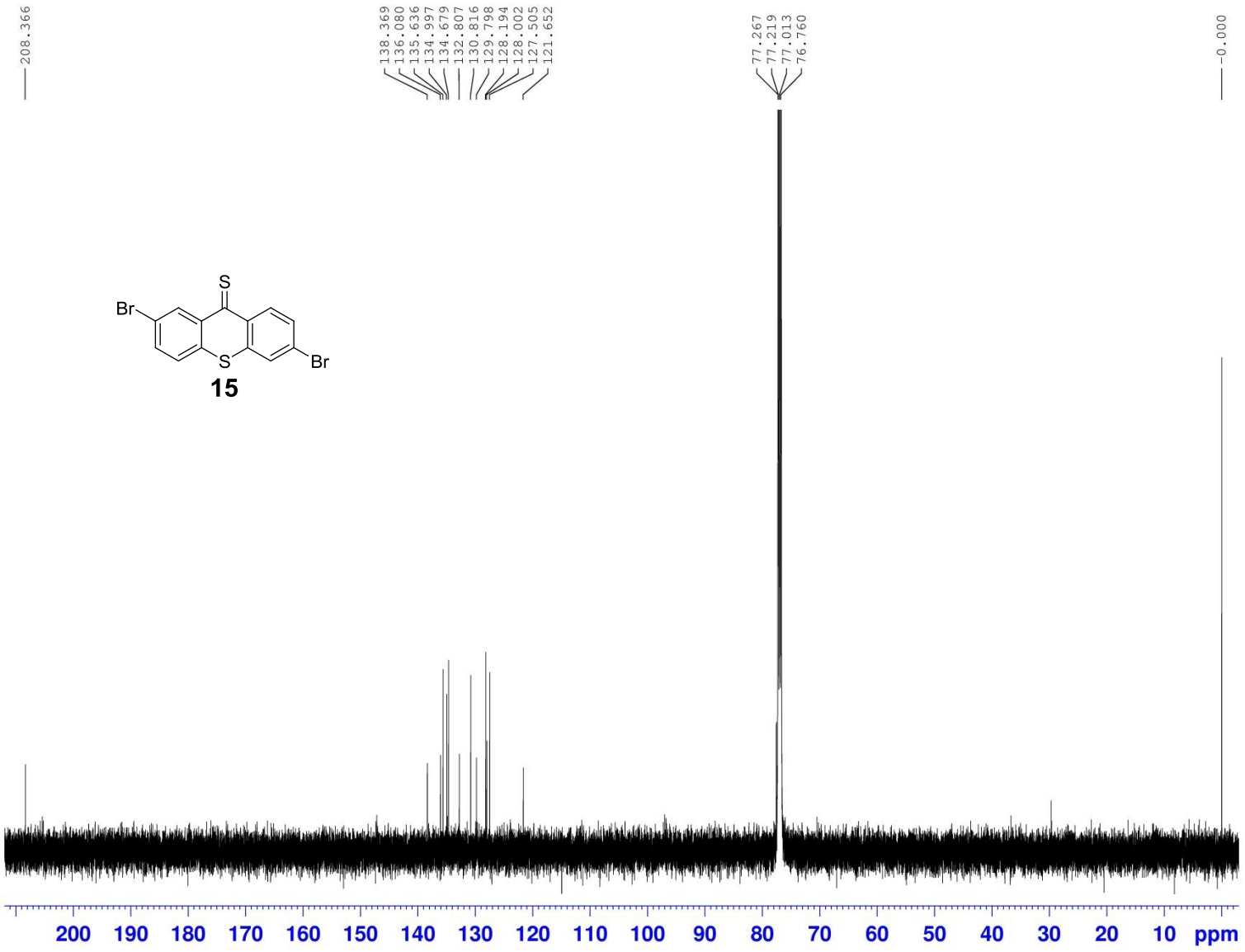
208.366
138.369
136.080
135.636
134.997
134.679
132.807
130.816
129.798
128.194
128.002
127.505
121.652
77.267
77.219
77.013
76.760
0.000
S
Br
S
Br
15
200 190 180 170 160 150 140 130 120 110 100 90 80 70 60 50 40 30 20 10 ppm

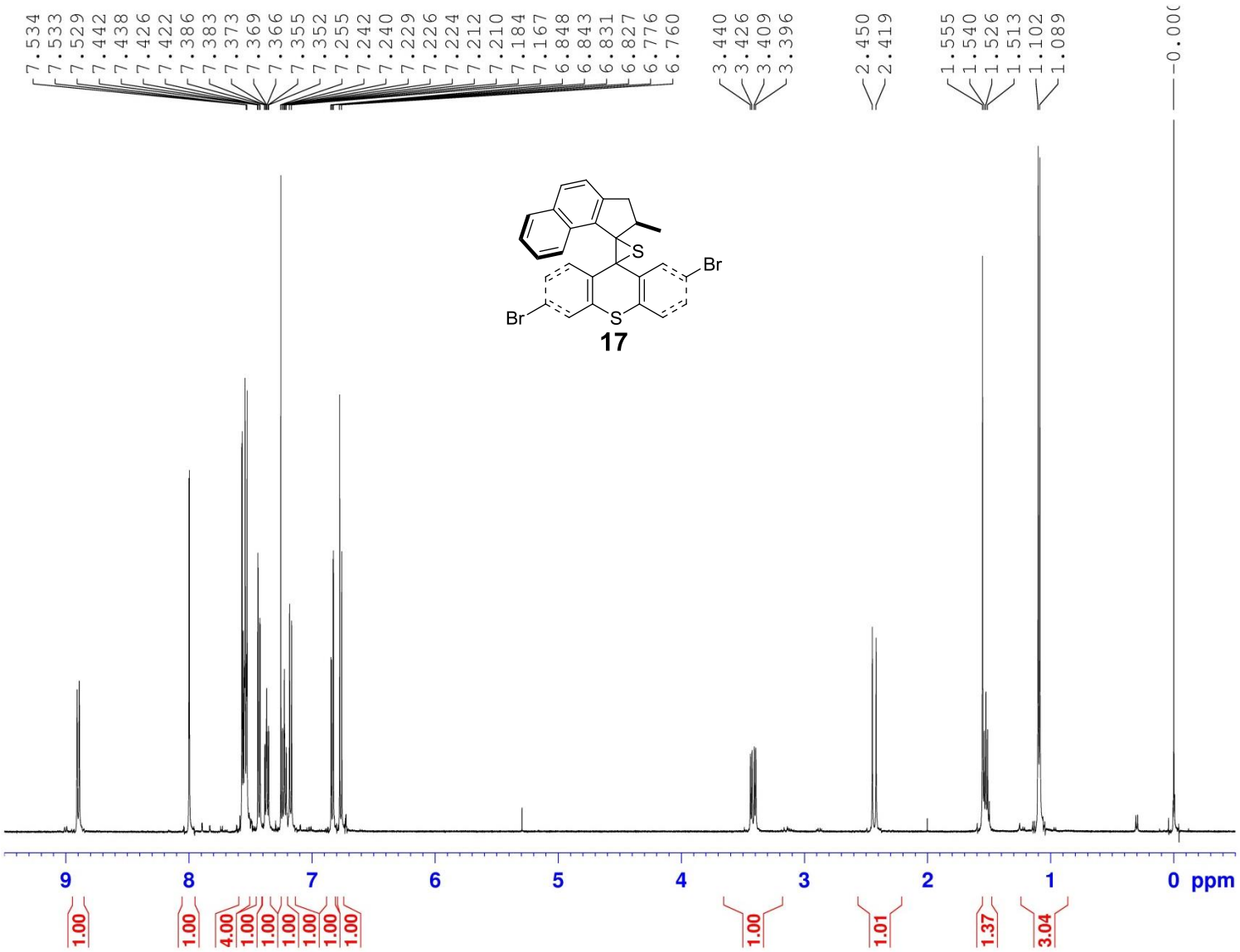
7.534
7.533
7.529
7.442
7.438
7.426
7.422
7.386
7.383
7.373
7.369
7.366
7.355
7.352
7.255
7.242
7.240
7.229
7.226
7.224
7.212
7.210
7.184
7.167
6.848
6.843
6.831
6.827
6.776
6.760
3.440
3.426
3.409
3.396
2.450
2.419
1.555
1.540
1.526
1.513
1.102
1.089
0.000
S
Br
Br
S
17
9
8
7
6
5
4
3
2
1
0 ppm
1.00
1.00
4.00
1.00
1.00
1.00
1.00
1.00
1.00
1.00
1.01
1.37
3.04

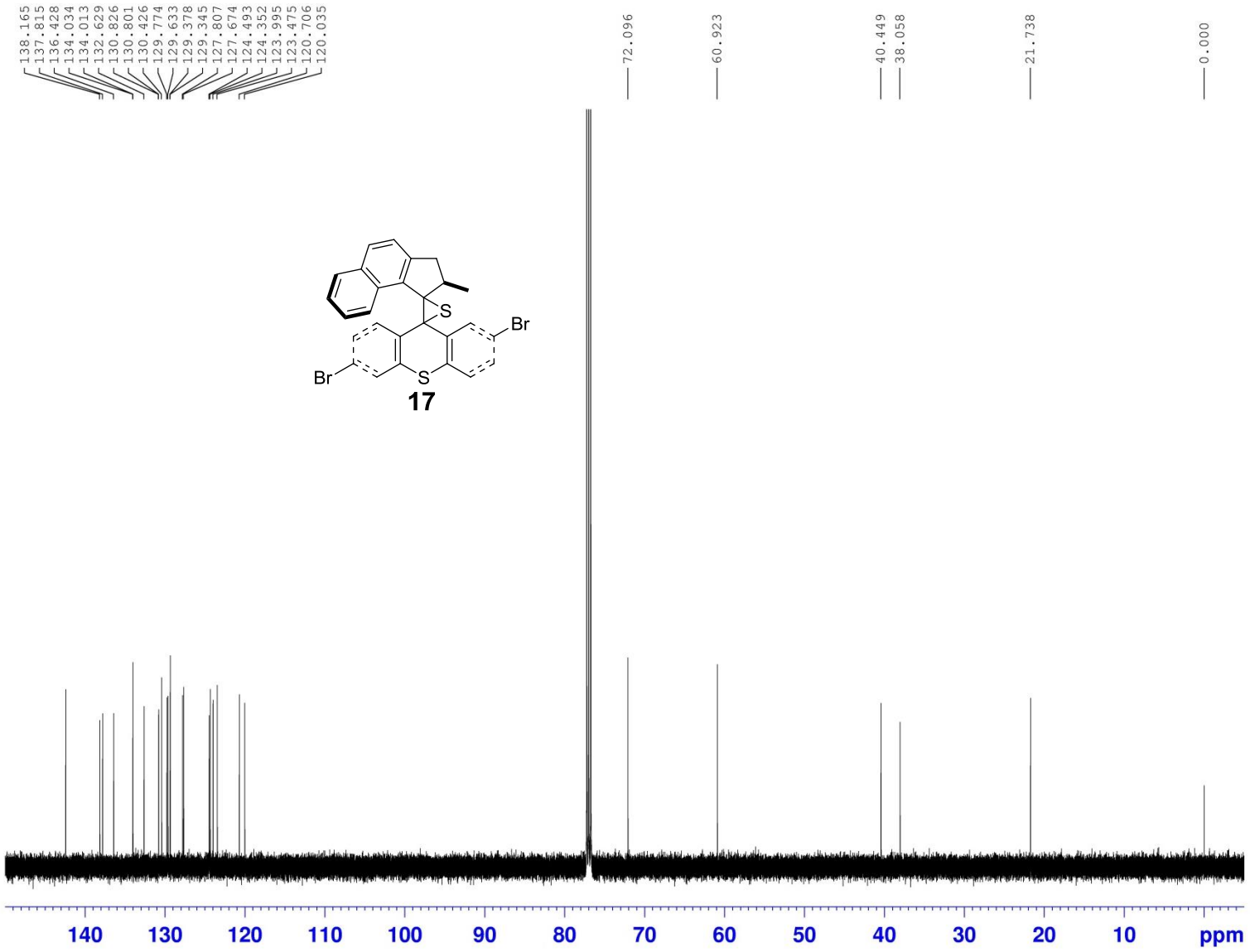
138.165
137.815
136.428
134.034
134.013
132.629
130.826
130.801
130.426
129.774
129.633
129.378
129.345
127.807
127.674
124.493
124.352
123.995
123.475
120.706
120.035
72.096
60.923
40.449
38.058
21.738
0.000
S
Br
Br
S
17
140
130
120
110
100
90
80
70
60
50
40
30
20
10
ppm

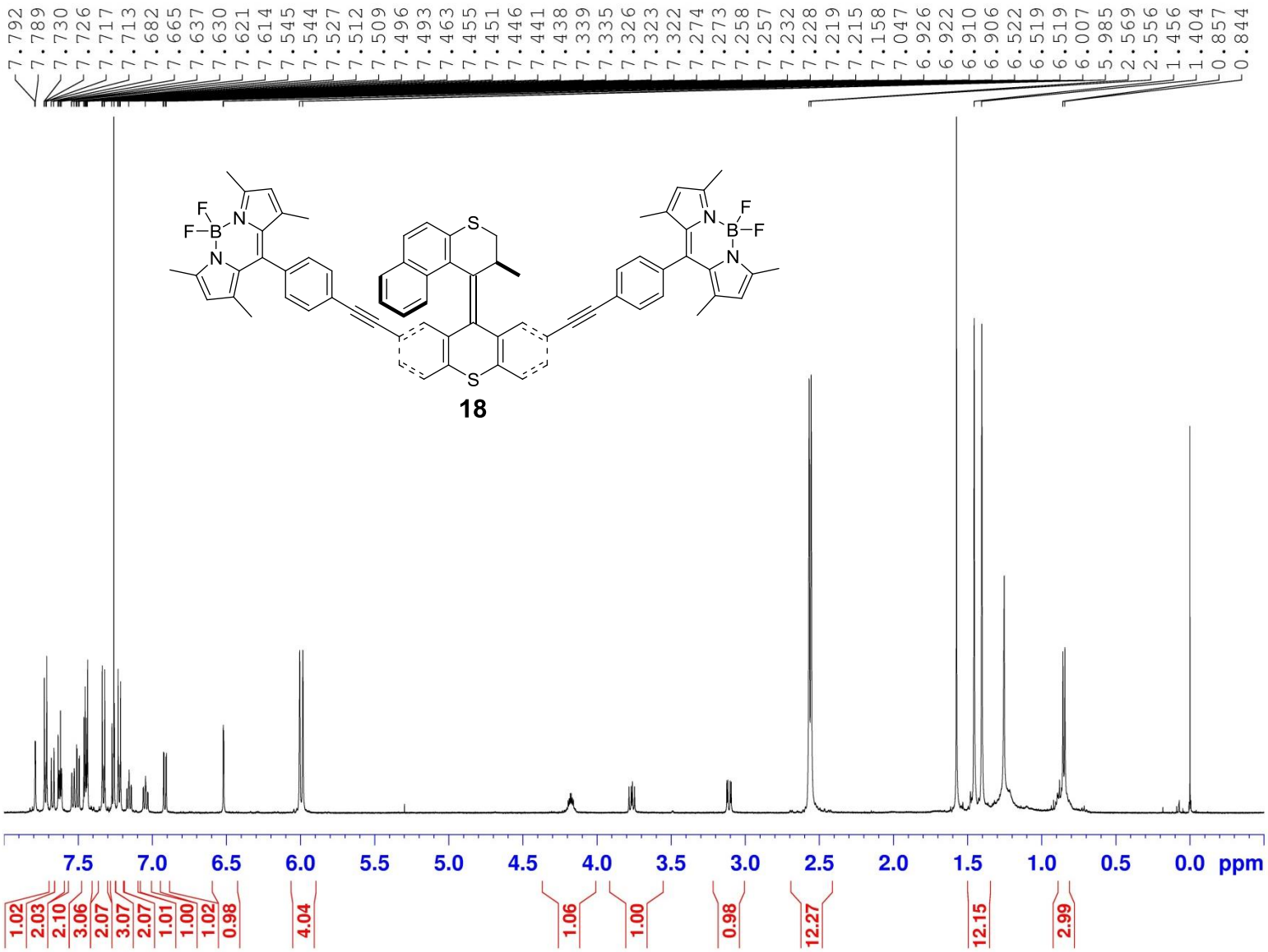
7.792
7.789
7.730
7.726
7.717
7.713
7.682
7.665
7.637
7.630
7.621
7.614
7.545
7.544
7.527
7.512
7.509
7.496
7.493
7.463
7.455
7.451
7.446
7.441
7.438
7.339
7.335
7.326
7.323
7.322
7.274
7.273
7.258
7.257
7.232
7.228
7.219
7.215
7.158
7.047
6.926
6.922
6.910
6.906
6.522
6.519
6.519
6.007
5.985
2.569
2.556
1.456
1.404
0.857
0.844
F
F–B
N
N
S
S
N
B–F
F
N
18
7.5
7.0
6.5
6.0
5.5
5.0
4.5
4.0
3.5
3.0
2.5
2.0
1.5
1.0
0.5
0.0
ppm
1.02
2.03
2.10
3.06
2.07
3.07
2.07
1.01
1.00
1.02
0.98
4.04
1.06
1.00
0.98
12.27
12.15
2.99

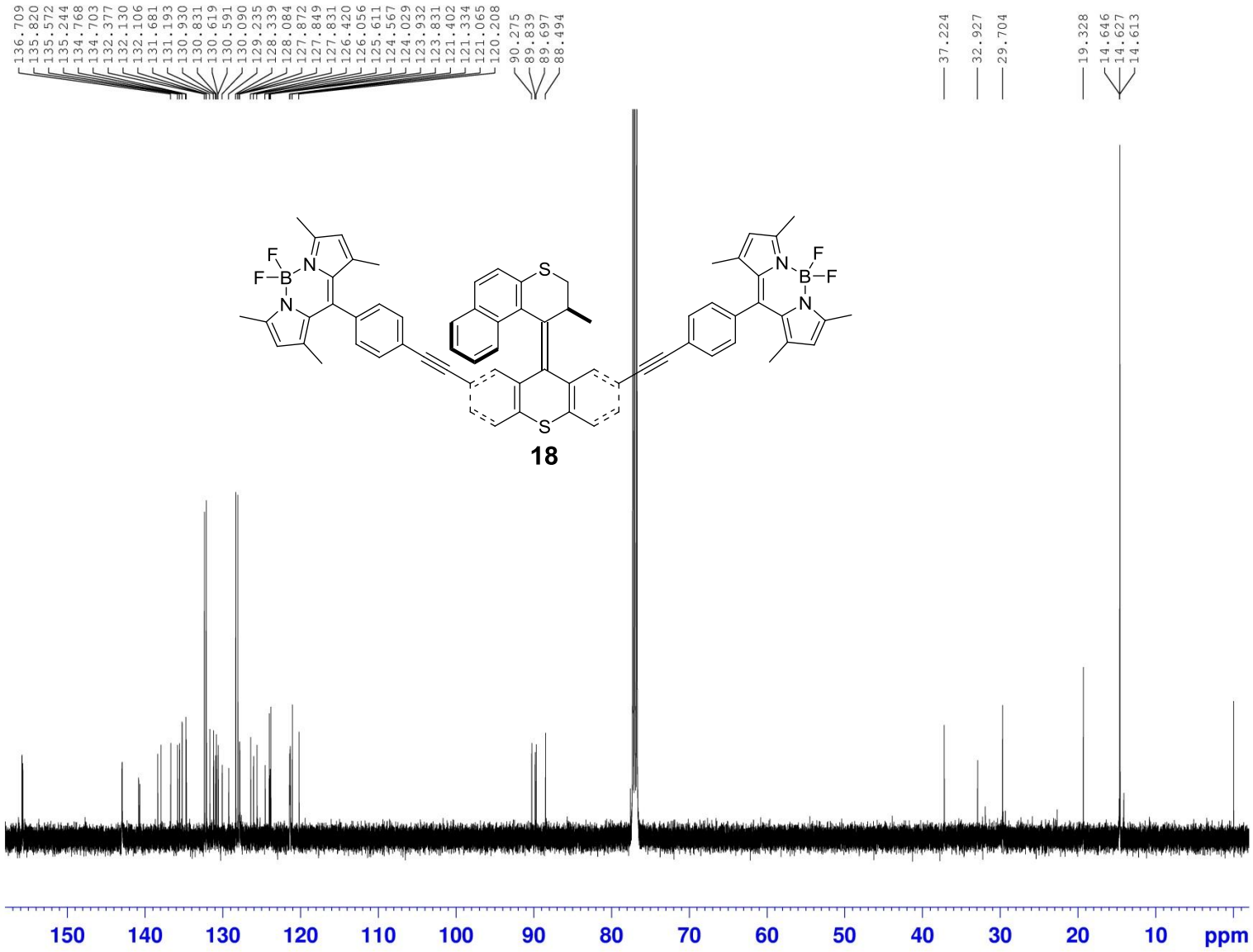
136.709
135.820
135.572
135.244
134.768
134.703
132.377
132.130
132.106
131.681
131.193
130.930
130.831
130.619
130.591
130.090
129.235
128.339
128.084
127.872
127.849
127.831
126.420
126.056
125.611
124.567
124.029
123.932
123.831
121.402
121.334
121.065
120.208
90.275
89.839
89.697
88.494
37.224
32.927
29.704
19.328
14.646
14.627
14.613
18
150
140
130
120
110
100
90
80
70
60
50
40
30
20
10
ppm

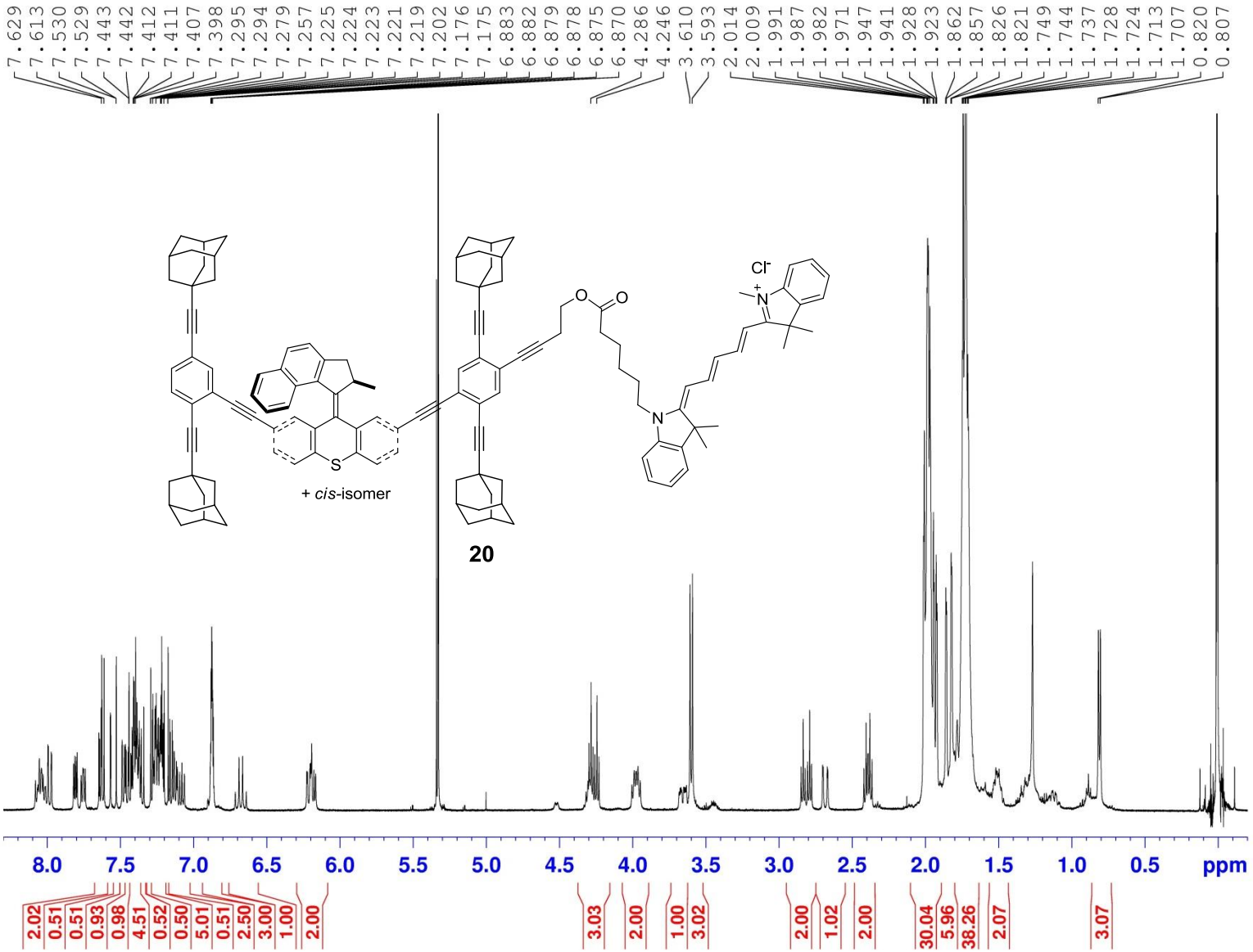
7.629
7.613
7.530
7.529
7.443
7.442
7.412
7.411
7.407
7.398
7.295
7.294
7.279
7.257
7.225
7.224
7.223
7.221
7.219
7.202
7.176
7.175
6.883
6.882
6.879
6.878
6.875
6.870
4.286
4.246
3.610
3.593
2.014
2.009
1.991
1.987
1.982
1.971
1.947
1.941
1.928
1.923
1.862
1.857
1.826
1.821
1.749
1.744
1.737
1.728
1.724
1.713
1.707
0.820
0.807
Cl-
+ cis-isomer
20
8.0
7.5
7.0
6.5
6.0
5.5
5.0
4.5
4.0
3.5
3.0
2.5
2.0
1.5
1.0
0.5
ppm
2.02
0.51
0.51
0.93
0.98
4.51
0.52
0.50
5.01
0.51
2.50
3.00
1.00
2.00
3.03
2.00
1.00
3.02
2.00
1.02
2.00
30.04
5.96
38.26
2.07
3.07

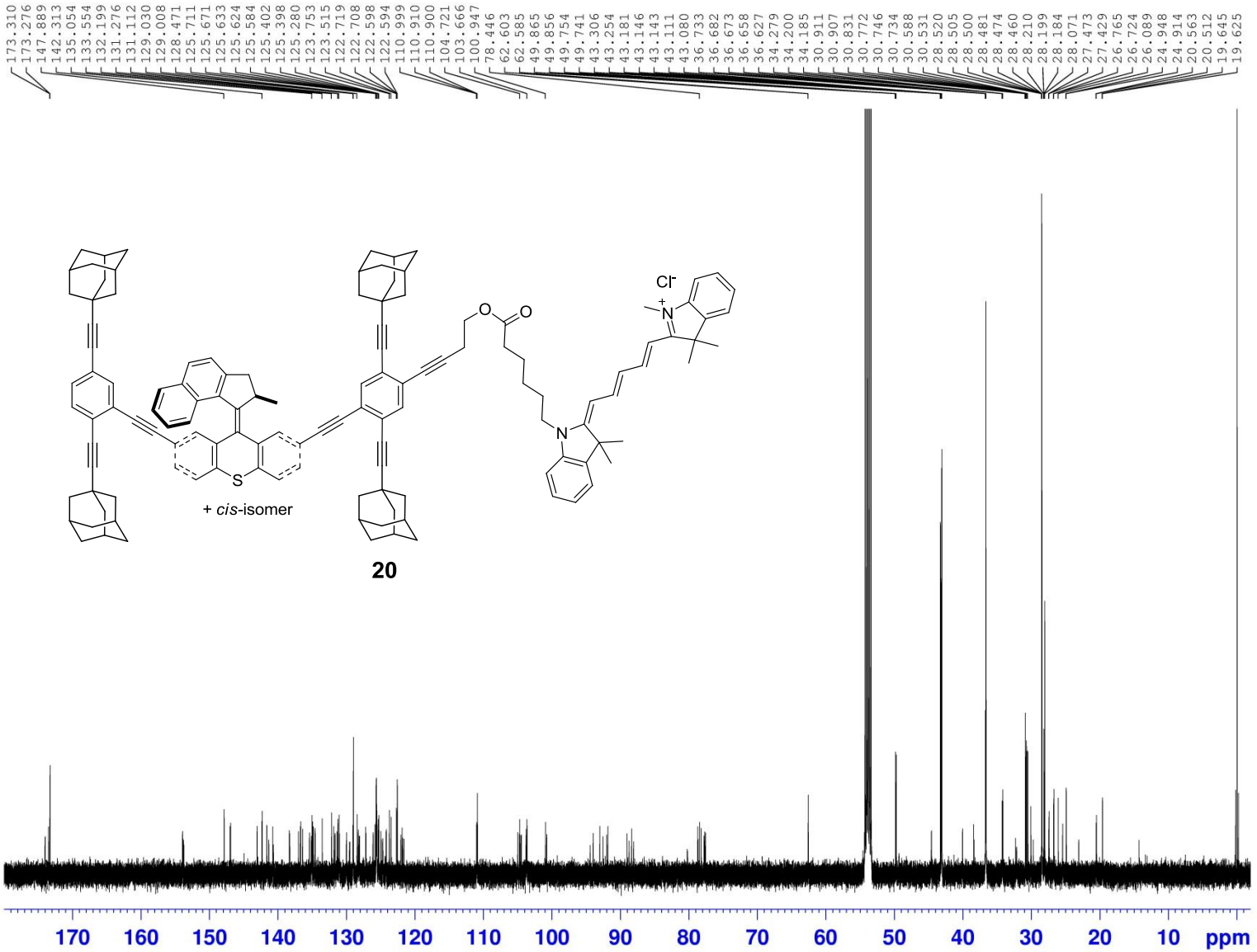
173.310
173.276
147.889
142.313
135.054
133.554
132.199
131.276
131.112
129.030
129.008
128.471
125.711
125.671
125.633
125.624
125.584
125.402
125.398
125.280
123.753
123.515
122.719
122.708
122.598
122.594
110.999
110.910
110.900
104.721
103.666
100.947
78.446
62.603
62.585
49.865
49.856
49.754
49.741
43.306
43.254
43.181
43.146
43.143
43.111
43.080
36.733
36.682
36.673
36.658
36.627
34.279
34.200
34.185
30.911
30.907
30.831
30.772
30.746
30.734
30.588
30.531
28.520
28.505
28.500
28.481
28.474
28.460
28.210
28.199
28.184
28.071
27.473
27.429
26.765
26.724
26.089
24.948
24.914
20.563
20.512
19.645
19.625
Cl-
+
N
O
O
N
S
+ cis-isomer
20
170
160
150
140
130
120
110
100
90
80
70
60
50
40
30
20
10
ppm

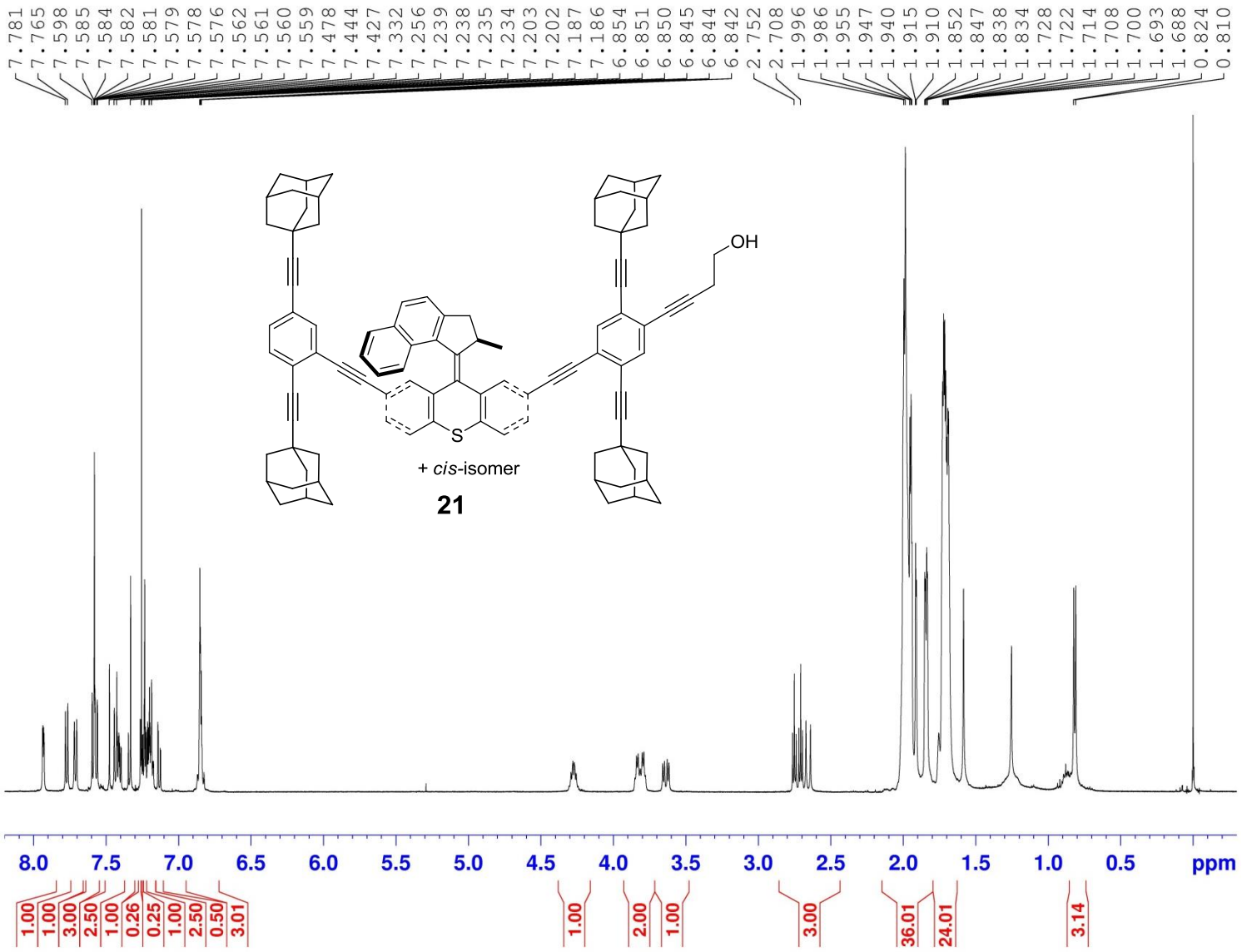
7.781
7.765
7.598
7.585
7.584
7.582
7.581
7.579
7.578
7.576
7.562
7.561
7.560
7.559
7.478
7.444
7.427
7.332
7.256
7.239
7.238
7.235
7.234
7.203
7.202
7.187
7.186
6.854
6.851
6.850
6.845
6.844
6.842
2.752
2.708
1.996
1.986
1.955
1.947
1.940
1.915
1.910
1.852
1.847
1.838
1.834
1.728
1.722
1.714
1.708
1.700
1.693
1.688
0.824
0.810
OH
S
+ cis-isomer
21
8.0
7.5
7.0
6.5
6.0
5.5
5.0
4.5
4.0
3.5
3.0
2.5
2.0
1.5
1.0
0.5
ppm
1.00
1.00
3.00
2.50
1.00
0.26
0.25
1.00
2.50
0.50
3.01
1.00
2.00
1.00
3.00
36.01
24.01
3.14

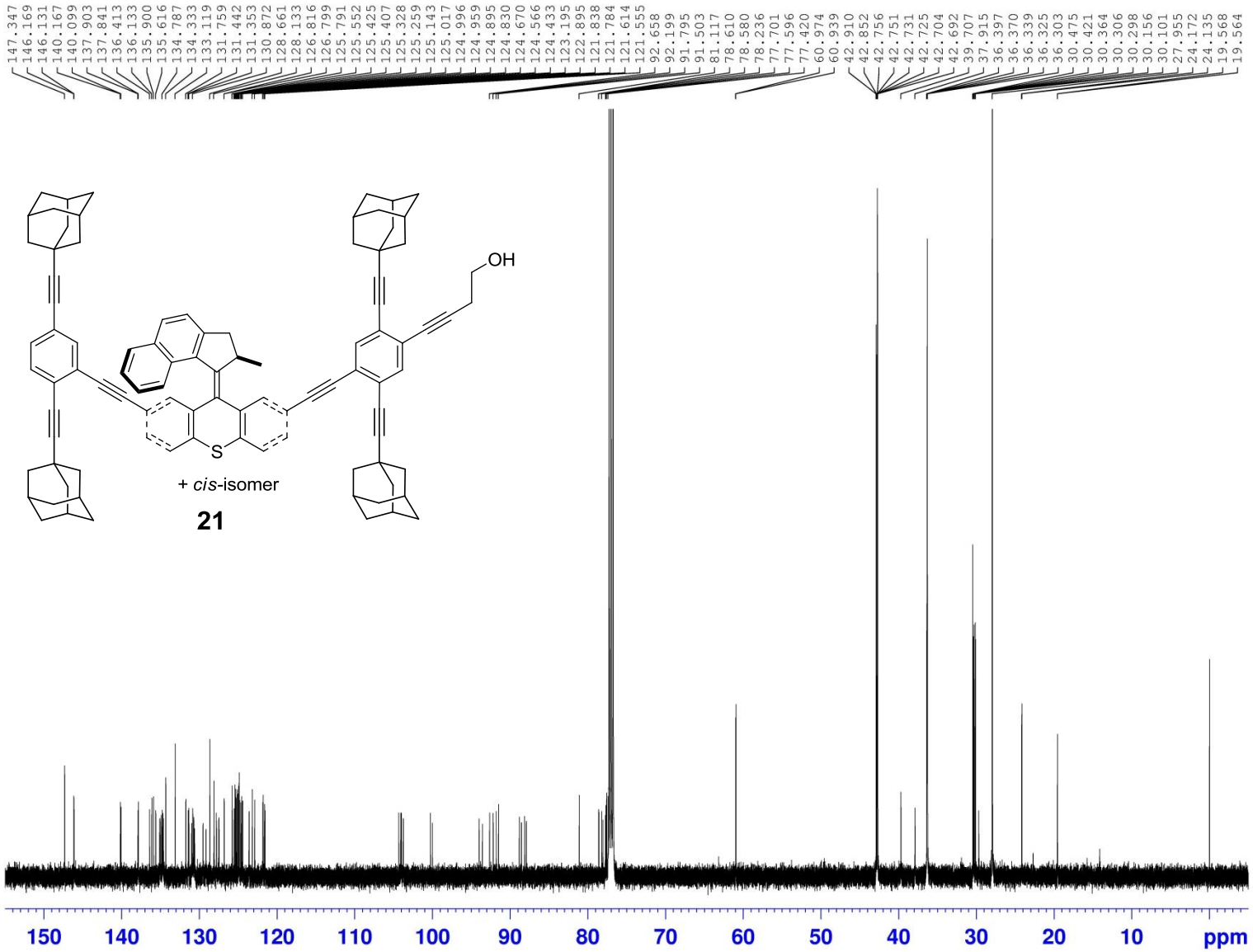
147.347
146.169
146.131
140.167
140.099
137.903
137.841
136.413
136.133
135.900
135.616
134.787
134.333
133.119
131.759
131.442
131.353
130.872
128.661
128.133
126.816
126.799
125.791
125.552
125.425
125.407
125.328
125.259
125.143
125.017
124.996
124.959
124.895
124.830
124.670
124.566
124.433
123.195
122.895
121.838
121.784
121.614
121.555
92.658
92.199
91.795
91.503
81.117
78.610
78.580
78.236
77.701
77.596
77.420
60.974
60.939
42.910
42.852
42.756
42.751
42.731
42.725
42.704
42.692
39.707
37.915
36.397
36.370
36.339
36.325
36.303
30.475
30.421
30.364
30.306
30.298
30.156
30.101
27.955
24.172
24.135
19.568
19.564
OH
S
+ *cis*-isomer
21
150
140
130
120
110
100
90
80
70
60
50
40
30
20
10
ppm

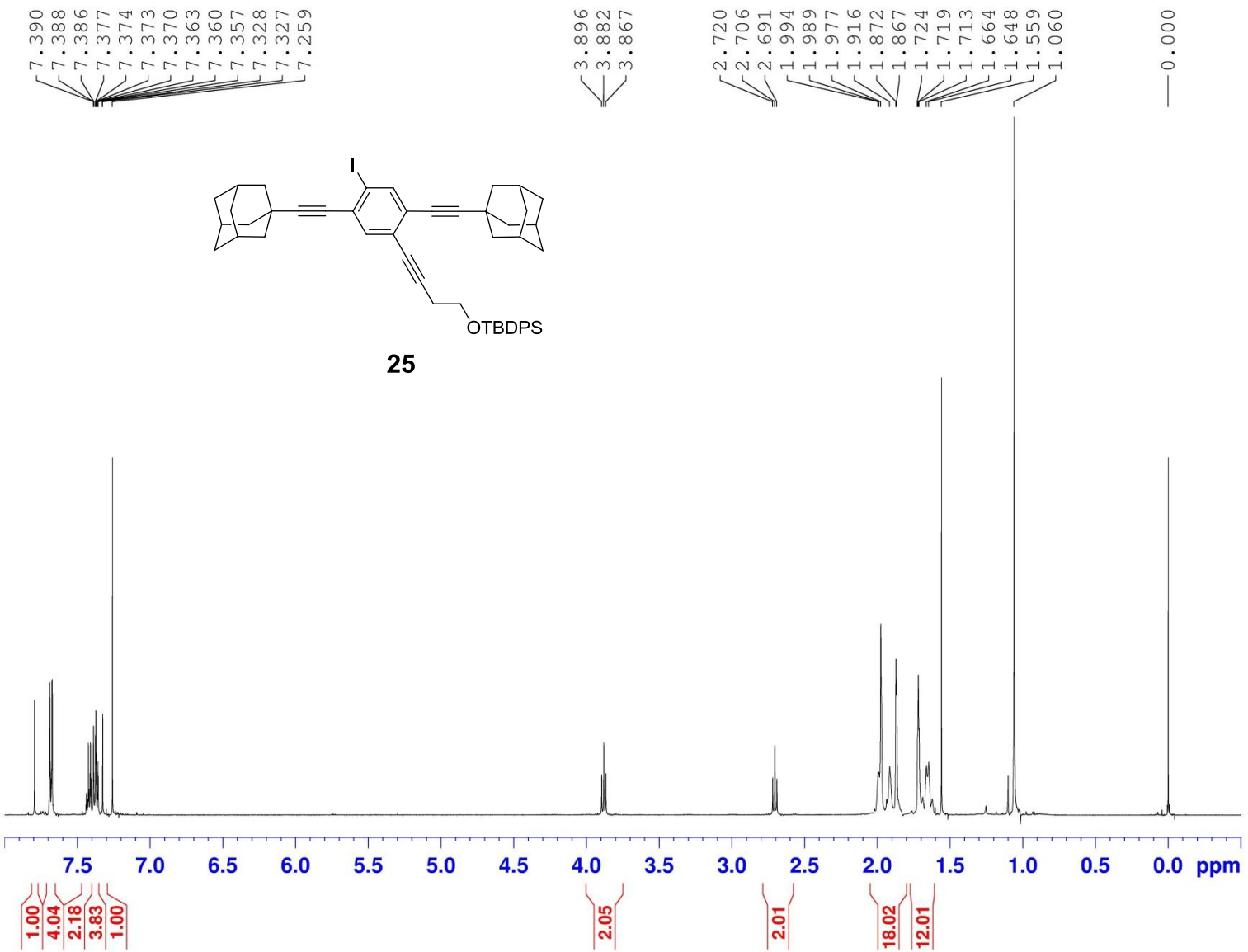
7.390
7.388
7.386
7.377
7.374
7.373
7.370
7.363
7.360
7.357
7.328
7.327
7.259
3.896
3.882
3.867
2.720
2.706
2.691
1.994
1.989
1.977
1.916
1.872
1.867
1.724
1.719
1.713
1.664
1.648
1.559
1.060
0.000
I
OTBDPS
7.5
7.0
6.5
6.0
5.5
5.0
4.5
4.0
3.5
3.0
2.5
2.0
1.5
1.0
0.5
0.0
ppm
1.00
4.04
2.18
3.83
1.00
2.05
2.01
18.02
12.01

25

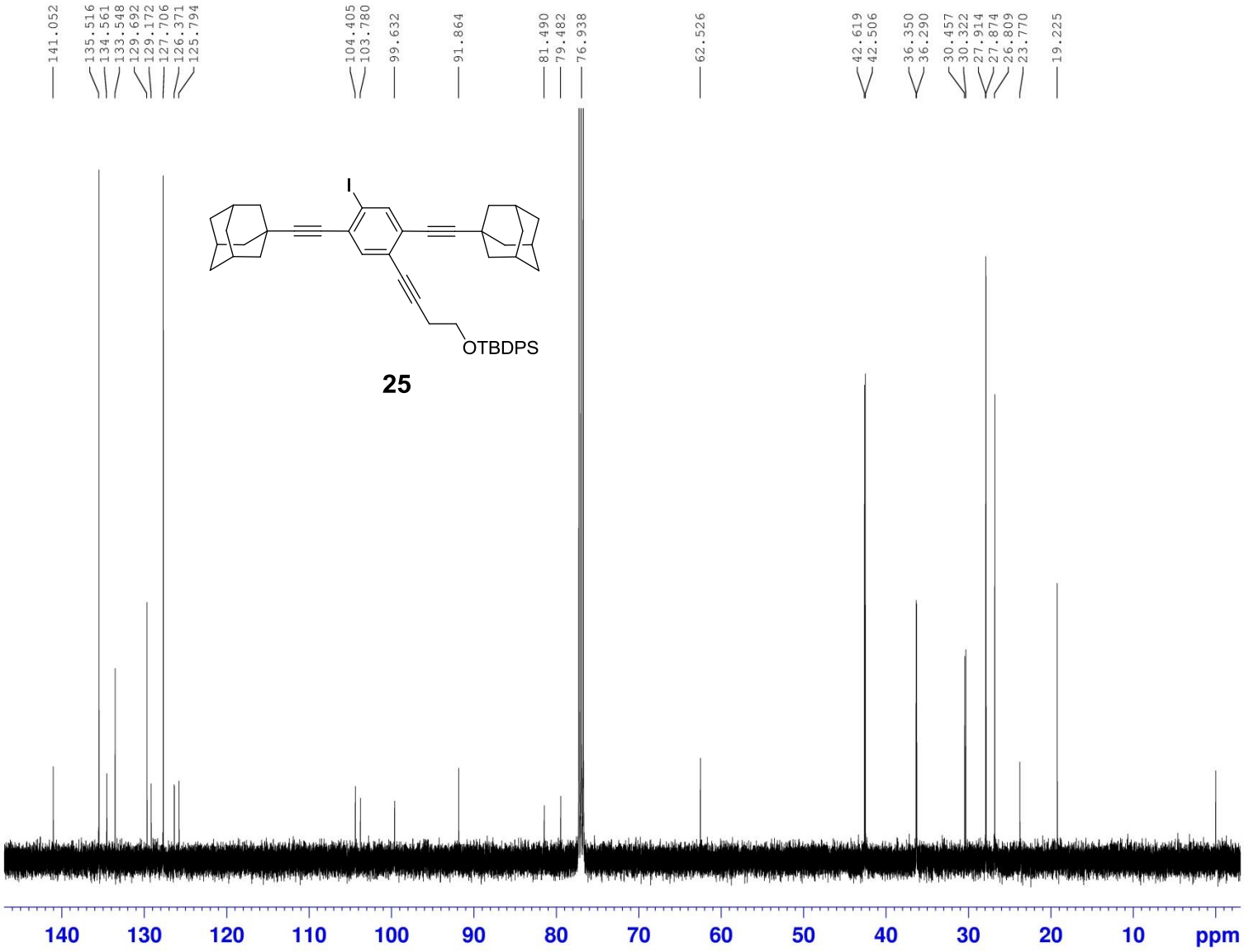
141.052
135.516
134.561
133.548
129.692
129.172
127.706
126.371
125.794
104.405
103.780
99.632
91.864
81.490
79.482
76.938
62.526
42.619
42.506
36.350
36.290
30.457
30.322
27.914
27.874
26.809
23.770
19.225
I
OTBDPS
25
140
130
120
110
100
90
80
70
60
50
40
30
20
10
ppm

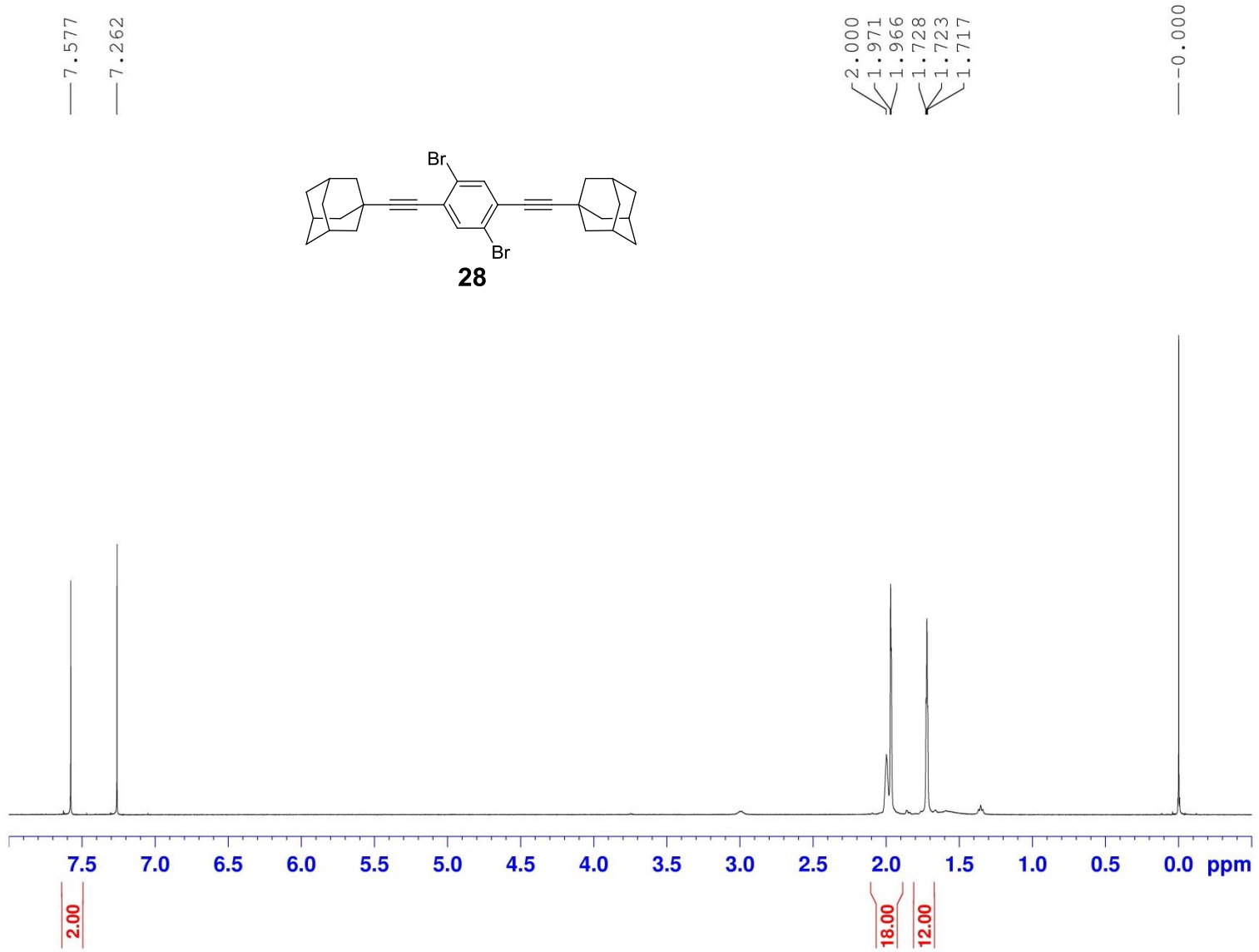
7.577
7.262
2.000
1.971
1.966
1.728
1.723
1.717
0.000
Br
Br
28
7.5
7.0
6.5
6.0
5.5
5.0
4.5
4.0
3.5
3.0
2.5
2.0
1.5
1.0
0.5
0.0
ppm
2.00
18.00
12.00

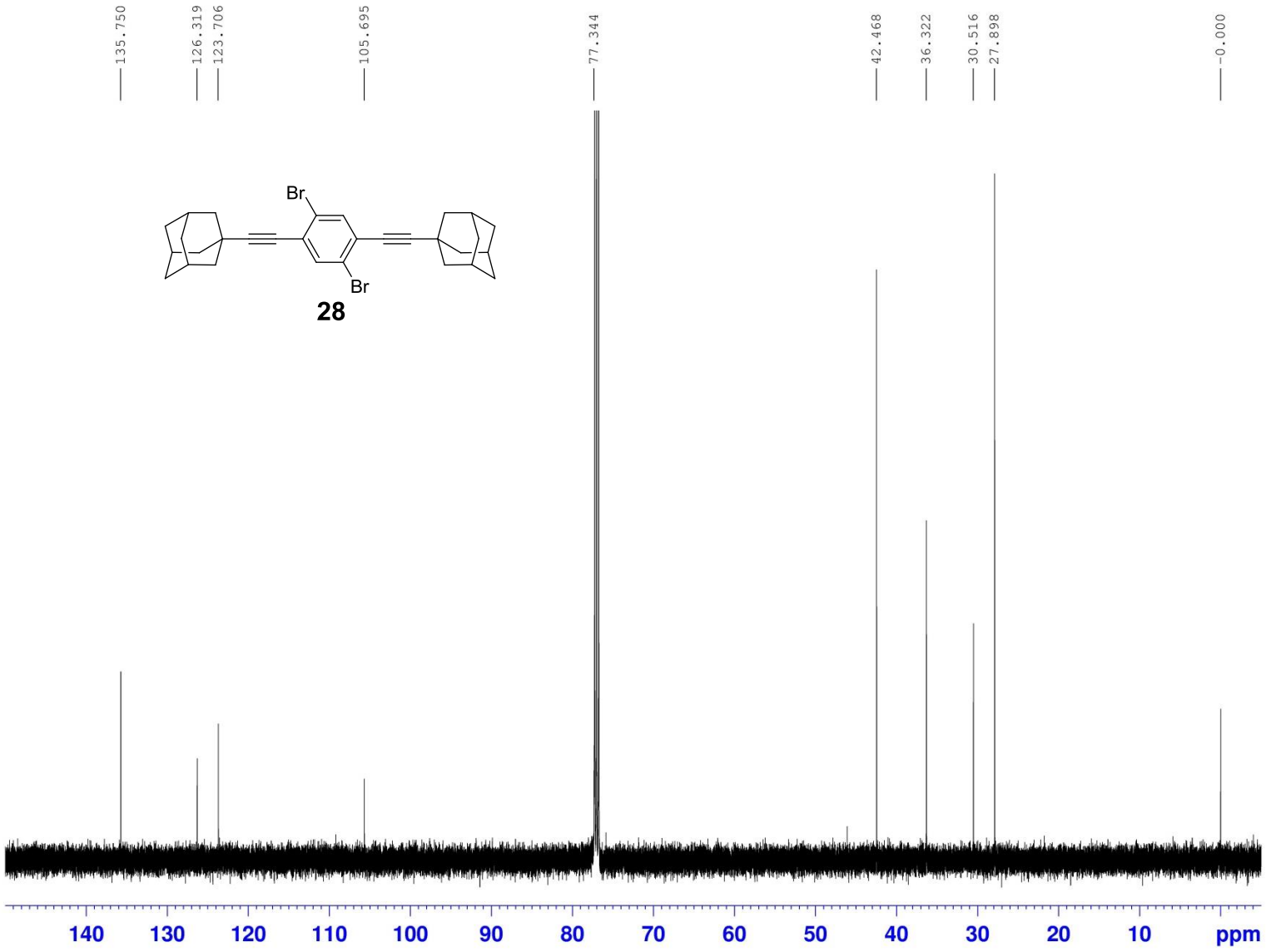
135.750
126.319
123.706
105.695
77.344
42.468
36.322
30.516
27.898
-0.000
Br
Br
28
140
130
120
110
100
90
80
70
60
50
40
30
20
10
ppm

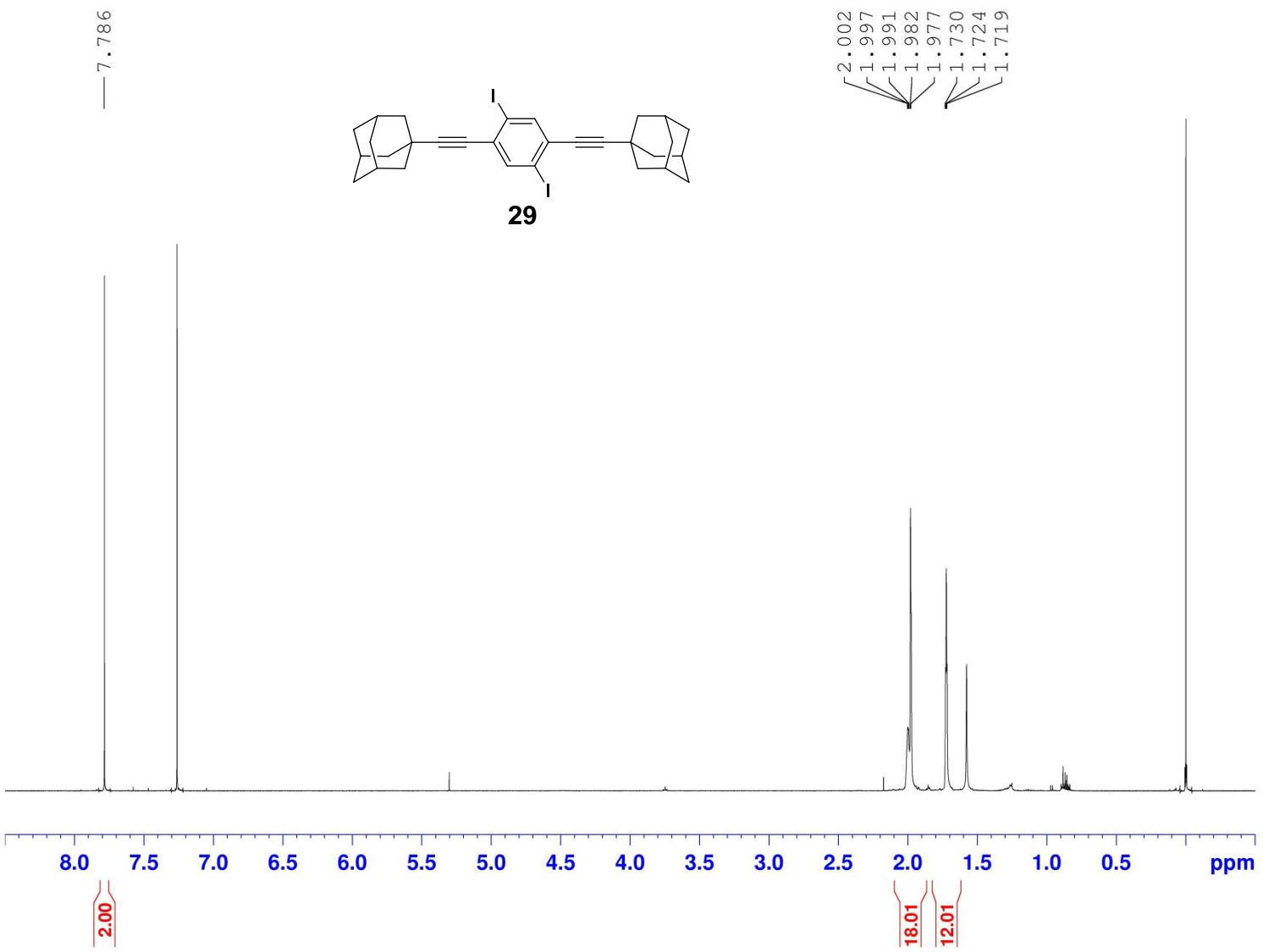
7.786
2.002
1.997
1.991
1.982
1.977
1.730
1.724
1.719
8.0
7.5
7.0
6.5
6.0
5.5
5.0
4.5
4.0
3.5
3.0
2.5
2.0
1.5
1.0
0.5
ppm
2.00
18.01
12.01

29

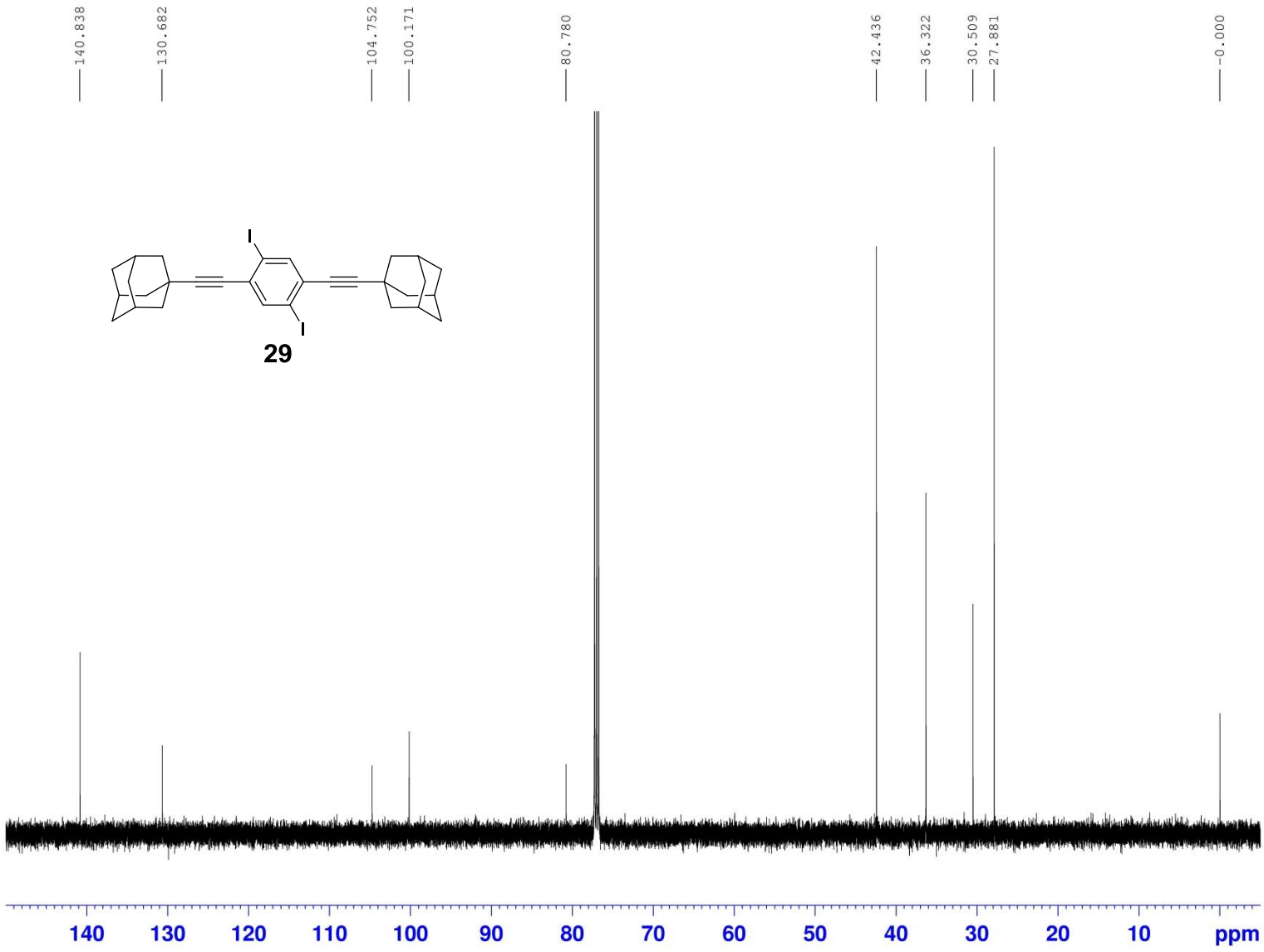
140.838
130.682
104.752
100.171
80.780
42.436
36.322
30.509
27.881
-0.000
I
I
29
140
130
120
110
100
90
80
70
60
50
40
30
20
10
ppm

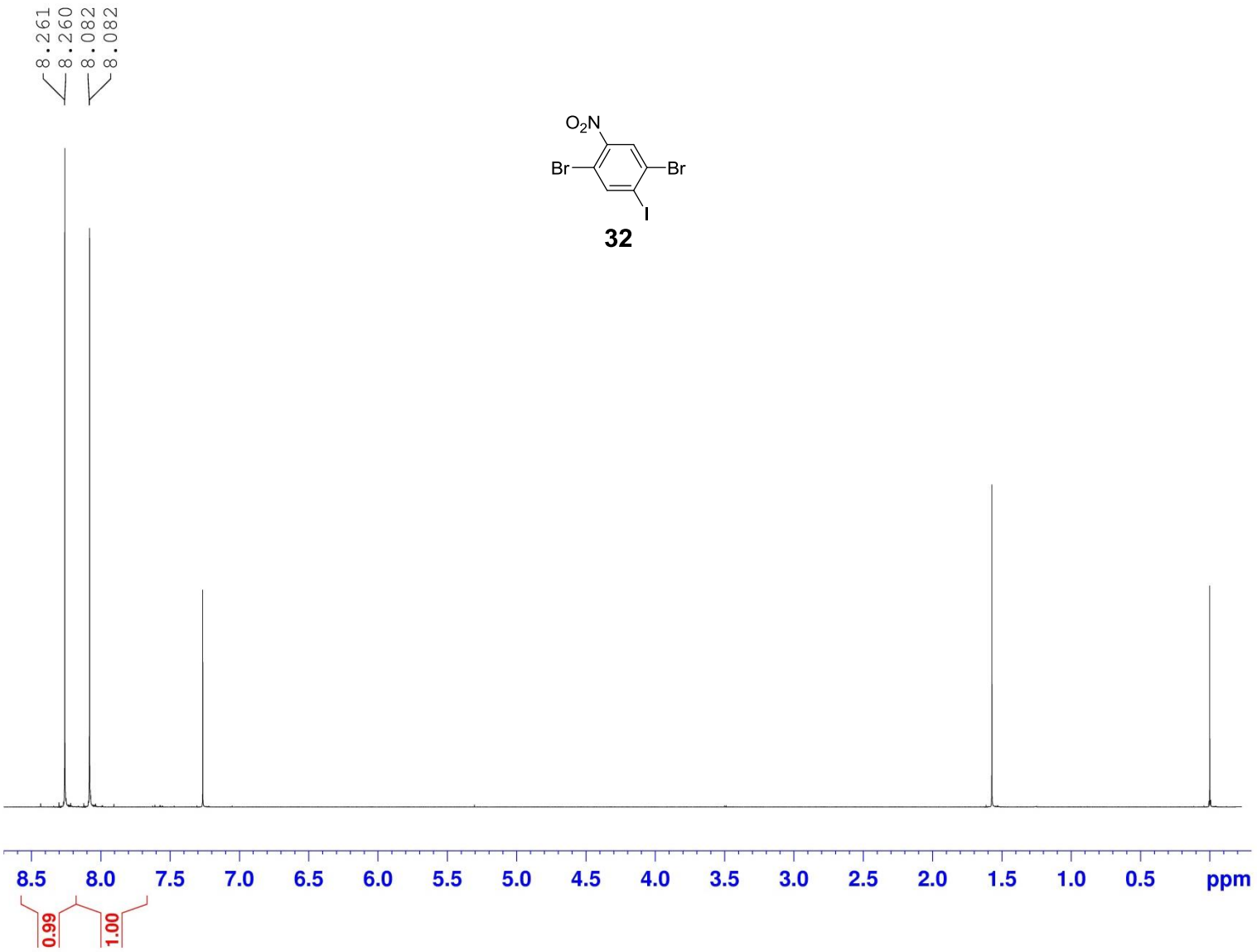
8.261
8.260
8.082
8.082
O2N
Br
Br
I
32
8.5
8.0
7.5
7.0
6.5
6.0
5.5
5.0
4.5
4.0
3.5
3.0
2.5
2.0
1.5
1.0
0.5
ppm
0.99
1.00

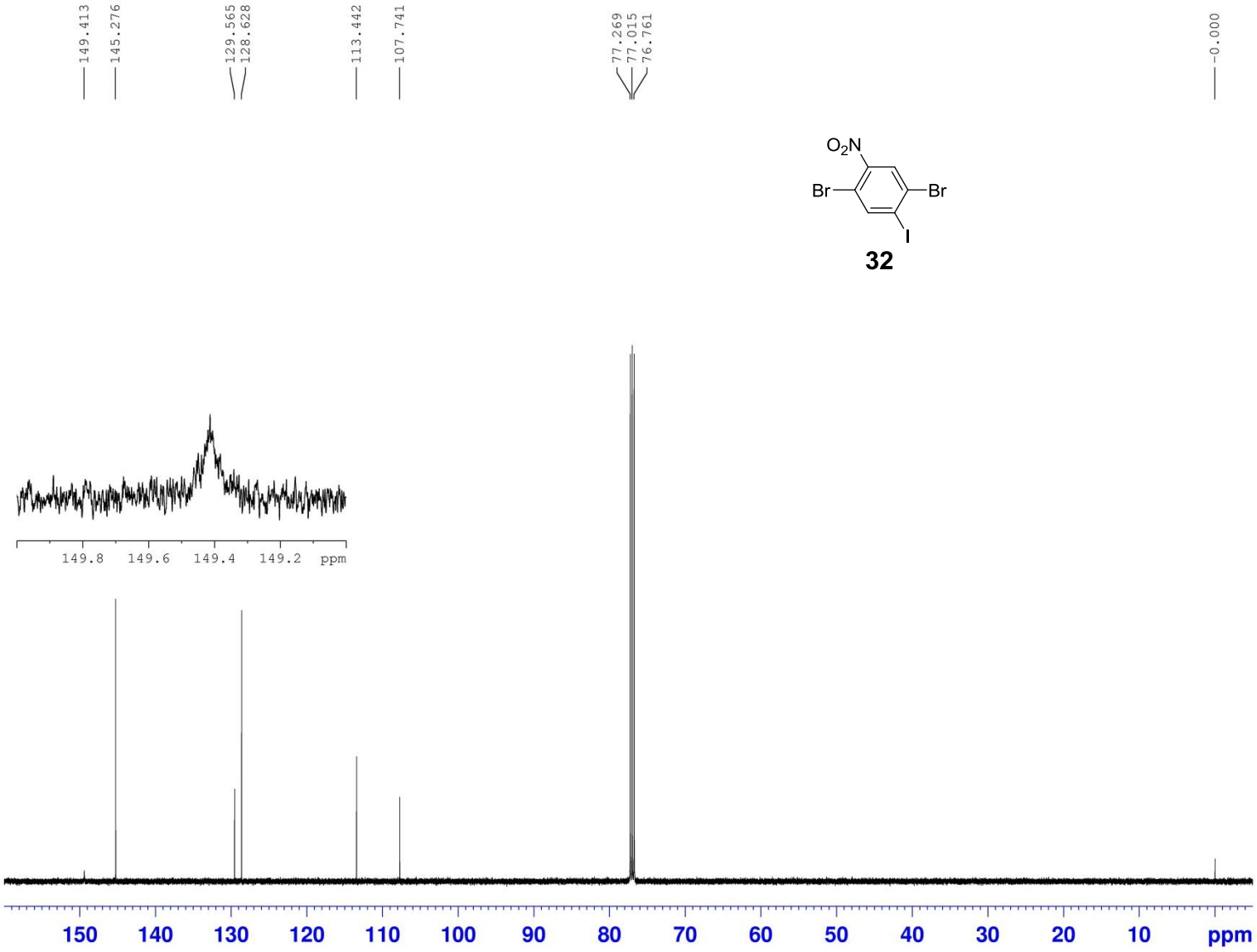
149.413
145.276
129.565
128.628
113.442
107.741
77.269
77.015
76.761
-0.000
O2N
Br
Br
I
32
149.8
149.6
149.4
149.2
ppm
150
140
130
120
110
100
90
80
70
60
50
40
30
20
10
ppm

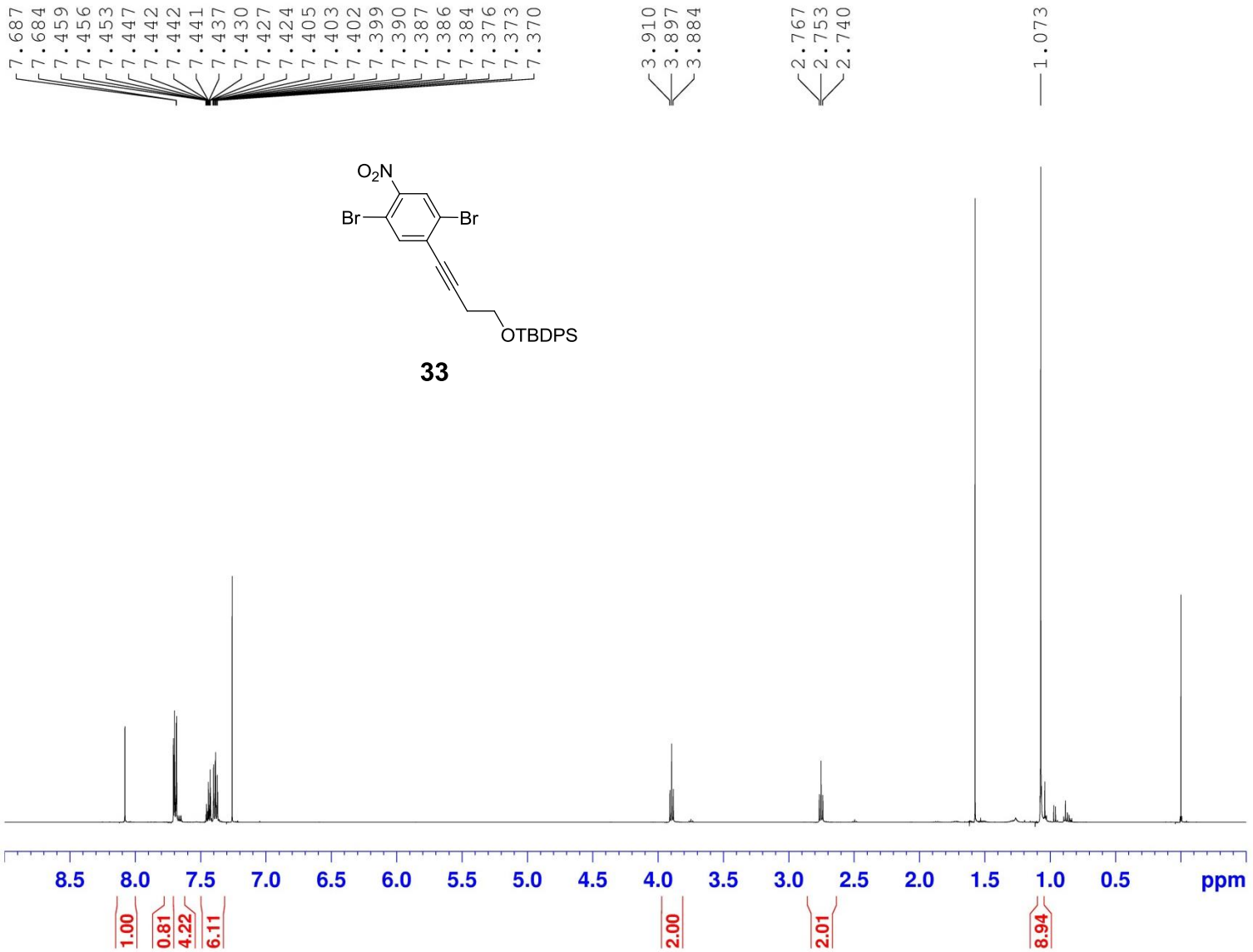
7.687
7.684
7.459
7.456
7.453
7.447
7.442
7.442
7.441
7.437
7.430
7.427
7.424
7.405
7.403
7.402
7.399
7.390
7.387
7.386
7.384
7.376
7.373
7.370
3.910
3.897
3.884
2.767
2.753
2.740
1.073
O2N
Br
Br
OTBDPS
8.5
8.0
7.5
7.0
6.5
6.0
5.5
5.0
4.5
4.0
3.5
3.0
2.5
2.0
1.5
1.0
0.5
ppm
1.00
0.81
4.22
6.11
2.00
2.01
8.94

33

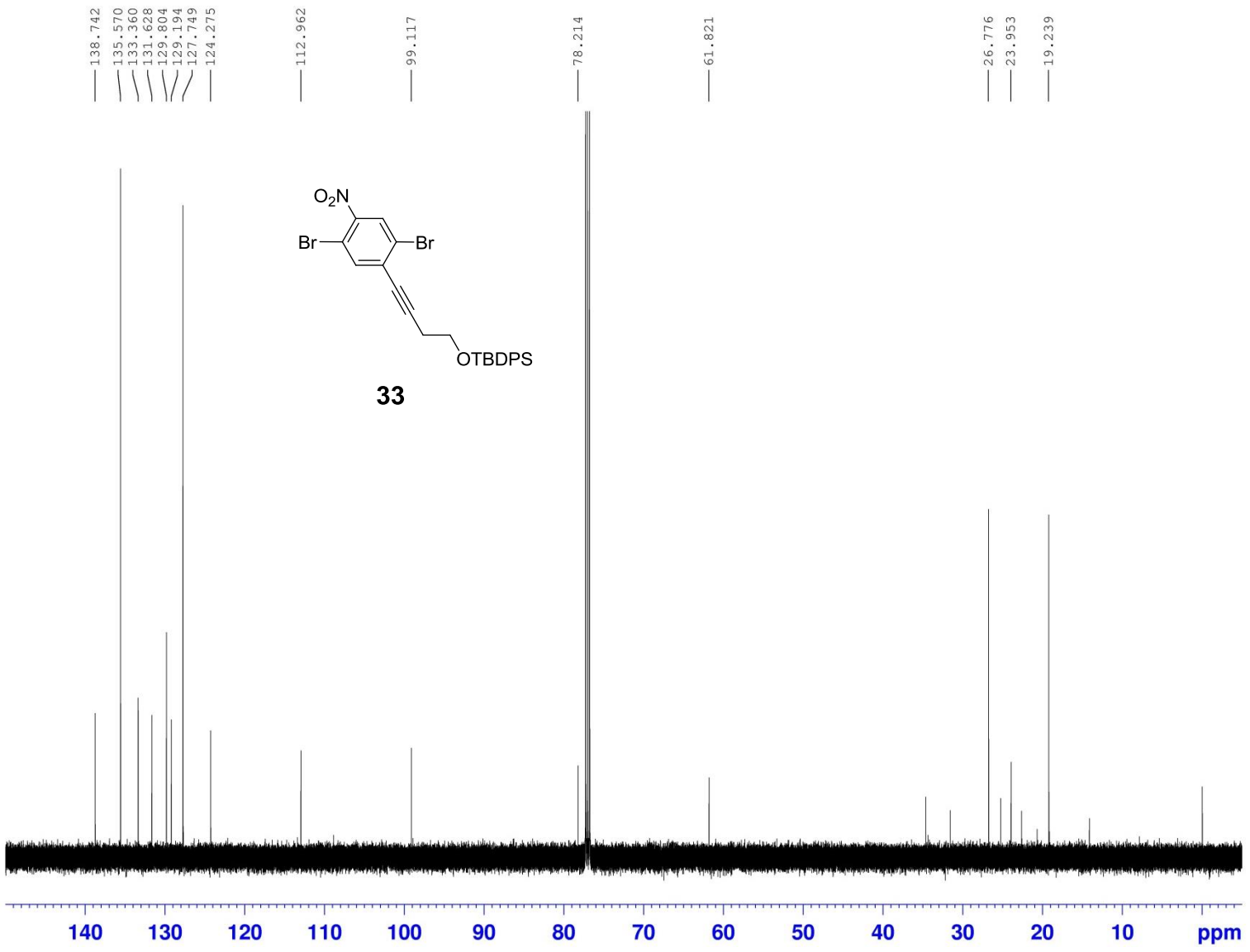
138.742
135.570
133.360
131.628
129.804
129.194
127.749
124.275
112.962
99.117
78.214
61.821
26.776
23.953
19.239
O2N
Br
Br
OTBDPS
33
140
130
120
110
100
90
80
70
60
50
40
30
20
10
ppm

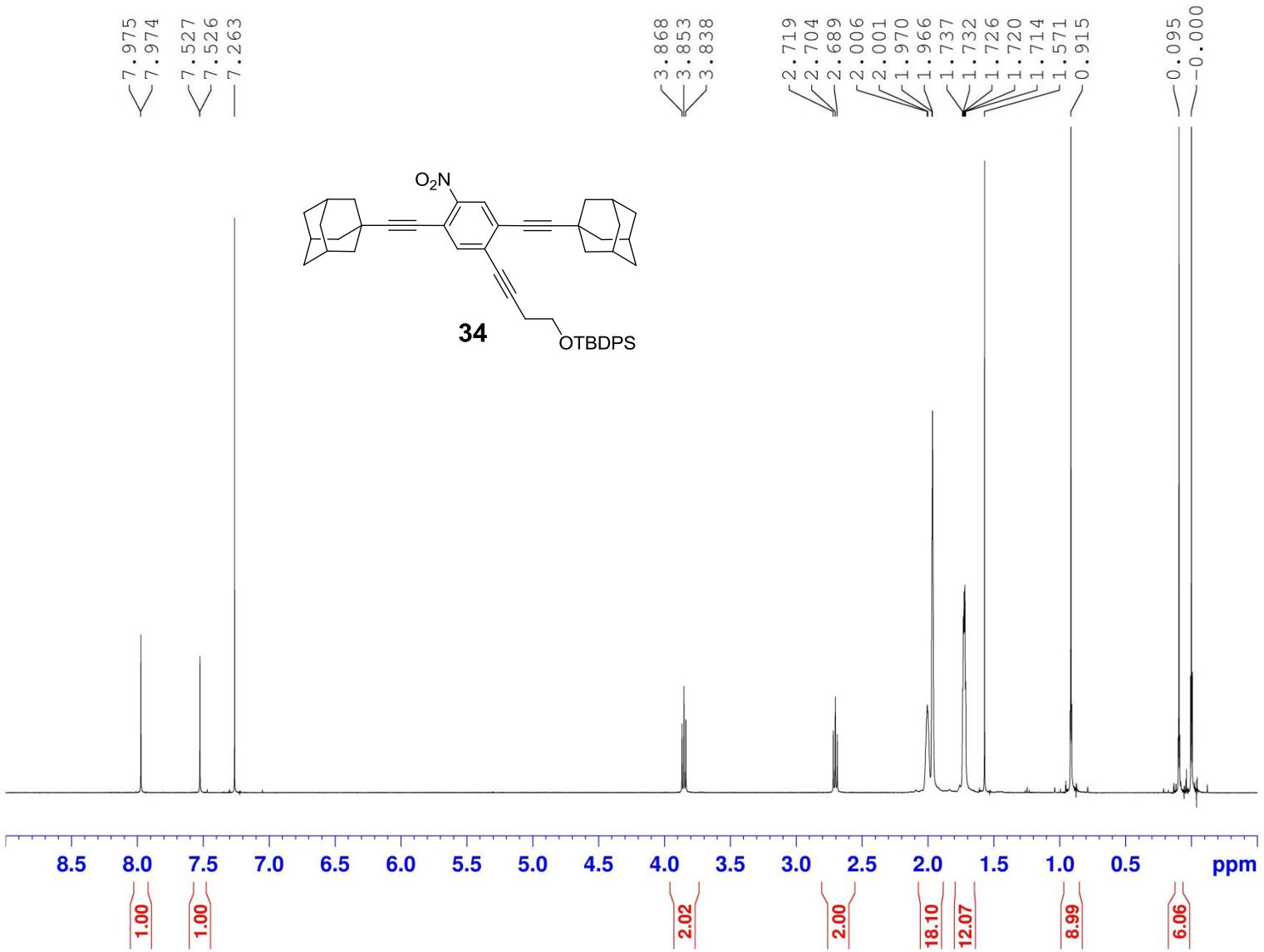
7.975
7.974
7.527
7.526
7.263
3.868
3.853
3.838
2.719
2.704
2.689
2.006
2.001
1.970
1.966
1.737
1.732
1.726
1.720
1.714
1.571
0.915
0.095
-0.000
O2N
34
OTBDPS
8.5
8.0
7.5
7.0
6.5
6.0
5.5
5.0
4.5
4.0
3.5
3.0
2.5
2.0
1.5
1.0
0.5
ppm
1.00
1.00
2.02
2.00
18.10
12.07
8.99
6.06

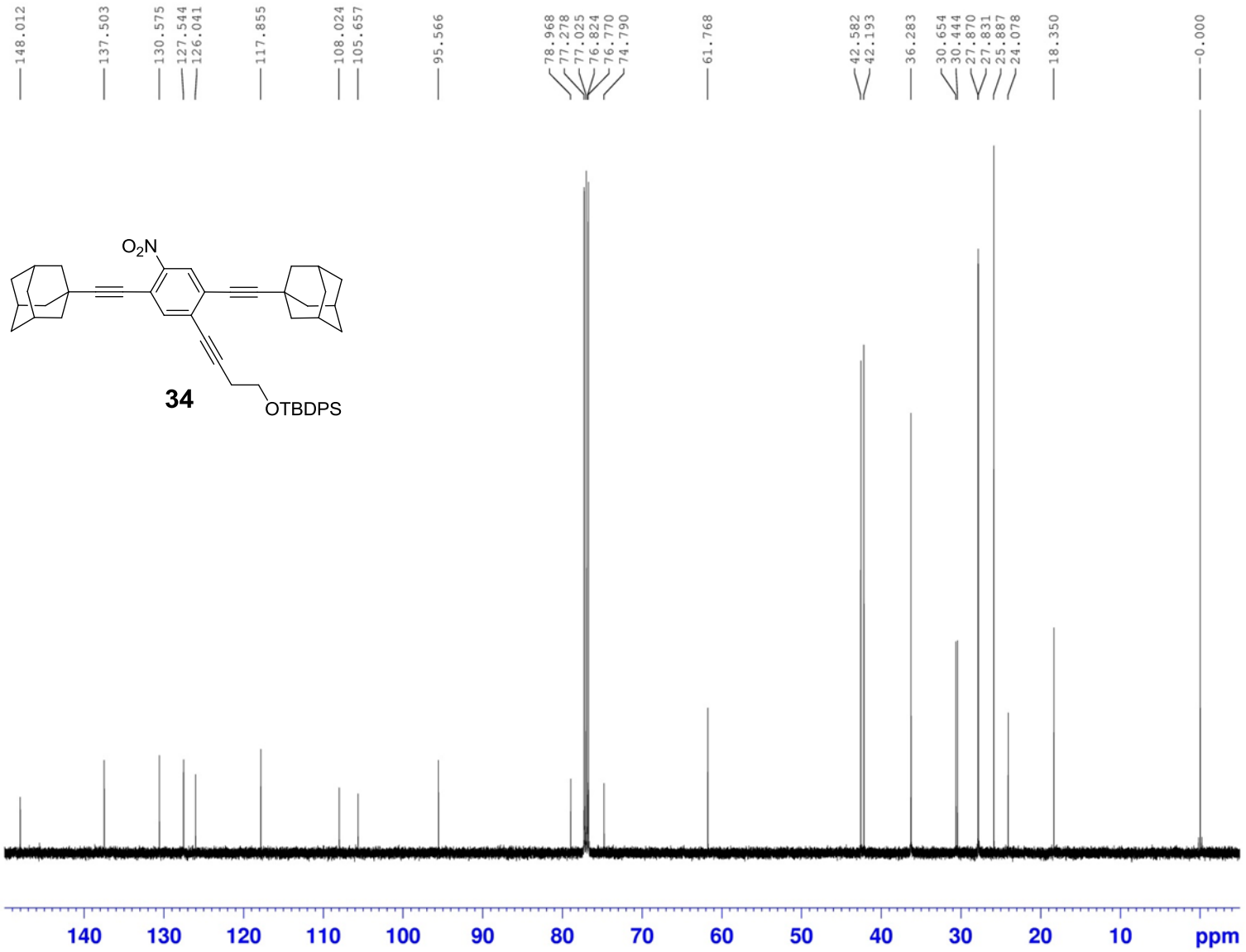
148.012
137.503
130.575
127.544
126.041
117.855
108.024
105.657
95.566
78.968
77.278
77.025
76.824
76.770
74.790
61.768
42.582
42.193
36.283
30.654
30.444
27.870
27.831
25.887
24.078
18.350
-0.000
O2N
OTBDPS
34
140
130
120
110
100
90
80
70
60
50
40
30
20
10
ppm

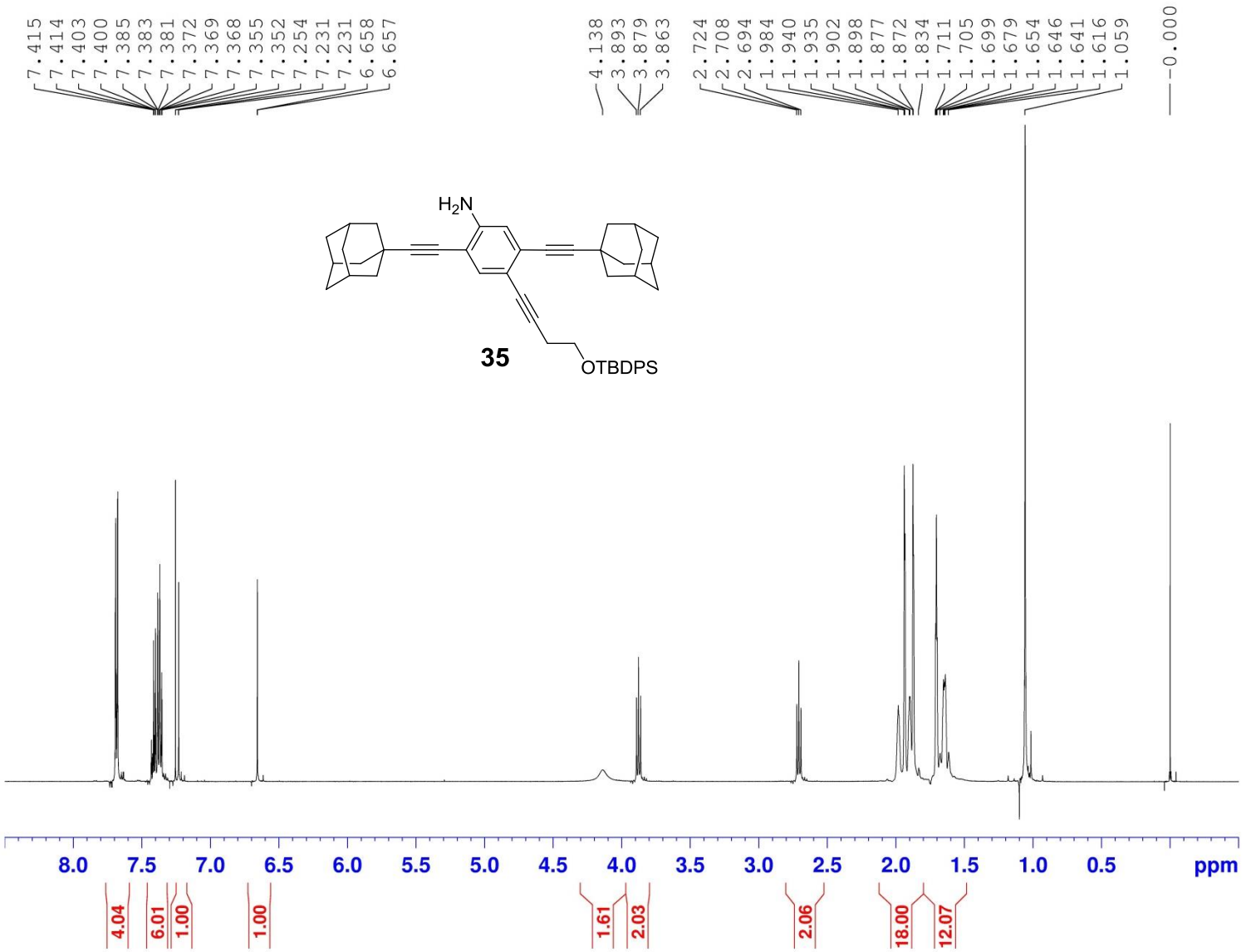
7.415
7.414
7.403
7.400
7.385
7.383
7.381
7.372
7.369
7.368
7.355
7.352
7.254
7.231
7.231
6.658
6.657
4.138
3.893
3.879
3.863
2.724
2.708
2.694
1.984
1.940
1.935
1.902
1.898
1.877
1.872
1.834
1.711
1.705
1.699
1.679
1.654
1.646
1.641
1.616
1.059
0.000
H2N
35
OTBDPS
8.0
7.5
7.0
6.5
6.0
5.5
5.0
4.5
4.0
3.5
3.0
2.5
2.0
1.5
1.0
0.5
ppm
4.04
6.01
1.00
1.00
1.61
2.03
2.06
18.00
12.07

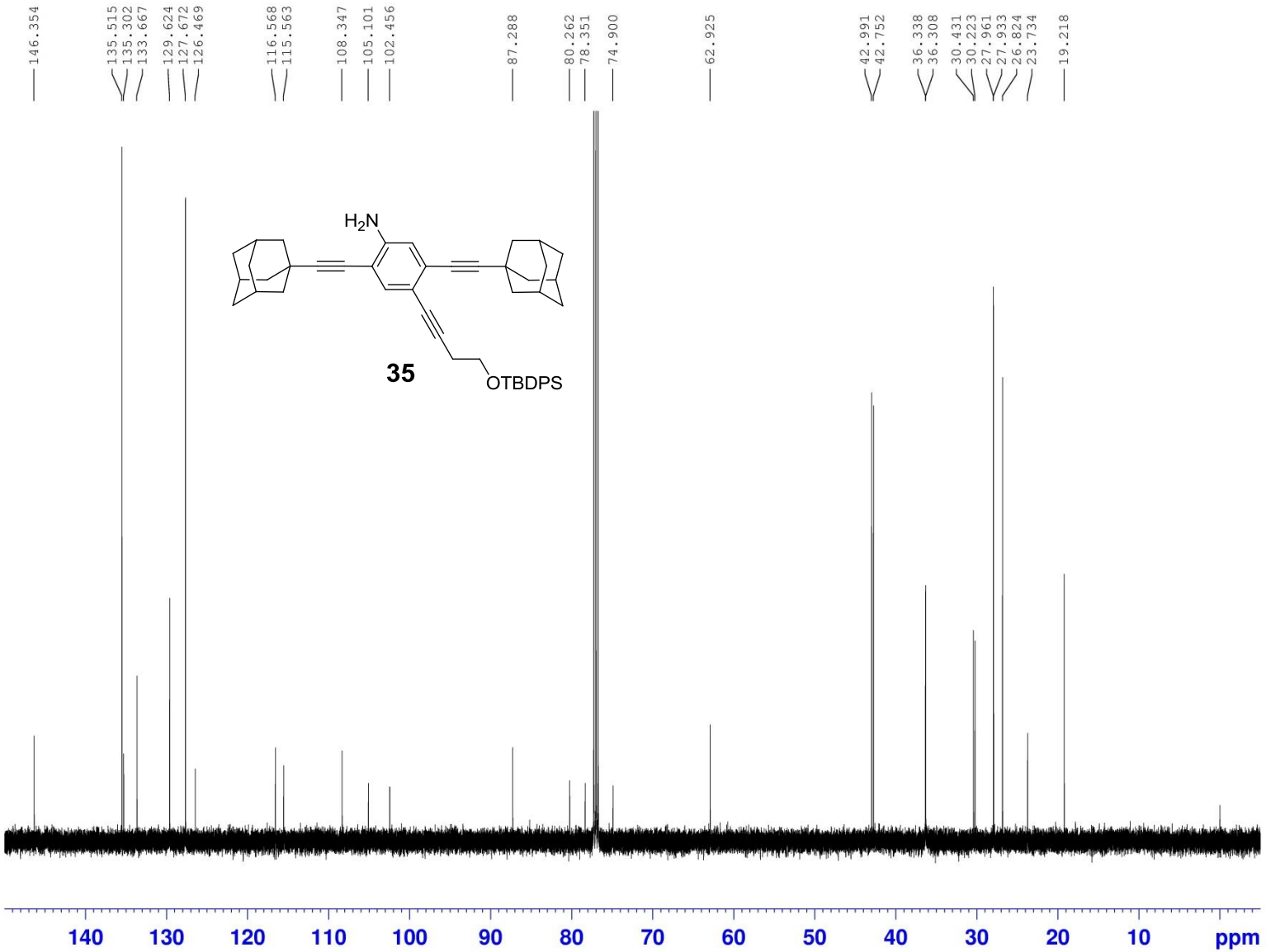
146.354
135.515
135.302
133.667
129.624
127.672
126.469
116.568
115.563
108.347
105.101
102.456
87.288
80.262
78.351
74.900
62.925
42.991
42.752
36.338
36.308
30.431
30.223
27.961
27.933
26.824
23.734
19.218
H2N
OTBDPS
35
140
130
120
110
100
90
80
70
60
50
40
30
20
10
ppm

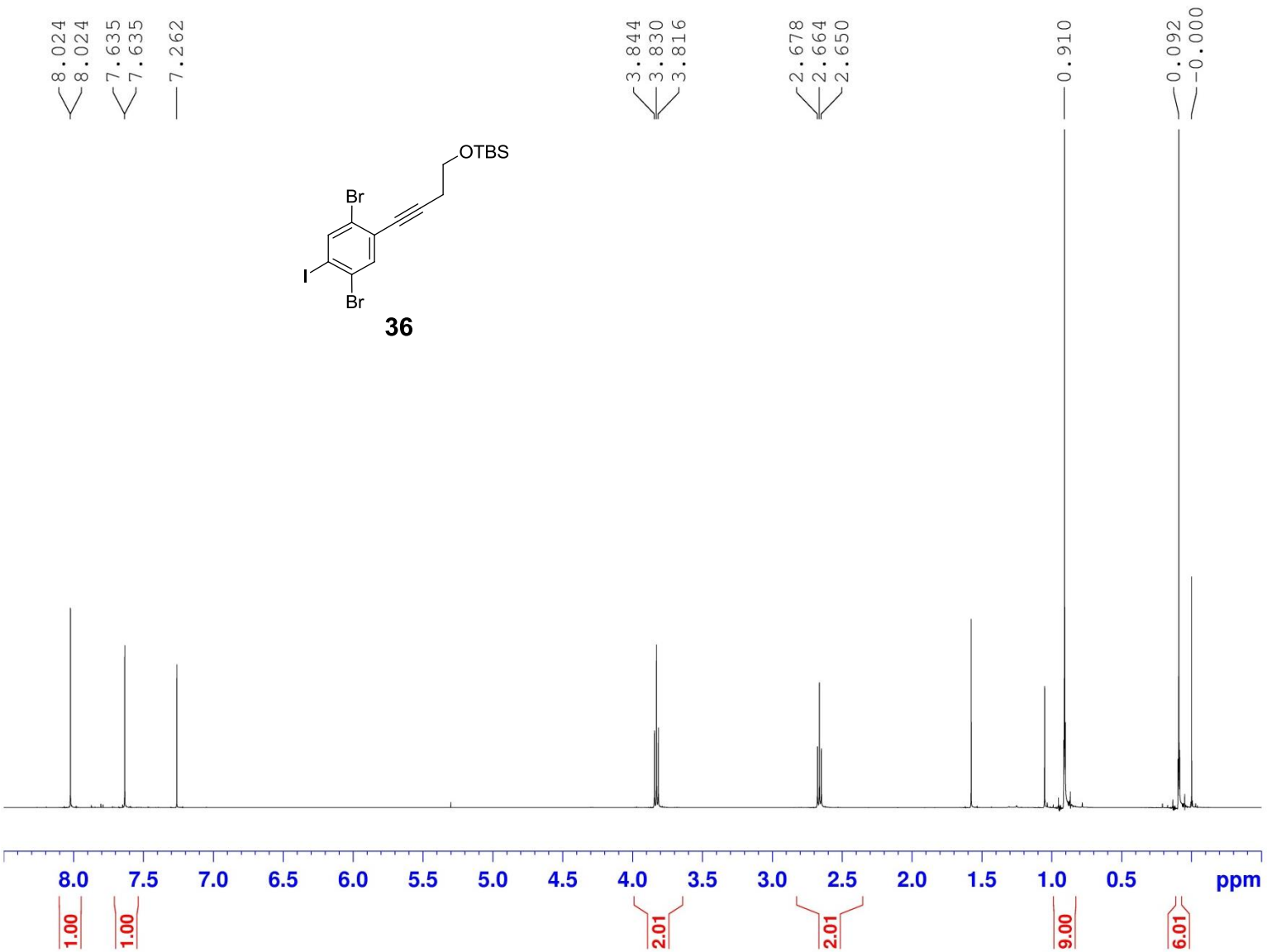
8.024
8.024
7.635
7.635
7.262
3.844
3.830
3.816
2.678
2.664
2.650
0.910
0.092
-0.000
OTBS
Br
I
Br
36
8.0
7.5
7.0
6.5
6.0
5.5
5.0
4.5
4.0
3.5
3.0
2.5
2.0
1.5
1.0
0.5
ppm
1.00
1.00
2.01
2.01
9.00
6.01

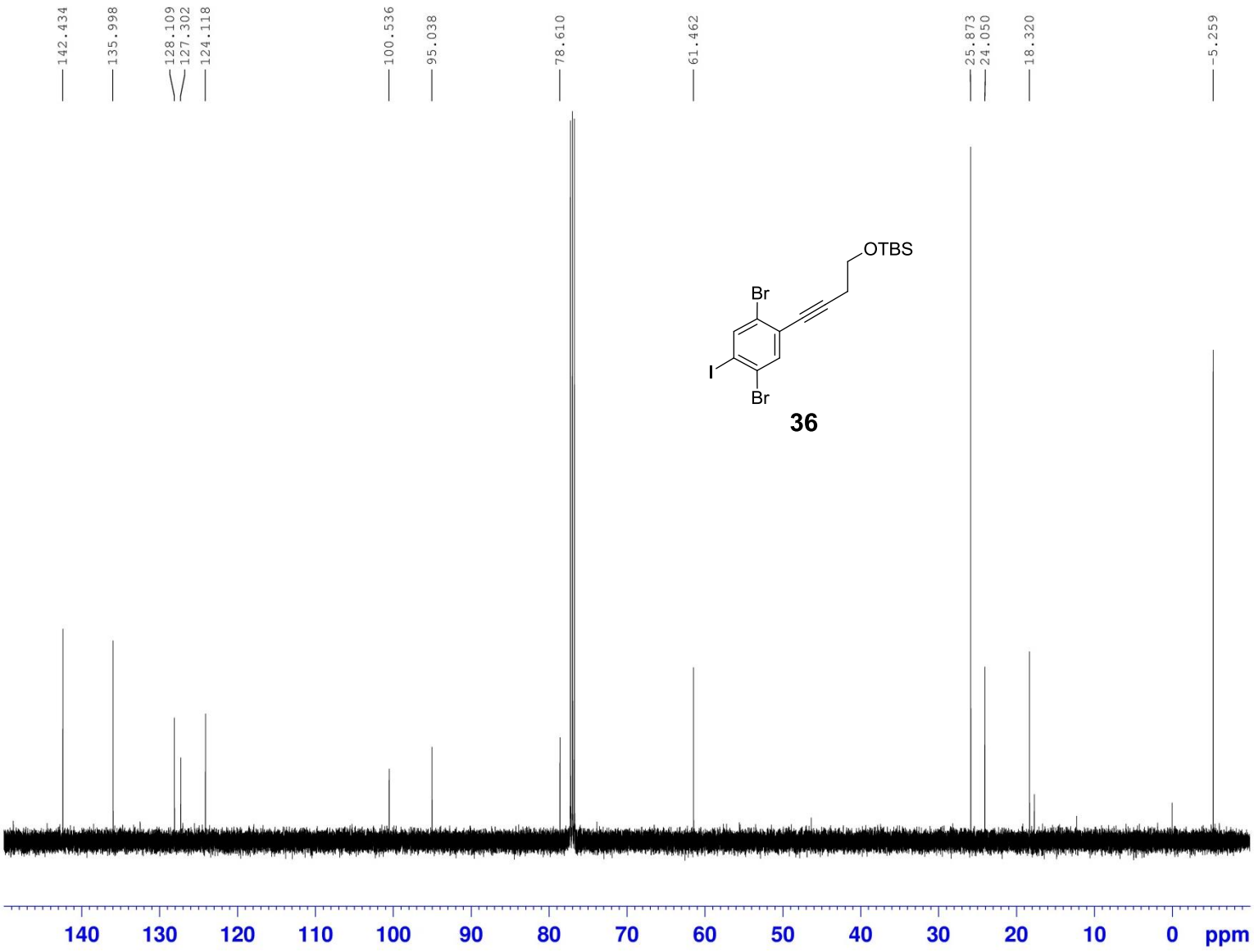
142.434
135.998
128.109
127.302
124.118
100.536
95.038
78.610
61.462
25.873
24.050
18.320
-5.259
OTBS
Br
I
Br
36
140
130
120
110
100
90
80
70
60
50
40
30
20
10
0
ppm

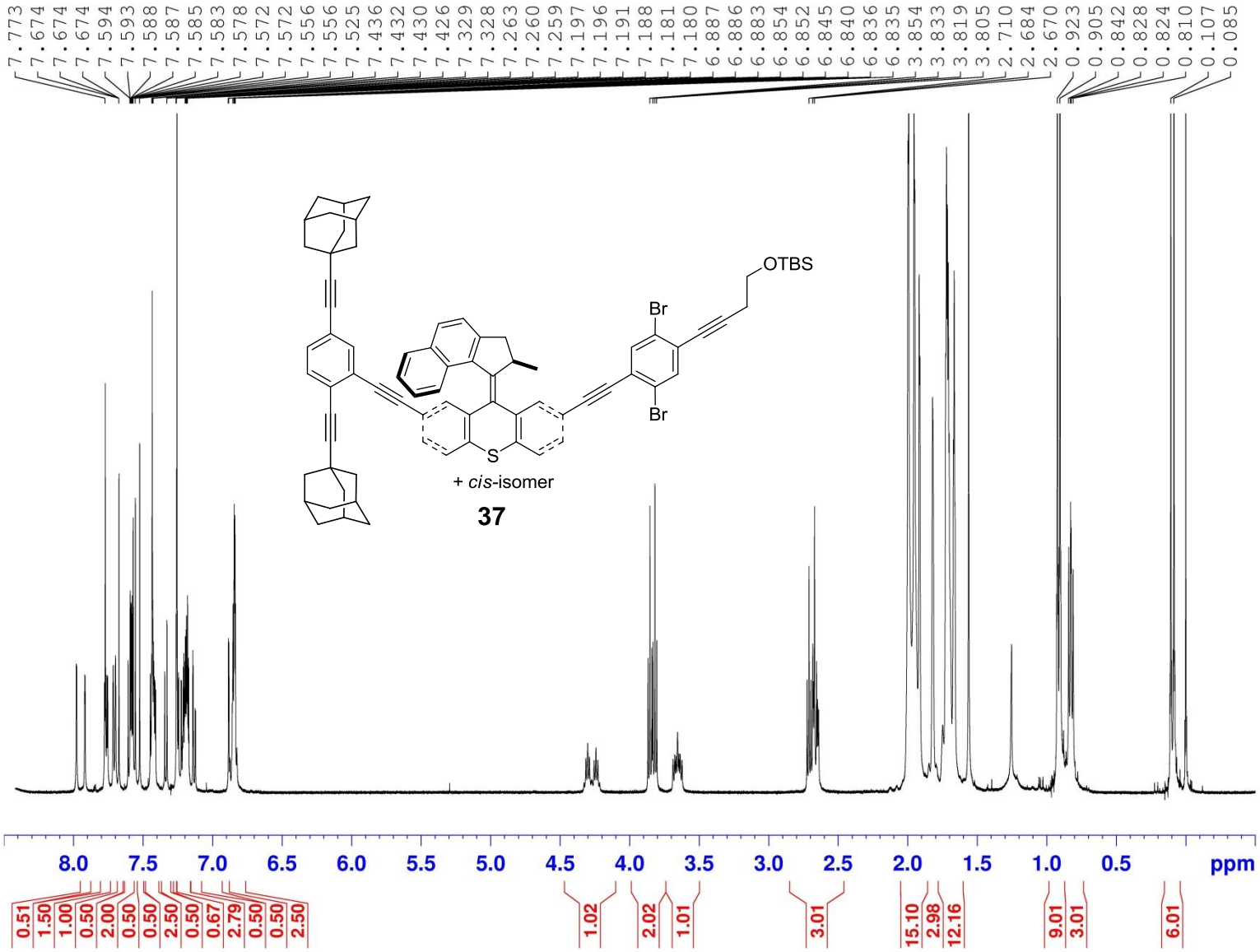
7.773
7.674
7.674
7.674
7.594
7.593
7.588
7.587
7.585
7.583
7.578
7.572
7.572
7.556
7.556
7.525
7.436
7.432
7.430
7.426
7.329
7.328
7.263
7.260
7.259
7.197
7.196
7.191
7.188
7.181
7.180
6.887
6.886
6.883
6.854
6.852
6.845
6.840
6.836
6.835
3.854
3.833
3.819
3.805
2.710
2.684
2.670
0.923
0.905
0.842
0.828
0.824
0.810
0.107
0.085
OTBS
Br
Br
S
+ cis-isomer
37
8.0
7.5
7.0
6.5
6.0
5.5
5.0
4.5
4.0
3.5
3.0
2.5
2.0
1.5
1.0
0.5
ppm
0.51
1.50
1.00
0.50
2.00
0.50
0.50
2.50
0.50
0.67
2.79
0.50
0.50
2.50
1.02
2.02
1.01
3.01
15.10
2.98
12.16
9.01
3.01
6.01

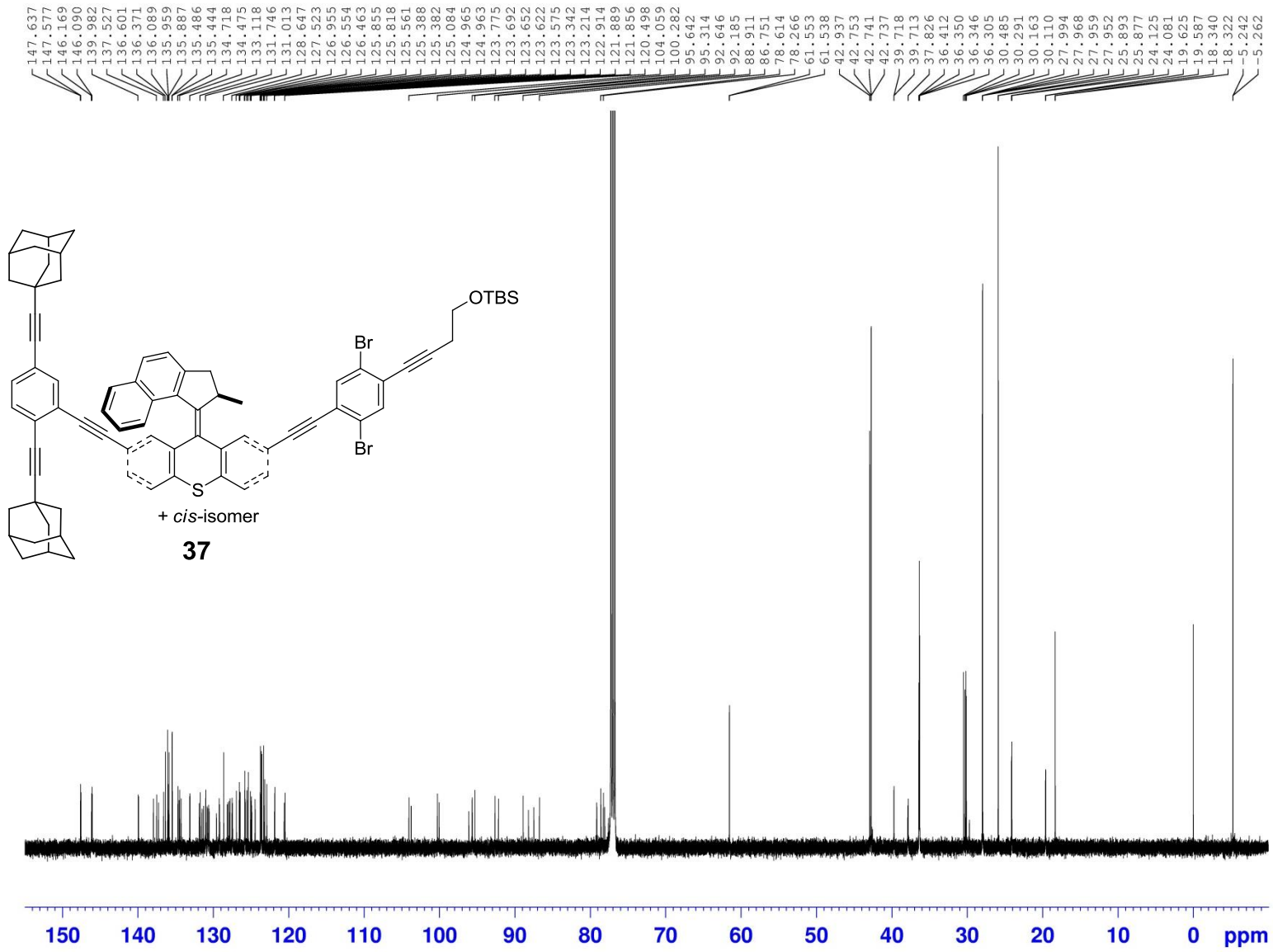
147.637
147.577
146.169
146.090
139.982
137.527
136.601
136.371
136.089
135.959
135.887
135.486
135.444
134.718
134.475
133.118
131.746
131.013
128.647
127.523
126.955
126.554
126.463
125.855
125.818
125.561
125.388
125.382
125.084
124.965
124.963
123.775
123.692
123.652
123.622
123.575
123.342
123.214
122.914
121.889
121.856
120.498
104.059
100.282
95.642
95.314
92.646
92.185
88.911
86.751
78.614
78.266
61.553
61.538
42.937
42.753
42.741
42.737
39.718
39.713
37.826
36.412
36.350
36.346
36.305
30.485
30.291
30.163
30.110
27.994
27.968
27.959
27.952
25.893
25.877
24.125
24.081
19.625
19.587
18.340
18.322
-5.242
-5.262
OTBS
Br
Br
S
+ cis-isomer
37
150
140
130
120
110
100
90
80
70
60
50
40
30
20
10
0
ppm

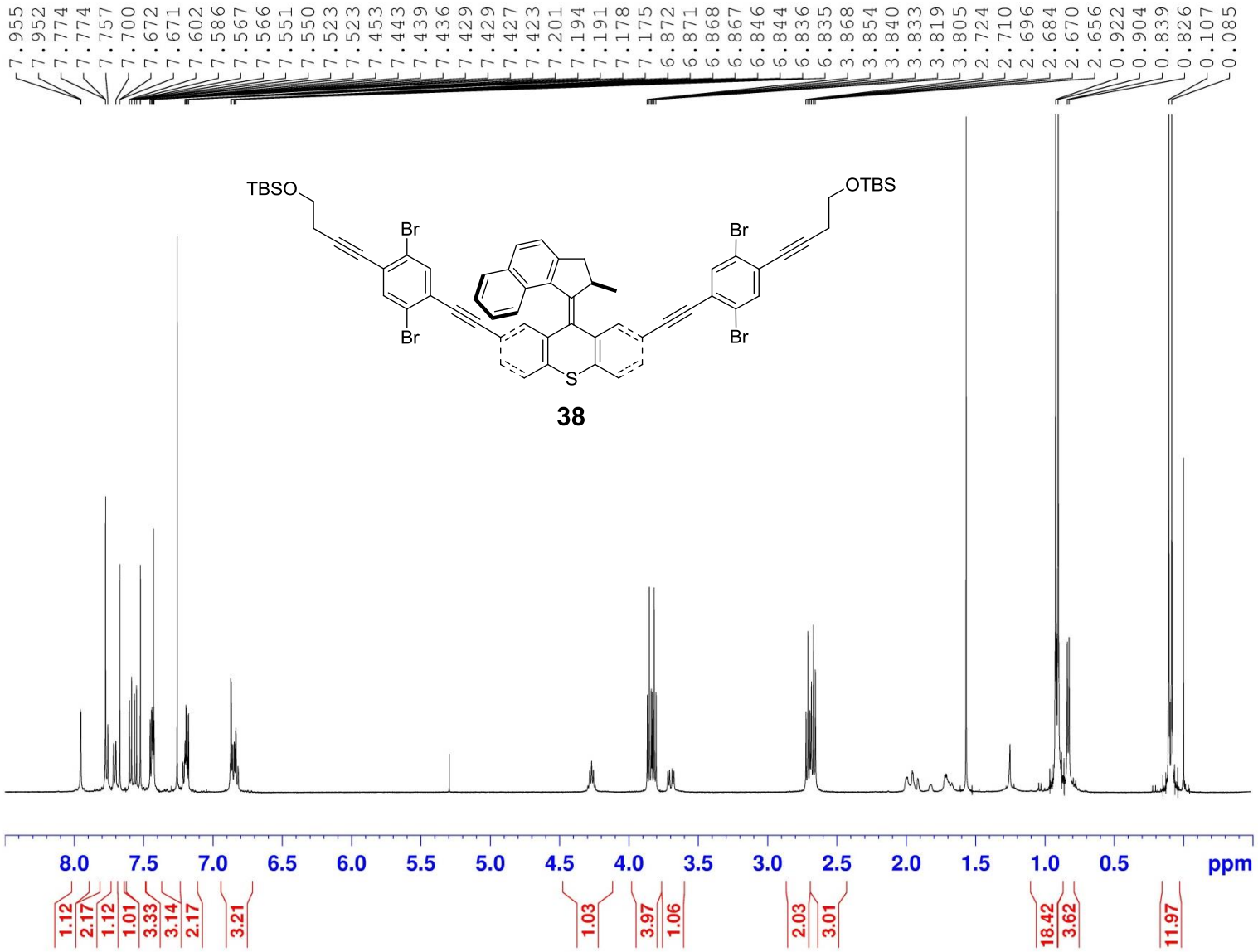
7.955
7.952
7.774
7.774
7.757
7.700
7.672
7.671
7.602
7.586
7.567
7.566
7.551
7.550
7.523
7.523
7.453
7.443
7.439
7.436
7.429
7.429
7.427
7.423
7.201
7.194
7.191
7.178
7.175
6.872
6.871
6.868
6.867
6.846
6.844
6.836
6.835
3.868
3.854
3.840
3.833
3.819
3.805
2.724
2.710
2.696
2.684
2.670
2.656
0.922
0.904
0.839
0.826
0.107
0.085
TBSO
OTBS
Br
Br
Br
Br
S
38
8.0
7.5
7.0
6.5
6.0
5.5
5.0
4.5
4.0
3.5
3.0
2.5
2.0
1.5
1.0
0.5
ppm
1.12
2.17
1.12
1.01
3.33
3.14
2.17
3.21
1.03
3.97
1.06
2.03
3.01
18.42
3.62
11.97

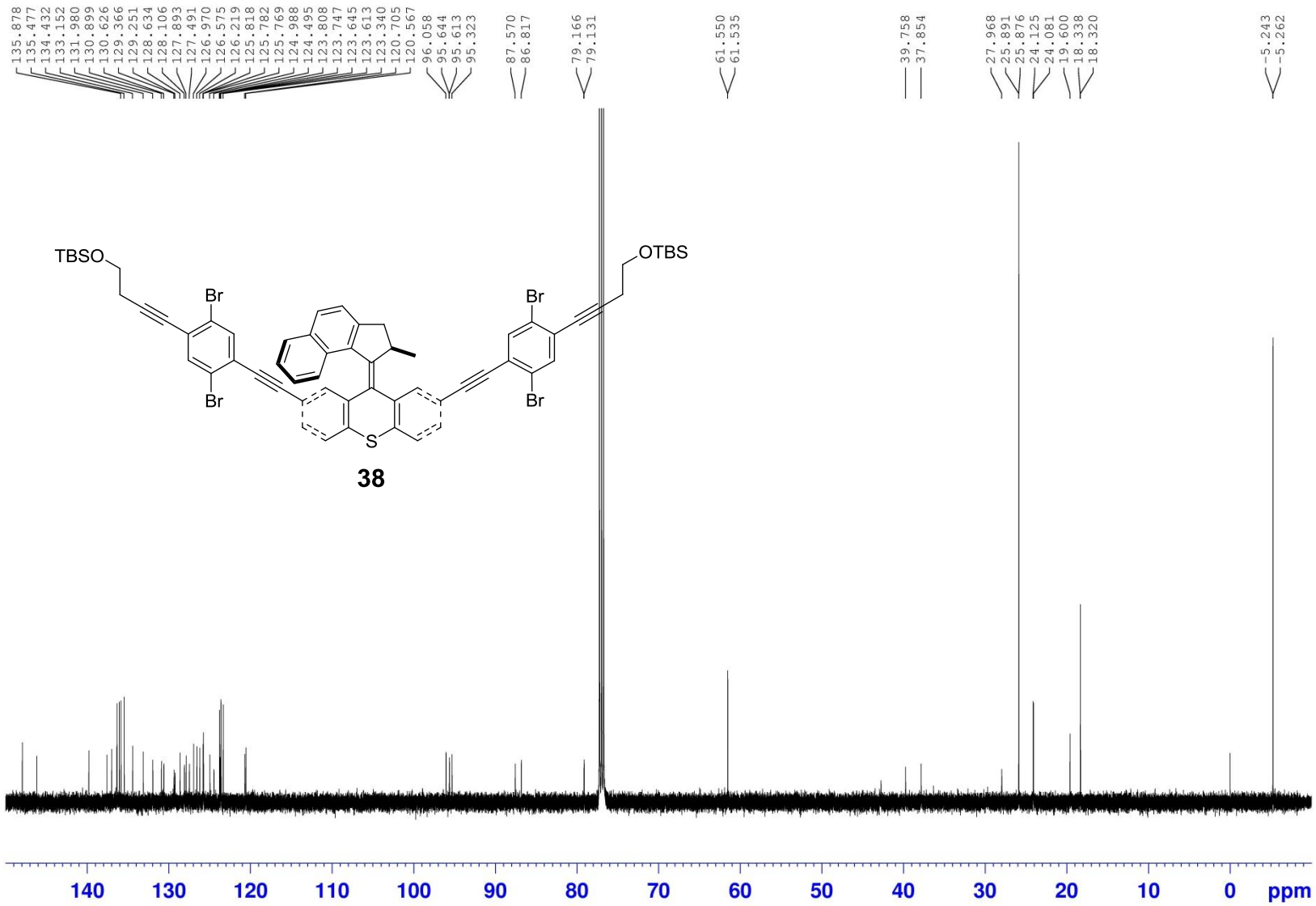
135.878
135.477
134.432
133.152
131.980
130.899
130.626
129.366
129.251
128.634
128.106
127.893
127.491
126.970
126.575
126.219
125.818
125.782
125.769
124.988
124.495
123.808
123.747
123.645
123.613
123.340
120.705
120.567
96.058
95.644
95.613
95.323
87.570
86.817
79.166
79.131
61.550
61.535
39.758
37.854
27.968
25.891
25.876
24.125
24.081
19.600
18.338
18.320
-5.243
-5.262
TBSO
OTBS
Br
Br
Br
Br
S
38
140
130
120
110
100
90
80
70
60
50
40
30
20
10
0
ppm

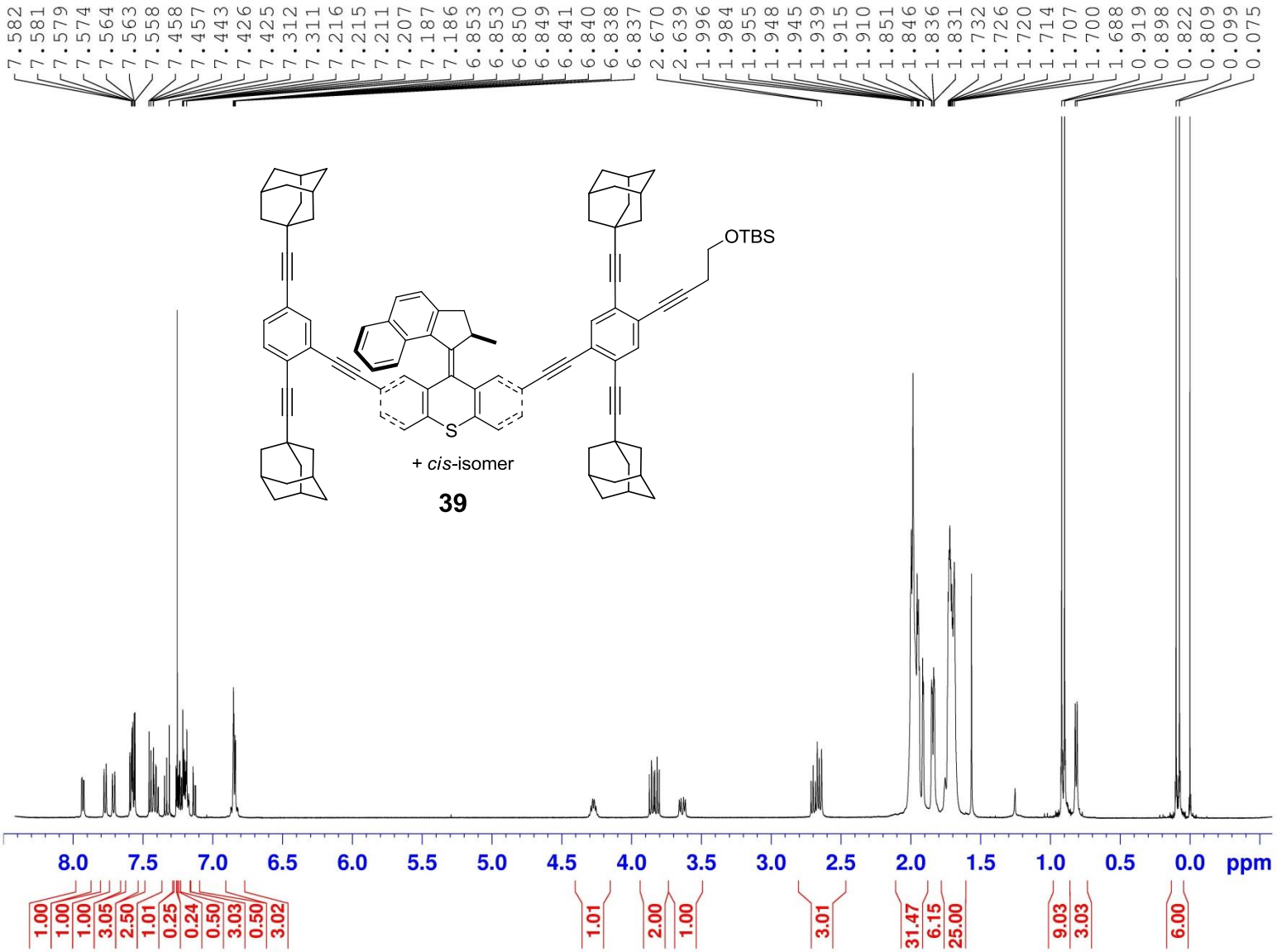
7.582
7.581
7.579
7.574
7.564
7.563
7.558
7.458
7.457
7.443
7.426
7.425
7.312
7.311
7.216
7.215
7.211
7.207
7.187
7.186
6.853
6.853
6.850
6.849
6.841
6.840
6.838
6.837
2.670
2.639
1.996
1.984
1.955
1.948
1.945
1.939
1.915
1.910
1.851
1.846
1.836
1.831
1.732
1.726
1.720
1.714
1.707
1.700
1.688
0.919
0.898
0.822
0.809
0.099
0.075
OTBS
S
+ cis-isomer
39
8.0
7.5
7.0
6.5
6.0
5.5
5.0
4.5
4.0
3.5
3.0
2.5
2.0
1.5
1.0
0.5
0.0
ppm
1.00
1.00
1.00
3.05
2.50
1.01
0.25
0.24
0.50
3.03
0.50
3.02
1.01
2.00
1.00
3.01
31.47
6.15
25.00
9.03
3.03
6.00

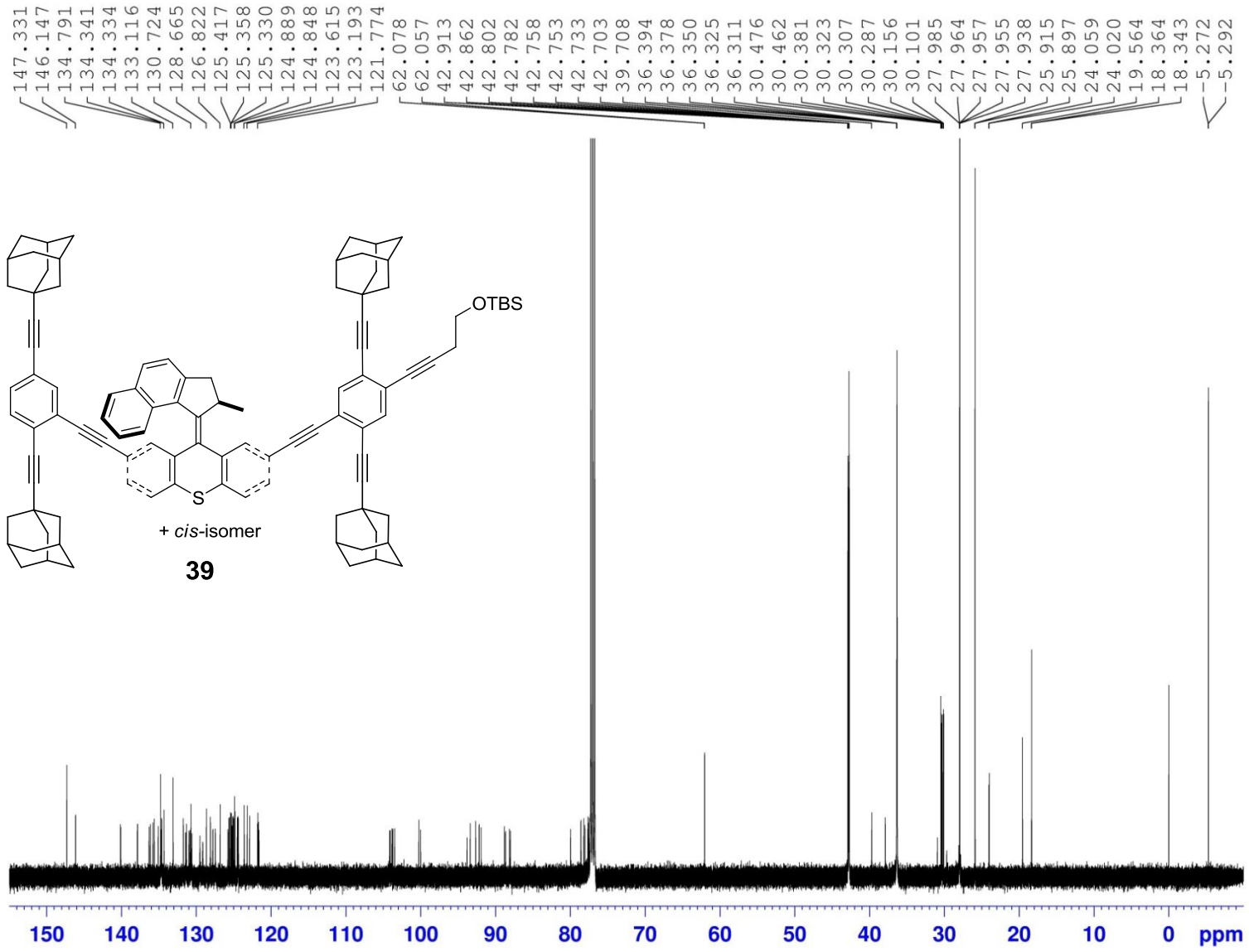
147.331
146.147
134.791
134.341
134.334
133.116
130.724
128.665
126.822
125.417
125.358
125.330
124.889
124.848
123.615
123.193
121.774
62.078
62.057
42.913
42.862
42.802
42.782
42.758
42.753
42.733
42.703
39.708
36.394
36.378
36.350
36.325
36.311
30.476
30.462
30.381
30.323
30.307
30.287
30.156
30.101
27.985
27.964
27.957
27.955
27.938
25.915
25.897
24.059
24.020
19.564
18.364
18.343
-5.272
-5.292
OTBS
S
+ cis-isomer
39
150
140
130
120
110
100
90
80
70
60
50
40
30
20
10
0
ppm

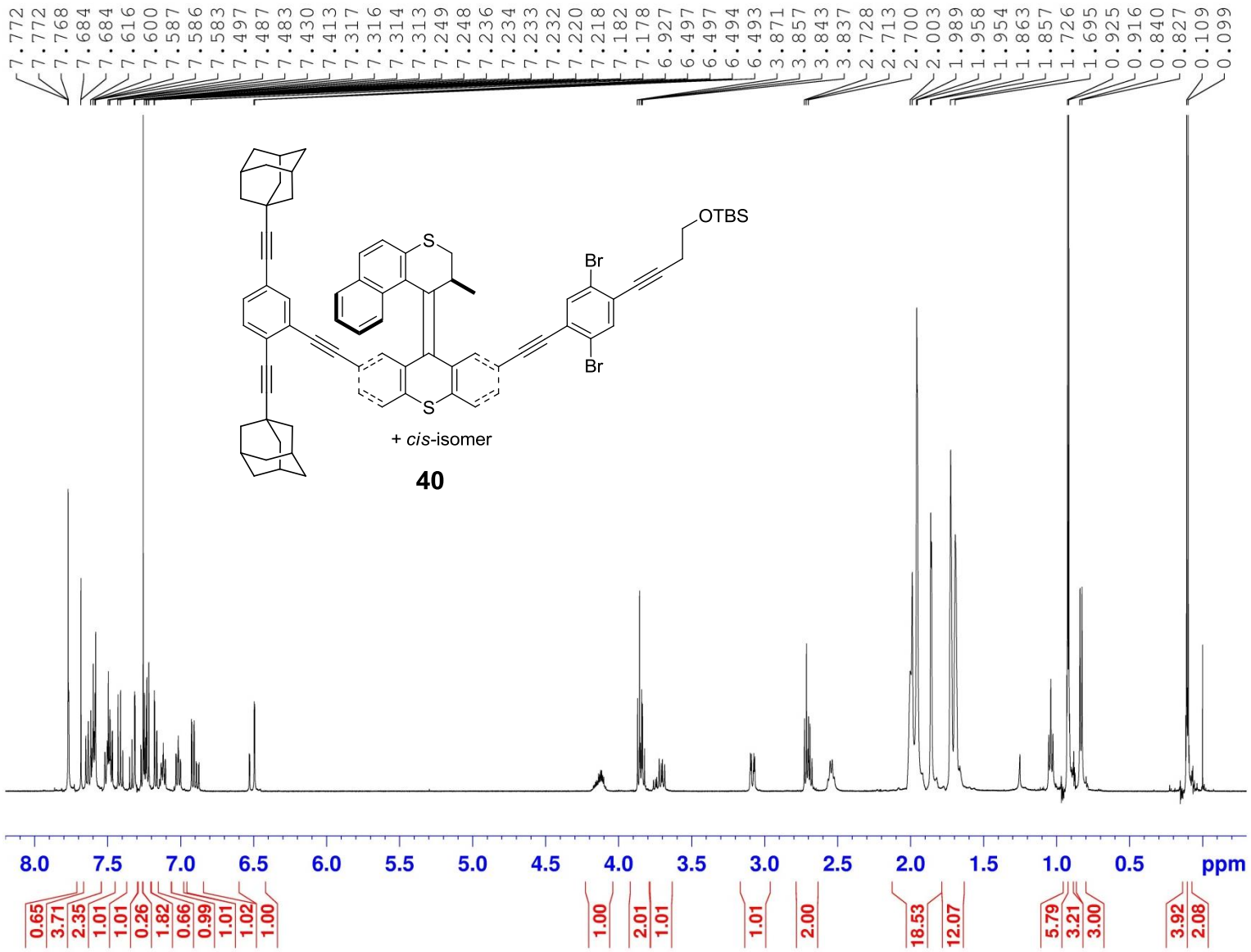
7.772
7.772
7.768
7.684
7.684
7.616
7.600
7.587
7.586
7.583
7.497
7.487
7.483
7.430
7.413
7.317
7.316
7.314
7.313
7.249
7.248
7.236
7.234
7.233
7.232
7.220
7.218
7.182
7.178
6.927
6.497
6.497
6.494
6.493
3.871
3.857
3.843
3.837
2.728
2.713
2.700
2.003
1.989
1.958
1.954
1.863
1.857
1.726
1.695
0.925
0.916
0.840
0.827
0.109
0.099
OTBS
Br
Br
S
S
+ cis-isomer
40
8.0
7.5
7.0
6.5
6.0
5.5
5.0
4.5
4.0
3.5
3.0
2.5
2.0
1.5
1.0
0.5
ppm
0.65
3.71
2.35
1.01
1.01
0.26
1.82
0.66
0.99
1.01
1.02
1.00
1.00
2.01
1.01
1.01
2.00
18.53
12.07
5.79
3.21
3.00
3.92
2.08

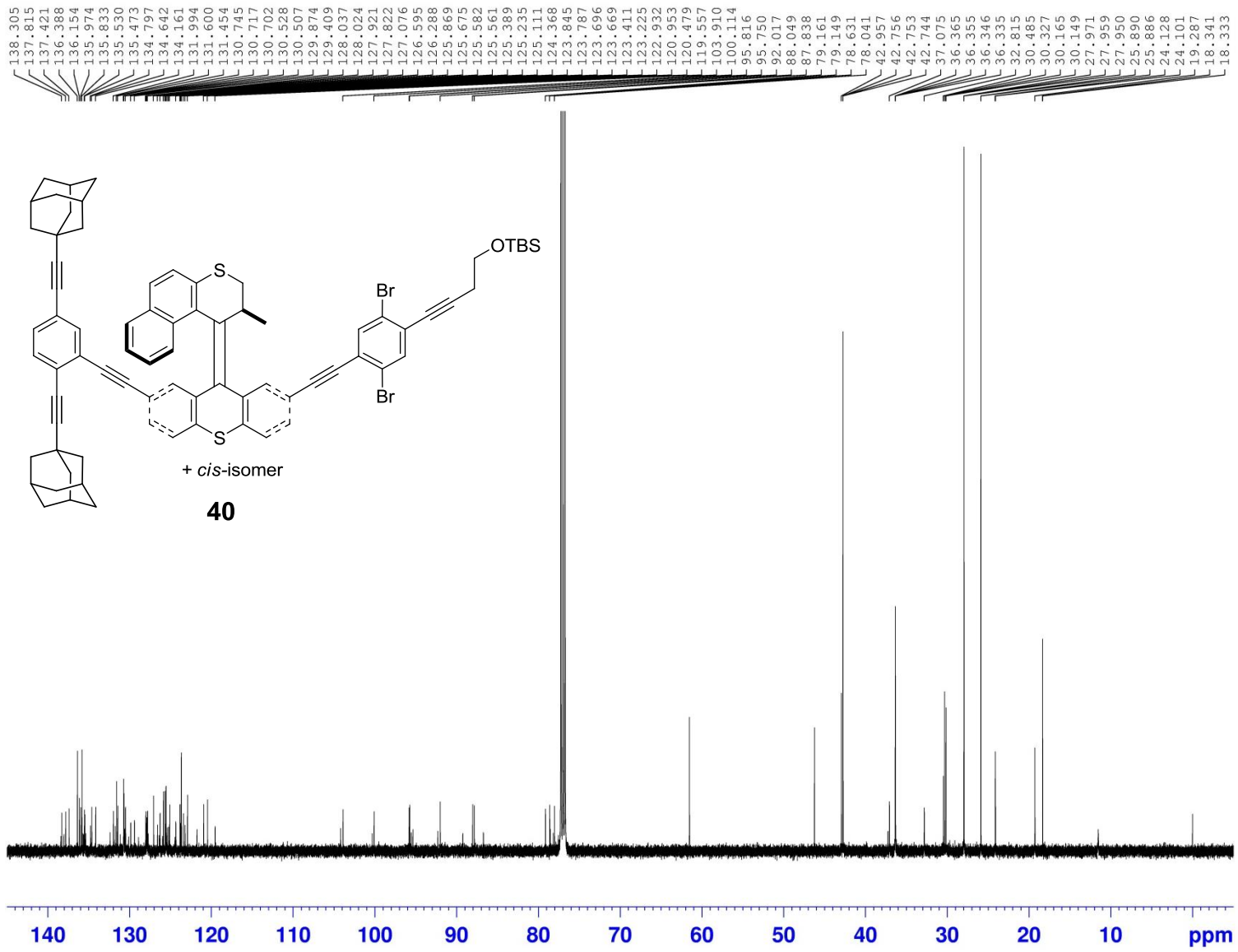
138.305
137.815
137.421
136.388
136.154
135.974
135.833
135.530
135.473
134.797
134.642
134.161
131.994
131.600
131.454
130.745
130.717
130.702
130.528
130.507
129.874
129.409
128.037
128.024
127.921
127.822
127.076
126.595
126.288
125.869
125.675
125.582
125.561
125.389
125.235
125.111
124.368
123.845
123.787
123.696
123.669
123.411
123.225
122.932
120.953
120.479
119.557
103.910
100.114
95.816
95.750
92.017
88.049
87.838
79.161
79.149
78.631
78.041
42.957
42.756
42.753
42.744
37.075
36.365
36.355
36.346
36.335
32.815
30.485
30.327
30.165
30.149
27.971
27.959
27.950
25.890
25.886
24.128
24.101
19.287
18.341
18.333
OTBS
Br
Br
S
S
+ cis-isomer
40
140
130
120
110
100
90
80
70
60
50
40
30
20
10
ppm

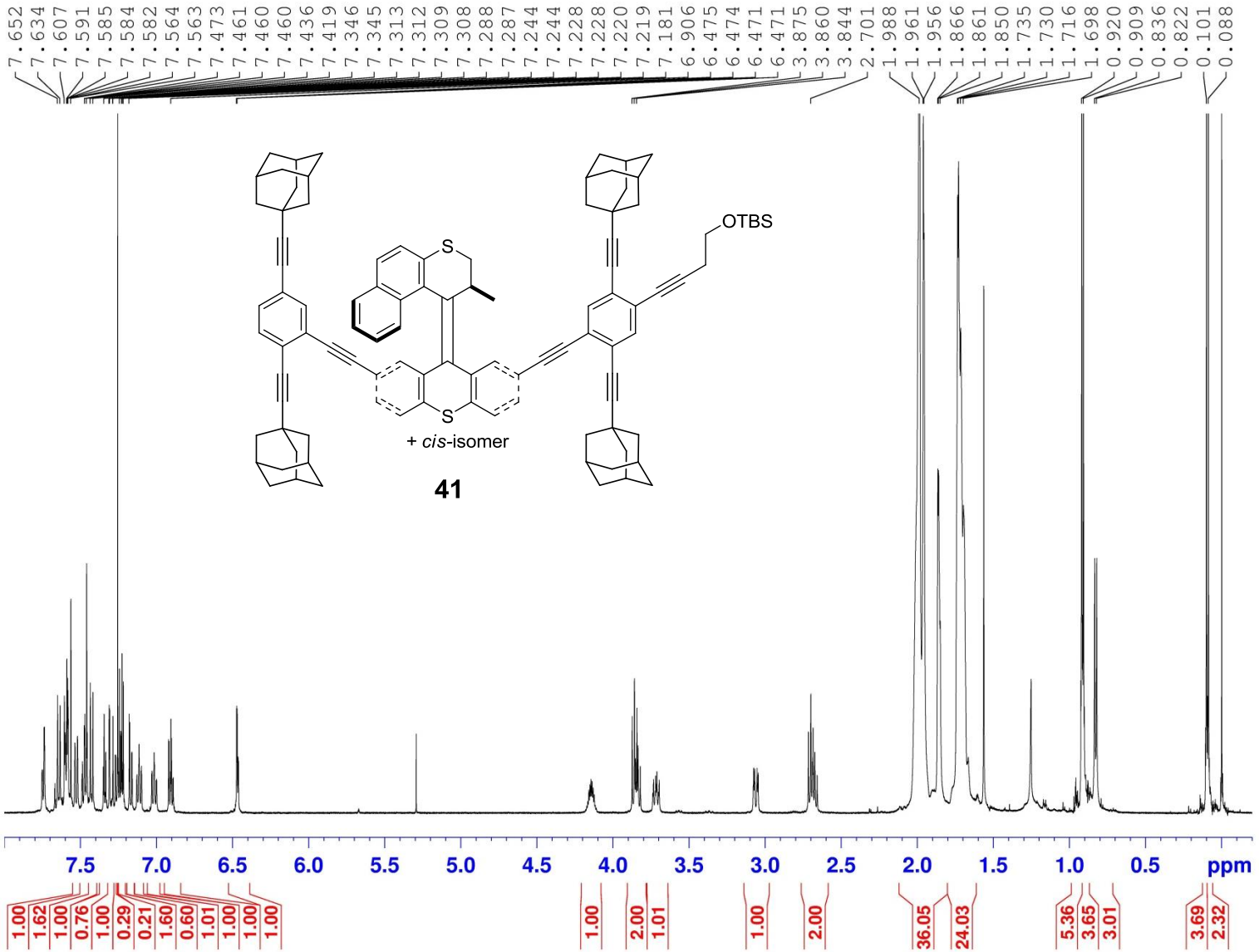
7.652
7.634
7.607
7.591
7.585
7.584
7.582
7.564
7.563
7.473
7.461
7.460
7.460
7.436
7.419
7.346
7.345
7.313
7.312
7.309
7.308
7.288
7.287
7.244
7.244
7.228
7.228
7.220
7.219
7.181
6.906
6.475
6.474
6.471
6.471
3.875
3.860
3.844
2.701
1.988
1.961
1.956
1.866
1.861
1.850
1.735
1.730
1.716
1.698
0.920
0.909
0.836
0.822
0.101
0.088
OTBS
S
S
+ cis-isomer
41
7.5
7.0
6.5
6.0
5.5
5.0
4.5
4.0
3.5
3.0
2.5
2.0
1.5
1.0
0.5
ppm
1.00
1.62
1.00
0.76
1.00
0.29
0.21
1.60
0.60
1.01
1.00
1.00
1.00
1.00
2.00
1.01
1.00
2.00
36.05
24.03
5.36
3.65
3.01
3.69
2.32

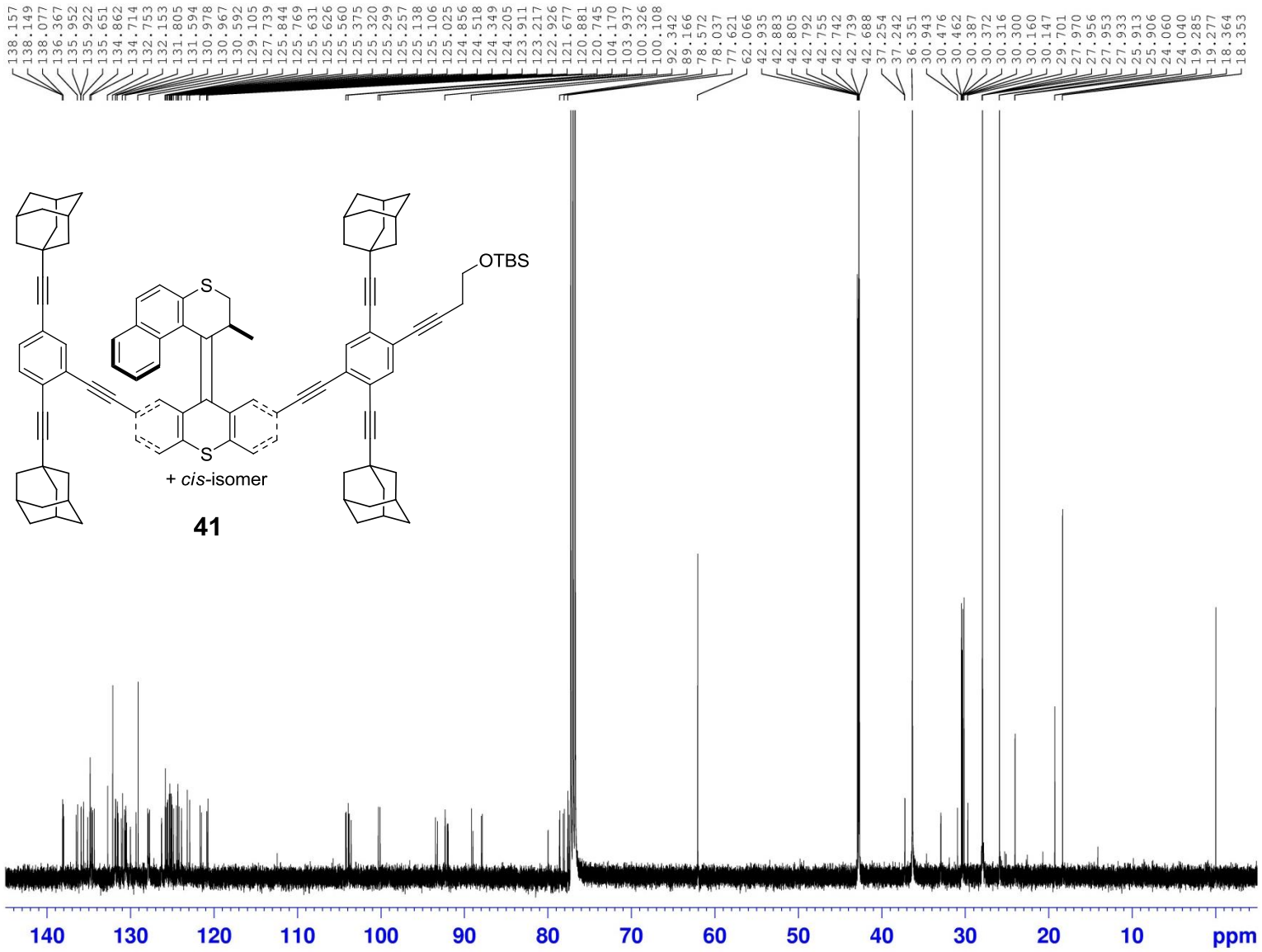
138.157
138.149
138.077
136.367
135.952
135.922
135.651
134.862
134.714
132.753
132.153
131.805
131.594
130.978
130.967
130.592
129.105
127.739
125.844
125.769
125.631
125.626
125.560
125.375
125.320
125.299
125.257
125.138
125.106
125.025
124.856
124.518
124.349
124.205
123.911
123.217
122.926
121.677
120.881
120.745
104.170
103.937
100.326
100.108
92.342
89.166
78.572
78.037
77.621
62.066
42.935
42.883
42.805
42.792
42.755
42.742
42.739
42.688
37.254
37.242
36.351
30.943
30.476
30.462
30.387
30.372
30.316
30.300
30.160
30.147
29.701
27.970
27.956
27.953
27.933
25.913
25.906
24.060
24.040
19.285
19.277
18.364
18.353
OTBS
S
S
+ cis-isomer
41
140
130
120
110
100
90
80
70
60
50
40
30
20
10
ppm

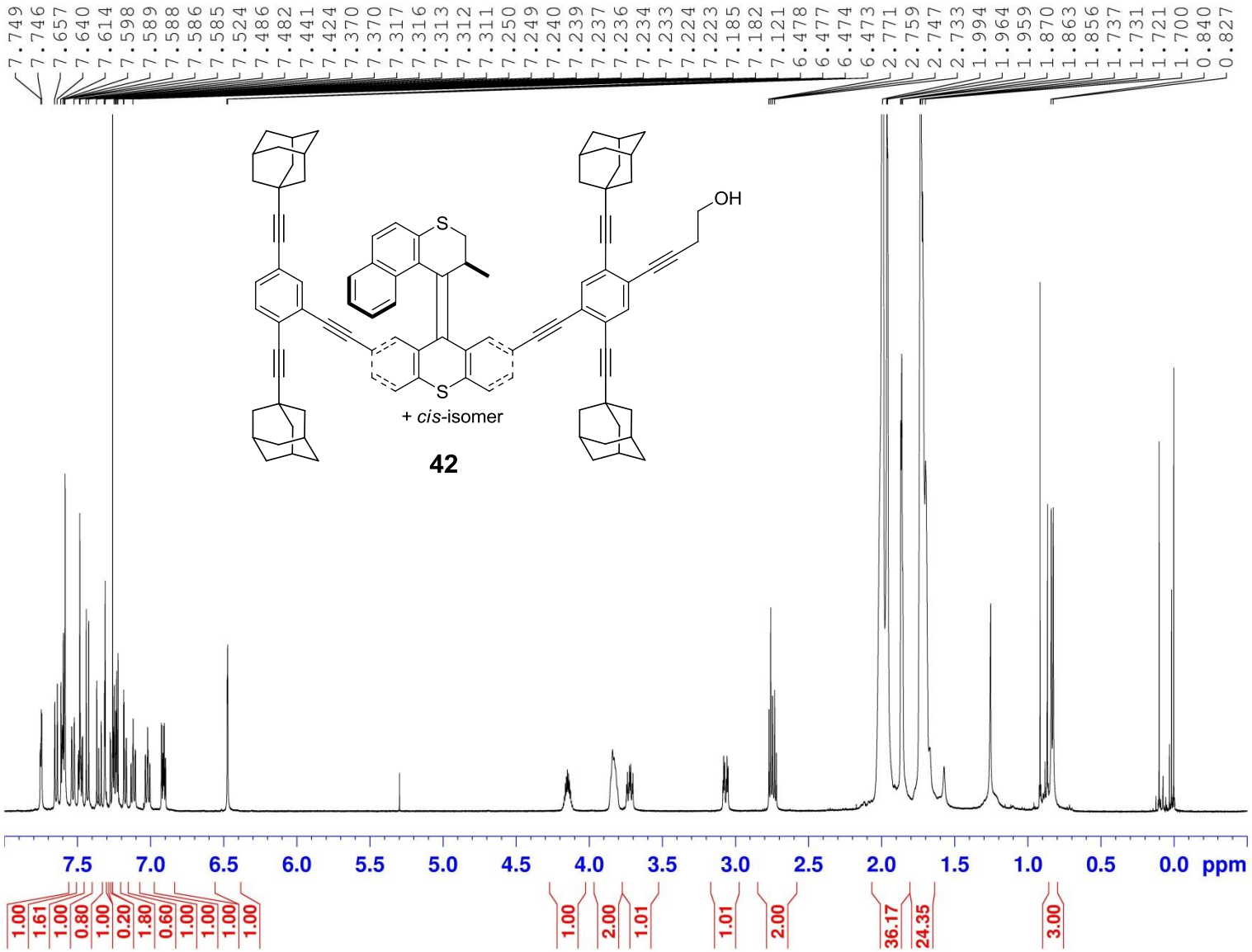
7.749
7.746
7.657
7.640
7.614
7.598
7.589
7.588
7.586
7.585
7.524
7.486
7.482
7.441
7.424
7.370
7.370
7.317
7.316
7.313
7.312
7.311
7.250
7.249
7.240
7.239
7.237
7.236
7.234
7.233
7.224
7.223
7.185
7.182
7.121
6.478
6.477
6.474
6.473
2.771
2.759
2.747
2.733
1.994
1.964
1.959
1.870
1.863
1.856
1.737
1.731
1.721
1.700
0.840
0.827
OH
S
S
+ cis-isomer
42
7.5
7.0
6.5
6.0
5.5
5.0
4.5
4.0
3.5
3.0
2.5
2.0
1.5
1.0
0.5
0.0
ppm
1.00
1.61
1.00
0.80
1.00
0.20
1.80
0.60
1.00
1.00
1.00
1.00
1.00
2.00
1.01
1.01
2.00
36.17
24.35
3.00

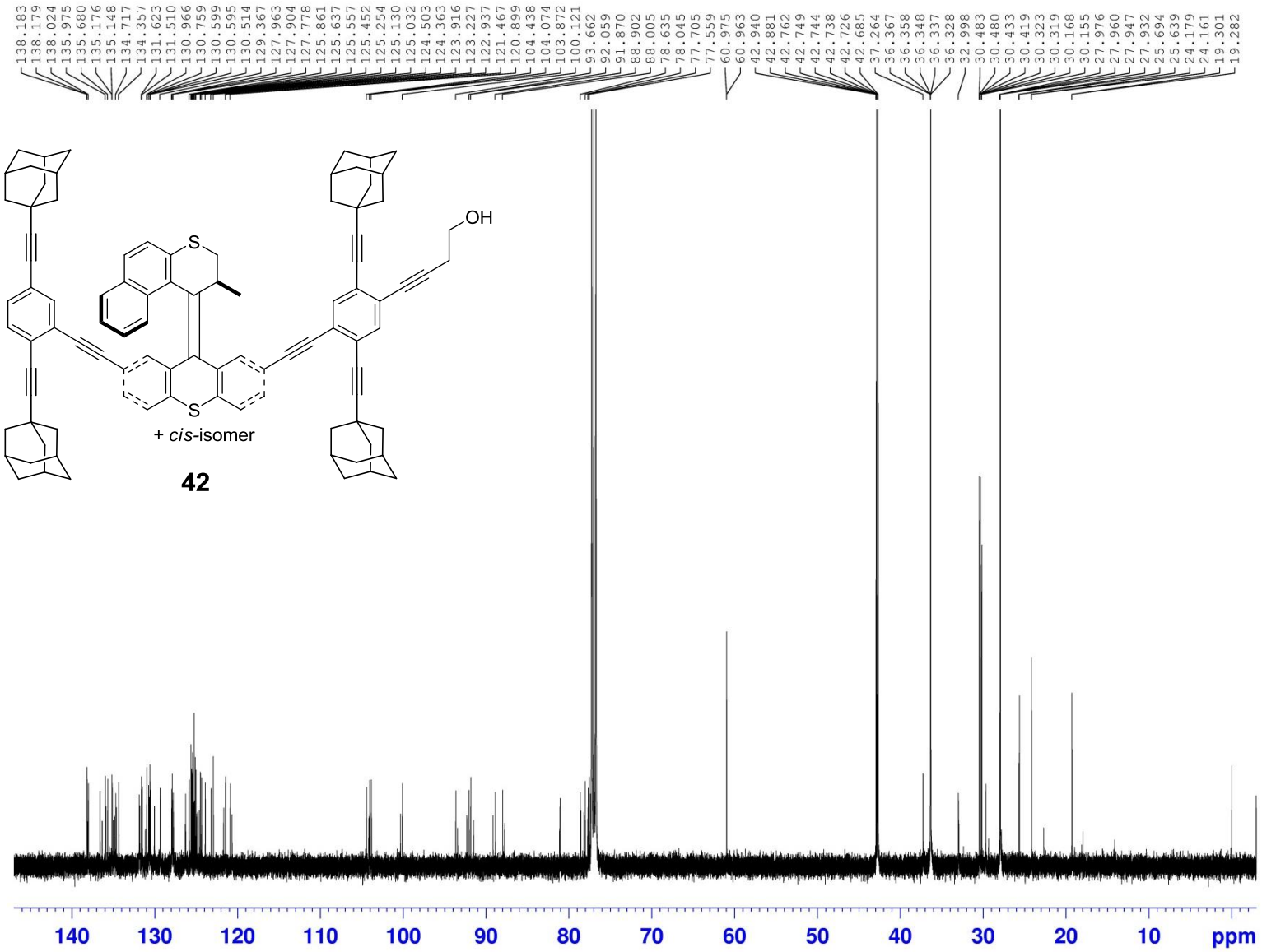
138.183
138.179
138.024
135.975
135.680
135.176
135.148
134.717
134.357
131.623
131.510
130.966
130.759
130.599
130.595
130.514
129.367
127.963
127.904
127.778
125.861
125.637
125.557
125.452
125.254
125.130
125.032
124.503
124.363
123.916
123.227
122.937
121.467
120.899
104.438
104.074
103.872
100.121
93.662
92.059
91.870
88.902
88.005
78.635
78.045
77.705
77.559
60.975
60.963
42.940
42.881
42.762
42.749
42.744
42.738
42.726
42.685
37.264
36.367
36.358
36.348
36.337
36.328
32.998
30.483
30.480
30.433
30.419
30.323
30.319
30.168
30.155
27.976
27.960
27.947
27.932
25.694
25.639
24.179
24.161
19.301
19.282
OH
S
S
+ cis-isomer
42
140
130
120
110
100
90
80
70
60
50
40
30
20
10
ppm

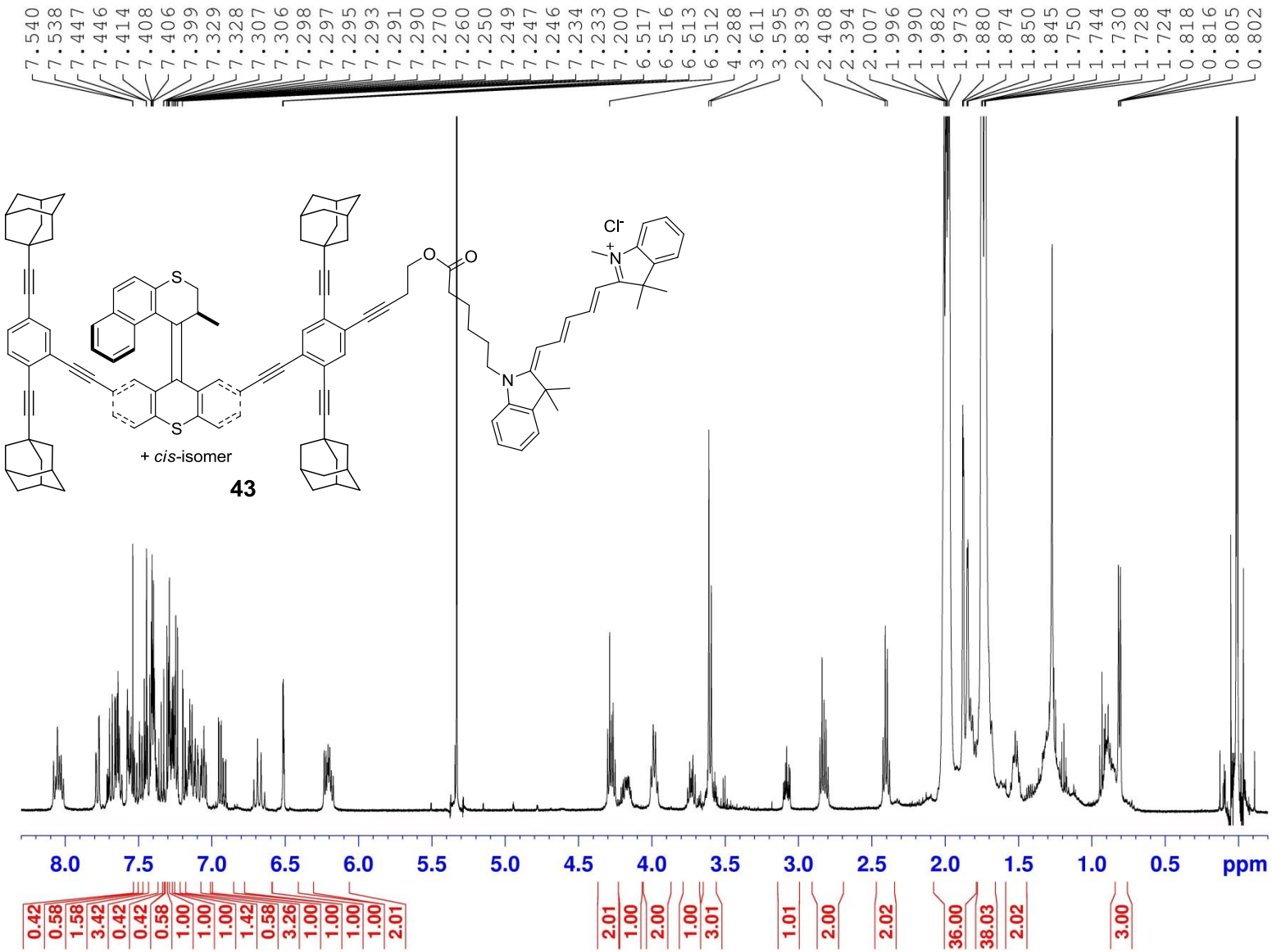
7.540
7.538
7.447
7.446
7.414
7.408
7.406
7.399
7.329
7.328
7.307
7.306
7.298
7.297
7.295
7.293
7.291
7.290
7.270
7.260
7.250
7.249
7.247
7.246
7.234
7.233
7.200
6.517
6.516
6.513
6.512
4.288
3.611
3.595
2.839
2.408
2.394
2.007
1.996
1.990
1.982
1.973
1.880
1.874
1.850
1.845
1.750
1.744
1.730
1.728
1.724
0.818
0.816
0.805
0.802
Cl-
+ cis-isomer
43
8.0
7.5
7.0
6.5
6.0
5.5
5.0
4.5
4.0
3.5
3.0
2.5
2.0
1.5
1.0
0.5
ppm
0.42
0.58
1.58
3.42
0.42
0.42
0.58
1.00
1.00
1.00
1.42
0.58
3.26
1.00
1.00
1.00
1.00
2.01
2.01
1.00
2.00
1.00
3.01
1.01
2.00
2.02
36.00
38.03
2.02
3.00

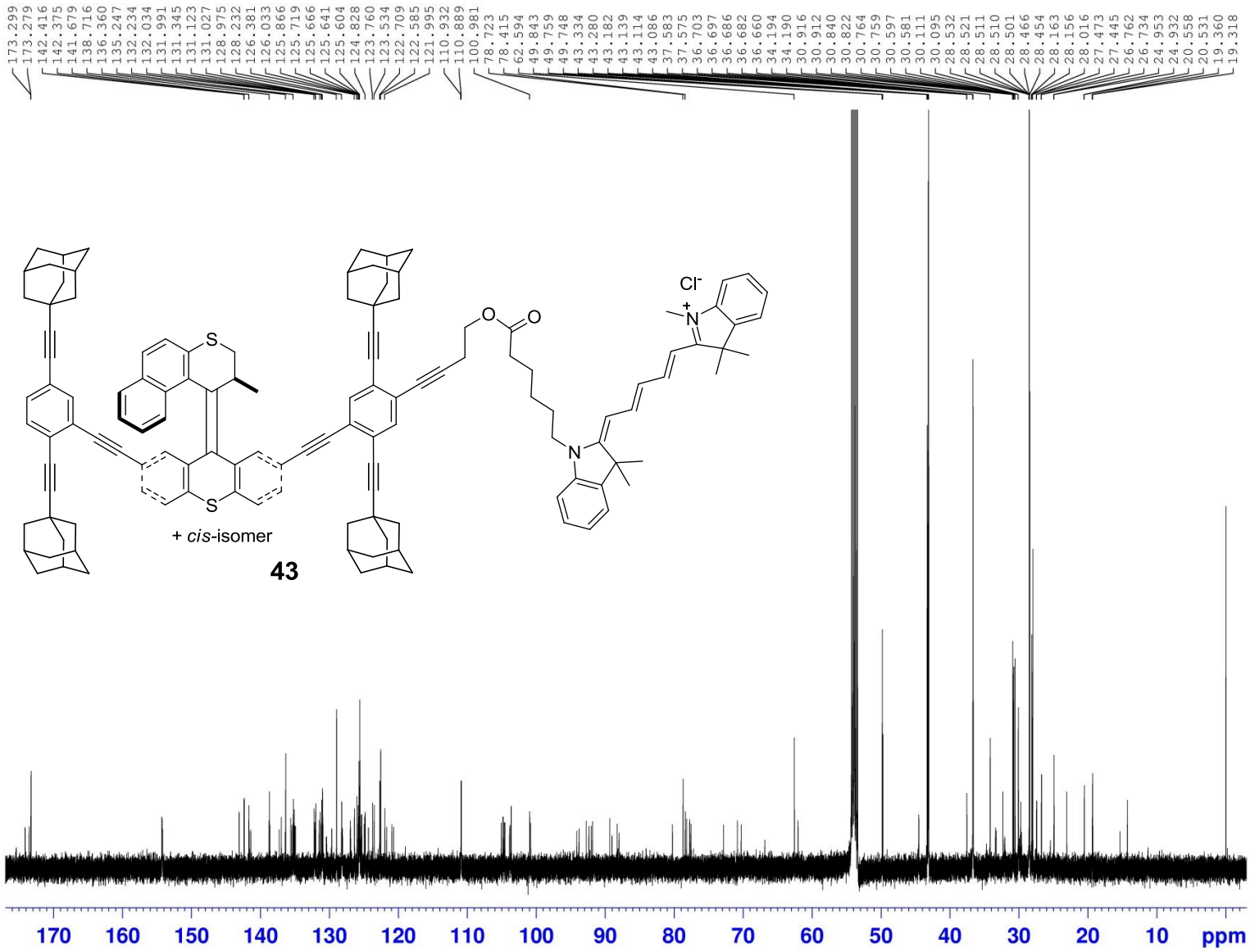
173.299
173.279
142.416
142.375
141.679
138.716
136.360
135.247
132.234
132.034
131.991
131.345
131.123
131.027
128.975
128.232
126.381
126.033
125.866
125.719
125.666
125.641
125.604
124.828
123.760
123.534
122.709
122.585
121.995
110.932
110.889
100.981
78.723
78.415
62.594
49.843
49.759
49.748
43.334
43.280
43.182
43.139
43.114
43.086
37.583
37.575
36.703
36.697
36.686
36.682
36.660
34.194
34.190
30.916
30.912
30.840
30.822
30.764
30.759
30.597
30.581
30.111
30.095
28.532
28.521
28.511
28.510
28.501
28.466
28.454
28.163
28.156
28.016
27.473
27.445
26.762
26.734
24.953
24.932
20.558
20.531
19.360
19.318
Cl-
+
N
O
O
S
S
N
+ cis-isomer
43
170
160
150
140
130
120
110
100
90
80
70
60
50
40
30
20
10
ppm

CHAPTER 4

Design, Synthesis, and Diffusion Study of Light-Activated Single-Molecule Nanosubmarines

4.1. Introduction

The studies of biological motor proteins[1-5] have stimulated the designs and syntheses of artificial molecular machines,[6,7] such as switches,[8,9] muscles,[10-12] and rotary motors.[13,14] These nanomachines respond to various external stimuli and perform a variety of functions at nanometer scale. Although the results are rich and fruitful, the area of artificial self-propelled micrometer-sized or nanometer-sized structures in solution was scarcely developed until the past decade.

Two main challenges for designing self-propelled nanostructure concern the supply of fuel and the conversion of fuel input into kinetic energy. Whitesides and co-workers overcame these problems on the millimeter scale by placing a metallic plate, consisting of a small area of platinum on one side, in a hydrogen peroxide aqueous solution to produce chemically-propelled autonomous movement. The locomotion of the plate was powered by the oxygen bubble burst produced during the platinum-catalyzed disproportionation of hydrogen peroxide ($H_2O_{2(l)} \rightarrow O_2 + H_2O_{(l)}$) in the solution.

This concept of chemically-propelled autonomous movement was subsequently applied to the designs of micrometer-sized objects.[15-17] Sen, Mallouk, Crespi, and co-workers created a platinum and gold (Pt/Au) segmented nanorod (~2 μm in size) that exhibited linear autonomous movement in a H_2O_2 aqueous solution.[18]

van Hest and co-workers also demonstrated a platinum-loaded polymeric stomatocytes (~0.2 μm in size) that achieved autonomous movement in H_2O_2 solution. These stomatocytes are bowl-shaped structure loaded with platinum nanoparticle (PtNP). The gases generated at the PtNP moved through the bowl opening and provided the thrust for autonomous movement.[19]

Ring-opening metathesis polymerization (ROMP) was also utilized for propelling autonomous movement for micrometer-sized object. Sen and co-workers prepared a gold-silica Janus particle (~0.5 μm in size) functionalized with a ROMP-catalyst. Upon addition of norbornene, the diffusion constant of the particles increased up to 70% due to the polymerization process.[20]

Despite these achievements of chemically propelled micrometer-sized object, the potential to promote solution-phased self-propulsion at the nanometer scale still faces major challenges, [16,17] namely tracking of object, designing of molecule, and mitigating the dominance of Brownian motion. In this chapter, we described designs and syntheses of signle-molecule nanosubmarines to address these challenges for self-propulsion at nanometer-scale.

4.2. Diffusion Studies of Single Molecules by Fluorescence Quenching

While micrometer-scale objects can be tracked directly in solution by an optical microscope, similar nanometer-scale single-molecule tracking techniques are not readily available.[21] In order to study the diffusion behavior of single molecules in solution, we used a fluorescence quenching approach to obtain the diffusion information desired. The fluorescence of tris(2,2'-bipyridine)ruthenium(II)$^{+2}$ (**1**, Ru(bpy)$_3^{+2}$) and the fluorescence quenching by methyl viologen^{+2} (**2**, MV^{+2}) have been extensively investigated.[22] The fluorescence of Ru(bpy)$_3^{+2}$ (Figure 4.1.) originates from absorbing 450 nm light (maximum absorption), and a metal to ligand charge transfer (MLCT) occurs between the Ru^{+2} atom and bipyridine ligands. The higher energy singlet state intermediate (^{1}MLCT) undergoes an intersystem crossing and forms a triplet state (^{3}MLCT) intermediate. The

$Ru(bpy)_3^{+2}$ triplet state intermediate relaxes back to the singlet ground state and generates fluorescence with much longer lifetime (610 nm, lifetime τ ~1 μs, quantum yield 0.07) compared to organic fluorophores (usually ranging from 1 to 10 ns). If the ^{3}MLCT intermediate of $Ru(bpy)_3^{+2}$ collides with MV^{+2}, the ^{3}MLCT intermediate can relax to the ground state without emitting fluorescence.

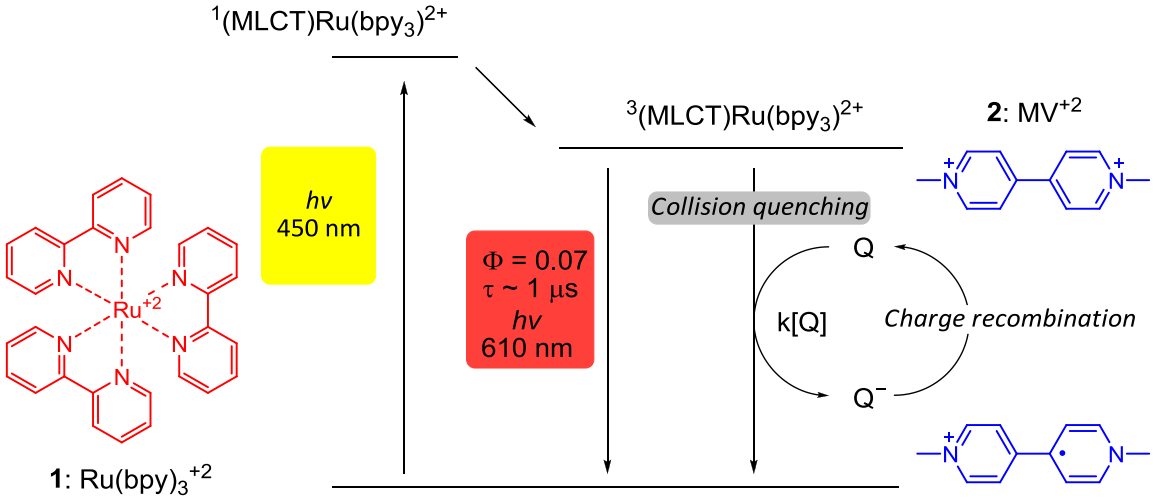

Figure 4.1. Structure of the tris(2,2'-bipyridine)ruthenium(II) (**1**, $Ru(bpy)_3^{+2}$) fluorophore, methyl vologen^{+2} (**2**, MV^{+2}), and the Jablonski diagram[23] for the fluorescence of $Ru(bpy)_3^{+2}$ and collision quenching by MV^{+2}.

The collision quenching is described by the Stern-Volmer equation:[24]

$$\frac{1}{\tau} = \frac{1}{\tau_0} + k_q[Q] \qquad (1).$$

A plot of the reciprocal fluorescence lifetime (τ) as a function of the concentration of quencher [Q] results in a straight line, and the slope is the bimolecular-quenching rate

constant (k_q). Then, using this rate constant, the diffusion coefficients of the molecules can be calculated by the Smoluchowski equation:[25,26]

$$\frac{k_q}{p} = k_0 = \frac{4\pi N_{av}}{1000}\left(R_l + R_Q\right)\left(D_l + D_Q\right) \quad (2)$$

where, p is the probability of quenching occurring upon each collision, R_l, D_l and R_Q, D_Q are the collision radii and diffusion coefficients of the fluorophore and the quencher, respectively, and N_{av} is Avogadro's number. Finally, the root mean square displacement in a defined time interval (t) can be derived by the Einstein-Smoluchowski equation:[27]

$$\Delta\sigma_{rms} = \langle \Delta x^2 + \Delta y^2 + \Delta z^2 \rangle^{1/2} = \sqrt{6Dt} \quad (3)$$

where $\Delta\sigma_{rms}$ is the square root of the squared mean displacement.

4.3. Design and Synthesis of the Methyl Viologen-Armed Nanosubmarine

A challenge to constructing an efficient self-propelled molecule is to overcome the dominant forces in its surroundings.[28] Inside a cell, for example, the viscous forces are ~1 pN. Translational biological motor proteins can generate a force ~10 pN per step by utilizing the energy from adenosine triphosphate (ATP) hydrolysis.[29] Therefore, they can be propelled.

We planned to use a synthetic light-driven rotary molecular motor that is capable of rotating like a propeller at 3 MHz.[14] With providing a significant amount of energy provided by photon excitement, a force generated by motor rotation might be able to overcome the viscous forces. The motors operate in a unidirectional rotational process that is most easily understood in this manner: there are two pre-existing elements of stereogenicity in the motor, the stereogenic center alpha to the methyl group and the twisted (atropisomeric) double bond. Once the motor is excited photochemically wherein

the alkene assumes an orthogonal conformation in its excited state, the two possible transition state routes to relaxation are diastereotopic. The motor keeps progressing over diastereotopic pathway of lower energy, leading to unidirectional rotation.

To study the diffusion behavior, we opted to use fluorescence quenching of $Ru(bpy)_3^{+2}$ by MV^{+2}. We proposed a structure of nanosubmarine **3** (Figure 4.2.) that was designed based on the light-driven MHz-rate unidirectional rotary motor with two methyl viologen motifs as fluorescence quenching arms. The rotary motor in **3** should exhibit a rotational frequency similar to its parent motor of 3 MHz, and the quenching properties of **3** should also be similar to those of MV^{+2}. The photochemically driven rotary motor in **3** rotates by irradiation of UV-light, and the motor rotation might propel the entire molecule and generate some measurable increase in the diffusion coefficient compared to the diffusion coefficient without irradiation of UV-light. Furthermore, the fluorescence lifetime of $Ru(bpy)_3^{+2}$ is long (~1 μs), which increases the probability of the occurrence of collision quenching and allows the system to reach thermal equilibrium.[30]

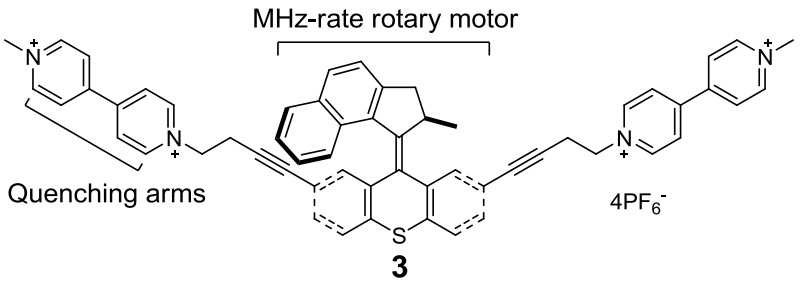

Figure 4.2. Structure of a light-driven methyl viologen-armed nanosubmarine **3**.

The collision quenching can also be described by simple collision theory, in which the k_q is expressed as:[31]

$$k_q(T) = p\pi b_{max}^2 v_r \exp\left(-\frac{\varepsilon}{kT}\right) \quad (4)$$

where, p is the probability of effective collision, $b_{max} = R_l + R_Q$, v_r is the relative speed between the fluorophore and quencher, ε is the energy barrier of the reaction, k is the Boltzmann constant, and T is the temperature. Note that in eq 5, the rate constant is proportional to the relative speed between the fluorophore and the quencher. The speed of $Ru(bpy)_3^{+2}$ remains constant with or without motor excitation. If an increase in k_q is observed, we can attribute the more rapid quenching to the higher speed of the nanosubmarine. Therefore, comparing the two k_q that are obtained with and without UV-light, a conclusion as to whether the nanosubmarine molecule accelerates under photoexcitation in solution will be reached.

According to simple collision theory, the k_q is proportional to the relative speed of the nanosubmarine and the $Ru(bpy)_3^{+2}$. Two k_q would be obtained: with, and without, UV-light that triggers the motor rotation. If a larger k_q is observed with UV-light irradiation, we can attribute the increase in the coefficient to the increase of speed of the nanosubmarine that resulted from motor rotation.

4.4. Synthesis of the Methyl Viologen-Tagged Nanosubmarine

The synthesis of the nanosubmarine **3** was based on the 2,7-dibromomotor **4** (Scheme 4.1).[32] A Sonogashira coupling using modified Fu's condition[32,33] between **4** and 4-(*tert*-butyldimethylsilyoxy)-but-1-yne was completed in moderate yield. Removal of the *tert*-butyldimethylsilyoxy (TBS) protecting group by a tetrabutylammonium fluoride (TBAF) solution in THF led to dialcohol **6**. Functional group interconversion of dialcohol **6** gave ditosylate **7**. Ditosylate **7** was alkylated with 4,4'-bipyridyl and the

nanosubmarine precursor **8** was produced. Finally, methylation of **8** with methyl tosylate yielded nanosubmarine **3**. The nanosubmarine was stable as a hexafluorophosphate (PF_6) salt, and was soluble in CH_3CN. Although **3** is tetracationic, it is not soluble in water when the anion is PF_6. To produce a water soluble version of nanosubmarine **3**, attempts to exchange the anion with chloride produced only decomposition.

Scheme 4.1. Synthesis of the methyl viologen-armed nanosubmarine

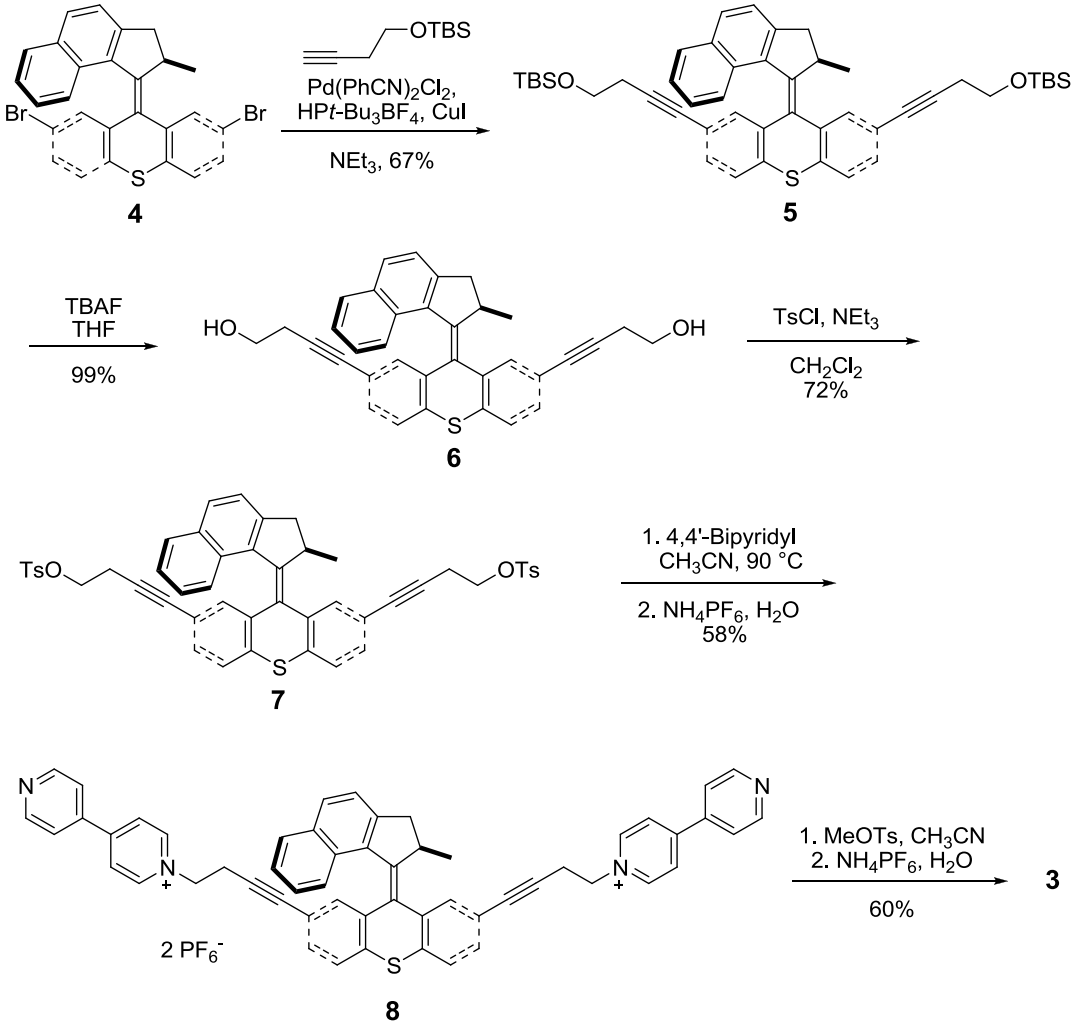

A control molecule equipped with a slow-rotating motor was also synthesized in a protocol similar to **3**. Motor **9**[34] was coupled with 4-(*tert*-butyldimethylsilyoxy)-but-1-yne to give **10**. The corresponding deprotected compound **11** was obtained by treating **10** with a TBAF solution in THF. Tosylate **12** was obtained in excellent yield. A substitution reaction with 4,4'-bipyridyl yielded control molecule precursor **13**. Final methylation and anion exchange led to the slow-motor control molecule **14**.

Scheme 4.2. Synthesis of the methyl viologen-armed slow-motor control molecule

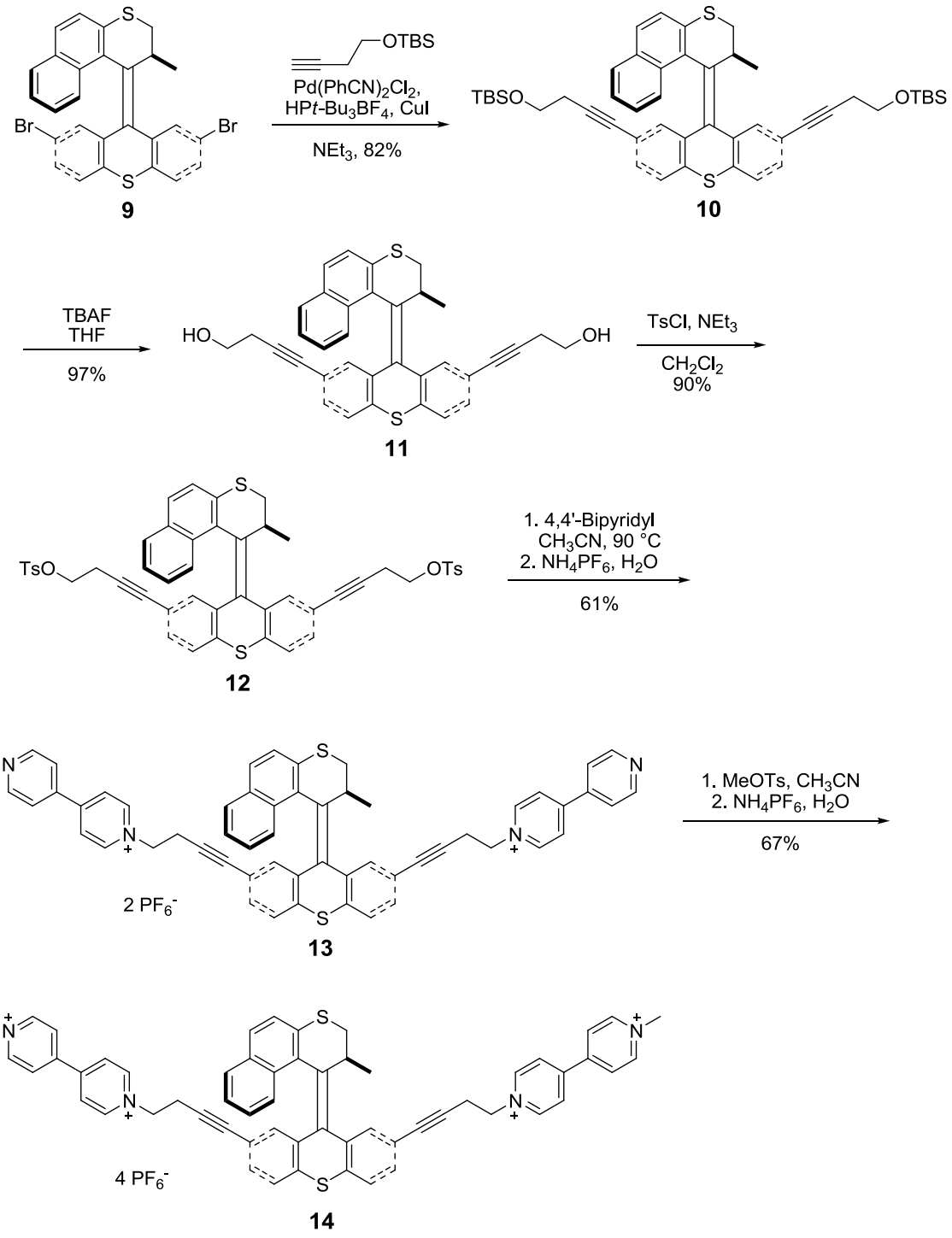

4.5. Diffusion Studies in Solution of the Methyl Viologen-Armed Nanosubmarine by Time-Resolved Fluorescence Spectroscopy

The $Ru(bpy)_3^{+2}$ fluorescence quenching experiments by the nanosubmarine **3** were carried out under two conditions (Figure 4.3.). In the presence of electrolyte (0.1 M tetrabutylammonium hexafluorophosphate ($TABPF_6$)), the fluorescence lifetimes were recorded by using 444 nm or 371 nm laser sources. Both sets of data were consistent with the eq 2, and $k_{q,444nm}$ and $k_{q,371nm}$ were obtained, respectively. The values of k_q were of the same order of magnitude when using MV^{+2} as the quencher.[22] However, the value of $k_{q,371nm}$ was not larger than $k_{q,444nm}$, indicating that no acceleration of **3** was observed. Another set of fluorescence quenching experiments was done without the electrolyte. The data points were not consistent with the Stern-Volmer eq (1) because of the changes in ionic strengths at different concentration of **3**. Thus, the lifetime data points obtained from different lasers did not show significant difference for any given concentration. The result can be attributed to the fact that Brownian motion is dominating the molecular diffusion and not the motor rotation.

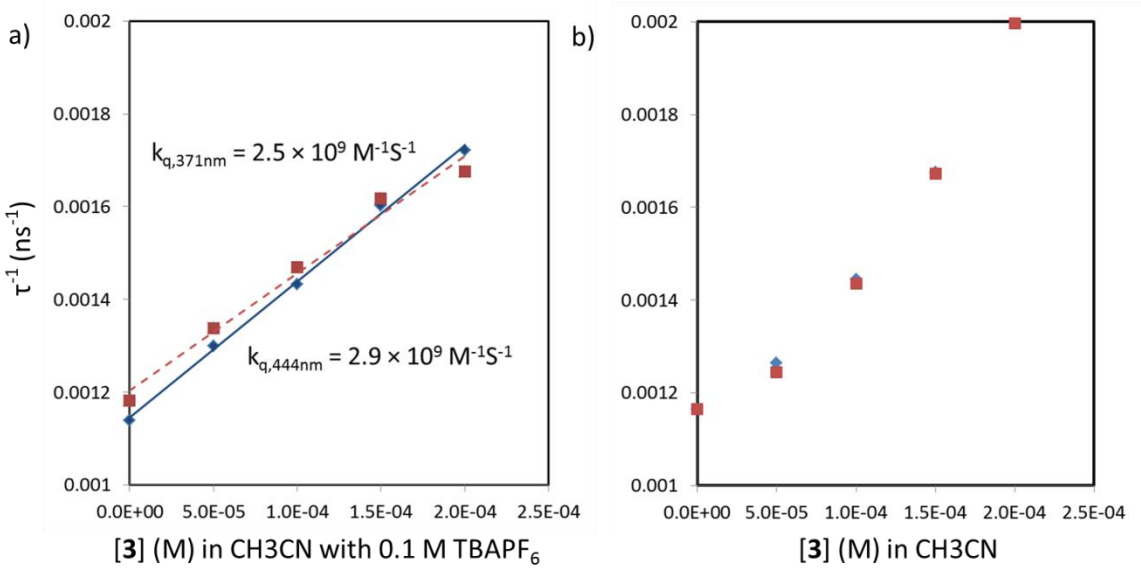

Figure 4.3. Fluorescence quenching of $Ru(bpy)_3^{+2}$ **1** by nanosubmarine **3** at 444 nm (red dashed line) and 371 nm (blue solid line) lasers excitation (298 K; laser pulse repetitive time: 5 μs). in (a) CH_3CN with 0.1 M $TBAPF_6$ as electrolyte for maintaining ionic strength. The fluorescence lifetime data points acquired by 444 nm laser and 371 nm laser were consistent with the Stern-Volmer eq (1), and $k_{q,444nm}$ and $k_{q,371nm}$ were obtained, respectively. However, the value of $k_{q,371nm}$ was not higher than $k_{q,444nm}$, which indicated no acceleration of **3**. (b) CH_3CN without electrolyte. The data points were not consistent with eq (1) because of the changes in ionic strength. The lifetime data points (444 nm laser: blue shields; 371 nm laser: red square) obtained from different lasers did not show significant differences at a given concentration.

4.6. Design of the Cy5-Armed Nanosubmarine

Another method to study diffusion is fluorescent correlation spectroscopy (FCS). FCS records the fluorescence fluctuations from a single light-emitting source in a small open volume and transforms the time traces into autocorrelation curves via a correlation

analysis. The intensity of the autocorrelation as a function of lagtime (τ) can be expressed in terms of experimental parameters as:

$$G(\tau) = \frac{1}{V_{eff}<C>} \cdot \frac{1}{\left(1+\frac{\tau}{\tau_D}\right)} \cdot \frac{1}{\left(1+\left(\frac{r_0}{z_0}\right)^2\left(\frac{\tau}{\tau_D}\right)\right)^{1/2}} \quad (5)$$

where V_{eff} is volume, r_0 is beam waist, z_0 is beam height, τ_D is characteristic diffusion time, and $<C>$ is analyte concentration. The experimental characteristic diffusion time can thus be obtained by fitting the autocorrelation curves with eq (5). Finally, the three-dimensional diffusion coefficient (D) can be calculated using the following equation:

$$\tau_D = \frac{r_0^2}{4D} \quad (6).$$

In chapter 3, a cy5-tagged motorized nanocar was designed and synthesized. A control molecule was synthesized, and the photoisomerization efficiency of the motor was studied. The result showed that the cy5 dye interfered minimally with the motor photoisomerization. Hence, we designed a cy5-armed nanosubmarine **15** that was incorporated with the MHz-rotary motor. In **15**, the fast motor was attached to two cy5 dyes. A control molecule **16**, equipped with a slow motor core, was also designed. The slow motor would allow the confirmation of photoisomerization efficiency of the cy5-armed nanosubmarines by NMR spectroscopy.[34] The slow rotation of the motor in **16** (~2 rotations per hour at 60 °C)[34,35] should not result in acceleration of molecule.

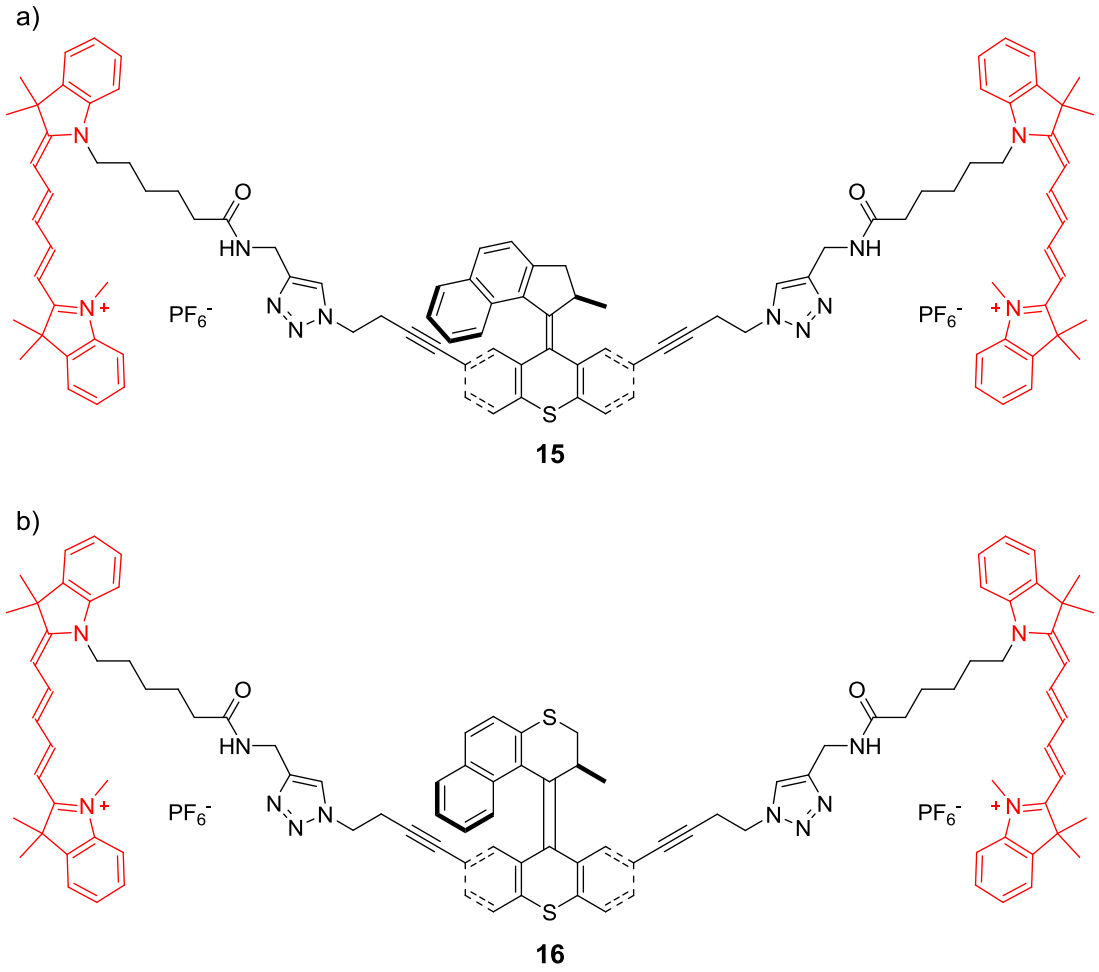

Figure 4.4. (a) Structure of the light-driven cy5-armed nanosubmarine **15** that bears two cy5 dyes, one on each side of the fast-turning motor. A double azide-alkyne Hüisgen cycloaddition was planned to connect the fast MHz motor and the cy5 dyes. (b) Structure of control molecule **16**. The control molecule would allow the study the photoisomerization efficiency of the motor since the motor only turns at ~2 rotations per hour at 60 ℃. It could also serve as a control molecule because the slow rotating motor should not contribute to accelerating the molecule.

4.7. Synthesis of the Cy5-Armed Nanosubmarine

A cy5 dye **17** with a carboxylic functional group was prepared according to a literature procedure.[36] A *N,N'*-dicyclohexylcarbodiimide promoted amidation between cy5 dye **17** and propargyl amine was carried out to give **18**. Subsequently, cy5 dye **18** with an alkyne ready for click chemistry was obtained in good yield. The skeleton of the cy5-armed nanosubmarine **15** was made as a substitution reaction converted ditosylate **6** into diazide **19**. The cy5-armed nanosubmarine **15** was obtained by a high yielding double azide-alkyne Hüisgen cycloaddition using CH_2Cl_2 and water as co-solvents.[37] Ditosylate **12** was converted into a diazide **20**, and the control cy5-armed molecule **16** was synthesized by a double azide-alkyne Huisgen cycloaddition.

Scheme 4.3. Synthesis of the cy5-armed nanosubmarine and control molecule

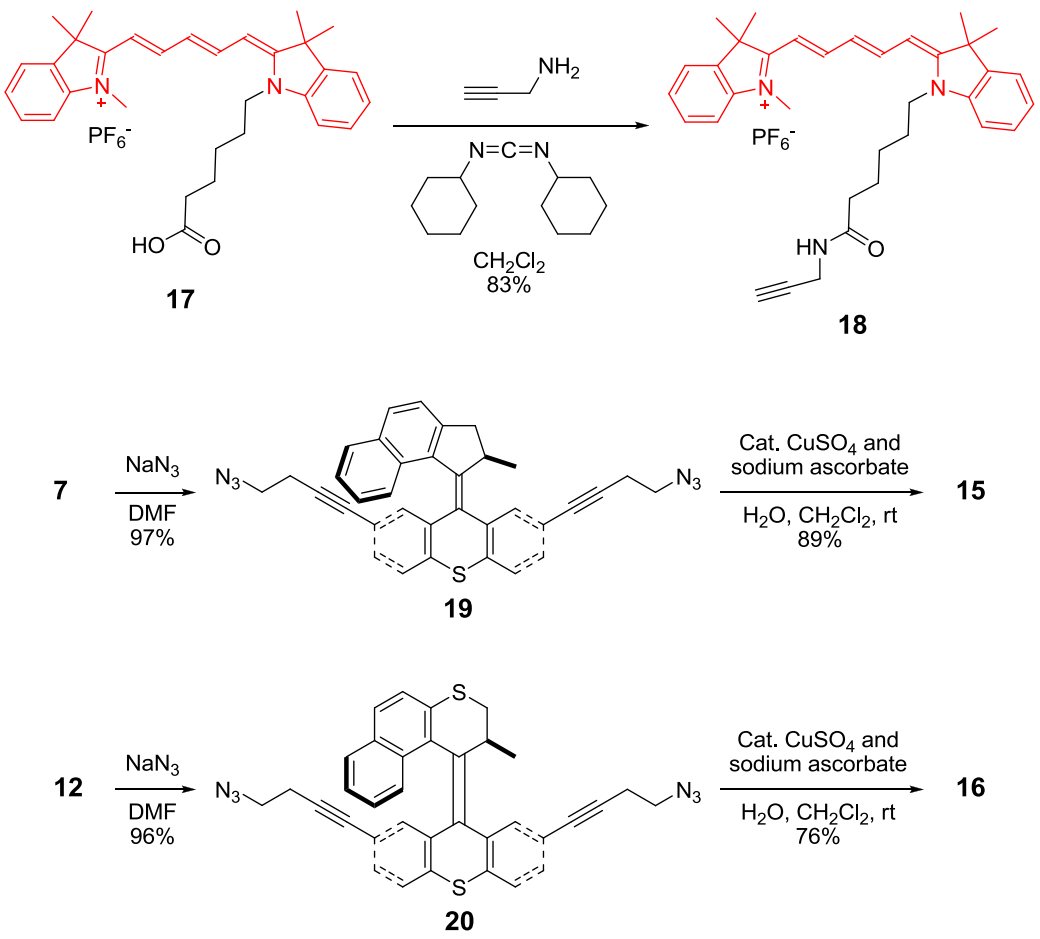

4.8. Diffusion Studies of the Cy5-Armed Nanosubmarine by FCS

The diffusion behavior of the cy5-armed nanosubmarine **15** was studied by FCS (Figure 4.5.) in a CH_3CN solution. A 638 nm laser source was used, and the correlation studies utilized the fluorescence from the cy5 dye. One correlation curve was obtained without irradiating UV light that triggers the motor rotation (Figure 4.5.a). Another correlation curve was obtained with irradiating UV light from a 371 nm picosecond diode laser that excites the motor rotation. Unfortunately, the diffusion coefficient (Figure 4.5.b) obtained in both cases did not show any significant difference.

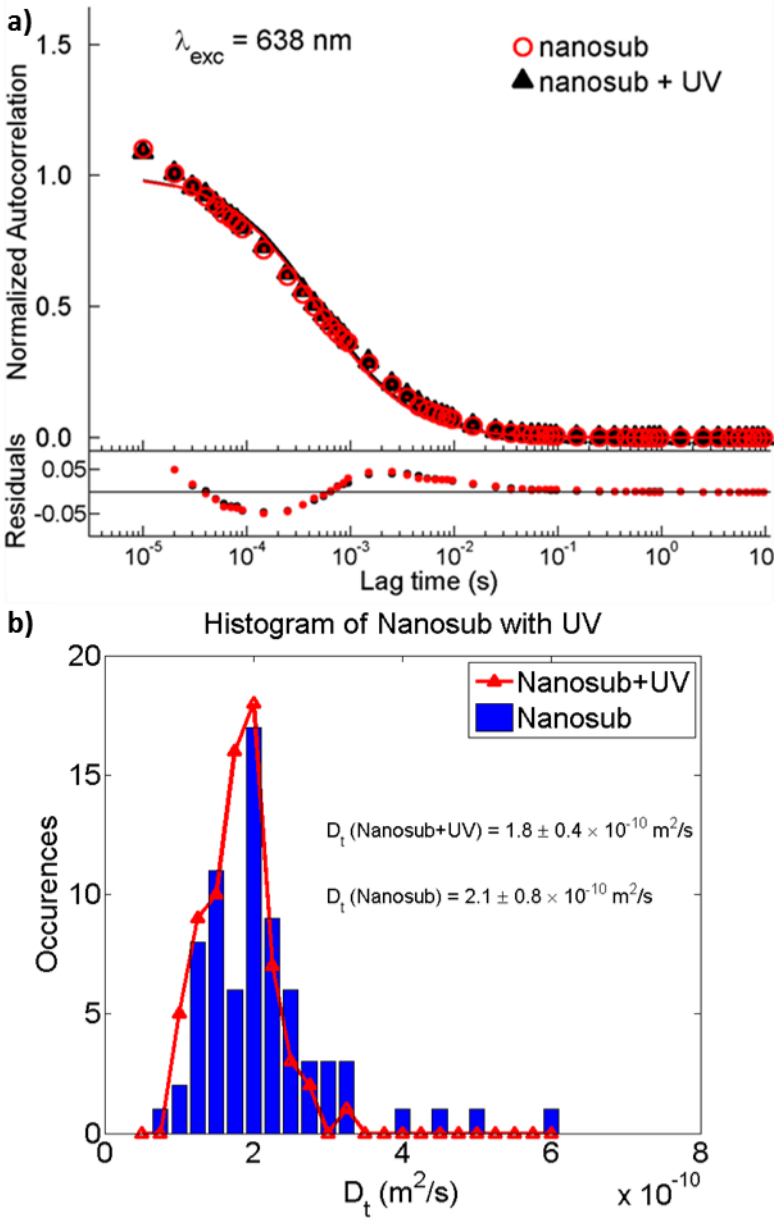

Figure 4.5. FCS studies of cy5-armed nanosubmarine **15** (CH_3CN, 295 K, 10^{-8} M). a) The autocorrelation curves of **15** without irradiation of 371 nm laser (red circles) and with irradiation of 371 nm laser (5 μs pulse period, black triangles). b) The distribution of the diffusion coefficients without irradiation of 371 nm laser (D = 2.1 (± 0.8) × 10^{-10} m^2/s,

red triangle) and with irradiation of 371 nm laser (D = 1.8 (± 0.4) × 10^{-10} m^2/s, blue column). No significant difference between the diffusion coefficients was found.

4.9. Minimizing the Effects of Brownian Motion by Confining Nanosubmarines in 1-D Channels

An increase in quenching rate was not found with the test between $Ru(bpy)_3^{+2}$ **1** and nanosubmarine **3** in an CH_3CN solution. A FCS study of a fluorescent cy5-armed nanosubmarine **15** also did not show an increase in diffusion coefficient. These results are attributed to the dominant Brownian motion, a constant displacement and random reorientation in solution. In nature, molecular motor proteins, such as myosin and kinesin, rely on binding to "tracks" to perform work.[3, 38] Myosin and kinesin, for example, utilize the energy released from ATP hydrolysis to break the equilibrium of the environment and generate translational motion. The track prevents displacement perpendicular to the track and constrains reorientation of the motor proteins. Therefore, if the molecules could be loaded in a 1-D channel-like environment, the diffusion behaviors are expected to be different.[39-42]

One approach to crerating a 1-D channel-like environment was to co-encapsulate nanosubmarines **3**, or **15** and $Ru(bpy)_3^{+2}$ in mesoporous materials, such as MCM-41[43,44] or SBA-15, and measure the fluorescence quenching of $Ru(bpy)_3^{+2}$. It has been demonstrated that the fluorescence of a ruthenium complex similar to $Ru(bpy)_3^{+2}$ can be efficiently quenched by cy5.[45] The decay law that governs the 1-D quenching process within the channels should provide direct information on the average diffusion coefficient of $Ru(bpy)_3^{+2}$ and nanosubmarines with respect to one another. The equations for the

diffusion-influenced fluorescence quenching in 1-D have been described by Szabo[46] and more recently by Medhage and Almgren:[47]

$$ln\frac{I(t)}{I(0)} = -k_0 t - a^3 c_q Q_{1D} \quad (7)$$

$$Q_{1D} = \frac{4\pi}{ha}\left\{\sqrt{\left(\frac{ha}{\sqrt{\tau_q}}\right)^2 \frac{t}{\pi}} + \frac{3}{4}\left[exp\left\{\left(\frac{ha}{\sqrt{\tau_q}}\right)^2 \frac{4t}{9}\right\} erfc\left\{\left(\frac{ha}{\sqrt{\tau_q}}\right)\sqrt{\frac{4t}{9}}\right\} - 1\right]\right\} \quad (8)$$

where I(t) is the time-dependent fluorescence intensity, k_0 is the natural fluorescence rate constant, c_q is the quencher concentration, a is the radius of the cylindrical reaction zone where the quenching occurs (that can be roughly estimated by the sum of the radii of $Ru(bpy)_3^{+2}$ and nanosubmarines), $\tau_q = a^2/D$, D is the sum of the diffusion coefficients of $Ru(bpy)_3^{+2}$ and nanosubmarines, and h is a parameter that weights reaction against diffusion. The two unknown variables are D and h, which requires the fitting of the time-decay data to this expression using non-linear least square methods, and the determination of the diffusion coefficient is straight forward. Simpler expressions can be obtained by making assumptions concerning the magnitude of the diffusion coefficient; however this is not fundamentally necessary. The system containing the $Ru(bpy)_3^{+2}$ and nanosubmarines would be excited using a 444 nm picosecond diode laser that will only excite $Ru(bpy)_3^{+2}$, and a 371 nm picosecond diode laser that will excite both $Ru(bpy)_3^{+2}$ and nanosubmarines. We anticipate obtaining a larger diffusion coefficient when the system is excited with 371 nm light (that will activate the rotation of the motor) than with 444 nm light (that will only excite $Ru(bpy)_3^{+2}$). Experimental conditions such as the concentrations of the species, the effects of different solvents, the amount of residual solvent within the channels, and the pore size of the mesoporous material will be varied.

Although several studies have been published to determine the diffusion coefficient of molecules by time-resolved fluorescence methods in 2-D and 3-D, studies in 1-D are scarce.[26,48-51] Nevertheless, work by Almgren's group has demonstrated the applicability of these equations to study the 1-D diffusion of pyrene in rod-like micelles.[52] The successful of the studies outlined here would increase the currently limited studies on 1-D diffusion using time-resolved fluorescence spectroscopy. The use of fluorescence lifetime measurements and mathematical analyses will be used to calculate the average diffusion coefficient of nanosubmarines within the channels of mesoporous materials such as MCM-41 and SBA-15.

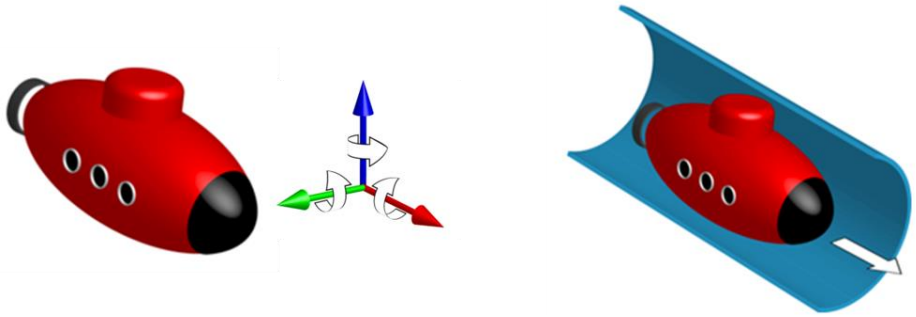

Figure 4.6. Schematic representation of a nanosubmarine in solution (left) and in a 1-D confinement environment (right). In solution, the nanosubmarine undergoes rapid reorientation and random displacement from Brownian motion. To create a track-like environment, the nanosubmarine will be co-encapsulated into mesoporous materials consisting of channels with diameters in the nanometer range. This 1-D confinement approach should prevent displacement perpendicular to the channel, constrain the reorientation of the molecules, and allow the nanosubmarine to move directionally inside the channels.

4.10. Preliminary Diffusion Studies of the Cy5-Armed Nanosubmarine in 1-D Channels

Initial experiments included co-encapsulation of $Ru(bpy)_3Cl_2$ and **15** in MCM-41 with a 3 nm pore size, which is close to the dimensions of the $Ru(bpy)_3Cl_2$ and **15**. Fluorescence quenching experiments of the co-encapsulated $Ru(bpy)_3Cl_2$ and **15** were done with irradiation of 444 nm laser and 371 nm laser. However, the lifetime obtained by different wavelength light sources did not show significant differences.

Another mesoporous material MSU-H, with a larger porous size of 7 nm was used for co-encapsulating $Ru(bpy)_3(PF_6)_2$ and/or **15**. Interestingly, when CH_2Cl_2 was used as the encapsulating solvent, both $Ru(bpy)_3(PF_6)_2$ and **15** were loaded inside the channel, but in contrast, when CH_3CN was used as the solvent, both $Ru(bpy)_3(PF_6)_2$ and **15** came out of the channel.

The fluorescence lifetime of $Ru(bpy)_3(PF_6)_2$ co-encapsulating with **15** in MSU-H mesoporous material were measured (Figure 4.7.). The fluorescent decay curve can be fitted biexponentially, and two lifetime components τ_1 and τ_2 were obtained. Compared to the τ_1 and τ_2 obtained by 444 nm and 371 nm lasers, significant decrease of lifetimes were observed in both when 371 nm light was used. As a control experiment, we studied the fluorescence quenching of $Ru(bpy)_3(PF_6)_2$ by the co-encapsulated control molecule **16** in MSU-H mesoporous material. Similarly, lasers of two different wavelengths were used in the quenching experiment, and no significant difference in lifetime was observed. This indicated that the nanosubmarine in the 1-D channel environment showed acceleration presumably because irradiation at 371 nm light triggers the rotation of the motor.

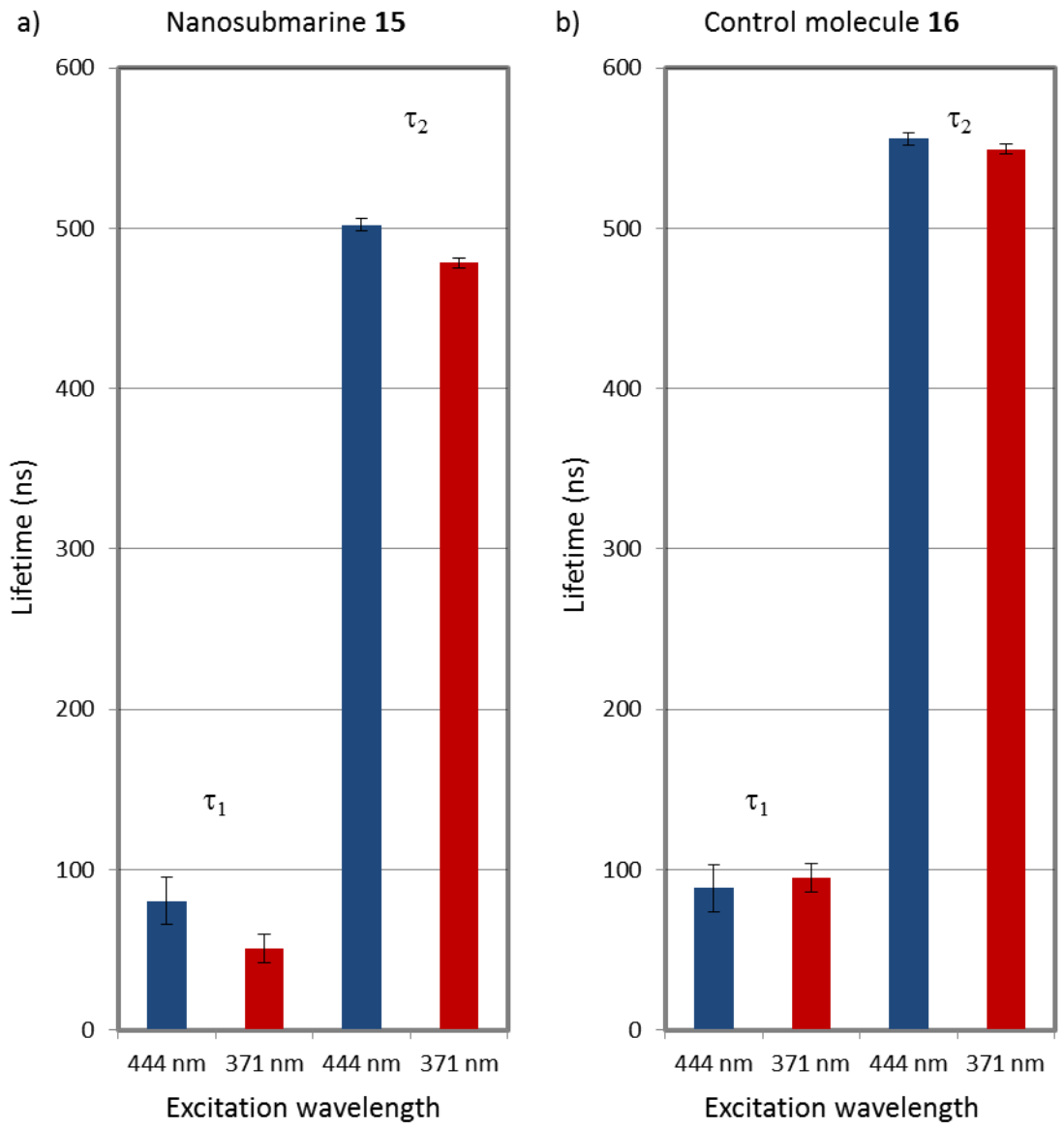

Figure 4.7. Biexponential fluorescent lifetime (τ_1 and τ_2) of $Ru(bpy)_3^{+2}$ co-encapsulating with nanosubmarine **15** (1:1), or control molecule **16** (1:1) in MSU-H with CH_2Cl_2 as solvent. Two sets of τ_1 and τ_2 were obtained with excitation wavelengths at 444 nm and 371 nm. a) Comparing τ_1 and τ_2 obtained by 444 nm and 371 nm excitation wavelengths, shorter τ_1 and τ_2 were obtained at 371 nm. b) Comparing τ_1 and τ_2 obtained by 444 nm and 371 nm excitation wavelengths, no significant difference in τ_1 and τ_2 were found.

4.11. Conclusion and Future Work

In this chapter, methyl viologen-armed nanosubmarine **3** and cy5-armed nanosubmarine **15** were designed and synthesized. In order to study the diffusion behavior, a series of fluorescence quenching experiments of $Ru(bpy)_3^{+2}$ by nanosubmarine **3** were carried out. Unfortunately, the fluorescence lifetimes of $Ru(bpy)_3^{+2}$ measured by using 444 mn and 371 nm laser excitations did not show significant difference, which means the motor rotation did not resulted in acceleration of the molecule. We also tried FCS to measure the diffusion coefficients of cy5-armed nanosubmarine **15**. However, the diffusion coefficients obtained with or without 371 nm laser irradiation did not show significant difference. These results were probably due to the very dominant Brownian motion in solution.

In nature, a track strategy is used for transporting molecules inside a cell. Mimicking nature's track approach, we encapsulated the nanosubmarine inside mesoporous materials to create a 1-D channel environment. This would decrease the effects of Brownian motion because the 1-D channel should restrict the molecules from rapid reorientation and the constant displacements perpendicular to the channel. Preliminary testing by fluorescence quenching of $Ru(bpy)_3^{+2}$ by **15** in MSU-H mesoporous material showed that the fluorescence lifetime decreases when irradiated with 371 nm laser. In contrast, the control molecule **16** showed no decrease of lifetime. The shortened lifetime is attributed to the acceleration of nanosubmarine **15** generated by motor rotation.

Future work will include in-depth studies of how different concentrations of molecules, solvents, and channel size affect the fluorescence lifetimes. We hope this

work can provide insights into the design of light-driven nanovehicles for performing autonomous movement.

4.12. Contribution

I conceived the designs of all nanosubmarine molecules and the 1-D channel approach. I synthesized all the nanosubmarine molecules and conducted the quenching experiments in solution. Victor Garcia repeated the synthesis and did all the fluorescence quenching experiments in 1-D mesoporous materials. Professor Angel Martí extracted information for the mathematical analyses. Lin-Yung Wang in the laboratory of Stephan Link at Rice University did the FCS experiments. E. Loïc Samuel made Figure 4.6.

4.13. Experimental Section

4.13.1. Fluorescent Monitoring

Fluorescence quenching experiment in solution. The fluorescence quenching experiments were conducted on an Edinburg instrument single photon counter (OB-920). All experiments were halted manually to ensure consistent initial photo count (~1000). HPLC grade CH_3CN was dried over CaH_2 and distilled. The freshly distilled CH_3CN was degassed by a stream of argon for 2 h in a round-bottom flask equipped with a stir bar. $Ru(bpy)_3^{+2}$ **1** and nanosubmarine **3** were weighed under ambient conditions. The CH_3CN, **1**, and **3** were introduced into a glovebox in which the oxygen level was lower than 2 ppm. The fluorescence lifetime experiments were obtained by an Edinburgh Instruments single-photon counter (Edinburgh Instrument OB-920) with detection wavelength at 600 nm. Two picosecond pulse diode lasers at 371 nm (Edinburgh Instrument ELP-375) and

444 nm (Edinburgh Instrument ELP-445) were used as the light source. The pulse repetition time was 5 μs.

With electrolyte (0.1 M $TBAPF_6$ in CH_3CN)

	444 nm	371 nm
[**3**] (M^{-1})	$1/\tau$ (ns^{-1})	$1/\tau$ (ns^{-1})
0	0.001139	0.001182
0.00005	0.001299	0.001337
0.0001	0.001433	0.001468
0.00015	0.001603	0.001618
0.0002	0.001721	0.001675

Without electrolyte (CH_3CN)

	444 nm	371 nm
[**3**] (M^{-1})	$1/\tau$ (ns^{-1})	$1/\tau$ (ns^{-1})
0	0.001164	0.001166
0.00005	0.001264	0.001244
0.0001	0.001445	0.001435
0.00015	0.001675	0.001672
0.0002	0.002008	0.001996

Table 4.1. Fluorescence quenching data of $Ru(bpy)_3^{+2}$ by **3** in CH_3CN with and without the presence of electrolyte.

Optical Setup for FCS. FCS was performed using a home-built inverted confocal microscope (Observer.D1, Zeiss). The light from a 638 nm laser was collimated and expanded to overfill the back aperture of a microscope objective (Fluar, Zeiss: 100×, NA = 1.3). The beam was circularly polarized using a λ/4 waveplate (Newport). The laser power was attenuated to ~150 nW using neutral density filters (Thorlabs). This power gave a signal to background ratio of ~10, yet ensured negligible heating of the sample. The focal plane of the objective was set to approximately ~6 μm inside the solution to avoid excessive scattered light from the glass−water interface. Polystyrene fluorospheres (100 nm in diameter, Molecular Probes) were used for alignment and calibration of the focal volume. The fluorescence was collected in the backward direction and redirected to

a 50 μm pinhole (Thorlabs) before focusing onto an avalanche photodetector (SPCM-AQRH, Perkin-Elmer).

Fluorescence quenching in MCM-41. $Ru(bpy)_3Cl_2·6H_2O$ was obtained from Sigma-Aldrich. The mesoporous material MCM-41 was first vacuum dried at 300 ℃ for 15 h and cooled to rt. A solution contained $Ru(bpy)_3Cl_2$ (1.56 mM) and/or cy5-armed nanosubmarine **15** (1.56 mM) in CH_3CN was mixed with the dried MCM-41 channel, and $Ru(bpy)_3Cl_2$ and **15** were successfully loaded into the mesoporous material. 1.5 mL of stock solution was added to the dried MCM-41, and the mixture was shaken for 18 h at 500 Hz. After shaking, the samples were centrifuged for 10 min and the supernatants were collected separately. The residues were washed with CH_3CN (3 mL) and centrifuged for 10 min. The washing procedure was repeated twice, and the organic phases were combined. The solution was analyzed by UV-Vis spectroscopy (Shimatzu UV-2450) and the amount of $Ru(bpy)_3Cl_2$ and nanosumbarine loaded in the MCM-41 was calculated by subtracting the amount in the supernatant fraction from amount in the original solution. The collected solid was dried under vacuum and the dried sample added CH_3CN to make a suspension at 0.04% w/V. The suspension was purged with Argon for 10 min.

Fluorescence quenching in MSU-H. $Ru(bpy)_3(PF_6)_2$ was prepared by an anion exchange from $Ru(bpy)_3Cl_2·6H_2O$ using NH_4PF_6, CH_3CN and water. CH_2Cl_2 was freshly distilled over CaH_2 before use. MSU-H was obtained from Sigma-Aldrich. The sample preparation process was identical to the MCM-41 samples.

	371 nm	ns	STD	Rel. %	444 nm	ns	STD	Rel. %
15	τ_1	80.2	14.7	2.27	τ_1	51.1	8.9	1.88
	τ_2	502	3.9	97.73	τ_2	478.4	2.9	98.12
16	τ_1	88.3	4.2	8.14	τ_1	94.6	4	9.9
	τ_2	555.8	4.9	91.86	τ_2	549.3	4.7	90.1

Table 4.2. Fluorescence lifetime of $Ru(bpy)^{+2}$ co-encapsulating with nanosubmarine **15** (1:1) or control molecule **16** (1:1) in MSU-H.

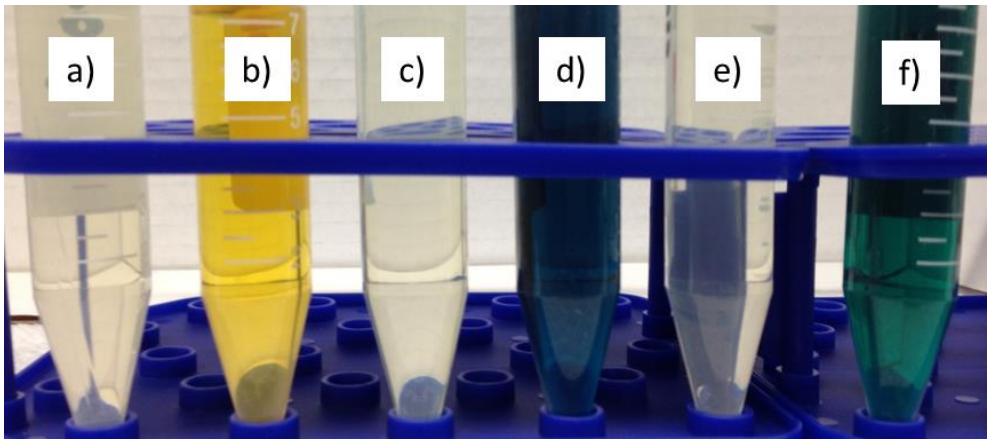

Figure 4.7. Picture of the supernatant after encapsulating $Ru(bpy)_3(PF_6)_2$ and/or nanosubmarine **15** into mesoporous silica MSU-H (7 nm porous size) using different solvents: a) $Ru(bpy)_3(PF_6)_2$ in CH_2Cl_2; b) $Ru(bpy)_3(PF_6)_2$ in CH_3CN; c) nanosubmarine **15** in CH_2Cl_2; d) nanosubmarine **15** in CH_3CN; e) mixture of $Ru(bpy)_3^{+2}$ and nanosubmarine **15** in CH_2Cl_2; f) mixture of $Ru(bpy)_3(PF_6)_2$ and nanosubmarine **15** in CH_3CN. Interestingly, when CH_2Cl_2 was used as the encapsulating solvent, both $Ru(bpy)_3^{+2}$ **1** and nanosubmarine **15** could be loaded into the MSU-H channels, which is at much larger than the molecule dimensions. However, the use of CH_3CN did not lead to inclusion of **1**

and **15**. The role of solvent and the molecule interactions with the channel will be further investigated in the future.

4.13.2. Experimental Data for Compounds 3, 5, 6, 7, 8, 10, 11, 12, 13, 14, 15, 16, 18, 19, and 20.

General Methods. ^{1}H NMR and ^{13}C NMR spectra were recorded at 400 or 500 and 100 or 125 MHz, respectively. Chemical shifts (δ) are reported in ppm from tetramethylsilane (TMS). FTIR spectra were recorded using a FTIR infrared microscope with ATR objective with 2 cm^{-1} resolution. All glassware was oven-dried overnight prior to use. Reagent grade tetrahydrofuran (THF) and ether (Et_2O) was distilled from sodium benzophenoneketyl under an N_2 atmosphere. Triethylamine (NEt_3), dichloromethane (CH_2Cl_2), and *N*,*N*'-dimethylforamide (DMF) were distilled from calcium hydride (CaH_2) under N_2 atmosphere. THF and NEt_3 were degassed with a stream of argon for 15 min before being used in the Sonogashira coupling reactions. All palladium-catalyzed reactions were carried out under argon atmosphere, while other reactions were performed under N_2 unless otherwise noted. All other chemicals were purchased from commercial suppliers and used without further purification. Flash column chromatography was performed using 230-400 mesh silica gel from EM Science. Thin layer chromatography (TLC) was performed using glass plates pre-coated with silica gel 40 F_{254} 0.25 mm layer thickness purchased from EM Science.

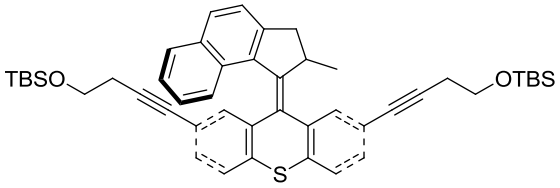

(4,4'-(9-(2-Methyl-2,3-dihydro-1*H*-cyclopenta[a]naphthalen-1-ylidene)-9*H*-thioxanthene-2,7-diyl)bis(but-3-yne-4,1-diyl))bis(oxy)bis(*tert*-butyldimethylsilane) (5). An oven dried Schlenk tube equipped with a stir bar was charged with motor **4**[32] (212 mg, 0.4 mmol), bis(benzonitrile)palladium(II) dichloride (7.7 mg, 0.02 mmol), tri-*tert*-butylphosphonium tetrafluoroborate (11.6 mg, 0.04 mmol), copper(I) iodide (7.6 mg, 0.04 mmol), and 4-(*tert*-butyldimethylsilyloxy)-but-1-yne (0.50 ml, 2.4 mmol). NEt_3 (4 mL) was added and the mixture was stirred at 45 °C overnight. The resulting mixture was partitioned between CH_2Cl_2 (20 mL) and saturated $NH_4Cl_{(aq)}$ (20 mL). The organic layer was dried over anhydrous $MgSO_4$, concentrated, and purified by column chromatography (silica gel; 30% CH_2Cl_2 in hexanes) to afford **5** as a pale-yellow solid (199 mg, 67%): mp 207–209 °C; FTIR (neat) 3052, 2954, 2930, 2856, 1588, 1472, 1454, 1388, 1362, 1252, 1218, 1100, 1058, 1006 cm^{-1}; ^1H NMR (500 MHz, $CDCl_3$) δ 7.79 (d, J = 1.7 Hz, 1H), 7.75 (d, J = 8.2 Hz, 1H), 7.69 (br d, J = 8.2 Hz, 1H), 7.49 (dd, J_1 = 8.0 Hz, J_2 = 0.3 Hz, 1H), 7.47 (dd, J_1 = 8.1 Hz, J_2 = 0.5 Hz, 1H), 7.43 (d, J = 8.2 Hz, 1H), 7.25 (dd, J_1 = 8.0 Hz, J_2 = 1.7 Hz, 1H), 7.19 (ddd, J_1 = 8.2 Hz, J_2 = 5.5 Hz, J_3 = 2.5 Hz, 1H), 7.03 (dd, J_1 = 8.1 Hz, J_2 = 1.8 Hz, 1H), 6.85–6.80 (m, 2H), 6.73 (dd, J_1 = 1.8 Hz, J_2 = 0.4 Hz, 1H), 4.24 (qd, J_1 = 6.8 Hz, J_2 = 6.1 Hz, 1H), 3.85 (t, J = 6.9 Hz, 2H), 3.63 (dd, J_1 = 15.5 Hz, J_2 = 6.1 Hz, 1H), 3.59–3.52 (m, 2H), 2.67 (t, J = 6.9 Hz, 2H), 2.63 (d, J = 15.5 Hz, 1H), 2.34 (t, J = 7.1 Hz, 2H), 0.94 (s, 9H), 0.84 (s, 9H), 0.78 (d, J = 6.8 Hz, 3 H), 0.13 (s, 6H), −0.02 (s, 3H), −0.03 (s, 3H). ^{13}C NMR (125 MHz, $CDCl_3$) δ 147.0, 146.1, 139.9, 137.7,

135.3, 134.8, 134.7, 133.1, 131.5 (CH), 130.7 (CH), 130.4 (CH), 129.3 (CH), 129.2 (CH), 128.7, 127.9 (CH), 127.6 (CH), 127.3 (CH), 127.1, 125.9 (CH), 124.9 (CH), 124.4 (CH), 123.6 (CH), 122.1, 122.0, 88.0, 87.0, 81.3, 80.6, 61.9 (CH_2), 61.7 (CH_2), 39.7 (CH_2), 37.9 (CH), 25.92 (CH_3), 25.85 (CH_3), 24.0 (CH_2), 23.6 (CH_2), 19.5 (CH_3), 18.4, 18.3, −5.19 (CH_3), −5.20 (CH_3), −5.31(CH_3), −5.32 (CH_3). HRMS (APCI) *m*/*z* calcd for $[M+H]^+$ $C_{47}H_{57}O_2SSi$ 741.3612, found 741.3584.

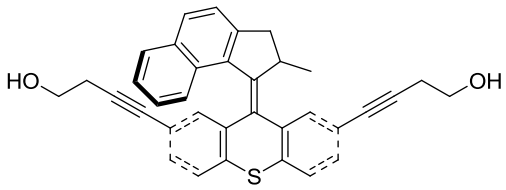

4,4'-(9-(2-Methyl-2,3-dihydro-1*H*-cyclopenta[a]naphthalen-1-ylidene)-9*H*-thioxanthene-2,7-diyl)dibut-3-yn-1-ol (6). A 25 mL round-bottomed flasked equipped with a stir bar was charged with **5** (371 mg, 0.5 mmol). THF (2 mL) and a solution of TBAF (1.5 mL, 1.5 mmol, 1.0 M in THF) were added, and the mixture was stirred at rt for 1 h. The mixture was poured into water (20 mL) and filtered. The solid was collected, washed by water (20 mL × 2), and dried under vacuum to afford desired product **6** as a pale-yellow solid (253 mg, 99%): mp 240 °C (decomp.); FTIR (neat) 3302, 3050, 2954, 2922, 2894, 2838, 1702, 1586, 1516, 1454, 1386, 1338, 1256, 1170, 1042, 1020 cm^{-1}; ^1H NMR (500 MHz, d_4-THF) δ 7.87 (d, J = 1.7 Hz, 1H), 7.76 (d, J = 8.2 Hz, 1H), 7.71–7.68 (m, 1H), 7.52 (dd, J_1 = 8.0 Hz, J_2 = 0.3 Hz, 1H), 7.50 (dd, J_1 = 8.1 Hz, J_2 = 0.8 Hz, 1H), 7.44 (d, J = 8.2 Hz, 1H), 7.25 (dd, J_1 = 8.1 Hz, J_2 = 1.8 Hz, 1H), 7.15 (ddd, J_1 = 8.1 Hz, J_2 = 6.6 Hz, J_3 = 1.4 Hz, 1H), 7.03 (dd, J_1 = 8.1 Hz J_2 = 1.8 Hz, 1H), 6.84–6.81 (m, 1H), 6.77 (ddd, J_1 = 8.6 Hz, J_2 = 6.6 Hz, J_3 = 1.3 Hz, 1H), 6.68 (dd, J_1 = 1.8 Hz, J_1 = 0.4 Hz,

1H), 4.27 (qd, J_1 = 6.9 Hz, J_2 = 6.3 Hz, 1H), 4.00 (br s, 1H), 3.72–3.64 (m, 4H), 3.42–3.35 (m, 2H), 2.63 (d, J = 15.5 Hz, 1H), 2.60 (t, J = 7.0 Hz, 2H), 2.25 (t, J = 7.2 Hz, 2H), 0.75 (d, J = 6.9 Hz, 3H); ^{13}C NMR (125 MHz, $CDCl_3$) δ 147.9, 147.2, 141.1, 138.7, 136.2, 135.8, 135.3, 134.3, 134.3, 132.2 (CH), 131.5 (CH), 131.4 (CH), 130.3 (CH), 130.1 (CH), 129.8, 128.7 (CH), 128.4 (CH), 128.3, 128.1 (CH), 126.6 (CH), 125.6 (CH), 125.0 (CH), 124.4 (CH), 123.5, 123.4, 89.1, 88.1, 81.6, 81.0, 61.6 (CH_2), 61.4 (CH_2), 40.3 (CH_2), 38.9 (CH), 24.7 (CH_2), 24.4 (CH_2), 19.6 (CH_3). HRMS (APCI) *m*/*z* calcd for $[M+H]^+$ $C_{35}H_{29}O_2S$ 513.1883, found 513.1879.

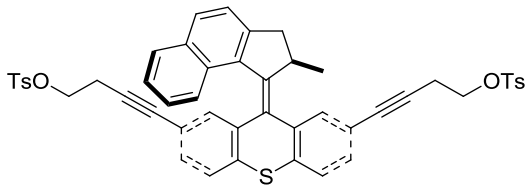

4,4'-(9-(2-Methyl-2,3-dihydro-1*H*-cyclopenta[a]naphthalen-1-ylidene)-9*H*-thioxanthene-2,7-diyl)bis(but-3-yne-4,1-diyl) bis(4-toluenesulfonate) (7).

An oven dried 25 mL round-bottom flask equipped with a stir bar was charged with dialcohol **6** (113 mg, 0.220 mmol), 4-toluenesulfonyl chloride (210 mg, 1.10 mmol), and CH_2Cl_2 (7 mL). After cooling to 0 °C, the round-bottom flask was added NEt_3 (0.30 mL, 2.2 mmol). The suspension was stirred vigorously for 16 h in the absence of light. The resulting yellow solution was partitioned between CH_2Cl_2 (20 mL) and water (30 mL). The organic phase was dried over anhydrous $MgSO_4$, concentrated, and purified by column chromatography (SiO_2; 20% hexanes in CH_2Cl_2) to afford **7** as a yellow solid (130 mg, 72%): mp 181–183 ℃; FTIR (neat) 3050, 2956, 2922, 1598, 1454, 1356, 1188, 1174, 1098, 1070, 1038 cm^{-1}; ^{1}H NMR (500 MHz, $CDCl_3$) δ 7.85–7.81 (m, 2H), 7.77–

7.74 (m, 2H), 7.73–7.68 (m, 3H), 7.50 (dd, J_1 = 8.0 Hz, J_2 = 0.3 Hz, 1H), 7.47 (dd, J_1 = 8.1 Hz, J_2 = 0.5 Hz, 1H), 7.44 (d, J = 8.2 Hz, 1H), 7.32–7.29 (m, 2H), 7.27–7.24 (m, 2H), 7.21–7.16 (m, 2H), 6.97 (dd, J_1 = 8.1 Hz, J_2 = 1.8 Hz, 1H), 6.81 (ddd, J_1 = 8.6 Hz, J_2 = 6.6 Hz, J_3 = 1.3 Hz, 1H), 6.78–6.75 (m, 2H), 6.66 (dd, J_1 = 1.8 Hz, J_2 = 0.4 Hz, 1H), 4.26–4.18 (m, 3H), 3.96–3.88 (m, 2H), 3.66 (dd, J_1 = 15.5 Hz, J_2 = 6.1 Hz, 1H), 2.83 (t, J = 7.0 Hz, 2H), 2.65 (d, J = 15.5 Hz, 1H), 2.48 (t, J = 7.2 Hz, 2H), 2.392 (s, 3H), 2.387 (s, 3H), 0.79 (d, J = 6.8 Hz, 3H); ^{13}C NMR (125 MHz, $CDCl_3$) δ 147.4, 146.2, 145.0, 144.8, 139.9, 137.7, 135.9, 135.4, 134.5, 133.1, 132.9, 132.8, 131.6 (CH), 130.8 (CH), 130.6 (CH), 129.9 (CH), 129.8 (CH), 129.4 (CH), 129.2 (CH), 128.7, 128.0 (overlapping of two signals, both CH carbons), 127.9 (CH), 127.7 (CH), 127.3 (CH), 126.7, 125.8 (CH), 124.9 (CH), 124.4 (CH), 123.7 (CH), 121.25, 121.21, 84.6, 83.6, 82.4, 81.8, 67.7 (CH_2), 67.5 (CH_2), 39.7 (CH_2), 37.9 (CH), 21.6 (overlapping of two signals, both CH_3 carbons), 20.5 (CH_2), 20.1 (CH_2), 19.5 (CH_3); HRMS (APCI) *m/z* calcd for $[M+H]^+$ $C_{49}H_{41}O_6S_3$ 821.2060, found 821.2066.

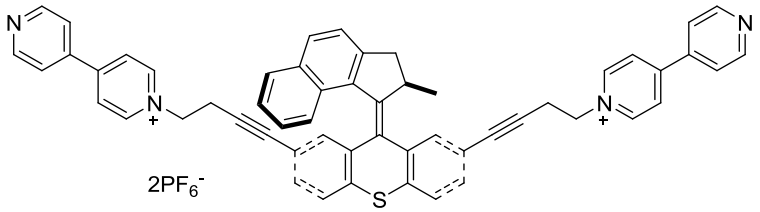

1,1'-(4,4'-(9-(2-Methyl-2,3-dihydro-1*H*-cyclopenta[a]naphthalen-1-ylidene)-9*H*-thioxanthene-2,7-diyl)bis(but-3-yne-4,1-diyl))bis(4-(pyridin-4-yl)pyridinium) (8).

In a glove box, anhydrous CH_3CN (16 mL) was added to a 100 mL screw-cap tube equipped with a stir bar. The tube was charged with **7** (162 mg, 0.200 mmol) and 4,4'-bipyridine (500 mg, 3.20 mmol). The cap was affixed and the tube was removed from the

glove-box. The mixture was stirred at 90 °C for 3 d. The reaction mixture was cooled to rt and NH_4PF_6 (250 mg, 1.53 mmol) was added. The mixture was transferred to a 250 mL round-bottom flask and rinsed with CH_3CN (20 mL) and water (50 mL), and the organic phase was removed under vacuum. The resulting precipitate was filtered and washed with water (5 mL × 2). The solid was purified by a reprecipitation process from a solution of CH_3CN (15 mL) and water (50 mL). The organic phase was removed under vacuum at 80 °C. The resulting precipitate was filtered while hot and washed with water (5 mL × 2). The reprecipitation process was repeated. The desired compound **8** was collected and dried under vacuum as a yellow-brownish solid (125 mg, 58%): m.p. 165 °C (decomp.); FTIR (neat) 3130, 3069, 2930, 1738, 1640, 1548, 1460, 1410, 1328, 1218, 1172 cm^{-1}; ^1H NMR (500 MHz, $CDCl_3$) δ 8.93–8.90 (m, 2H), 8.90–8.87 (m, 2H), 8.83–8.80 (m, 2H), 8.56–8.53 (m, 2H), 8.38–8.35 (m, 2H), 8.12–8.08 (m, 2H), 7.79 (d, J = 8.3 Hz, 1H), 7.79–7.77 (m, 2H), 7.76–7.71 (m, 4H), 7.59 (dd, J_1 = 8.1 Hz, J_2 = 0.4 Hz, 1H), 7.58 (dd, J_1 = 8.1 Hz, J_2 = 0.5 Hz, 1H), 7.44 (d, J = 8.2 Hz, 1H), 7.27 (dd, J_1 = 8.1 Hz, J_2 = 1.8 Hz, 1H), 7.19 (ddd, J_1 = 8.1 Hz, J_2 = 6.8 Hz, J_3 = 1.1 Hz, 1H), 7.05 (dd, J_1 = 8.1 Hz, J_2 = 1.8 Hz, 1H), 6.83 (ddd, J_1 = 8.6 Hz, J_2 = 6.8 Hz, J_3 = 1.3 Hz, 1H), 6.72–6.69 (m, 1H), 6.53 (dd, J_1 = 1.8 Hz, J_2 = 0.5 Hz, 1H), 4.87–4.77 (m, 2H), 4.62–4.49 (m, 2H), 4.09 (qd, J_1 = 6.9 Hz, J_2 = 6.2 Hz, 1H), 3.48 (dd, J_1 = 15.7 Hz, J_2 = 6.2 Hz, 1H), 3.23 (t, J = 6.3 Hz, 2H), 2.91 (J = 6.3 Hz, 2H), 2.51 (d, J = 15.7 Hz, 1H), 0.63 (d, J = 6.9 Hz, 3H); ^{13}C NMR (125 MHz, $CDCl_3$) δ 155.7, 155.6, 152.3 (CH), 152.2 (CH), 148.6, 148.1, 146.3 (CH), 145.9 (CH), 142.2, 142.1, 141.1, 138.6, 136.99, 136.96, 135.1, 134.0, 132.0 (CH), 131.6 (CH), 131.5 (CH), 130.7 (CH), 130.4 (CH), 129.5, 129.2 (CH), 129.0 (CH), 128.9 (CH), 127.6, 126.9 (CH), 126.7 (CH), 126.4 (CH), 126.1 (CH), 125.5 (CH), 125.2 (CH), 122.92

(CH), 122.91 (CH), 122.0, 121.5, 85.6, 85.3, 84.9, 84.8, 60.6 (CH_2), 60.4 (CH_2), 40.2 (CH_2), 38.9 (CH), 22.7 (CH_2), 22.4 (CH_2), 19.5 (CH_3); HRMS (ESI) *m*/*z* calcd for $[M-2PF_6]^{2+}$ $C_{55}H_{42}N_4S$ 395.1560, found 395.1546.

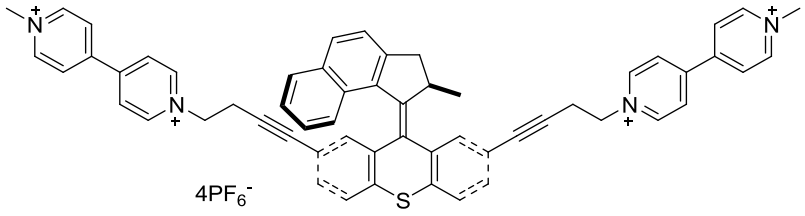

1',1''-(4,4'-(9-(2-Methyl-2,3-dihydro-1*H*-cyclopenta[a]naphthalen-1-ylidene)-9*H*-thioxanthene-2,7-diyl)bis(but-3-yne-4,1-diyl))bis(1-methyl-4,4'-bipyridine-1,1'-diium) tetrakis(hexafluorophosphate) (Quenching nanosubmarine 3). A 5 mL round-bottom flask equipped with a stir bar was charged with **8** (65 mg, 0.060 mmol). CH_3CN (1.5 mL) and MeOTs (0.10 mL; 0.66 mmol) was added and the mixture was stirred at 60 °C for 16 h. After cooling to rt, CH_2Cl_2 (10 mL) was added and the solid was filtered, collected, and washed thoroughly with CH_2Cl_2 (10 mL × 2). To the solid was added NH_4PF_6 (100 mg, 0.61 mmol) and the mixture was dissolved in CH_3CN (10 mL) and water (20 mL). The organic phase was removed under vacuum, and the suspension in water was filtered, and washed with water (10 mL). The solid was collected and dried under vacuum to afford the desired product as a brown solid (50 mg, 60%): m.p. 180 ℃ (decomp.); FTIR (neat) 3138, 3070, 2960, 2918, 2850, 1726, 1640, 1564, 1452, 1376, 1224 cm^{-1}; ^1H NMR (500 MHz, CD_3CN) δ 9.06–9.03 (m, 2H), 8.90–8.85 (m, 4H), 8.73–8.70 (m, 2H), 8.48–8.45 (m, 2H), 8.41–8.35 (m, 4H), 8.28–8.24 (m, 2H), 7.90 (d, J = 1.8 Hz, 1H), 7.82 (br d, J = 8.2 Hz, 1H), 7.78–7.74 (m, 1H), 7.61 (dd, J_1 = 8.1 Hz, J_2 = 0.3 Hz, 1H), 7.59 (dd, J_1 = 8.1 Hz, J_2 = 0.5 Hz, 1H), 7.51 (br d, J = 8.2 Hz, 1H), 7.29 (dd, J_1

= 8.1 Hz, J_2 = 1.8 Hz, 1H), 7.21 (ddd, J_1 = 8.2 Hz, J_2 = 6.7 Hz, J_3 = 1.2 Hz, 1H), 7.06 (dd, J_1 = 8.1 Hz, J_2 = 1.8 Hz, 1H), 6.85 (ddd, J_1 = 8.6 Hz, J_2 = 6.7 Hz, J_3 = 1.8 Hz, 1H), 6.77–6.73 (m, 1H), 6.66 (dd, J_1 = 1.8 Hz, J_1 = 0.4 Hz, 1H), 4.92–4.83 (m, 2H), 4.68–4.55 (m, 2H), 4.43 (s, 3H), 4.41 (s, 3H), 4.20 (qd, J_1 = 6.9 Hz, J_2 = 6.1 Hz, 1H), 3.65 (dd, J_1 = 15.7 Hz, J_2 = 6.1 Hz, 1H), 3.25 (t, J = 6.3 Hz, 2H), 2.98–2.86 (m, 2H), 2.62 (d, J = 15.7 Hz, 1H), 0.69 (d, J = 6.9 Hz, 3H); ^{13}C NMR (125 MHz, CD_3CN) δ 151.6, 151.5, 150.6, 150.5, 148.7, 148.2, 147.6 (overlapping of two signals, both CH carbons), 146.9 (CH), 146.6 (CH), 141.2, 138.6, 137.00, 136.96, 135.2, 134.1, 132.1 (CH), 131.7 (CH), 131.5 (CH), 130.8 (CH), 130.6 (CH), 129.6, 129.2 (CH), 129.0 (CH), 128.9 (CH), 128.1 (CH), 127.94 (CH), 127.91 (CH), 127.87 (CH), 127.6, 126.4 (CH), 126.1 (CH), 125.5 (CH), 125.3 (CH), 122.0, 121.5, 85.4, 85.3, 84.9, 84.7, 61.2 (CH_2), 61.0 (CH_2), 49.70 (CH_3), 49.67 (CH_3), 40.3 (CH_2), 39.0 (CH), 22.8 (CH_2), 22.5 (CH_2), 19.5 (CH_3); HRMS (ESI) *m*/*z* calcd for $[M-3PF_6]^{+3}$ $C_{57}H_{48}N_4SPF_6$ 321.7750, found 321.7752.

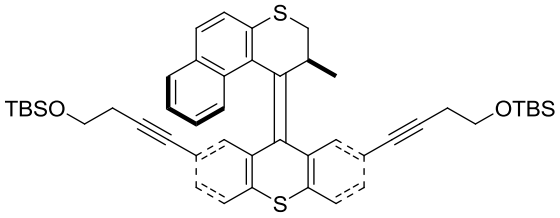

(4,4'-(9-(2-Methyl-2,3-dihydro-1*H*-benzo[f]thiochromen-1-ylidene)-9*H*-thioxanthene-2,7-diyl)bis(but-3-yne-4,1-diyl))bis(oxy)bis(tert-butyldimethylsilane) (10). Following the procedure described in the synthesis of **5**, motor **9** (700 mg, 1.24 mmol), bis(triphenylphosphine)palladium(II) dichlodride (88 mg, 0.13 mmol), copper(I) iodide (48 mg, 0.26mmol), 4-(*tert*-butyldimethylsilyloxy)-1-butyne (1.02 mL, 4.96 mmol), and triethyl amine (6.5 mL) were used in the reaction to yield **10** as a white solid

(782 mg, 82%): m.p. 72–74 °C; FTIR (neat) 3052, 2952, 2928, 2856, 1588, 1504, 1456, 1388, 1360, 1332, 1250, 1102, 1058, 1006 cm^{-1}; ^1H NMR (500 MHz, $CDCl_3$) δ 7.62–7.56 (m, 3H), 7.51 (dd, J_1 = 8.0 Hz, J_2 = 0.3 Hz, 1H), 7.50–7.47 (m, 1H), 7.38 (d, J = 8.5 Hz, 1H), 7.31 (dd, J_1 = 8.0 Hz, J_2 = 1.7 Hz, 1H), 7.15 (dd, J_1 = 8.1 Hz J_2 = 0.5 Hz, 1H), 7.12 (ddd, J_1 = 8.1 Hz, J_2 = 6.8 Hz, J_3 = 1.2 Hz, 1H), 6.99 (ddd, J_1 = 8.5 Hz, J_2 = 6.8 Hz, J_3 = 1.3 Hz, 1H), 6.73 (dd, J_1 = 8.1 Hz, J_1 = 1.8 Hz, 1H), 6.35 (dd, J_1 = 1.8 Hz, J_2 = 0.3 Hz, 1H), 4.10 (dqd, J_1 = 7.4 Hz, J_2 = 6.8 Hz, J_3 = 3.5 Hz, 1H), 3.85 (t, J = 6.9 Hz, 2H), 3.70 (dd, J_1 = 11.4 Hz, J_2 = 7.4 Hz, 1H), 3.62 (t, J = 7.1 Hz, 2H), 3.06 (dd, J_1 = 11.4 Hz, J_2 = 3.5 Hz, 1H), 2.67 (t, J = 6.9 Hz, 2H), 2.39 (t, J = 7.1 Hz, 2H), 0.94 (s, 9H), 0.88 (s, 9H), 0.79 (d, J = 6.8 Hz, 3H), 0.12 (s, 6H), 0.04 (s, 6H); ^{13}C NMR (125 MHz, $CDCl_3$) δ 137.9, 137.6, 135.8, 135.6, 135.2, 133.6, 132.0 (CH), 131.6, 131.2, 130.9, 130.6, 130.5 (CH), 130.0 (CH), 129.2 (CH), 127.71 (CH), 127.69 (CH), 127.5 (CH), 126.1 (CH), 125.8 (CH), 125.5 (CH), 124.4 (CH), 124.0 (CH), 121.9, 121.1, 88.4, 86.8, 81.1, 80.5, 61.84 (CH_2), 61.82 (CH_2), 37.2 (CH_2), 32.6 (CH), 25.93 (CH_3), 25.90 (CH_3), 24.0 (CH_2), 23.7, 19.2 (CH_3), 18.4, 18.3, −5.17 (CH_3), −5.18 (CH_3), −5.22 (CH_3), −5.23 (CH_3); HRMS (APCI) *m*/*z* calcd for $[M+H]^+$ $C_{47}H_{57}O_2S_2Si_2$ 773.3333, found 773.3331.

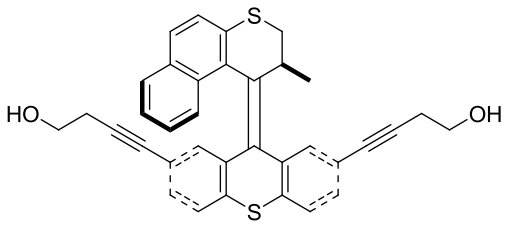

4,4'-(9-(2-Methyl-2,3-dihydro-1*H*-benzo[f]thiochromen-1-ylidene)-9*H*-thioxanthene-2,7-diyl)dibut-3-yn-1-ol (11). Following the procedure described in the synthesis of **6**, **10** (386 mg, 0.5 mmol), THF (2 mL), and TBAF (1.5 mL, 1.0 M in THF) were used in

the reaction to yield **11** as a white solid (220 mg, 97%): m.p. 190 ℃ (decomp.); FTIR (neat) 3286, 3046, 2918, 2878, 2228, 1616, 1588, 1550, 1504, 1454, 1388, 1328, 1242, 1166, 1136, 1076, 1044, 1022 cm^{-1}; ^1H NMR (500 MHz, d_4-THF) δ 7.66 (d, J = 1.6 Hz, 1H), 7.64 (br d, J = 8.4 Hz, 1H), 7.59–7.56 (m, 1H), 7.54 (dd, J_1 = 8.0 Hz, J_2 = 0.3 Hz, 1H), 7.53–7.49 (m, 1H), 7.37 (d, J = 8.6 Hz, 1H), 7.32 (dd, J_1 = 8.0 Hz, J_2 = 1.7 Hz, 1H), 7.16 (dd, J_1 = 8.1 Hz J_2 = 0.5 Hz, 1H), 7.06 (ddd, J_1 = 8.1 Hz, J_2 = 6.8 Hz, J_3 = 1.1 Hz, 1H), 6.94 (ddd, J_1 = 8.5 Hz, J_2 = 6.8 Hz, J_3 = 1.3 Hz, 1H), 6.72 (dd, J_1 = 8.1 Hz, J_1 = 1.8 Hz, 1H), 6.33 (d, J = 1.7 Hz, 1H), 4.09 (dqd, J_1 = 7.2 Hz, J_2 = 6.7 Hz, J_3 = 3.4 Hz, 1H), 4.00 (t, J = 5.7 Hz, 1H), 3.77 (dd, J_1 = 11.5 Hz, J_2 = 7.3 Hz, 1H), 3.73 (t, J = 5.9 Hz, 1H), 3.68 (dt, J_1 = 7.0 Hz, J_2 = 5.7 Hz, 2H), 3.45 (dd, J_1 = 7.2 Hz, J_2 = 5.9 Hz, 1H), 3.05 (dd, J_1 = 11.5 Hz, J_2 = 3.4 Hz, 1H), 2.59 (t, J = 7.0 Hz, 2H), 2.30 (t, J = 7.2 Hz, 2H), 0.75 (d, J = 6.7 Hz, 3H); ^{13}C NMR (125 MHz, d_4-THF) δ 139.0, 138.8, 136.8, 136.7, 136.4, 134.6, 132.7, 132.6 (CH), 132.1, 131.7, 131.6, 131.3 (CH), 130.8 (CH), 130.1 (CH), 128.6 (CH), 128.5 (CH), 128.4 (CH), 127.0 (CH), 126.6 (CH), 126.1 (CH), 125.1 (CH), 124.7 (CH), 123.3, 122.4, 89.5, 87.9, 81.4, 80.9, 61.6 (CH_2), 61.5 (CH_2), 37.5 (CH_2), 33.6 (CH), 24.7 (CH_2), 24.4 (CH_2), 19.2 (CH_3); HRMS (APCI) *m*/*z* calcd for $[M+H]^+$ $C_{35}H_{29}O_2S_2$ 545.1603, found 545.1591.

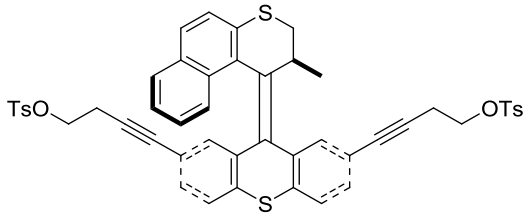

4,4'-(9-(2-Methyl-2,3-dihydro-1*H*-benzo[f]thiochromen-1-ylidene)-9*H*-thioxanthene-2,7-diyl)bis(but-3-yne-4,1-diyl) bis(4-toluenesulfonate) (12). Following the procedure

described in the synthesis of **7**, **11** (164 mg, 0.3 mmol), 4-toluenesulfonyl chloride (172 mg, 0.9 mmol), NEt_3 (0.17 mL, 1.2 mmol), and CH_2Cl_2 (6 mL) were used in the reaction to yield **12** as a pale-yellow solid (230 mg, 90%): m.p. 84–86 °C; FTIR (neat) 3052, 2960, 2924, 1598, 1454, 1188, 1174, 1098, 1066 cm^{-1}; ^1H NMR (500 MHz, $CDCl_3$) δ 7.86–7.81 (m, 2H), 7.76–7.72 (m, 2H), 7.61 (d, J = 8.4 Hz, 1H), 7.59–7.55 (m, 2H), 7.51 (d, J = 8.1 Hz, 1H), 7.48–7.44 (m, 1H), 7.39 (d, J = 8.6 Hz, 1H), 7.35–7.31 (m, 2H), 7.28–7.24 (m, 3H), 7.15 (dd, J_1 = 8.1 Hz, J_2 = 0.4 Hz, 1H), 7.11 (ddd, J_1 = 8.0 Hz, J_2 = 6.8 Hz, J_3 = 1.2 Hz, 1H), 6.99 (ddd, J_1 = 8.5 Hz, J_2 = 6.8 Hz, J_3 = 1.3 Hz, 1H), 6.65 (dd, J_1 = 8.1 Hz, J_1 = 1.8 Hz, 1H), 6.29 (d, J = 1.5 Hz, 1H), 4.27–4.18 (m, 2H), 4.07 (dqd, J_1 = 7.5 Hz, J_2 = 6.8 Hz, J_3 = 3.5 Hz, 1H), 4.03–3.98 (m, 2H), 3.69 (dd, J_1 = 11.5 Hz, J_2 = 7.5 Hz, 1H), 3.05 (dd, J_1 = 11.5 Hz, J_2 = 3.5 Hz, 1H), 2.84 (t, J = 7.0 Hz, 2H), 2.59–2.49 (m, 2H), 2.41 (s, 3H), 2.40 (s, 3H), 0.80 (d, J = 6.8 Hz, 3H). ^{13}C NMR (125 MHz, $CDCl_3$) δ 145.0, 144.8, 138.1, 137.8, 136.1, 135.7, 134.1, 132.9, 132.8, 132.2 (CH), 131.6, 130.4, 130.9, 130.8, 130.7 (CH), 130.5, 130.0 (CH), 129.93 (CH), 129.87 (CH), 129.2 (CH), 128.0 (CH), 127.9 (CH), 127.83 (CH), 127.82 (CH), 127.6 (CH), 126.1 (CH), 125.9 (CH), 125.6 (CH), 124.4 (CH), 123.9 (CH), 121.1, 120.2, 85.0, 83.5, 82.2, 81.6, 67.61 (CH_2), 67.56 (CH_2), 37.1 (CH_2), 32.8 (CH), 21.7 (CH_3), 21.6 (CH_3), 20.6 (CH_2), 20.2 (CH_2), 19.3 (CH_3); HRMS (APCI) *m*/*z* calcd for $[M+H]^+$ $C_{49}H_{41}O_6S_4$ 853.1780, found 853.1773.

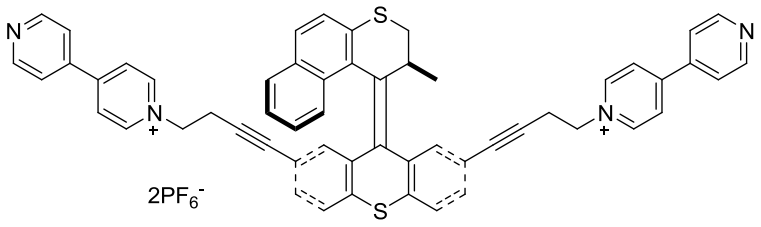

1,1'-(4,4'-(9-(2-Methyl-2,3-dihydro-1*H*-benzo[f]thiochromen-1-ylidene)-9*H*-

thioxanthene-2,7-diyl)bis(but-3-yne-4,1-diyl))bis(4-(pyridin-4-yl)pyridinium) bis(hexafluorophosphate) (13). Following the procedure described in the synthesis of **8**, **12** (171 mg, 0.2 mmol), 4,4'-bipyridine (500 mg, 3.2 mmol), and CH_3CN (16 mL) were used in the reaction to yield compound **13** as a yellow-brownish solid (135 mg, 61%): m.p. 185 ℃ (decomp.); FTIR (neat) 3642, 3120, 3072, 1642, 1602, 1548, 1524, 1458, 1412, 1328, 1220, 1174, 1136, 1070 cm^{-1}; ^1H NMR (500 MHz, CD_3CN) δ 8.94–8.91 (m, 2H), 8.88–8.86 (m, 2H), 8.85–8.82 (m, 2H), 8.69–8.65 (m, 2H), 8.39–8.36 (m, 2H), 8.31–8.28 (m, 2H), 7.82–7.78 (m, 4H), 7.68–7.65 (m, 1H), 7.61 (dd, J_1 = 8.1 Hz, J_2 = 0.3 Hz, 1H), 7.62–7.59 (m, 1H), 7.46 (d, J = 1.7 Hz, 1H), 7.46–7.43 (m, 1H), 7.34 (dd, J_1 = 8.1 Hz, J_2 = 1.8 Hz, 1H), 7.32 (d, J = 8.6 Hz, 1H), 7.26 (dd, J_1 = 8.1 Hz, J_2 = 0.5 Hz, 1H), 7.12 (ddd, J_1 = 8.1 Hz, J_2 = 6.8 Hz, J_3 = 1.2 Hz, 1H), 7.00 (ddd, J_1 = 8.5 Hz, J_2 = 6.8 Hz, J_3 = 1.3 Hz, 1H), 6.74 (dd, J_1 = 8.1 Hz, J_1 = 1.8 Hz, 1H), 6.19 (br d, J = 1.7 Hz, 1H), 4.88–4.78 (m, 2H), 4.63 (t, J = 6.4 Hz, 2H), 3.94 (dqd, J_1 = 7.0 Hz, J_2 = 6.7 Hz, J_3 = 3.2 Hz, 1H), 3.55 (dd, J_1 = 11.5 Hz, J_2 = 7.1 Hz, 1H), 3.24 (t, J = 6.3 Hz, 2H), 2.97 (t, J = 6.4 Hz, 2H), 2.96 (dd, J_1 = 11.5 Hz, J_2 = 3.2 Hz, 1H), 0.65 (d, J = 6.7 Hz, 3H); ^{13}C NMR (125 MHz, CD_3CN) δ 155.7, 155.6, 152.28 (CH), 152.26 (CH), 146.3 (CH), 146.0 (CH), 142.14, 142.12, 139.3, 139.2, 137.2, 136.6, 136.5, 136.0, 132.5 (CH), 132.4, 131.52 (CH), 131.46, 131.42 (CH), 131.3 (CH), 131.1, 130.3 (CH), 129.0 (CH), 128.9 (CH), 128.8 (CH), 127.9 (CH), 127.2 (CH), 126.9 (CH), 126.8, 126.2 (CH), 125.6 (CH), 124.7 (CH), 123.0 (CH), 122.9 (CH), 121.9, 120.6, 85.9, 85.1, 84.8, 84.6, 60.5 (CH_2), 60.3 (CH_2), 37.6 (CH_2), 32.9 (CH), 22.7 (CH_2), 22.4 (CH_2), 18.9 (CH_3); HRMS (ESI) *m*/*z* calcd for $[M-2PF_6]^{+2}$ $C_{55}H_{42}N_4S_2$ 414.1120, found 414.1114.

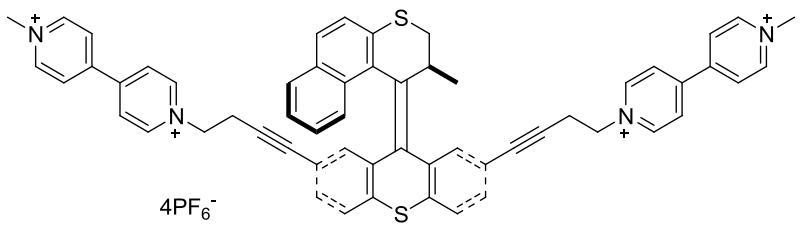

1',1''-(4,4'-(9-(2-Methyl-2,3-dihydro-1*H*-benzo[f]thiochromen-1-ylidene)-9*H*-thioxanthene-2,7-diyl)bis(but-3-yne-4,1-diyl))bis(1-methyl-4,4'-bipyridine-1,1'-diium) tetrakis(hexafluorophosphate) (14). Following the procedure described in the synthesis of **3**, **13** (33 mg, 0.03 mmol), methyl tosylate (0.05 mL; 0.33 mmol), and CH_3CN (1.2 mL) were used in the reaction to yield **14** as a yellow solid (29 mg, 67%): m.p. 170 °C (decomp.); FTIR (neat) 3314, 3070, 2918, 1726, 1640, 1564, 1510, 1454, 1180, 1000 cm^{-1}; ^1H NMR (500 MHz, $CDCl_3$) δ 9.06–9.02 (m, 2H), 8.89–8.85 (m, 4H), 8.82–8.78 (m, 2H), 8.49–8.45 (m, 2H), 8.42–8.35 (m, 6H), 7.72–7.68 (m, 1H), 7.65–7.62 (m, 1H), 7.63 (dd, J_1 = 8.1 Hz, J_2 = 0.3 Hz, 1H), 7.59 (d, J = 1.6 Hz, 1H), 7.50–7.47 (m, 1H), 7.39 (d, J = 8.6 Hz, 1H), 7.35 (dd, J_1 = 8.1 Hz, J_2 = 1.7 Hz, 1H), 7.28 (dd, J_1 = 8.1 Hz, J_2 = 0.5 Hz, 1H), 7.14 (ddd, J_1 = 8.1 Hz, J_2 = 6.9 Hz, J_3 = 1.2 Hz, 1H), 7.02 (ddd, J_1 = 8.5 Hz, J_2 = 6.8 Hz, J_3 = 1.3 Hz, 1H), 6.76 (dd, J_1 = 8.1 Hz, J_1 = 1.8 Hz, 1H), 6.32 (br d, J = 1.7 Hz, 1H), 4.88 (t, J = 6.3 Hz, 2H), 4.68 (t, J = 6.5 Hz, 2H), 4.42 (br s, 6H), 4.00 (dqd, J_1 = 7.0 Hz, J_2 = 6.7 Hz, J_3 = 3.0 Hz, 1H), 3.71 (dd, J_1 = 11.5 Hz, J_2 = 7.0 Hz, 1H), 3.25 (t, J = 6.3 Hz, 2H), 3.06 (dd, J_1 = 11.5 Hz, J_2 = 3.0 Hz, 1H), 2.98 (t, J = 6.4 Hz, 2H), 0.69 (d, J = 6.7 Hz, 3H); ^{13}C NMR (125 MHz, CD_3CN) δ 151.6, 151.5, 150.6, 150.5, 147.6 (overlapping of two signals, both CH carbons), 146.9 (CH), 146.7 (CH), 139.34, 139.28, 137.3, 136.7, 136.5, 136.1, 132.54 (CH), 132.47, 131.6, 131.5, 131.43 (CH), 131.39 (CH), 131.2, 130.4 (CH), 129.0 (CH), 128.9 (overlapping of two signals, both CH carbons), 128.2 (CH), 128.0 (CH), 127.920 (CH), 127.916 (CH), 127.89 (CH), 127.2

(CH), 126.3 (CH), 125.7 (CH), 124.7 (CH), 121.9, 120.6, 85.7, 85.1, 84.7, 84.6, 61.2 (CH_2), 61.0 (CH_2), 49.7 (CH_3), 37.6 (CH_2), 33.0 (CH), 22.8 (CH_2), 22.5 (CH_2), 18.9 (CH_3); HRMS (ESI) *m*/*z* calcd for $[M-4PF_6]^{4+}$ $C_{57}H_{48}N_4S_2$ 213.0825, found 213.0816.

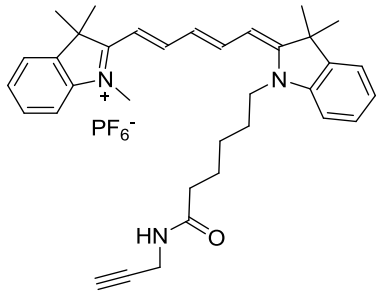

2-((1E,3E,5Z)-5-(3,3-Dimethyl-1-(6-oxo-6-(prop-2-ynylamino)hexyl)indolin-2-ylidene)penta-1,3-dienyl)-1,3,3-trimethyl-3*H*-indolium hexafluorophosphate (18). An oven-dried round-bottom flask equipped with a stir bar was charged with cy5 dye **17** (153 mg, 0.25 mmol) and *N*,*N'*-dicyclohexylcarbodiimide (54 mg, 0.26 mmol), to which CH_2Cl_2 (2 mL) and propargyl amine (19 μL, 0.3 mmol) was added in sequence. The solution was allowed to stir at rt overnight in the absence of light. The solution was purified by column chromatography (SiO_2, 2% MeOH in CH_2Cl_2) to afford the desired cy5 dye **18** as a blue solid (135 mg, 83%): m.p. 98 °C (decomp.); FTIR (neat) 3426, 3320, 3286, 2928, 2850, 1480, 1446, 1367, 1332, 1213, 1142, 1086, 1036, 1014 cm^{-1}; ^1H NMR (500 MHz, CD_2Cl_2) δ 8.15–8.08 (m, 2H), 7.51–7.47 (m, 2H), 7.43–7.37 (m, 2H), 7.28–7.23 (m, 4H), 6.90 (br t, *J* = 5.7Hz, 1H), 6.59 (t, *J* = 12.5 Hz, 1H), 6.25 (d, *J* = 13.8 Hz, 1H), 6.21 (d, *J* = 13.9 Hz, 1H), 4.02 (t, *J* = 7.6Hz, 2H), 3.89 (dd, J_1 = 5.7 Hz, J_2 = 2.5 Hz, 2H), 3.55 (s, 3H), 2.41 (t, *J* = 2.5 Hz, 1H), 2.16 (t, *J* = 7.4 Hz, 2H), 1.81–1.74 (m, 2H), 1.687 (s, 6H), 1.686 (s, 6H), 1.66–1.60 (m, 2H), 1.47–1.40 (m, 2H); ^{13}C NMR (125 MHz, CD_2Cl_2) δ 174.9, 174.3, 173.3, 154.9 (CH), 154.8 (CH), 144.1, 143.4, 142.5, 142.3,

129.6 (CH), 129.5 (CH), 125.960 (CH), 125.957 (CH), 125.7 (CH), 123.3 (CH), 123.2 (CH), 112.1 (CH), 111.8 (CH), 103.2 (CH), 104.1 (CH), 81.8 (CH), 71.6 (CH), 50.24, 50.19, 44.9 (CH_2), 36.3 (CH_2), 32.2 (CH_3), 29.0 (CH_2), 27.83 (CH_3), 27.77 (CH_2), 27.7 (CH_3), 27.0 (CH_2), 25.9 (CH_2); HRMS (APCI) *m*/*z* calcd for $[M-PF_6]^+$ $C_{35}H_{42}N_3O$ 520.3322, found 520.3328.

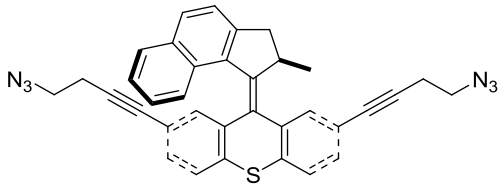

2,7-Bis(4-azidobut-1-ynyl)-9-(2-methyl-2,3-dihydro-1*H*-cyclopenta[a]naphthalen-1-ylidene)-9*H*-thioxanthene (19). An oven-dried round-bottom flask equipped with a stir bar was charged with ditosylate **7** (190 mg, 0.23 mmol) and NaN_3 (60 mg, 1.0 mmol). DMF (5 mL) was added, and the mixture was stirred at 80 °C overnight. After cooled to rt, the mixture was partitioned between Et_2O (20 mL) and water (30 mL × 3). The organic phase was dried over anhydrous $MgSO_4$, and concentrated under vacuum to afford **19** as a pale yellow solid (125 mg, 97%): m.p. 199–200 °C; FTIR (neat) 3048, 2922, 2190, 1738, 1586, 1452, 1336, 1270, 1066 cm^{-1}; ^1H NMR (500 MHz, $CDCl_3$) δ 7.81 (d, J = 1.7 Hz, 1H), 7.76 (br d, J = 8.1 Hz, 1H), 7.73–7.69 (m , 1H), 7.51 (dd, J_1 = 8.0 Hz, J_2 = 0.4 Hz, 1H), 7.48 (dd, J_1 = 8.1 Hz, J_2 = 0.5 Hz, 1H), 7.43 (br d, J = 8.2 Hz, 1H), 7.27 (dd, J_1 = 8.0 Hz, J_2 = 1.7 Hz, 1H), 7.21 (ddd, J_1 = 8.2 Hz, J_2 = 6.5 Hz, J_3 = 1.4 Hz, 1H), 7.05 (dd, J_1 = 8.1 Hz, J_2 = 1.8 Hz, 1H), 6.83 (ddd, J_1 = 8.6 Hz, J_2 = 6.5 Hz, J_3 = 1.3 Hz, 1H), 6.81–6.77 (m, 1H), 6.73 (dd, J_1 = 1.7 Hz, J_2 = 0.4 Hz, 1H), 4.23 (qd, J_1 = 6.8 Hz, J_2 = 6.1 Hz, 1H), 3.64 (dd, J_1 = 15.5 Hz, J_2 = 6.1 Hz, 1H), 3.51 (t, J = 6.7 Hz, 2H), 3.22 (t, J =

6.9 Hz, 2H), 2.76 (t, J = 6.7 Hz, 2H), 2.63 (d, J = 15.5 Hz, 1H), 2.42 (t, J = 6.9 Hz, 2H), 0.75 (d, J = 6.8 Hz, 3H); ^{13}C NMR (125 MHz, $CDCl_3$) δ 147.3, 146.1, 139.9, 137.7, 135.8, 135.3, 134.6, 133.1, 131.6 (CH), 130.8 (CH), 130.4 (CH), 129.3 (CH), 129.2 (CH), 128.7, 127.9 (CH), 127.7 (CH), 127.3 (CH), 126.8, 125.9 (CH), 124.9 (CH), 124.4 (CH), 123.7 (CH), 121.4, 121.4, 86.5, 85.6, 82.3, 81.6, 49.9 (CH_2), 49.7 (CH_2), 39.7 (CH_2), 37.9 (CH), 20.8 (CH_2), 20.4 (CH_2), 19.6 (CH_3); HRMS (APCI) m/z calcd for $[M+Na]^+$ $C_{35}H_{26}N_6SNa$ 585.1832, found 585.1839.

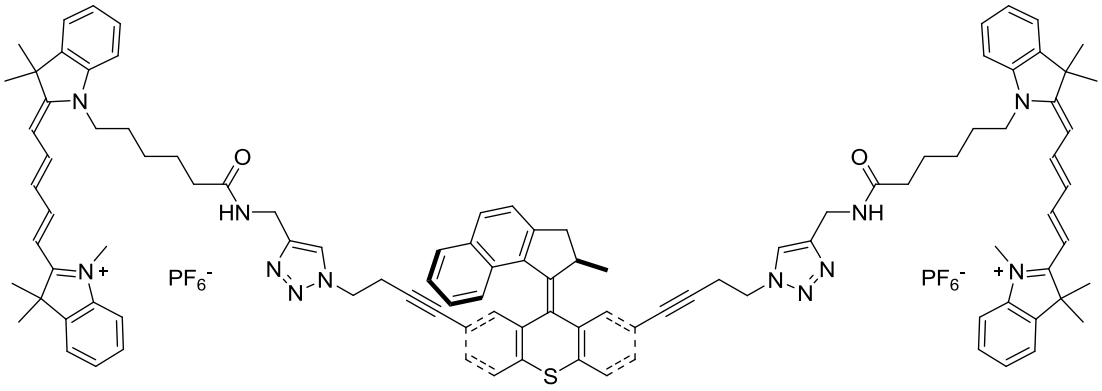

Cy5-armed nanosubmarine 15. A 2 mL vial charged with diazide **19** (18 mg, 0.032 mmol), cy5 dye **18** (47 mg, 0.071 mmol), $CuSO_{4(s)}$ (0.8 mg, 0.0032 mmol), and sodium ascorbate (1.9 mg, 0.0096 mmol) was sealed with a rubber septum cap. A well degassed mixture of CH_2Cl_2 (0.08 mL) and water (0.08 mL) was added to the vial, and the vial was shaken by a wrist-action shaking machine for 48 h. The mixture was partitioned between CH_2Cl_2 (5 mL) and water (5 mL). The organic phase was dried over anhydrous $MgSO_4$, filtered, and the filtrate was concentrated under vacuum. The crude product was purified by column chromatography (silica gel, 2% to 3% MeOH in CH_2Cl_2) to afford the desired cy5-armed nanosubmarine **15** as a blue solid (56 mg, 89%): m.p. 165 ℃ (decomp.); FTIR (neat): 3426, 2954, 2922, 2852, 1480, 1446, 1368, 1332, 1216, 1144, 1084, 1038,

1014 cm^{-1}; ^{1}H NMR (500 MHz, CD_3CN) δ 8.08–8.00 (m, 4H), 7.84 (d, J = 1.5 Hz, 1H), 7.82 (br s, 1H), 7.78 (d, J = 8.3 Hz, 1H), 7.76–7.72 (m, 1H), 7.50 (s, 1H), 7.48 (s, 1H), 7.49–7.32 (m, 10H), 7.26–7.10 (m, 10H), 6.98 (dd, J_1 = 8.1 Hz, J_2 = 1.8 Hz, 1H), 6.95 (br t, J = 5.5 Hz, 1H), 6.84 (br t, J = 5.6 Hz, 1H), 6.80 (ddd, J_1 = 8.5 Hz, J_2 = 6.7 Hz, J_3 = 1.3 Hz, 1H), 6.75–6.71 (m, 1H), 6.61 (d, J = 1.6 Hz, 1H), 6.52–6.43 (m, 2H), 6.17–6.09 (m, 4H), 4.56 (t, J = 6.4 Hz, 2H), 4.46–4.20 (m, 6H), 4.19 (qd, J_1 = 6.9 Hz, J_2 = 6.2 Hz, 1H), 3.92–3.80 (m, 4H), 3.71 (dd, J_1 = 15.6 Hz, J_2 = 6.2 Hz, 1H), 3.51 (s, 3H), 3.49 (s, 3H), 2.99 (t, J = 6.4 Hz, 2H), 2.65 (t, J = 6.5 Hz, 2H), 2.61 (d, J = 15.6 Hz, 1H), 2.07–2.03 (m, 4H), 1.68–1.59 (m, 28H), 1.56–1.46 (m, 4H), 1.36–1.24 (m, 4H), 0.65 (d, J = 6.9 Hz, 3H); ^{13}C NMR (125 MHz, CD_3CN) δ 174.98, 174.96, 174.14, 174.10, 173.4, 173.4, 154.8 (overlapping of four signals, all CH carbons), 148.5, 148.2, 146.3, 146.0, 144.07, 144.06, 143.28, 143.26, 142.40, 142.39, 142.300, 142.296, 141.2, 138.6, 136.443, 136.436, 135.2, 134.1, 132.1 (CH), 131.59 (CH), 131.57 (CH), 130.6 (CH), 130.3 (CH), 129.57, 129.56 (overlapping of four signals, all CH carbons), 129.2 (CH), 128.8 (CH), 128.7 (CH), 127.7, 126.3 (CH), 126.0 (overlapping of three signals, all CH carbons), 125.972 (CH), 125.966 (CH), 125.59 (CH), 125.55 (CH), 125.4 (CH), 125.2 (CH), 123.9 (CH), 123.7 (CH), 123.3 (overlapping of two signals, both CH carbons), 123.2 (overlapping of two signals, both CH carbons), 122.6, 122.2, 112.0 (CH), 111.9 (CH), 111.850 (CH), 111.846 (CH), 104.15 (CH), 104.14 (CH), 103.93 (CH), 103.91 (CH), 87.9, 87.2, 83.2, 82.8, 50.19, 50.184, 50.177 (overlapping of two signal, both quaternary carbons), 49.6 (CH_2), 49.4 (CH_2), 44.83 (CH_2), 44.82 (CH_2), 40.4 (CH_2), 39.0 (CH), 36.4 (CH_2), 36.3 (CH_2), 35.6 (CH_2), 35.5 (CH_2), 32.03 (CH_3), 32.01 (CH_3), 27.81 (CH_3), 27.80 (CH_3), 27.7 (CH_2), 27.64 (CH_2), 27.61 (overlapping of two signals, both CH_3 carbons),

27.0 (overlapping of two signals, both CH_2 carbons), 25.94 (CH_2), 25.92 (CH_2), 22.1 (CH_2), 21.8 (CH_2), 19.6 (CH_3); HRMS (ESI) *m*/*z* calcd for $[M-2PF_6]^{+2}$ $C_{105}H_{110}N_{12}S$ 801.4292, found 801.4268.

Note: 1. Two pairs of considerably broader and consequently shorter signals at δ 146.4 (quaternary carbon) and 146.0 (quaternary carbon), and δ 123.9 (CH) and 123.7 (CH) were observed. These signals to the carbons in the 1,2,3-triazole rings, with the breadth resulting from rapid relaxation caused by the directly attached ^{14}N (a quadrupolar nucleus).[53,54] These assignments were consistent with the observation in the ^{13}C NMR spectrum of **16**. 2. The assignments were tentatively determined by comparing ^{13}C NMR spectrum and DEPT-135 spectra of **15**, **16**, **18**, and **19**. Further experiments and/or the use of higher frequency NMR instrument maybe required to confirm the assignments.

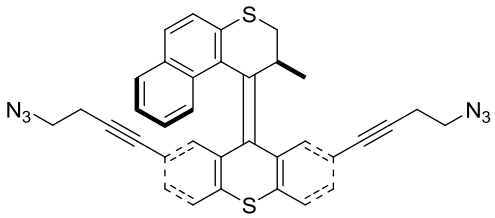

(2,7-Bis(4-azidobut-1-ynyl)-9*H*-thioxanthen-9-ylidene)-2-methyl-2,3-dihydro-1*H*-benzo[f]thiochromene (20). Following the procedure described in the synthesis of **19**, **12** (111 mg, 0.100 mmol), NaN_3 (20 mg, 0.31 mmol), and DMF (3 mL) were used in the reaction to yield **20** as a pale yellow solid (mg, 96%): m.p. 96–98 °C; FTIR (neat) 3052, 2870, 2926, 2088, 1738, 1586, 1444, 1426, 1414, 1366, 1218, 1064 cm^{-1}; ^1H NMR (500 MHz, $CDCl_3$) δ 7.64–7.56 (m, 3H), 7.51 (dd, J_1 = 8.0 Hz, J_2 = 0.3 Hz, 1H), 7.49–7.46 (m, 1H), 7.39 (d, J = 8.5 Hz, 1H), 7.32 (dd, J_1 = 8.0 Hz, J_2 = 1.7 Hz, 1H), 7.15 (dd, J_1 = 8.1 Hz, J_2 = 0.5 Hz, 1H), 7.11 (ddd, J_1 = 8.1 Hz, J_2 = 6.8 Hz, J_3 = 1.2 Hz, 1H), 6.99 (ddd, J_1

= 8.5 Hz, J_2 = 6.8 Hz, J_3 = 1.2 Hz, 1H), 6.75 (dd, J_1 = 8.1 Hz, J_2 = 1.8 Hz, 1H), 6.37 (d, J = 1.6 Hz, 1H), 4.09 (dqd, J_1 = 7.4 Hz, J_2 = 6.8 Hz, J_3 = 3.4 Hz, 1H), 3.70 (dd, J_1 = 11.5 Hz, J_2 = 7.4 Hz, 1H), 3.50 (t, J = 6.6 Hz, 1H), 3.27 (t, J = 6.9 Hz, 1H), 3.05 (dd, J_1 = 11.5 Hz, J_2 = 3.4 Hz, 1H), 2.76 (t, J = 6.6 Hz, 1H), 2.47 (t, J = 6.9 Hz, 1H), 0.79 (d, J = 6.8 Hz, 1H); ^{13}C NMR (125 MHz, $CDCl_3$) δ 137.92, 137.85, 136.00, 135.72, 135.37, 133.99, 132.12 (CH), 131.56, 130.92, 130.81, 130.58 (CH), 130.55, 129.92 (CH), 129.12 (CH), 127.72 (CH), 127.70 (CH), 127.61 (CH), 126.18 (CH), 125.87 (CH), 125.52 (CH), 124.41 (CH), 123.92 (CH), 121.30, 120.46, 86.94, 85.45, 82.13, 81.43, 49.79 (CH_2), 49.73 (CH_2), 37.09 (CH_2), 32.56 (CH), 20.88 (CH_2), 20.40 (CH_2), 19.22 (CH_3); HRMS (APCI) *m*/*z* calcd for $[M+Na]^+$ $C_{35}H_{26}N_6S_2Na$ 617.1553, found 617.1570.

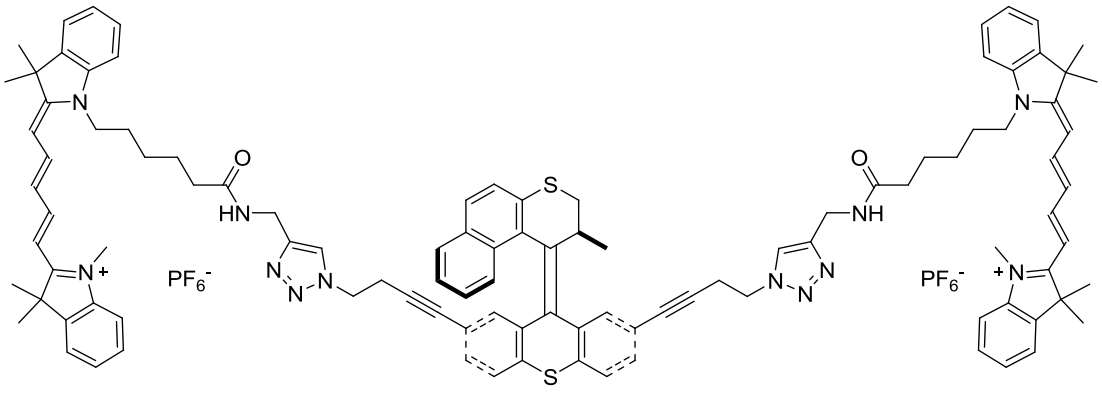

Cy5-armed control molecule 16. Following the procedure described in the synthesis of **15**, **20** (11.9 mg, 0.02 mmol), **18** (29.3 mg, 0.044 mmol), $CuSO_4 \cdot 5H_2O$ (0.5 mg, 0.002 mmol), sodium ascorbate (1.5 mg, 0.06 mmol), CH_2Cl_2 (0.05 mL), and water (0.05 mL) were used in the reaction to yield **20** as a blue solid (29 mg, 76%): m.p. 155 ℃ (decomp.); FTIR (neat) 3426, 2926, 2854, 1480, 1446, 1368, 1332, 1216, 1144, 1088, 1038, 1014 cm^{-1}; ^{1}H NMR (500 MHz, CD_3CN) δ 8.10–8.00 (m, 4H), 7.81 (br s, 1H), 7.68-7.65 (m, 1H), 7.63–7.60 (m, 1H), 7.56 (d, J = 1.5 Hz, 1H), 7.55 (s, 1H), 7.51 (d, J = 8.0 Hz, 1H),

7.48–7.43 (m, 5H), 7.42–7.34 (m, 5H), 7.27–7.20 (m, 7H), 7.19-7.15 (m, 3H), 7.11 (ddd, J_1 = 8.1 Hz, J_2 = 6.8 Hz, J_3 = 1.1 Hz, 1H), 6.97 (ddd, J_1 = 8.6 Hz, J_2 = 6.8 Hz, J_3 = 1.3 Hz, 1H), 6.87 (br t, J = 5.7 Hz, 1H), 6.83 (br t, J = 5.7 Hz, 1H), 6.68 (dd, J_1 = 8.1 Hz, J_2 = 1.8 Hz, 1H), 6.53–6.44 (m, 2H), 6.28 (d, J = 1.7 Hz, 1H), 6.18–6.10 (m, 4H), 4.57 (t, J = 6.4 Hz, 2H), 4.43–4.29 (m, 6H), 3.99 (dqd, J_1 = 7.2 Hz, J_2 = 6.7 Hz, J_3 = 3.0 Hz, 1H), 3.91–3.85 (m, 4H), 3.82 (dd, J_1 = 11.5 Hz, J_2 = 7.2 Hz, 1H), 3.50 (br s, 6H), 3.10 (dd, J_1 = 11.5 Hz, J_2 = 3.0 Hz, 1H), 3.00 (t, J = 6.3 Hz, 2H), 2.72 (t, J = 6.5 Hz, 2H), 2.07–2.03 (m, 4H), 1.71–1.60 (m, 28H), 1.56–1.47 (m, 4H), 1.36–1.28 (m, 4H), 0.67 (d, J = 6.7 Hz, 3H); ^{13}C NMR (125 MHz, $CDCl_3$) δ 175.01, 175.00, 174.18, 174.15, 173.44, 173.40, 154.8 (overlapping of four signals, all CH carbons), 144.1 (overlapping of two signals), 143.30, 143.29, 142.43, 142.41, 142.314, 142.310, 139.22, 139.20, 136.7, 136.6, 136.5, 135.4, 132.7, 132.5, 131.7, 131.6, 131.5, 131.4, 131.1, 130.2, 129.6 (overlapping of four signals, all CH carbons), 129.0, 128.9, 128.7, 127.7, 127.0, 126.4, 126.1 (overlapping of two signals), 125.994, 125.985, 125.6 (overlapping of three signals, all CH carbons), 124.7, 123.9 (very broad signal), 123.7 (very broad signal), 123.282, 123.280, 123.2 (overlapping of two signals, both CH carbons), 122.5, 121.3, 111.98, 111.96, 111.86 (overlapping of two signals, both CH carbons), 104.16, 104.15, 103.94, 103.93, 88.2, 87.1, 83.1, 82.5, 55.4, 50.21, 50.20, 49.6, 49.5, 44.9, 37.7, 36.37, 36.34, 35.6, 35.5, 33.1, 32.0, 27.8, 27.7, 27.6, 27.02, 27.00, 25.9, 22.2, 21.8, 19.1; HRMS (APCI) *m*/*z* calcd for $[M-2PF_6]^{+2}$ $C_{105}H_{110}N_{12}S_2$ 817.4153, found 817.4147.

Note: 1. Two considerably broader and consequently shorter signals at δ 123.9 (CH) and 123.6 (CH) were observed. These signals to the carbons in the 1,2,3-triazole rings, with the breadth resulting from rapid relaxation caused by the directly attached ^{14}N (a

quadrupolar nucleus). Compared to the signals at δ 123.9 and δ 123.7 in the ^{13}C NMR of **15**, the signals at δ 123.9 (CH) and 123.6 (CH) were even more severely broadened. In the ^{13}C spectrum of **16**, we did not observe any carbon signals at the δ ~146.5 region corresponding to the quaternary carbon in the 1,2,3-triazole rings, which were found in the case of **15**. 2. The assignments were tentatively determined by comparing ^{13}C and DEPT-135 spectra of **15**, **16**, **18**, and **20**.

4.14. References

1. Bustamante, C.; Chemla, Y. R.; Forde, N. R.; Izhaky, D. Mechanical Processes in Biochemistry. *Annu. Rev. Biochem.* **2004**, *73*, 705–748.

2. Spudich, J. A. How Molecular Motors Work. *Nature* **1994**, *372*, 515–518.

3. Vale, R. D.; Milligan, R. A. The Way Things Move: Looking under the Hood of Molecular Motor Proteins. *Science* **2000**, *288*, 88–95.

4. Courty, S.; Luccardini, C.; Bellaiche, Y.; Cappello, G.; Dahan, M. Tracking Individual Kinesin Motors in Living Cells Using Single Quantum-Dot Imaging. *Nano Lett.* **2006**, *6*, 1491–1495.

5. von Delius, M.; Leigh, D. A. Walking Molecules. *Chem. Soc. Rev.* **2011**, *40*, 3656–3676.

6. Special issue on molecular machines: *Acc. Chem. Res.* **2001**, *32*, 410–522.

7. Balzani, V.; Credi, A.; Venturi, M. Molecular Devices and Machines– Concepts and Perspectives for the Nanoworld; Wiley–VCH: Weinheim, 2008.

8. Chiang, P.-T.; Cheng, P.-N.; Lin, C.-F.; Liu, Y.-H.; Lai, C.-C.; Peng, S.-M.; Chiu, S.-H. A Macrocycle/Molecular-Clip Complex That Functions as a Quadruply Controllable Molecular Switch. *Chem. –Eur. J.* **2006**, *12*, 865–876.

9. von Delius, M.; Geertsema, E. M.; Leigh, D. A. A Synthetic Small Molecule That Can Walk Down a Track. *Nat. Chem.* **2010**, *2*, 96–101.

10. Chuang, C.-J.; Li, W.-S.; Lai, C.-C.; Liu, Y.-H.; Peng, S.-M.; Chao, I.; Chiu, S.-H. A Molecular Cage-Based [2]Rotaxane That Behaves as a Molecular Muscle. *Org. Lett.* **2008**, *11*, 385–388.

11. Huang, T. J.; Brough, B.; Ho, C.-M.; Liu, Y.; Flood, A. H.; Bonvallet, P. A.; Tseng, H.-R.; Stoddart, J. F.; Baller, M.; Magonov, S. A Nanomechanical Device Based on Linear Molecular Motors. *Appl. Phys. Lett.* **2004**, *85*, 5391–5393.

12. Liu, Y.; Flood, A. H.; Bonvallet, P. A.; Vignon, S. A.; Northrop, B. H.; Tseng, H.-R.; Jeppesen, J. O.; Huang, T. J.; Brough, B.; Baller, M.; Magonov, S.; Solares, S. D.; Goddard, W. A.; Ho, C.-M.; Stoddart, J. F. Linear Artificial Molecular Muscles. *J. Am. Chem. Soc.* **2005**, *127*, 9745–9759.

13. van Delden, R. A.; ter Wiel, M. K. J.; Pollard, M. M.; Vicario, J.; Koumura, N.; Feringa, B. L. Unidirectional Molecular Motor on a Gold Surface. *Nature* **2005**, *437*, 1337–1340.

14. Klok, M.; Boyle, N.; Pryce, M. T.; Meetsma, A.; Browne, W. R.; Feringa, B. L. Mhz Unidirectional Rotation of Molecular Rotary Motors. *J. Am. Chem. Soc.* **2008**, *130*, 10484–10485.

15. Paxton, W. F.; Sundararajan, S.; Mallouk, T. E.; Sen, A. Chemical Locomotion. *Angew. Chem. Int. Ed.* **2006**, *45*, 5420–5429.

16. Qin, L.; Banholzer, M. J.; Xu, X.; Huang, L.; Mirkin, C. A. Rational Design and Synthesis of Catalytically Driven Nanorotors. *J. Am. Chem. Soc.* **2007**, *129*, 14870–14871.

17. Fournier-Bidoz, S.; Arsenault, A. C.; Manners, I.; Ozin, G. A. Synthetic Self-Propelled Nanorotors. *Chem. Commun.* **2005**, 441–443.

18. Paxton, W. F.; Kistler, K. C.; Olmeda, C. C.; Sen, A.; St. Angelo, S. K.; Cao, Y.; Mallouk, T. E.; Lammert, P. E.; Crespi, V. H. Catalytic Nanomotors: Autonomous Movement of Striped Nanorods. *J. Am. Chem. Soc.* **2004**, *126*, 13424–13431.

19. Wilson, D. A.; Nolte, R. J. M.; van Hest, J. C. M. Autonomous Movement of Platinum-Loaded Stomatocytes. *Nat. Chem.* **2012**, *4*, 268–274.

20. Pavlick, R. A.; Sengupta, S.; McFadden, T.; Zhang, H.; Sen, A. A Polymerization-Powered Motor. *Angew. Chem. Int. Ed.* **2011**, *123*, 9546–9549.

21. Moerner, W. E. New Directions in Single-Molecule Imaging and Analysis. *Proc. Natl. Acad. Sci.* **2007**, *104*, 12596–12602.

22. Hoffman, M. Z.; Bolletta, F.; Moggi, L.; Hug, G. L. Rate Constants for the Quenching of Excited States of Metal Complexes in Fluid Solution. *J. Phys. Chem. Ref. Data* **1989**, *18*, 219–543.

23. Juris, A.; Balzani, V.; Barigelletti, F.; Campagna, S.; Belser, P.; von Zelewsky, A. Ru(II) Polypyridine Complexes: Photophysics, Photochemistry, Eletrochemistry, and Chemiluminescence. *Coord. Chem. Rev.* **1988**, *84*, 85–277.

24. Lakowicz, J. R. Principles of Fluorescence Spectroscopy, 2nd ed.; Kluwer Academics / Plenum Publishers: New York, 1999.

25. Colon, J. L.; Yang, C. Y.; Clearfield, A.; Martin, C. R. Photophysics and Photochemistry of Tris(2,2'-Bipyridyl)Ruthenium(II) within the Layered Inorganic Solid Zirconium Phosphate Sulfophenylphosphonate. *J. Phys. Chem.* **1990**, *94*, 874–882.

26. Martí, A. A.; Colón, J. L. Photophysical Characterization of the Interactions among Tris(2,2'-Bipyridyl)Ruthenium(II) Complexes Ion-Exchanged within Zirconium Phosphate. *Inorg. Chem.* **2010**, *49*, 7298–7303.

27. Einstein, A. On the Motion of Small Particles Suspended in Liquids at Rest Required by the Molecular-Kinetic Theory of Heat. In Einstein's Miraculous Year, Stachel, J., Ed. Princeton University Press: New Jersey, 1998; pp 85–98.

28. Astumian, R. D. Design Principles for Brownian Molecular Machines: How to Swim in Molasses and Walk in a Hurricane. *Phys. Chem. Chem. Phys.* **2007**, *9*, 5067–5083.

29. Veigel, C.; Schmidt, C. F. Moving into the Cell: Single-Molecule Studies of Molecular Motors in Complex Environments. *Nat. Rev. Mol. Cell Biol.* **2011**, *12*, 163–176.

30. Bock, C. R.; Connor, J. A.; Gutierrez, A. R.; Meyer, T. J.; Whitten, D. G.; Sullivan, B. P.; Nagle, J. K. Estimation of Excited-State Redox Potentials by Electron-Transfer Quenching. Application of Electron-Transfer Theory to Excited-State Redox Processes. *J. Am. Chem. Soc.* **1979**, *101*, 4815–4824.

31. Houston, P. L. Chemical Kinetics and Reaction Dynamics, 1st ed.; McGraw-Hill: New York, 2001; pp 95–99.

32. Chiang, P.-T.; Mielke, J.; Godoy, J.; Guerrero, J. M.; Alemany, L. B.; Villagómez, C. J.; Saywell, A.; Grill, L.; Tour, J. M. Toward a Light-Driven Motorized Nanocar: Synthesis and Initial Imaging of Single Molecules. *ACS Nano* **2012**, *6*, 592–597.

33. Hundertmark, T.; Littke, A. F.; Buchwald, S. L.; Fu, G. C. $Pd(PhCN)_2Cl_2/P(t\text{-}Bu)_3$: A Versatile Catalyst for Sonogashira Reactions of Aryl Bromides at Room Temperature. *Org. Lett.* **2000**, *2*, 1729–1731.

34. Morin, J.-F.; Shirai, Y.; Tour, J. M. En Route to a Motorized Nanocar. *Org. Lett.* **2006**, *8*, 1713–1716.

35. Koumura, N.; Geertsema, E. M.; van Gelder, M. B.; Meetsma, A.; Feringa, B. L. Second Generation Light-Driven Molecular Motors. Unidirectional Rotation Controlled by a Single Stereogenic Center with near-Perfect Photoequilibria and Acceleration of the Speed of Rotation by Structural Modification. *J. Am. Chem. Soc.* **2002**, *124*, 5037–5051.

36. Kvach, M. V.; Ustinov, A. V.; Stepanova, I. A.; Malakhov, A. D.; Skorobogatyi, M. V.; Shmanai, V. V.; Korshun, V. A. A Convenient Synthesis of Cyanine Dyes: Reagents for the Labeling of Biomolecules. *Eur. J. Org. Chem.* **2008**, *2008*, 2107–2117.

37. Lee, B.-Y.; Park, S. R.; Jeon, H. B.; Kim, K. S. A New Solvent System for Efficient Synthesis of 1,2,3-Triazoles. *Tetrahedron Lett.* **2006**, *47*, 5105–5109.

38. Astumian, R. D. Thermodynamics and Kinetics of Molecular Motors. *Biophys. J.* **2010**, *98*, 2401–2409.

39. Banerjee, A.; Kihm, K. D. Experimental Verification of near-Wall Hindered Diffusion for the Brownian Motion of Nanoparticles Using Evanescent Wave Microscopy. *Phys. Rev. E* **2005**, *72*, 042101.

40. Sharma, P.; Ghosh, S.; Bhattacharya, S. Microrheology of a Sticking Transition. *Nat. Phys.* **2008**, *4*, 960–966.

41. Huang, P.; Breuer, K. S. Direct Measurement of Anisotropic near-Wall Hindered Diffusion Using Total Internal Reflection Velocimetry. *Phys. Rev. E* **2007**, *76*, 046307.

42. Sharma, P.; Ghosh, S.; Bhattacharya, S. A High-Precision Study of Hindered Diffusion near a Wall. *Appl. Phys. Lett.* **2010**, *97*, 104101–104103.

43. Bhattacharyya, S.; Lelong, G.; Saboungi, M. L. Recent Progress in the Synthesis and Selected Applications of Mcm-41: A Short Review. *J. Exp. Nanosci.* **2006**, *1*, 375–395.

44. Saha, A.; Ghosh, S.; Behabtu, N.; Pasquali, M.; Martí, A. A. Single-Walled Carbon Nanotubes Shell Decorating Porous Silicate Materials: A General Platform for Studying the Interaction of Carbon Nanotubes with Photoactive Molecules. *Chem. Sci.* **2011**, *2*, 1682–1687.

45. Martí, A. A.; Puckett, C. A.; Dyer, J.; Stevens, N.; Jockusch, S.; Ju, J.; Barton, J. K.; Turro, N. J. Inorganic−Organic Hybrid Luminescent Binary Probe for DNA Detection Based on Spin-Forbidden Resonance Energy Transfer. *J. Am. Chem. Soc.* **2007**, *129*, 8680–8681.

46. Szabo, A. Theory of Diffusion-Influenced Fluorescence Quenching. *J. Phys. Chem.* **1989**, *93*, 6929–6939.

47. Medhage, B.; Almgren, M. Diffusion-Influenced Fluorescence Quenching Dynamics in One to Three Dimensions. *J. Fluoresc.* **1992**, *2*, 7–21.

48. Miller, D. D.; Evans, D. F. Fluorescence Quenching in Double-Chained Surfactants. 1. Theory of Quenching in Micelles and Vesicles. *J. Phys. Chem.* **1989**, *93*, 323–333.

49. Turró, C.; Zaleski, J. M.; Karabatsos, Y. M.; Nocera, D. G. Bimolecular Electron Transfer in the Marcus Inverted Region. *J. Am. Chem. Soc.* **1996**, *118*, 6060–6067.

50. Martins, J.; Melo, E. Molecular Mechanism of Lateral Diffusion of Py10-Pc and Free Pyrene in Fluid Dmpc Bilayers. *Biophys. J.* **2001**, *80*, 832–840.

51. Naqvi, K. R.; Martins, J.; Melo, E. Recipes for Analyzing Diffusion-Controlled Reactions in Two Dimensions: Time-Resolved and Steady-State Measurements. *J. Phys. Chem. B* **2000**, *104*, 12035–12038.

52. Almgren, M.; Alsins, J.; Mukhtar, E.; Van Stam, J. Fluorescence Quenching Dynamics in Rodlike Micelles. *J. Phys. Chem.* **1988**, *92*, 4479–4483.

53. The quaternary carbon signal of nitrobenzene is ^{14}N broadened. See: Levy, G. C.; Nelson, G. L. Carbon-13 Nuclear Magnetic Resonance for Organic Chemists, 1st ed.; John Wiley & Sons, Inc.l: New York, 1972.

54. Another example of ^{14}N broadened signal: see ^{13}C spectrum of 1,4-dibromo-2-iodo-5-nitrobenzene (**32** in chapter 3, signal at δ 149.41).

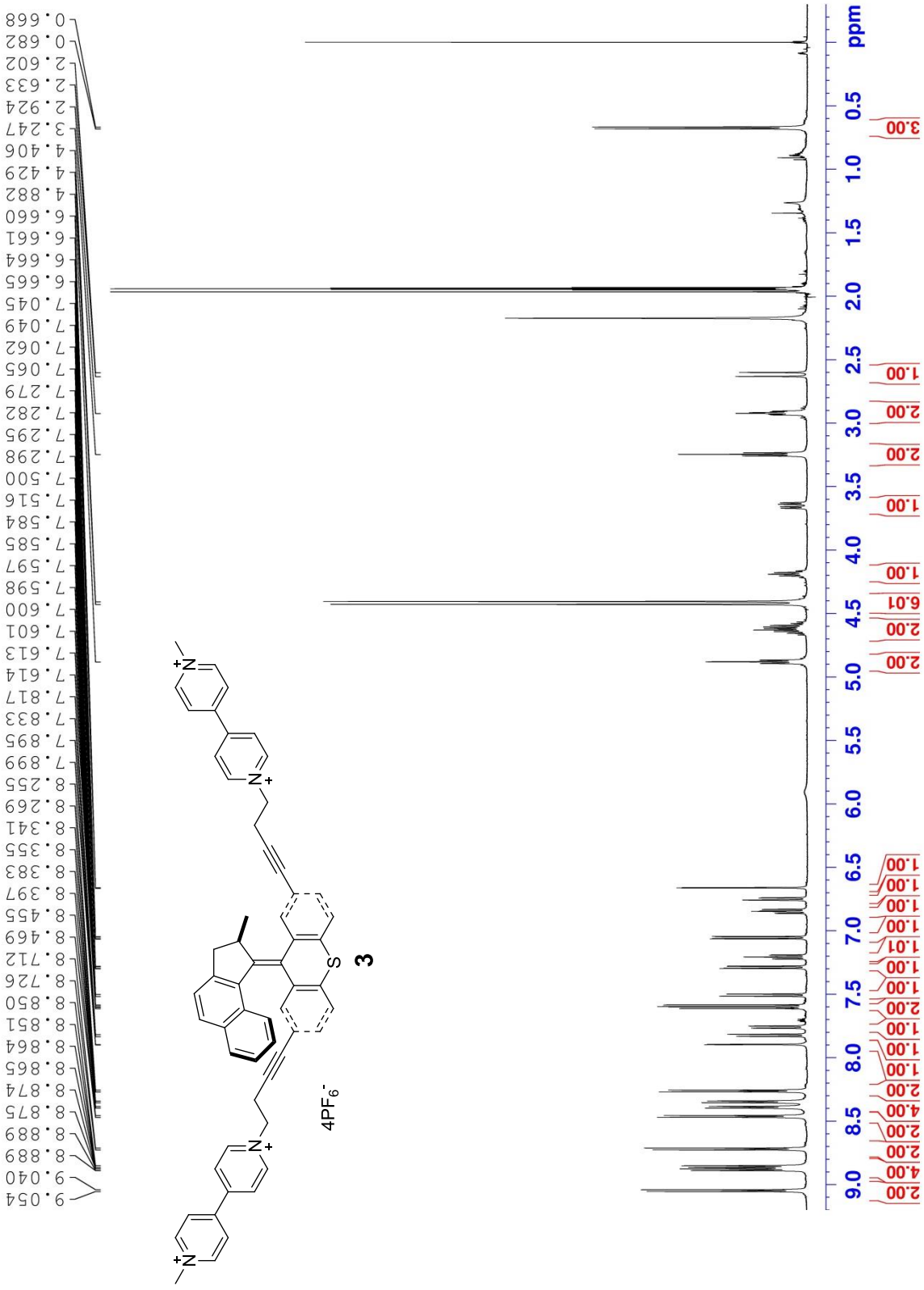
3
4PF6-
ppm

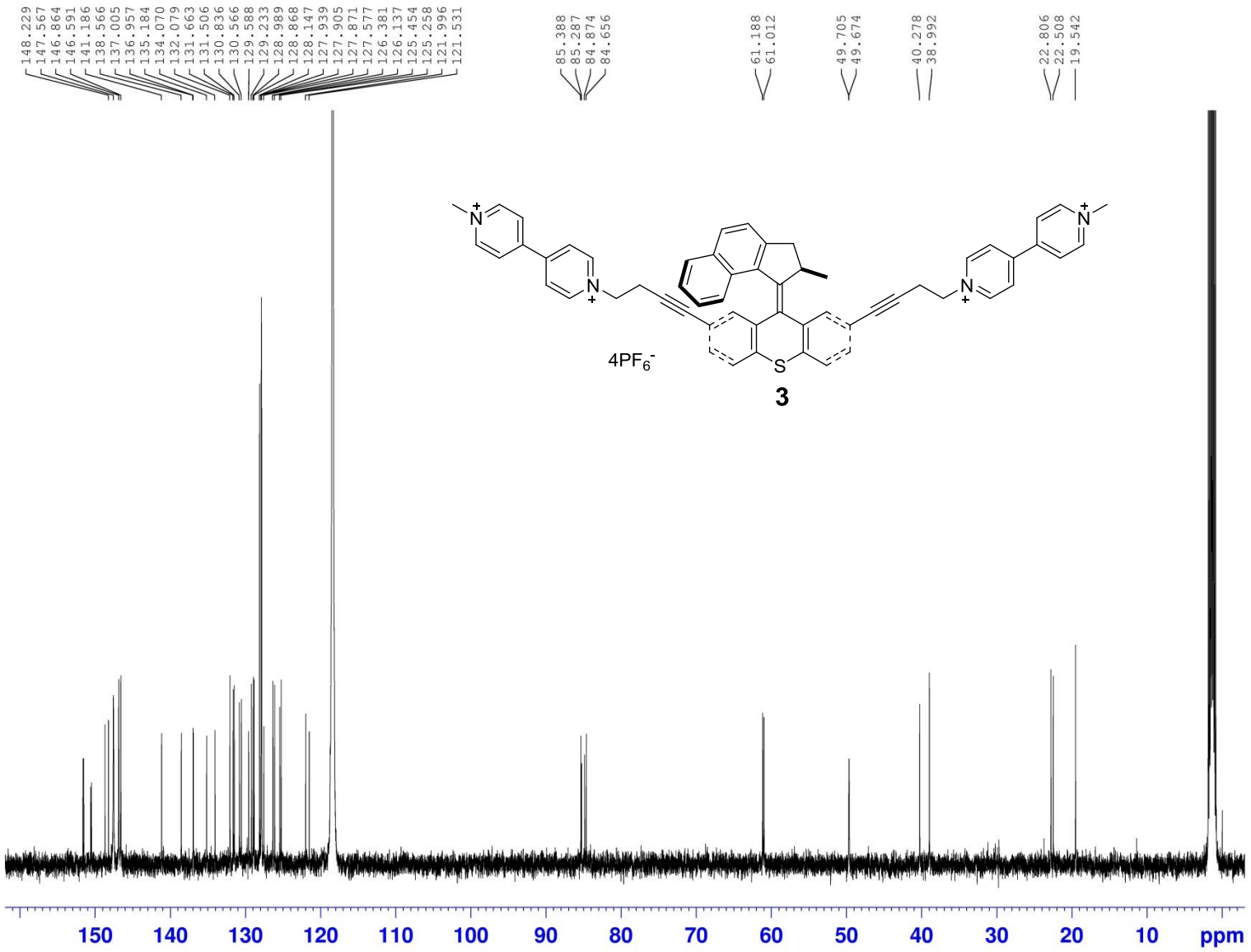
148.229
147.567
146.864
146.591
141.186
138.566
137.005
136.957
135.184
134.070
132.079
131.663
131.506
130.836
130.566
129.588
129.233
128.989
128.868
128.147
127.939
127.905
127.871
127.577
126.381
126.137
125.454
125.258
121.996
121.531
85.388
85.287
84.874
84.656
61.188
61.012
49.705
49.674
40.278
38.992
22.806
22.508
19.542
4PF6-
3
150
140
130
120
110
100
90
80
70
60
50
40
30
20
10
ppm

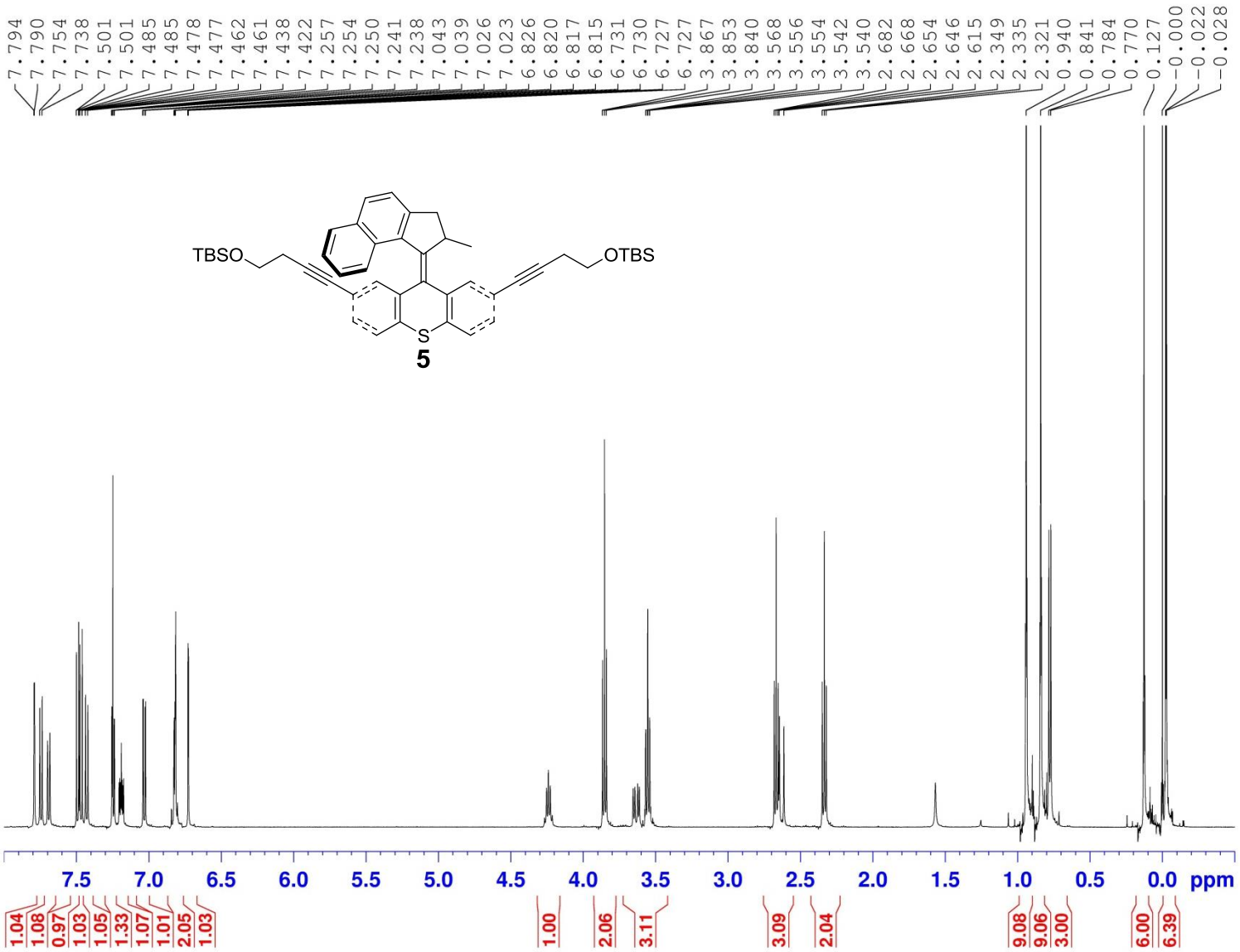
7.794
7.790
7.754
7.738
7.501
7.501
7.485
7.485
7.478
7.477
7.462
7.461
7.438
7.422
7.257
7.254
7.250
7.241
7.238
7.043
7.039
7.026
7.023
6.826
6.820
6.817
6.815
6.731
6.730
6.727
6.727
3.867
3.853
3.840
3.568
3.556
3.554
3.542
3.540
2.682
2.668
2.654
2.646
2.615
2.349
2.335
2.321
0.940
0.841
0.784
0.770
0.127
-0.000
-0.022
-0.028
TBSO
OTBS
S
5
7.5
7.0
6.5
6.0
5.5
5.0
4.5
4.0
3.5
3.0
2.5
2.0
1.5
1.0
0.5
0.0
ppm
1.04
1.08
0.97
1.03
1.05
1.33
1.07
1.01
2.05
1.03
1.00
2.06
3.11
3.09
2.04
9.08
9.06
3.00
6.00
6.39

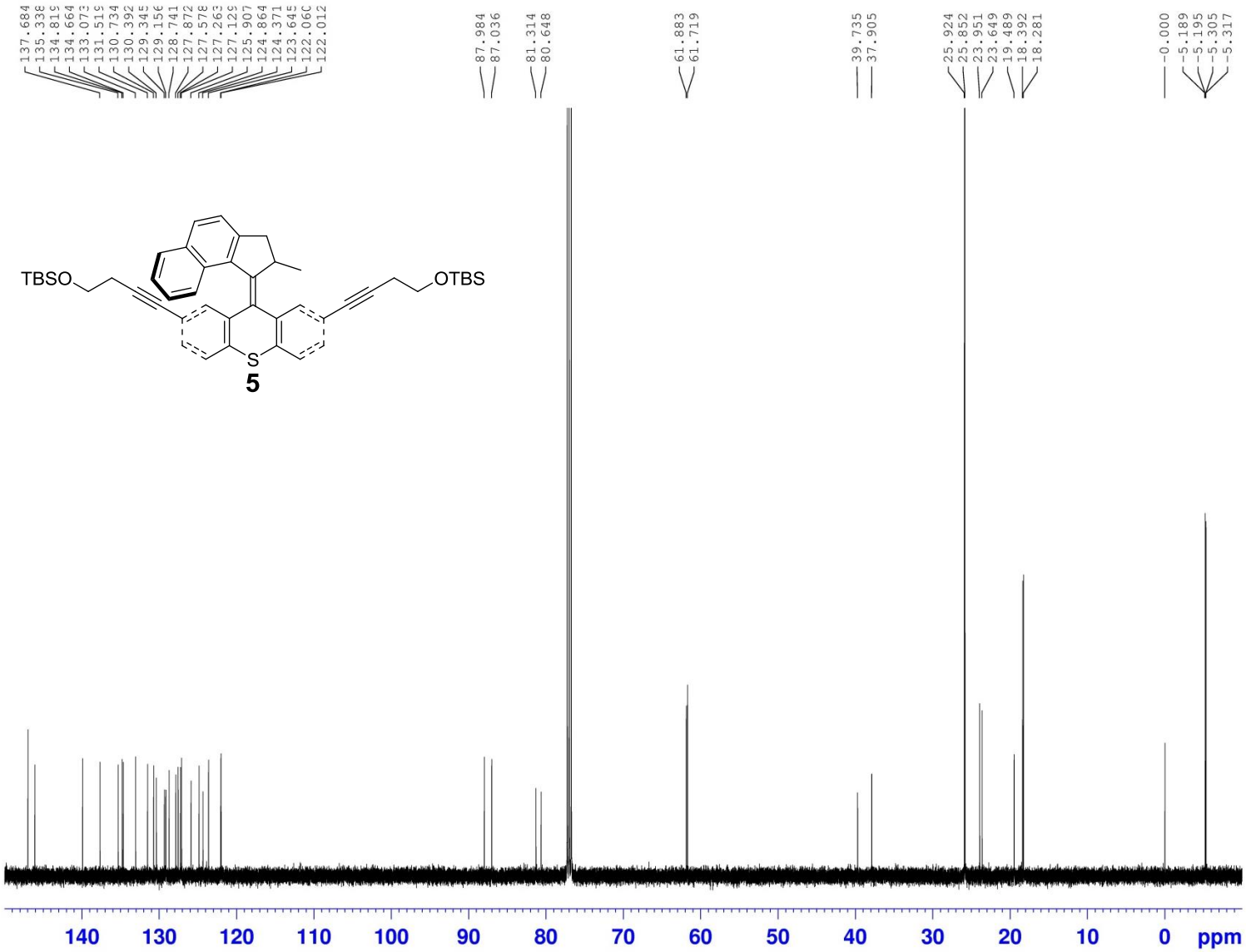
137.684
135.338
134.819
134.664
133.073
131.515
130.734
130.392
129.345
129.156
128.741
127.872
127.578
127.263
127.129
125.907
124.864
124.371
123.645
122.060
122.012
87.984
87.036
81.314
80.648
61.883
61.719
39.735
37.905
25.924
25.852
23.951
23.649
19.489
18.392
18.281
-0.000
-5.189
-5.195
-5.305
-5.317
TBSO
OTBS
S
5
140
130
120
110
100
90
80
70
60
50
40
30
20
10
0
ppm

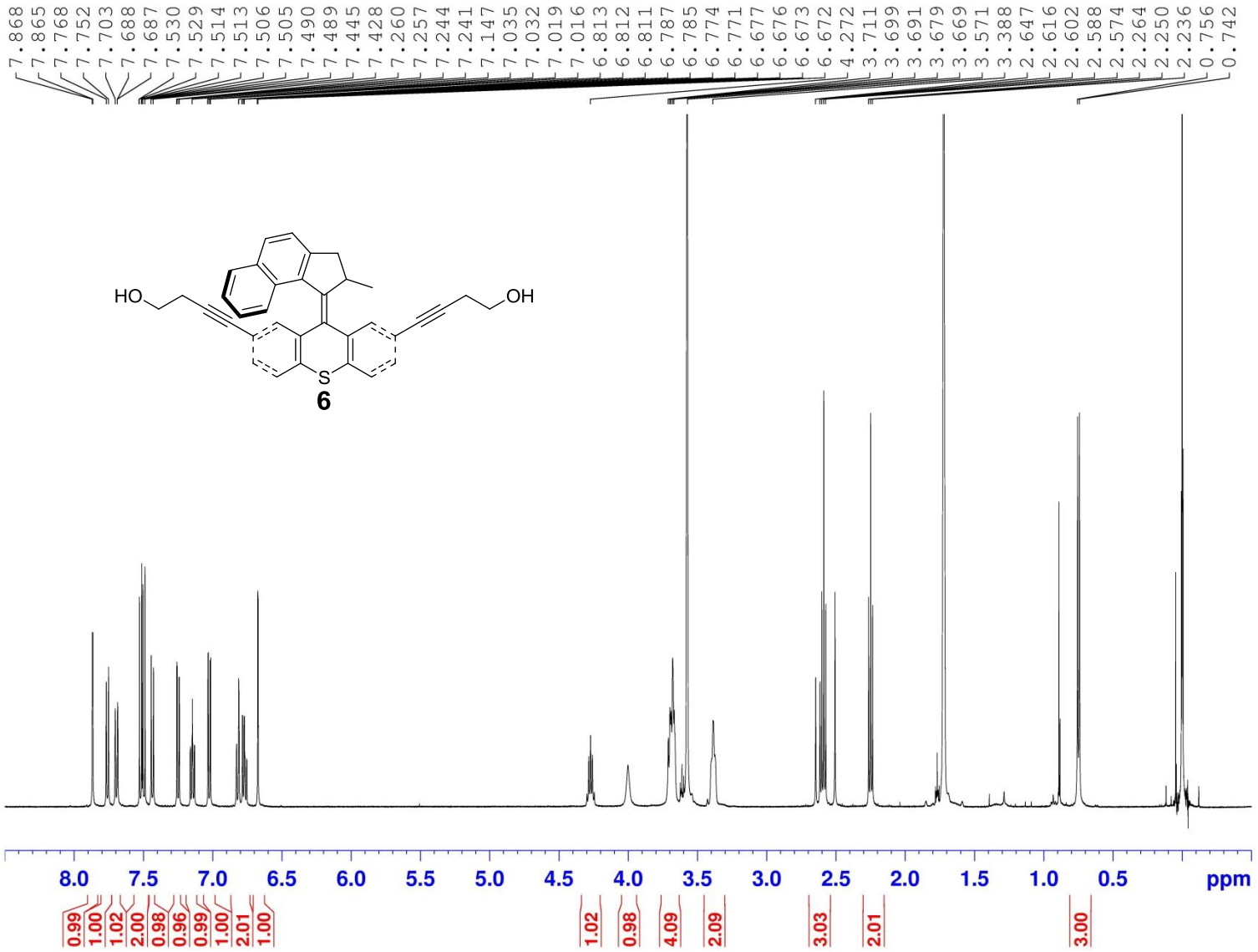
7.868
7.865
7.768
7.752
7.703
7.688
7.687
7.530
7.529
7.514
7.513
7.506
7.505
7.490
7.489
7.445
7.428
7.260
7.257
7.244
7.241
7.147
7.035
7.032
7.019
7.016
6.813
6.812
6.811
6.787
6.785
6.774
6.771
6.677
6.676
6.673
6.672
4.272
3.711
3.699
3.691
3.679
3.669
3.571
3.388
2.647
2.616
2.602
2.588
2.574
2.264
2.250
2.236
0.756
0.742
HO
OH
S
6
8.0
7.5
7.0
6.5
6.0
5.5
5.0
4.5
4.0
3.5
3.0
2.5
2.0
1.5
1.0
0.5
ppm
0.99
1.00
1.02
2.00
0.98
0.96
0.99
1.00
2.01
1.00
1.02
0.98
4.09
2.09
3.03
2.01
3.00

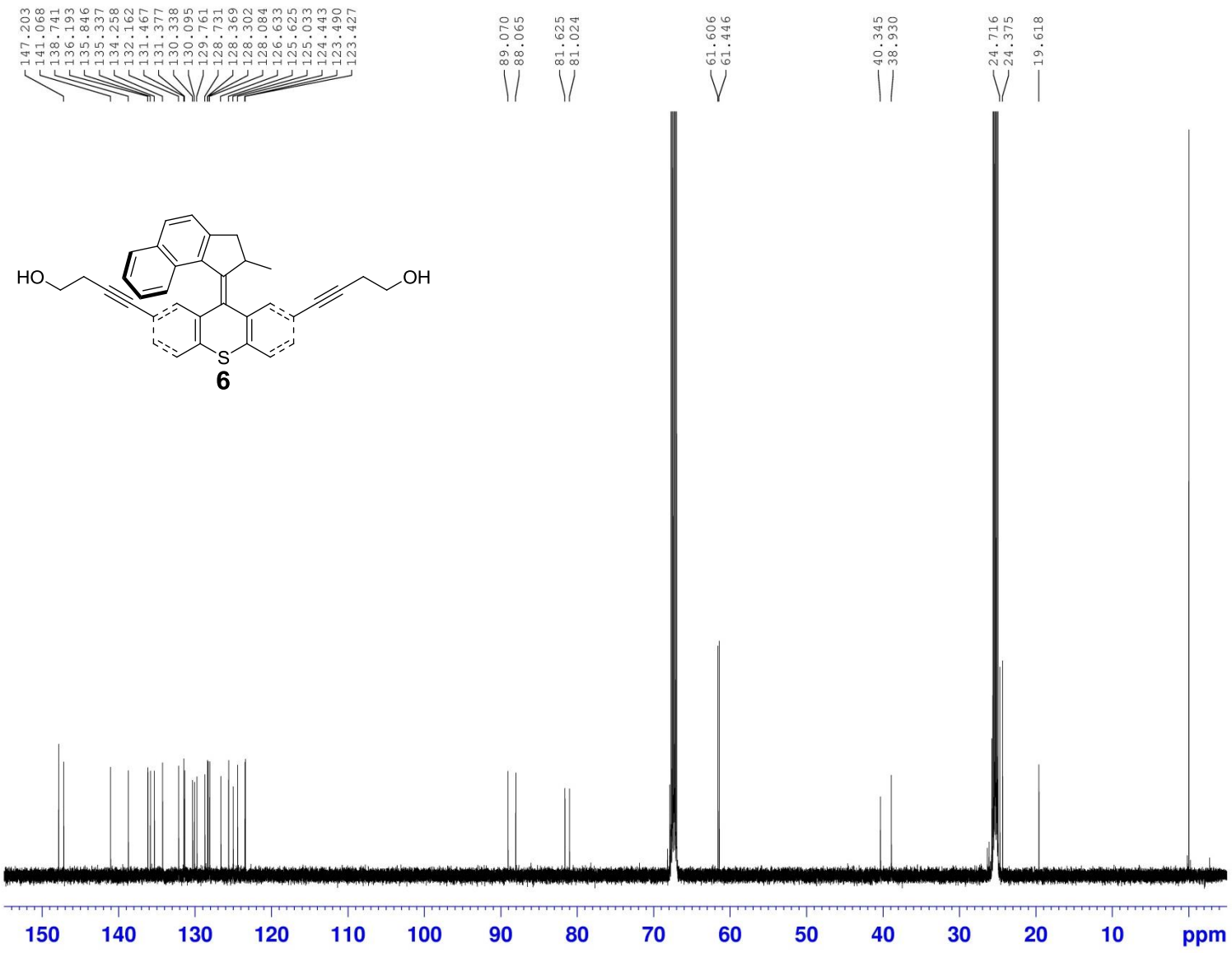
147.203
141.068
138.741
136.193
135.846
135.337
134.258
132.162
131.467
131.377
130.338
130.095
129.761
128.731
128.369
128.302
128.084
126.633
125.625
125.033
124.443
123.490
123.427
89.070
88.065
81.625
81.024
61.606
61.446
40.345
38.930
24.716
24.375
19.618
HO
OH
S
6
150
140
130
120
110
100
90
80
70
60
50
40
30
20
10
ppm

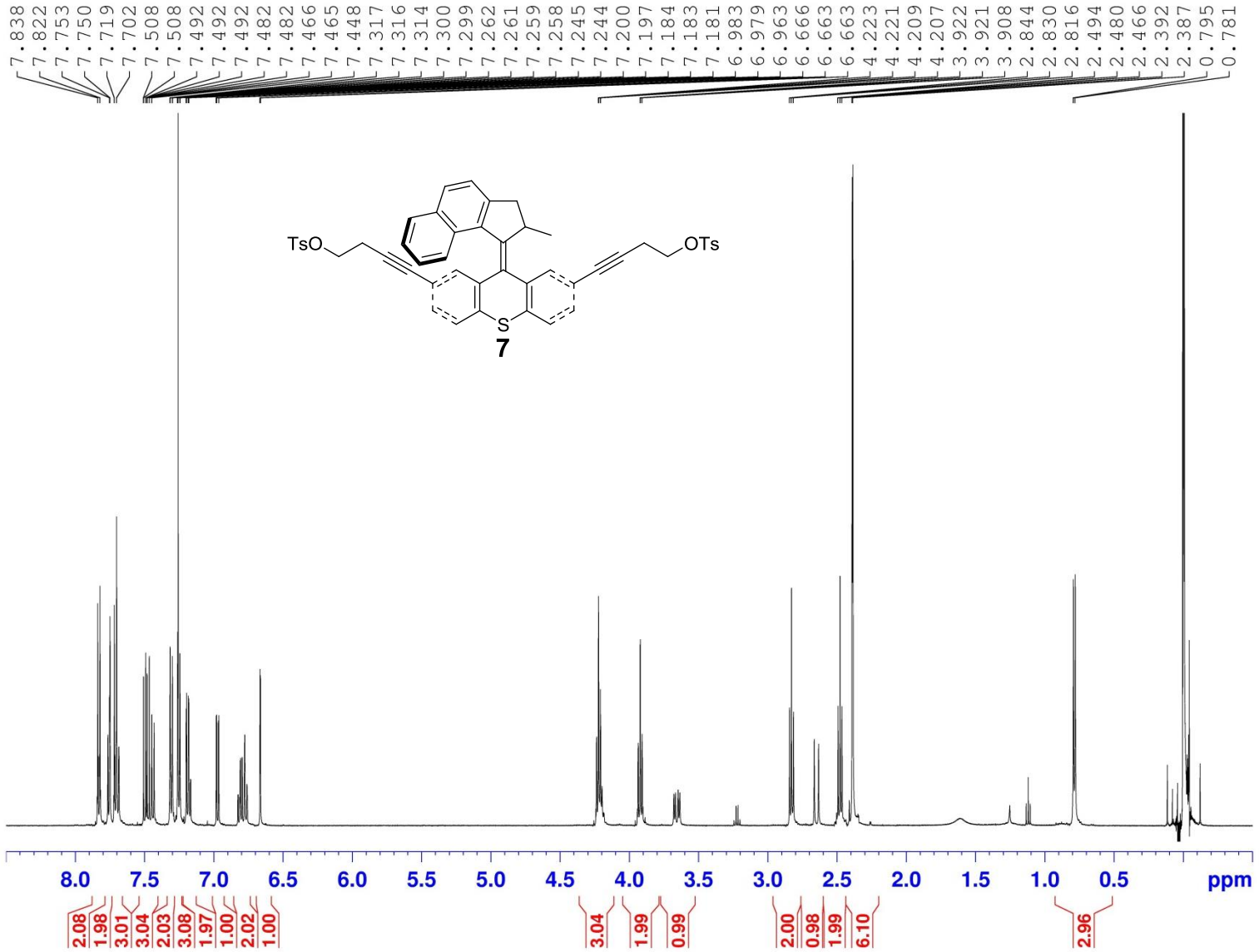
7.838
7.822
7.753
7.750
7.719
7.702
7.508
7.508
7.492
7.492
7.492
7.482
7.482
7.466
7.465
7.448
7.317
7.316
7.314
7.300
7.299
7.262
7.261
7.259
7.258
7.245
7.244
7.200
7.197
7.184
7.183
7.181
6.983
6.979
6.963
6.666
6.663
6.663
4.223
4.221
4.209
4.207
3.922
3.921
3.908
2.844
2.830
2.816
2.494
2.480
2.466
2.392
2.387
0.795
0.781
TsO
OTs
S
7
8.0
7.5
7.0
6.5
6.0
5.5
5.0
4.5
4.0
3.5
3.0
2.5
2.0
1.5
1.0
0.5
ppm
2.08
1.98
3.01
3.04
2.03
3.08
1.97
1.00
2.02
1.00
3.04
1.99
0.99
2.00
0.98
1.99
6.10
2.96

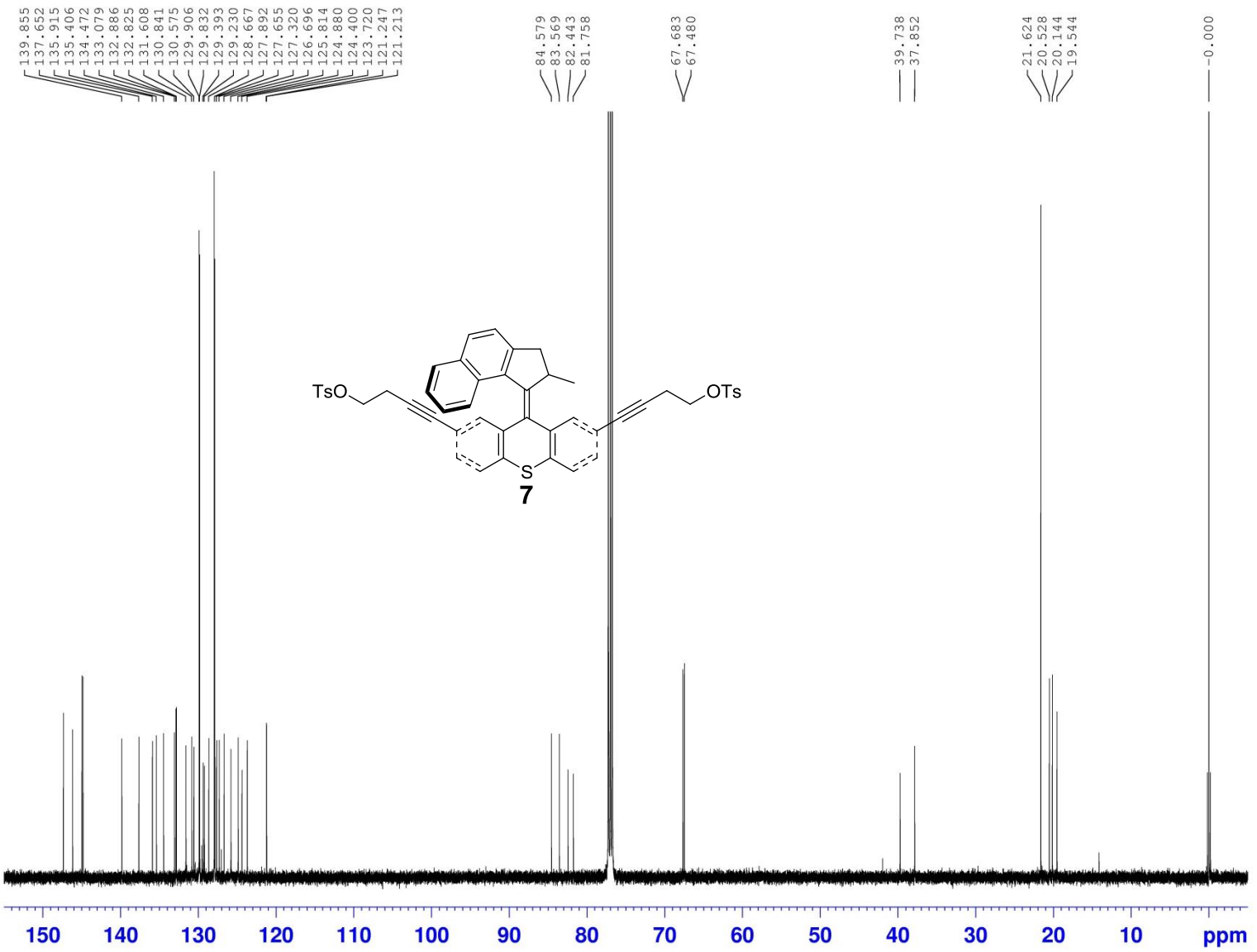
139.855
137.652
135.915
135.406
134.472
133.079
132.886
132.825
131.608
130.841
130.575
129.906
129.832
129.393
129.230
128.667
127.892
127.655
127.320
126.696
125.814
124.880
124.400
123.720
121.247
121.213
84.579
83.569
82.443
81.758
67.683
67.480
39.738
37.852
21.624
20.528
20.144
19.544
0.000
TsO
OTs
S
7
150
140
130
120
110
100
90
80
70
60
50
40
30
20
10
ppm

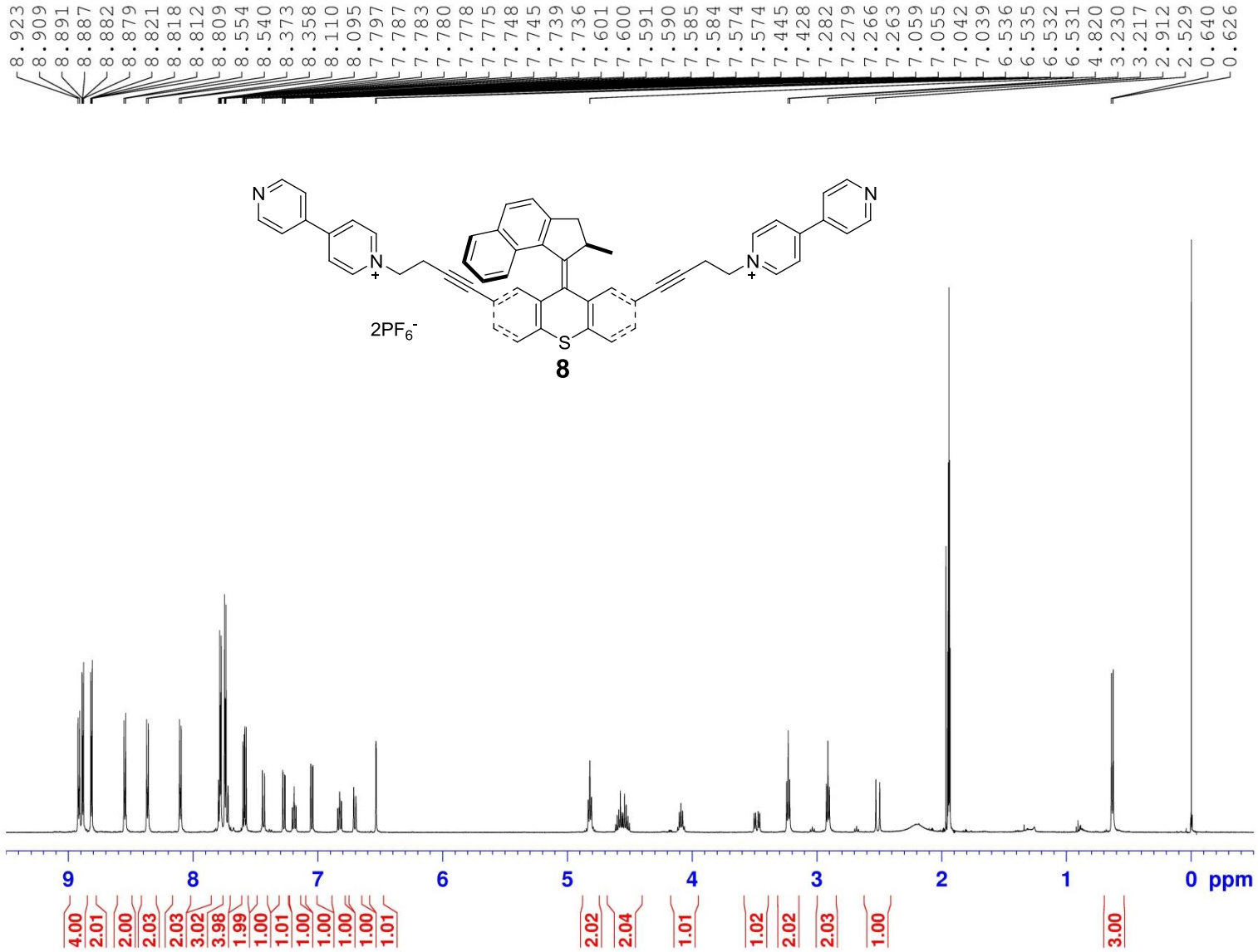
8.923
8.909
8.891
8.887
8.882
8.879
8.821
8.818
8.812
8.809
8.554
8.540
8.373
8.358
8.110
8.095
7.797
7.787
7.783
7.780
7.778
7.775
7.748
7.745
7.739
7.736
7.601
7.600
7.591
7.590
7.585
7.584
7.574
7.574
7.445
7.428
7.282
7.279
7.266
7.263
7.059
7.055
7.042
7.039
6.536
6.535
6.532
6.531
4.820
3.230
3.217
2.912
2.529
0.640
0.626
N
N
N
2PF6-
S
8
9
8
7
6
5
4
3
2
1
0 ppm
4.00
2.01
2.00
2.03
2.03
3.02
3.98
1.99
1.00
1.01
1.00
1.00
1.00
1.00
1.01
2.02
2.04
1.01
1.02
2.02
2.03
1.00
3.00

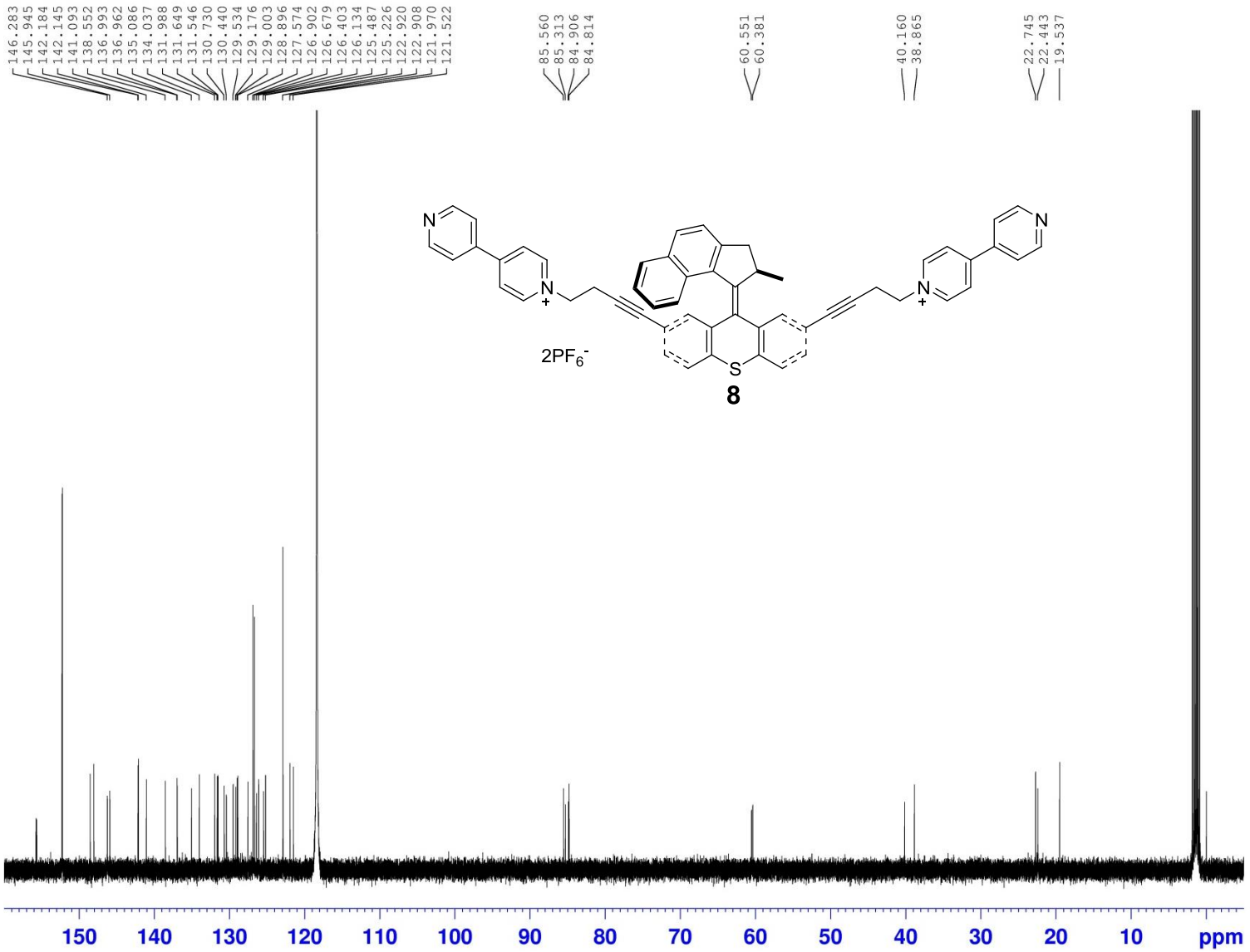
146.283
145.945
142.184
142.145
141.093
138.552
136.993
136.962
135.086
134.037
131.988
131.649
131.546
130.730
130.440
129.534
129.176
129.003
128.896
127.574
126.902
126.679
126.403
126.134
125.487
125.226
122.920
122.908
121.970
121.522
85.560
85.313
84.906
84.814
60.551
60.381
40.160
38.865
22.745
22.443
19.537
N
N
N
S
2PF6-
8
150
140
130
120
110
100
90
80
70
60
50
40
30
20
10
ppm

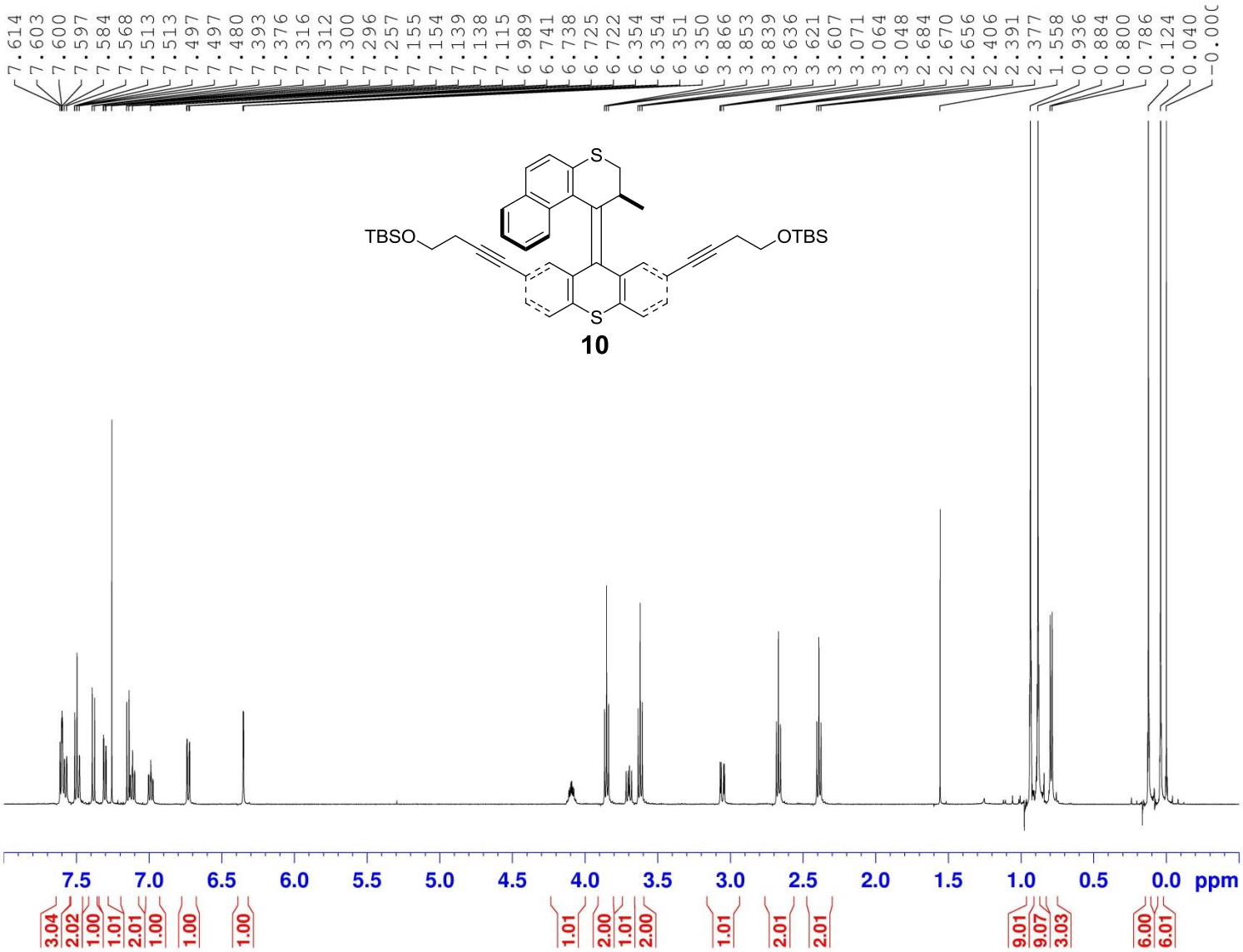
7.614
7.603
7.600
7.597
7.584
7.568
7.513
7.497
7.497
7.480
7.393
7.376
7.316
7.312
7.300
7.296
7.257
7.155
7.154
7.139
7.138
7.115
6.989
6.741
6.738
6.725
6.722
6.354
6.354
6.351
6.350
3.866
3.853
3.839
3.636
3.621
3.607
3.071
3.064
3.048
2.684
2.670
2.656
2.406
2.391
2.377
1.558
0.936
0.884
0.800
0.786
0.124
0.040
-0.000
S
TBSO
OTBS
S
10
7.5
7.0
6.5
6.0
5.5
5.0
4.5
4.0
3.5
3.0
2.5
2.0
1.5
1.0
0.5
0.0
ppm
3.04
2.02
1.00
1.01
2.01
1.00
1.00
1.00
1.01
2.00
1.01
2.00
1.01
2.01
2.01
9.01
9.07
3.03
6.00
6.01

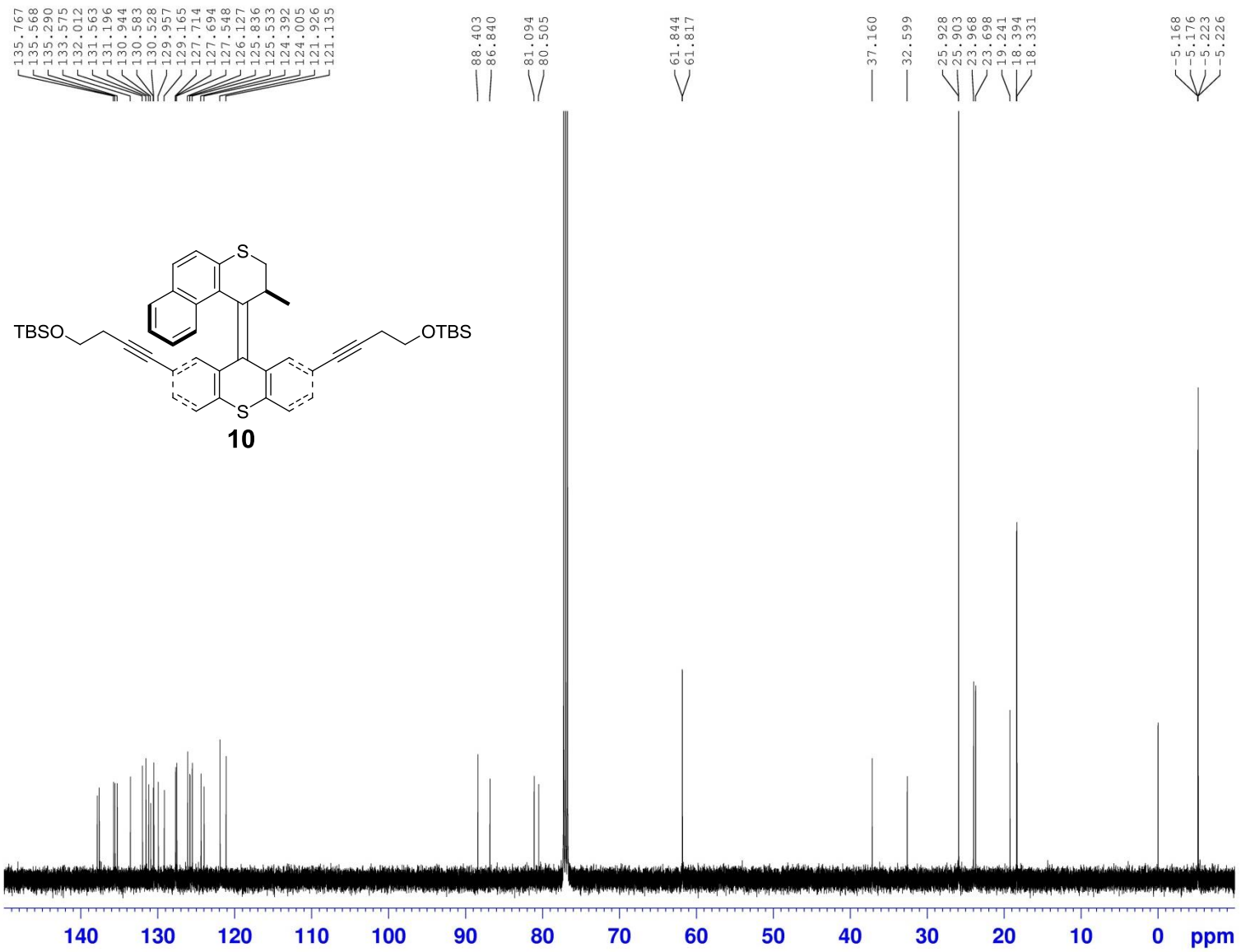
135.767
135.568
135.290
133.575
132.012
131.563
131.196
130.944
130.583
130.528
129.957
129.165
127.714
127.694
127.548
126.127
125.836
125.533
124.392
124.005
121.926
121.135
88.403
86.840
81.094
80.505
61.844
61.817
37.160
32.599
25.928
25.903
23.968
23.698
19.241
18.394
18.331
-5.168
-5.176
-5.223
-5.226
TBSO
OTBS
S
S
10
140
130
120
110
100
90
80
70
60
50
40
30
20
10
0
ppm

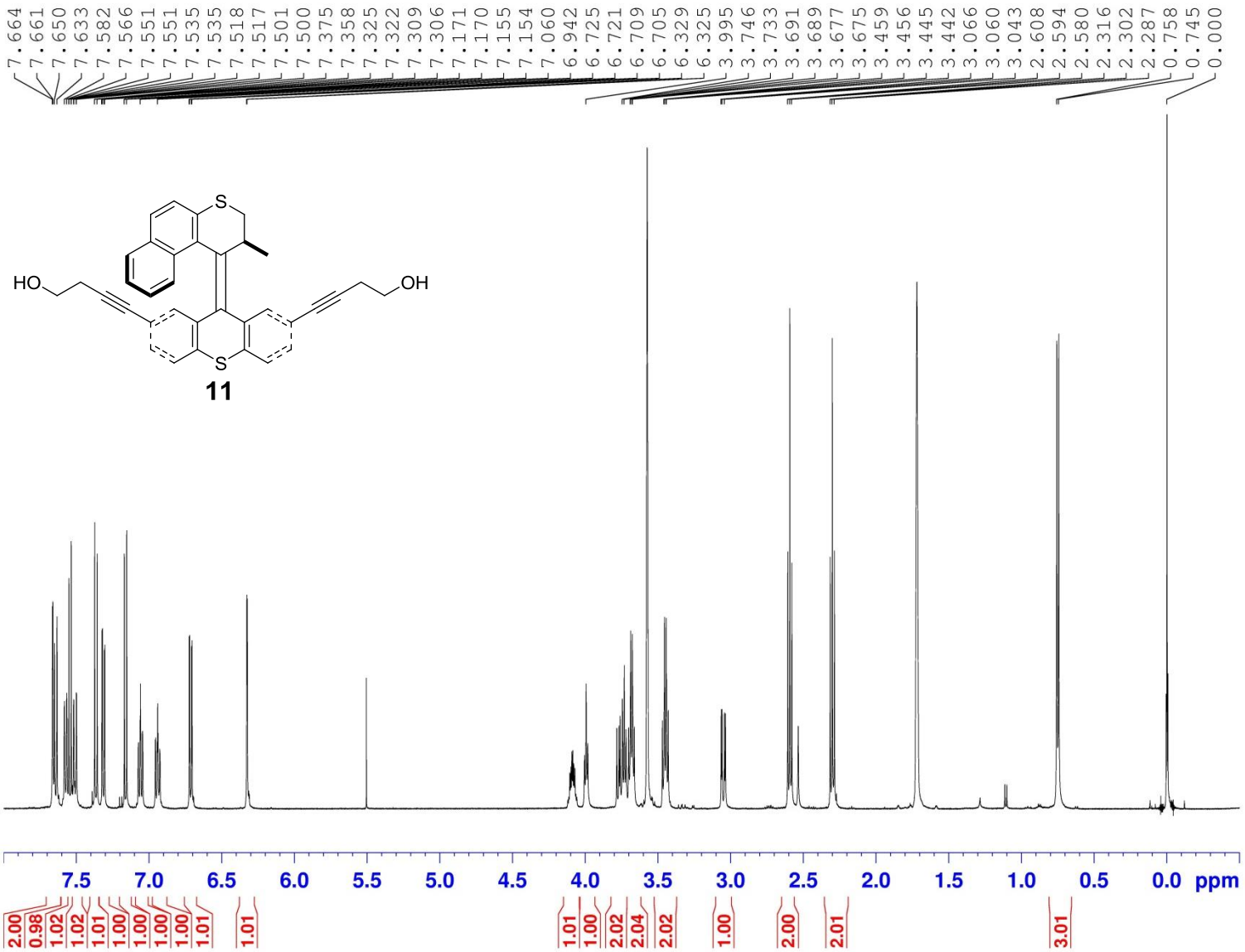
7.664
7.661
7.650
7.633
7.582
7.566
7.551
7.535
7.535
7.518
7.517
7.501
7.500
7.375
7.358
7.325
7.322
7.309
7.306
7.171
7.170
7.155
7.154
7.060
6.942
6.725
6.721
6.709
6.705
6.329
6.325
3.995
3.746
3.733
3.691
3.689
3.677
3.675
3.459
3.456
3.445
3.442
3.066
3.060
3.043
2.608
2.594
2.580
2.316
2.302
2.287
0.758
0.745
0.000
HO
OH
S
S
11
7.5
7.0
6.5
6.0
5.5
5.0
4.5
4.0
3.5
3.0
2.5
2.0
1.5
1.0
0.5
0.0
ppm
2.00
0.98
1.02
1.02
1.01
1.00
1.00
1.00
1.00
1.01
1.01
1.01
1.00
2.02
2.04
2.02
1.00
2.00
2.01
3.01

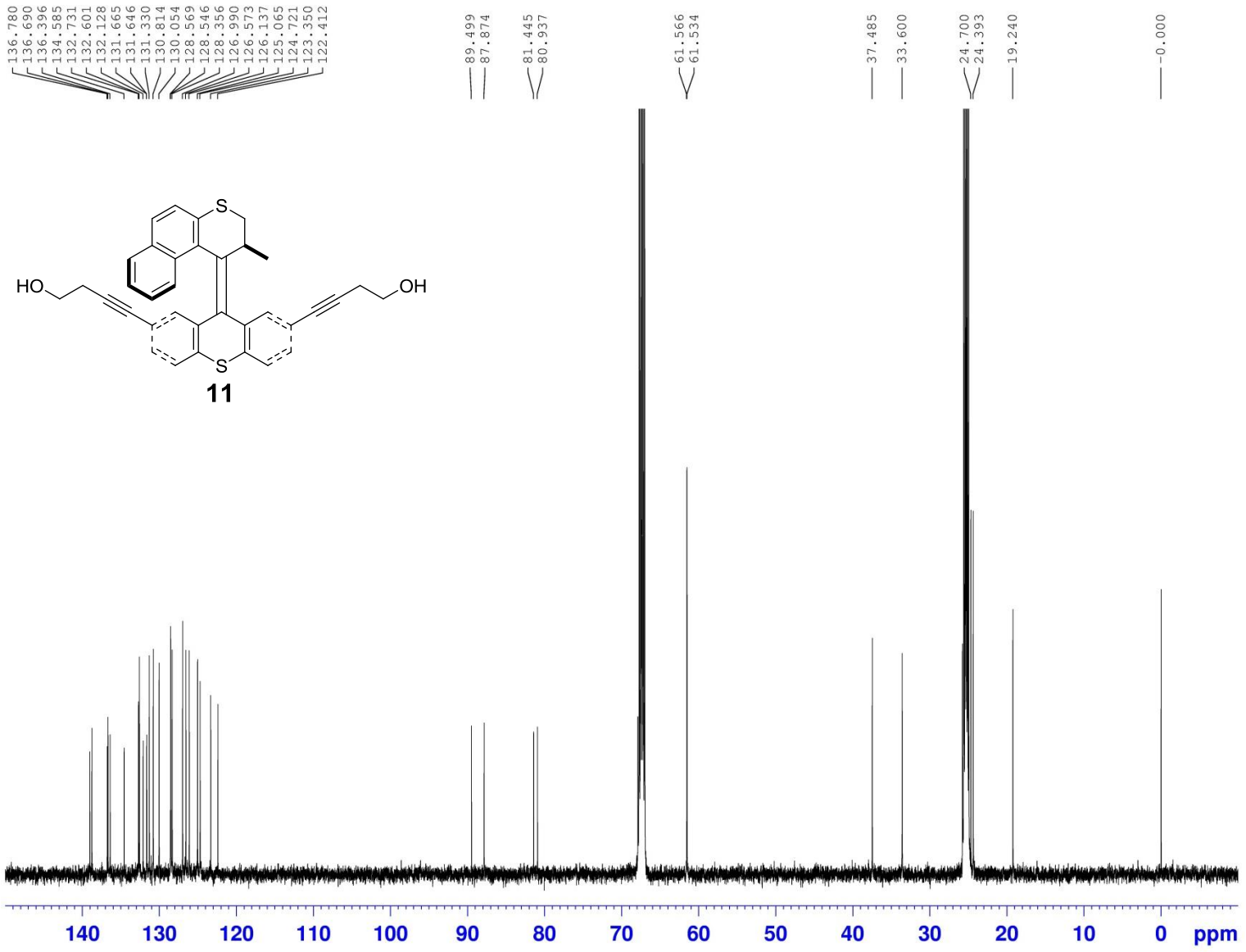
136.780
136.690
136.396
134.585
132.731
132.601
132.128
131.665
131.646
131.330
130.814
130.054
128.569
128.546
128.356
126.990
126.573
126.137
125.065
124.721
123.350
122.412
89.499
87.874
81.445
80.937
61.566
61.534
37.485
33.600
24.700
24.393
19.240
0.000
HO
OH
S
S
11
140
130
120
110
100
90
80
70
60
50
40
30
20
10
0
ppm

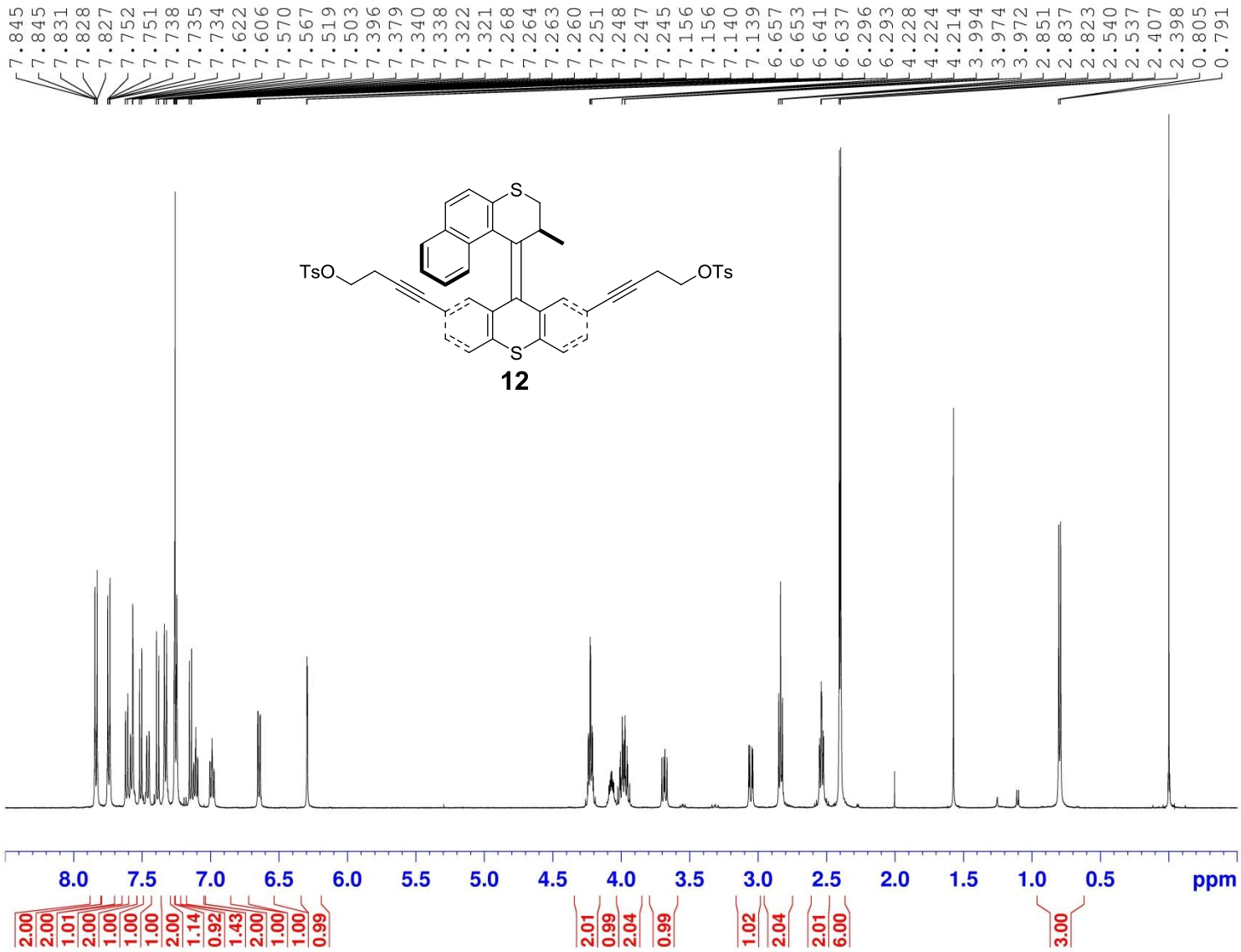
7.845
7.845
7.831
7.828
7.827
7.752
7.751
7.738
7.735
7.734
7.622
7.606
7.570
7.567
7.519
7.503
7.396
7.379
7.340
7.338
7.322
7.321
7.268
7.264
7.263
7.260
7.251
7.248
7.247
7.245
7.156
7.156
7.140
7.139
6.657
6.653
6.641
6.637
6.296
6.293
4.228
4.224
4.214
3.994
3.974
3.972
2.851
2.837
2.823
2.540
2.537
2.407
2.398
0.805
0.791
TsO
OTs
S
S
12
8.0
7.5
7.0
6.5
6.0
5.5
5.0
4.5
4.0
3.5
3.0
2.5
2.0
1.5
1.0
0.5
ppm
2.00
2.00
1.01
2.00
1.00
1.00
1.00
2.00
1.14
0.92
1.43
2.00
1.00
1.00
0.99
2.01
0.99
2.04
0.99
1.02
2.04
2.01
6.00
3.00

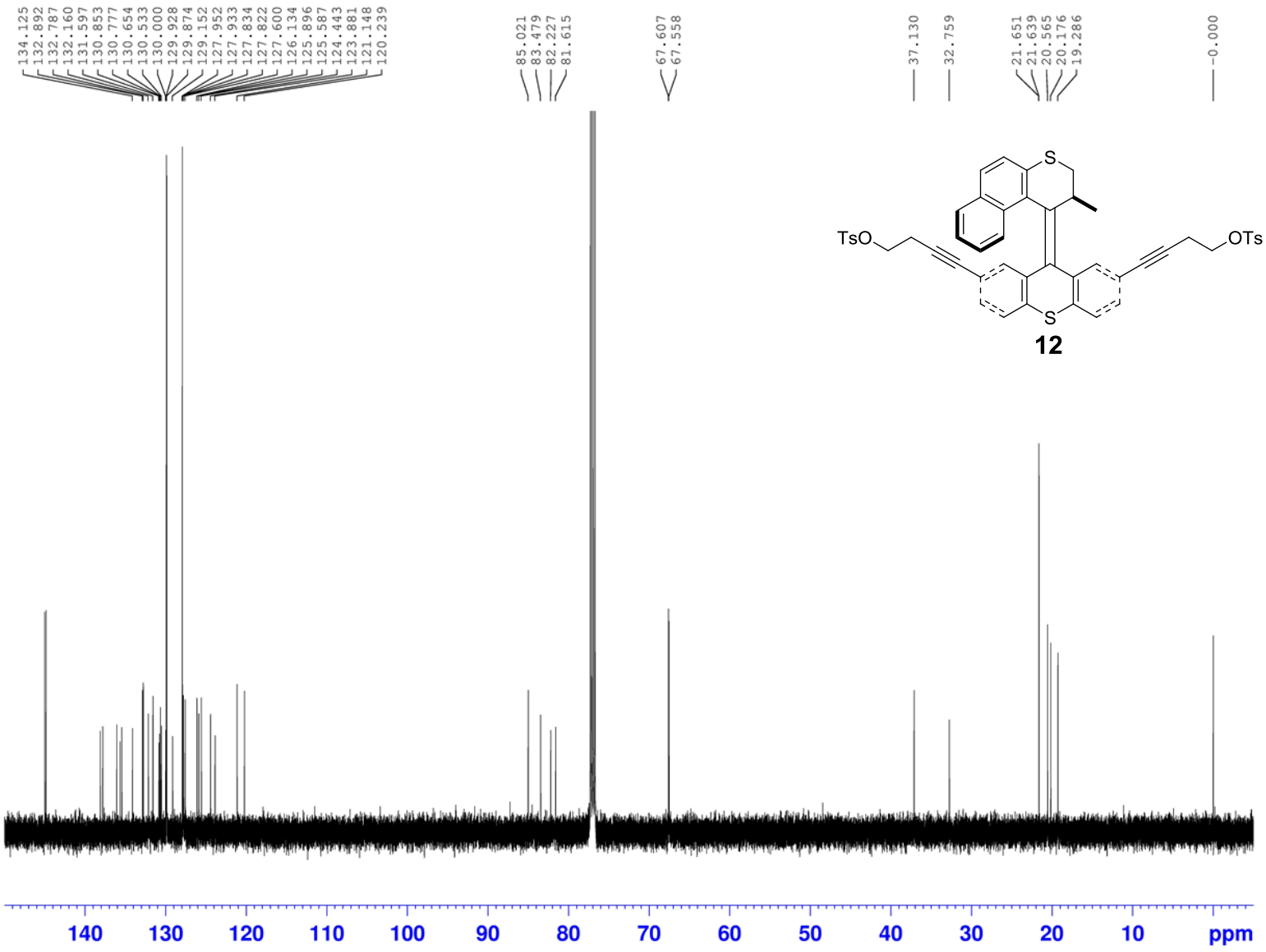
134.125
132.892
132.787
132.160
131.597
130.853
130.777
130.654
130.533
130.000
129.928
129.874
129.152
127.952
127.933
127.834
127.822
127.600
126.134
125.896
125.587
124.443
123.881
121.148
120.239
85.021
83.479
82.227
81.615
67.607
67.558
37.130
32.759
21.651
21.639
20.565
20.176
19.286
-0.000
TsO
OTs
S
S
12
140
130
120
110
100
90
80
70
60
50
40
30
20
10
ppm

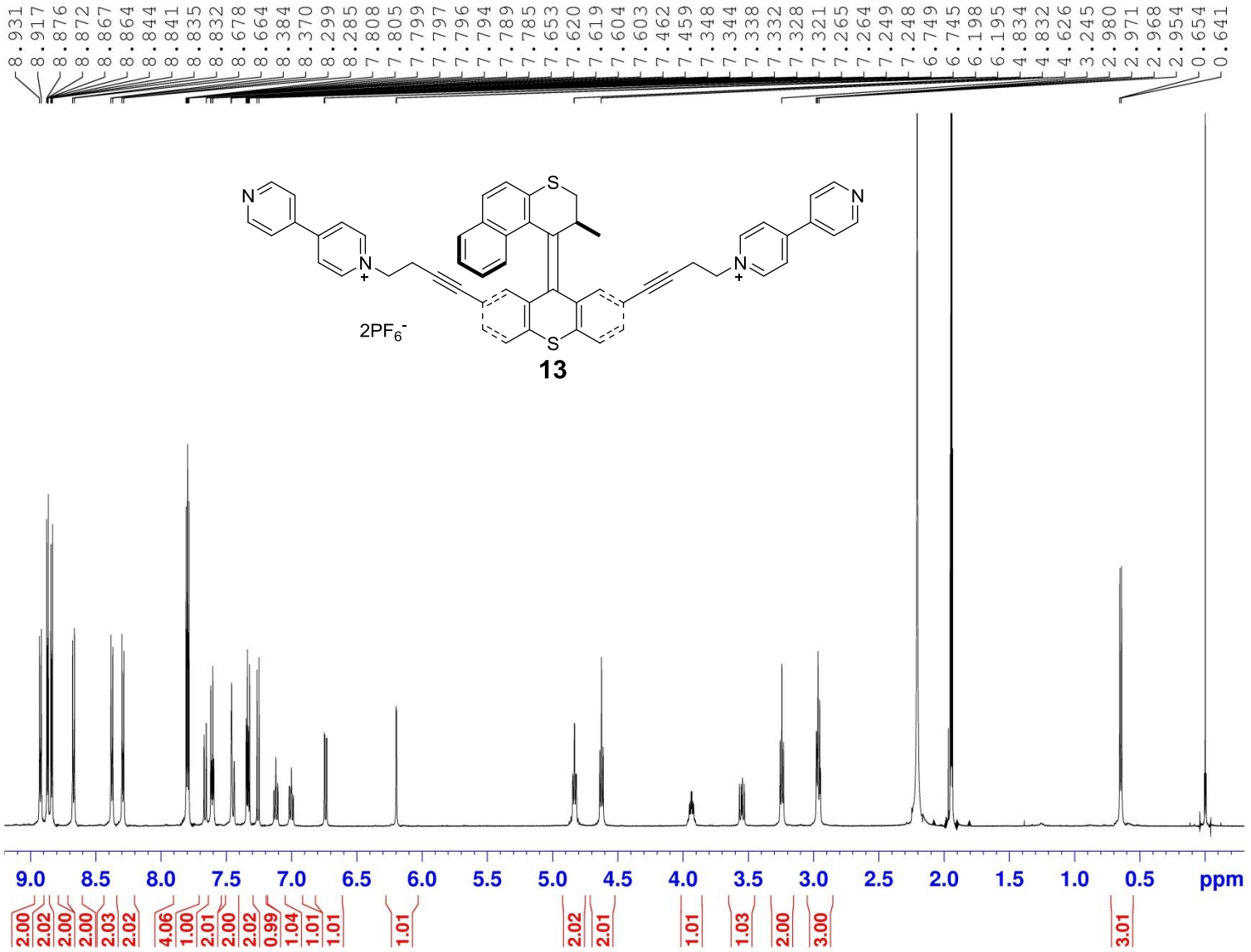
8.931
8.917
8.876
8.872
8.867
8.864
8.844
8.841
8.835
8.832
8.678
8.664
8.384
8.370
8.299
8.285
7.808
7.805
7.799
7.797
7.796
7.794
7.789
7.785
7.653
7.620
7.619
7.604
7.603
7.462
7.459
7.348
7.344
7.338
7.332
7.328
7.321
7.265
7.264
7.249
7.248
6.749
6.745
6.198
6.195
4.834
4.832
4.626
3.245
2.980
2.971
2.968
2.954
0.654
0.641
N
S
N
N
S
N
2PF6-
13
9.0
8.5
8.0
7.5
7.0
6.5
6.0
5.5
5.0
4.5
4.0
3.5
3.0
2.5
2.0
1.5
1.0
0.5
ppm
2.00
2.02
2.00
2.00
2.03
2.02
4.06
1.00
2.01
2.00
2.02
0.99
1.04
1.01
1.01
1.01
2.02
2.01
1.01
1.03
2.00
3.00
3.01

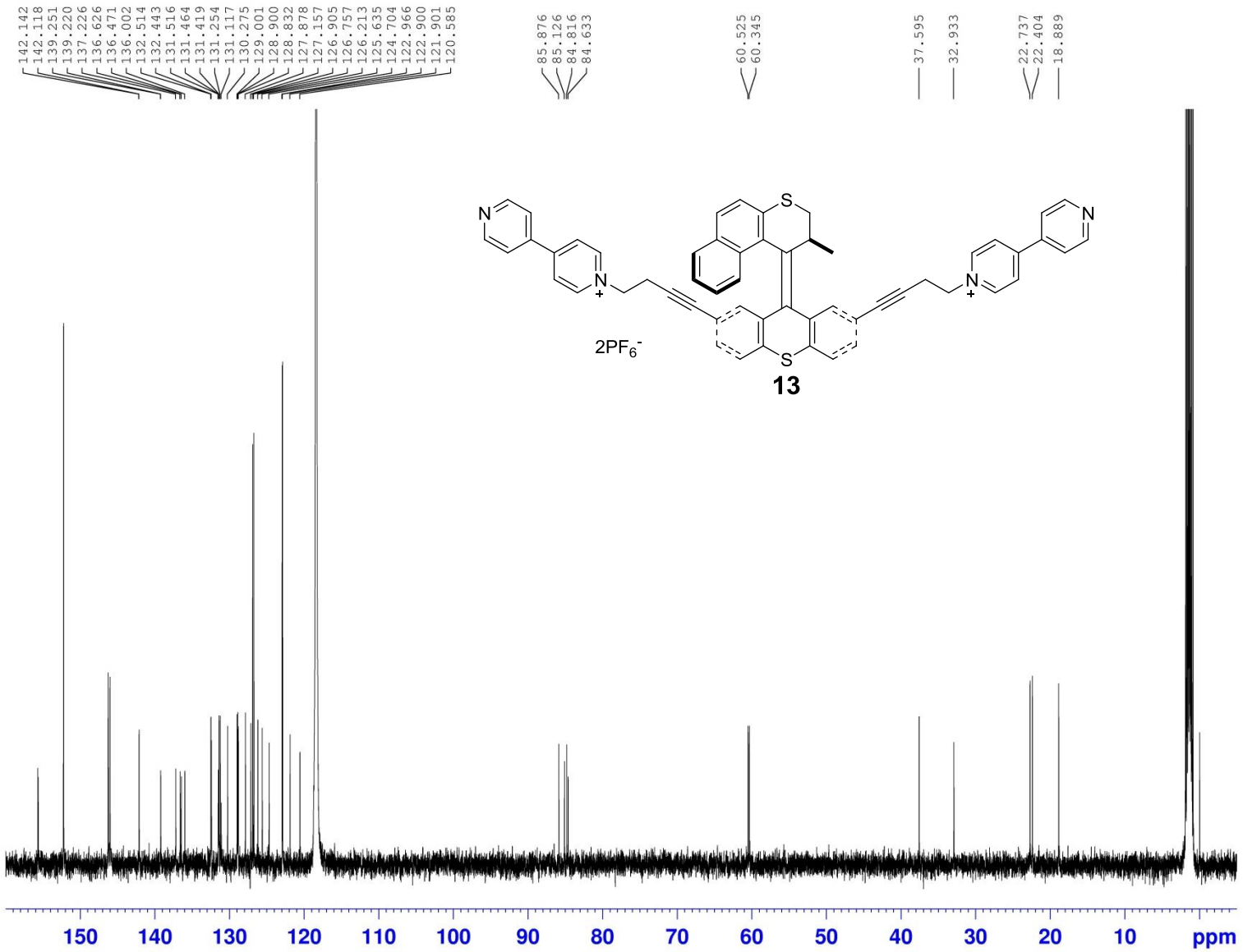
142.142
142.118
139.251
139.220
137.226
136.626
136.471
136.002
132.514
132.443
131.516
131.464
131.419
131.254
131.117
130.275
129.001
128.900
128.832
127.878
127.157
126.905
126.757
126.213
125.635
124.704
122.966
122.900
121.901
120.585
85.876
85.126
84.816
84.633
60.525
60.345
37.595
32.933
22.737
22.404
18.889
N
S
N
N
S
2PF6-
13
150
140
130
120
110
100
90
80
70
60
50
40
30
20
10
ppm

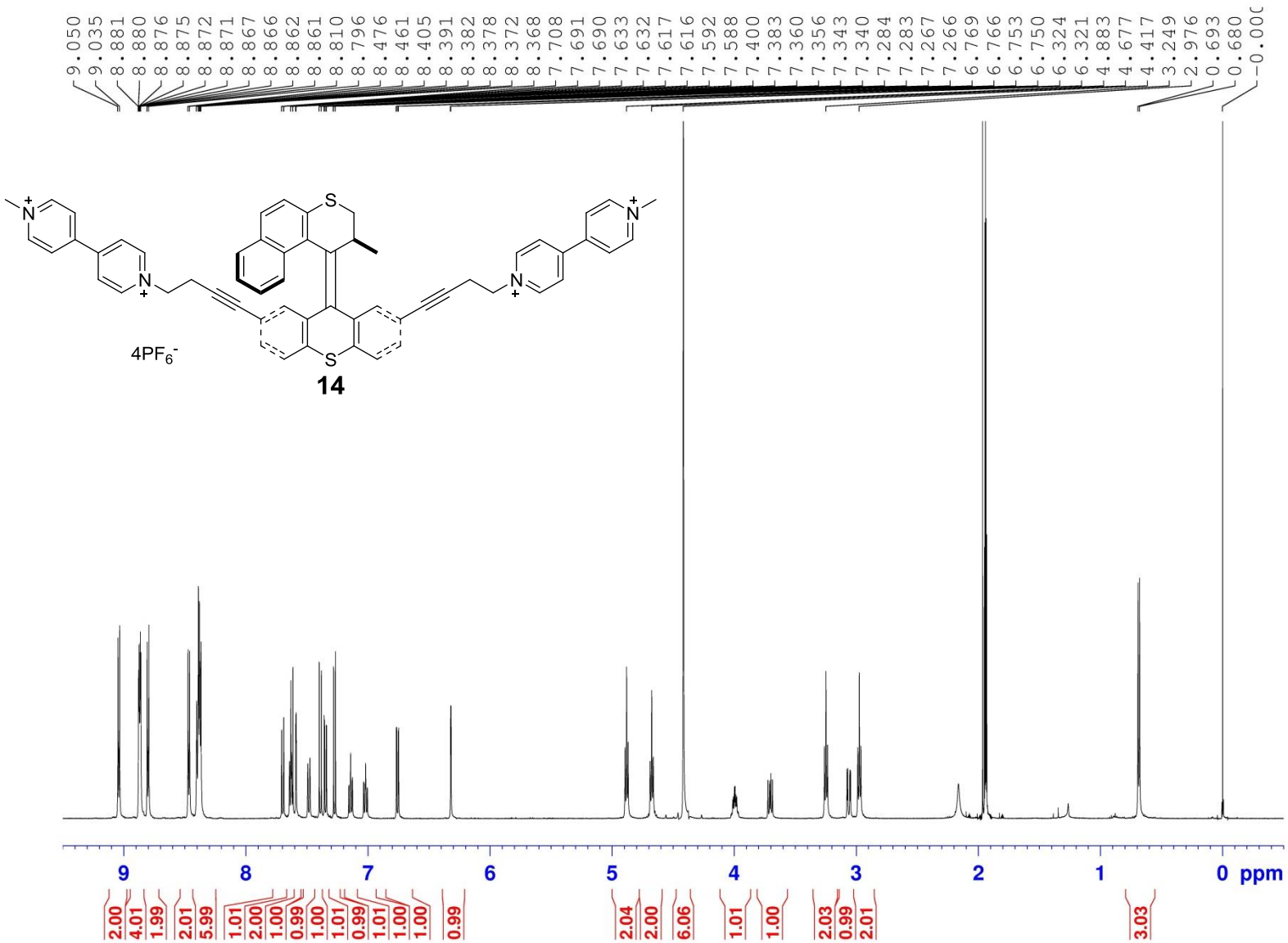
9.050
9.035
8.881
8.880
8.876
8.875
8.872
8.871
8.867
8.866
8.862
8.861
8.810
8.796
8.476
8.461
8.405
8.391
8.382
8.378
8.372
8.368
7.708
7.691
7.690
7.633
7.632
7.617
7.616
7.592
7.588
7.400
7.383
7.360
7.356
7.343
7.340
7.284
7.283
7.267
7.266
6.769
6.766
6.753
6.750
6.324
6.321
4.883
4.677
4.417
3.249
2.976
0.693
0.680
0.000
4PF6-
14
9
8
7
6
5
4
3
2
1
0 ppm
2.00
4.01
1.99
2.01
5.99
1.01
2.00
1.00
0.99
1.00
1.01
0.99
1.01
1.00
1.00
0.99
2.04
2.00
6.06
1.01
1.00
2.03
0.99
2.01
3.03

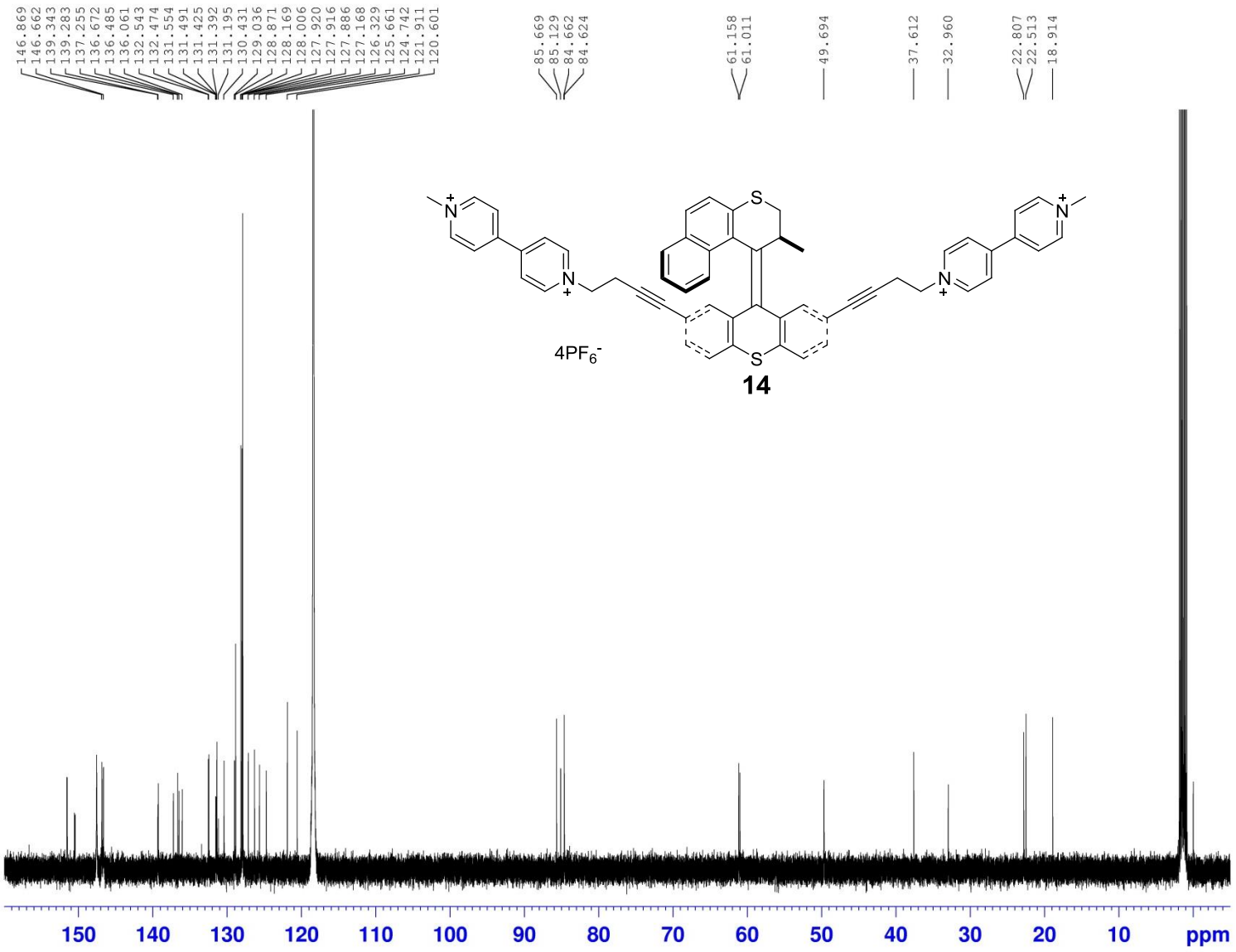
146.869
146.662
139.343
139.283
137.255
136.672
136.485
136.061
132.543
132.474
131.554
131.491
131.425
131.392
131.195
130.431
129.036
128.871
128.169
128.006
127.920
127.916
127.886
127.168
126.329
125.661
124.742
121.911
120.601
85.669
85.129
84.662
84.624
61.158
61.011
49.694
37.612
32.960
22.807
22.513
18.914
4PF6-
14
150
140
130
120
110
100
90
80
70
60
50
40
30
20
10
ppm

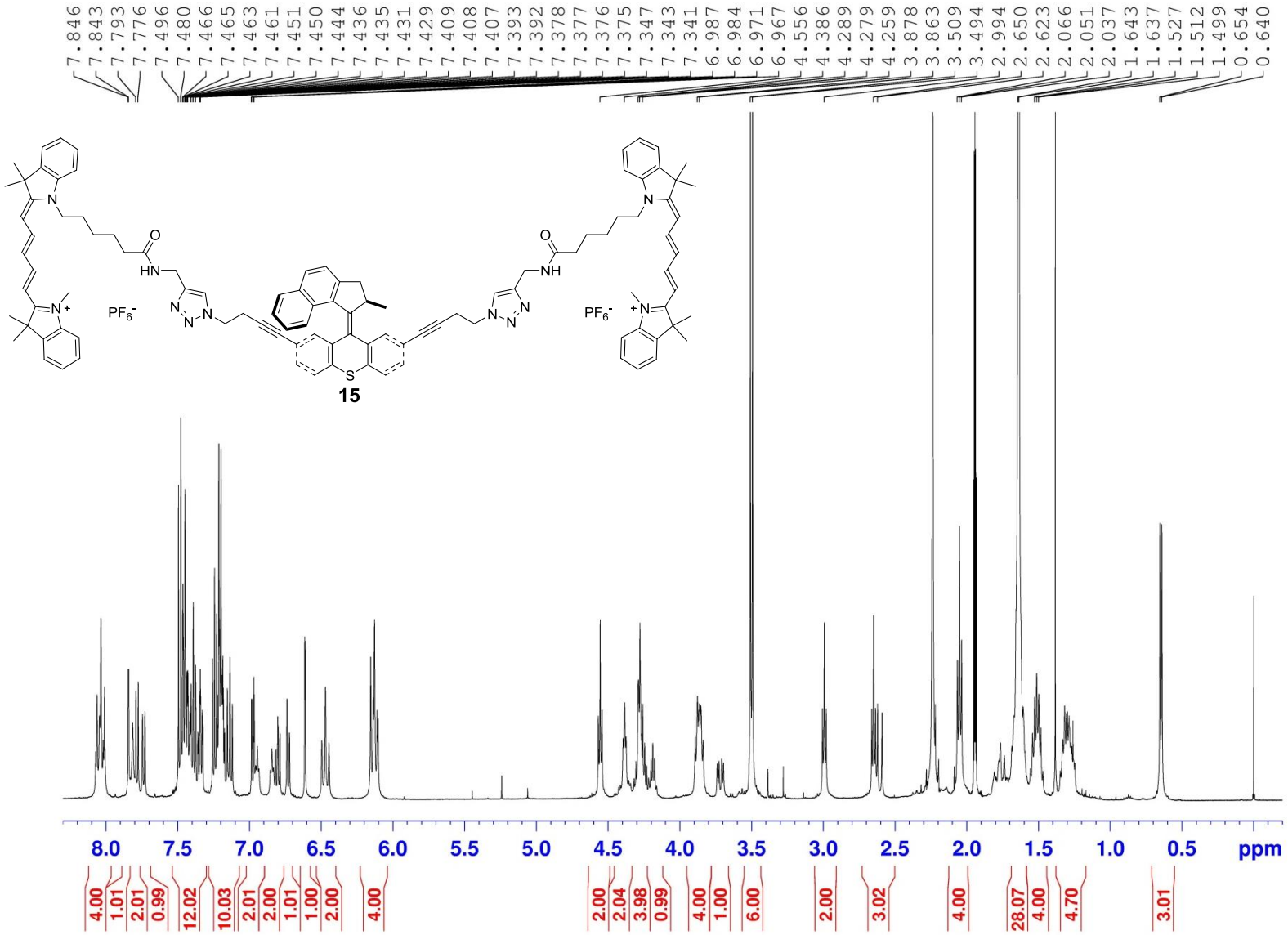
7.846
7.843
7.793
7.776
7.496
7.480
7.466
7.465
7.463
7.461
7.451
7.450
7.444
7.436
7.435
7.431
7.429
7.409
7.408
7.407
7.393
7.392
7.378
7.377
7.376
7.375
7.347
7.343
7.341
6.987
6.984
6.971
6.967
4.556
4.386
4.289
4.279
4.259
3.878
3.863
3.509
3.494
2.994
2.650
2.623
2.066
2.051
2.037
1.643
1.637
1.527
1.512
1.499
0.654
0.640
PF6-
PF6-
15
8.0
7.5
7.0
6.5
6.0
5.5
5.0
4.5
4.0
3.5
3.0
2.5
2.0
1.5
1.0
0.5
ppm
4.00
1.01
2.01
0.99
12.02
10.03
2.01
2.00
1.01
1.00
2.00
4.00
2.00
2.04
3.98
0.99
4.00
1.00
6.00
2.00
3.02
4.00
28.07
4.00
4.70
3.01

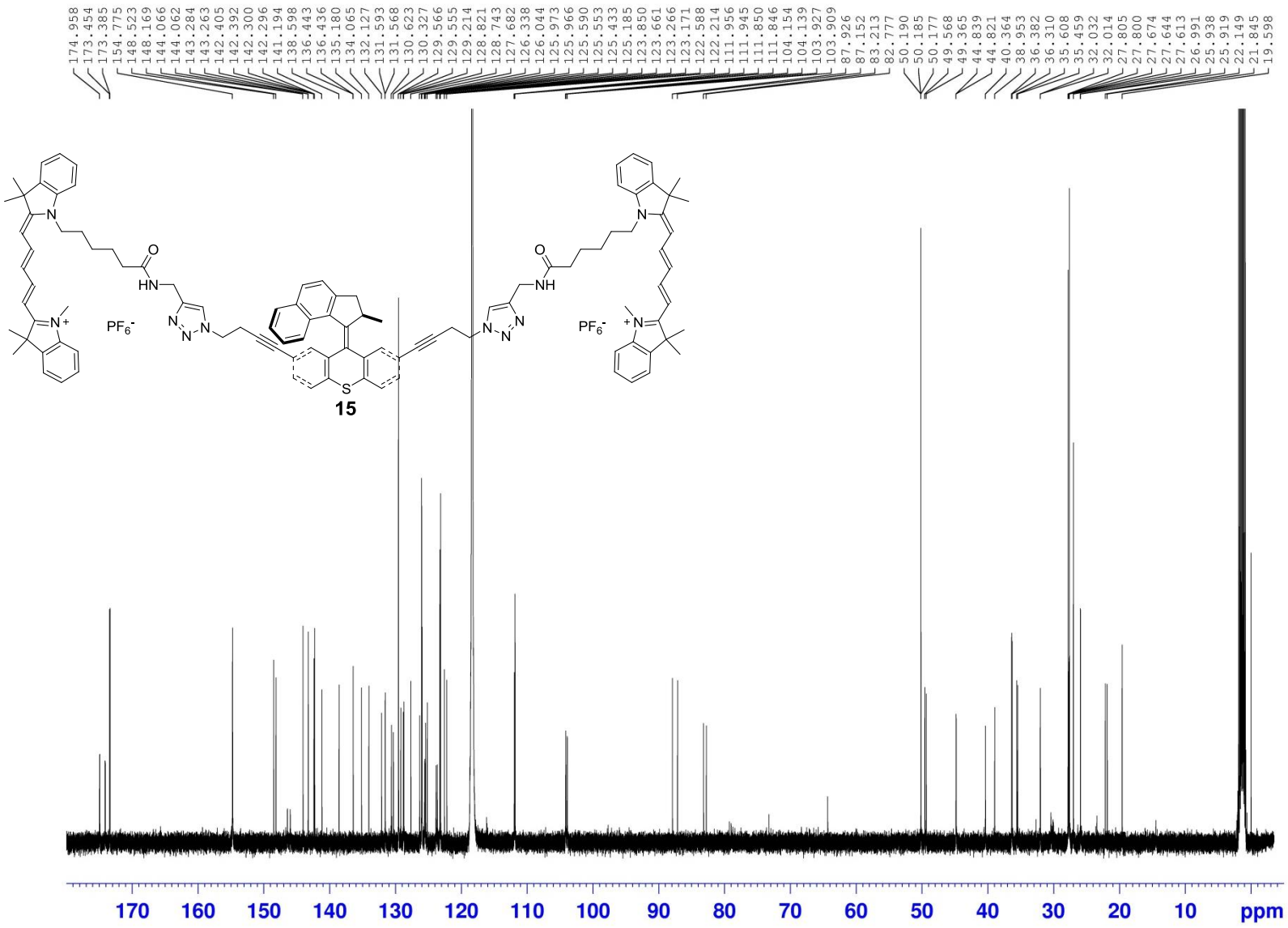
174.958
173.454
173.385
154.775
148.523
148.169
144.066
144.062
143.284
143.263
142.405
142.392
142.300
142.296
141.194
138.598
136.443
136.436
135.180
134.065
132.127
131.593
131.568
130.623
130.327
129.566
129.555
129.214
128.821
128.743
127.682
126.338
126.044
125.973
125.966
125.590
125.553
125.433
125.185
123.850
123.661
123.266
123.171
122.588
122.214
111.956
111.945
111.850
111.846
104.154
104.139
103.927
103.909
87.926
87.152
83.213
82.777
50.190
50.185
50.177
49.568
49.365
44.839
44.821
40.364
38.953
36.382
36.310
35.608
35.459
32.032
32.014
27.805
27.800
27.674
27.644
27.613
26.991
25.938
25.919
22.149
21.845
19.598
PF6-
PF6-
15
170
160
150
140
130
120
110
100
90
80
70
60
50
40
30
20
10
ppm

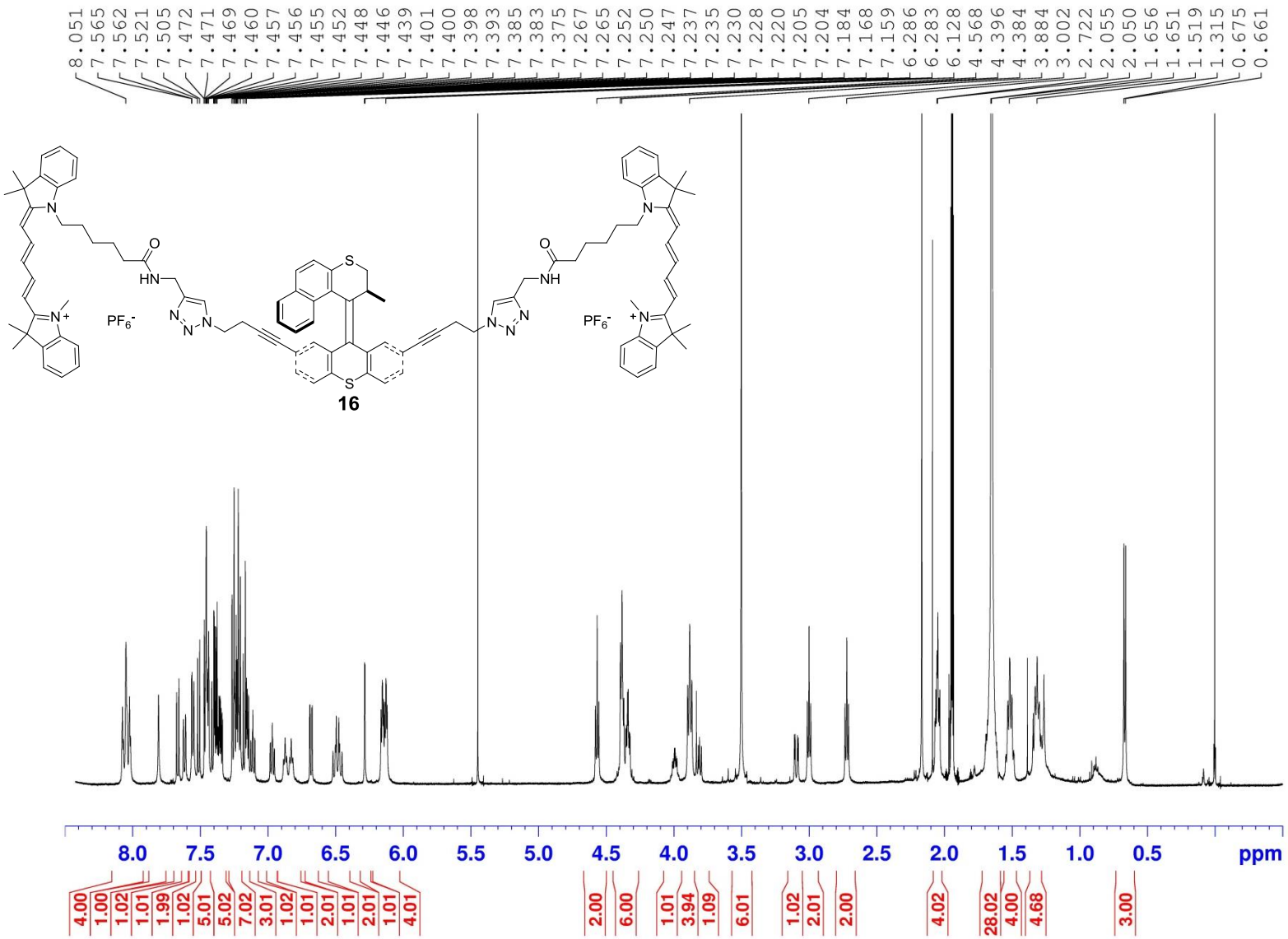
8.051
7.565
7.562
7.521
7.505
7.472
7.471
7.469
7.460
7.457
7.456
7.455
7.452
7.448
7.446
7.439
7.401
7.400
7.398
7.393
7.385
7.383
7.375
7.267
7.265
7.252
7.250
7.247
7.237
7.235
7.230
7.228
7.220
7.205
7.204
7.184
7.168
7.159
6.286
6.283
6.128
4.568
4.396
4.384
3.884
3.002
2.722
2.055
2.050
1.656
1.651
1.519
1.315
0.675
0.661
PF6-
PF6-
16
8.0
7.5
7.0
6.5
6.0
5.5
5.0
4.5
4.0
3.5
3.0
2.5
2.0
1.5
1.0
0.5
ppm
4.00
1.00
1.02
1.01
1.99
1.02
5.01
5.02
7.02
3.01
1.02
1.01
2.01
1.01
2.01
1.01
4.01
2.00
6.00
1.01
3.94
1.09
6.01
1.02
2.01
2.00
4.02
28.02
4.00
4.68
3.00

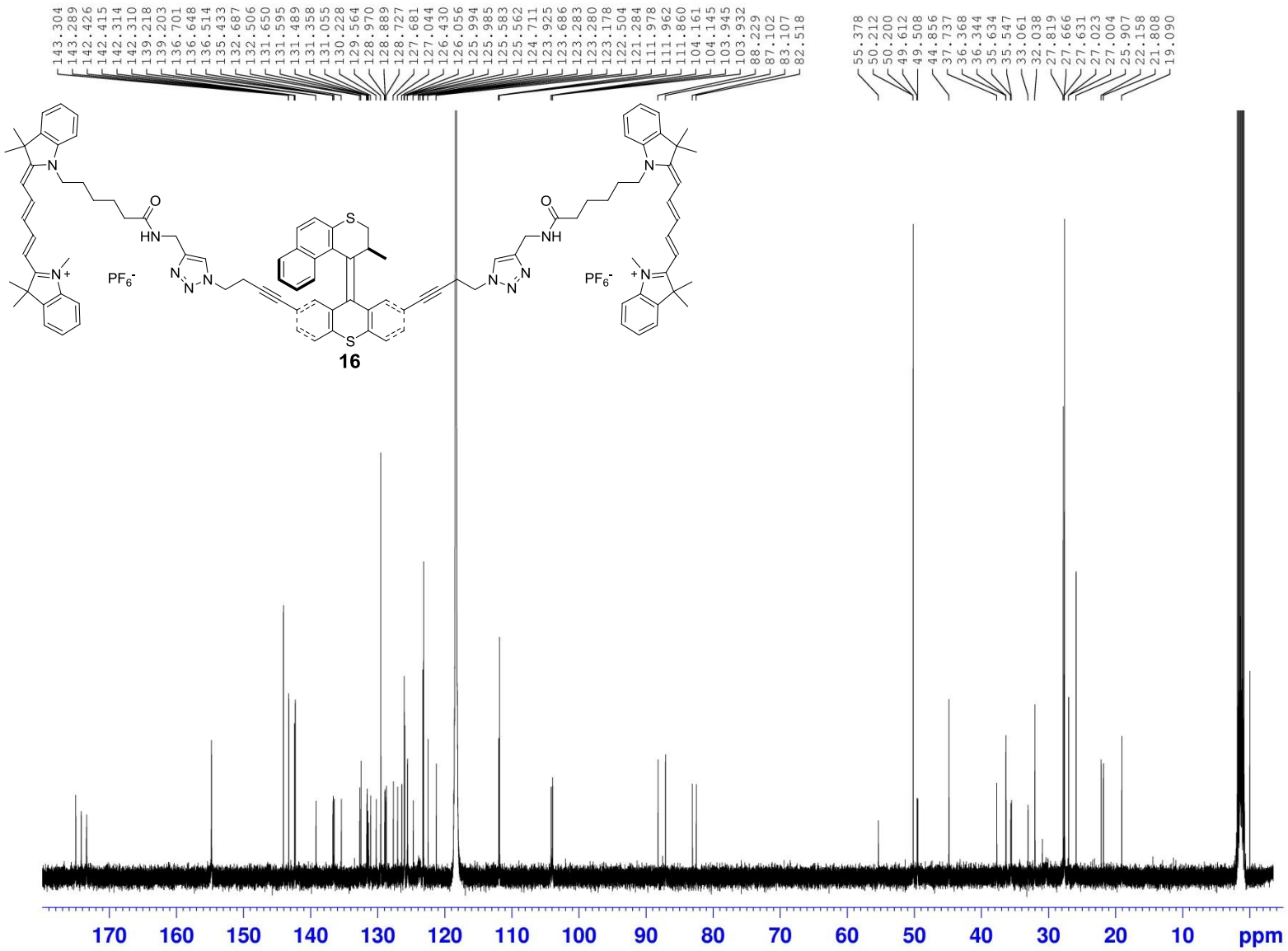
143.304
143.289
142.426
142.415
142.314
142.310
139.218
139.203
136.701
136.648
136.514
135.433
132.687
132.506
131.650
131.595
131.489
131.358
131.055
130.228
129.564
128.970
128.889
128.727
127.681
127.044
126.430
126.056
125.994
125.985
125.583
125.562
124.711
123.925
123.686
123.283
123.280
123.178
122.504
121.284
111.978
111.962
111.860
104.161
104.145
103.945
103.932
88.229
87.102
83.107
82.518
55.378
50.212
50.200
49.612
49.508
44.856
37.737
36.368
36.344
35.634
35.547
33.061
32.038
27.819
27.666
27.631
27.023
27.004
25.907
22.158
21.808
19.090
PF6-
PF6-
16
170
160
150
140
130
120
110
100
90
80
70
60
50
40
30
20
10
ppm

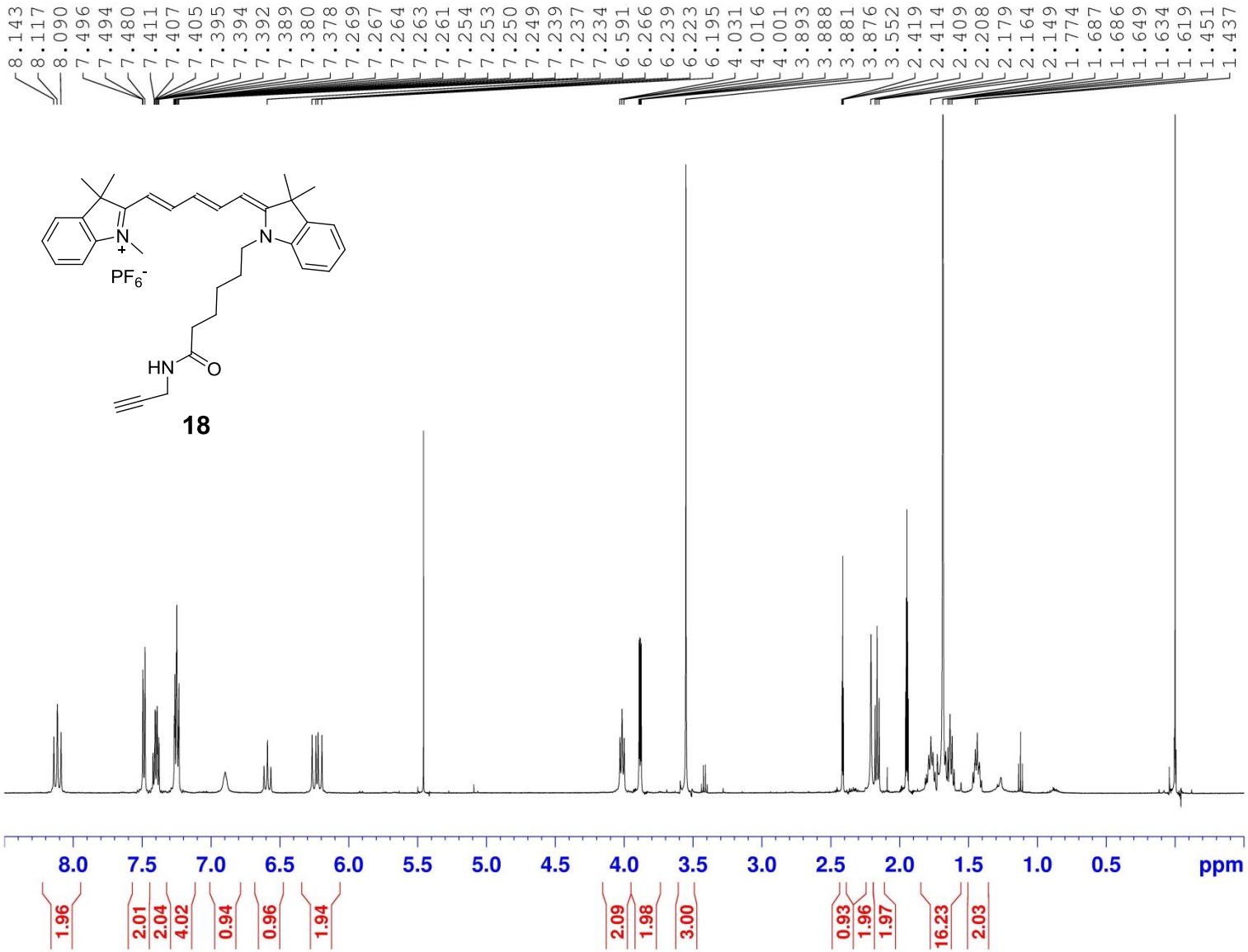
8.143
8.117
8.090
7.496
7.494
7.480
7.411
7.407
7.405
7.395
7.394
7.392
7.389
7.380
7.378
7.269
7.267
7.264
7.263
7.261
7.254
7.253
7.250
7.249
7.239
7.237
7.234
6.591
6.266
6.239
6.223
6.195
4.031
4.016
4.001
3.893
3.888
3.881
3.876
3.552
2.419
2.414
2.409
2.208
2.179
2.164
2.149
1.774
1.687
1.686
1.649
1.634
1.619
1.451
1.437
PF6-
HN
O
18
8.0
7.5
7.0
6.5
6.0
5.5
5.0
4.5
4.0
3.5
3.0
2.5
2.0
1.5
1.0
0.5
ppm
1.96
2.01
2.04
4.02
0.94
0.96
1.94
2.09
1.98
3.00
0.93
1.96
1.97
16.23
2.03

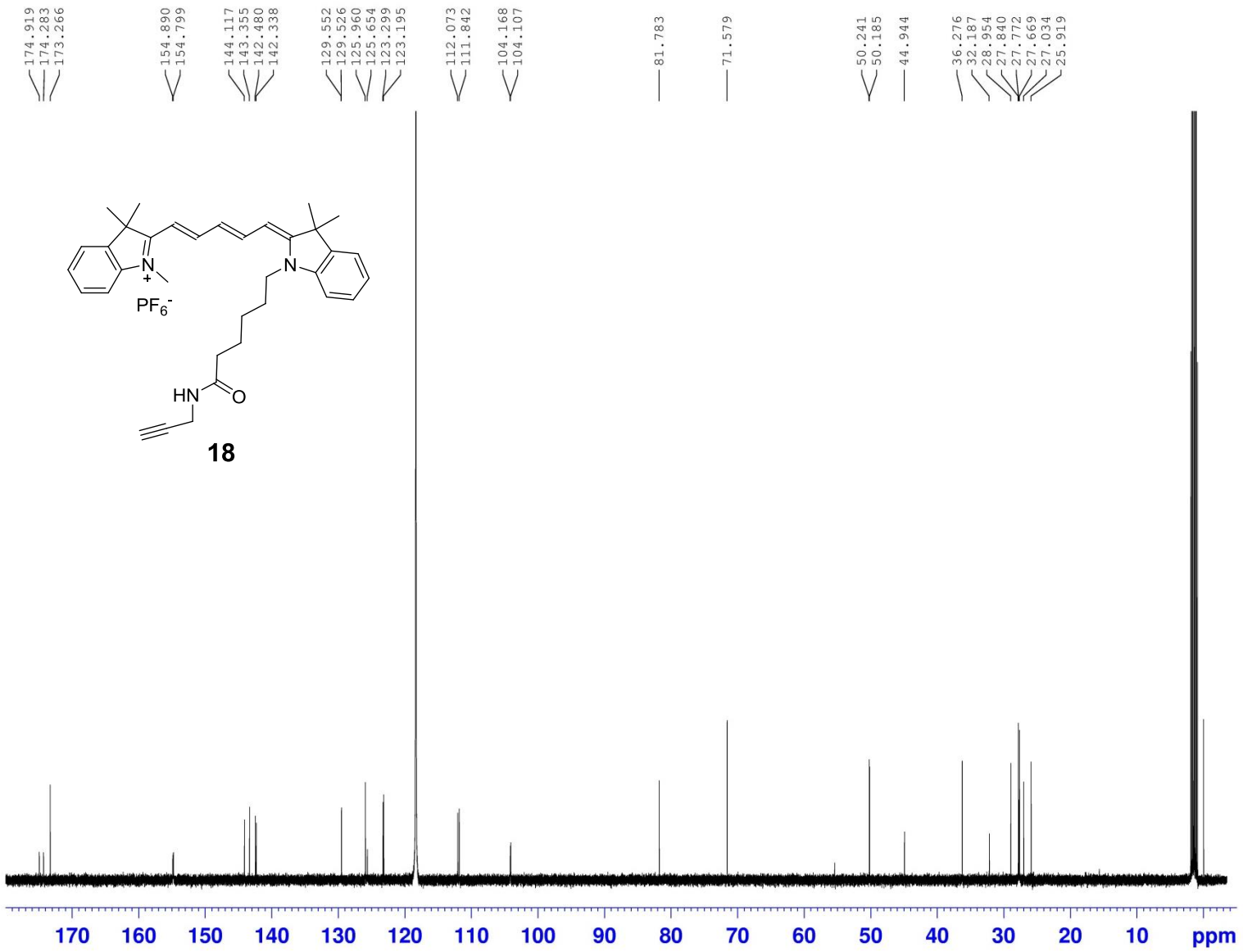
174.919
174.283
173.266
154.890
154.799
144.117
143.355
142.480
142.338
129.552
129.526
125.960
125.654
123.299
123.195
112.073
111.842
104.168
104.107
81.783
71.579
50.241
50.185
44.944
36.276
32.187
28.954
27.840
27.772
27.669
27.034
25.919
PF6-
HN
O
18
170
160
150
140
130
120
110
100
90
80
70
60
50
40
30
20
10
ppm

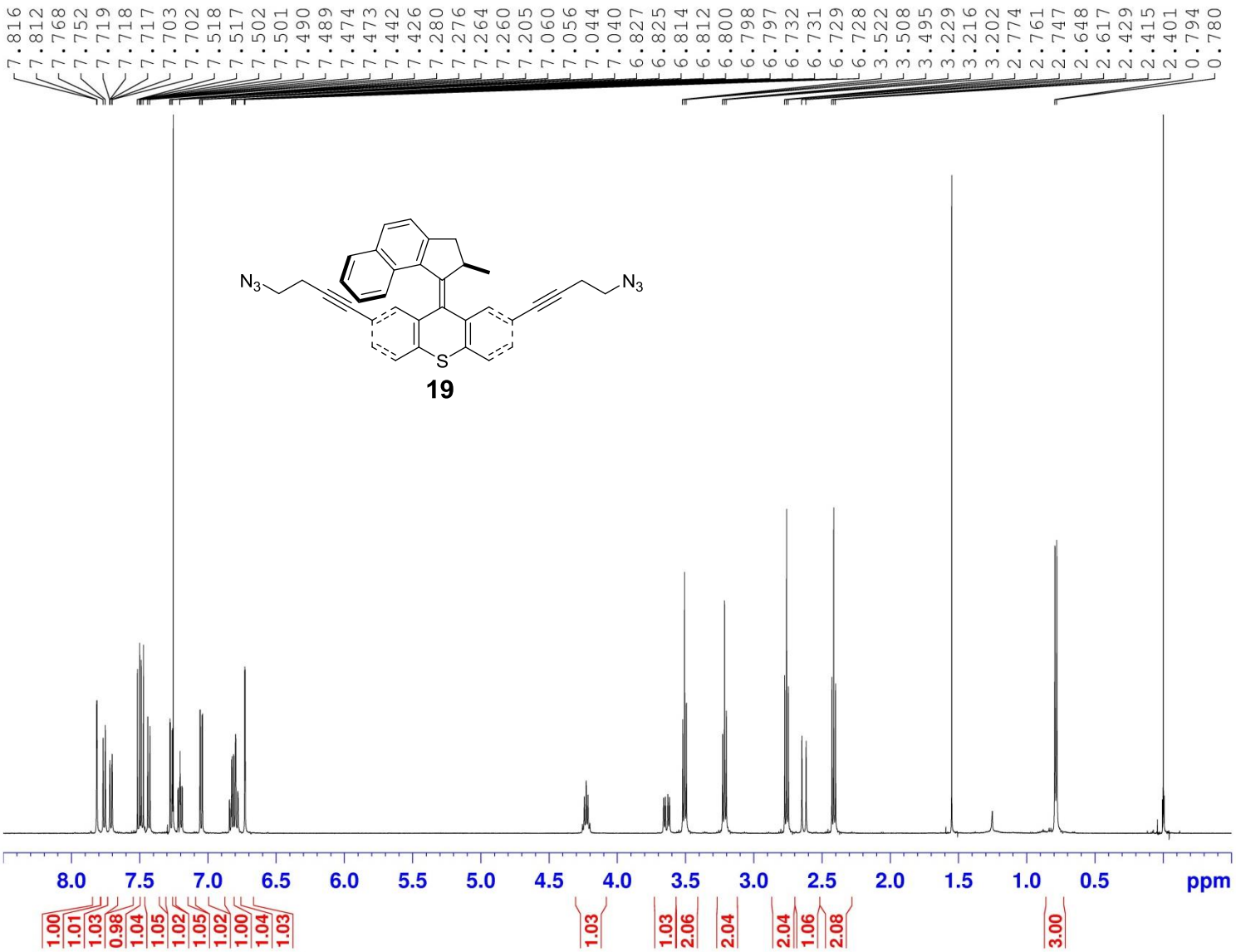
7.816
7.812
7.768
7.752
7.719
7.718
7.717
7.703
7.702
7.518
7.517
7.502
7.501
7.490
7.489
7.474
7.473
7.442
7.426
7.280
7.276
7.264
7.260
7.205
7.060
7.056
7.044
7.040
6.827
6.825
6.814
6.812
6.800
6.798
6.797
6.732
6.731
6.729
6.728
3.522
3.508
3.495
3.229
3.216
3.202
2.774
2.761
2.747
2.648
2.617
2.429
2.415
2.401
0.794
0.780
N3
N3
S
19
8.0
7.5
7.0
6.5
6.0
5.5
5.0
4.5
4.0
3.5
3.0
2.5
2.0
1.5
1.0
0.5
ppm
1.00
1.01
1.03
0.98
1.04
1.05
1.02
1.05
1.02
1.00
1.04
1.03
1.03
1.03
2.06
2.04
2.04
1.06
2.08
3.00

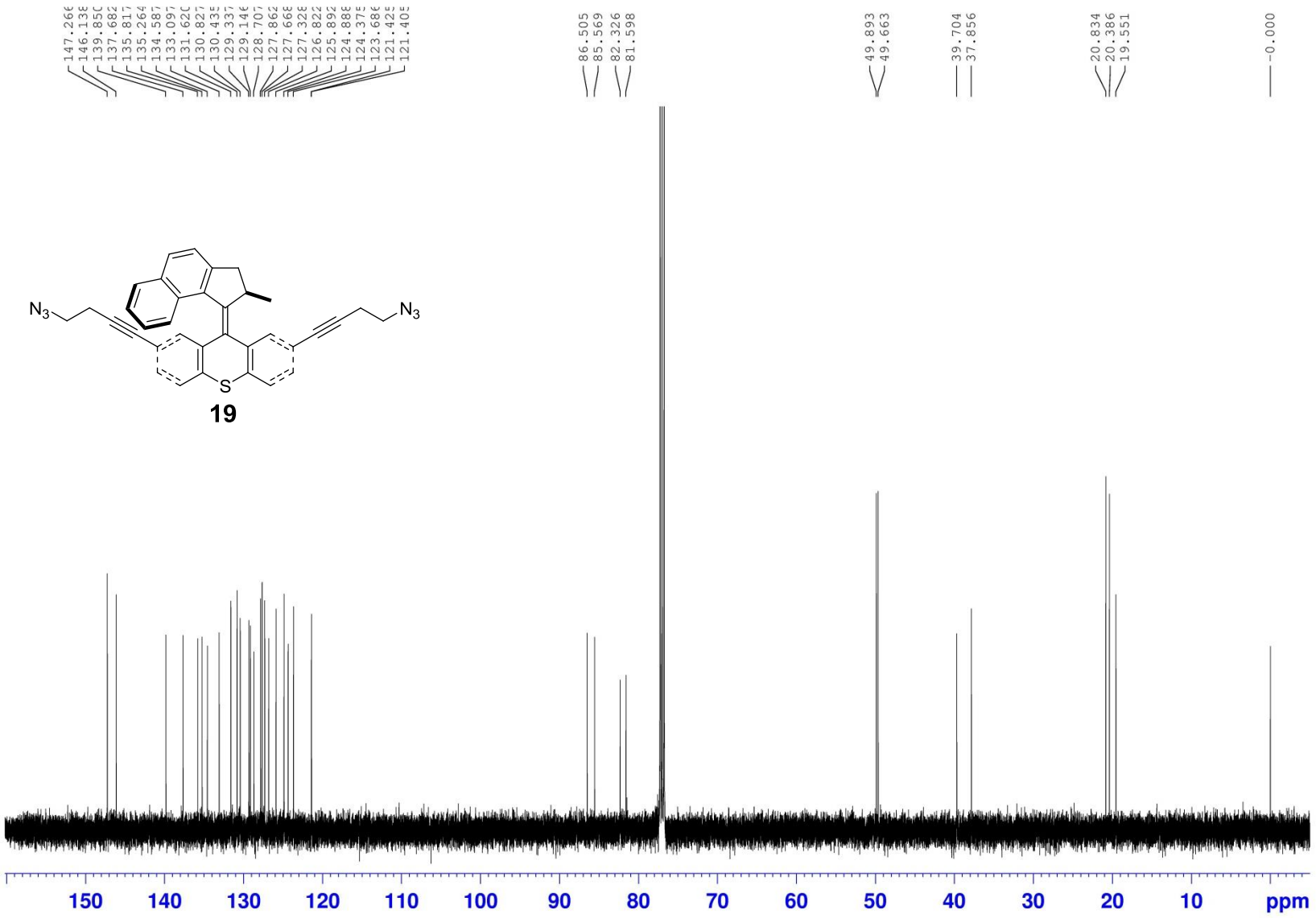
147.266
146.138
139.850
137.682
135.817
135.264
134.587
133.097
131.620
130.827
130.435
129.337
129.146
128.707
127.862
127.668
127.328
126.822
125.892
124.888
124.375
123.686
121.425
121.405
86.505
85.569
82.326
81.598
49.893
49.663
39.704
37.856
20.834
20.386
19.551
-0.000
N3
N3
S
19
150
140
130
120
110
100
90
80
70
60
50
40
30
20
10
ppm

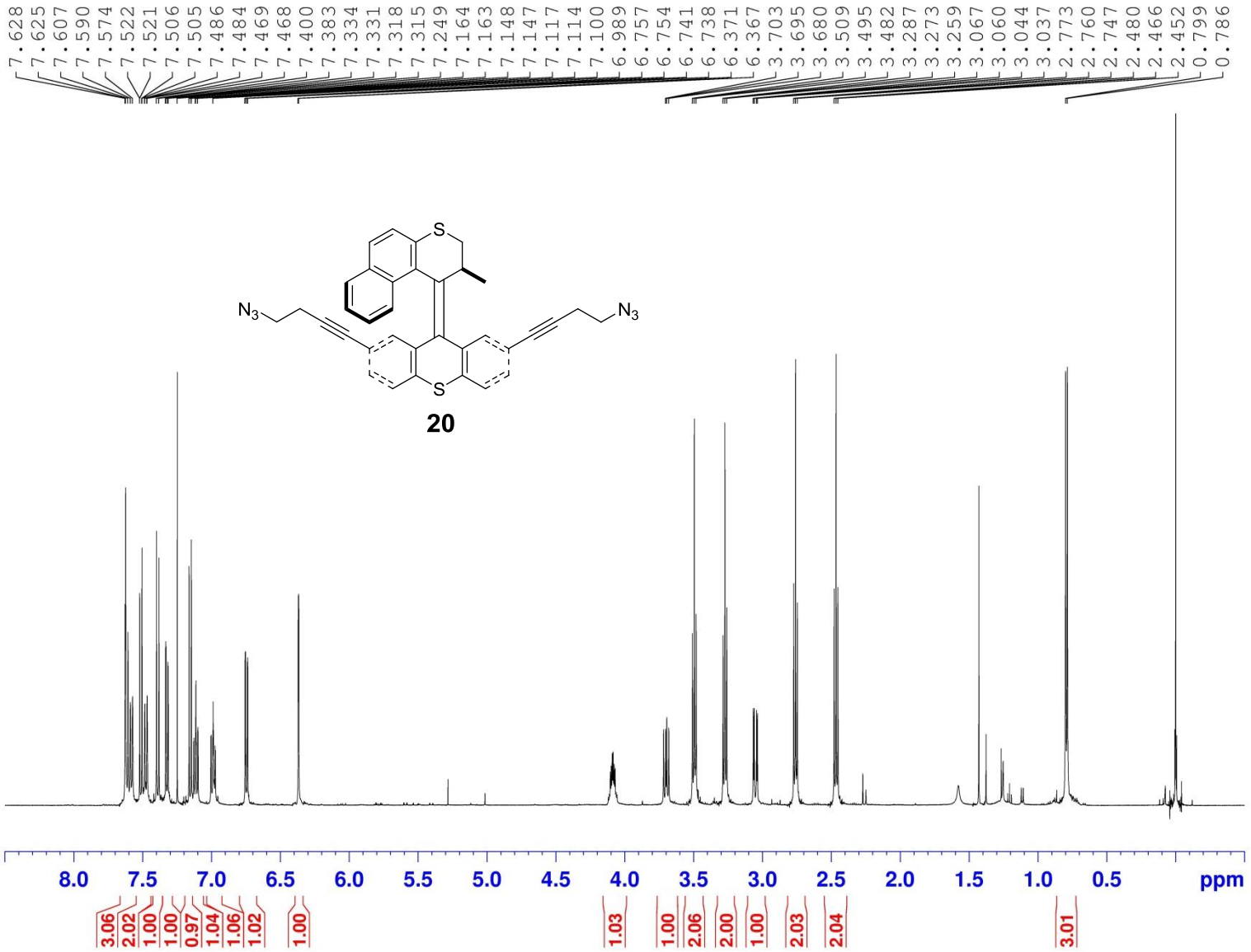
7.628
7.625
7.607
7.590
7.574
7.522
7.521
7.506
7.505
7.486
7.484
7.469
7.468
7.400
7.383
7.334
7.331
7.318
7.315
7.249
7.164
7.163
7.148
7.147
7.117
7.114
7.100
6.989
6.757
6.754
6.741
6.738
6.371
6.367
3.703
3.695
3.680
3.509
3.495
3.482
3.287
3.273
3.259
3.067
3.060
3.044
3.037
2.773
2.760
2.747
2.480
2.466
2.452
0.799
0.786
S
N3
N3
S
20
8.0
7.5
7.0
6.5
6.0
5.5
5.0
4.5
4.0
3.5
3.0
2.5
2.0
1.5
1.0
0.5
ppm
3.06
2.02
1.00
1.00
0.97
1.04
1.06
1.02
1.00
1.03
1.00
2.06
2.00
1.00
2.03
2.04
3.01

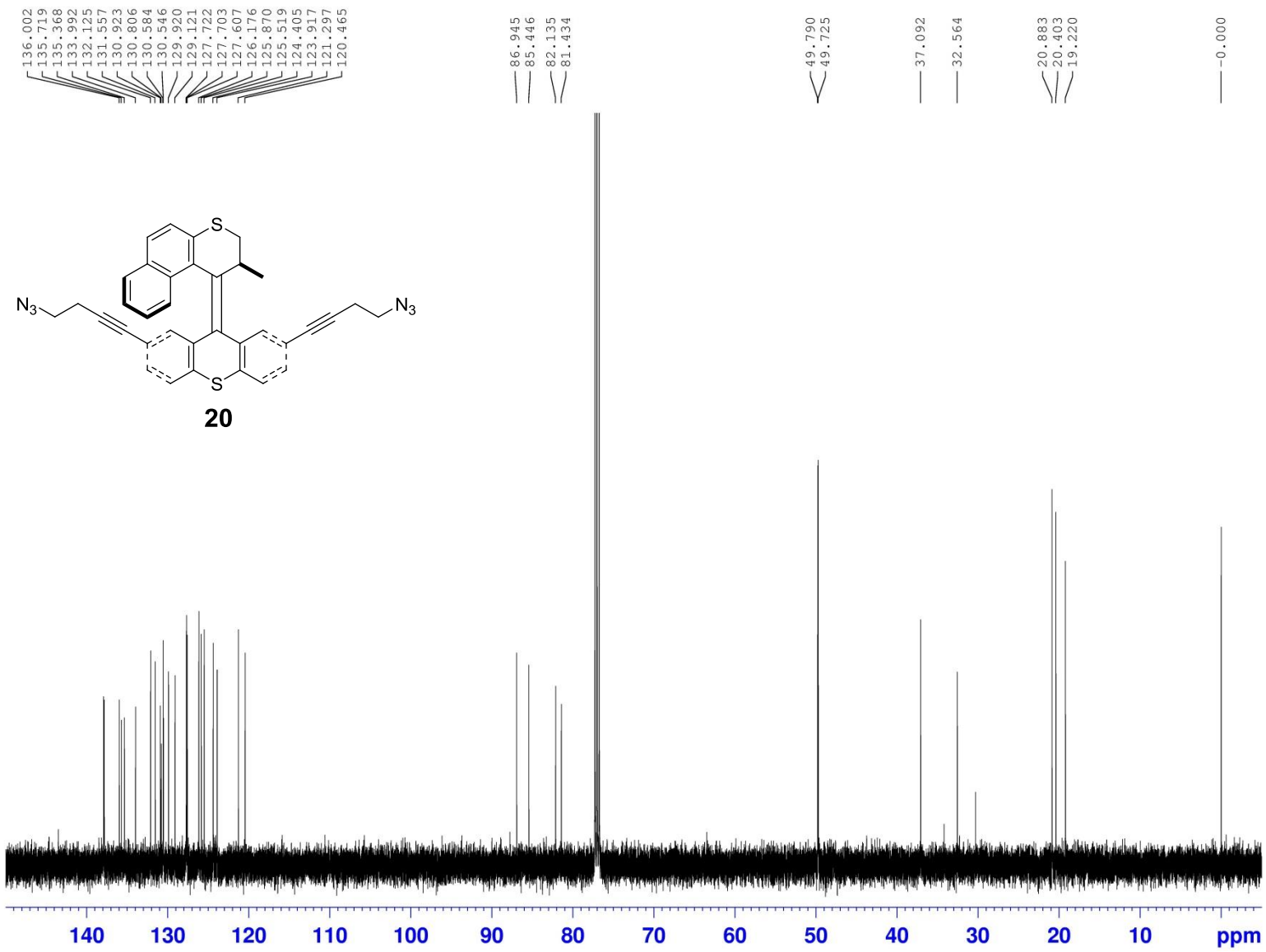
136.002
135.719
135.368
133.992
132.125
131.557
130.923
130.806
130.584
130.546
129.920
129.121
127.722
127.703
127.607
126.176
125.870
125.519
124.405
123.917
121.297
120.465
86.945
85.446
82.135
81.434
49.790
49.725
37.092
32.564
20.883
20.403
19.220
0.000
S
N3
N3
S
20
140
130
120
110
100
90
80
70
60
50
40
30
20
10
ppm